

DEVELOPMENT OF AN $Al(OH)_3$ CRYSTALLIZATION
MODEL BASED ON POPULATION BALANCE

by



PIETER G. GROENEWEG, B. Eng.

A Thesis

Submitted to the School of Graduate Studies

in Partial Fulfilment of the Requirements

for the Degree

Doctor of Philosophy

McMaster University

December 1980

DOCTOR OF PHILOSOPHY (1980)
(Chemical Engineering)

McMASTER UNIVERSITY
Hamilton, Ontario

TITLE: Development of an $Al(OH)_3$ Crystallization
Model Based on Population Balance

AUTHOR: Pieter G. Groeneweg, B. Eng.
McMaster University

SUPERVISOR: Dr. T.W. Hoffman

Number of
Pages: XIX, 526

ABSTRACT

The overall objective of this program was to develop mathematical and experimental techniques, and thus obtain a mathematical model, capable of predicting the crystal size distribution as a function of batch time, for a seeded batch crystallizer in which alumina trihydrate was crystallizing in a supersaturated aqueous solution of sodium aluminate.

In this regard, a 2l bench-scale crystallizer was designed so as to operate in a similar way (with respect to mechanisms and rates) as industrial crystallizers in that gentle mixing allowed significant agglomeration to occur during the crystallization. Thus, nucleation, growth and agglomeration rates had to be predicted in the crystallizer model as a function of the crystallizer operation conditions.

Reproducible and representative samples were extracted from this crystallizer by a developed sampling system which did not contaminate or affect the sample nor the crystallizer contents. Analytical techniques were developed to obtain sodium aluminate and solids concentration. Crystal size distribution was measured for each sample by a special Coulter counter equipped with a Channelizer and a Log-Transformer apparatus. This equipment measured crystal volume with a resolution of 100 size intervals over a spherical equivalent diameter range of 4 to 80 μm . The lack of measurements below 4 μm was a source of trouble in the modeling program, and was the main source of error in the mathematical analyses using the particle size distribution data.

A special mathematical method based on the population balance was developed to investigate and determine each of the rate equations for the processes growth, agglomeration, and nucleation individually from the obtained batch data. The method is termed here the 'method of pseudo moments'. It allows for investigation within feasible computer resources and circumvents the confounding of each of these processes with each other.

The growth rate was modeled by a two-dimensional birth and spread mechanism, while the model for the agglomeration rate was based on a mechanism of free-in-space binary collisions with an agglomeration effectiveness kernel. This kernel was modeled by the product of a crystal environment term and a crystal size effect term. The form of the environment term suggests that the agglomeration rate is related to the growth rate lending support to the concept that alumina trihydrate crystals after collision are grown together to form true polycrystalline crystals and are not a 'flock' of crystals held together by physical attractive forces. The size-dependent term is made up of an inertial impaction mechanism term which accounts for the collision frequency, and a term which accounts for the efficiency of the collision. It was shown that crystals in the intermediate size range (ca. 10 to 30 μm) agglomerate most effectively. The expression for the nucleation rate, which was also developed using the pseudo-moment method suggests that the formation of nuclei in this experimental crystallizer at 85°C was not via normal homogeneous or heterogeneous nucleation mechanisms but rather occurred through attrition of very small particles from the seed particles (a sort of 'dusting-off' of nuclei-sized particles). These rate expressions still need to be expanded for the effect of

temperature, of intensity of agitation, and of impurities.

Although the method of pseudo moments allows for the determination of rate expressions from size distribution data, it does not provide a means of predicting the evolution of size distributions. To this end a model based on the population balance, mass balances, and rate equations was formulated. However, such a model, if it includes agglomeration, is impractical for investigation of rate equations due to long numerical solution times.

Because of the significance of the three rate processes the resulting model was made up of a set of algebraic equations and an integro-first order non-linear hyperbolic partial differential equation, with one of the integrals being a convolution integral. Numerical solution schemes of such an equation are prone to exhibit stability, accuracy, and long solution time problems. The stability and accuracy problems were solved and the long solution time problem minimized by the development of two numerical solution schemes. One was based on a developed weighted central difference approximation for the partial derivative with respect to crystal size and integrating by the Runge-Kutta Merson technique along a rectangular grid with respect to batch time. The other was based on solution along the characteristics of the equation and interpolating between the 'characteristic grid' and a specially developed rectangular grid for the integral terms. This grid allows for the convolution nature of one of the integrals. The resultant quadrature was fast and accurate. Depending on the type of crystallization process and the shape of the evolving size distribution either one or the other is best suited with regard to speed of solution and accuracy.

The method of pseudo moments and numerical solution schemes allow for any growth, agglomeration, and nucleation expressions and any form of size distributions. Thus the numerical methods developed here for the determination of rate equations and prediction of size distributions are applicable to any particulate process, such as polymerization, microbial reactions, etc.

ACKNOWLEDGEMENTS

Many people have contributed either directly or indirectly to this work. Dr. P.C. Chakravarti from the McMaster Applied Mathematics Department contributed his time and knowledge in the form of many helpful discussions on the numerical solution problems encountered in this work. The efforts of my thesis supervisor, Dr. T.W. Hoffman, are gratefully acknowledged. His assistance in this work was unlimited and he provided me with an invaluable research experience. The many stimulating discussions with my co-graduate students also contributed significantly to this work. The encouragement and understanding of my CIL co-workers and CIL management aided greatly in the completion of this dissertation. The efforts and skills of Helen Rousseau, who transferred an illegible manuscript into a very well-typed, readable thesis, are really appreciated. Lastly, a special thanks is in order to my wife Laurie for her continued support, patience, and encouragement throughout my undergraduate, graduate student years, and full time employment years during which in our spare time and holidays this dissertation was written.

TABLE OF CONTENTS

	<u>Page</u>
CHAPTER 1. INTRODUCTION	1
1.1 General Issue	1
1.2 Specific Objectives	4
CHAPTER 2. CRYSTALLIZATION THEORY, LITERATURE REVIEW	6
2.1 Introduction	6
2.2 Crystallization Processes	6
2.2.1 Alumina Trihydrate Crystallization Process	7
2.3 Fundamental Crystallization Process Concepts	8
2.3.1 Rate Processes	9
2.3.2 Process Variables	12
2.3.3 Crystallizer Performance	12
2.4 Crystal Growth Rate	13
2.4.1 Diffusion Controlled Growth	14
2.4.2 Surface Reaction Controlled Growth	14
2.4.3 Effect of Crystal Size on Growth	16
2.4.4 Observations of Growth Rates for the Alumina Trihydrate System	18
2.4.5 Review of Growth Rate Models for the Alumina Trihydrate System	19
2.4.6 Effect of Poisons on the Crystal Growth Rate of Alumina Trihydrate	26
2.4.7 Summary of the Available Information on the Growth Rates for the Alumina Trihydrate System	27
2.5 Nucleation Rate	28
2.5.1 Homogeneous Nucleation	30
2.5.2 Heterogeneous Nucleation	30
2.5.3 Secondary Nucleation	31
2.5.3.1 Secondary Nucleation Rate Correlations	34
2.5.4 Observations on the Nucleation Rates of the Alumina Trihydrate System	36

	<u>Page</u>
2.5.5 Estimate of the Minimum Nuclei Size for the Alumina Trihydrate System	37
2.5.6 Summary of the Available Information on Nucleation for the Alumina Trihydrate System	38
2.6 Agglomeration Rate	39
2.6.1 General Agglomeration Rate Model	40
2.6.2 Review of Observations on Agglomeration and Agglomeration Rate Models for the Alumina Trihydrate System	43
2.6.3 Summary of the Available Information on Agglomeration for the Alumina Trihydrate System	45
2.7 Attrition Rate	45
2.7.1 General Attrition Rate Model	46
2.7.2 Observations on the Attrition Rates for the Alumina Trihydrate System	47
2.8 Induction Period	49
2.8.1 Effect of the Induction Phenomenon on the Alumina Trihydrate Rate Processes	49
2.9 Crystal Habit	50
2.9.1 Alumina Trihydrate Crystal Shape	51
2.10 Modelling of a Crystallizer	51
2.10.1 Mechanistic Model	52
2.10.1.1 Conservation Laws	53
2.10.1.1.1 Conservation Laws for the Batch Alumina Trihydrate System	54
2.10.1.2 Constitutive Relations: Alumina Trihydrate System Relations	57
2.10.1.3 Empirical Correlations; Alumina Trihydrate System Correlations	58

	<u>Page</u>
CHAPTER 3. EXPERIMENTAL; MEASUREMENT OF PROCESS VARIABLES	62
3.1 Crystallization Experiments; Introduction	62
3.1.1 Experimental Features of the Alumina Trihydrate System	62
3.1.2 Experimental Variables	64
3.1.3 Batch vs. Continuous Experiments	64
3.1.4 Mixing of the Crystal Suspension	66
3.1.5 Pure vs. Impure Solutions	66
3.1.6 Caking and Corrosion Problems	67
3.1.7 Initial Batch Conditions and Batch Sampling	67
3.1.8 Sample Analysis Difficulties	68
3.2 Bench-Scale Crystallizer Apparatus	69
3.2.1 Development of Crystallizer Apparatus	71
3.2.2 The Experimental Crystallizer	77
3.3 Preparation of a Supersaturated Solution of Sodium Aluminate	79
3.4 Preparation of Alumina Trihydrate Seed Crystals	82
3.5 Alumina Trihydrate Batch System Process Variables	84
3.6 Batch Crystallizer Sampling Procedure	87
3.7 Analysis of the Sodium Aluminate Solution Sample	93
3.8 Analysis of the Alumina Trihydrate Crystals. Suspension Sample	94
3.9 Experimental Procedure	97
CHAPTER 4. EXPERIMENTAL PLAN AND EXPERIMENTAL RESULTS	102
4.1 Introduction; Experimental Plan	102
4.2 Presentation and Discussion of Experimental Data	113
4.2.1 Solution Density and Equilibrium Alumina Concentration	113
4.2.2 Typical Experimental Batch Data	115
4.2.2.1 Solution Concentration Measurements	115
4.2.2.2 Crystallizer Operating Temperature	117
4.2.2.3 Crystal Size Distribution	119
4.3 Consistency Check of the Measurements	130
4.4 Different Presentations of the Crystal Size Distribution	136
4.5 Moments of the Crystal Size Distribution	142

	<u>Page</u>
CHAPTER 5. DEVELOPMENT OF THE MODEL EQUATIONS FOR A SEEDED BATCH CRYSTALLIZER FOR ALUMINA TRIHYDRATE	148
5.1 Introduction	148
5.2 Population Balance Derivation	149
5.2.1 Use of the General Population Balance Equation to Describe a Batch Crystallizer	155
5.2.2 Boundary and Initial Condition for the Batch Crystallizer Population Balance	158
5.2.2.1 Initial Condition	158
5.2.2.2 Boundary Condition	159
5.3 Derivation of the Functional Relationship for Growth, Nucleation, Agglomeration, and Attrition	162
5.4 Mathematical Manipulation of the Population Balance Equations; Including the Functional Relationships	168
5.4.1 The Symmetric Property of the Agglomeration Convolution Integral	168
5.4.2 Spatial Averaged Number Density Population Balance for a Batch System with the Rate Processes Growth, Nucleation, Agglomeration, and Attrition	170
5.4.3 Spatial Averaged Number Cumulative Population Balance for a Batch System with Growth, Nucleation, Agglomeration, and Attrition	171
5.5 Pseudo Moment Equations for a Batch System with the Rate Processes, Growth, Nucleation, Agglomeration, and Attrition	178
5.6 Mass Balances and Auxiliary Relations for the Batch Alumina Trihydrate System	192
5.6.1 Mass Balances	192
5.6.2 Auxiliary and Empirical Relationships	194
5.6.3 Relationships between Population Balance and Mass Balances	195
5.6.4 Number of Independent Mass Balance Equations	196
5.6.5 Mass Balances for a Batch Alumina Trihydrate System with Approximate Constant Suspension Volume	198
5.6.6 Mass Balances for a Batch Alumina Trihydrate System with a Given Empirical Solution Density Correlation	199
5.6.7 Mass Balances for a Batch Alumina Trihydrate System with a Given Empirical Alumina Concentration Model	201

	<u>Page</u>
CHAPTER 6. NUMERICAL SOLUTION OF THE MECHANISTIC BATCH CRYSTALLIZATION MODEL	204
6.1 Introduction	204
6.2 Mechanistic Model for the Batch Crystallization of Alumina Trihydrate	205
6.3 Solution of the Model Equations	218
6.3.1 General	218
6.3.2 Solution of the Population Balance Equation	218
6.3.2.1 Survey of Previous Solutions of the Population Balance Equation	219
6.3.2.2 Initial Investigation of Different Numerical Solutions	221
6.3.2.2.1 Successive Approximations Combined with the Method of Characteristics	222
6.3.2.2.2 Method of Moments and Pseudo Moments	225
6.3.2.2.3 Finite Difference Solutions using a Fixed Grid	227
6.3.3 Strategy for Obtaining a Solution for the Population Balance Equation	228
6.3.3.1 Solution of the Integro Part of the Integro-Partial Differential Equation	229
6.3.3.1.1 Special Grid and Quadrature Expressions for the Evaluation of the Agglomeration Term	231
6.3.3.1.2 Investigation of the Numerical Accuracy of the Quadrature Expressions for the Agglomeration Term	238
6.3.3.2 Solution of the Partial Differential Part of the Integro-Partial Differential Equa- tion	243
6.3.3.2.1 Evaluation of the Accuracy of the Numerical Solution of the Population Balance for a Growth-only Process	244
6.4 Solution of the Full Model	250
6.4.1 Correction for Quadrature Approximation Errors	255

	<u>Page</u>
6.5 Investigation of the Two Numerical Solution Methods	259
6.6 Solution Procedure for the Alumina Trihydrate System	263
6.7 Comments on and Problems Arising Out of the Solution Difficulties of the Full Model	264
CHAPTER 7. DEVELOPMENT OF CONSTITUTIVE RELATIONSHIPS BY MEANS OF THE METHOD OF PSEUDO MOMENTS	266
7.1 Introduction	266
7.2 Method of Pseudo Moments	266
7.2.1 Change in the Crystal Size Distribution Due to the Growth Process	268
7.2.2 Change in the Crystal Size Distribution Due to the Agglomeration Process	273
7.2.3 Change in the Crystal Size Distribution Due to the Nucleation Process	280
7.3 Constitutive Relationships for Growth, Agglomeration, and Nucleation	284
7.3.1 Smoothing of Experimental Data	285
7.3.1.1 Solution Concentration Variables	285
7.3.1.2 Smoothing Formula for the Experimental Crystal Size Distribution Data	291
7.3.1.3 Estimation of the Number of Crystals with a Size Less Than the Cut-off Size	296
7.3.2 Implementation of the Pseudo Moment Equations	302
7.3.2.1 Kinetic Growth Rate Expression	304
7.3.2.2 Kinetic Agglomeration Rate Expression	309
7.3.2.2.1 Estimation of the Parameters in the Models	313
7.3.2.3 Kinetic Nucleation Rate Expressions	317
7.3.2.3.1 Estimation of Parameters	325
7.4 Summary of the Rate Models for Growth, Agglomeration and Nucleation	332

	<u>Page</u>
CHAPTER 8. BATCH CRYSTALLIZATION MODEL FOR THE ALUMINA TRIHYDRATE SYSTEM: COMPARISON WITH EXPERIMENTAL OBSERVATIONS AND RESULTS FROM OTHER STUDIES	354
8.1 Introduction	354
8.2 Size Distribution of Seed	355
8.3 Comparison between Predictions and Experimental Data	342
8.3.1 The Problem of Correlation of Models and Model Parameters	352
8.4 Comparison with Other Studies	353
8.5 Summary	356
CHAPTER 9. SUMMARY, CONCLUSIONS, AND RECOMMENDATIONS	358
9.1 General	358
9.2 Experimental	358
9.3 Determination of the Rate Equations	362
9.4 Numerical Solution of a Population Balance for an Unsteady State Process with Growth, Nucleation, and Agglomeration Terms	363
9.5 Model for the Seeded Batch Crystallization of Alumina Trihydrate	367
NOTATION	375
REFERENCES	377
APPENDIX A. Raw Data, Experiment #13	382
APPENDIX B. Preparation of and Analysis of a Supersaturated Solution of Sodium Aluminate	427
B.1 Preparation of a Supersaturated Solution of NaAlO ₂	427
B.2 Solution Concentration Analysis Procedure	430
APPENDIX C. Crystal Size Analysis System	433
C.1 Operating Principle of a Coulter Counter Apparatus (Model Z _p)	433
C.2 Function of Peripheral Coulter Counter Apparatus	435
C.2.1 Coulter Channelyzer, Model C-1000	435
C.2.1.1 Channelyzer Log Transformer	435
C.2.1.2 Teleprinter Interface, Teletype	436
C.2.2 Constant Voltage Transformer	437

	<u>Page</u>
C.5 Coulter Counter Channelyzer Calibration	437
C.3.1 Channelyzer in Linear Mode	438
C.3.2 Channelyzer in Log Mode	440
C.4 Coulter Counter Count Corrections	441
C.4.1 Coincidence Correction Coulter Counter Equation	441
C.4.2 An Agglomeration Type of Equation for Coincidence Correction	442
C.4.3 Background Count Interference	444
C.5 Channelyzer Number Rejection Losses	445
C.6 Coulter Counter Electrolyte	448
C.7 Particle Size Distribution Measurement with a Coulter Counter Analysis System	449
APPENDIX D. Derivation of Auxiliary Equations and Relationships	453
D.1 Calculation of Crystallizer Solids Concentra- tion	453
D.2 Shape Factor Functions	458
APPENDIX E. Computer Listing of the Major Programs	463

LIST OF FIGURES

<u>Figure #</u>	<u>Title</u>	<u>Page</u>
2.5.1-A	Crystallization Rate Processes	11
2.5-A	Line Diagram of Different Nucleation Mechanisms	29
3.2.1-A	Stainless Steel Scaled Down Industrial Batch Crystallizer	72
3.2.1-B	Glass Batch Crystallizer with Air Lift	73
3.2.1-C	Polypropylene Batch Crystallizer with Semi-Automatic Sampling System	75
3.2.2-A	Experimental Batch Crystallizer	78
3.2.2-B	Crystallizer Suspension Sampler	80
3.3-A	Alumina Trihydrate Digester	81
3.6-A	Crystallizer Suspension Sample Sampler	89
3.6-B	Crystallizer Suspension Sample Filtering Apparatus	91
4.2.2.1-A	Solution Concentration Measurements	116
4.2.2.2-A	Batch Crystallizer Operating Temperature	118
4.2.2.3-A	Number Density Function with Respect to Crystal Volume	120-125
4.2.2.3-B	Number Density Function with Respect to Crystal Volume at Selected Batch Times	129
4.3-A	Calculated Crystallizer Solids Concentration	133
4.4-A	Number Density Function with Respect to Spherical Equivalent Diameter for Selected Batch Times	137
4.4-B	Area Density Function with Respect to Spherical Equivalent Diameter for Selected Batch Times	140
4.4-C	Electron Micrographs of Typical Alumina Trihydrate Crystals	141

<u>Figure #</u>	<u>Title</u>	<u>Page</u>
4.4-D	Weight Density Function with Respect to Spherical Equivalent Diameter for Selected Batch Times	143
4.5-A	Moments of the Crystal Size Distribution	145
6.3.3.1-A	Grid to Facilitate the Repeated Calculation of the Agglomeration Rate Expression	234
6.4-A	Grid for the Solution of the Full Model	252
7.2.2-A	Schematic of the Weighting Functions used in the Investigation of Agglomeration Kernel Models Superimposed on a Number Density Function	275
7.3.1.1-A	Experimental and Smoothed Alumina and Caustic Solution Concentrations	290
7.3.1.2-A	Experimental Density Function Data and Smoothed Cubic Splines Predictions	297-298
7.3.1.3-A	Measured Number, Area, and Weight of Crystals with Sizes Greater than the Cut-off Size and Estimated Values Over All Sizes	303
7.3.2.1-A	Fit of the Growth Rate Model in Terms of the Pseudo Moments	308
7.3.2.2.1-A	Fit of the Agglomeration Rate Model in Terms of the Pseudo Moments	318-321
7.3.2.2.1-B	Size Dependent Term of the Agglomeration Effectiveness Kernel, $\phi_{V,a}$ vs. $D(l)$ and $D(p)$	322-323
7.3.2.3-A	Fit of the Nucleation Rate Model in Terms of the Pseudo Moments	329
8.1-A	Change in the Crystal Size Distribution due to Different Crystallization Processes	336
8.2-A	Fit of the Full Model with an Exponential Initial Distribution	340
8.2-B	Fit of the Full Model with a Log-Normal Initial Distribution	341
8.3-A to I	Mechanistic Batch Model Solution and Raw Size Distribution Data	343-351

<u>Figure #</u>	<u>Title</u>	<u>Page</u>
C-1	Coulter Counter Sampling Section	434
C-2	Different Resolution of a Crystal Size Density Function	436
C-3	Channelyzer Number Rejection Losses	447
C-4	Automatic Batch Filtration Apparatus	450

LIST OF TABLES

<u>Table #</u>	<u>Title</u>	<u>Page</u>
4.1-A	Range of Alumina Trihydrate Batch Process Variables	103
4.1-B	Experimental Conditions and Type of Experimental Apparatus	104-112
4.2.1-A	Spot Checks on Misra's Solution Density and Equilibrium Alumina Solution Concentration Correlations	114
4.3-A	Consistency Check of the Measurements by Means of the Variable Solids Concentration	134
6.2-A	Summary of Model Equations	215-217
6.3.3.1.2-A	Comparison between the Analytical and Developed Numerical Approximation Solution of an Unsteady State Agglomeration Model	241-242
6.5-A	Number of Required Function Evaluations and Required Central Processing Time for the Numerical Solution over an Integration Interval of Fifteen Minutes	260
7.3.1.2-A	Relative Percentage Difference between Experimental Density Function Data and Smoothed Predictions	293-295
7.3.2.1-A	Fit of Different Growth Rate Models	306
7.3.2.2-A	Fit of Different Agglomeration Effectiveness Kernel Models	311
7.3.2.3-A	Fit of Different Models for the Crystals Environment Term of the Nucleation Rate Expression	326
A-1	Raw Data; Experiment #13	383
A-2 to 15	Raw Data from the Model Z_B Coulter Counter; Experiment #13, Sample #1 ^B to #14	385-426
C-1	Calibration of 200 (240 depth) Coulter Counter Orifice Tube	439
C-2	Channelyzer Number Rejection Losses	446

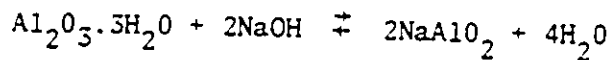
CHAPTER 1

INTRODUCTION

1.1 General Issue

Most of the alumina produced industrially is obtained by extracting it from bauxite ore using the Bayer process (pl). The essential features of this process are the same as they were when the process was invented by Karl Josef Bayer in Austria and patented by him in 1888. This process resolves into five basic steps:

1. Digestion, in which the alumina trihydrate in the bauxite ore is dissolved in a caustic solution according to



leaving a residue called 'red mud'.

2. Filtration of the red mud, leaving a clear concentrated solution.
3. Concentration of the solution by flash vaporization of the water and by cooling to produce a supersaturated solution.
4. Crystallization of the sodium aluminate to alumina trihydrate in a seeded batch crystallizer according to the reverse reaction above.
5. Separation of the solid to provide both recycle seed material and product. This product is then calcined in a kiln to provide α -alumina for the reduction cells.

This study is concerned with the fundamental phenomena associated with the crystallization process.

One of the most important variables in determining the characteristics of any crystallization process is the size distribution of the crystal hold-up in the crystallizer. This distribution indirectly governs the crystallizer production rate and directly determines the size distribution of the product. For example, crystallization rate depends on the surface area of the crystals in the crystallizer; hence, for a given mass hold-up in the crystallizer, the highest rate occurs when the crystals have the smallest average size. However, the advantage of this high production rate would be offset by the disadvantage of the handling or separating difficulties associated with further processing of small crystals. Thus, in most crystallization processes there is usually a need to produce crystals with a desired size distribution at a desired production rate. To understand how this objective can best be achieved in any given situation requires knowledge of the underlying fundamental crystallization processes which are occurring in any given system.

Most crystallizers are now operated based on 'state-of-the-art' or operating experience. An attempt is usually made to control the operation over a narrow range of operating conditions and the personnel in charge usually only have a qualitative feel for the effect of changing operating conditions on the resultant crystal production rate and product size distribution.

Several laboratory and pilot plant studies involving the crystallization of alumina trihydrate have been reported (m3,h1,g1,b6). Since these studies are discussed later, it suffices to say at this point that

these studies were either carried out under conditions which were not representative of industrial operation (m3), or carried out over a very narrow range of operating conditions (h1), or concerned mainly with observations on single crystals (b6), or based on detailed experimental observations without attempting to explain the underlying crystallization processes (g1,g4). All of these studies are difficult to compare because of the dependence of the overall crystallization process on the type and operation of the crystallizer employed in the study. Industrial crystallizers operate with only slight to moderate agitation and it is this intensity of agitation which affects the crystal attrition and agglomeration processes in the crystallizer. Systems with or without agglomeration behave quite differently. Certainly, a model based on laboratory data with insignificant agglomeration has little relation to the industrial systems where agglomeration occurs. A narrow range of operating conditions for laboratory experiments usually leads to a model which may have limited applicability outside this operating range. Single crystal studies on the other hand provide valuable fundamental insight with regard to growth rate and possibly nucleation rate (t1), but they do not shed much light on the overall performance of a crystallizer. Straight observations of the system under lab conditions without explanation of the underlying processes will be confusing, at best, because of the high dimensionality of the problem.

These studies illustrate the two basic approaches to crystallization investigations: first, the study of the behaviour of single crystals and second, the study of the whole crystal population in a crystallizer using the population balance equation to unravel the various phenomena occurring therein. The first is a more fundamental study which provides direct basic information with regard to the rate and type of

growth process, nucleation rates and factors affecting these processes (see, for example, Garside (g5)). The second also provides basic information on growth and nucleation rates, although more on an average or overall basis; but, in addition, provides some measure of the agglomeration and attrition rates existing in a given system, and most important the interaction of all of these processes. This approach leads readily to the description of an industrial type of crystallizer and is the approach taken for this work as illustrated by the following objectives.

1.2 Specific Objectives

The objectives of this work are:

1. To provide a mathematical model for a batch crystallizer which will predict the solid production rate and the crystal size distribution as a function of process variables.
2. To develop a bench-scale experimental crystallizer which will behave similar to an industrial type of crystallizer and which will allow the mathematical model to be tested. This requires the development of sampling and measurement techniques for the variables of the process.
3. To define the required form of the constitutive equations or rate expressions in the model and evaluate their parameters from the bench-scale experimental program.

Since it is recognized that some of the parameters in the kinetic rate expressions depend upon geometry and operation of a crystallizer (for example, agitation), it is realized that a model developed from a bench-scale apparatus will not apply directly to an industrial crystallizer.

It is expected, however, that the model for an industrial crystallizer will at least be of similar form and that this work will provide the mathematical and experimental procedures necessary to effect a mathematical model for an industrial crystallizer.

A secondary benefit of this study arises by virtue of the nature of this crystallization process. Since the study involves studying all crystal growth, nucleation, attrition and agglomeration processes simultaneously and involves modelling all of these processes within the population balance equation, the rather complex non-linear integro-partial differential equation which results must be integrated numerically. The techniques developed for this will have widespread application in other than crystallization work, such as for instance: cloud physics, microbial processes, polymerization, liquid-liquid extraction, etc. This shows the broad applicability of the modelling technique which is used in this work.

CHAPTER 2

CRYSTALLIZATION THEORY, LITERATURE REVIEW

2.1 Introduction

Although the main topic of this thesis is the crystallization of alumina trihydrate, considerable discussion and reference will be made to general crystallization phenomena as well. This will lead into the mathematical description of these rate processes and how they fit into the general approach to modelling a crystallizer which has been adopted here. Throughout this discussion the pertinent information which is available in the literature will be delineated.

Although the literature survey will be relatively extensive, it will not be exhaustive. That which is included is, in the author's opinion, the most relevant to this work. The emphasis will be on the underlying fundamentals of crystallization which are common to most crystallization systems.

2.2 Crystallization Processes

Crystallization is a very common unit operation in the chemical industry as well as in others. Synonyms of crystallization are precipitation and deposition (pl). This operation is used to separate, to purify, to combine, to produce, or to improve the handling and appearance of a certain compound. Crystallization is the process whereby a certain component transfers from either the vapor phase to the solid phase or from

the liquid to the solid phase. The liquid phase is either described as a solution or a melt, the latter being more common in the metallurgical industries. The operation can be carried out either in a crystallizer which is operated batch-wise, or on a continuous basis.

There are many different crystallizer designs; each depends on practical considerations and in many instances on the available 'know-how' for a certain crystallization system. Recently, substantial progress has been made in obtaining quantitative models for the crystallization process associated with many practical crystallization systems (r1). However, for most systems, it is still necessary to base the design on inadequate empirical (or semi-empirical) equations and other practical considerations (m1). Inadequate knowledge of the fundamental phenomena occurring and the important variables in a crystallization process usually leads to over-design of equipment, the addition of extra equipment and/or inadequate control schemes to maintain the product on the required quality specification. This semi-empiricism is a result of the complex nature of and interaction in most crystallization processes.

2.2.1 Alumina Trihydrate Crystallization Process

Pearson (p1) has provided a detailed description of the alumina trihydrate crystallization chemistry and process. Essentially, it involves the crystallization of alumina trihydrate from a supersaturated solution of sodium aluminate. Unseeded precipitate tends to be gelatinous or made up of very small crystals which are very difficult, if not impossible, to separate by filtering and washing. A seeded solution, however, forms a much larger sized precipitate which is convenient for handling and further treatment.

The most common crystallizer in industry consists of a very large cylindrical vessel in which the 'magma' or slurry suspension is agitated either by an external or internal air-lift or by slowly rotating agitators. The supersaturated solution and seed crystals (the fine material separated from the coarse crystal product) are charged and the crystallizer operated batch-wise for approximately 24 hours. These large crystallizers and long processing time are required because the crystal growth rate for this alumina trihydrate system is very slow relative to most other systems.

2.3 Fundamental Crystallization Process Concepts

The basic processes that govern a crystallization process are complex, varied, and encompass a broad spectrum of problems which can satisfy a variety of interests, tastes, and backgrounds of workers in the field. The emphasis and direction of the research depends to a large extent on the long range interests and aims of the researcher. For example, here the emphasis is on predicting the performance of an industrial crystallizer and therefore the transport and kinetic phenomena associated with a magma of crystals are important. In this case, for example, it is desired to represent the overall average crystal growth rate by a simple (perhaps empirical) function of supersaturation with some empirical expression to account for major impurities; on the other hand, a solid-state physicist would represent or correlate crystal growth on a much more fundamental basis, looking for such additional effects as surface structure, particular crystal faces, interfacial tension, etc. However important these fundamental scientific studies

are, they do not shed any light on the interactions occurring among all the transport and kinetic phenomena occurring in a large-scale crystallizer.

2.3.1 Rate Processes

The main rate processes associated with most solution crystallization processes, as exemplified by the alumina trihydrate system, are:

1. Crystal Growth

This is the process whereby solute molecules in solution are incorporated into the crystal lattice of a solid.

2. Nucleation

This is the process of formation or birth of new crystals.

These crystals either form spontaneously (homogeneous nucleation) or result from larger crystals being subjected to some stress such as occurs on impact of a crystal with another solid object or the crystal contained in a high shear field in the solution.

3. Agglomeration

This is the process whereby two or more crystals combine to form one crystal. This means the death of the crystals which combine and the birth of the resultant crystal.

4. Attrition

Here, attrition will be considered the process in which a crystal breaks through impact with other crystals or solid

objects into relatively large fragments. The process where very small fragments are chipped off a large crystal will be considered a form of nucleation since this process cannot be distinguished from secondary nucleation, as described above. Mathematically, the rates at which the fragments are formed are represented by birth attrition functions and the rate of attrition of the original crystal by a death attrition expression.

5. Induction Period

This is the period in which the growth, nucleation and agglomeration rates are still influenced by prior treatment of the crystal mass and/or the supersaturated solution. For instance, prior treatment of crystalline seed might influence the initial growth rate, while the prior temperature history of the solution may have an effect on the initial nucleation rate.

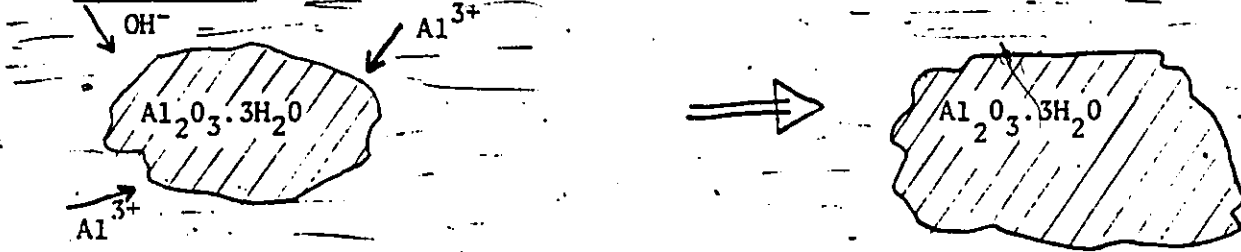
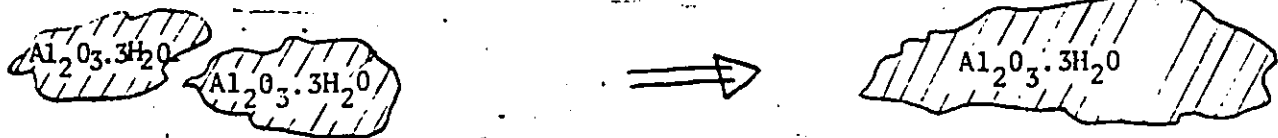
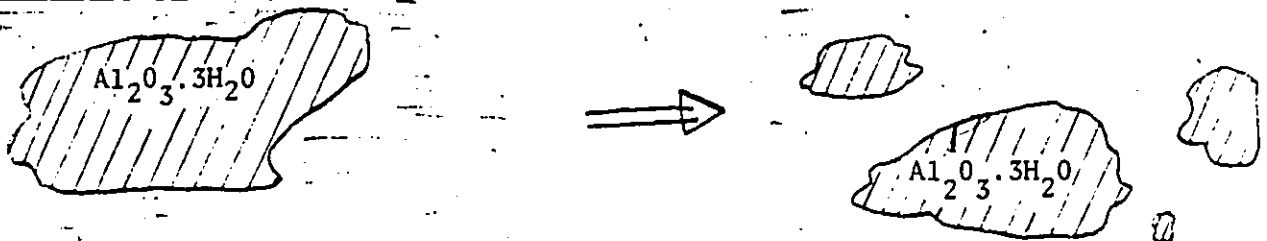
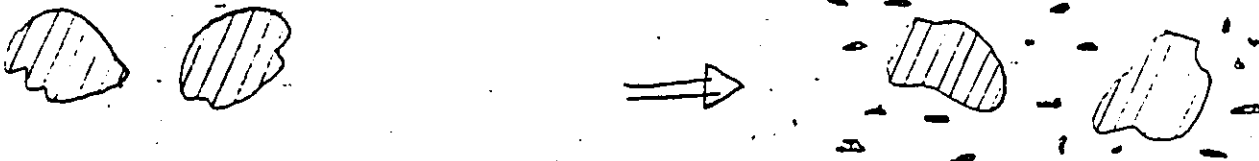
6. Crystal Habit

Crystal habit is the term used to describe the variation of shape of crystals which may be determined indirectly by a number of operating variables. These operating variables affect the crystal growth rate of different crystal surfaces and in so doing determine the shape of the resultant crystals.

A conceptual representation of the first four of these processes is presented in Figure 2.5.1-A. All six processes are discussed in detail in the next sub-sections.



FIGURE 2.3.1-A Crystallization Rate Processes

GROWTH RATE *AGGLOMERATION RATEATTRITION RATENUCLEATION RATE

*Representing the sodium aluminate solution by Al^{3+} and OH^- ions is an oversimplification. The nature of the actual aluminate complex(es) in solution is not well understood. (21)

2.3.2 Process Variables

The crystallization rate processes are indirectly or directly a function of the following process variables:

1. Solution Supersaturation

Supersaturation is defined as the difference between the actual concentration of the solution and the equilibrium concentration, that is, the solubility of the solute under the conditions that pertain at that instant. The equilibrium concentration is a function of temperature and concentration of other species that may be present. The actual correlation for the alumina solution will be presented in section 2.10.1.3.

2. Temperature

Temperature is an important variable in that it affects the crystal growth rate; its dependence is often expressed through an Arrhenius type relationship.

3. Other Variables

Other variables which influence the crystallization processes are: impurities, type of solvent, degree of agitation in a crystallizer. These variables may affect any one or all of the basic phenomena. In a crystallizer, however, an effect on any one of the basic processes, indirectly affects the others.

2.3.3 Crystallizer Performance

The above-mentioned operating conditions affect the rates of the various crystallization processes and these rates and the interaction

between the various processes will determine the capacity of a crystallizer, the resultant crystal size distribution, and the shape and purity of the individual crystals. Because of these interactions, the description of all the processes becomes difficult and complex. The problem deserves considerable attention considering the importance of this unit operation to the chemical and related industries.

2.4 Crystal Growth Rate

Crystal growth rate from solution is the rate at which solute molecules are transferred from the solution to the solids phase. These rates are measured or obtained either by direct measurement on single crystals (sl) or indirectly by studying mixed suspension systems (rl,m3). Growth rate models consist either of empirical correlations or equations based on physical concepts of the growth process. These physical models are most often based on the screw dislocation theory of Burton et al. or on the theory that postulates two-dimensional nucleation on the crystal surface (sl).

As with other mass transfer processes with chemical reaction, the crystal growth rate may be controlled by the diffusion or mass transfer of solute molecules through the solvent to the crystal-solution interface or by the reaction or incorporation of the solute into the crystal lattice. In some instances, both rate processes may be of equal importance in determining growth rate.

2.4.1 Diffusion Controlled Growth

The diffusional process is determined by the hydrodynamics of the system. It is most often correlated by an equation of the form (g2):

$$Sh = f(Sc, Re) \quad (2.1)$$

Many different functional forms have appeared in the chemical industry and in the main, they depend on the fluid mechanic regime. Garside (g2) discusses methods of measuring these mass transfer coefficients and the effects of neglecting diffusion on growth rate correlations.

Growth rates for the alumina trihydrate system are relatively quite slow and have been measured to be of the order of only several micrometres per hour. Moreover, since agitation does not affect this growth rate, it can be said that the growth rate is surface-reaction controlled (m2, l1). This means that the growth rate does not depend on the hydrodynamics of the suspension, the type of the apparatus or the method of agitation, but is only a function of the surface phenomena associated with the incorporation of solute molecules into the alumina trihydrate crystal lattice.

2.4.2 Surface Reaction Controlled Growth

In general, a surface reaction controlled growth rate is a function of the following variables:

- temperature
- solution supersaturation
- crystal size (r4)
- type of crystal face (b2)

- crystal surface structure (w2)
- solution impurities concentration (b1)

There are a relatively large number of ways of correlating growth rates (ol,rl). These correlations incorporate all of the above variables or only some of them depending on the extent of empiricism. For a given crystal-solution system, however, the growth rate may be suitably correlated with temperature and supersaturation. Without elaborating on the details of the models, the main correlating equations may have the following forms:

$$(1) \quad G = b_1 \times (\Delta C)^{b_2} \quad (2.2)$$

$$(2) \quad G = b_1 \times \sigma^{b_2} \quad (2.3)$$

$$(3) \quad G = b_1 \times \sigma^2 \times \tanh(b_2/\sigma) \quad (2.4)$$

$$(4) \quad G = b_1 \times \sigma^{5/6} \times \exp(-b_2/\sigma) \quad (2.5)$$

where G - rate at which the faces of the crystal advance;
 Z - distances measured normal to the faces
 $\Delta C = C - C_e$ - a measure of supersaturation
 $\sigma = \Delta C/C_e$ - also a measure of supersaturation
 b_1, b_2 - model parameters which, depending on the theory of the underlying model, incorporate a large number of variables, such as: surface diffusion, thickness of growth layer, absolute temperature, activation energy, etc.

Models 1 and 2 are widely used in the engineering literature. They are empirical power-laws which fit growth rate data reasonably well depending on the accuracy and range of the data (g2). Model 4 follows from the 'nuclei above nuclei' theory or in other words, from the theory of the 'birth and spread of two-dimensional nucleation' (s1,01,b2). Simply, it is based on the concept that crystals grow by the formation of one or several nuclei on a surface. These nuclei mark the start of the formation of a new layer of atoms on the crystal face, this layer forming quite rapidly after it is initiated. Model 3 follows from the BCF or Burton, Cabrera, Frank theory of dislocation growth. It is based on the concept of growth on ledges, in particular, on spiral ledges formed by screw dislocations. This forms a self propagating mechanism and circumvents the need for nuclei formation. This model reduces to:

$$G = b_1 \times \sigma^2 \quad (2.6)$$

for low supersaturation, and to:

$$G = 2 b_1 \times b_2 \times \sigma \quad (2.7)$$

for high supersaturation. The above theories and modifications thereof have been discussed and investigated extensively (s1,b1,01).

2.4.3 Effect of Crystal Size on Growth

Another well-established concept has been forwarded by McCabe (m1), referred to as the 'McCabe ΔL Law'. This 'law' states that the

linear growth rate or rate at which the crystal surfaces grow or increase in the direction normal to the surface is independent of the size of the individual crystals. In other words, all crystals regardless of size increase in size at the same linear rate, expressed for example as micrometres per second. This concept is reasonable if the growth rate is surface reaction controlled, that is, controlled by the mechanisms suggested earlier. In many instances, this law represents the observed average behaviour quite well. Single crystal studies, however, have indicated that the growth rate may be different on different faces of the crystal; in fact, it is this variation which gives crystals their characteristic shape (needles, flat disk-like shape, etc.). If the crystal surface structure changes with size, then the average growth rate is expected to change with size. If the shape remains the same throughout the growth period, then the average growth rate may be expected to remain constant independent of size as long as the growth rate is surface reaction rate controlled. It is worthwhile noting here that if diffusion of solute to the surface is important, then mass transfer rate considerations would suggest that the growth rate is proportional to the size of the crystal.

Randolph (r1) has proposed a model for growth rate which suggests a linear dependence on size, viz.

$$G = G_0(1 + b_1 D_p)^{b_2} \quad (2.8)$$

He shows (r4) that for the system potassium sulfate-water a size dependent model represents his experimental data better than the McCabe

ΔL law. It must be recognized, however, that this apparent size dependence may be due to the wrong choice of the characteristic linear dimension of the crystal. As mentioned, it may be a true dependence that may have reflected the importance of mass transfer or an apparent dependence which results from the interaction of the other processes which may be occurring - for example, agglomeration and attrition. These latter processes probably do depend on size. From these arguments it is seen that the growth rate might well depend on crystal size, but on the other hand, a plot of growth rate vs. a linear crystal dimension might be very misleading and should be analyzed with care.

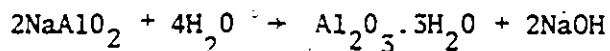
2.4.4 Observations of Growth Rates for the Alumina Trihydrate System

Although electron micrographs of some types of crystals have shown the prominent spiral ledges which have been hypothesized by the BCF model, this type of dislocation has not been observed with the alumina trihydrate system. Brown (b7) has observed instead surface layer type of defects. These observations led Brown to conclude that the growth rate of alumina trihydrate does not follow the BCF model but rather a mechanism involving surface nucleation followed by a surface spreading.

As pointed out by Garside (g2), it is difficult to discriminate among any of the models for growth on the basis of observed growth rate variation with supersaturation since all models may be approximated by a parabolic type function. Very accurate growth rate data over a wide range of supersaturation is needed in order to effect any discrimination among the models which have been proposed.

2.4.5 Review of Growth Rate Models for the Alumina Trihydrate System

The crystallization of alumina trihydrate follows the chemical reaction:



A number of studies of crystal growth of alumina trihydrate have appeared in the literature. These are discussed in turn below.

(a) Misra and White (m3)

Misra (m3) conducted bench-scale seeded batch crystallization experiments of the alumina trihydrate in an impeller-agitated vessel. They concluded that the growth rate appeared to be independent of size and from the same data, White (w2) made the observation that the difference in growth rate as a result of differences in crystal surface structure is negligible for this system. Their observations and hence conclusions are confounded, however, by the high level of agitation in their crystallizer which probably led to considerable attrition of the crystals in the crystallizer.

Their growth rate expression is:

$$G_D = \frac{dD}{d\tau} = k_{G,M} \times (CA - CA_e)^2 \quad (2.9)$$

where $k_{G,M}$ = reaction rate constant ($\mu\text{m}^2/\text{h g}^2$)

D = spherical equivalent diameter (μm)

τ = batch time (h)

- CA - alumina solution concentration (g Al_2O_3 /l sol.)
 CA_e - equilibrium concentration
 R - 8.314 J/mol K
 T - absolute temperature (K)

The reaction rate constant, $k_{G,M}$, is expressed as a function of temperature through the Arrhenius relationship:

$$k_{G,M} = 1.96 \times 10^6 \times \exp(-\Delta E/RT) \quad (2.10)$$

where the activation energy is 5.98×10^4 J/mol (14.5×10^3 cal/mol).

The above correlation for growth rate was based on experiments in which the impurities in the solution were negligible. Impurities are expected to affect both growth rate and equilibrium concentration (pl).

(b) Pearson (pl)

Pearson (pl) reports that the rate of decrease of the molar concentration of sodium aluminate in a batch seeded solution is given by the expression:

$$\frac{dx}{d\tau} = -k_1 \times A \times \frac{\{x - x_e\}^2}{\{a_e + x_e\}^2} \quad (2.11)$$

- where $x(\tau)$ - molar concentration of $NaAlO_2$
 $a(\tau)$ - molar concentration of NaOH
 $A(\tau)$ - crystal surface area (m^2/l sol.)

- k_1 - parameter dependent on temperature
 τ - batch time (h)
 e - subscript denoting equilibrium

For comparison between Pearson's growth rate expression and Misra's expression, equation (2.11) is transformed as follows:

1. First x is expressed in terms of the total crystal weight, W_T , as follows:

$$\frac{d(W_T/V_L)}{d\tau} \left(\frac{\text{g Al}_2\text{O}_3 \cdot 3\text{H}_2\text{O}}{\text{h l sol.}} \right) \times \frac{1}{156} \left(\frac{\text{mol Al}_2\text{O}_3 \cdot 3\text{H}_2\text{O}}{\text{g Al}_2\text{O}_3 \cdot 3\text{H}_2\text{O}} \right) \times \frac{2}{1} \left(\frac{\text{mol NaAlO}_2}{\text{mol Al}_2\text{O}_3 \cdot 3\text{H}_2\text{O}} \right) = - \frac{dx}{d\tau}$$

Therefore, for approximate constant V_L with respect to τ :

$$\frac{dW_T}{d\tau} \times \frac{1}{V_L} \times \frac{1}{156} \times \frac{2}{1} = - \frac{dx}{d\tau}$$

2. Similarly for the Al^{3+} concentration, the relationship between CA and x is equal to:

$$\text{CA} \left(\frac{\text{g Al}_2\text{O}_3}{\text{l sol.}} \right) \times \frac{1}{102} \left(\frac{\text{mol Al}_2\text{O}_3}{\text{g Al}_2\text{O}_3} \right) \times \frac{2}{1} \left(\frac{\text{mol NaAlO}_2}{\text{mol Al}_2\text{O}_3} \right) = x$$

$$\text{CA} \times \frac{2}{102} = x$$

and for the Na^+ concentration the relationship between CN and a is given by:

$$\text{CN} \left(\frac{\text{g Na}_2\text{O}}{\ell \text{ sol.}} \right) \times \frac{1}{62} \left(\frac{\text{mol Na}_2\text{O}}{\text{g Na}_2\text{O}} \right) \times \frac{2}{1} \left(\frac{\text{mol NaOH}}{\text{mol Na}_2\text{O}} \right)$$

$$= \text{CN} \times \frac{2}{62} \left(\frac{\text{mol NaOH}}{\ell \text{ sol.}} \right)$$

which is equal to the total Na^+ concentration expressed as NaOH, or in Pearson's nomenclature, equal to the 'free' sodium ion concentration which is defined as:

$$" \text{Na}_2\text{O (free)} = \text{Na}_2\text{O equivalent to NaAlO}_2 + \text{NaOH} "$$

Therefore:

$$\text{CN} \times \frac{2}{62} - \text{CA} \times \frac{2}{102} = a$$

3. Substitution of x and a by CA and CN in equation (2.11) gives:

$$\frac{dW_T}{d\tau} \times \frac{1}{V_L} \times \frac{1}{156} \times \frac{2}{1} = k_1 \times A \times \frac{\left\{ \text{CA} \times \frac{2}{102} - \text{CA}_e \times \frac{2}{102} \right\}^2}{\left\{ \text{CN}_e \times \frac{2}{62} - \text{CA}_e \times \frac{2}{102} + \text{CA}_e \times \frac{2}{102} \right\}^2}$$

or

$$\frac{dW_T}{d\tau} = \left\{ 57.6 \times k_1 \times \frac{1}{(\text{CN}_e)^2} \times (\text{CA} - \text{CA}_e)^2 \right\} \times \frac{A}{2} \times V_L$$

4. Comparison of this equation with the first moment of the population balance which can be written as:

$$\frac{dW_T}{d\tau} \left(\frac{g}{h} \right) = G_D \left(\frac{\mu m}{h} \right) \times 2.42 \left(\frac{g}{cm^3} \right) \times \frac{A}{2} \left(\frac{m^2}{l \text{ sol.}} \right)$$

$$\times V_L (l \text{ sol.}) \times \frac{10^4}{1} \left(\frac{cm^2}{m^2} \right) \times \frac{1}{10^4} \left(\frac{cm}{\mu m} \right)$$

or

$$\frac{dW_T}{d\tau} = \{2.42 \times G_D\} \times \frac{A}{2} \times V_L$$

shows that:

$$G_D = k_{G,P} \times (CA - CA_e)^2 \quad (2.12)$$

$$\text{where } k_{G,P} = 2.38 \times 10^1 \times \frac{k_1}{(CN_e)^2} \quad (2.13)$$

The factor $k_{G,P}$ is approximately constant for an isothermal crystallization process. Therefore, equation (2.12) is of the same form as the generally used expression for a size independent crystal growth rate.

Pearson (p1) states the factor k_1 increases by a factor of 2.25 for every $10^\circ C$ temperature increase. This compares to a factor of ~ 1.90 for every $10^\circ C$ increase for Misra's growth rate expression, equation (2.10).

(c) Halfon and Kaliaguine, Model A (h1)

Halfon and Kaliaguine report on crystallization in an impeller-agitated 400 l tank from solutions which contained very low supersaturations

and had an impurity level 'equivalent to that of plant liquor'. Their growth rate expression is:

$$G_D = k_{G,H} \times (CA - CA_e)^2 \quad (2.14)$$

where $k_{G,H} = 3.6 \times 10^{-4}$ @ 60°C

All experiments were carried out at 60°C so no temperature dependence was reported. Pearson's $k_{G,P}$ value at this temperature and at Halfon's caustic concentration of about 110 g $\text{Na}_2\text{O}/\text{l}$ sol. is 3.1×10^{-4} , while Misra's is 8.1×10^{-4} at this temperature and concentration. Note that these rate constants are all of the same order of magnitude but do differ by as much as a 62% , i.e. 3.1×10^{-4} as compared to 8.1×10^{-4} , in absolute value. These differences may be due to the influence of impurities on the growth rate. On the other hand, they might be due to different procedures used in calculating the growth rate G_D . The main difficulty in this experimental work is the measurement or definition of the actual crystal's surface area at every instant of time.

(d) Halfon and Kaliaguine, Model B (h1)

Halfon states that the previous models, all of which are of the same general form, fail to account for the induction period, which is known to occur with this system. His second model for the growth rate of alumina trihydrate is purported to account for an induction period. It is given by:

$$G_D = 1.62 \times 10^{-20} \times s_u \times (CA - CA_e)^2 \quad (\mu\text{m/h}) \quad (2.15)$$

where G_D - linear growth rate ($\mu\text{m/h}$)
 CA - alumina concentration ($\text{g Al}_2\text{O}_3/\text{l sol.}$)
 CA_e - equilibrium concentration of alumina ($\text{g Al}_2\text{O}_3/\text{l sol.}$)
 s_u - number of nucleation sites per unit surface area (dm^{-2})

The variable s_u is calculated from:

$$\frac{ds_u}{d\tau} = \left\{ 3.52 \times 10^{-3} \times \frac{N_{cc}^2}{S} \right\} - 1.55 \times 10^{-4} \times s_u \times (CA - CA_e)^2 \quad \dots (2.16)$$

where S - external surface area of crystal per unit volume of suspension at time τ ($\text{dm}^2/\text{l susp.}$)
 N_{cc} - number of crystals with a size greater than $2 \mu\text{m}$ per unit volume of suspension (number $> 2 \mu\text{m}/\text{l susp.}$)
 s_0 - maximum value for s_u

This equation holds as long as $s_u(\tau) < s_0$, while otherwise $s_u(\tau)$ is a constant equal to s_0 . The model reduces to model A for $s_u = s_0$ with s_0 equal to 2.11×10^{-16} . Model B in essence reduces the available crystal surface area for growth by means of the variable s_u . These authors describe s_u as the "number of vacant sites per unit surface area of crystals". They hypothesize that during the induction period, growth takes place on only part of the available crystal surface area, while the rest of the surface inhibits growth presumably due to poisoning of that part of the surface.

Although this is a reasonable argument the actual determination of the number of vacant sites per unit area of crystals seems a very difficult problem. Another weakness of the model is the use of the number of crystals with a size greater than the minimum size that could be measured with the particle counter which they used. This means that with another type of measuring device the equation for s_u could very well have different parameters or, indeed, have a completely different form. Moreover, the use of the surface area variable S introduces uncertainty since surface area is a difficult variable to measure and strongly depends on the method of surface area measurement. Thus, although this model predicts the smaller growth rates during the induction period, the development of it seems somewhat arbitrary especially in the use of the variables N_{cc} and s_u .

2.4.6 Effect of Poisons on the Crystal Growth Rate of Alumina Trihydrate

Pearson (pl) discusses the effects of impurities or poisons on the growth rate of alumina trihydrate crystals. He lists as effective poisons: "saponin, gum arabic, cane sugar and numerous other organic substances containing hydroxyl groups". As inorganic poisons he states that dissolved iron and calcium salts are the most common. The overall effect of these poisons is to retard the crystal growth rate.

Pearson (pl) expresses this poisoning effect through a 'poison factor' which he presents graphically as a function of temperature. This poisoning factor corrects the equilibrium concentrations of sodium, a_e , and aluminate, x_e , for the poisons and thus allows the growth rate to be

calculated under these contaminated conditions by use of the same expression, equation (2.12). The reduction in growth rate arising from poisons becomes less as the temperature increases up to and above about 80°C, at which temperature the effect of the poisons becomes negligible.

2.4.7 Summary of the Available Information on the Growth Rates for the Alumina Trihydrate System

From the literature the following is known or concluded from experimental observations with regard to the crystal growth rate of alumina trihydrate from a supersaturated sodium aluminate solution.

- The growth rate is surface reaction controlled, not diffusion controlled.
- Surface reaction or growth takes place by surface nucleation followed by the fairly rapid spreading of a molecular solid layer over the surface.
- McCabe's ΔL law seems to be valid.
- Differences in the growth rate due to structural differences in the crystal surface are negligible for this system.
- Poisons or impurities slow the growth rate, the fractional decrease being a definite function of temperature up to about 80°C; at higher temperatures this effect is negligible.
- The alumina trihydrate system exhibits an induction period which is probably a function of seed treatment and crystallizer operating conditions.
- The growth rate models which have been developed to date are empirical (or semi-empirical) and are all of the form:

$$G_D = k_G \times (CA - CA_e)^2 \quad (2.17)$$

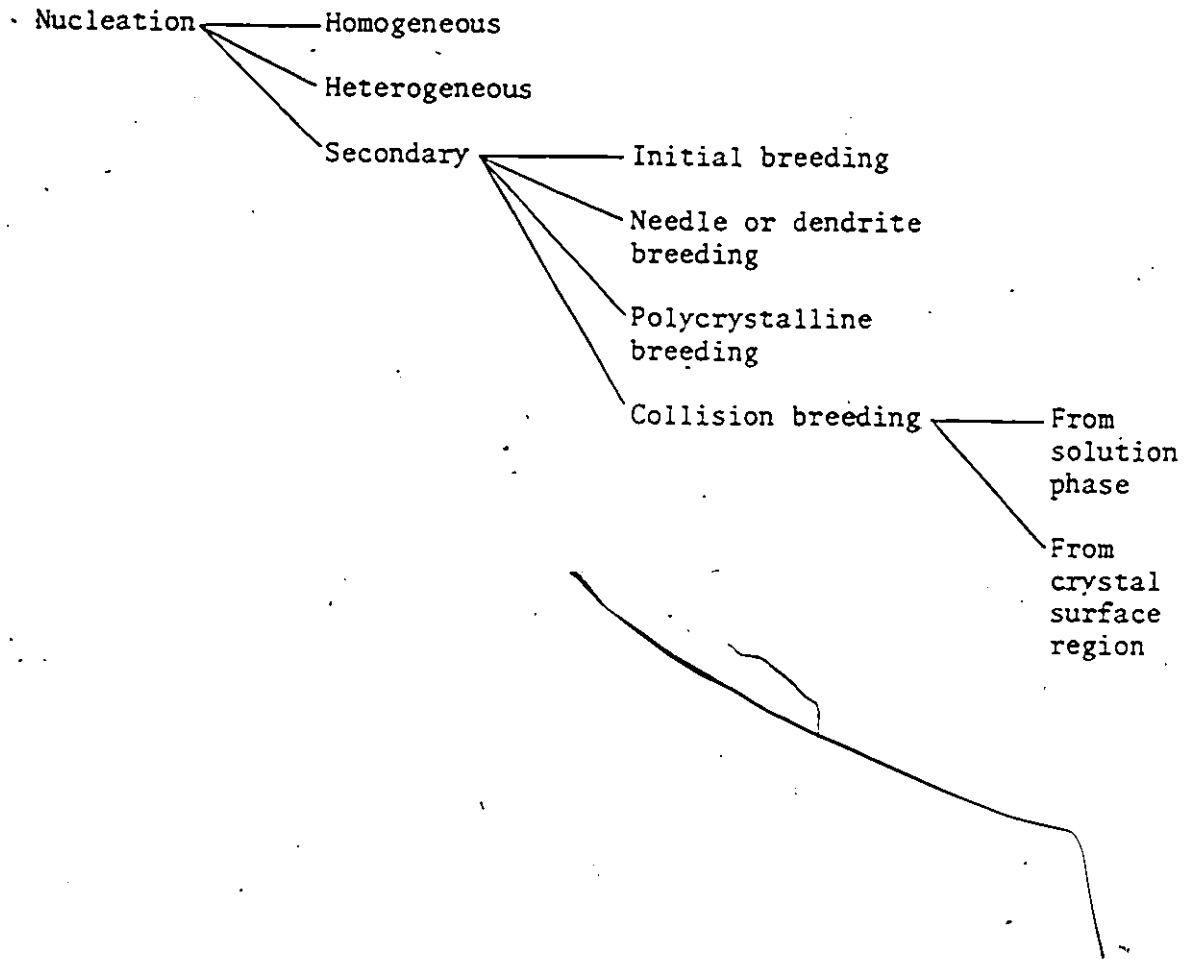
The rate parameter, k_G , has been estimated from experiments and although various different estimates have been reported, these differences may reflect the shortcomings of the experiments and/or modelling procedure for the complete crystallization process.

It is known that an induction period of varying duration occurs in this seeded crystallization process. One attempt at modelling this induction phenomena has been reported but the model is shown to have a number of shortcomings.

2.5 Nucleation Rate

Nucleation rate in the context of this work denotes the rate at which new crystals are generated other than by attrition; however, it is difficult to distinguish between nucleation and attrition when very small crystals are formed by attrition. Attrition is most often thought to result from mechanical fracture of the crystal which in turn arises from impact on the crystal causing internal stresses. On the other hand, nucleation is governed by chemical and physical phenomenon. Although in theory this distinction can be made, in practice, since there are so many different mechanisms for nucleation, the formation of small crystals by attrition is really another mechanism by which small, nuclei-sized, crystals are formed. The various mechanisms of nucleation are discussed below, and presented in Figure 2.5-A. The classification presented here, although general, is by no means the only classification (b5).

FIGURE 2.5-A Line Diagram of Different Nucleation Mechanisms



2.5.1 Homogeneous Nucleation

This is the process whereby a solid or liquid is formed from the solution or vapour phase with a size greater than some 'critical size'. The critical size is one where crystals greater than this size remain crystals and crystals less than this size will dissolve or disappear. For homogeneous nucleation as opposed to heterogeneous nucleation, the phase transformation takes place without the benefit of the lower energy barrier which results when a foreign solid surface with the correct crystal structure and interatomic distances is present. Classical nucleation theory predicts the size of the critical nucleus and its rate of formation or nucleation (m_l, s_l). The theory shows that homogeneous nucleation is strongly dependent on supersaturation. In general, relatively very high supersaturation levels are required for any significant nucleation rate. It is either the predominant mechanism for nuclei formation or its contribution is insignificant.

2.5.2 Heterogeneous Nucleation

This refers to the formation of crystals as a result of lowering of the nuclei formation energy barrier by the presence of foreign solid matter. Because traces of insoluble matter are difficult to eliminate and, in any event, the container walls are a foreign surface upon which crystals may form, heterogeneous nucleation can become a primary or predominant mode of forming new crystals (nuclei). Moreover, heterogeneous nucleation requires much lower levels of supersaturation than homogeneous nucleation. The mechanism of heterogeneous nucleation is complex. It is probably a function of the following variables: temperature, supersatura-

tion, type of solid-liquid interface, crystal structure of the foreign substance, etc. (r2). Besides the molecular form of the interface, other interface variables such as an electrostatic double layer and/or trace amounts of poisons might significantly influence the rate of heterogeneous nucleation (r2).

From a practical viewpoint, heterogeneous nucleation is in general undesirable since it causes scaling, or in industrial terms salting out on or fouling of vessel walls and heat exchanger surfaces. This results in additional maintenance costs and poorer average performance of a crystallizer. One way to minimize this is by specially treating the heat exchanger surfaces. For instance, electropolishing of cooling coils has met with some success.

2.5.3 Secondary Nucleation

Secondary nucleation refers to the production of nuclei crystals in the presence of suspended parent crystals. It takes place at high and low to relatively very low supersaturation levels. The rate being still large at supersaturation levels far below those for any significant heterogeneous or homogeneous nucleation rates (m1). It is generally accepted that the superfluous production of nuclei in crystallizers at very low supersaturations results from some mechanism of secondary nucleation. Conceptually, secondary nucleation might take place by one or a combination of the following mechanisms (s2).

(a) Initial Breeding

This might occur when seed crystals are introduced into a super-

saturated solution. The seed surfaces are thought to have attached to it, in a 'loose way' very fine crystals which are washed off and then grow as new crystals. This would result in an initial 'shower' of nuclei the quantity of which would depend on the pretreatment of the seed, and to a small extent on the supersaturation level and temperature which would determine the size of surviving crystals. Equation (2.21) shows the relationship between the minimum crystal size and the variables, saturation and temperature.

(b) Needle or Dendrite Breeding

This occurs when crystals grow needles or dendrites which might then break off due to external forces, and grow as new crystals. Growth of dendrites most often occurs under conditions of high supersaturation and temperature and relatively mild agitation.

(c) Polycrystalline Breeding

As in needle growth, this formation of nuclei is due to imperfect crystal growth. At high supersaturations the crystals might grow imperfectly forming 'polycrystalline' or crystalline masses which are loosely held together and which might break up when subjected to external forces. The conditions favouring this nucleation mechanism are similar to those for dendrite formation. Both mechanisms might be classed as a special kind of attrition rather than nucleation; however, when the resulting crystals are of the same order of size as those produced by other nucleation processes, this process is referred to as nucleation as well.

(d) Collision Breeding

This occurs very readily when a crystal is subjected to external forces, either from contact or near contact with other crystals and/or foreign objects such as stirrers and vessel walls. Large numbers of crystals are produced even at low supersaturations by this mechanism. It appears that this is the principle mechanism of nucleation in most agitated seeded crystallizers. Two conceptual mechanisms of collision breeding are (s2):

From Solution Phase

The hypothesis is that clusters of molecules form in the liquid phase and these grow while being loosely held to the parent crystal by physical attractive forces. Strickland-Constable (s2) describes these molecules as being 'associated with the parent crystal surface'. After the clusters of molecules grow to a stable nuclei size, they usually detach by virtue of some relatively small or weak external force; thereafter they grow and are observed as new crystals. This phenomenon is enhanced at higher supersaturations.

From Crystal Surface Region

This mechanism assumes that instead of being associated with the surface, the cluster of molecules is actually attached by chemical bonds to the crystal surface. These crystalline masses of nuclei size are then detached by means of relatively high shearing forces. Indeed, McCabe et al. (j2) found that collision breeding does not occur by contact between a rubber surface and a crystal. It was hypothesized that if one of the approaching surfaces is elastic it will accommodate the hydrostatic forces on both faces and consequently reduce the shearing action on the crystal face.

It is thought that the rate of collision breeding is a function of (b4):

- temperature
- level of supersaturation
- size of contacted crystals
- crystal hardness
- hardness of contacting matter
- magnitude of forces on crystals or agitation intensity

2.5.3.1 Secondary Nucleation Rate Correlations

A typical correlation for secondary nucleation is given by. (o2):

$$BF_n = k'_n \times D^{b1'} \times (C - C_e)^{b2'} \times \phi_D \times E_D \times F_D \quad (2.18)$$

which when integrated over all crystal sizes gives the total nucleation rate, viz:

$$BN_n \Delta \int_{D_0}^{D_m} BF_n \times dD$$

- where
- BF_n - crystal birth rate density function (number / (h dm³ sol. μm))
 - BN_n - secondary nucleation rate (number / (h dm³ sol.))
 - D - linear crystal dimension (μm)
 - $C - C_e$ - supersaturation (g/dm³ sol.)
 - ϕ_D - collision frequency density function (number / (h μm))
 - E_D - surface impact energy density function (J/μm)
 - F_D - crystal number density function (number / (dm³ sol. μm))
 - k'_n - rate constant which includes the effect of temperature, type of collision, and birth size distribution of formed nuclei

$b1', b2'$ - model parameters

Ottens et al. (o2) related the collision frequency and surface impact energy variables to the total mass of crystals and a variable related to the dissipated energy per unit mass of crystals giving:

$$BN_n = k_n \times \psi_n \times W_t^{b1} \times (C - C_e)^{b2} \quad (2.19)$$

where ψ_n - variable related to the dissipated energy per unit mass of crystals

W_t - crystal mass per unit suspension

$b1$ - model parameter related to the domineering mode of collision breeding; it is 1 for crystal-wall collisions and 2 for crystal-crystal collisions

$b2$ - model parameter

k_n - rate constant which might differ depending on the type of collision breeding

$C - C_e, BN_n$ - same as in equation (2.18)

Evans et al. (e1) also suggest a value for $b1$ of about unity for crystal-wall collisions. However, for crystal-crystal collisions they make a distinction between crystal-crystal collisions due to gravity and turbulence driving forces; $b1$ is equal to 2 for gravity and 1 for turbulence, respectively.

Randolph (r1) also proposes a relationship of the same form as equation (2.19) for the secondary nucleation rate, i.e.

$$BN_n = k_n'' \times W_t^{b1''} \times (C - C_e)^{b2''} \quad (2.20)$$

Here the variable related to impact energy, ψ , and the rate constant k_n are lumped into the one parameter, k_n'' . This circumvents the difficult and ambiguous problem of determining ψ ; however, it means that this equation is only valid for a particular type of crystallizer and a particular intensity of agitation.

2.5.4 Observations on the Nucleation Rates of the Alumina Trihydrate System

At the supersaturations normally encountered in industrial practice, it is quite unlikely that homogeneous nucleation takes place for the alumina trihydrate system (p1). Heterogeneous nucleation probably takes place to some extent depending on supersaturation as well as on the type and concentration of impurities in solution, and type of material from which the crystallizer is made.

In industrial practice, it is well known that a considerable rate of nucleation exists even at low levels of supersaturation. All laboratory work suggests that the dominating mechanism for the formation of these nuclei must be the secondary one, probably involving the collision breeding mechanism.

At present there is essentially no quantitative information available on the nucleation rate for the alumina trihydrate system. Some very limited information is provided by Misra (m2,m3). He states that nucleation does not occur at 75°C and above. However, it must be remembered that secondary nucleation depends very much on the crystallizer apparatus

and intensity of agitation. Therefore, there is a real question as to whether Misra's observations may be of general applicability. Certainly, his apparatus was extremely well agitated. Moreover, the limitations of his experimental work and data analysis did not allow definitive statements on this subject to be made.

2.5.5 Estimate of the Minimum Nuclei Size for the Alumina Trihydrate System

In the above discussion nothing has been said about the size distribution of the nuclei as they are formed. Unfortunately, these nuclei are so small that they cannot be easily observed until they have grown to a relatively much larger size. Therefore, their actual size distribution is unknown. Thermodynamic considerations suggest a critical or minimum nuclei size, as given by (ml):

$$D_o = \{4 \times M \times \sigma\} / \{R \times T \times \rho_s \times \ln\left(\frac{CA}{CA_e}\right)\} \times 10^6 \quad (2.21)$$

Several assumptions are made in the derivation of this equation.

For a typical case of the alumina trihydrate system:

- M - molecular weight, = 0.078 kg/mol
- σ - solid solution interfacial tension, $\approx 1.25 \text{ J/m}^2$
- R - gas constant, = 8.31 J/(mol K)
- T - absolute temperature, = 328 K
- ρ_s - solids density, $\approx 2420 \text{ kg/m}^3$
- CA_e - equilibrium alumina concentration, $\approx 44 \text{ g Al}_2\text{O}_3/\ell \text{ sol.}$
for CNC $\approx 200 \text{ g Na}_2\text{CO}_3/\ell \text{ sol.}$ and T = 328 K
- D_o - critical nuclei size (μm)

Therefore, for typical values of CA the minimum size nuclei are:

CA (g Al ₂ O ₃ /l sol.)	CA _e	D ₀ (μm)
140	44	0.05
88	44	0.09
46	44	1.3

This provides an order of magnitude calculation for D₀. Nuclei of a size greater than the critical will continue to grow while those smaller than D₀ will dissolve. This is known as the 'survival theory'.

2.5.6 Summary of the Available Information on Nucleation for the Alumina Trihydrate System

Thus, from the literature, it follows that:

- The nucleation of alumina trihydrate probably occurs by a secondary nucleation mechanism.
- No quantitative nucleation rate expressions are available for this system. Other nucleation studies suggest that the secondary nucleation rate might be modelled by expressions such as given by equation (2.20).
- No information is available with regard to the size distribution of alumina trihydrate nuclei. An order of magnitude estimate of the smallest nuclei size is given by equation (2.21).

2.6 Agglomeration Rate

Agglomeration is the process whereby two or more particles combine to form one particle. This means the loss or death of the particles which combine and the birth of the resultant particle. This combining process consists essentially of two main steps in series. First, the particles need to collide and second, they need to remain joined after collision. Frequency and intensity of collision is determined by the hydrodynamics of the suspension and by the size distribution of the particles involved. Joining or bonding of the collided particles may consist of the breaking of droplet interfaces, in the case of a liquid dispersed in a gas or liquid phase, or be due to physical forces which hold the particles together to form a loosely agglomerated floc. On the other hand, the bonding may involve the same chemical forces which bind the molecules in the colliding particles. The agglomeration of crystals which then form true crystals is an example of the latter case.

The phenomenon of agglomeration reduces the total number of particles and the total surface area available for growth. This in turn results in a reduced production rate even for the same growth rate, while simultaneously the particle size distribution shifts to the larger size and at a rate considerably above that due to growth. Thus, the net effect of agglomeration is that it slows down transfer of solute from solution to the solids phase and that it makes the resulting particle size distribution broader.

The agglomeration process in crystallization systems has not been investigated very extensively either experimentally or in modelling work. In fact, if a crystallizing system exhibits only a relatively small

agglomeration rate and the experimental conditions are changed only over a small range, then the resultant change in the size distribution might mistakenly be modelled by a size dependent growth rate, with the largest rate being associated with the largest particles. Modelling of the agglomeration process is avoided by many because of the non-linear partial integrodifferential equation which results when growth, nucleation and agglomeration exist and the severe difficulties which arise in trying to obtain a numerical solution.

Considerable work has been done on the agglomeration process, when it is the only process, in the field of aerosol science - in particular, in the branch of cloud physics (h5). In this system, the increase in size of droplets results from vapour to liquid mass transfer (growth process) and also from agglomeration or coagulation of droplets (d1,d2). In addition, agglomeration has been considered in some detail in such fields as emulsion polymerization (w3), liquid-liquid or gas-liquid mass transfer processes (r5), and microbial systems (t2). Pure agglomeration occurs in the granulation production step in making ammonium nitrate fertiliser. In this case, small particles are upgraded to larger ones to improve their further processability. Thus, there is a very broad applicability of any general modelling procedure for the agglomeration phenomenon.

2.6.1 General Agglomeration Rate Model

Regardless of the differences in the systems in which agglomeration occurs, the agglomeration process should be modelled by an equation of

the same general form. This equation should reflect the rate of collision between two different sized particles which in turn is determined by the relative size and concentration of the two particles in question. Moreover, the effectiveness of the collision in producing a stable agglomerate must be included and this effectiveness is expected to be determined by the prime variables, such as supersaturation and temperature as well as such crystallizer (apparatus) variables as level of agitation, etc. The total agglomeration rate is the sum of all agglomerations which occur between all particle pairs, viz.:

$$\left\{ \frac{\partial (F_{V,T}(V,\tau))}{\partial \tau} \right\}_a = \frac{1}{\{V_L(\tau)\}} \times \underbrace{\left\{ \frac{1}{2} \int_{V_0}^{V-V_0} k_{V,a}(V',V-V',\tau) F_{V,T}(V',\tau) F_{V,T}(V-V',\tau) dV' \right\}}$$

$$\underbrace{F_{V,T}(V-V',\tau) dV'}$$

number of crystals that
agglomerate into size V
per hour

$$- \underbrace{F_{V,T}(V,\tau) \int_{V_0}^{V_u} k_{V,a}(V',V,\tau) F_{V,T}(V',\tau) dV'}$$

number of crystals that
agglomerate out of size
V per hour

..... (2.22)

where $k_{V,a}$ - agglomeration rate effectiveness kernel

- 0 for $(V + V') > V_u$

$V < V_0$

$V' < V_0$

$$\geq 0 \text{ for } (V + V') \leq V_u$$

$$V \geq V_o$$

$$V' \geq V_o$$

- $F_{V,\tau}$ - number density function with respect to particle volume
 V_L - solution volume
 V - particle volume
 τ - batch or residence time

The above kernel incorporates the effects of the variables:

- temperature
- particle size
- supersaturation
- suspension hydrodynamics

The assumption made in the formulation of this model is that the agglomeration rate of crystals of volume V' and $V-V'$ is proportional to the product of the number densities $F_V(V',\tau)$ and $F_V(V - V',\tau)$; that is, it is a binary process only. This model is developed in detail in Chapter 5.

Sastry (s3) makes a distinction between 'free-in-space type' and 'restricted-in-space type' agglomeration process models. The distinction being that in the free-in-space case each particle has an equal probability of encountering any other particle, while restricted-in-space means that each particle can encounter only those particles in its immediate vicinity. His free-in-space model is identical to the general equation presented before, while the restricted-in-space concept leads to:

$$\begin{aligned}
 \left\{ \frac{\partial}{\partial \tau} (F_{V,T}(V, \tau)) \right\}_a &= \frac{1}{\{V_L(\tau)\}} \times \frac{1}{N_L(\tau)} \times \left\{ \frac{1}{2} \int_{V_0}^{V-V_0} k_{V,a}(V', V - V', \tau) \right. \\
 &\quad \left. F_{V,T}(V', \tau) F_{V,T}(V - V', \tau) dV' \right. \\
 &\quad \left. - F_{V,T}(V, \tau) \int_{V_0}^{V_u} k_{V,a}(V', V, \tau) F_{V,T}(V', \tau) dV' \right\} \\
 &\dots\dots (2.25)
 \end{aligned}$$

Where the variables are the same as those in equation (2.22); here the additional variable, $N_L(\tau)$, denotes the total number of crystals per unit volume of solution.

The model function $k_{V,a}$ is usually split into two factors. One factor incorporates the effect of temperature and supersaturation, the other the effect of particle size and the hydrodynamics of the suspension on the agglomeration rate. The strong dependence on the hydrodynamics means that agglomeration, like nucleation, is very dependent on the type of vessel and mode or intensity of agitation.

2.6.2 Review of Observations on Agglomeration and Agglomeration Rate Models for the Alumina Trihydrate System

For the alumina trihydrate system, plant experience indicates that under normal operating conditions the occurrence of agglomeration is an established fact. Moreover, plant experience suggests that it occurs for all supersaturations and that smaller crystals agglomerate at a faster rate than larger ones. Pearson (pl) suggests that agglomeration is favoured by:

- fine seed
- high seed concentration
- high temperature
- high supersaturation
- slow stirring rates

Gnyra (g4) concluded from electron micrograph observations that agglomerated crystals are true crystals and not flocs held together by physical attractive forces. This is in accord with the concept that alumina trihydrate crystals form an agglomerate by being 'grown' together after collision. In the alumina industry this is referred to as 'welding' (k1) or 'cementing' (p1) of a pair of crystals.

The only quantitative work on the agglomeration for this system has been reported by Halfon (h2). He found that the general type of model (equation (2.22)) fitted his data with an agglomeration rate constant or agglomeration rate effectiveness kernel given by:

$$k_{V,a)H} = 2.1 \times 10^{-16} \times (CA - CA_e)^4 \frac{\text{g susp}}{\text{h}} \left(\frac{\text{g sol.}}{\text{g}} \right)^4 \quad (2.24)$$

60°C

Unfortunately this function was developed without taking into account the effects of growth and nucleation on the size distribution. In addition, no attempt was made to include the effects of the unknown number of crystals of a size less than that which could be measured. Moreover, their numerical solution of the agglomeration equation was only approximate and their data, from which the function (equation (2.24)) was developed, covered only a very narrow range of operating conditions. All of these factors would tend to confound the form and values of this

agglomeration kernel and explain why this function does not reflect the expected dependence of the agglomeration rate on the crystal size distribution.

2.6.3 Summary of the Available Information on Agglomeration for the Alumina Trihydrate System

In summary, the following can be deduced from the literature with regard to agglomeration of alumina trihydrate crystals:

1. Agglomerated crystals are true crystals and not a cluster of crystals held together by other than primary chemical bonds.
2. Agglomeration is favoured by:
 - fine seed
 - high seed concentration
 - high temperature
 - high supersaturation
 - slow stirring rates
3. One agglomeration model with a size independent kernel has been reported, but as discussed here, the development of this model has several shortcomings which explains why the kernel does not show the expected size dependence.

2.7 Attrition Rate

Attrition is the process whereby a particle breaks into two or more fragments. If the fracture results in relatively large particles, it is a clear attrition process. If on the other hand, it results in an original particle of essentially the same size and chipped off particles

of nuclei size, the distinction between attrition and nucleation is at best vague. Attrition as compared to nucleation requires probably more force, and the resultant number of particles formed is in general less than that arising from secondary nucleation. From a population balance standpoint, attrition means the death of the fractured particle and the birth of the resultant particles. Depending on the field of study attrition is also referred to as: breakage and comminution.

Attrition is most often thought to result from mechanical forces only which give rise to excessive stresses within the particle. The mechanical stresses to which the particle is subjected will depend primarily on the operating conditions within the crystallizer, particularly the intensity of agitation within it. In addition, the strength of the particles will determine their ability to withstand these stresses. Such operating conditions as crystallizer temperature and level of supersaturation will determine the shape (habit) and strength of the crystals so formed.

2.7.1 General Attrition Rate Model

A general model describing the population balance on size V in a process where only attrition occurs is:

$$\left\{ \frac{\partial}{\partial \tau} F_{V,T}(V, \tau) \right\}_b = 2 \int_{V+V_0}^{V_u} k_{V,b}(V', V, V' - V, \tau) F_{V,T}(V', \tau) dV' \\ - \int_{V_0}^{V-V_0} k_{V,b}(V, V', V - V', \tau) F_{V,T}(V', \tau) dV' \quad \dots (2.25)$$

Here $k_{V,b}$ is a rate function denoting the rate at which crystals of size V break into two fragments of sizes V' and $V - V'$. Its value is:

$$\begin{aligned}
 &= 0 \text{ for } V < 2V_0 \\
 & \quad V > V_u \\
 & \quad V' < V_0 \\
 & \quad V' > (V - V_0)
 \end{aligned}$$

$$\begin{aligned}
 &\geq 0 \text{ for } V \geq 2V_0 \\
 & \quad V \leq V_u \\
 & \quad V' \geq V_0 \\
 & \quad V' \leq V - V_0
 \end{aligned}$$

This equation is based on the concept that the attrition rate for particles of size V is proportional to the number of particles of that size. The rate function $k_{V,b}$ is a function of the interaction of these particles with its environment (for example, intensity of agitation, strength of particles); it is not thought to be a function of the interaction between different particles. This latter assumption means that the attrition process is a first-order process and thus becomes easier to deal with mathematically than the agglomeration process which is a second-order one.

2.7.2 Observations on the Attrition Rates for the Alumina Trihydrate System

Not much is known with regard to the attrition of alumina trihydrate crystals. The attrition process for this system is confounded

by nucleation and agglomeration. However, some quantitative information in the form of crystal size distribution graphs has been obtained (g3,r6) for the attrition of alumina trihydrate particles suspended in a saturated solution of sodium aluminate. In such a solution, nucleation and agglomeration do not take place, and the shift towards the lower end of the size distribution is solely due to attrition. As might be expected, it was found that attrition is related to the intensity of agitation and the residence time of the crystals in this agitated system. After a considerable time interval, the attrition rate became negligible. This suggested that a stable size distribution corresponding to a certain intensity of agitation had been obtained.

Attrition under these conditions is of course not the same as that under crystallization operating conditions. The intensity of agitation could be the same for both systems but a saturated solution environment is definitely different from a supersaturated solution environment in which growth and agglomeration take place simultaneously.

As mentioned earlier these rate processes will affect the strength of the particles and hence the rate of attrition will depend on the rates of growth and agglomeration in a specified system. This interaction among these processes suggests that it is impossible to obtain information on any one of them in independent experiments and therein lies the experimental problem. To date, no quantitative or qualitative information on attrition in a crystallizer is available. It is known, however, for the alumina trihydrate system that:

1. Attrition takes place under relatively intense conditions of agitation.

2. Given that no growth and agglomeration take place a stable size distribution results after a certain time interval of agitation.
3. No information is available for attrition under crystallizer operating conditions.

2.8 Induction Period

The induction period refers to that initial batch time interval over which the rates of growth, nucleation, agglomeration, and attrition are different, that is, slower or faster as compared to the rates which would occur at the crystallizer operating conditions after the crystallization processes had been proceeding for a long period. This induction process is a poorly understood phenomenon. Generally, it is thought to be related to the state or properties of the crystal surfaces. The dominant property is probably the number and size of surface ledges and/or imperfections. From the point of view of a research program which is attempting to study the normal crystallization processes, this induction period should be minimized as much as possible. In this study, this is achieved by pretreating the seed material.

2.8.1 Effect of the Induction Phenomenon on the Alumina Trihydrate Rate Processes

If the seed is not pretreated the alumina trihydrate system exhibits prominent induction effects (g3,m2,h1,p1). These effects are a function of temperature as well as other operating conditions. In general, it has been observed that the higher the temperature the smaller

the induction effects, both in the duration of the period and in the magnitude of rate changes. The effect on the growth rate has been observed qualitatively by several authors (e.g., g3,p1). As indicated earlier, Halfon modelled this growth rate change over very limited conditions (h1). No information is available on the effects of induction on the other rate processes of nucleation, agglomeration, and attrition.

2.9 Crystal Habit

The shape or form of the individual crystals making up the crystalline product is referred to as the crystal habit. The structure of the crystals is a regular, three-dimensional pattern of atoms in space. These patterns are made up of repeated identical units, or unit cells, which are joined together by either primary or secondary bonds in either a regular or irregular way. The irregularities are referred to as lattice defects. In practice, most crystals are imperfect and it is these defects which determine some of the important properties of the crystals, such as: resistivity, purity and strength. The geometry of a unit cell remains invariant for a particular crystal system, regardless of changing environmental conditions. On the other hand, the relative areas of the different faces of a unit cell are strongly influenced by the crystal's environment, with the slowest growing faces dominating the shape or habit of the crystal. What actually influences and/or controls crystal habit is poorly understood; certainly it is unique for each crystal system. It has been observed that habit has been influenced by type of solvent, pH of solution, impurities (particularly surface active agents), degree of supersaturation, rate of cooling, temperature of crystallization, and degree of agitation (ml):

2.9.1 Alumina Trihydrate Crystal Shape

The unit cell for the alumina trihydrate crystal has a monoclinic shape (m6), i.e. three axes of unequal lengths with two axes intersecting at right angles. Figure 4.4-C shows a photo micrograph of typical alumina trihydrate crystals. It shows that the crystal is made up from regularly shaped monoclinic structures which are joined together to form an irregularly shaped crystal. The regular shapes are joined together by primary bonds (g4) to form 'true' crystals, as opposed to for instance graphite, which is made up of layers held together by secondary molecular forces.

2.10 Modelling of a Crystallizer

As for any process, two basic modelling approaches can be followed for the modelling of a crystallizer. One is a purely empirical approach and the other is based on mechanistic concepts of the underlying process. The empirical approach is very limited in scope and only suitable for modelling of small dimensional problems without providing any extrapolative power. A mechanistic approach on the other hand allows one to deal with large dimensional problems, as it pertains in many crystallization systems, and given that the mechanistic concepts of the underlying processes are correct a model based on fundamental mechanisms allows for extrapolation and possibly even transfer to other crystallization systems. The mechanistic approach has the following advantages over an empirical one:

- It allows the modelling of large dimensional problems with complex interactions among the variables.

- It allows for predictions with reasonable confidence beyond the range of the modelled variables. Thus this approach most often leads to models with extrapolative powers.
- It provides for model development with a minimum of experimental effort.
- It provides a means of furthering or developing knowledge of the underlying processes that govern the overall behaviour of a particular system.

In view of these advantages and the fact that the alumina trihydrate crystallization problem is complex with highly interactive processes, a mechanistic approach was adopted for this work. The trend in crystallization work seems to be towards the increased use of mechanistic models (r1,h4,m1,n1). The difference among different investigators is in the complexity of the proposed mechanistic models and the corresponding extent of empiricism.

2.10.1 Mechanistic Model

In general, a mechanistic model which will allow prediction of crystal production as well as crystal size distribution, requires application and development of:

A. Conservation Laws

1. Mass balances.
2. Energy balance.
3. Momentum balance.
4. ~~Crystal~~ population balance.

B. Constitutive Relations

1. Crystal growth kinetics.
2. Crystal nucleation kinetics.
- 3. Crystal agglomeration kinetics.
4. Crystal attrition kinetics.

C. Empirical Semi-Empirical Correlations

1. Solubility data.
2. Solution density data.
3. Crystal geometry data.

Each of these will be discussed in turn as they apply to the alumina trihydrate system under study.

2.10.1.1 Conservation Laws

The conservation equations are of the general form:

$$\text{Accumulation} = \text{Input} - \text{Output} + \text{Net Generation} \quad (2.26)$$

where the conserved quantities are:

- mass
- energy
- momentum
- crystal numbers.

The first three are the familiar conservation equations that are often considered in process design where flows of material, energy, and

momentum into and out of equipment have to be accounted for. Vessel hydrodynamics determine the spatial distribution of these quantities with plug flow behaviour at one extreme and well mixed flow behaviour at the other.

The fourth conservation law, the crystal population balance, accounts for all crystals, as they are removed or introduced into a vessel and nucleated, agglomerated, attritted, and grown out of and into different size ranges. This 'keeping track of' individual species is not usually done in chemical unit operations. Depending on the type of operation it might or might not provide additional information over that obtained by application of the usual conservation laws. However, the unit operation of crystallization, among others, is a definite candidate for the application of the population balance. Crystallization models that are not based on the population balance will provide at best the crystallizer production rate and some average or mean product size. Such models are largely empirical and applicable only over a narrow range of operating conditions. Use of the population balance, on the other hand, will result in models that predict the production rate as well as the crystal size distribution at any instant in time and place. This provides a means of optimizing the crystallizer operation and at the same time produce a product with an acceptable size range for further processing or handling.

2.10.1.1.1 Conservation Laws for the Batch Alumina Trihydrate System

For the alumina trihydrate batch crystallization operation the conservation equations are:

1. Mass Balances(i) Overall

$$\frac{d}{d\tau} \{V_L \rho_L + W_T\} = 0 \quad (2.27)$$

(ii) Alumina Component

$$\frac{d}{d\tau} \{V_L CA + .654 W_T\} = 0 \quad (2.28)$$

(iii) Caustic Component

$$\frac{d}{d\tau} \{V_L CN\} = 0 \quad (2.29)$$

where $\frac{d}{d\tau} W_T$ is obtained from the population balance and ρ_L is related to CA and CN by an empirical relationship presented later. These equations are derived and discussed in detail in Chapter 5.

2. Energy Balance

In this work the energy balance is not required since the batch experiments will be carried out isothermally.

3. Momentum Balance

In this experimental program, the batch crystallizer is operated with constant agitation; thus, the internal and external forces are maintained essentially constant and the momentum balance does not play a direct role in the model. It must be remembered, however, that although

the momentum balance is neglected in the model, the intensity and mode of agitation indirectly affect the crystallization process since many of the parameters in the model will be a function of the intensity of agitation. These effects are beyond the scope of this study.

4. Population Balance

This balance provides the framework for a particulate mechanistic model. The success of developing such a model will depend to a large extent on an ability to solve the mathematical complexities and difficulties associated with the population balance equation. For the batch alumina trihydrate system and under certain not too restricting assumptions this balance is given by:

$$\underbrace{\frac{\partial}{\partial \tau}(F_{V,T})}_{\substack{\text{accumulation} \\ \text{of crystals} \\ \text{of size } V}} = \underbrace{-\frac{\partial}{\partial V}(G_V F_{V,T})}_{\substack{\text{output-input} \\ \text{into size } V \\ \text{due to crystal} \\ \text{growth}}} + \underbrace{V_L(BF_{V,\ell,n} + BF_{V,\ell,a} - DF_{V,\ell,a} + BF_{V,\ell,b} - DF_{V,\ell,b})}_{\substack{\text{output-input into size } V \text{ due} \\ \text{to crystal birth and death} \\ \text{processes, e.g. nucleation,} \\ \text{agglomeration, and attrition}} \quad (2.30)$$

The initial and boundary conditions for this equation are respectively:

$$F_{V,T}(V,0) = F_{V,T,0}(V) \quad (2.31)$$

and

$$F_{V,T}(V_0,\tau) = 0 \quad (2.32)$$

This equation is derived in Chapter 5. It can be solved once the constitutive relationships are known. The complexity and corresponding difficulty of solution depend on the form of these relationships.

2.10.1.2 Constitutive Relations; Alumina Trihydrate System Relations

These relationships relate the basic crystallization phenomenon, as discussed in Sections 2.4, 2.5, 2.6 and 2.7, to the process variables. They indicate the kinetic behaviour of each crystal while the population balance keeps track of the change in number of crystals of each size.

In general terms, the constitutive relationships are given by the following functionals:

(I) Growth Rate

$$G_V = \phi_g \{V, \theta, (CA - CA_e)\} \quad (2.33)$$

(II) Nucleation Birth Rate

$$BF_{V,\ell,n} = \phi_n \{V, \theta, W_t, (CA - CA_e), APA\} \quad (2.34)$$

(III) Agglomeration Birth and Death Rate

$$\begin{aligned} BF_{V,\ell,a} - DF_{V,\ell,a} = & \phi_{b,a} \{V', (V - V'), \theta, (CA - CA_e), \\ & F_{V,T}(V'), F_{V,T}(V - V'), APA\} - \\ & - \phi_{d,a} \{V, V', \theta, (CA - CA_e), F_{V,T}(V), F_{V,T}(V'), APA\} \\ & \dots \dots \dots (2.35) \end{aligned}$$

(IV) Attrition Birth and Death Rate

$$\begin{aligned}
 BF_{V,\lambda,b} - DF_{V,\lambda,b} &= \phi_{b,b}\{V',V,(V' - V),\theta,(CA - CA_e),F_{V,T}(V'),APA\} \\
 &\quad - \phi_{d,b}\{V,V',V - V',\theta,(CA - CA_e),F_{V,T}(V),APA\} \\
 &\quad \dots\dots(2.36)
 \end{aligned}$$

where

V	-	crystal volume
F	-	crystal size density function
θ	-	temperature
W_t	-	crystal mass weight per unit suspension
$CA - CA_e$	-	supersaturation
APA	-	variable related to type of apparatus and intensity of agitation

The first three of these functionals will be developed in this work. Sections 2.4, 2.5 and 2.6 present the information which is currently available in the literature with regard to these functions for crystallization systems in general and for the alumina trihydrate system in particular. The behaviour of the alumina trihydrate system during the induction period and the effect of operating variables on the crystal habit will not be investigated in detail in this program, although obviously, their effect will affect the course of the batch crystallizations.

2.10.1.3 Empirical Correlations; Alumina Trihydrate System Correlations

These type of correlations provide basic information with regard to such variables as solubility, solution density, and crystal area-volume relationships.

A. Solute Solubility

Solute solubility is required to establish the level of supersaturation at any instant or under any given operating condition. Supersaturation is one of the basic operating variables and is the driving force for the crystallization processes of growth and nucleation and also indirectly affects agglomeration and attrition. The relationship of solubility to solute concentration, temperature and the concentration of other solute and/or impurities is a basic requirement in any mechanistic model for a crystallization process.

Misra (m4) developed the following relationship for a pure alumina trihydrate-sodium aluminate system:

$$CA_e = CN \times \exp\{6.2106 + [((1.08753 \times CN) - 2486.7)/(273.16 + \theta)]\} \dots\dots (2.37)$$

with a range of applicability of: θ 25 + 100°C

CN 30 + 320 g Na₂O/l sol.

B. Solution Density

Solution density is required to relate the solution volume and concentration variables to the mass balances. Misra (m2) developed the following empirical relationship for solution density of this system:

$$\rho_l = 1.051 + (9.92 \times 10^{-4} - 1.1 \times 10^{-7} \times CN) \times CN + 5.66 \times 10^{-4} \times CA + (-9.4 \times 10^{-4} + 5.1 \times 10^{-6} \times \theta) \times \theta \dots\dots (2.38)$$

With a range of:

θ 20 + 100°C

CN 50 → 250 g Na₂O/l sol.

CA 15 + 300 g Al₂O₃/l sol.

C. Crystal Geometry Relationship

Crystal geometry establishes a relationship between crystal volume and crystal area. Crystal volume and density are required to establish a relationship between size and mass; crystal surface area is required in any crystal growth rate model. In this work, the crystal volume distribution of the crystals is measured by a Coulter Counter; hence some relationship is required between this measurement and the surface area of the crystals. This relationship is difficult to establish since it depends on the shape of the crystals, which in turn depends on the agglomeration and attrition effects in the crystallizer. Moreover, these effects may cause a change in shape with crystal size.

Scott (gl) has attempted to relate crystal volume and surface area through a variable ψ which he calls an angularity factor, which is defined as:

$$\psi = \frac{\text{surface area of particle}}{\text{surface area of sphere of equal volume}}$$

It is noted that this angularity factor is the inverse of the 'sphericity' which is a shape factor used in flow through porous media (fl) and in sedimentation theory (w4).

Scott (gl) determined ψ by measuring the specific surface area by air permeability and by calculating the area from particle size distri-

tion measurements assuming perfect spheres. Particle sizes were determined by sieving and by sedimentation. He presented a table of values of ψ vs. D which were correlated by the expression:

$$\psi(D) = 1.9055 - (1.0562 \times 10^{-2} + 2.924 \times 10^{-5} \times D) \times D \quad (2.39)$$

where D = equivalent sieving or sedimentation diameter (μm)

Although ψ probably varies with other process variables, here it is assumed that it is only a function of particle size.

The system of empirical, constitutive, and conservation equations which has been presented constitute a mechanistic model for the batch crystallization of alumina trihydrate. It predicts the crystal production rate as well as the crystal size distribution at any instant of batch time.

CHAPTER 3

EXPERIMENTAL; MEASUREMENT OF PROCESS VARIABLES

3.1 Crystallization Experiments; Introduction

During the development of any mathematical model for a system, the formulation of its mathematical equations should be directed by experimental observations and the desire to explain these observations by the model. This procedure ensures that the final model will include most, if not all, of the important phenomena occurring in the system. In addition, experimental measurements/observations are required to discriminate among alternative models which are possible and/or allow the evaluation of parameters within the overall model. This procedure should ensure that the 'best' fit of the experimental data by the model ensues and the confidence intervals on the parameters and the 'goodness of fit' of the model are determined. The experimental program which is described herein was designed to provide the required information for the model development which is described in later chapters.

3.1.1 Experimental Features of the Alumina Trihydrate System

The alumina trihydrate system has several features which affect the choice of a bench-scale experimental apparatus. For example, it is known that the crystal growth rate is relatively slow, that is of the order of a few micrometres per hour. This results in relatively long batch or continuous crystallization experiments, and this in turn means that the system conditions change relatively slowly with time. This also

means that it is not critical to control the sampling and sample analysis procedure to very short times. It is also known that the agglomeration of crystals occurs at a measureable rate. This phenomenon does not present any serious experimental difficulties except that the crystal size distribution covers a wide range of particle sizes. It is also known that the alumina trihydrate system does not nucleate readily from a supersaturated homogeneous solution (highly supersaturated solutions may be stored for very long times without nucleation), but does exhibit very significant secondary nucleation. Whether this is true secondary nucleation or a manifestation of very friable (weak) crystals which exhibit high attrition rates is open to conjecture. Because of these phenomena and the basic mechanisms involved, it is expected that the observations on the crystallization of this system will be very apparatus dependent. For example, it can be expected that very vigorous agitation will promote secondary nucleation or attrition. Thus, if it is desirable to minimize the nucleation rate, agitation should be as gentle as practically possible. On the other hand, reasonable mixing of the system is required to ensure that the crystal suspension and solute are uniform throughout the solution.

The fact that supersaturated solutions are very stable, means that preparation and handling (preparation, cooling, filtering) of this solution is quite easy. It does mean, however, that in order to carry out the crystallization process, the supersaturated solution must be 'seeded' with alumina trihydrate crystals and thus, the size distribution of this seed must be known.

3.1.2 Experimental Variables

The basic variables for a crystallization process are solution supersaturation, temperature, and crystal size distribution. Solution concentration determines the driving force for the rate of crystallization processes. Temperature determines the equilibrium condition at the crystal-solution interface and the rate of the different processes. The crystal size distribution and the total mass or number of crystals determines the interfacial surface area and thus indirectly governs these rate processes. Thus it is important to measure crystal size distribution for a mathematical model which is capable of predicting not only the crystal production rate but also the size distribution of the product. Such a model cannot be developed without knowledge of or a direct measurement of crystal size distribution with time. It is to be noted that although solution concentration and temperature are straightforward measurements, the measurement of crystal size distribution can be rather difficult. This difficulty is related in part to the range of crystal sizes that must be measured and to the strength of the crystals, their shape, etc.

3.1.3 Batch vs. Continuous Experiments

The experiments may be carried out in a batch or a continuous crystallizer. Each processing scheme has its advantages and disadvantages. In most cases, the batch system is easier and cheaper to set up. On the other hand, since the conditions in a batch system change continuously, it is more difficult to extract representative samples. In the alumina trihydrate system, the batch system is ideal since the solution needs to

be seeded and the changes occur relatively slowly and hence little difficulty is experienced with it. On the other hand, mathematical modeling is more difficult for the batch system if agglomeration takes place to any extent. This difficulty arises since for a batch system an integro-partial differential equation needs to be solved in order to predict the crystal-size distribution with time. For the continuous system, it is necessary to solve an integro-ordinary differential equation. Both systems present difficult numerical problems although the batch problem is probably more difficult.

Randolph (r1,r8) has pointed out another possible difficulty with a continuous process; that is, the fact that such a process may exhibit cyclic behaviour under certain conditions. This means that the system is never at a true steady-state condition but keeps changing continuously with time. The problem of replicating results is an obvious difficulty but may not be serious if the variation is relatively small.

It is to be noted that a continuous crystallization process may take a relatively long time to reach steady state and then this steady state provides one set of data at one particular operating condition. This leads to tedious and expensive experimental work. In the batch system, each experiment covers a wide range of experimental conditions and hence provides a lot more information from each experiment.

In this work with the alumina trihydrate system, a batch system does not present any particular disadvantage from an experimental standpoint. Certainly, it is expected that this bench-scale apparatus should not necessarily behave as the full-scale industrial batch plant because some of the crystallization processes are apparatus dependent.

3.1.4 Mixing of the Crystal Suspension

In the design of the batch system, it must be kept in mind that the mode and degree of mixing are important. In general, vigorous agitation enhances secondary nucleation, and probably slows down agglomeration. It is probably for this reason that in the industrial plant mixing is carried out relatively gently by means of an air-lift system. Thus, in order to have the rate processes of the same relative importance in the bench-scale model, it is important that the mixing be relatively gentle. Practically this may be achieved by using an air-lift or by slowly tumbling a partly-filled crystallizer through 360° in an oscillatory manner. The action of the air bubble in this container provides sufficient mixing to maintain a homogeneous suspension while subjecting the crystals to minimal forces. Both methods of mixing should closely approximate the plant mixing method, and therefore have a similar effect on the crystallization rate processes. If this was not done it is conceivable that the agglomeration would be small or insignificant in the bench-scale while in the actual process, it could be an overriding effect. The model for the bench-scale experiment would thus not be applicable at all to the actual full-scale operation.

3.1.5 Pure vs. Impure Solutions

In this type of research work, it is possible to work with pure solutions, or with solutions which might more closely represent the solution as it exists in the plant. A pure solution contains only sodium hydroxide and sodium aluminate dissolved in water, whereas the plant solution contains, in addition, such chemicals as iron, silicates, organic

material such as oxalic acid, sodium carbonate, etc. Since these impurities add another dimension to an already large and difficult problem, it was decided to use pure solutions in this research program. The effect of impurities can thus be determined independently later. It is expected that the mathematical models will have the same form, but the parameter values may be different in the impure system; certainly the equilibrium solubility is expected to be affected by the impurity level.

3.1.6 Caking and Corrosion Problems

A problem of particular importance in this crystallization work is the 'caking' problem which results in a crystal mass growing on the walls of the container. In a small bench scale apparatus with large surface-to-volume ratio, this crystal layer can affect the overall crystallization process significantly. At the same time, it is difficult to model and its effect will not be nearly as important in the large-scale system. Thus, the bench-scale apparatus should be comprised of material which has a 'non-sticking' characteristic for the crystals (this implies that imperfections, etc. will not cause nucleation of crystals on the walls). Moreover, the material must also be inert to a hot sodium aluminate solution.

3.1.7 Initial Batch Conditions and Batch Sampling

In a batch system, it is important to be able to control the initial conditions; such as the supersaturation level, temperature, seed concentration, seed size distribution. The seed must be prepared in a

standard way so that the initial induction period is approximately the same for each run. The control of initial conditions is necessary if reasonable replication of any of the experimental runs is to be achieved. Without replication model discrimination is more difficult.

The sampling procedure of the batch system has to be well thought out. It is necessary to obtain a representative sample from the crystallizer in a short time without affecting the sample or the suspension in the crystallizer. The sampling procedure must not affect the crystallizer operation or else all subsequent measurements could be correlated with it, which would introduce additional problems in the analysis of the results and in the estimation of parameters.

3.1.8 Sample Analysis Difficulties

Once a representative sample has been extracted from the crystallizer, there still remains the difficult task of sample analysis. First, after the crystallizer contents are sampled, it will be necessary to extract a relatively small representative sample from this sample for crystal size analysis. The remainder of the sample is then used for solution analysis.

The analysis of the solution can be done by well established titration procedures. On the other hand, a particle size analysis is tedious and difficult to obtain without considerable care and expertise. The problem with the present system is that the crystals are relatively weak and hence the particle size distribution must be obtained in a short time with gentle treatment of the sample. In addition, it is important to measure the distribution over as wide a range of sizes as possible.

This will facilitate the modelling work. The next sections show how these experimental difficulties have been tackled and solved.

3.2 Bench-Scale Crystallizer Apparatus

Since the bench-scale apparatus was to provide experience in testing and modelling a large-scale unit, it was desirable to design the bench-scale unit so that it would behave similarly to the plant crystallizer. This behaviour is directly related to the mixing characteristics within the crystallizer since the degree of mixing probably affects the rates of nucleation, attrition and agglomeration in this chemical system.

Thus, the basic requirements for the bench-scale crystallizer are:

1. Gentle Mixing

The industrial crystallizer employs an air-lift within or outside of the crystallizer. In the bench-scale apparatus, the gentle mixing is achieved by rotating the entire crystallizer slowly backward and forward through 360° . The air bubble within the crystallizer provides the required mixing.

2. Temperature Control

The crystallization reaction is slightly exothermic. In industry, the crystallizations are usually carried out at about 60°C . Some cooling is provided; however, the solution may increase several degrees during the initial stages when the rate of crystallization is relatively high. In the bench-scale apparatus, isothermal operation is relatively easily

achieved by surrounding the crystallizer with a temperature-controlled water bath. The large surface-to-volume ratio ensures isothermal operation over the entire crystallization period.

3. Rapid Charging of Chemicals

A method of charging the seed and solution rapidly and achieving intimate mixing rapidly is required to establish known initial conditions. This is important in any unsteady-state operation. The requirements here are not too stringent because the batch times are in the order of 24 h.; however, much of the crystallization occurs over the first hour or two and if a good initial condition is not achieved, this can affect all subsequent processes.

4. Representative Sampling

It is required to obtain representative samples in order to determine the instantaneous supersaturation level, the particle-size distribution, and the solids concentration, all of which are required in the latter modelling work.

5. Negligible Caking

The main crystallization processes should occur in solution. This means that any nucleation and subsequent growth of crystals on the walls of the small crystallizer should be avoided as much as possible since this behaviour would add further complications to a process which is complex already.

3.2.1 Development of Crystallizer Apparatus

The development of a suitable apparatus for these seeded batch crystallization experiments is reviewed here since many of the salient features of the final apparatus grew out of this program. The development program involved the designing and testing of four bench-scale crystallizers. A brief description of the design and operating features of each of them is presented below along with their major operating problems.

Figure 3.2.1-A shows the first crystallizer tested. This unit was a scaled-down version of one type of industrial crystallizer. The external air lift system, which provides the mixing, is a common mixing arrangement in the industry. In its operation in the laboratory, the air flow was adjusted to provide near maximum pump-around rate (as observed directly). The air was saturated with water at the crystallizer operating temperature before it was fed to the crystallizer. As crystallization of the seeded solution occurred, it was observed, however, that a significant amount of alumina trihydrate deposited on the stainless steel walls of the crystallizer. Thus, because of the modelling difficulties discussed earlier, this crystallizer design had to be abandoned.

To overcome this deposition problem, a second crystallizer was constructed, as shown in Figure 3.2.1-B. This apparatus had the following design features:

1. It was made from pyrex glass which, although attacked slightly by the caustic solutions at the concentrations and temperatures employed, was not expected to provide a surface to which alumina trihydrate crystals would adhere.

FIGURE 5.2.1-A Stainless Steel Scaled Down Industrial Batch Crystallizer

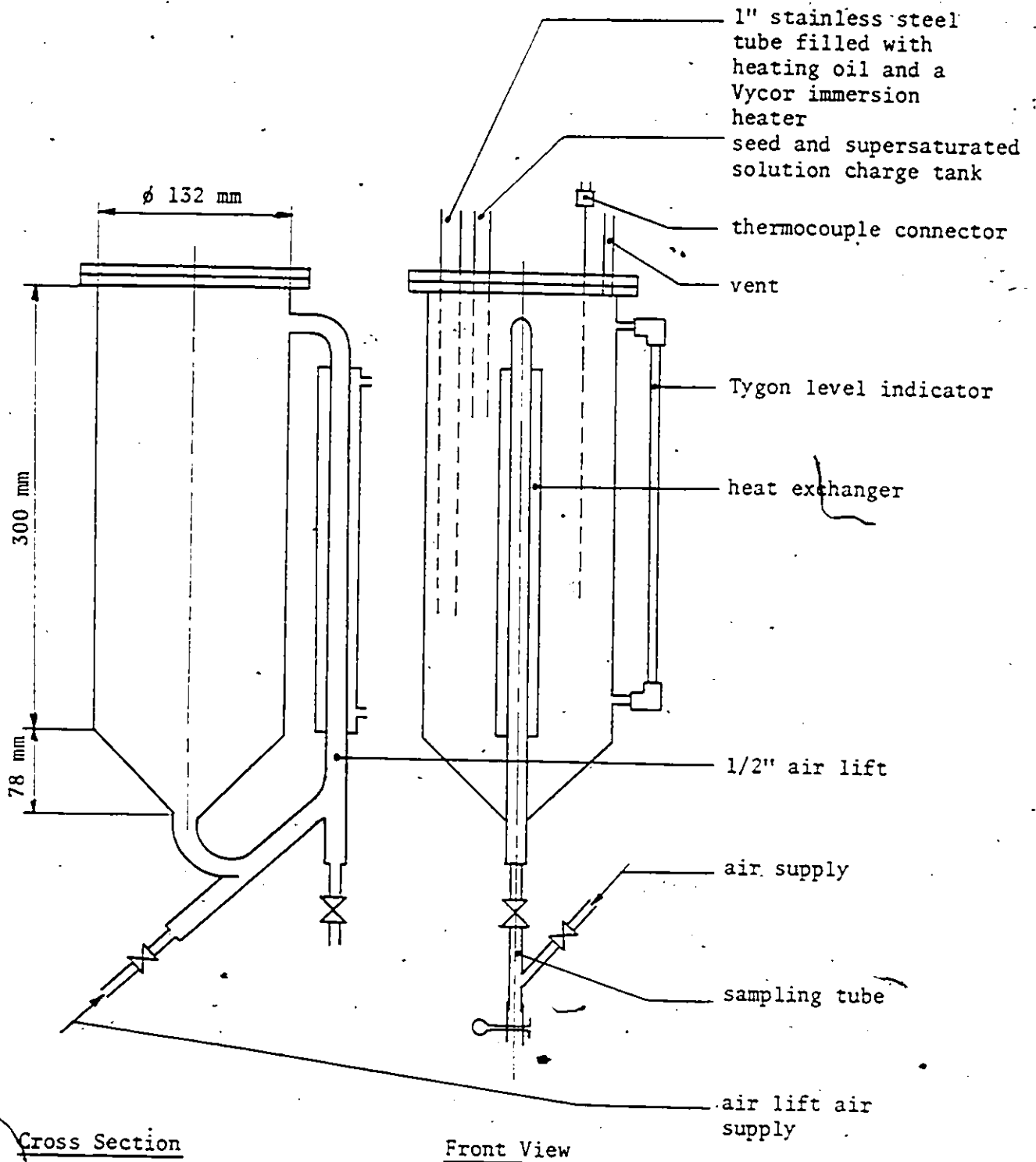
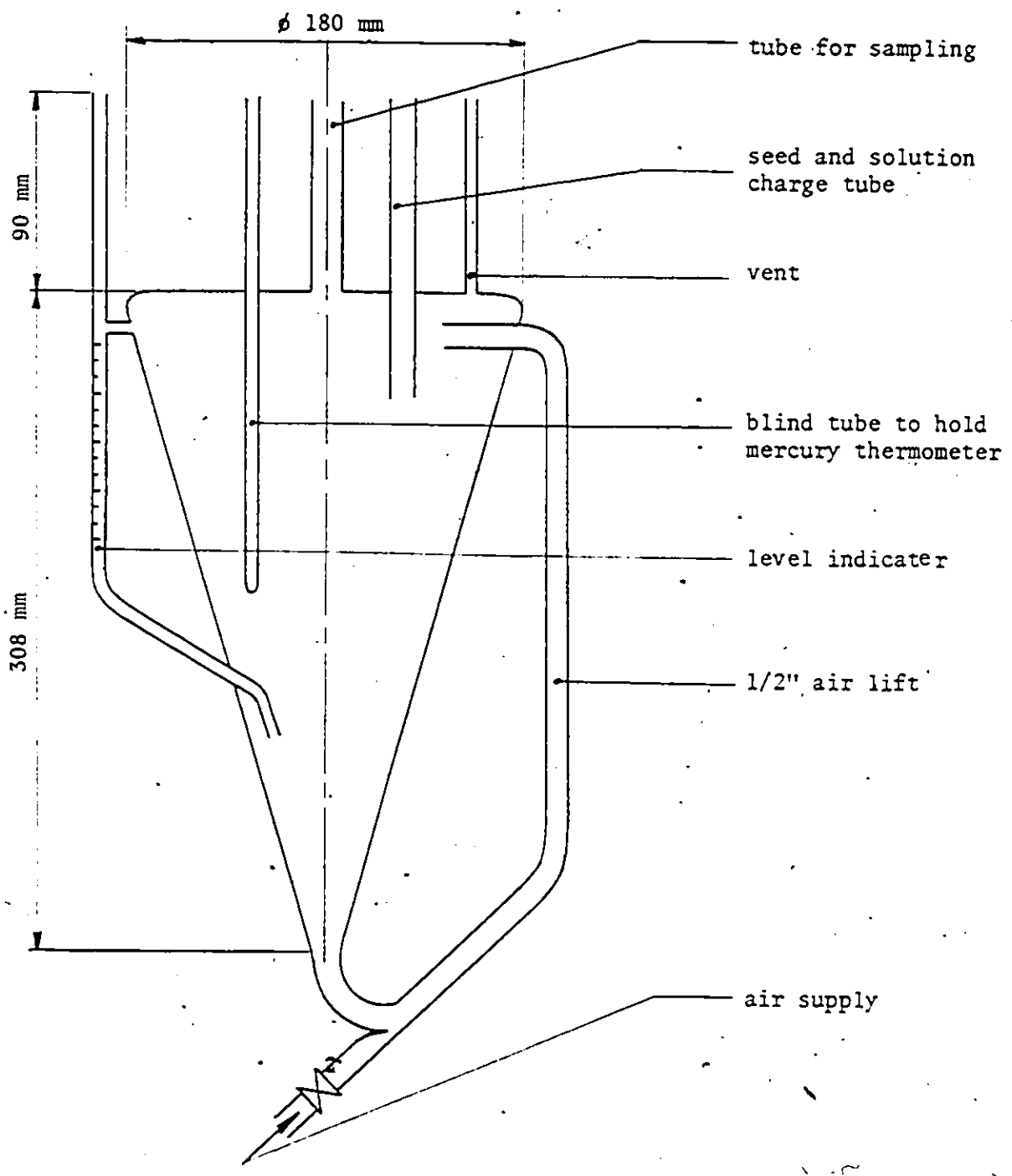


FIGURE 3.2.1-B Glass Batch Crystallizer with Air Lift



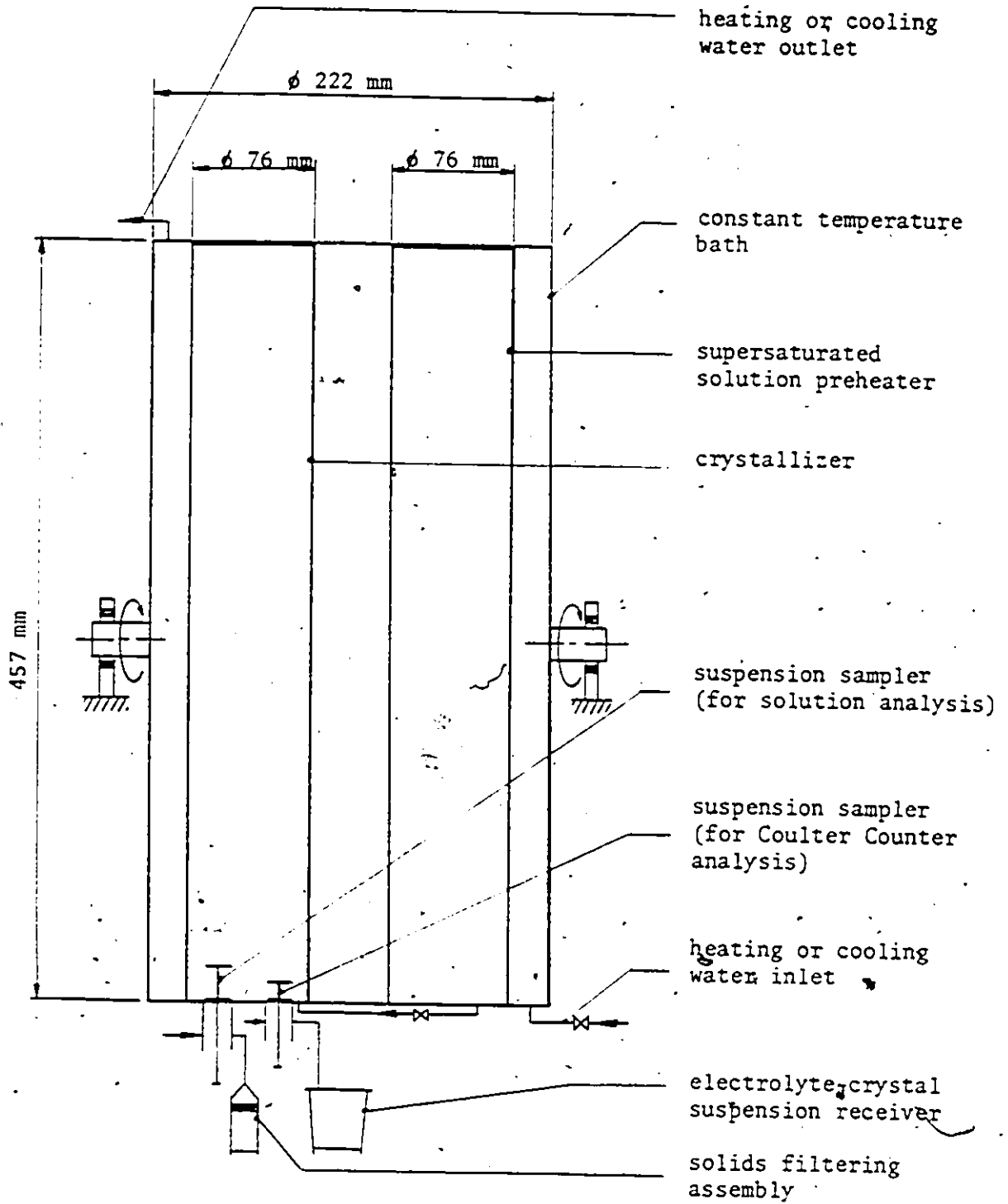
2. It was easily constructed and its cost was relatively small. Moreover, it could be easily modified.
3. The steep cone angle kept the solids moving rapidly downward, thus reducing the probability of crystals sticking to the walls.
4. It was also mixed by an air lift system. The off-center position of the air lift return imparted a swirling movement to the slurry. This facilitated mixing and at the same time hindered settling of solids on the crystallizer walls.

However, it was found that for high solids loading the air lift capacity was insufficient to remove the solids from the bottom of the crystallizer at the required rate. This resulted in blockage of the elbow connecting the vessel and air lift tube. Also, it was observed that after a few experiments some 'caking' on the walls started to occur. Deposits were formed on locations where the glass had become 'rough'. Thus, although the caking on the walls had been reduced, it still presented a serious problem with this apparatus. The problem seemed to be associated with the material and finish of the walls of the crystallizer. For this reason, the use of plastic was investigated.

The third crystallizer, shown in Figure 3.2.1-C, was made entirely of plastic material. It had the following design features:

1. It was constructed entirely of plastic which is inert towards the caustic solution at all operating conditions. The plastics in contact with the caustic solution were polypropylene and teflon while the constant temperature bath was made from polycarbonate.

FIGURE 3.2.1-C Polypropylene Batch Crystallizer with Semi-Automatic Sampling System



2. It was rocked backward and forward through 360° , thus providing quite good mixing (from the air bubble which moved up and down through the suspension), while at the same time not subjecting the suspension to destructive agitation.
3. The sampling arrangement allowed for the extraction of separate known volumes of suspension from the crystallizer for solute analysis and for crystal size distribution analysis on an absolute basis.
4. The sample which was used for crystal size analysis could be brought into contact with an inert solution very quickly, thus quenching the crystallization processes.
5. The sample used for solute analysis was filtered on line, thus providing fast separation of the supersaturated solution from the crystals. These sampling procedures meant that the sampling time was well defined.

Although this crystallizer performed satisfactorily in all ways relative to the previously observed problems (no caking on the walls, good mixing), it failed in other respects as follows:

1. The plastic crystallizer and supersaturated solution pre-heater 'buckled' at the process operating conditions. This was caused by the loss of strength of the polypropylene at the operating temperature.
2. A discontinuity in the solute concentration-time curve was observed at about each time of sampling. This was attributed to contamination which was introduced when the solid sample

was extracted, since this procedure could have introduced a small amount of the electrolyte used to quench the reaction and provide the media for the Coulter Counter particle size analysis. This electrolyte probably affected the crystallization processes.

In spite of these negative features, this design had the following very significant positive points:

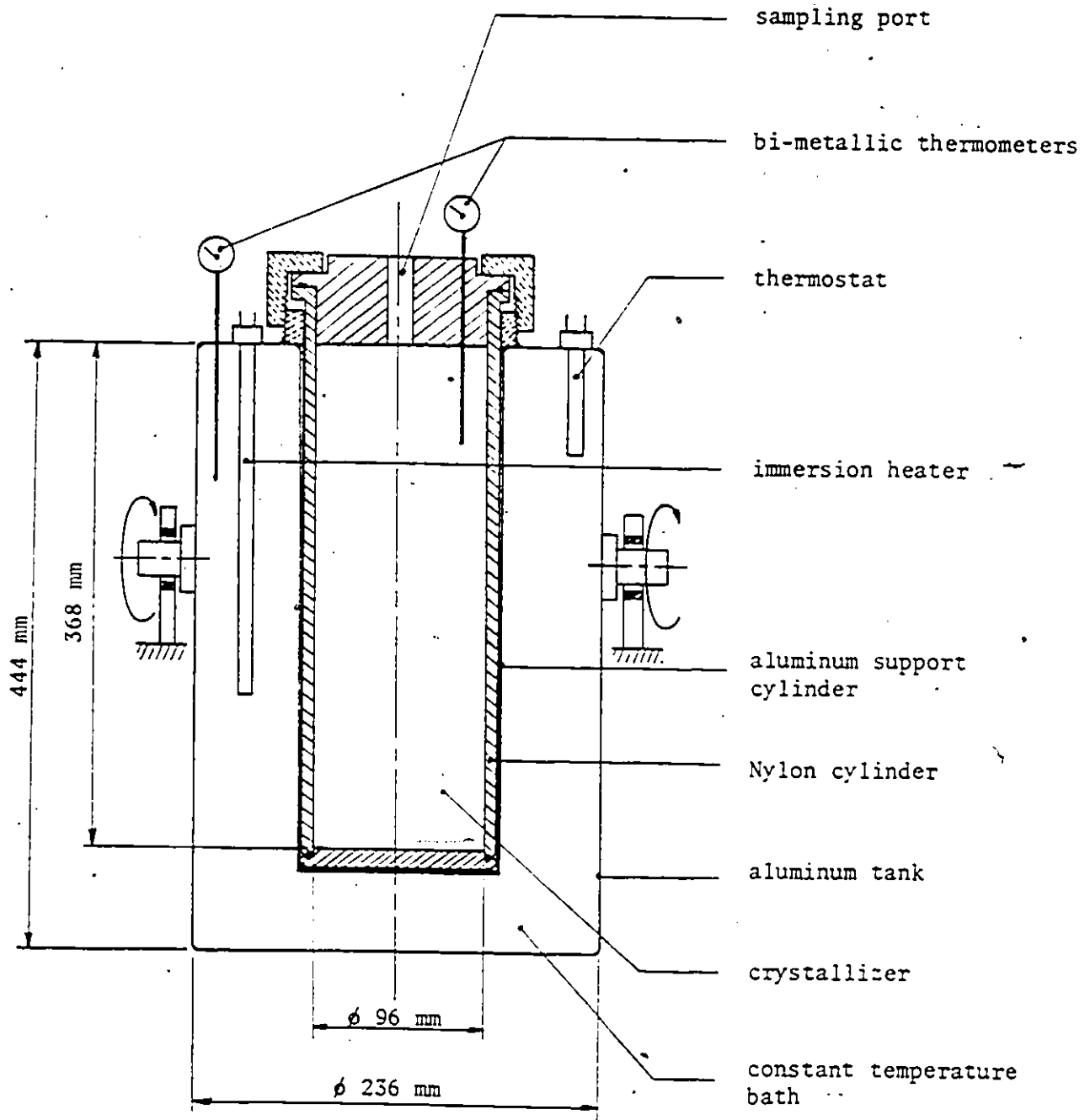
1. The method of mixing was satisfactory.
2. Caking did not occur.

3.2.2 The Experimental Crystallizer

The final design of the experimental crystallizer was based on the experience gained during the development stages. Thus, the experimental crystallizer, as shown in Figure 3.2.2-A, was made of nylon supported by an aluminum casing; it also was equipped with a modified sampling system. The design and construction details were as follows:

The crystallizer consisted of a 3.8" diameter by 14.5" long, closed plastic (nylon) cylinder which, because of its lack of strength at the operating temperature, was enclosed in an aluminum cylinder. Fortunately, aluminum and nylon have about the same coefficient of thermal expansion. The crystallizer was contained in another closed vessel containing thermostatically-controlled water. The entire system was held at its balance point by an axle as shown and rotated at about 5 to 6 RPM first through 360° in a clockwise and then through 360° in a counter-clockwise direction.

FIGURE 3.2.2-A Experimental Batch Crystallizer



A gentle mixing action resulted mainly from the action of the air bubble in the crystallizer although some crystal motion would occur because of the changing gravitational force and the effect of the small centrifugal force. Direct observation in a transparent system indicated that the mixing action of the air bubble was good but relatively gentle.

The crystallizer was equipped with a sample port which was plugged during normal operation. When a sample of the suspension was to be extracted, the crystallizer was stopped in an upright position, the sample port plug removed and a dip-stick type sampler, as shown in Figure 3.2.2-B, was inserted. So as not to affect the crystallization processes in the crystallizer, it was rinsed with distilled water and heated to the crystallizer operating temperature before sampling. The extracted sample was processed separate from the crystallizer in order to avoid the contamination problem which was encountered previously.

The crystallizer and sampling scheme was found to be completely satisfactory from all standpoints.

3.3 Preparation of a Supersaturated Solution of Sodium Aluminate

The batch crystallization experiments required a supersaturated solution of sodium aluminate. This supersaturated solution was prepared by digesting a known amount of $\text{Al}_2\text{O}_3 \cdot 3\text{H}_2\text{O}$ in a hot caustic solution.

The $\text{Al}_2\text{O}_3 \cdot 3\text{H}_2\text{O}$ crystals were dissolved or digested at about 300°F in the apparatus shown diagrammatically in Figure 3.3-A. The temperature was obtained and maintained by passing steam at 100 psig through a copper coil which was wrapped around the outside of the cylindrical part of the stainless steel tank. To prevent settling of the $\text{Al}_2\text{O}_3 \cdot 3\text{H}_2\text{O}$ crystals,

FIGURE 3.2.2-B Crystallizer Suspension Sampler

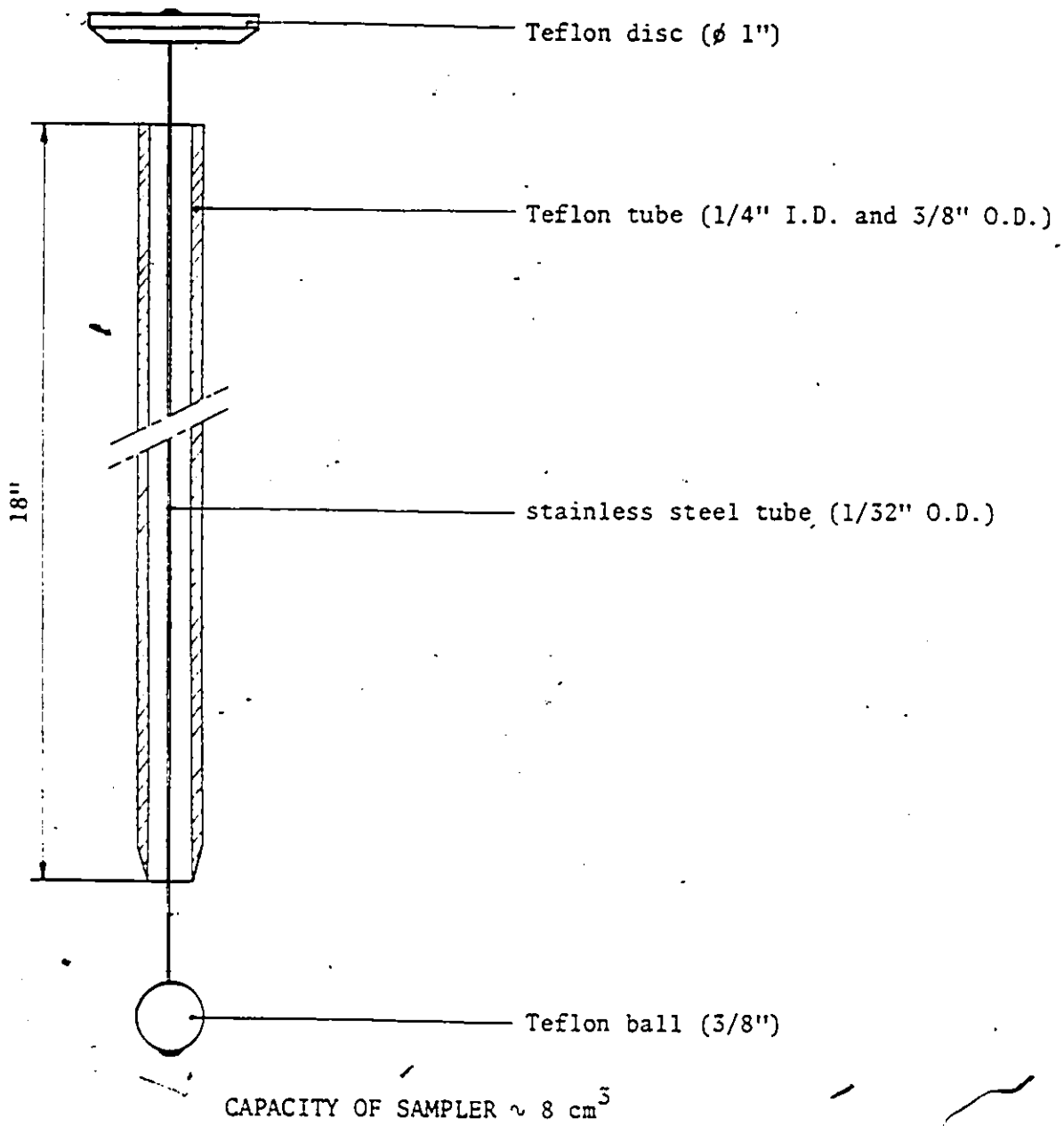
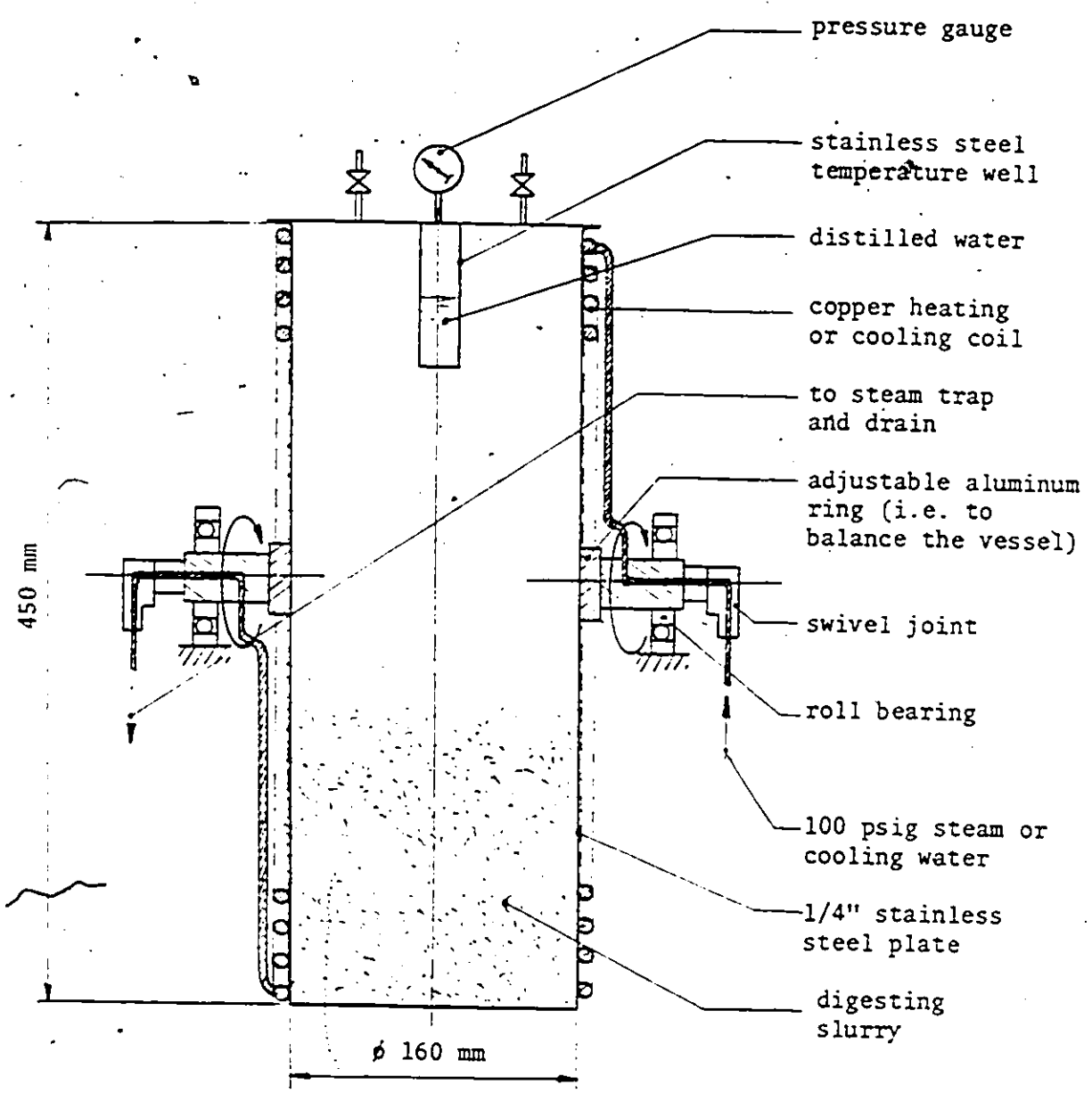


FIGURE 3.3-A Alumina Trihydrate Digester



the whole apparatus was rotated at about 50 rpm while the steam flowed through the coil. After the solution was digested at temperature for about an hour, it was cooled, filtered and stored for future use.

This supersaturated solution was very stable and could usually be kept in its supersaturated state for up to a few days depending upon the supersaturation level. Just before a crystallization experiment, it was preheated to the crystallizer operating temperature and then transferred to the crystallizer.

A computer program which calculates the required quantities of water, caustic and alumina trihydrate to make up a desired composition is presented in Appendix E. This program accounts for temperature effects by means of a dilution factor.

3.4 Preparation of Alumina Trihydrate Seed Crystals

It is well known with this crystallizing system that the pre-treatment of the seed material can affect the crystallization processes during the initial stages of batch crystallization (m2). Therefore, the seed material for this batch crystallization experimental program was prepared in an identical manner before each experiment. This procedure, as described below, was developed by experimentation to ensure that the initial attrition in the crystallizer would be a minimum.

Initial seed crystals were obtained either from a very highly supersaturated solution through heterogeneous and secondary nucleation, or from chemically pure alumina trihydrate crystals as obtained from a supplier. In each case, the size distribution was relatively wide and the average diameter was quite small (of the order of a few micrometres).

Because of the limitations of the Coulter Counter (to be discussed later) which was used to measure the crystal size distribution, only the upper part of the seed size distribution could be measured; the lower end of the distribution (less than 4 μm) was unknown. This presented a considerable difficulty in the modelling work, since this initial condition in the model was ill-defined. The only recourse was to assume some size distribution function over the unmeasured size interval and estimate parameters in this function (in a least-squares sense) so that the overall weight of seed as calculated from the distribution was the same as measured. To minimize the error in this procedure, the fraction of seed with size less than the smallest measured value had to be minimized. To achieve this result the fine seed material was introduced into a gently stirred supersaturated solution and thus causing the crystals to increase in size by growth and agglomeration. The resulting crystal suspension was either:

- (a) filtered and dried at 110°C and then stored, or
- (b) diluted with water to achieve a saturated solution in which the crystals were stored until required for use.

It was observed, however, that if these crystals were subjected to agitation their size distribution would shift progressively towards the smaller end. That is, by direct measurement it was determined that the number of crystals in the upper size intervals would decrease while the number in the lower intervals would increase. It was determined experimentally (g3) that after approximately two hours of intense stirring of this seed material, no further attrition took place; therefore, crystals so treated were regarded as 'stable'. It was hoped that this procedure

would minimize the complications which could arise at the start of a crystallization experiment as a result of an unknown attrition rate which would be difficult to reproduce.

Before the start of each experiment, therefore, a predetermined amount of seed was weighed and suspended in a saturated solution, and then vigorously stirred for approximately two hours. Afterwards, the seed suspension was preheated to the crystallizer operating temperature, and at the start of a batch experiment transferred to the crystallizer.

3.5 Alumina Trihydrate Batch System Process Variables

To define this two-phase, four component system, the Gibbs Phase Rule indicates that at equilibrium four variables must be specified.

These are:

1. Solids concentration, W_s
2. Alumina concentration, CA
3. Caustic concentration, CN
4. System pressure, P

In addition to these intensive variables, it is necessary to specify the extensive variable: total suspension volume, V_T , in order to specify total quantities.

For a batch system, it is necessary to measure these variables at known times from the start of the crystallization. This information gives the rate of change of these variables with time for any given process condition.

The solids concentration can either be measured directly or calculated indirectly from crystal size distribution measurements. The advantage

of crystal size distribution measurement is that it can be related to the basic crystallization processes, such as growth, nucleation, agglomeration, and attrition. For example, the overall growth rate, which is reflected in the rate of decrease in solute concentration, will depend on the total surface area of the particles which, in turn, is related to the total mass of solid and its size distribution. The solids concentration measurement, on the other hand, will allow only the development of empirical models and such models would require a large experimental effort for a relatively small return in information. Moreover, model development work based on crystal size distribution will greatly enhance the understanding of the overall crystallization process, and the relative significance of and interaction between the different crystallization phenomena.

For this reason, the variables which were measured or held constant for this work are:

- seed weight and initial solution volume
- batch crystallization time
- suspension temperature
- crystal size distribution (on an absolute basis)
- solids concentration
- alumina concentration
- caustic concentration
- method of seed preparation
- type of crystallizer
- intensity of agitation
- impurities concentration.

During the experiments in this program the following conditions prevailed:

- (a) The temperature during any one experiment was maintained at a constant value by the thermostatically controlled water bath. This meant that in the model formulations, the energy balance, with all the complications of predicting heat transfer rates, could be disregarded.
- (b) Use of the same type of crystallizer and mode of mixing meant that those processes, such as attrition agglomeration and to some extent nucleation, which depend on geometry and intensity of agitation, should not vary as a result of these variables.
- (c) As indicated earlier, the seed was prepared in an identical way to reduce the effect of a highly variable seed quality which could not be measured.
- (d) Although impurities are present in industrial processes, this complicating effect was avoided here by using a chemically pure reacting system.

The variables which were measured for each experiment as a function of time were: suspension temperature, crystal-size distribution (on an absolute basis, - number of a given size per unit volume), solids concentration, dissolved alumina concentration, and caustic concentration. The range of these variables in the experiments was as wide as practically possible and certainly included that of industrial importance. This wide range ensured that the model which was to be developed from the experimental data would have a broad range of applicability and also be tested

over a wide range of conditions where all crystallization phenomena would be interacting and proceeding at a significant rate. In this way also the likelihood of formulating the correct model is improved and the parameter estimates in the model should be good.

3.6 Batch Crystallizer Sampling Procedure

In developing a sampling procedure for this batch crystallization experimental program, it was necessary to satisfy the following features:

1. The extracted sample must be a representative sample, that is, it should not introduce any bias into the result.
2. The time to remove and isolate a sample must be insignificantly small compared to the time of the experiment.
3. The sampling procedure should not interfere with the course of the crystallization process.
4. The sampling procedure should not affect the sample in any way.

Based on a number of tests, the following sampling equipment and procedure were found to satisfy these criteria.

First, the crystallizer was momentarily stopped in an upright position; the sample port plug was removed; and the sampler shown in Figure 3.2.2-B was inserted. This sampler was made of teflon since previously it had been determined that the alumina trihydrate suspension did not stick to teflon either on the inside or outside of the tube. This apparatus and procedure did not interfere with the crystallizer suspension and moreover, it was demonstrated by experimentation that it did not introduce any bias in the extracted sample. The end of the

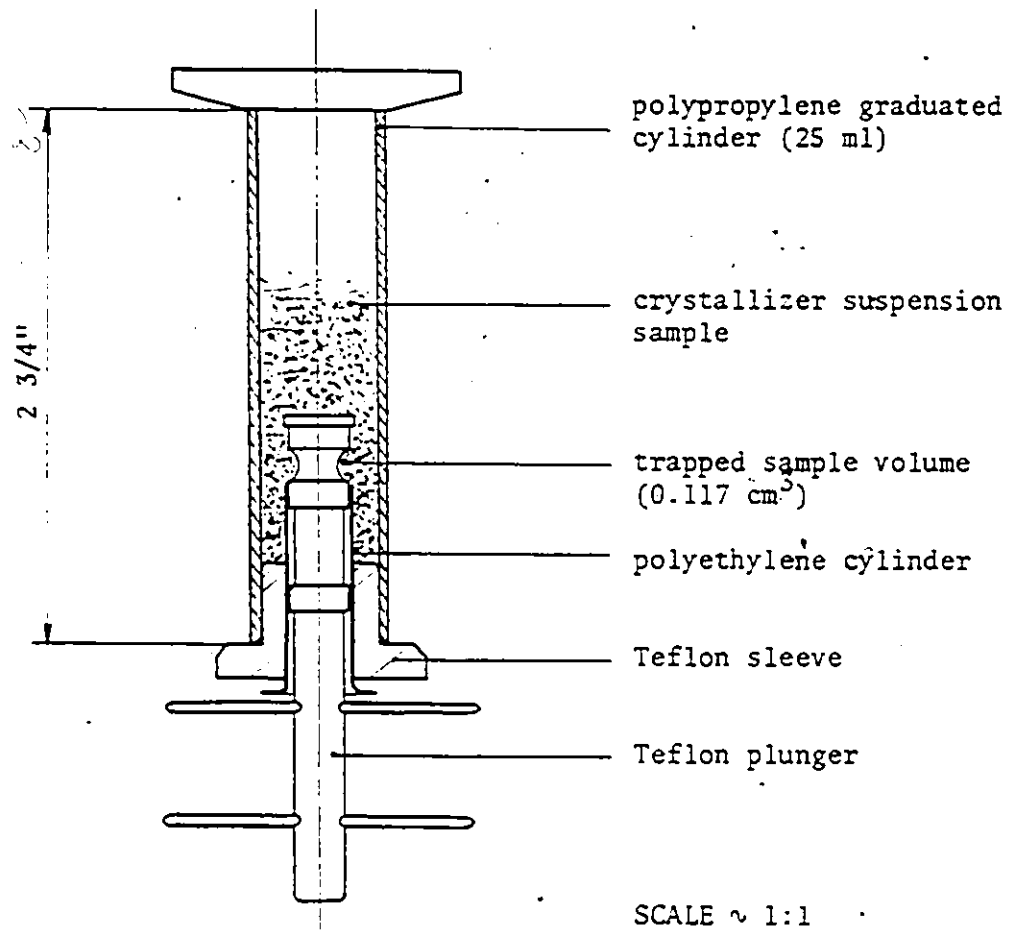
sampler, where the sample entered the sampler, and the ball valve were designed so as to minimize any segregation effects while the sampler was being inserted, again to minimize any sampling bias introduced in this way. Before taking each sample, the sampler was preheated to the suspension temperature so as to prevent thermal-shock and a resulting local increase in supersaturation near the sampler. In particular, this procedure minimized the secondary nucleation effects that could be expected to occur if a cold sampler were inserted.

After the sampler was inserted, the teflon ball was raised to trap a sample of the suspension. This sample was then transferred to the secondary sampling system, the sample port closed and the crystallizer tumbling resumed. This entire procedure only required a fraction of a minute.

The system for extracting samples from the overall sample (the secondary sampling system) is shown in Figure 3.6-A. This system provided a sample for particle-size analysis using a Coulter Counter model Z_B and another for solute analysis and for determining the solids concentration of the suspension.

The sample for the Coulter Counter analysis was extracted with the secondary sampler by gently shaking this device and then trapping a known volume of the suspension in the annulus of the plunger system shown in Figure 3.6-A (this sampling device was preheated as well). This suspension was then transferred to a jar filled with the electrolyte used in the Coulter Counter. The plunger was washed with this electrolyte by immersing it directly into it and shaking gently. The electrolyte quenched the crystallization process since the sodium aluminate solute

FIGURE 3.6-A Crystallizer Suspension Sample Sampler

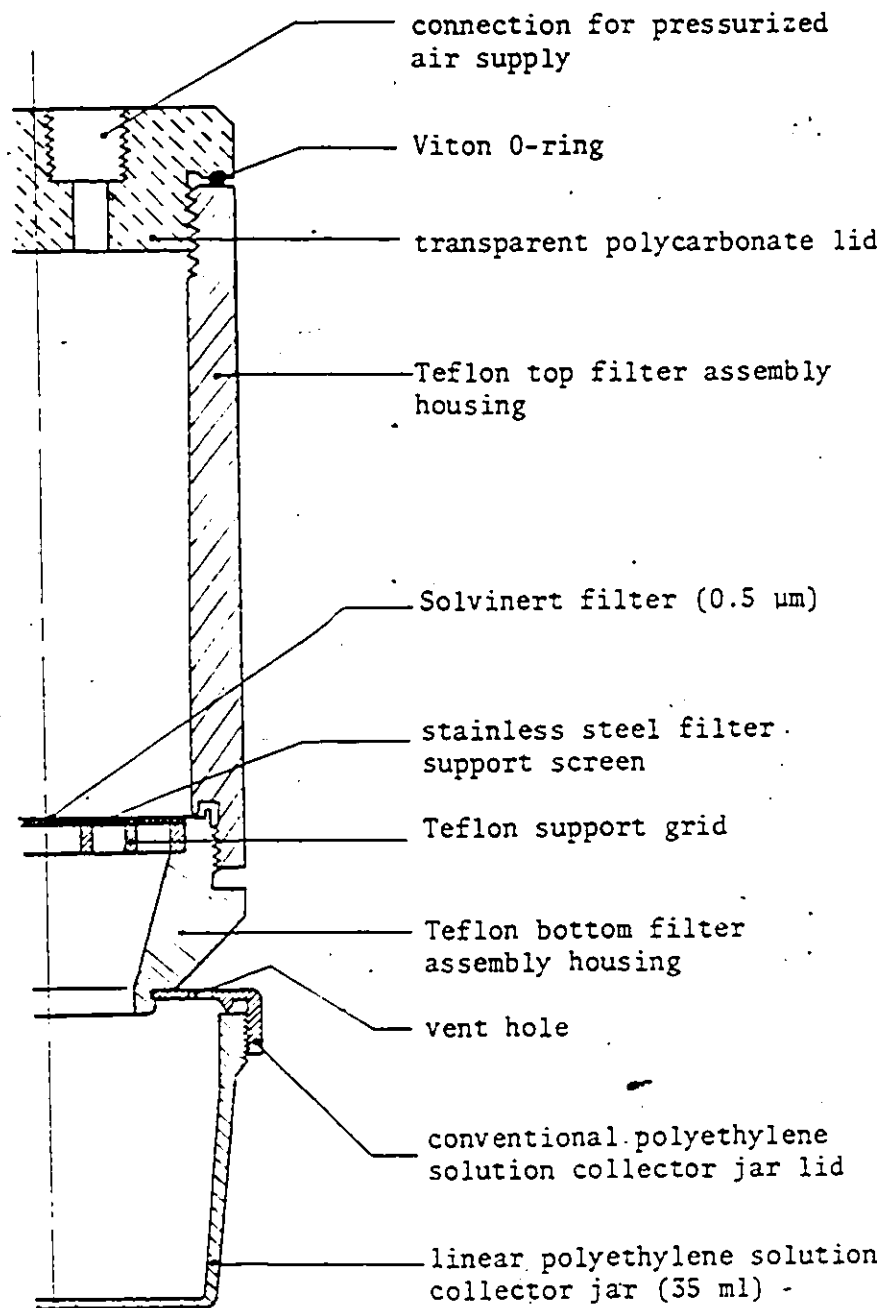


was dispersed in it. The crystals were stored in this inert solution until their size distribution could be determined at a later convenient time. It was demonstrated that these samples could be stored for extended times (a day or more) without a detectable change in size distribution. The detailed procedure for determining the particle-size distribution using the Model Z_B Coulter Counter is presented in Appendix C. It should be pointed out that considerable effort went into developing this sampling system. Other systems which were tried (g3) were found to bias either the larger or the smaller particles or to affect the suspension concentration. It was demonstrated by experiment that the secondary sampler system employed here allowed a fast extraction of a representative sample of a few drops of suspension as required for the Coulter Counter analysis.

The sample suspension which remained after extracting the Coulter Counter sample was then transferred to the filtering apparatus shown in Figure 3.6-B. This suspension was filtered under air pressure through a 0.5 μ m Solvinert* filter. Most of the filtrate in the cake was removed by an air blow. The filtrate was collected, weighed and stored in a closed bottle for solute analysis at a later time. Because the solution was filtered, further crystallization did not occur. The cake was then washed three times with distilled water, after which it was dried for at least 24 hours at 110°C. The dried filter cake was weighed and stored for future possible use, that is, as a check on the size distribution analysis.

*Trade name which is used by the Millipore Corporation for a membrane structure type of filter resistant to acids and alkalis.

FIGURE 3.6-B Crystallizer Suspension Sample Filtering Apparatus



SCALE ~ 1:1

All of these sampling and filtering procedures were developed so that with a skilled operator sampling, separation or quenching could be achieved in a very short overall time (ca. 1 minute). Hence the time of sampling was very short relative to the time of the overall crystallization process and could be considered essentially instantaneous. Furthermore, it was determined by experimentation that all of the criteria required of the sampling system were satisfied.

This procedure provided the following information at each sampling time during the batch run:

- (i) Size distribution of the crystals per unit suspension volume.
- (ii) A direct measurement of the solid concentration of the suspension.
- (iii) The concentration of alumina and total sodium ion.

These data could be checked for consistency in the following way:

The solids concentration per unit suspension volume may be calculated from the size distribution data, since the Coulter Counter measures particle volume, by the relationship

$$CS_3 \approx \frac{1}{2} \times 10^{-12} \times \rho_s \times D_2 t_\tau \times \left\{ \sum_{j=1}^m \Delta n_{a,j} \times (V_{j+1} + V_j) \right\}_\tau \quad (3.1)$$

Also the mass of solids in suspension at any time may be obtained by the material balance on alumina, viz:

$$CS_1 = \{ [(V_{L,o} \times CA_o) / .654] - [(V_{L,o} \times CN_o / CN_T) \times (CA_T / .654)] + W_{T,o} \} / \{ [V_{L,o} \times CN_o / CN_T] + [W_{T,T} / (1000 \times \rho_s)] \} \quad (3.2)$$

Equations (3.1) and (3.2) are derived in Appendix D where also the symbols are defined.

The direct measurement of solids concentration may be compared with these derived values to test the consistency of the data.

The actual analytical procedures are discussed in the following sections and described in detail in Appendices B and C.

3.7 Analysis of the Sodium Aluminate Solution Sample

The concentration of a particular ion in solution can either be measured directly or indirectly by measuring solution properties corresponding to a certain ion concentration. Examples of the indirect method are: solution density (g6), refractive index (m7), and solution conductivity (m3). For this work the solution density change with ion concentration change is much too insensitive to allow reliable measurements. Similarly refractive index is relatively insensitive to concentration changes; moreover, it is quite sensitive to temperature changes. The measurement of conductivity has been tried for this system (m3) but considerable difficulties due to deposition on the electrodes were encountered.

Examples of the direct method are: atomic absorption and titrimetric methods. Atomic absorption has been used for estimating caustic and alumina concentrations (m3). The method used for this work was a

volumetric titration procedure (w5). This is a well established method of analysis in the aluminum industry, while its reproducibility has been demonstrated in previous work (g3). A thermometric titration method which allows fast and accurate concentration measurements has been developed by Alcan (k2). It was decided, however, that the slight gain in speed of analysis and in the accuracy of the measurement of solution concentration, could not justify the relatively large expense for this study.

The volumetric titration procedure or wet analysis* used in this study is described in all details in Appendix B. The standard deviation of the wet analysis for the measurement of Al^{3+} expressed as equivalent grams of Al_2O_3 per litre of solution, was found through replicate tests of several samples to be 0.6, while that for the sodium concentration expressed as equivalent grams sodium carbonate per litre of solution was 0.7 (g3). Caustic concentration has also been expressed as equivalent Na_2O^{**} in some instances in this work in order to compare the results of this study with those of others where this concentration has been used.

3.8 Analysis of the Alumina Trihydrate Crystals Suspension Sample

Some well established methods of particle size analysis are: microscopy, sieving, sedimentation, and 'Coulter Counter' (b8,d3). Based

* "Wet analysis", is the usual term used in industry for the chemical analysis of a sodium aluminate solution, which in turn is referred to as "liquor".

** Note: 1 g/l sol. Na_2O = 1.712 g/l sol. Na_2CO_3

on these methods several devices are commercially available, each measuring a particular characteristic of the particle. For this research work all four methods are possible (b8), but the Coulter Counter appeared most suitable. The reliability of the Coulter Counter in comparison with other instruments has been demonstrated repeatedly by several workers (m8,d3), while its reproducibility for the alumina trihydrate system has been shown to be satisfactory (see Chapter 4, Section 4.5.2).

Some features of the Coulter Counter are:

1. It has a very fast analysis time, i.e. of the order of 15 seconds for one crystal size distribution analysis.
2. The instrument response is proportional to the particle volume which is an unambiguous particle size measurement.
3. The measurement obtained is total particle count (in a specified small size range) per unit volume of suspension per size fraction and hence relates directly to the probability density function for the particle mixture.
4. It has been found that the lower cut-off size is related to orifice diameter by the relationship:

$$d_{\min} \approx 0.02 \times d_{\text{orifice}}$$

For particles less than this size, the noise-to-signal ratio is too large to allow meaningful measurements to be made.

This lower size limit also relates to the cleanliness of the test solution since the electrolyte or test solution must be

relatively free of foreign particles. The ramifications of this feature are discussed in detail in Chapters 4 and 7.

The choice of the Coulter Counter over other instruments was based mainly on the advantages offered by items 1 and 3 above. The details of the operating principle, calibration technique, function of peripheral equipment, and count correction equations for the equipment used in this work are presented in Appendix C.

The main feature of the Model Z_B Coulter Counter equipped with a Channelyzer and channel 'Log Transformer' is that it automatically records the number of particles in each of 100 size groups on one pass of the suspension through the orifice. This 'one-pass' feature meant that the suspension was agitated for a very short time (\sim 30 seconds) and hence the amount of attrition of these very fragile particles was reduced accordingly. The addition of the 'log-size transformation' device meant that the size groups were concentrated at the lower end of the size spectrum, that is, the ΔV size intervals were smaller for the smaller sizes and progressively increased as the size increased. This feature was very important in this work, since the size distribution changed rapidly over the smaller particle sizes but not over the larger sizes; as a result, good resolution was obtained for the distribution. This resultant well-defined measurement of particle size distribution greatly facilitated the subsequent model development work. In addition to crystal size distribution on an absolute basis, the Coulter Counter analysis provided an indirect measurement of the variable solids concentration.

3.9 Experimental Procedure

The previous sections presented the rationale for the experimental system and procedures; the details of the actual procedure for a batch crystallization experimental run are presented below in point form.

1. Before the start of an experiment the following preparatory work was carried out:
 - (a) A sufficient quantity of sample jars was filled with 250 ml of the electrolyte used in the Coulter Counter. These jars were capped to prevent dust contamination.
 - (b) The crystallizer sampling tube, the Coulter Counter sampler and the sample filtration assembly were preheated in an oven to the crystallizer operating temperature.
 - (c) The supersaturated solution for the crystallization trial was prepared as follows: The caustic required for a specified supersaturation level, as determined by the computer program presented in Appendix E, was dissolved, with cooling on the outside of a stainless steel beaker in about three-quarters of the required water. The required alumina trihydrate was added to the caustic solution. The suspension was then transferred to the digester shown in Figure 3.3-A. The stainless steel beaker was rinsed repeatedly with the remaining water, which was transferred to the digester also. The digester was closed and then rotated at about 40 rpm. Steam, at 115 psia was passed into the copper coil, which

is wound around the digester and imbedded in Thermon cement (a graphite base material used to conduct heat in such situations). The contents were thus heated at about 300°F in this closed container for about one hour. After this digestion period, the solution was cooled by passing water through the coils. The solution was then transferred to a Buchner type filter for filtration and preheated to the crystallizer operating temperature in a hot water bath. Extensive use of plastic ware was made in these operations because polyethylene, nylon or teflon are inert to the chemicals and, since plastics are non-wetting, accurate measurement and transfer of solutions and suspension were easily accomplished.

The crystallizer which has already been described was preheated to the desired operating temperature by the water bath surrounding it. The crystallizer was then tumbled at approximately 6 rpm to ensure a uniform temperature throughout.

- (d) The seed for the batch crystallization was prepared as follows: A predetermined amount of alumina trihydrate was weighed out and mixed with a quantity of distilled water (about 2 l). This suspension was stirred vigorously with a stainless steel turbine for about two hours in order to ensure that the seed crystals which were to be

charged into the crystallizer would not readily break up in the crystallizer. This ensured that any ensuing nucleation, attrition or agglomeration arose out of the crystallization processes which followed and did not arise from the seed material. At the end of the two-hour period, the water was decanted to give the final desired concentration of solids at the start of the crystallization run.

- (e) Samples of the supersaturated solution and seed suspension were taken and stored for future analysis.
2. An experiment was started by transferring first the seed water suspension and then the supersaturated solution into the crystallizer. This charging and mixing was completed within about 30 seconds and this marked the start of the experiment. Samples were taken at predetermined times: first, at very short time intervals (ca. 10 min. apart), and later at longer intervals (ca. every 2 or 3 hours). These sampling periods were necessary since about 80 per cent of the crystallization occurred within the first hour; the actual crystallization trial continued for 24 to 48 hours or until the rate of change of solution concentration was very small.
3. Each sample was processed as follows:
 - (a) After extraction of the sample from the crystallizer it was transferred to the graduated cylinder of the Coulter Counter sampling assembly, and a Coulter Counter sample was extracted by pulling the sampler plunger

while shaking the assembly. This sample was transferred to the Coulter Counter electrolyte in the plastic jars by pushing the plunger back while in the electrolyte, and shaking it to make certain all of the sample was transferred. The electrolyte solution was then stirred with a teflon stick to hasten the diffusion of mother liquor from the crystal surface. The electrolyte-crystal suspension was stored for Coulter Counter analysis.

- (b) The remaining sample in the graduated cylinder of the Coulter Counter sampling assembly was transferred to the filter assembly, and filtered under air pressure. After this the filtered solution was weighed by difference, and a sample extracted by pipetting 5 ml into a polyethylene sample bottle and diluted to 50 ml with distilled water. This bottle was stored for the 'wet analysis'.
- (c) Before weighing of the solution, the filter cake was washed repeatedly (at least three times) with distilled water and put aside to dry first at room temperature and then after the completion of the experiment in an oven for at least 24 hours at 110°C. This dried the cake and left the cake in the alumina trihydrate form ($\text{Al}_2\text{O}_3 \cdot 3\text{H}_2\text{O}$). For this process it was essential that the filter cake was properly washed, otherwise a solid cake of crystals and solution would form when dried. The dried filter cake was weighed by difference and stored for possible future use.

- (d) The sampling procedure was completed by rinsing the crystallizer sampler, the Coulter Counter sampler, and the filtering apparatus with distilled water, and then drying them at the crystallizer operating temperature.
4. The prepared samples were analyzed when convenient according to the procedures outlined in Appendices B and C. The wet analyses were carried out during the later part of the experiment, while the Coulter Counter particle-size analyses were performed after the experiment was completed.

The experimental results are presented in the next chapter, where also the large amount of data obtained in each batch experiment is processed.

CHAPTER 4

EXPERIMENTAL PLAN AND EXPERIMENTAL RESULTS

4.1 Introduction; Experimental Plan

Typical industrial operating conditions and the range of experimental conditions over which the experiments in this study were performed are indicated in Table 4.1-A. The actual experimental conditions for each of the experiments conducted in the various bench-scale equipment are summarized in Table 4.1-B. This series of runs traces the development of the experimental apparatus and although considerable useful data were obtained, not all of it was self-consistent because of sampling and analysis problems, as discussed. The last and most successful experiments were carried out at about 85°C, at which temperature the initial induction effects were observed to be negligible. Thus, the data obtained during the early stages of these experiments were not confounded by this phenomena and the problems associated with predicting the initial condition at the start of the 'normal' behaviour period were avoided. Moreover, all of the data from this run were self consistent (e.g. crystal mass per unit volume as measured checked the particle size distribution and the mass of solute which crystallized); consequently, these data were used to develop and test the mathematical models which are to be presented in Chapter 7.

The main difficulty in obtaining good (consistent) experimental data was in obtaining a reliable measurement of the crystal size distribution for each sample. These measurements were only possible using the

TABLE 4.1-A

Range of Alumina Trihydrate Batch Process Variables

Variables	Plant	Laboratory
temperature ($^{\circ}\text{C}$)	50 + 70	40 + 90
caustic concentration- (g $\text{Na}_2\text{CO}_3/\ell$ sol.)	150 + 250	150 + 250
alumina concentration (g $\text{Al}_2\text{O}_3/\ell$ sol.)	150 + 40	150 + 40
seed charge (g $\text{Al}_2\text{O}_3 \cdot 3\text{H}_2\text{O}/$ ℓ susp.)	100 + 300	10 + 300
residence time (h)	20 + 40	+ 60
type of mixing	gentle	gentle + vigorous

TABLE 4.1-B

Experimental Conditions and Type of Experimental Apparatus



<p>Experiment #</p> <p><u>Experimental Conditions</u></p> <p>batch temperature ($^{\circ}\text{C}$)</p> <p>seed concentration (g/l susp.)</p> <p>alumina concentration (g Al_2O_3/l sol.)</p> <p>caustic concentration (g Na_2CO_3/l sol.)</p> <p>suspension volume (l)</p> <p>batch time (h)</p> <p><u>Type of Experimental Apparatus</u></p> <p>type of crystallizer</p> <p>crystallizer material</p> <p>type of crystallizer sampler</p> <p>method of mixing</p> <p>method of crystal size measurement</p> <p><u>Remarks</u></p>	<p>1</p> <p>70.4</p> <p>102</p> <p>72.1 + 47.8</p> <p>156.2 + 150.2</p> <p>3.6</p> <p>5.1</p> <p> , Figure 3.2.1-A</p> <p>stainless steel</p> <p> , drain on air lift</p> <p>external air lift</p> <p>Coulter Counter Model B</p> <p>-apparatus and sample analysis development experiment</p>
<p>Experiment #</p> <p><u>Experimental Conditions</u></p> <p>batch temperature ($^{\circ}\text{C}$)</p> <p>seed concentration (g/l susp.)</p> <p>alumina concentration (g Al_2O_3/l sol.)</p> <p>caustic concentration (g Na_2CO_3/l sol.)</p> <p>suspension volume (l)</p> <p>batch time (h)</p>	<p>2</p> <p>75.3</p> <p>43.1</p> <p>106.9 + 85.9</p> <p>193.0 + 187.4</p> <p>3.6</p> <p>5.6</p> <p>.....(cont'd.)</p>

TABLE 4.1-B (cont'd.)





<p><u>Type of Experimental Apparatus</u></p> <p>type of crystallizer</p> <p>crystallizer material</p> <p>type of crystallizer sampler</p> <p>method of mixing</p> <p>method of crystal size measurement</p> <p><u>Remarks</u></p>	 , Figure 3.2.1-A stainless steel  , drain on air lift external air lift Coulter Counter Model B - apparatus and sample analysis development experiment
<p>Experiment #</p> <p><u>Experimental Conditions</u></p> <p>batch temperature ($^{\circ}\text{C}$)</p> <p>seed concentration (g/l susp.)</p> <p>alumina concentration (g Al_2O_3/l sol.)</p> <p>caustic concentration (g Na_2CO_3/l sol.)</p> <p>suspension volume (l)</p> <p>batch time (h)</p> <p><u>Type of Experimental Apparatus</u></p> <p>type of crystallizer</p> <p>crystallizer material</p> <p>type of crystallizer sampler</p> <p>method of mixing</p> <p>method of crystal size measurement</p> <p><u>Remarks</u></p>	<p>3</p> <p>25.3</p> <p>22.2</p> <p>11.8 + 12.4</p> <p>151.2 + 151.0</p> <p>3.6</p> <p>24.6</p>  , Figure 3.2.1-A stainless steel  , drain on air lift external air lift Coulter Counter Model B - attrition experiment - developed a sample system consisting of: 'dip stick' (Figure 3.2.2-B) and 'plunger' (Figure 3.6-A)
	<p>.....(cont'd.)</p>

TABLE 4.1-B (cont'd.)



<p>Experiment #</p> <p><u>Experimental Conditions</u></p> <p>batch temperature (°C)</p> <p>seed concentration (g/l susp.)</p> <p>alumina concentration (g Al₂O₃/l sol.)</p> <p>caustic concentration (g Na₂CO₃/l sol.)</p> <p>suspension volume (l)</p> <p>batch time (h)</p> <p><u>Type of Experimental Apparatus</u></p> <p>type of crystallizer</p> <p>crystallizer material</p> <p>type of crystallizer sampler</p> <p>method of mixing</p> <p>method of crystal size measurement</p> <p><u>Remarks</u></p>	<p>4</p> <p>85.8</p> <p>13.9</p> <p>128.7 + 127.8</p> <p>276.2 + 276.0</p> <p>3.6</p> <p>19.0</p> <p> , Figure 3.2.1-A</p> <p>stainless steel</p> <p> , Figure 3.2.2-B</p> <p>external air lift</p> <p>Coulter Counter Model B</p> <p>- attrition and equilibrium concentration experiment</p>
<p>Experiment #</p> <p><u>Experimental Conditions</u></p> <p>batch temperature (°C)</p> <p>seed concentration (g/l susp.)</p> <p>alumina concentration (g Al₂O₃/l sol.)</p> <p>caustic concentration (g Na₂CO₃/l sol.)</p> <p>suspension volume (l)</p> <p>batch time (h)</p>	<p>5</p> <p>74.0</p> <p>13.8</p> <p>123.8 + 74.2</p> <p>199.0 + 195.1</p> <p>3.6</p> <p>26.0</p> <p>.....(cont'd.)</p>

TABLE 4.1-B (cont'd.)





<p><u>Type of Experimental Apparatus</u></p> <p>type of crystallizer</p> <p>crystallizer material</p> <p>type of crystallizer sampler</p> <p>method of mixing</p> <p>method of crystal size measurement</p> <p><u>Remarks</u></p>	 , Figure 3.2.1-A stainless steel  , Figure 3.2.2-B external air lift Coulter Counter Model B and Model TA — last experiment with this type of crystallizer due to severe 'caking' on the crystallizer walls under supersaturated conditions
<p>Experiment #</p> <p><u>Experimental Conditions</u></p> <p>batch temperature ($^{\circ}\text{C}$)</p> <p>seed concentration (g/l susp.)</p> <p>alumina concentration (g Al_2O_3/l sol.)</p> <p>caustic concentration (g Na_2CO_3/l sol.)</p> <p>suspension volume (l)</p> <p>batch time (h)</p> <p><u>Type of Experimental Apparatus</u></p> <p>type of crystallizer</p> <p>crystallizer material</p> <p>type of crystallizer sampler</p> <p>method of mixing</p> <p>method of crystal size measurement</p> <p><u>Remarks</u></p>	<p>6</p> <p>54.8</p> <p>24.8</p> <p>124.6 → 70.5</p> <p>194.2 → 201.3</p> <p>2.1</p> <p>16.0</p>  , Figure 3.2.1-B glass  , Figure 3.2.2-B external airlift Coulter Counter Model TA — further improved crystal size distribution analysis technique

TABLE 4.1-B (cont'd.)






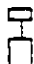


<p>Experiment #</p> <p><u>Experimental Conditions</u></p> <p>batch temperature ($^{\circ}\text{C}$) seed concentration (g/l susp.) alumina concentration (g Al_2O_3/l sol.) caustic concentration (g Na_2CO_3/l sol.) suspension volume (l) batch time (h)</p> <p><u>Type of Experimental Apparatus</u></p> <p>type of crystallizer crystallizer material type of crystallizer sampler method of mixing method of crystal size measurement</p> <p><u>Remarks</u></p>	<p>7</p> <p>54.8 24.2 141.8 + 80.2 186.0 + 203.0 2.0 9.0</p> <p> , Figure 3.2.1-B glass</p> <p> , Figure 3.2.2-B external air lift</p> <p>Coulter Counter Model TA</p> <ul style="list-style-type: none"> - developed a 'two tube' Coulter Counter analysis procedure - discontinued the use of this type of crystallizer due to severe caking on the glass surface of this crystallizer
<p>Experiment #</p> <p><u>Experimental Conditions</u></p> <p>batch temperature ($^{\circ}\text{C}$) seed concentration (g/l susp.) alumina concentration (g Al_2O_3/l sol.) caustic concentration (g Na_2CO_3/l sol.) suspension volume (l) batch time (h)</p>	<p>8</p> <p>54.5 7.28 86.2 + 52.2 164.5 - 172.4 1.7 10.2</p> <p>.....(cont'd.)</p>

TABLE 4.1-B (cont'd.)

<p><u>Type of Experimental Apparatus</u></p> <p>type of crystallizer</p> <p>crystallizer material</p> <p>type of crystallizer sampler</p> <p>method of mixing</p> <p>method of crystal size measurement</p> <p><u>Remarks</u></p>	<p> , Figure 3.2.1-C</p> <p>polypropylene</p> <p> , plunger type of sampler</p> <p>tumbled partially filled crystallizer back & forth</p> <p>Coulter Counter Model TA</p> <ul style="list-style-type: none"> - designed a more automated type of experimental set-up - the results were invalidated due to crystallizer contents contamination with Coulter Counter electrolyte
<p>Experiment #</p> <p><u>Experimental Conditions</u></p> <p>batch temperature ($^{\circ}\text{C}$)</p> <p>seed concentration (g/l susp.)</p> <p>alumina concentration (g Al_2O_3/l sol.)</p> <p>caustic concentration (g Na_2CO_3/l sol.)</p> <p>suspension volume (l)</p> <p>batch time (h)</p> <p><u>Type of Experimental Apparatus</u></p> <p>type of crystallizer</p> <p>crystallizer material</p> <p>type of crystallizer sampler</p> <p>method of mixing</p> <p>method of crystal size measurement</p>	<p>9</p> <p>55.2</p> <p>4.9</p> <p>103.9 + 68.3</p> <p>192.1 + 200.1</p> <p>1.8</p> <p>30.3</p> <p> , Figure 3.2.1-C</p> <p>polypropylene</p> <p> , plunger type of sampler</p> <p>tumbled partially filled crystallizer back & forth</p> <p>Coulter Counter Model TA</p>

.....(cont'd.)

TABLE 4.1-B (cont'd.)

<u>Remarks</u>	- discontinued the use of this type of crystallizer for contents contamination and crystallizer material buckling reasons
<u>Experiment #</u> <u>Experimental Conditions</u> batch temperature ($^{\circ}\text{C}$) seed concentration (g/l susp.) alumina concentration (g Al_2O_3 /l sol.) caustic concentration (g Na_2CO_3 /l sol.) suspension volume (l) batch time (h) <u>Type of Experimental Apparatus</u> type of crystallizer crystallizer material type of crystallizer sampler method of mixing method of crystal size measurement <u>Remarks</u>	10  , Figure 3.2.2-A nylon supported by an aluminum casing  , Figure 3.2.2-B tumbled partially filled crystallizer back & forth Coulter Counter Model TA - designed more robust type of plastic crystallizer - further improved sampling and Coulter Counter analysis techniques
<u>Experiment #</u> <u>Experimental Conditions</u> batch temperature ($^{\circ}\text{C}$) seed concentration (g/l susp.) alumina concentration (g Al_2O_3 /l sol.) caustic concentration (g Na_2CO_3 /l sol.)	11 84.8 10.0 134.7 + 82.4 196.6 + 188.7

.....(cont'd.)

TABLE 4.1-B (cont'd.)







<p>suspension volume (ℓ) batch time (h)</p> <p><u>Type of Experimental Apparatus</u></p> <p>type of crystallizer crystallizer material type of crystallizer sampler method of mixing method of crystal size measurement</p> <p><u>Remarks</u></p>	<p>2.7 24.0</p> <p> , Figure 3.2.2-A nylon supported by an aluminum casing</p> <p> , Figure 3.2.2-B tumbled partially filled crystallizer back & forth Coulter Counter Model TA</p> <p>— results were invalidated by contamination of crystallizer contents by water from the hot water jacket</p>
<p>Experiment #</p> <p><u>Experimental Conditions</u></p> <p>batch temperature (°C) seed concentration (g/ℓ susp.) alumina concentration (g Al₂O₃/ℓ sol.) caustic concentration (g Na₂CO₃/ℓ sol.) suspension volume (ℓ) batch time (h)</p> <p><u>Type of Experimental Apparatus</u></p> <p>type of crystallizer crystallizer material type of crystallizer sampler</p>	<p>12</p> <p>85.3 10.0 137.1 + 96.3 206.7 + 215.2 2.5 20.2</p> <p> , Figure 3.2.2-A nylon supported by an aluminum casing</p> <p> , Figure 3.2.2-B</p> <p>.....(cont'd.)</p>

TABLE 4.1-B (cont'd.)

method of mixing	tumbled partially filled crystallizer back & forth
method of crystal size measurement	Coulter Counter Model TA
<u>Remarks</u>	— further improved the Coulter Counter analysis technique for the size distribution measurement on an absolute basis
Experiment #	13
<u>Experimental Conditions</u>	
batch temperature ($^{\circ}\text{C}$)	85.1
seed concentration (g/l susp.)	9.94
alumina concentration (g Al_2O_3 /l sol.)	136.4 + 94.7
caustic concentration (g Na_2CO_3 /l sol.)	212.8 + 219.4
suspension volume (l)	2.5
batch time (h)	44.0
<u>Type of Experimental Apparatus</u>	
type of crystallizer	 , Figure 3.2.2-A
crystallizer material	nylon supported by an aluminum casing
type of crystallizer sampler	 , Figure 3.2.2-B
method of mixing	tumbled partially filled crystallizer back & forth
method of crystal size measurement	Coulter Counter Model TA and by Coulter Counter Model Z _B with a Channelyzer and channel size Log Transformer
<u>Remarks</u>	— obtained size distribution measurements on an absolute basis suitable for mathematical analysis

Coulter Counter Model Z_B equipped with Channelyzer and Log Transformer. Although other less sophisticated Coulter Counters were used, each required too much processing time in the instrument because of the requirement for multiple pass of the solution through the orifice. Other problems such as caking on the crystallizer walls, extracting unrepresentative samples, non-homogeneous mixing, contaminating the crystallizer contents through the sampling procedure were all eliminated by progressively improving the experimental system.

4.2 Presentation and Discussion of Experimental Data

All the experimental conditions and actual observations of the one experimental run which has been thoroughly tested and analyzed in this study are presented in Appendix A. These data are typical of the information which may be obtained from the experimental equipment.

These experimental observations are presented here in different forms with particular emphasis on the different ways that the raw measurements of the crystal size distribution may be presented. It will also be shown how the various observations may be used to test them for consistency among them. Also, some of the significant overall observations with regard to system behaviour will be delineated to indicate the type of crystallizer model which has to be developed.

4.2.1 Solution Density and Equilibrium Alumina Concentration

Misra's solution density and equilibrium alumina solution concentration correlations (m_2, m_4) for a pure solution were checked by making some spot measurements. The results are presented in Table 4.2.1-A. The

TABLE 4.2.1-A

Spot Checks on Misra's Solution Density and
Equilibrium Alumina Solution Concentration Correlations

experiment #	3	4	9
suspension temperature ($^{\circ}\text{C}$)	25.0	83.8	-
solution temperature ($^{\circ}\text{C}$)	-	-	24.0
caustic concentration (g $\text{Na}_2\text{O}/\ell$ sol.)	88.3	161.2	116.2
alumina concentration (g $\text{Al}_2\text{O}_3/\ell$ sol.)	-	-	118.2
equilibrium alumina concentration (measured) (g $\text{Al}_2\text{O}_3/\ell$ sol.)	12.17	127.8	-
solution density (measured) (g/cm 3)	-	-	1.210
Misra's equilibrium correlation (g $\text{Al}_2\text{O}_3/\ell$ sol.)	14.46	123.7	-
Misra's solution density correlation (g/cm 3)	-	-	1.212
percentage deviation (%)	16	3	.2

agreement was found to be reasonable and it was not deemed necessary to check his correlations more thoroughly.

4.2.2 Typical Experimental Batch Data

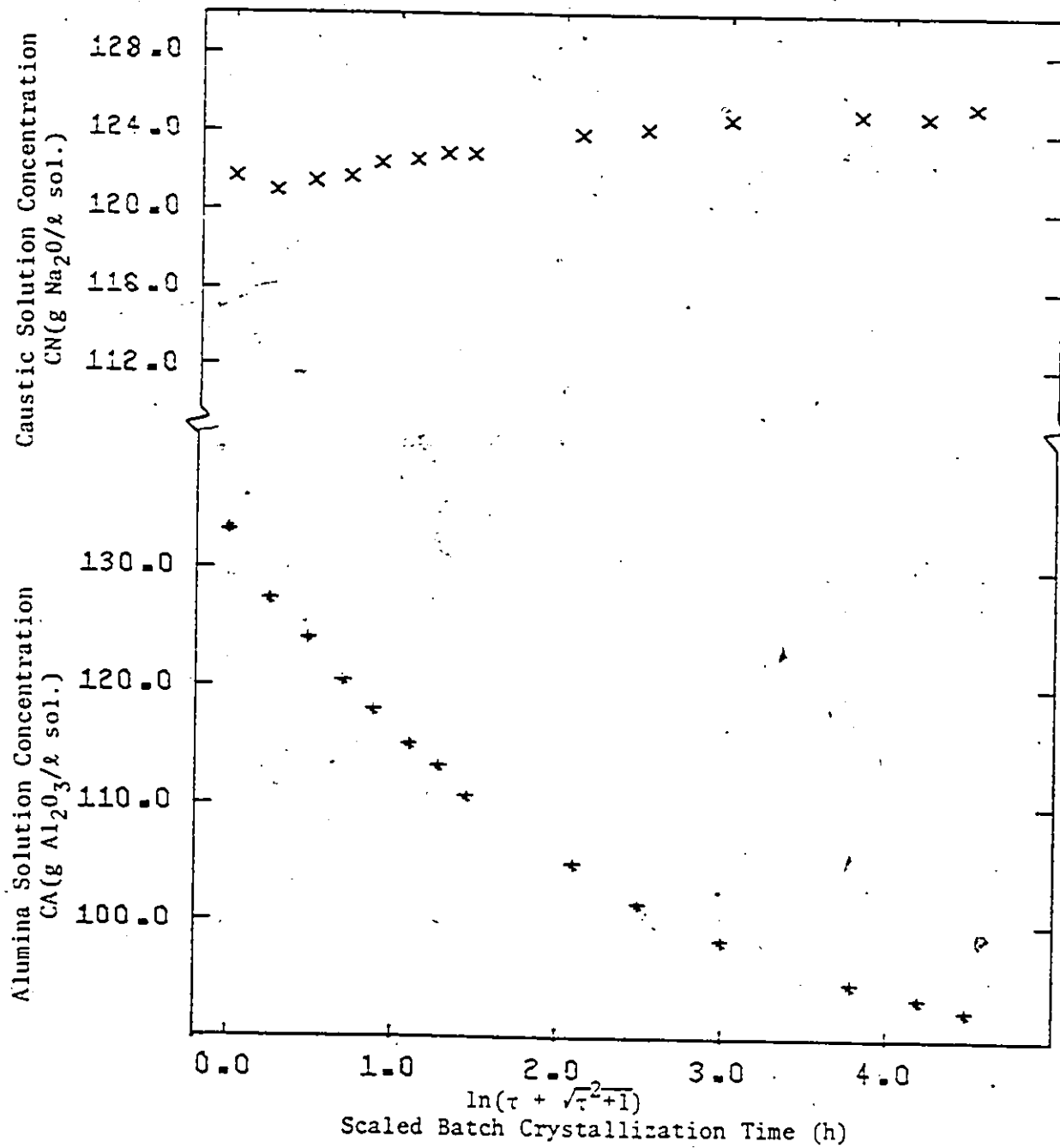
The data from the analyzed batch run, experiment number 13, are presented and discussed in the next sub-sections.

4.2.2.1 Solution Concentration Measurements

The alumina and sodium (as sodium carbonate) concentrations as measured as a function of time are shown in Figure 4.2.2.1-A. It is seen that the total sodium concentration changed little during the run because the change in volume of the solution due to solute crystallization was small for these relatively dilute suspensions. The decrease of the alumina concentration provides a measure of the rate of depletion of Al(OH)_3 from solution due to crystal growth. Again, however, to achieve this exact equivalence, the small change in volume of the solution must be taken into account. Moreover, a temperature correction must be applied, since the solution density changes with temperature and the measurements of solution concentration were made at room temperature which was lower than the crystallizer operating temperature. This difference in volume is proportional to the temperature difference and this proportionality, which is derived in Appendix B, may be expressed by:*

*Subscript 1 refers to the concentrations at room temperature, while 2 refers to those at the crystallizer operating temperature.

FIGURE 4.2.2.1-A Solution Concentration Measurements



$$CA = CA_2 = CA_1/\alpha \quad (4.1)$$

$$CN = CN_2 = CN_1/\alpha \quad (4.2)$$

where $\alpha = \{-C2 + [(C2)^2 - (4 \times C1 \times C3)]^{1/2}\} / (2 \times C1)$

$$C1 = 1.051 + (5.1 \times 10^{-6} \times \theta_2 - 9.4 \times 10^{-4}) \times \theta_2$$

$$C2 = (9.92 \times 10^{-4} \times CN_1) + (5.66 \times 10^{-4} \times CA_1) - \rho_{2,1}$$

$$C3 = -1.1 \times 10^{-7} \times (CN_1)^2$$

$$\rho_{2,1} = 1.051 + (-1.1 \times 10^{-7} \times CN_1 + 9.92 \times 10^{-4}) \times CN_1 \\ + 5.66 \times 10^{-4} \times CA_1 + (5.1 \times 10^{-6} \times \theta_1 - 9.4 \times 10^{-4}) \times \theta_1$$

CA = alumina concentration (g Al₂O₃/l sol.)

CN = caustic concentration (g Na₂O/l sol.)

θ_1 = room temperature (°C)

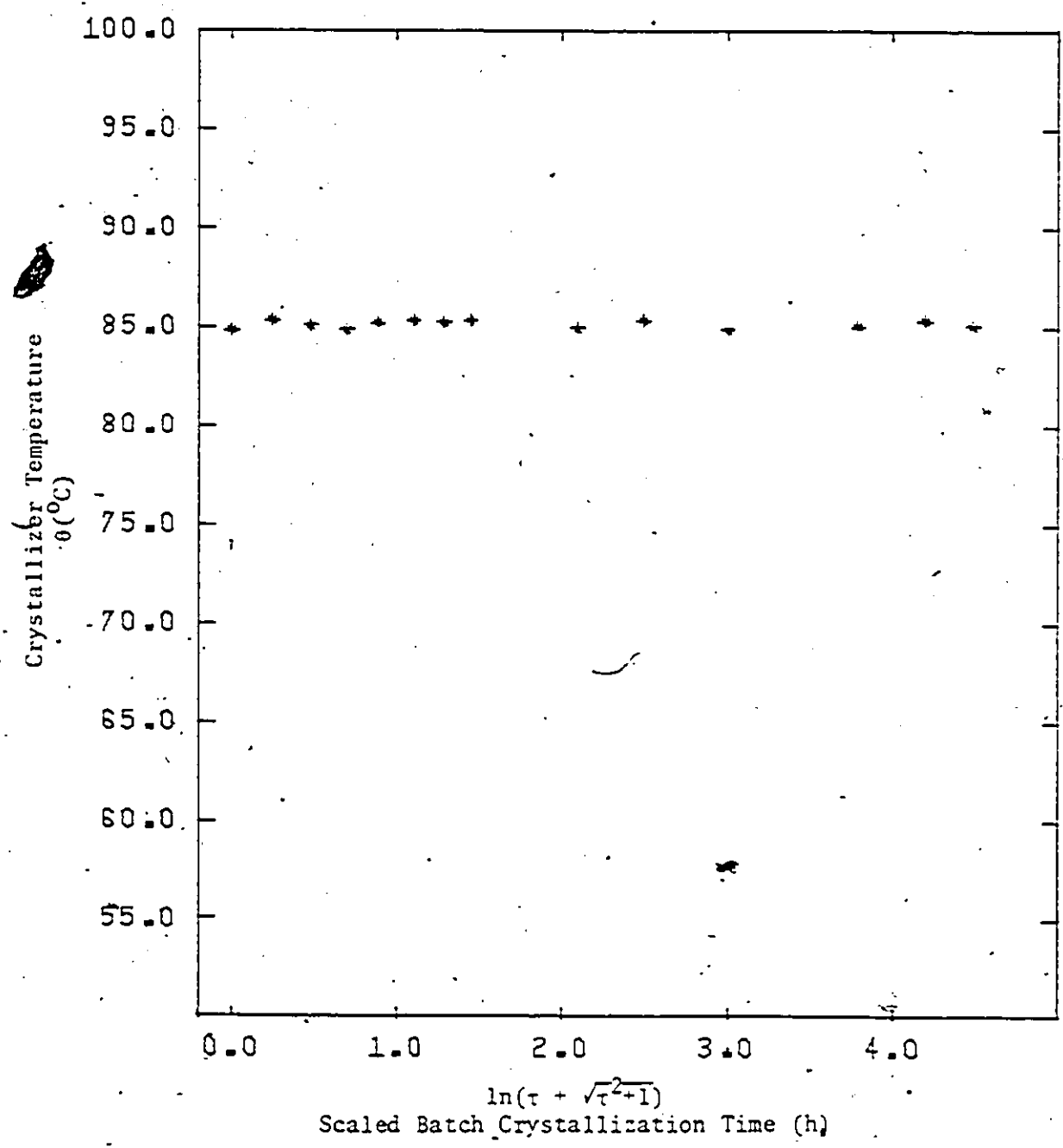
θ_2 = crystallizer operating temperature (°C)

This derivation is based on the density correlation which was developed by Misra (m2).

4.2.2.2 Crystallizer Operating Temperature

Figure 4.2.2.2-A shows the change in crystallizer temperature with time for this typical experiment. The temperature was practically kept constant by initially cooling the bench scale crystallizer and then by heating to make up for heat losses to the environment during the later stages of the batch experiment. If no cooling had been provided the operating temperature would have increased due to the slightly exothermic

FIGURE 4.2.2.2-A Batch Crystallizer Operating Temperature



nature of the crystallization process. For a well insulated bench scale batch crystallizer or for an industrial crystallizer with a much larger ratio of volume-to-surface area, cooling is required throughout to maintain an approximate constant operating temperature.

4.2.2.3 Crystal Size Distribution

The crystal size distribution as measured by the Coulter Counter and auxiliary equipment for a typical experiment is shown in Figure 4.2.2.3-A. In order that a comparison on an absolute scale can be effected between different batch samples to provide a true indication of the change of the crystal size distribution with time, a number of corrections have to be applied, namely:

(1) Channelyzer Number Rejection Losses

As a result of the electronics design of the Coulter Counter and Channelyzer, the channelyzer cannot process the signals or pulses as fast as they are sensed by and then sent from the Coulter Counter; this results in low channelyzer counts. To correct for this, the following equation was developed for this work (see Appendix C):

$$\Delta n_{cc} = \Delta n_{ch} + \left(\frac{bl_{ch}}{100} \times \Delta n_{ch} \right) / i \quad (4.3)$$

where $bl_{ch} = 2 \times e^{6.95 \times 10^{-5} \times N_{ch}}$

N_{ch} - total channelyzer count

$\Delta n_{ch,i}$ - channelyzer count in each channel

$\Delta n_{cc,i}$ - corrected channelyzer count for each channel

FIGURE 4.2.2.3-A Number Density Function with Respect to Crystal Volume

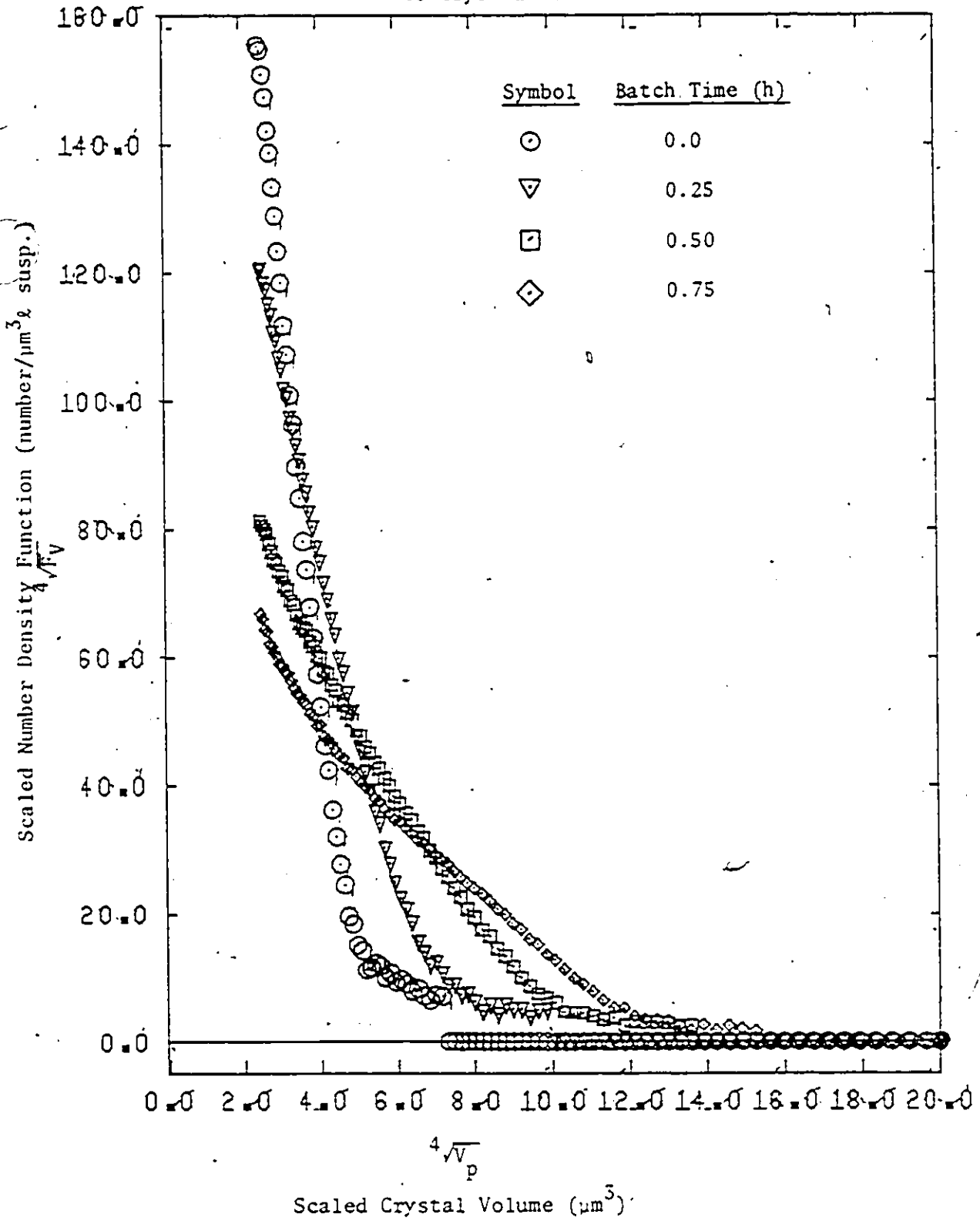


FIGURE 4.2.2.3-A (cont'd.)

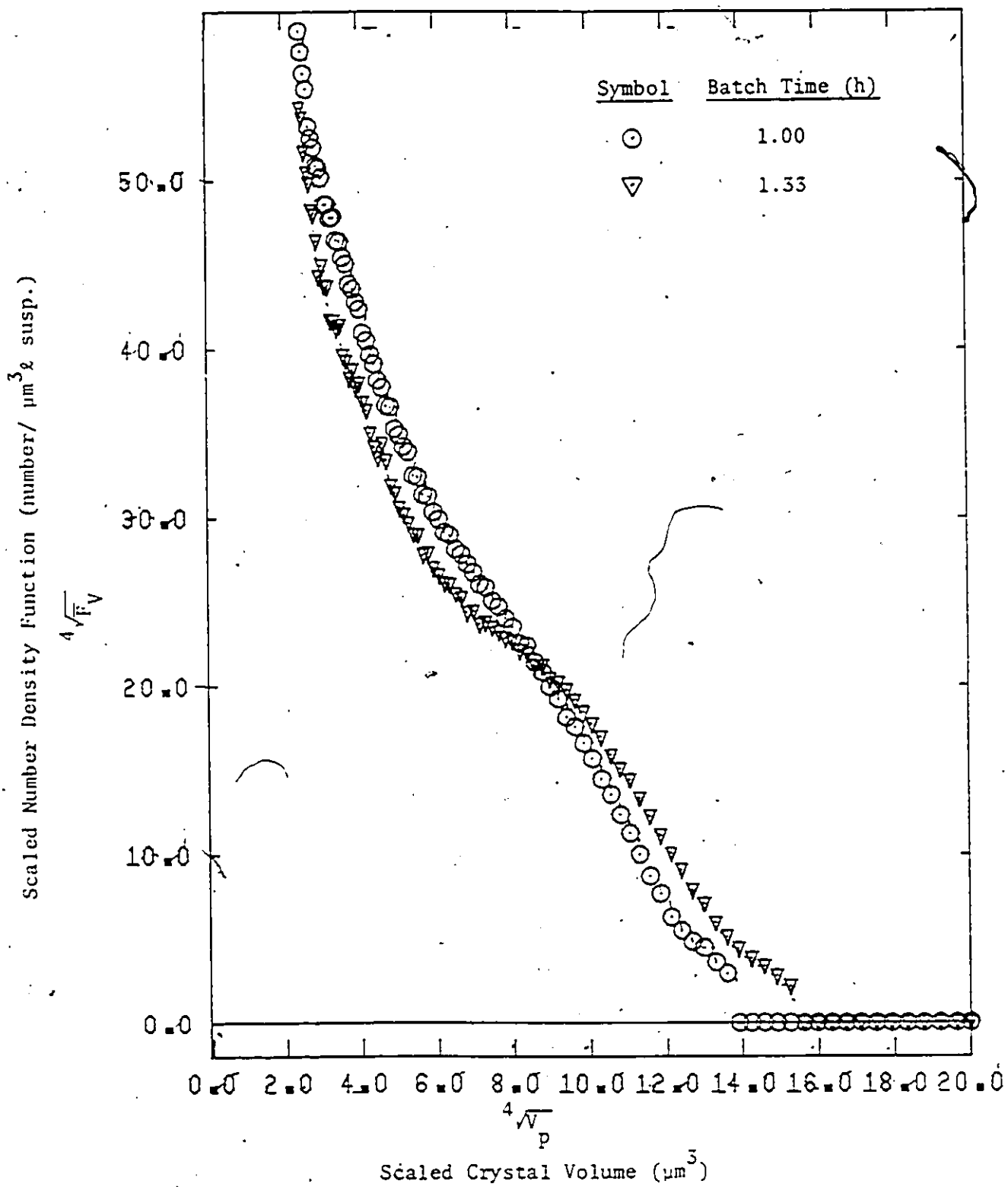


FIGURE 4.2.2.3-A (cont'd.)

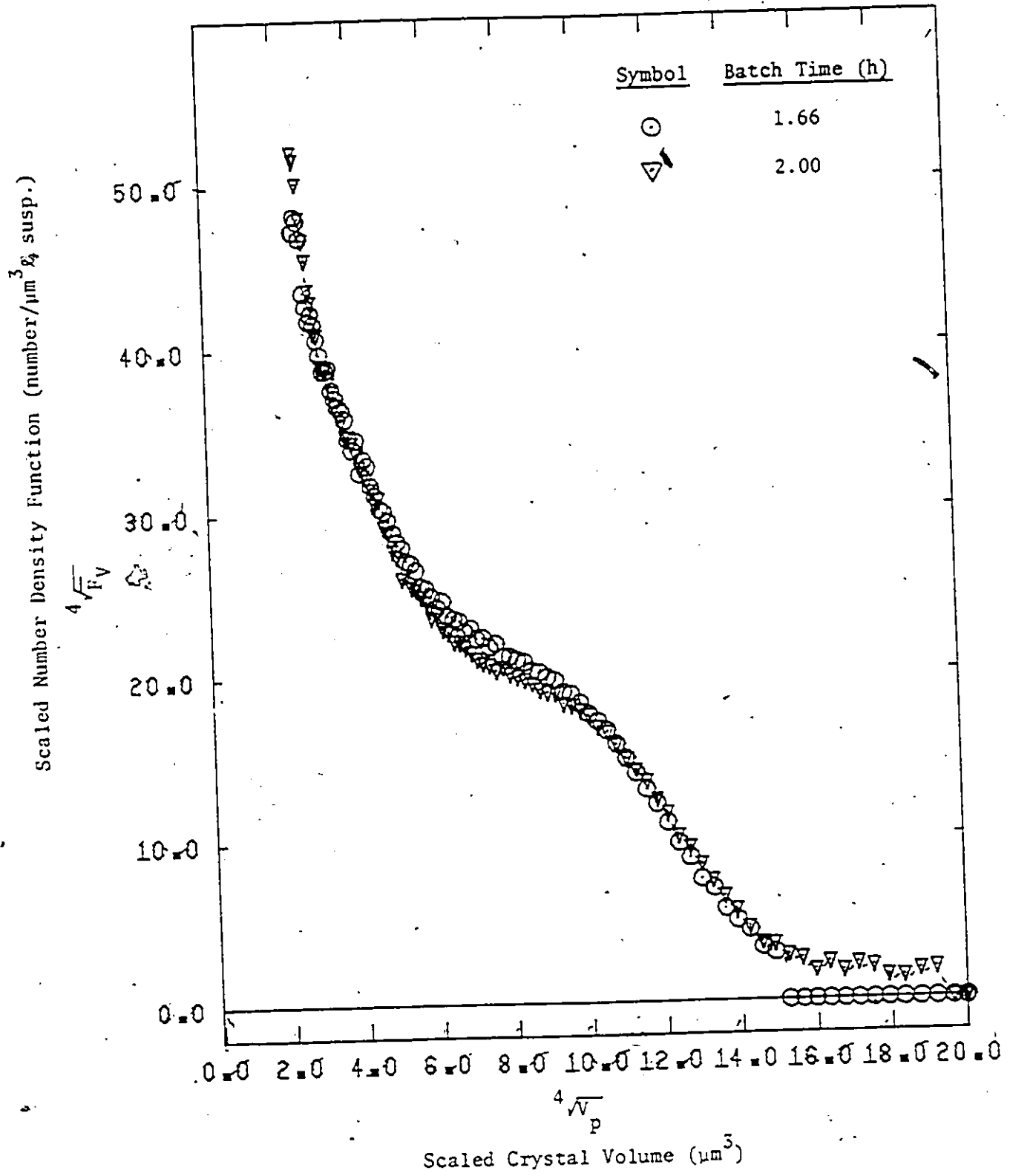


FIGURE 4.2.2.3-A (cont'd.)

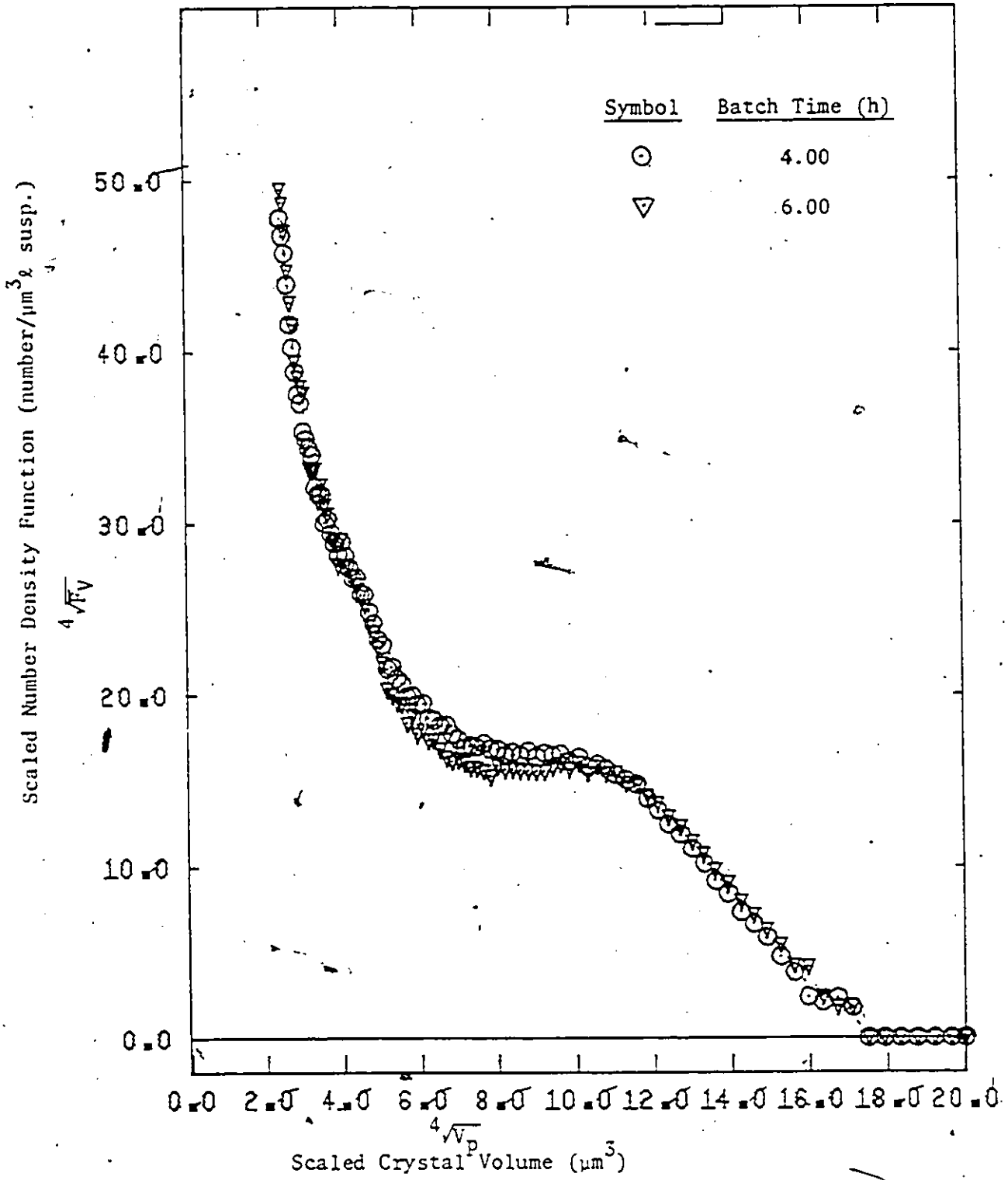


FIGURE 4.2.2.3-A (cont'd.)

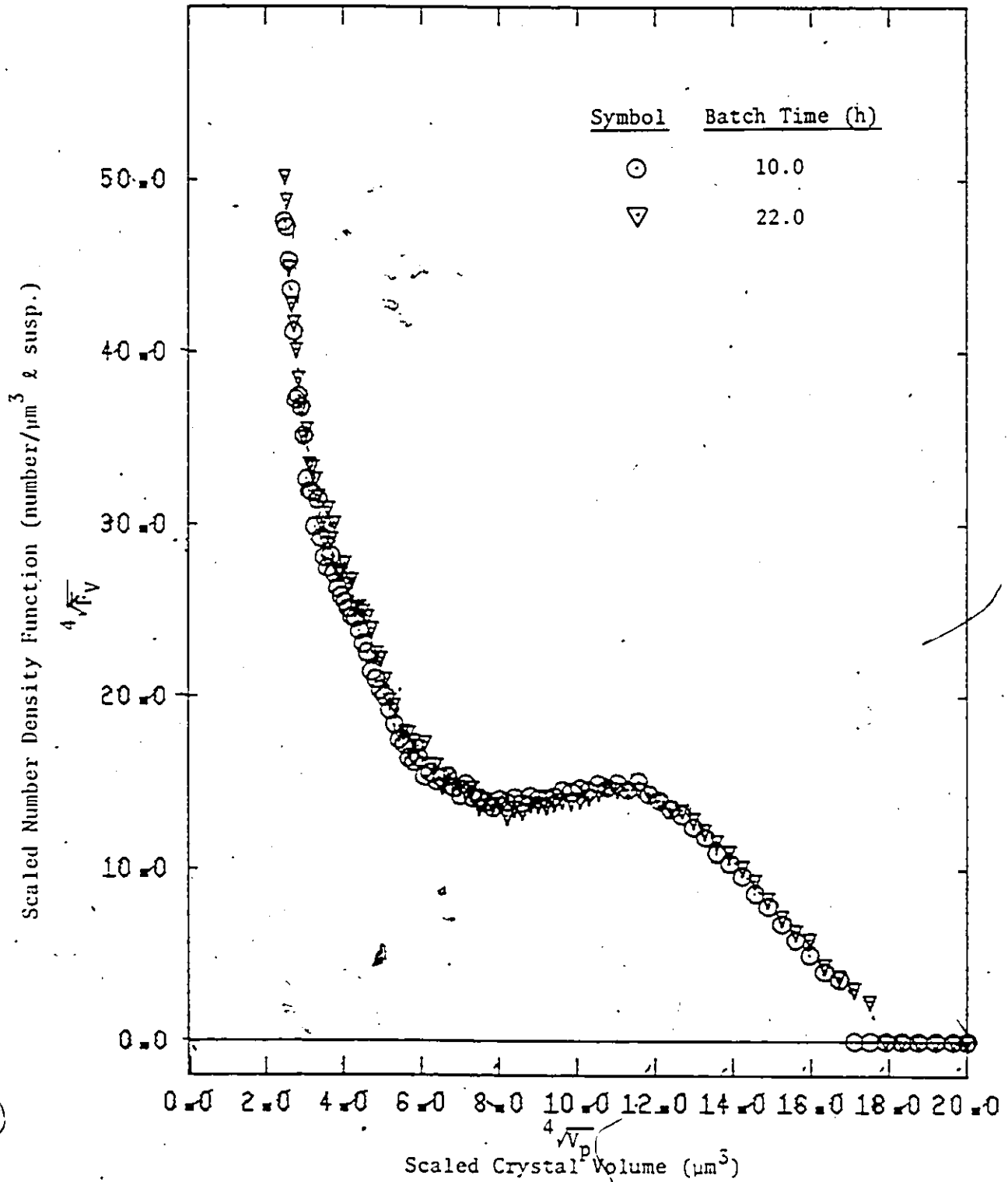
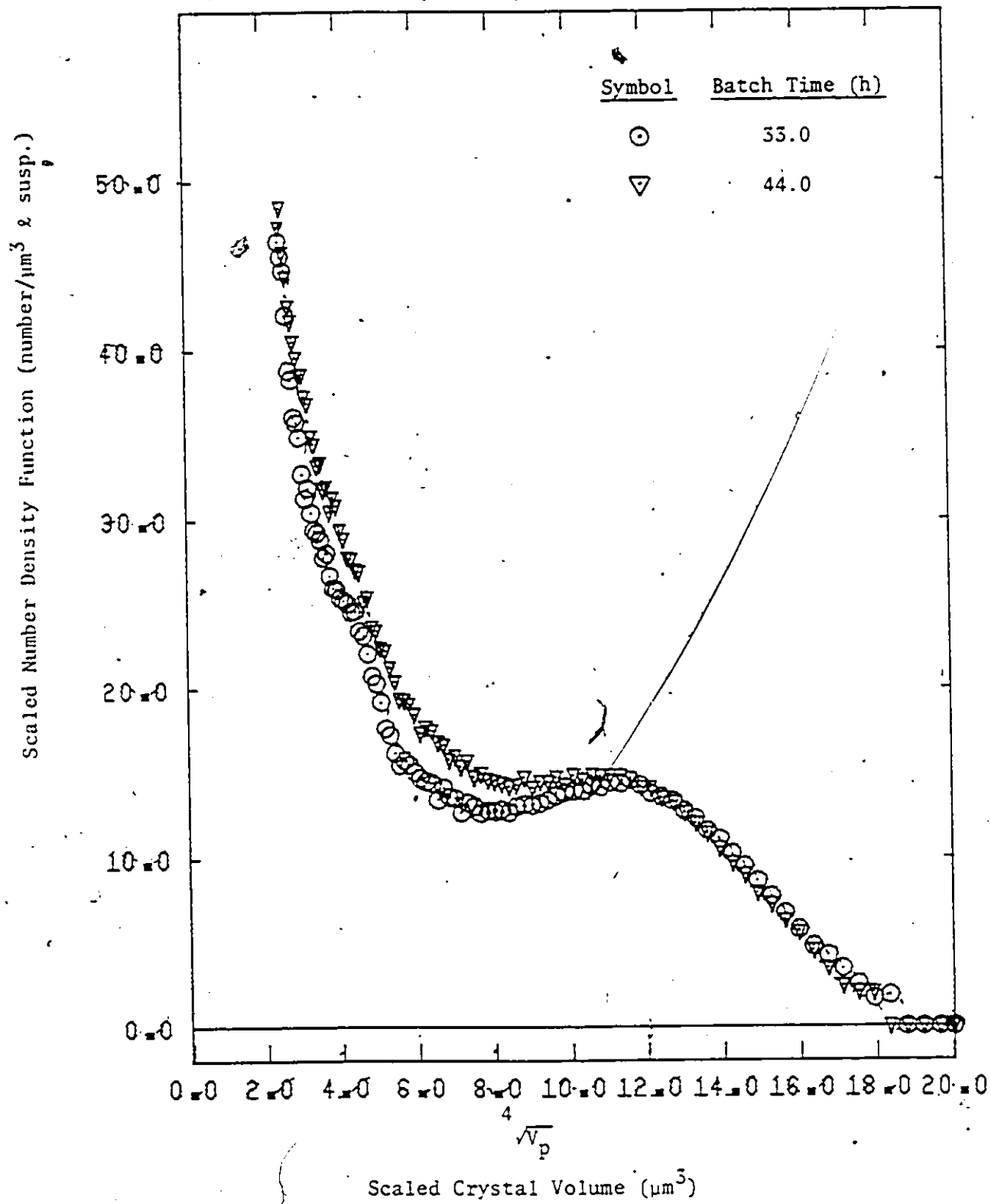


FIGURE 4.2.2.3-A (cont'd.)



(2) Coulter Counter Coincidence Losses

The following equation, which is developed in Appendix C, corrects for the fact that in some of the Coulter Counter counts a loss of count may occur, due to two or more particles passing through the sampling aperture simultaneously; thus only a single pulse or count is registered.

$$\Delta n_{a,i} = \{(\Delta n_{cc,i}/\Delta V_i) + b_{cc} \times [(\Delta n_{cc,i}/\Delta V_i) \times \sum_{l=1}^{100} \Delta n_{cc,l} - (\sum_{l=i-6}^i \Delta n_{cc,l}/\Delta V_l)/7 \times \sum_{l=1}^{i-7} \Delta n_{cc,l}]\} \times \Delta V_i \dots (4.4)$$

where $\Delta n_{cc,i}$ = corrected channelzyer count or Coulter Counter measured number of particles in channel i
 $\Delta n_{a,i}$ = 'actual' or corrected number count for channel i
 ΔV_i = volume size interval of channel i
 b_{cc} = experimentally determined coincidence correction parameter

In most instances, replicate samples of particles were measured and these measurements were averaged, viz.:

$$\overline{\Delta n}_{a,i,j} = [\sum_{l=1}^{m_{cc}} \Delta n_{a,i,j,l}] / m_{cc} \quad (4.5)$$

where m_{cc} = number of repeat Coulter Counter measurements
 $\overline{\Delta n}_{a,i,j}$ = averaged corrected number count for volume interval i for batch sample j

These average counts were then converted to the number of particles in the size interval per unit volume of suspension by relating the counts in the volume of electrolyte sampled in the Coulter Counter sample to the original volume sampled from the crystallizer. This was done through a dilution factor, Dlt:

$$\Delta N_{i,j} = \bar{\Delta n}_{a,i,j} \times Dlt_j \quad (4.6)$$

where

- Dlt_j = (VB_j/VM_j) × (CS_{2,j}/W_{cc,j})
- ΔN_{i,j} = number of crystals in volume interval i for batch sample j per l suspension
- VB_j = electrolyte volume to which sample j was added (cm³)
- VM_j = sampled Coulter Counter manometer volume (cm³)
- CS_{2,j} = crystallizer solids concentration calculated by method 2 which is described in Appendix D (g/l susp.)
- W_{cc,j} = weight of solids added to electrolyte (g)

ΔN_{i,j} is equal to the number of crystals in volume interval ΔV_{p,i}. Note, ΔN_{i,j} will change if the volume interval over which the measurements are made is changed. To remove this dependence it is necessary to express size distributions in terms of a density function which is defined by:

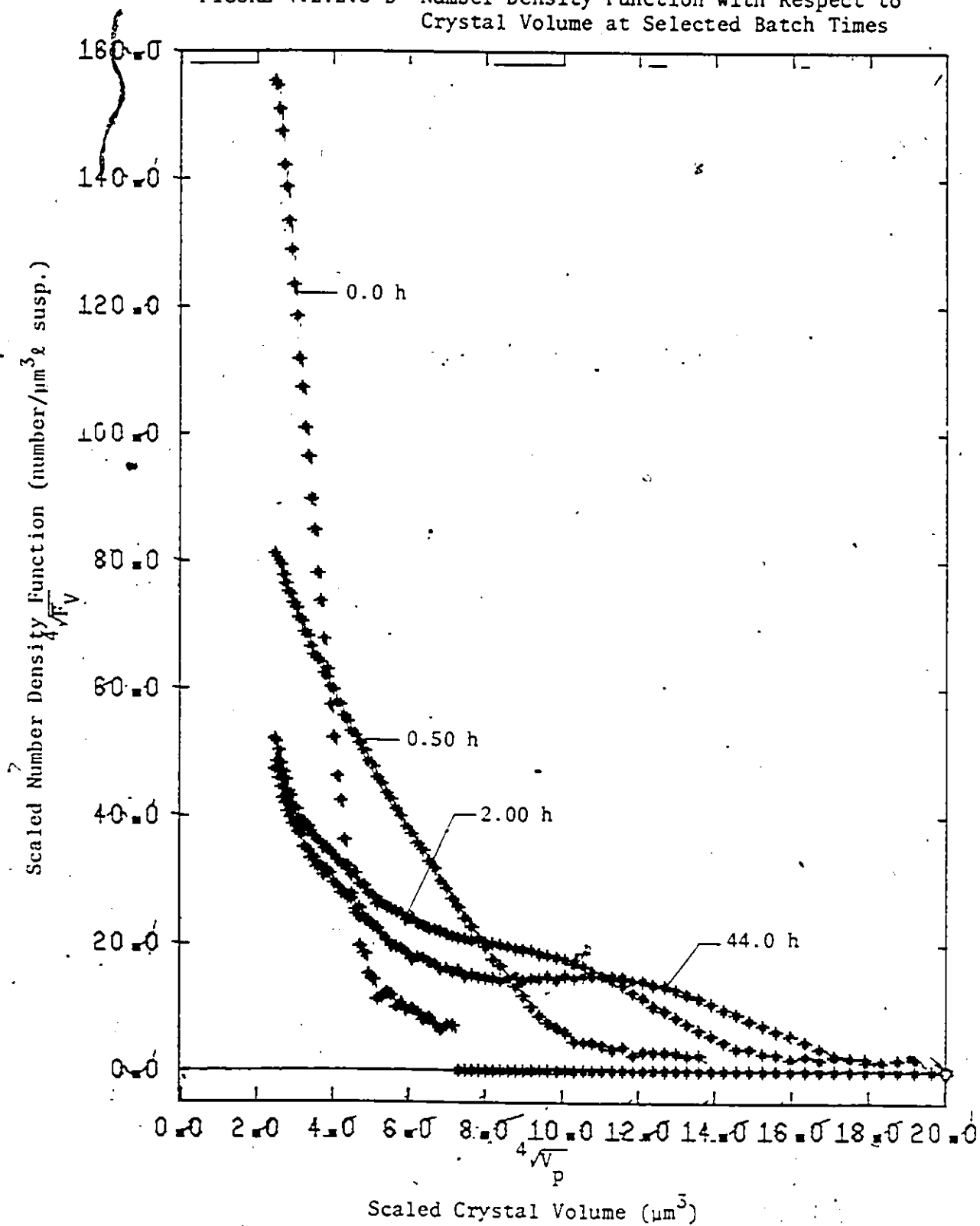
$$\bar{F}_{V,i,j} = \frac{\Delta N_{i,j}}{\Delta V_{p,i}} \quad (4.7)$$

where $\bar{F}_{V,i,j}$ = number density function with respect to crystal volume on a unit suspension volume basis averaged here over size interval i (number/ μm^3 & susp.)

The data presented in Figure 4.2.2.3-A are the \bar{F}_V values which are calculated as described above. Note that there are no data on the density function below about 39 cubic micrometres, the cut-off size on the Coulter Counter. This limitation of the Coulter Counter causes considerable difficulties in using these size measurements as will be described from time to time during the course of this dissertation.

The size measurements do show the excellent resolution that is obtained with the Coulter Counter-Log Transformation-Channelyzer combination, particularly over the lower size range where there is considerable variation in the size distribution. Normally probability density functions are normalized by dividing by the total number of crystals. This is not done here because due to the unknown number of crystals below the cut-off size the total number of crystals is unknown and such a division would thus confound the measured size distribution by a variable dependent on the cut-off size. Instead, for this work, the density function has been measured on a 'per unit suspension volume' basis and this allows a direct comparison of a distribution at one time with that at another time during the batch crystallization. This is demonstrated by the number density functions presented in Figure 4.2.2.3-B for this experiment at selected times. This figure demonstrates how fast the distribution spreads from the relatively narrow seed distribution and also shows the creation of a bimodal distribution which is characteristic

FIGURE 4.2.2.3-B Number Density Function with Respect to Crystal Volume at Selected Batch Times



of an agglomeration process. Note also that most of the change occurs within the first few hours of the experiment during which time the alumina concentration is at its highest, thus suggesting a strong dependence of all processes on supersaturation.

4.3 Consistency Check of the Measurements

A consistency check of the measurements was made by means of calculating and then comparing the same variable, namely solids concentration, from three independent measurements. The three ways are:

(i) from a material balance involving the seed and the measured dissolved alumina and sodium concentrations, (ii) the direct measurement of undissolved solids concentration and (iii) from the crystal size distribution on an absolute concentration basis. The basis of the calculations for each of these methods is described below in turn.

(i) The Solute Material Balance

As described in detail in Appendix D the solids concentration can be calculated from the Al_2O_3 , Na_2CO_3 , and seed weight measurements from the equation:

$$CS_1 = C1 / \{ (V_{L,o} \times CN_o / CN_\tau) + (C1 / \rho_s \times 1000) \} \quad (4.8)$$

where $C1 = \{ (V_{L,o} \times CA_o / .654) - (V_{L,o} / x \times CN_o / CN_\tau \times CA_\tau / .654) \} + W_{T,o}$

CS_1 = solids concentration (g/l susp.)

$W_{T,o}$ = seed weight (g)

CN - sodium concentration (g Na₂O/ℓ sol.)

CA - alumina concentration (g Al₂O₃/ℓ sol.)

(ii) Direct Measurement of Solids Concentration from Sample

As described, a sample of the suspension was filtered and the mass of dried solids and filtrate were measured separately. The solids concentration was then calculated from:

$$CS_2 = (W_{S,spl} \times 10^3) / (W_{L,spl} / \rho_{\ell,2} + W_{S,spl} / \rho_s) \quad (4.9)$$

where CS_2 - solids concentration (g/ℓ susp.)

$W_{S,spl}$ - sample solids weight (g)

$W_{L,spl}$ - sample filtrate weight (g)

(iii) Integration of the Measured Crystal Size Distribution

In this case, the crystal size distribution of the solid in a known volume of suspension (as taken directly from the crystallizer) was measured in the Coulter Counter. This measurement then gave the concentration of the crystals in each small size interval (number per unit suspension volume); this is what is referred to as 'on an absolute basis'. The total undissolved solids concentration is obtained by integrating this observed crystal size distribution over the entire range of measured sizes, viz.:

$$CS_3 \approx \frac{1}{2} \times 10^{-12} \times \rho_s \times Dlt \times \left\{ \sum_{i=1}^m [\Delta n_{a,i} \times (V_{i+1} + V_i)] \right\} \quad (4.10)$$

where CS_3 = solids concentration (g/l susp.)

This approximation is also derived in detail in Appendix D, while the other symbols in this relationship have been defined in the previous sub-sections.

These three completely separate means of determining solids concentration provide a way of testing the internal consistency of each of the measurements; indeed, it provides a severe test of the sampling and analytical procedures. The comparison among these methods is indicated on Figure 4.3-A and Table 4.3-A. It is seen that the relative difference between methods 1 and 3 is considerable over the first quarter hour of the experiment. The solute analysis is expected to be very accurate, as is the measurement of total seed and liquid added at the beginning of the experiment; method 1 should, therefore, be the most accurate measurement. Thus, this comparison of solids concentration gives a good indication of the accuracy of the particle size measurements and/or of the goodness of the sampling and analysis procedures for it. Error in method 3 may be either purely random or random plus systematic. Certainly, if the crystallizer suspension is non-homogeneous particularly with respect to solids, then differences among these methods would show up. The difficulty of extracting a representative sample from the crystallizer, then a representative sample from this sample (for the size distribution measurement) should not be underestimated. The fact that the differences between the three methods are much less after the first quarter of an hour suggests that these difficulties were overcome.

FIGURE 4.3-A Calculated Crystallizer Solids Concentration

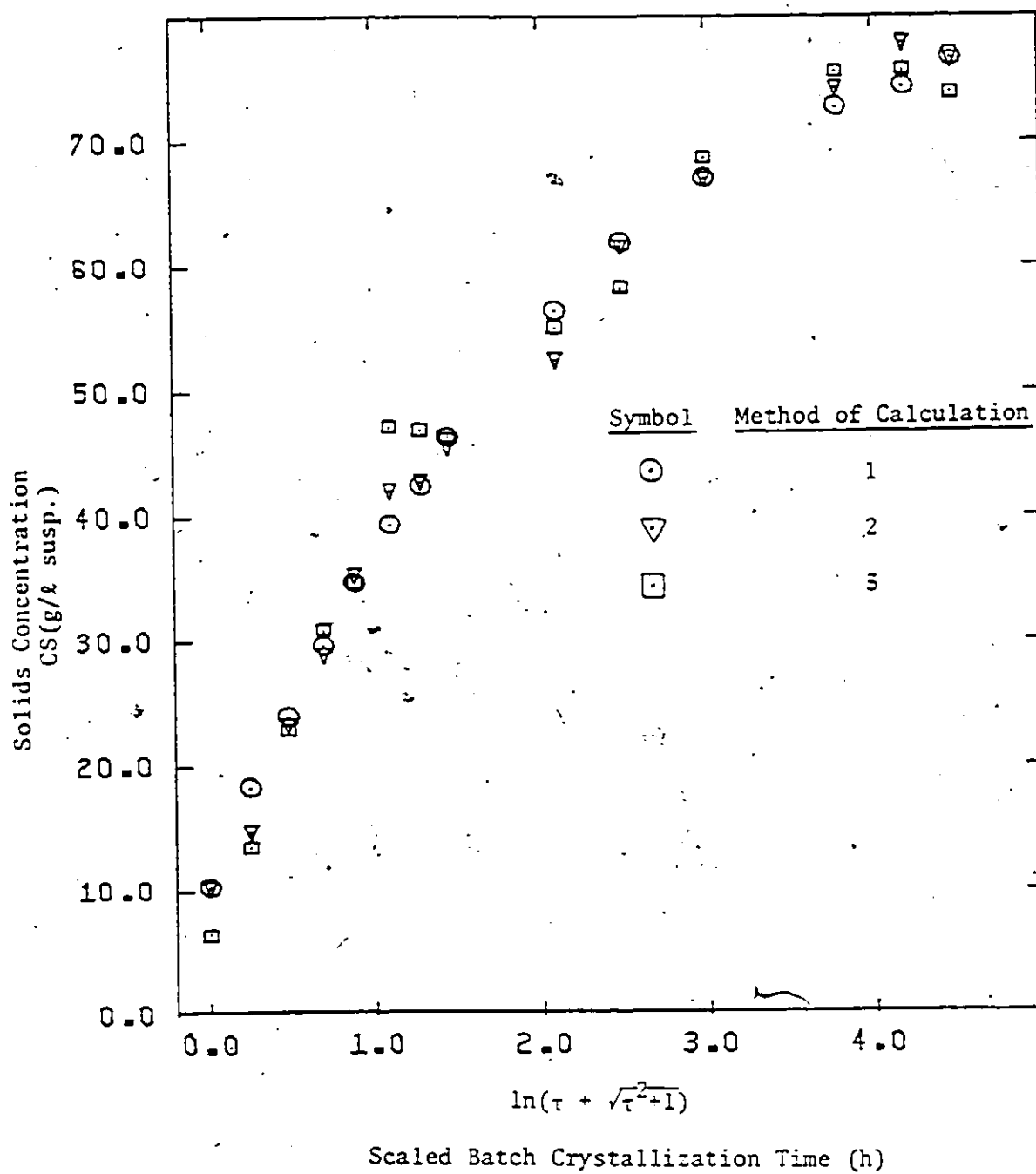


TABLE 4.3-A

Consistency Check of the Measurements
by means of the Variable Solids Concentration

Sample #	Batch Time τ (h)	Solids Concentration			Relative Difference	
		CS ₁	CS ₂ (g/2 susp.)	CS ₃	$\Delta CS_{1,2}^*$ (%)	$\Delta CS_{1,3}$
1	0	10.2	10.2	6.30	0.0	-38
2	0.25	18.2	14.7	13.4	-19	-26
3	0.50	23.9	23.3	22.8	- 2.6	- 4.4
4	0.75	29.6	28.8	30.8	- 2.4	4.3
5	1.0	34.6	35.2	34.6	1.7	0.0
6	1.33	39.3	42.0	47.0	6.9	20
7	1.66	42.3	42.7	46.8	0.92	10
8	2.0	46.2	45.5	46.1	- 1.6	- 0.29
9	4.0	56.4	52.5	55.0	- 6.9	- 2.4
10	6.0	61.8	61.5	58.2	- 0.44	- 5.8
11	10.0	67.0	67.0	68.6	0.0	2.4
12	22.0	72.6	74.2	75.5	2.1	3.9
13	33.0	74.3	77.8	75.6	4.7	1.8
14	44.0	76.6	76.5	73.7	- 0.21	- 3.8

$$* \Delta CS_{1,2} \triangleq \left(\frac{CS_2 - CS_1}{CS_1} \right) \times 100\%$$

On the other hand, the Coulter Counter has many possible sources of error, such as:

- (i) A non-representative sample passes through the Coulter Counter orifice.
- (ii) The agitation of the Coulter Counter suspension may have caused attrition of the sample. This would not cause a problem if all crystal sizes were measured since the Coulter Counter measures volume directly.
- (iii) There are inherent errors associated with the Coulter Counter, such as incorrect volume-to-current relationship while the particle passes through the orifice due to unknown effects such as 'shadowing' or non-centre passage of the crystals (d_4, k_3). Moreover, compensation corrections must be made for coincidence in the Counter and the Channelizer may lose pulse counts as discussed in Appendix C. A systematic error could also be introduced by using an incorrect calibration.

Notwithstanding these many sources of error, it is felt, however, that the greatest source of the differences indicated between methods 1 and 3 is that caused by not measuring the crystal size distribution below the Counter's cut-off size. This source is strongly suggested by the decrease in difference in the solids concentration as the crystals grow in size and a smaller fraction of the crystal distribution is contained in a size less than the cut-off size.

The conclusion from this analysis is that the Coulter Counter measures with high accuracy the size distribution of a representative sample

from the crystallizer, but that a considerable fraction of the crystals, during the initial period at least, is of a size less than the cut-off size of the Counter. The cut-off size is necessarily relatively high because of the need to have a relatively large orifice in the Counter to accommodate the relatively large crystal sizes which result from the agglomeration process.

4.4 Different Presentations of the Crystal Size Distribution

For a better appreciation of the size distribution change with batch time the number density functions with respect to crystal volume were transformed into the following related density functions.

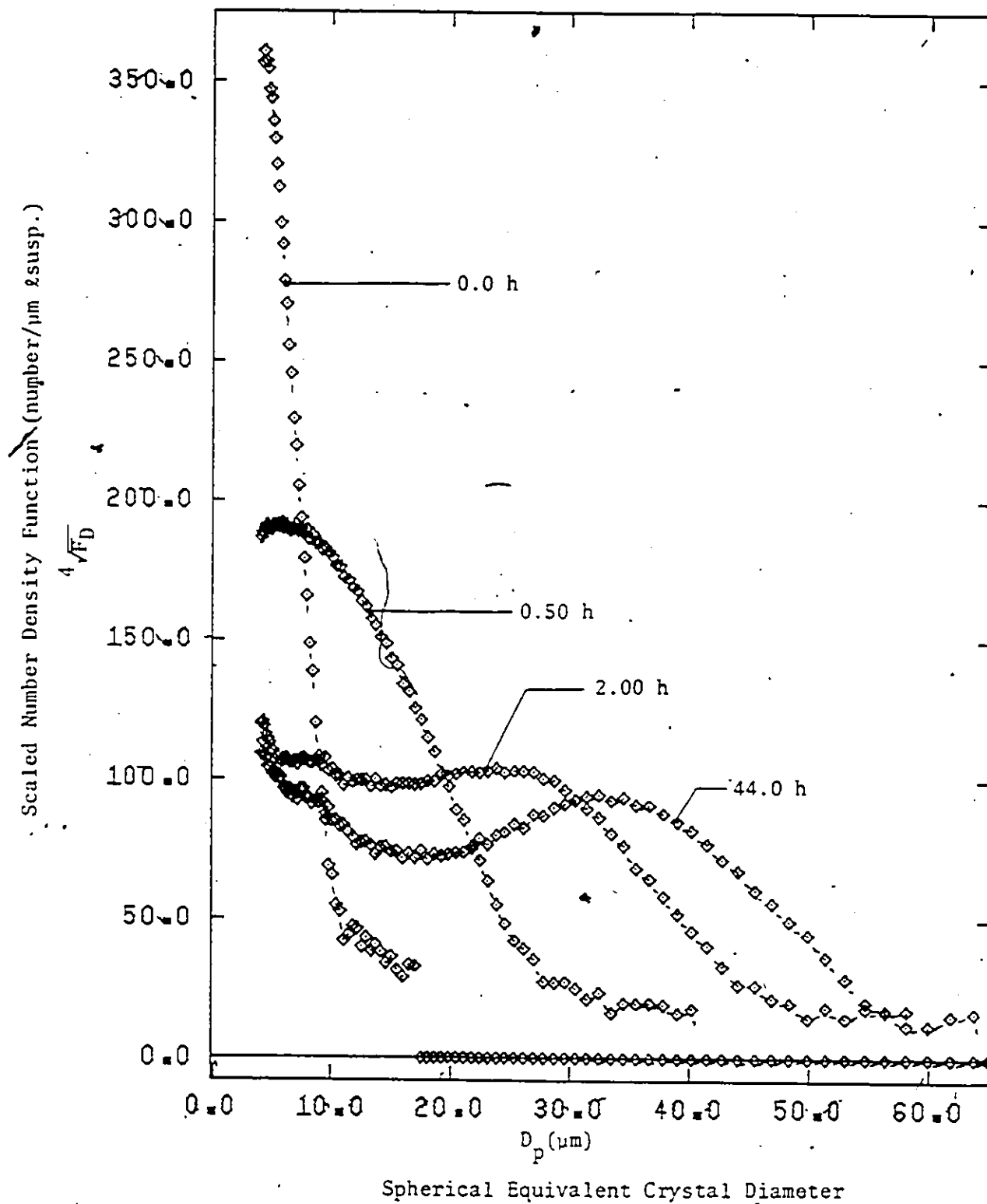
1. Number Density Function with Respect to Spherical Equivalent Diameter

Expressing the number density function with respect to spherical equivalent diameter provides for direct visual information with regard to the number of crystals within particular diameter intervals and the change with batch time. This density function is defined by:

$$\bar{F}_{D,i,j} = \Delta N_{i,j} / \Delta D_{p,i} \quad (4.11)$$

where $\Delta N_{i,j}$ is the number of crystals in the spherical equivalent diameter interval $\Delta D_{p,i}$. The \bar{F}_D values are plotted for selected batch times in Figure 4.4-A.

FIGURE 4.4-A Number Density Function with Respect to Spherical Equivalent Diameter for Selected Batch Times



2. Area Density Function with Respect to Spherical Equivalent Diameter

A density function may be calculated which indicates the surface area of the crystals in any particular size interval. It can be calculated by first calculating the areas of the crystals in each size interval via the formula:

$$\Delta A_{p,i} = 10^{-8} \int_{V_i}^{V_{i+1}} \psi_{AV} V_p^{2/3} \bar{F}_V dV_p \quad (4.12)$$

where $\Delta A_{p,i}$ = crystal area in crystal volume interval $V_{i+1} - V_i$
(cm^2/ℓ susp.)

ψ_{AV} = area volume shape factor (dimensionless)

10^{-8} = unit equalization constant

V_p = crystal volume (μm^3)

If it is assumed that the density function, \bar{F}_V , is constant and equal to the average value over the interval, then this equation may be easily integrated to give the reasonable approximation:

$$\Delta A_{p,i} \approx 3/5 \pi^{1/3} 6^{2/3} (10^{-8}) \bar{F}_{V,i} (V_{p,i+1}^{5/3} - V_{p,i}^{5/3}) \quad (4.13)$$

where ψ_{AV} has been assumed to be equal to $\pi(6/\pi)^{2/3}$. Thus, the area density function as defined by:

$$\bar{F}_{A,D,i,j} = \Delta A_{p,i,j} / \Delta D_{p,i} \quad (4.14)$$

is a close approximation to the 'true' value since the Coulter Counter measurements were made over a large number of small size intervals with good resolution. This area density function at selected batch times is plotted against the spherical volume equivalent diameter in Figure 4.4-B.

Note that by defining the area volume shape factor equal to $\pi(6/\pi)^{2/3}$, the crystal area is defined as the area of a sphere with a volume equivalent to the volume of the crystal. Since a crystal of alumina trihydrate is formed from a number of platelets (as shown by the excellent electron micrographs published by Brown (b6) and reproduced here in Figure 4.4-C), the crystal area calculated from equation (4.13) can only be an approximation, at best. What is needed is an area-to-volume shape factor, ψ_{AV} . Although Misra (m2) attempted to determine this shape factor from adsorption measurements, there is still the question whether this area for adsorption is the appropriate area for crystal growth. If the shape of the crystals remains essentially the same regardless of crystal size and the environment from which it was grown, then the area distribution density function as calculated from equation (4.14) is a good approximation and will only be incorrect by a constant factor. Plots such as that on Figure 4.4-B will give a good indication of the evolution of crystal surface area with time.

3. Mass Density Function with Respect to Spherical Equivalent Diameter

Another useful density function in this work is the mass or weight density function which may be defined by:

$$\overline{FW}_{D,i,j} \approx \Delta W_{p,i,j} / \Delta D_{p,i} \quad (4.15)$$

FIGURE 4.4-B Area Density Function with Respect to Spherical Equivalent Diameter for Selected Batch Times

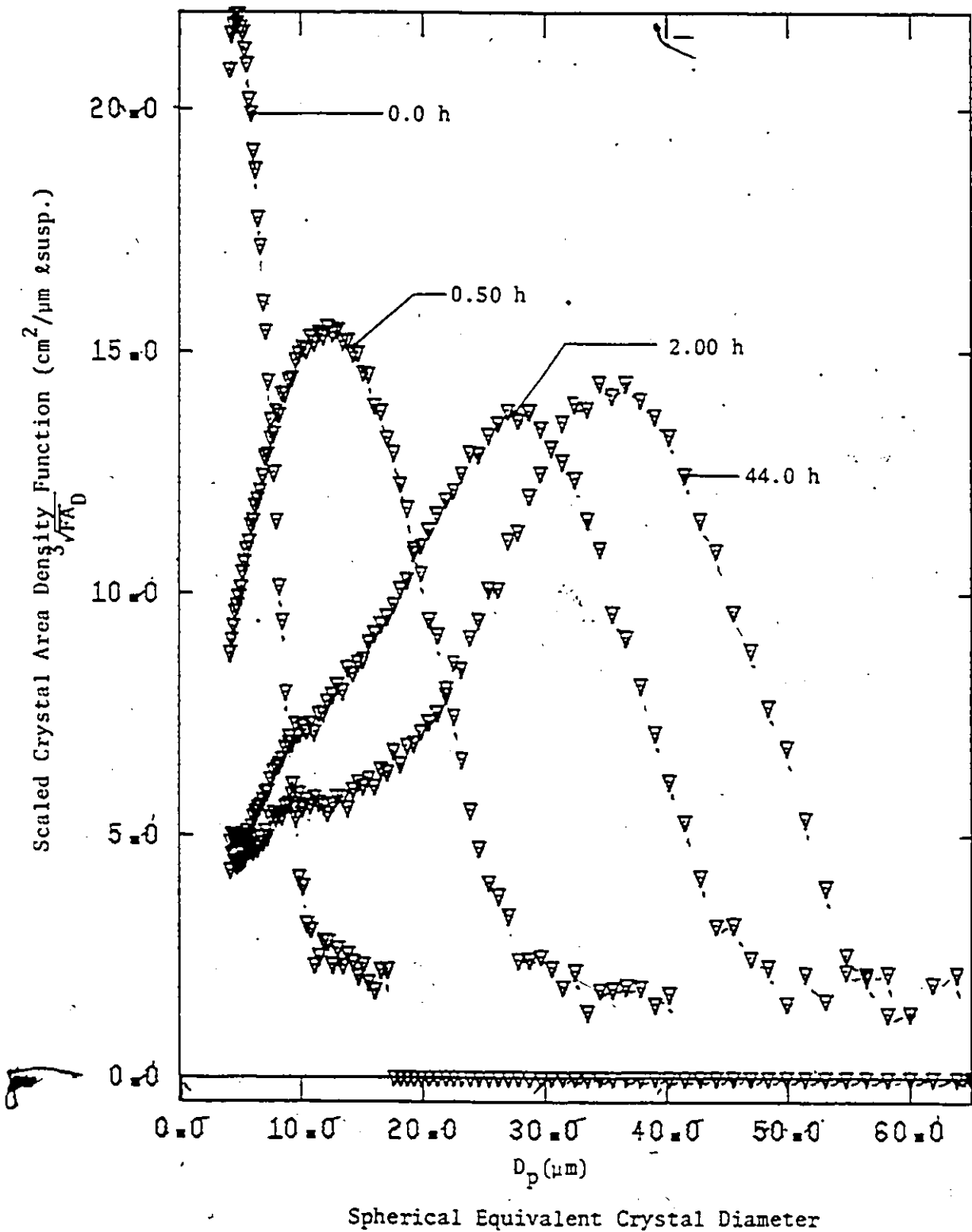


FIGURE 4.4-C Electron Micrographs of
Typical Alumina Trihydrate
Crystals (from Brown (b6))



$$\text{where } \Delta W_{p,i,j} \approx 10^{-12} \rho_s \int_{V_i}^{V_{i+1}} F_V V_p^3 dV_p$$

or with F_V assumed to be constant over the interval V_i to V_{i+1}

$$\Delta W_{p,i,j} \approx 10^{-12} \rho_s \bar{F}_{V,i,j} (V_{p,i+1}^2 - V_{p,i}^2)/2 \quad (4.16)$$

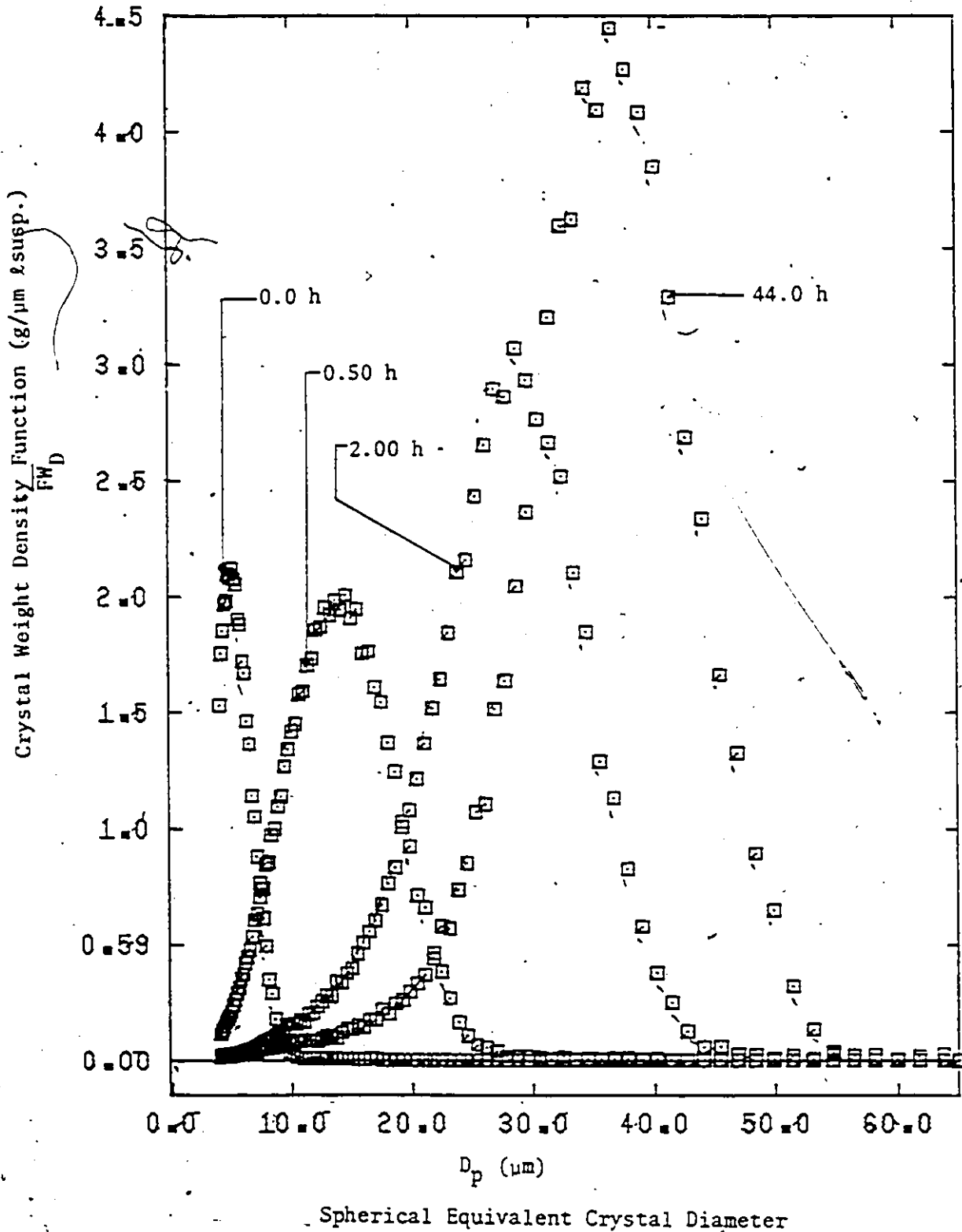
A plot of \bar{F}_D versus D_p for selected batch times as shown in Figure 4.4-D, gives a good indication of the relative crystal mass in each size interval and the distribution of the crystal mass.

These distribution function plots allow for a very good visual observation of how the crystal size distribution is changing with time during the batch crystallization under any given operating condition. They show that the number distribution changes from a unimodal narrow size distribution to a bimodal wide spread distribution. In addition, it is seen that on a number basis the part of the distribution below the Coulter Counter cut-off size was quite significant, especially during the earlier stages of a batch experiment. The difficulties which arise due to this cut-off size will be discussed in detail later. Note, however, that the area and mass distributions show that, especially after the initial stages of the crystallization, the crystals below the cut-off size contribute relatively little to the total area and mass of the total suspension.

4.5 Moments of the Crystal Size Distribution

As described previously, the total mass of crystals per unit suspension volume may be easily calculated from the measured crystal size

FIGURE 4.4-D Weight Density Function with Respect to Spherical Equivalent Diameter for Selected Batch Times



distribution, subject to the limitations imposed by the cut-off size of the Coulter Counter. This total mass is calculated directly from the first moment with respect to the crystal volume, viz.:

$$W_{t,j} = \int_0^{\infty} V_p F_p dV_p \approx \sum_{i=1}^m \Delta W_{p,i,j} \quad (4.17)$$

Thus the total mass as a function of time may be followed by this integration, as was shown in Figure 4.4-D. The crystal size distribution measurements also allow the calculation of the total crystal surface area and the total number of crystals as a function of time by defining, respectively, the two-thirds moment and the zero moment relative to crystal volume; that is:

$$A_{t,j} = \int_0^{\infty} V_p^{2/3} F_p dV_p \approx \sum_{i=1}^m \Delta A_{p,i,j} \quad (4.18)$$

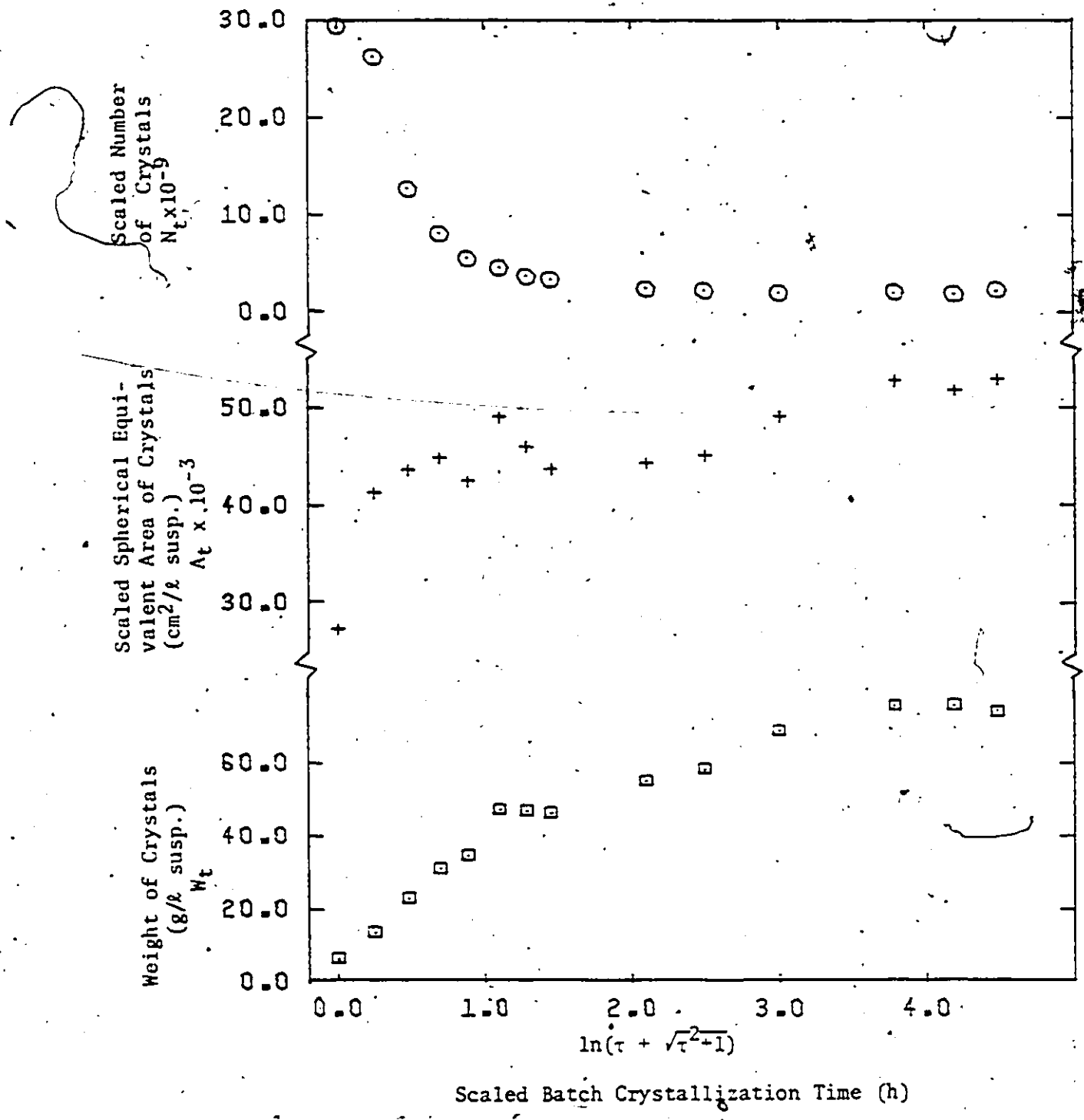
and

$$N_{t,j} = \int_0^{\infty} F_p dV_p \approx \sum_{i=1}^m \Delta N_{i,j} \quad (4.19)$$

These variables are plotted in Figure 4.5-A.

Although these variables are subject to the errors associated with the finite difference approximation to the integral and specifically the cut-off size problem, the plots shown on Figure 4.5-A do provide some significant observations relating to this crystallization process. First, the decrease of the total number of crystals during the initial period of the crystallization indicates that agglomeration occurred to a significant extent. If only growth had taken place, the total number above the cut-off size would have increased because minute crystals originally

FIGURE 4.5-A. Moments of the Crystal Size Distribution



in the seed (but not measured at the outset) would have grown into the measurable size range. This increase in number would have continued until all crystals would have grown to a size greater than the cut-off size; thereafter, the number of crystals would have remained constant. If in addition to growth significant nucleation of new crystals would have occurred, then the total number of crystals in the measurable region would have increased continuously as the nuclei grew to a size which could be measured by the Coulter Counter. This same increase would occur if considerable attrition of large crystals had occurred. If, on the other hand, attrition of small crystals had occurred and the fragments had been small enough not to be measurable, then a decrease in number with time would have been observed. This process, however, seems highly unlikely since it would have required small particles to break up preferentially to large ones. This is most unlikely particularly considering the pretreatment of the seed and the mixing action in the crystallizer.

Thus, it can be concluded from the shape of the total number-time plot that significant agglomeration of the particles did take place. The decrease in number and subsequent levelling off of the number is a result of a high rate of agglomeration, particularly during the early stages of the process. Note that the total area of the crystal suspension is decreased by agglomeration and this is observed on Figure 4.5-A as well, thus adding credence to the conclusion relating to agglomeration:

These particular observations are pertinent here since they suggest that the agglomeration process must be included in any model to be proposed for the crystallizer. This is important since, as we shall see,

including a description of agglomeration in addition to growth and nucleation in the mathematical model, makes the modelling mathematics much more difficult. Thus, in general, when modelling a process, it is important to have pertinent experimental observations to indicate in a qualitative way what processes of the many that could occur need be included in the mathematical description.

CHAPTER 5

DEVELOPMENT OF THE MODEL EQUATIONS FOR A SEEDED BATCH CRYSTALLIZER FOR ALUMINA TRIHYDRATE

5.1 Introduction

The mathematical model for the seeded batch crystallizer is comprised of a large number of mathematical equations. Some of these are derived from the fundamental conservation laws; others are constitutive relationships based on empirical curve fittings of experimental observations or based on our theoretical understanding of the phenomena involved. Particular emphasis is placed on the derivation of the population balance equation and its appropriate boundary conditions for use in the present context. Also, a constitutive relationship for the agglomeration process is derived in detail since it is particularly important in this work. The intent of presenting these derivations is to delineate the importance and interaction of the phenomena associated with crystallization processes.

The population balance equation, derived in terms of the number density function, is then transformed into terms of the cumulative number distribution function in anticipation of the solution method presented in Chapter 6. Also, from the population balance equation, a set of equations are derived which weight the number density function by a general weighting function. These equations are named 'pseudo moment equations' in this work and they are used in Chapter 7 to develop appropriate constitutive relationships for the crystallization rate processes for growth,

agglomeration, and nucleation. Lastly, mass balance and auxiliary equations are presented; these complete the full set of model equations for a seeded batch crystallizer for alumina trihydrate.

5.2 Population Balance Derivation*

The population balance equation is a general conservation law that accounts for the number of crystals (particles, chemical species) of a particular size. It may also be referred to as the particle-number continuity equation or as an equation of change for the number of particles. The derivation is similar to the technique one adopts in deriving the conventional equations of change. In this case the entity for which a balance is derived is the number of particles in a certain control volume. A convenient way of expressing the number of particles in this control volume is by the use of a particle density function, $F_{Q,t}(\underline{x}, \tau)$, defined on an $(m+4)$ dimensional set. Here, \underline{x} is the set of external and internal coordinates comprising the particle phase space Q . The value of $F_{Q,t}$ thus depends on its location given by three spatial dimensions, time and on the m independent internal particle dimensions or properties. Some typical internal dimensions (properties) are: particle volume, spherical equivalent diameter, chemical activity, particle age, particle growth activity, etc.

The number of particles existing at time τ in the differential or incremental volume of particle phase space dQ is:

*Although, the population balance has been derived by several other authors (rl,h4), a particular derivation is presented here for completeness and clarity.

$$dN_t = F_{Q,t} dQ \quad (5.1)$$

This equation assumes that the particles behave as a continuum. The total number of particles in some fixed subregion of Q, say Q1, is:

$$N_t(Q1) = \int_{Q1} F_{Q,t} dQ \quad (5.2)$$

Taking the Eulerian viewpoint*, an accounting of the particles in volume Q1 leads to the general equation:

$$\begin{aligned} \text{accumulation} &= \text{input} - \text{output} + \text{net generation} \\ &= \text{net inflow} + \text{net generation} \end{aligned} \quad (5.3)$$

The accumulation term is the rate of storage of the number of particles in the control volume Q1.

$$\frac{\partial}{\partial \tau} \int_{Q1} F_{Q,t} dQ \quad (5.4)$$

Applying the Leibnitz rule for differentiating an integral, with $\frac{d}{d\tau} Q1 = 0$ (since the Eulerian viewpoint has been taken), this integral becomes:

$$\int_{Q1} \frac{\partial}{\partial \tau} F_{Q,t} dQ \quad (5.5)$$

*An excellent derivation of the population balance is given by Randolph and Larson (rl) who took the Lagrangian viewpoint.

The flow of particles by convection across a boundary area element, dA , of Q_1 is:

$$F_{Q,t} = \underline{v} \cdot \underline{n} \, dA \quad (5.6)$$

The net inflow is expressed through the surface integral:

$$-\int_{A_1} F_{Q,t} = \int_{A_1} \underline{v} \cdot \underline{n} \, dA \quad (5.7)$$

where \underline{n} is an outward directed unit vector normal to the surface, and \underline{v} is defined as the particle phase-space velocity vector. This vector is made up of external, \underline{v}_{ext} , and internal, \underline{v}_{int} , velocity components, i.e.

$$\begin{aligned} \underline{v} &= (v_x \underline{\delta x}) + (v_y \underline{\delta y}) + (v_z \underline{\delta z}) + (v_1 \underline{\delta l}) + (v_2 \underline{\delta 2}) \\ &\quad + \dots + (v_m \underline{\delta m}) \\ &= \underline{v}_{ext} + \underline{v}_{int} \end{aligned} \quad (5.8)$$

Taking v_x and v_1 as examples, v_x could be the medium or fluid velocity in the x direction given that the slip velocity between particle and fluid in this direction is zero, while v_1 might describe the time rate of change of the spherical volume equivalent particle diameter, $\frac{d}{d\tau}D$. Thus if the linear crystal growth rate, G_D , is defined as: $G_D \triangleq \frac{d}{d\tau}D$, then it is seen that G_D is the convective velocity of a particle along the internal D axis.

Similarly, the net rate of diffusion into the region Q_1 is:

$$-\int_{A1} \frac{\psi_A}{\tau} \cdot \frac{n}{\tau} dA \quad (5.9)$$

where $\frac{\psi_A}{\tau}$ is the number diffusive flux vector of particles. The vector $\frac{\psi_A}{\tau}$ is taken to represent a convective velocity which is proportional to $\nabla F_{Q,t}$, resulting in second order partial differentials.

The net generation term is made up of birth, $BF_{Q,t}$, and death, $DF_{Q,t}$, rate density functions, and is:

$$\int_{Q1} (BF_{Q,t} - DF_{Q,t}) dQ \quad (5.10)$$

The birth and death rate density functions account for the rate of change of N_t as a result of particles entering the volume $Q1$ without crossing the boundary; that is, there is a source of particles (generation) or sink for particles (loss) within the control volume $Q1$. Substituting these terms into equation (5.3) gives:

$$\begin{aligned} \int_{Q1} \frac{\partial}{\partial \tau} (F_{Q,t}) dQ &= -\int_{A1} F_{Q,t} \frac{v \cdot n}{\tau} dA - \int_{A1} \frac{\psi_A}{\tau} \cdot \frac{n}{\tau} dA \\ &+ \int_{Q1} (BF_{Q,t} - DF_{Q,t}) dQ \quad \dots (5.11) \end{aligned}$$

The two surface integrals in equation (5.11) can be converted to volume integrals by use of the Gauss divergence theorem:

$$\begin{aligned} \int_{Q1} \frac{\partial}{\partial \tau} (F_{Q,t}) dQ &= -\int_{Q1} \nabla \cdot \frac{v}{\tau} F_{Q,t} dQ - \int_{Q1} \nabla \cdot \frac{\psi_A}{\tau} dQ \\ &+ \int_{Q1} (BF_{Q,t} - DF_{Q,t}) dQ \quad \dots (5.12) \end{aligned}$$

Rearranging terms, the population balance can be written for the volume Q1 as:

$$\int_{Q1} \left[\frac{\partial}{\partial \tau} (F_{Q,t}) + \nabla \cdot (\underline{v}_{\text{ext}} F_{Q,t}) + \nabla \cdot (\underline{v}_{\text{int}} F_{Q,t}) + \nabla \cdot \underline{\psi}_A + DF_{Q,t} - BF_{Q,t} \right] dQ = 0 \quad \dots (5.13)$$

As the region Q1 was arbitrary, the integrand must be identically zero.

$$\frac{\partial}{\partial \tau} (F_{Q,t}) + \nabla \cdot (\underline{v}_{\text{ext}} F_{Q,t}) + \nabla \cdot (\underline{v}_{\text{int}} F_{Q,t}) + \nabla \cdot \underline{\psi}_A + DF_{Q,t} - BF_{Q,t} = 0 \quad \dots (5.14)$$

Equation (5.14) is the general microscopic population balance subject to the assumption that the particle concentration is dense enough to approximate a continuum.

If the system under consideration behaves as a well-mixed or homogeneous suspension, then equation (5.14) can be averaged over the external phase space to yield an equation which is distributed only in the internal phase space. Multiplying equation (5.14) by dV and integrating over the total suspension volume, which might be some function of time, $V_T(\tau)$, gives:

$$\int_{V_T(\tau)} \left[\frac{\partial}{\partial \tau} (F_{Q,t}) + \nabla \cdot (\underline{v}_{\text{ext}} F_{Q,t}) + \nabla \cdot (\underline{v}_{\text{int}} F_{Q,t}) + \nabla \cdot \underline{\psi}_A + DF_{Q,t} - BF_{Q,t} \right] dV = 0 \quad \dots (5.15)$$

Since, under the above assumption, $F_{Q,t}$, $DF_{Q,t}$, $BF_{Q,t}$ and the internal region divergence term $\nabla \cdot (\underline{v}_{int} F_{Q,t})$ are independent of V they can be taken out of the integration. Also, for this well-mixed suspension the contribution of the diffusion term is neglected, therefore:

$$\begin{aligned} \frac{\partial}{\partial \tau}(F_{Q,t})V_T + \nabla \cdot \underline{v}_{int} F_{Q,t} V_T + DF_{Q,t} V_T - BF_{Q,t} V_T \\ + \int_{V_T(\tau)} \nabla \cdot \underline{v}_{ext} F_{Q,t} dV = 0 \end{aligned} \quad \dots (5.16)$$

Converting the volume integral into the following surface integral

$$\int_{V_T(\tau)} \nabla \cdot \underline{v}_{ext} F_{Q,t} dV = \int_{A_T(\tau)} \underline{v} \cdot \underline{n} F_{Q,t} dA$$

facilitates its interpretation, and shows that this term represents the rate of change of $F_{Q,t}$ due to particle suspension inflow and outflow of streams k to the system volume V_T , represented by

$$\sum_k U_{t(k)} F_{Q,t(k)} \quad (5.17)$$

Also, since $A_T(\tau)$ is a function of time this term accounts for the rate of change of the total suspension volume, represented by $F_{Q,t} \frac{d}{d\tau}(V_T)$. That is, the volume V_T expands or contracts in time $d\tau$ making it necessary for $F_{Q,t} dV_T$ particles to cross the boundary A_T to still be in the system at time $\tau + d\tau$. Thus:

$$\int_{A_T(\tau)} \underline{v} \cdot \underline{n} F_{Q,t} dA = \sum_k U_{t(k)} F_{Q,t(k)} + F_{Q,t} \frac{d}{d\tau}(V_T) \quad (5.18)$$

Collecting terms, rearranging, and dividing by V_T allows equation (5.16) to be written as:

$$\frac{\partial}{\partial \tau}(F_{Q,t}) + \nabla \cdot v_{int} F_{Q,t} + F_{Q,t}/V_T \times \frac{d}{d\tau}(V_T) - BF_{Q,t} - DF_{Q,t} - \sum_k U_{t(k)} F_{Q,t(k)}/V_T \quad (5.19)$$

Equation (5.19) is the external, spacially-averaged, macroscopic population balance subject to the following assumptions:

- particle continuum
- homogeneous suspension

5.2.1 Use of the General Population Balance Equation to Describe a Batch Crystallizer

It is assumed that the internal state of the crystals is completely defined by one internal coordinate, namely crystal volume, V . This implies that the surface activity or whatever else determines the crystal growth rate is uniform and independent of time. This assumption, therefore, also implies that the observed induction period has been excluded in this mathematical description.

Equation (5.19) is applicable to a well-mixed batch crystallizer. Considering each term of this equation, it is seen that the term,

$$(\sum_k U_{t(k)} F_{Q,t(k)})/V_T$$

is zero because a batch system has no inflow or outflow of crystals. The

$\nabla \cdot \underline{v}_{int} F_{V,t}$ term can be written by the above assumption as:

$$\frac{\partial}{\partial V}(G_V F_{V,t}), \text{ where } G_V \triangleq \frac{dV}{d\tau}.$$

Thus, equation (5.19) reduces to:

$$\frac{\partial}{\partial \tau}(F_{V,t}) + \frac{\partial}{\partial V}(G_V F_{V,t}) + (F_{V,t} \frac{d}{d\tau}(V_T))/V_T = BF_{V,t} - DF_{V,t}$$

or

$$\frac{\partial}{\partial \tau}(F_{V,t} V_T) + \frac{\partial}{\partial V}(G_V F_{V,t} V_T) = V_T(BF_{V,t} - DF_{V,t}) \quad (5.20)$$

For mathematical convenience, that is, to avoid implicit equations, the number density function, $F_{V,t}$, is redefined on the basis of total operating volume of the system; therefore:

$$F_{V,T} \triangleq F_{V,t} V_T$$

The total birth and death rate density term, $V_T(BF_{V,t} - DF_{V,t})$ is redefined on a solution volume (mother liquor) basis. This seems at least reasonable for the pure birth processes, because crystals come only into being in the solution phase and not in the solids phase. In this context, a pure birth process refers to the rate at which crystals enter size interval $[V, V + dV]$ from the solution phase as opposed to those that enter from another size interval, i.e. from the solids phase. Thus,

$$V_L(BF_{V,\ell} - DF_{V,\ell}) \Delta V_T(BF_{V,t} - DF_{V,t})$$

The birth and death processes for most crystallization systems are the nucleation, agglomeration, and attrition rates. Thus each of these processes may be accounted for by their particular birth and death functions, viz:

$$BF_{V,\ell,n} + BF_{V,\ell,a} + BF_{V,\ell,b} - DF_{V,\ell,a} - DF_{V,\ell,b} \Delta BF_{V,\ell} - DF_{V,\ell}$$

- where $BF_{V,\ell,n} dV$ - nucleation rate into size interval $[V, V + dV]$
- $BF_{V,\ell,a} dV, DF_{V,\ell,a} dV$ - agglomeration rate into and out of size interval $[V, V + dV]$
- $BF_{V,\ell,b} dV, DF_{V,\ell,b} dV$ - attrition rate into and out of size interval $[V, V + dV]$

Using these definitions, equation (5.20) becomes:

$$\frac{\partial}{\partial \tau}(F_{V,T}) + \frac{\partial}{\partial V}(G_V F_{V,T}) = V_L(BF_{V,\ell,n} + BF_{V,\ell,a} - DF_{V,\ell,a} + BF_{V,\ell,b} - DF_{V,\ell,b}) \quad (5.21)$$

Equation (5.21) is the population balance for a batch crystallizer subject to the assumptions made and the definitions employed.

5.2.2 Boundary and Initial Condition for the Batch Crystallizer Population Balance

A complete mathematical statement of a problem requires specification of boundary conditions around the domain under consideration. The initial and boundary condition for the population balance, equation (5.21), for a batch crystallizer requires some careful consideration since there are some subtleties which are not immediately obvious.

5.2.2.1 Initial Condition

The initial condition for the population balance equation as applied to a seeded batch crystallizer is $F_{V,T}(\tau, V) = F_{V,T,0}(V)$, the number density function of the seed crystals introduced to the crystallizer at time zero. The problem arises, however, in that this expression does not account for the 'activity' of the seed which manifests itself as an induction period in the crystallization process. This difference in initial crystal activity could lead to quite different behaviour of batch crystallizations which could be identical in all other respects; hence, this activity must be characterized.

There are two ways of dealing with this problem. One is to try to include the seed activity as a function of internal properties, ξ , to account for the effect on activity of the crystallizer operating conditions and/or pretreatment of the seed. This approach requires a detailed knowledge and understanding of the crystallization kinetics during the induction period which is a major study in itself. The second way is to specify as time zero some finite time after the introduction of the seed crystals at which point the seed activity is no longer a function of the

seed pretreatment. After this time, the crystallization processes should proceed at a rate determined only by the system operating conditions.

5.2.2.2 Boundary Condition

The boundary condition cannot be stated a priori without some consideration of the physical system and the mathematical equations involved. The difficulty is in how the nucleation phenomenon is expressed mathematically. In many instances, modellers of the overall crystallization process have treated nucleation as a boundary condition. This means that all the nuclei formed at a time τ are of size V_0 . On the other hand, nucleation may be expressed as a birth density function which allows for nuclei to be formed with a distribution of sizes over a finite size range, viz:

$$BN_{l,n,o}(\tau) = \int_{V_0}^u BF_{V,l,n}(V,\tau)dV \quad (5.22)$$

where $BN_{l,n,o}$ - number of crystals formed per hour per litre solution
 $BF_{V,l,n}$ - number of crystals of volume $V \text{ } \mu\text{m}^3$ formed per hour per litre solution

The latter method is adopted here.

The general approach to obtain the boundary condition in this case is to rederive the equation over a differential control volume, the boundaries of which include the system boundaries. This procedure has been suggested by Smith and Pike (s4) for the type of problem encountered here.

Thus, rederiving equation (5.21) on the system boundary V_0 for a number balance over the internal size interval $[V_0, V_0 + \Delta V]$ over the increment of time $\Delta \tau$ with:

$$\text{accumulation} - \text{input} - \text{output} + \text{net generation}$$

gives for each term:

$$F_{V,T}(V, \tau + \Delta \tau) \Delta V - F_{V,T}(V, \tau) \Delta V \quad \text{accumulation}$$

$$G_V(V_0 + \Delta V, \tau) F_{V,T}(V_0 + \Delta V, \tau) \Delta \tau \quad \text{output due to growth}$$

$$V_L BF_{V,\ell,n}(V, \tau) \Delta V \Delta \tau \quad \text{generation due to nucleation}$$

$$V_L [BF_{V,\ell,a}(V, \tau) - DF_{V,\ell,a}(V, \tau)] \Delta V \Delta \tau \quad \text{generation due to agglomeration}$$

$$V_L [BF_{V,\ell,b}(V, \tau) - DF_{V,\ell,b}(V, \tau)] \Delta V \Delta \tau \quad \text{generation due to attrition}$$

Collecting terms and dividing by $\Delta V \Delta \tau$ gives:

$$\begin{aligned} [F_{V,T}(V, \tau + \Delta \tau) - F_{V,T}(V, \tau)] / \Delta \tau &= -[G_V(V_0 + \Delta V, \tau) F_{V,T}(V_0 + \Delta V, \tau)] / \Delta V \\ &+ V_L [BF_{V,\ell,n}(V, \tau) + BF_{V,\ell,a}(V, \tau) \\ &- DF_{V,\ell,a}(V, \tau) + BF_{V,\ell,b}(V, \tau) \\ &- DF_{V,\ell,b}(V, \tau)] \dots\dots (5.23) \end{aligned}$$

Taking the limit as $\Delta\tau \rightarrow 0$ and multiplying by ΔV gives:

$$\frac{\partial}{\partial \tau}(F_{V,T})\Delta V = -G_V(V_0 + \Delta V, \tau)F_{V,T}(V_0 + \Delta V, \tau) + V_L [\dots] \Delta V$$

Now, taking the limit as $\Delta V \rightarrow 0$, gives:

$$0 = -[G_V F_{V,T}]_{V_0} + 0$$

From this equation it follows that

$$F_{V,T}(V_0, \tau) = 0 \quad \text{since} \quad G_V(V_0, \tau) \neq 0 \quad (5.24)$$

In the above derivation, as in the derivation of equation (5.21), the nucleation, agglomeration, and attrition rate processes are expressed by means of rate density functions. Expressing agglomeration and attrition rates in this manner is common practice; however, this is not the case for the nucleation rate which, as indicated earlier, is quite often treated as a boundary condition. The boundary condition definition leads to the following expression for $F_{V,T}(V_0, \tau)$:

$$F_{V,T}(V_0, \tau) = V_L(\tau)BN_{\ell,n,o}(\tau)/G_V(V_0, \tau) \quad (5.25)$$

That is, the term $V_L BF_{V,\ell,n}(V, \tau)$ in equation (5.23) has been replaced by $V_L BN_{\ell,n,o}/\Delta V$ after which the same steps were followed as in the derivation of $F_{V,T}(V_0, \tau) = 0$. Note that the use of the variable, $BN_{\ell,n,o}$, modifies equation (5.23) in that it excludes the nucleation term, $V_L BF_{V,\ell,n}$.

In this work, the density function definition has been adopted since it is consistent with the definition of the other generation terms (agglomeration, and attrition). Moreover, it allows for a more general model in that it has the capability of handling the birth of nuclei crystals over a particular size range.

To summarize, the initial and boundary conditions for equation (5.21) are, respectively:

$$F_{V,T}(V,0) = F_{V,T,0}(V) \quad (5.26)$$

$$F_{V,T}(V_0,\tau) = 0 \quad (5.27)$$

5.3 Derivation of the Functional Relationship for Growth, Nucleation, Agglomeration, and Attrition

The population balance equation (equation (5.21)) contains general functional relationships for attrition, agglomeration, nucleation, and growth. It is desirable to derive general relationships based on postulated mechanisms which are expressed only as functions of the dependent variable, $F_{V,T}$ and the independent variables V and τ . Those factors which are functions of concentration, temperature, etc. are indicated as functions of time. It is through the external material, energy and momentum balances that the experimental conditions are related to time. This method of formulation maintains flexibility in the modeling procedure. The derivations of the general functional relationships are presented below.

(a) Growth Rate

The average growth rate, $G(V, \tau) = \frac{dV}{d\tau}$, may be expressed as the product of two functions, each of which depends on only one of the independent variables, viz:

$$G_V(V, \tau) = G_D(\tau) \cdot \phi_g(V) \quad (5.28)$$

where G_D is the constitutive relationship expressing the dependence of the growth rate on the instantaneous concentrations, temperature, etc., and $\phi_g(V)$ expresses how this growth rate varies with the size of the crystals.

(b) Nucleation Rate

In a similar manner, the nucleation rate density function may be written as:

$$BF_{V,\ell,n}(V, \tau) = BF_{\ell,n}(\tau) \cdot \phi_n(V) \quad (5.29)$$

The birth function $BF_{\ell,n}(\tau)$ accounts for the external conditions, whereas the function $\phi_n(V)$ accounts for the crystal size dependence of the nucleation rate (for example, through the secondary nucleation phenomena).

(c) Agglomeration

In deriving a mathematical model for the agglomeration rate process, an attempt is made to include a description of the mechanisms which are expected to be involved. In this way, it is assumed that only

binary collisions take place and the crystal concentration is dilute enough that only 'free-in-space' type agglomeration takes place (§3).

To derive the functional form of the agglomeration rate function based on these assumptions, consider the rate of change of the number of crystals per unit volume of solution in the crystal size interval V to $V + \Delta V$ over an incremental time $\Delta\tau$ due to agglomeration only. The accumulation term is:

$$[F_{V,T}(V, \tau + \Delta\tau)\Delta V - F_{V,T}(V, \tau)\Delta V]/V_L(\tau)$$

The birth of the number of crystals into this size range in time $\Delta\tau$ is equal to the number of 'successful' binary collisions in time $\Delta\tau$ that have a combined volume of V . Based on the assumptions concerning the agglomeration process, the total number of binary collisions between crystals of volume size range V' to $V' + \Delta V'$ and V'' to $V'' + \Delta V''$ in time $\Delta\tau$ are:

$$k_{V,a}^*(V', V'', \tau) [F_{V,T}(V', \tau)\Delta V'/V_L(\tau)] [F_{V,T}(V'', \tau)\Delta V''/V_L(\tau)] \Delta\tau$$

where $k_{V,a}^*(V', V'', \tau)$ is the collision frequency rate function. The number of 'successful' binary collisions or the number of agglomerated crystals are:

$$k_{V,a}(V', V'', \tau) [F_{V,T}(V', \tau)\Delta V'/V_L(\tau)] [F_{V,T}(V'', \tau)\Delta V''/V_L(\tau)] \Delta\tau$$

where $k_{V,a}$ is the combined collision frequency rate-agglomeration rate function which designates the fraction per unit time of the theoretical total number of collisions which result in agglomeration. The function $k_{V,a}$ will be referred to in this work as the 'agglomeration rate effectiveness kernel'.

Since the crystal mass (volume) is conserved during agglomeration, $V = V' + V''$ and the expression becomes:

$$k_{V,a}(V', V-V', \tau) [F_{V,T}(V', \tau) \Delta V' / V_L(\tau)] [F_{V,T}(V-V', \tau) \Delta V / V_L(\tau)] \Delta \tau$$

where it is to be noted that $\Delta V'' = \Delta V$ for constant V' . Summing over all possible combinations of V' and $V-V'$ that give V , the term for the rate of input is:

$$\frac{1}{2} \sum_{\substack{V' = V - V_0 \\ V' = V_0}}^{\substack{V' = V - V_0 \\ V' = V_0}} k_{V,a}(V', V-V', \tau) [\dots] [\dots] \Delta \tau$$

where V_0 is the volume of the smallest particle in the system and the factor $\frac{1}{2}$ accounts for the fact that a collision between two particles of sizes V'' and V''' , and a collision between V''' and V'' constitute only one collision and not two.

The loss of the number of crystals in size range V to $V + \Delta V$ due to agglomeration over time $\Delta \tau$ is equal to all 'successful' binary collisions over time $\Delta \tau$ between crystals of volume V to $V + \Delta V$ and all other crystals, including those in this size range. Thus, the death rate term for the agglomeration process is:

$$[F_{V,T}(V, \tau) \Delta V / V_L(\tau)] \sum_{V'=V_0}^{V'=V_u} k_{V,a}(V', V, \tau) [F_{V,T}(V', \tau) \Delta V / V_L(\tau)] \Delta \tau$$

where V_0 and V_u are the volume of the smallest and largest particles in the system, respectively. Equating accumulation to birth-death and dividing by $\Delta V \Delta \tau$ gives:

$$\begin{aligned} & [(F_{V,T}(V, \tau + \Delta \tau) - F_{V,T}(V, \tau)) / V_L(\tau)] / \Delta \tau - \\ & 1/[V_L(\tau)]^2 \times \left[\frac{1}{2} \sum_{V'=V_0}^{V'=V-V_0} k_{V,a}(V', V-V', \tau) F_{V,T}(V', \tau) F_{V,T}(V-V', \tau) \Delta V' \right. \\ & \left. - F_{V,T}(V, \tau) \sum_{V'=V_0}^{V'=V_u} k_{V,a}(V, V', \tau) F_{V,T}(V', \tau) \Delta V' \right] \end{aligned}$$

Taking the limits as $\Delta \tau \rightarrow 0$ and $\Delta V' \rightarrow 0$

$$\begin{aligned} & 1/V_L(\tau) \times \frac{\partial}{\partial \tau} F_{V,T}(V, \tau) - \\ & 1/[V_L(\tau)]^2 \times \left[\frac{1}{2} \int_{V_0}^{V-V_0} k_{V,a}(V', V-V', \tau) F_{V,T}(V', \tau) F_{V,T}(V-V', \tau) dV' \right. \\ & \left. - F_{V,T}(V, \tau) \int_{V_0}^{V_u} k_{V,a}(V, V', \tau) F_{V,T}(V', \tau) dV' \right] \end{aligned}$$

and thus:

$$\begin{aligned} BF_{V,\ell,a}(V, \tau, F_{V,T}) &= 1/[V_L(\tau)]^2 \times \left[\frac{1}{2} \int_{V_0}^{V-V_0} k_{V,a}(V', V-V', \tau) \right. \\ & \left. F_{V,T}(V', \tau) F_{V,T}(V-V', \tau) dV' \right] \dots (5.30) \end{aligned}$$

$$DF_{V,\ell,a}(V,\tau,F_{V,T}) = 1/[V_L(\tau)]^2 \times [F_{V,T} \int_{V_0}^{V_u} k_{V,a}(V',V,\tau)F_{V,T}(V',\tau)dV'] \dots (5.31)$$

where

$$k_{V,a}(V,V',\tau) = 0 \quad \text{for } (V + V') > V_u \text{ and} \\ \text{for } V \text{ and/or } V' < V_0$$

$$\geq 0 \quad \text{for } (V + V') \leq V_u \text{ and} \\ \text{for } V \text{ and } V' \geq V_0$$

(d) Attrition

If it is assumed that the attrition of crystals arises solely as a result of the environment (collision with container walls, agitator, high shear fields) and not through the interaction or collision with other crystals, then the attrition rate of crystals in the size range to $V + \Delta V$ will be directly proportional to the number of crystals per unit volume of solution in that size interval and independent of the number of crystals in any other size range.

The attrition rate functions may be derived in the same way as that for the agglomeration process. In this case, the following expression results:

$$BF_{V,\ell,b}(V,\tau,F_{V,T}) - DF_{V,\ell,b}(V,\tau,F_{V,T}) = \\ 1/V_L(\tau) \times [2 \int_{-V+V_0}^V k_{V,b}(V',V,V'-V,\tau)F_{V,T}(V',\tau)dV' \\ - \int_{V_0}^{V-V_0} k_{V,b}(V,V',V-V',\tau)F_{V,T}(V,\tau)dV'] \dots (5.32)$$

where $k_{V,b}(V, V', V-V', \tau)$ is the rate function denoting the rate at which crystals of size V break into two fragments of sizes V' and $V-V'$. Its value is equal to zero for: $V < 2V_0$; $V > V_u$; $V' < V_0$; $V' > (V-V_0)$; and it is ≥ 0 for $V \geq 2V_0$; $V \leq V_u$; $V' \geq V_0$; and $V' \leq V-V_0$. The factor 2 in equation (5.32) accounts for the fact that the breakage (attrition) of a particle with a volume V' into two fragments of volumes (V) and $(V'-V)$ leads to one particle of size V while the breakage into fragments $(V'-V)$ and (V) leads to another particle of size V .

5.4 Mathematical Manipulation of the Population Balance Equations; Including the Functional Relationships

In order to facilitate the solution of the population balance equation, it is worthwhile recognizing some fundamental mathematical properties of the equation and the terms in it. These mathematical manipulations are discussed in the following subsections.

5.4.1 The Symmetric Property of the Agglomeration Convolution Integral

The value of the convolution integral in the agglomeration birth function must be approximated using numerical methods. In most cases, it is faster and more accurate to solve the following equivalent equation:

$$BF_{V,l,a}(V, \tau, F_{V,T}) = 1/[V_L(\tau)]^2 \times \left[\int_{V_0}^{V/2} k_{V,a}(V', V-V', \tau) F_{V,T}(V', \tau) F_{V,T}(V-V', \tau) dV' \right]$$

The following derivation shows that this convolution integral is equivalent to equation (5.30). Starting with equation (5.30),

first the independent variable V' is changed to $V'' = V' - (V/2)$, which gives $V' = V/2 + V''$, $V - V' = (V/2) - V''$, $dV' = dV''$ and the limits of the integration equal to $-(V/2) + V_0$ to $(V/2) - V_0$. With this transformation the right-hand side of equation (5.30) becomes:

$$\frac{1}{[V_L(\tau)]^2} \times \left[\frac{1}{2} \int_{-V/2+V_0}^{V/2-V_0} k_{V,a}(V/2 + V'', V/2 - V'', \tau) F_{V,T}(V/2 + V'', \tau) F_{V,T}(V/2 - V'', \tau) dV'' \right]$$

From this equation it is seen that if V'' is replaced by $-V''$ the integrand has the same value, i.e. it is symmetric with respect to $V/2$, given that $k_{V,a}$ is symmetric, therefore it may be written as:

$$\frac{1}{[V_L(\tau)]^2} \times \left[\int_{-V/2+V_0}^0 k_{V,a}(V/2 + V'', V/2 - V'', \tau) F_{V,T}(V/2 + V'', \tau) F_{V,T}(V/2 - V'', \tau) dV'' \right]$$

Changing the independent variable V'' back to V' gives the desired result, i.e.

$$\frac{1}{[V_L(\tau)]^2} \times \left[\frac{1}{2} \int_{V_0}^{V-V_0} k_{V,a}(V', V-V', \tau) F_{V,T}(V', \tau) F_{VT}(V-V', \tau) dV' \right] =$$

$$\frac{1}{[V_L(\tau)]^2} \times \left[\int_{V_0}^{V/2} k_{V,a}(V', V-V', \tau) F_{V,T}(V', \tau) F_{VT}(V-V', \tau) dV' \right] \dots (5.33)$$

5.4.2 Spatially Averaged Number Density Population Balance for a Batch System with the Rate Processes Growth, Nucleation, Agglomeration, and Attrition

Substitution of the general rate expressions from sub-section 5.3 into equation (5.21) gives the following integro-partial differential equation:

$$\begin{aligned}
 \frac{\partial}{\partial \tau} [F_{V,T}(V, \tau)] + G_D(\tau) \frac{\partial}{\partial V} [\phi_g(V) F_{V,T}(V, \tau)] - V_L(\tau) \times \\
 \{ + B F_{2,n}(\tau) \phi_n(V) \\
 + 1/[V_L(\tau)]^2 \times \int_{V_0}^{V/2} k_{V,a}(V', V-V', \tau) F_{V,T}(V', \tau) \\
 F_{V,T}(V-V', \tau) dV' \} - 1/[V_L(\tau)]^2 \times \\
 [F_{V,T}(V, \tau) \int_{V_0}^{V_u} k_{V,a}(V', V, \tau) F_{V,T}(V', \tau) dV'] \\
 + 1/V_L(\tau) \times [2 \int_{V+V}^{V_u} k_{V,b}(V', V, V'-V, \tau) F_{V,T}(V', \tau) dV' \\
 - 1/V_L(\tau) \times \int_{V_0}^{V-V_0} k_{V,b}(V, V', V-V', \tau) F_{V,T}(V, \tau) dV'] \} \\
 \dots (5.34)
 \end{aligned}$$

I.C. $F_{V,T}(V, 0) = F_{V,T,0}(V)$

B.C. $F_{V,T}(V_0, \tau) = 0$

Equation (5.34) is the population balance for the number density function for crystals in a batch crystallizer which includes general models for the rate processes of growth, nucleation, agglomeration, and attrition.

5.4.5 Spatial-Averaged-Number-Cumulative Population Balance for a Batch System with Growth, Nucleation, Agglomeration, and Attrition

All attempts to find a successful (accurate) numerical solution of equation (5.34) have failed. It has been found, however, that a successful numerical solution of the population balance equation can be effected if equation (5.34) is expressed in terms of the cumulative number distribution function, $H_T(V, \tau)$. The cumulative number and number density functions are related by:

$$H_T(V, \tau) \triangleq \int_{V_0}^V F_{V,T}(V'', \tau) dV'' \quad (5.35)$$

which, when differentiated, shows that:

$$F_{V,T}(V, \tau) = \frac{\partial}{\partial V} H_T(V, \tau) \quad (5.36)$$

Also, from the boundary condition for $F_{V,T}(V_0, \tau)$, it follows that:

$$H_T(V_0, \tau) = 0 \quad (5.37)$$

The transformation of the population balance equation (equation (5.34)) from the number density function to the cumulative distribution

function is carried out by integrating each term over the interval V_0 to V as follows:

(a) Accumulation Term

$$\int_{V_0}^V \frac{\partial}{\partial \tau} [F_{V,T}(V'', \tau)] dV'' = \frac{\partial}{\partial \tau} H_T(V, \tau) \quad (5.38)$$

by definition of $H_T(V, \tau)$.

(b) Growth Term

$$\begin{aligned} \int_{V_0}^V G_D(\tau) \frac{\partial}{\partial V''} [\phi_g(V''') F_{V,T}(V'', \tau)] dV'' &= G_D(\tau) [\phi_g(V''') F_{V,T}(V'', \tau)] \Big|_{V_0}^V \\ &= G_D(\tau) \phi_g(V) F_{V,T}(V, \tau) \\ &\quad - G_D(\tau) \phi_g(V_0) F_{V,T}(V_0, \tau) \\ &= G_D(\tau) \phi_g(V) \left[\frac{\partial}{\partial V} H_T(V, \tau) \right] - 0 \\ &\dots\dots (5.39) \end{aligned}$$

The second term on the right-hand side of this equation is zero because $F_{V,T}(V_0, \tau) = 0$ is the boundary condition (5.27).

(c) Nucleation Term

$$\int_{V_0}^V V_L(\tau) B_{L,n}(\tau) \phi_n(V'') dV'' = V_L(\tau) B_{L,n}(\tau) \phi_n(V) \quad (5.40)$$

where $\phi_n(V) \triangleq \int_{V_0}^V \phi_n(V'') dV''$

(d) Agglomeration Input Term

The integration of the agglomeration input term requires the evaluation of the following expression:

$$\int_{V_0}^V V_L(\tau) \frac{1}{V_L(\tau)^2} \int_{V_0}^{V''/2} k_{V,a}(V', V''-V', \tau) F_{V,T}(V', \tau) F_{V,T}(V''-V', \tau) dV' dV''$$

- (...)

This double integral is transformed into a double integral of a more tractable form with respect to the integration limits and order of integration with the aid of the Heaviside unit functions ϕ_1 and ϕ_2 as follows:

$$(\dots) = \int_{V_0}^V \int_{V_0}^{V''/2} \phi_1(V'', V) \phi_2(V', V) \phi(V''-V', V', \tau) dV' dV''$$

where $\phi(V''-V', V', \tau) \triangleq \frac{1}{V_L(\tau)} k_{V,a}(V', V''-V', \tau) F_{V,T}(V', \tau) F_{V,T}(V''-V', \tau)$

$$\phi_1(V'', V) = \begin{cases} 1 & , \quad V_0 \leq V'' \leq V \\ 0 & , \quad V'' < V_0, V'' > V \end{cases}$$

$$\phi_2(V', V) = \begin{cases} 1 & , \quad V_0 \leq V' \leq V''/2 \\ 0 & , \quad V' < V_0, V' > V''/2 \end{cases}$$

Therefore, with these definitions, the integrations can be extended to cover the full range from zero to infinity, i.e.:

$$(\dots) = \int_0^{\infty} \int_0^{\infty} \phi_1(V'', V) \phi_2(V', V) \phi(V''-V', V', \tau) dV' dV''$$

which when changing the order of integration becomes:

$$(\dots) = \int_0^{\infty} \int_0^{\infty} \phi_1(V'', V) \phi_2(V', V) \phi(V''-V', V', \tau) dV'' dV'$$

The integration limits of this integral are now reduced such that the only region covered is that for which both ϕ_2 and ϕ_1 are equal to one. Thus ϕ_2 and $\phi_1 = 1$ for $V \geq V''$, $V'' \geq 2V'$, $2V' \geq 2V_0$ and, therefore, $V \geq V'' \geq 2V' \geq 2V_0$ or $V/2 \geq V''/2 \geq V' \geq V_0$. Also $\phi_2 = 1$ for $V'' \geq 2V'$ and $\phi_1 = 1$ for $V'' \leq V$ which shows that the integration limits for V'' are $[2V', V]$. For V' , $\phi_2 = 1$ for $V' \geq V_0$ and $\phi_1 = 1$ for $V' \leq V''/2$ and since $V'' \leq V$ or $V''/2 \leq V/2$ for ($\phi_1 = 1$) it follows that $V' \leq V''/2 \leq V/2$, while from the integration limits for V'' the only possible values for V'' are those for which $V''/2 \geq V'$, thus $V' \leq V''/2$ is not a constraint on V' , and $V' \leq V/2$. The integration limits for V' are, therefore, $[V_0, V/2]$, and the integral term becomes:

$$(\dots) = \frac{V_L(\tau)}{[V_L(\tau)]^2} \times \int_{V_0}^{V/2} \int_{2V'}^V k_{V,a}(V', V''-V', \tau) F_{V,T}(V', \tau) F_{V,T}(V''-V', \tau) dV'' dV'$$

which by means of the variable V''' such that: $V''' \triangleq V'' - V'$, $dV'' = dV'''$, $V''' [V', V - V']$, gives:

$$\begin{aligned}
 (\dots) &= V_L(\tau) / [V_L(\tau)]^2 \times \int_{V_0}^{V/2} \int_{V'}^{V-V'} k_{V,a}(V', V''', \tau) \\
 &F_{V,T}(V', \tau) F_{V,T}(V''', \tau) dV''' dV' \dots (5.41)
 \end{aligned}$$

which is the desired result.

(e) Agglomeration Output Term

$$\begin{aligned}
 &\int_{V_0}^V - V_L(\tau) / [V_L(\tau)]^2 \times F_{V,T}(V'', \tau) \int_{V_0}^u k_{V,a}(V', V'', \tau) F_{V,T}(V', \tau) dV' dV'' \\
 &- - V_L(\tau) / [V_L(\tau)]^2 \int_{V_0}^V \int_{V_0}^u k_{V,a}(V', V'', \tau) F_{V,T}(V'', \tau) F_{V,T}(V', \tau) dV' dV'' \\
 &\dots (5.42)
 \end{aligned}$$

(f) Attrition Input Term

$$\begin{aligned}
 &\int_{V_0}^V 2V_L(\tau) / V_L(\tau) \times \int_{V+V_0}^u k_{V,b}(V', V'', V' - V'', \tau) F_{V,T}(V', \tau) dV' dV'' \\
 &- 2V_L(\tau) / V_L(\tau) \times \int_{V_0}^V \int_{V+V_0}^u k_{V,b}(V', V'', V' - V'', \tau) F_{V,T}(V', \tau) dV' dV'' \\
 &\dots (5.43)
 \end{aligned}$$

(g) Attrition Output Term

$$\int_{V_0}^V -V_L(\tau)/V_L(\tau) \times \int_{V_0}^{V-V_0} k_{V,b}(V'',V',V''-V',\tau) F_{V,T}(V'',\tau) dV' dV''$$

$$- -V_L(\tau)/V_L(\tau) \times \int_{V_0}^V \int_{V_0}^{V-V_0} k_{V,b}(V'',V',V''-V',\tau) F_{V,T}(V'',\tau) dV' dV''$$

..... (5.44)

Collecting terms shows that:

$$\frac{\partial}{\partial \tau} [H_T(V,\tau)] + G_D(\tau) \phi_g(V) \left[\frac{\partial}{\partial V} H_T(V,\tau) \right] -$$

$$+ V_L(\tau) B F_{z,n}(\tau) \phi_n(V)$$

$$+ V_L(\tau) / [V_L(\tau)]^2 \times \int_{V_0}^{V/2} \int_{V'}^{V-V'} k_{V,a}(V',V'',\tau) F_{V,T}(V',\tau) F_{V,T}(V'',\tau) dV'' dV'$$

$$- V_L(\tau) / [V_L(\tau)]^2 \times \int_{V_0}^V \int_{V_0}^{V_u} k_{V,a}(V',V'',\tau) F_{V,T}(V',\tau) F_{V,T}(V'',\tau) dV' dV''$$

$$+ 2V_L(\tau) / V_L(\tau) \times \int_{V_0}^V \int_{V+V_0}^{V_u} k_{V,b}(V',V'',V'-V'',\tau) F_{V,T}(V',\tau) dV' dV''$$

$$- V_L(\tau) / V_L(\tau) \times \int_{V_0}^V \int_{V_0}^{V-V_0} k_{V,b}(V'',V',V''-V',\tau) F_{V,T}(V'',\tau) dV' dV''$$

..... (5.45)

$$\text{B.C. } H_T(V_0,\tau) = 0 \quad (5.46)$$

$$\text{I.C. } H_T(V,0) = H_{T,0}(V) \quad (5.47)$$

where $F_{V,T}(V', \tau) = \frac{\partial}{\partial V} H_T(V', \tau)$

$$F_{V,T}(V'', \tau) = \frac{\partial}{\partial V} H_T(V'', \tau)$$

Equation (5.45) is the population balance for a batch system with growth, nucleation, agglomeration, and attrition-rate processes, expressed indirectly in terms of the cumulative number distribution function $H_T(V, \tau)$ *. The I.C. is subject to the same arguments that were presented in sub-section 5.2.2.1 for the I.C. of equation (5.21). The B.C. follows directly from the definition of the cumulative number distribution function. The assumptions made in the derivation of equation (5.45) are repeated here for clarity. Thus, it has been assumed that:

- The crystals concentration is dense enough to be approximated by a number continuum.
- The batch system behaves as a homogeneous suspension.
- The internal state of the crystals is completely defined by the one internal coordinate, crystal volume.
- The growth and nucleation rate functions can be split into two factors, one depending on the crystal environment and the other on the crystal dimensions.
- The crystal concentration is dense enough to allow for a deter-

*Although, $F_{V,T}$ still appears in this equation, it appears only in the integrand expressions which when integrated out are proportional to H_T by definition of H_T , i.e. $\int_V F_{V,T} dV = H_T(V)$. If the integrand expression is too complex for an analytical solution, the $F_{V,T}$ or $\partial H_T / \partial V$ values can be numerically approximated and the integrals evaluated by quadrature.

ministic formulation of the agglomeration rate process, but at the same time is dilute enough to have "free-in-space type" agglomeration, and to have only binary collisions take place.

- The attrition rate of crystals in the size range V to $V + \Delta V$ is independent of the number of crystals in any other size range.
- The volume of agglomerating crystals is conserved in the agglomeration process.

5.5 Pseudo Moment Equations for a Batch System with the Rate Processes, Growth, Nucleation, Agglomeration, and Attrition

Although the cumulative number expression, equation (5.45), might present fewer numerical problems than the number density function expression, equation (5.34), it still is an integro-partial differential equation which in most cases requires considerable computer power (time and storage) to effect a satisfactory numerical solution. To alleviate this problem the number density function expression can be transformed to a set of 'pseudo moment' equations.

Pseudo moment equations are obtained by multiplying equation (5.34) by a general weighting function, $X_i(V)$, and integrating over the independent variable V . The resulting equations are called 'pseudo moment equations', instead of merely 'moment equations', for the following two reasons. First, the weighting functions can be any function of V and are not restricted to the particular forms, $X_i(V) \triangleq V^i$, which are the weighting functions commonly used for the moment transformation of the population balance equation. Secondly, the resulting equations might for certain

$X_i(V)$ functions not be a set of equations exclusively in terms of the pseudo moments, that is, they still contain functions of the independent variable V .

These types of equations, where V has not been integrated out completely can be used to advantage, however, as is explained later in this section. On the other hand, if the independent variable V can be integrated out of the equation, then the solution is simplified greatly because writing the population balance equation in terms of the moments or pseudo moments transforms the integro-partial differential equation into a relatively small set of ordinary differential or algebraic equations, which are relatively easier to solve. The derivation of these pseudo moment equations is demonstrated below.

The i^{th} pseudo moment of the number distribution is defined as:

$$n_i(\tau) \triangleq \int_{V_0}^{V_u} X_i(V) F_{V,T}(V,\tau) dV \quad (5.48)$$

Therefore, multiplying equation (5.34) by $X_i(V)$ and integrating over V from V_0 to V_u gives for each term the following expressions:

(a) Accumulation

$$\int_{V_0}^{V_u} X_i(V) \frac{\partial}{\partial \tau} [F_{V,T}(V,\tau)] dV = \frac{\partial}{\partial \tau} \left[\int_{V_0}^{V_u} X_i(V) F_{V,T}(V,\tau) dV \right] \\ = \frac{d}{d\tau} n_i(\tau) \quad \dots (5.49)$$

(b) Growth

Integration by parts yields:

$$\begin{aligned}
 & \int_{V_0}^{V_u} X_i(V) G_D(\tau) \frac{\partial}{\partial V} [\phi_g(V) F_{V,T}(V, \tau)] dV \\
 & - G_D(\tau) \{ [\phi_g(V) F_{V,T}(V, \tau)] [X_i(V)] / \Big|_{V_0}^{V_u} \\
 & - \int_{V_0}^{V_u} [\phi_g(V) F_{V,T}(V, \tau)] \frac{d}{dV} [X_i(V)] dV \} \\
 & - G_D(\tau) \{ \phi_g(V_u) F_{V,T}(V_u, \tau) X_i(V_u) - \phi_g(V_0) F_{V,T}(V_0, \tau) X_i(V_0) \\
 & - \int_{V_0}^{V_u} [\phi_g(V) F_{V,T}(V, \tau)] \frac{d}{dV} [X_i(V)] dV \} \dots (5.50)
 \end{aligned}$$

The second and first terms on the right-hand side of this equation are zero because $F_{V,T}(V_0, \tau)$ and $F_{V,T}(V_u, \tau)$ have zero values, respectively. The zero value of the density function at V_0 is the boundary condition (5.27), while at V_u it follows from the fact that the value of V_u must always be large enough such that the solution domain contains the whole size distribution at all times (i.e. V_u is defined by $F(V, \tau) = 0$ for all $V \geq V_u$). Hence,

$$\begin{aligned}
 & \int_{V_0}^{V_u} X_i(V) G_D(\tau) \frac{\partial}{\partial V} [\phi_g(V) F_{V,T}(V, \tau)] dV \\
 & - - G_D(\tau) \int_{V_0}^{V_u} \phi_g(V) F_{V,T}(V, \tau) \frac{d}{dV} [X_i(V)] dV \dots (5.51)
 \end{aligned}$$

The possibility of expressing (5.51) in terms of the pseudo moments, $n_i(\tau)$, will depend on the functional forms of $\phi_g(V)$ and $X_i(V)$.

(c) Nucleation

$$\int_{V_0}^{V_u} X_i(V) V_L(\tau) B F_{i,n}(\tau) \phi_n(V) dV = V_L(\tau) B F_{i,n}(\tau) \int_{V_0}^{V_u} X_i(V) \phi_n(V) dV \quad \dots (5.52)$$

where $\int_{V_0}^{V_u} X_i(V) \phi_n(V) dV$ must be a known function of i in order that a meaningful solution can be effected.

(d) Agglomeration Input

$$\int_{V_0}^{V_u} X_i(V) \frac{1}{2} V_L(\tau) / [V_L(\tau)]^2 \times \int_{V_0}^{V-V_0} k_{V,a}(V', V-V', \tau) F_{V,T}(V', \tau) F_{V,T}(V-V', \tau) dV' dV' = (\dots)$$

This integral expression is transformed into a more manageable form with regard to the integration limits with the aid of the functions ϕ_1 and ϕ_2 as follows:

$$\text{Define: } \phi_1(\xi, \tau) = \phi_2(\xi, \tau) \triangleq F_{V,T}(\xi, \tau) \quad , \quad V_u \geq \xi \geq V_0$$

$$\triangleq 0 \quad , \quad \xi < V_0 \quad , \quad \xi > V_u$$

For convenience the independent variable τ is dropped in the following derivation. Thus:

$$(\dots) = \frac{1}{2} \frac{1}{V_L} \int_{V_0}^{V_u} \int_{V_0}^{V-V_0} [k_{V,a}(V', V-V') X_1(V) \phi_1(V') \phi_2(V-V')] dV' dV$$

and since $\phi_2(V') = 0$ for $V' < V_0$ this equation becomes:

$$= \frac{1}{2} \frac{1}{V_L} \int_{V_0}^{V_u} \int_{V_0}^{\infty} [\dots] dV' dV$$

while, from the relationship

$$\int_{V_0}^{V_u} \frac{\partial}{\partial \tau} [F_{V,T}(V, \tau)] dV = \int_{V_0}^{\infty} \frac{\partial}{\partial \tau} [F_{V,T}(V, \tau)] dV$$

it follows that the integration limits can be written as:

$$= \frac{1}{2} \frac{1}{V_L} \int_{V_0}^{\infty} \int_{V_0}^{\infty} [\dots] dV' dV$$

Changing the order of integration yields:

$$= \frac{1}{2} \frac{1}{V_L} \int_{V_0}^{\infty} \int_{V_0}^{\infty} [\dots] dV dV'$$

and, again from $\phi_2(V') = 0$ for $V' < V_0$, the integration limits can be changed to:

$$= \frac{1}{2} \frac{1}{V_L} \int_{V_0}^{\infty} \int_{V'+V_0}^{\infty} [\dots] dV dV'$$

and changing to the new variable $V'' = V - V'$ gives:

$$= \frac{1}{2} \frac{1}{V_L} \int_{V_0}^{\infty} \int_{V_0}^{\infty} [k_{V,a}(V', V'') X_i(V'' + V') \phi_1(V') \phi_2(V'')] dV'' dV'$$

which, since $\phi_1(V') = \phi_2(V') = 0$ for $V' > V_u$, becomes:

$$= \frac{1}{2} \frac{1}{V_L} \int_{V_0}^{V_u} \int_{V_0}^{V_u} [\dots] dV'' dV'$$

Therefore,

$$\begin{aligned} (\dots) &= \frac{1}{2} \frac{1}{V_L} \int_{V_0}^{V_u} \int_{V_0}^{V_u} k_{V,a}(V', V'', \tau) X_i(V'' + V') \\ &\quad F_{V,T}(V', \tau) F_{V,T}(V'', \tau) dV'' dV' \quad \dots (S.53) \end{aligned}$$

which is the desired expression for the agglomeration rate input term.

(e) Agglomeration Output

$$\begin{aligned} &\int_{V_0}^{V_u} X_i(V) \left[- \frac{V_L(\tau)}{[V_L(\tau)]^2} F_{V,T}(V, \tau) \int_{V_0}^{V_u} k_{V,a}(V', V, \tau) F_{V,T}(V', \tau) dV' \right] dV \\ &= - \frac{1}{V_L(\tau)} \int_{V_0}^{V_u} \int_{V_0}^{V_u} k_{V,a}(V', V, \tau) X_i(V) F_{V,T}(V', \tau) F_{V,T}(V, \tau) dV' dV \\ &\quad \dots (S.54) \end{aligned}$$

Combining the agglomeration input and output terms gives for the net agglomeration rate the expression:

(f) Net Agglomeration

$$\frac{1}{V_L(\tau)} \int_{V_0}^{V_u} \int_{V_0}^{V_u} k_{V,a}(V', V'', \tau) \left[\frac{1}{2} X_i(V'' + V') - X_i(V'') \right] F_{V,T}(V', \tau) F_{V,T}(V'', \tau) dV'' dV' \dots (5.55)$$

The possibility of expressing (5.55) in terms of the pseudo moments, $\eta_i(\tau)$, will depend on the functional forms of $k_{V,a}(V', V'', \tau)$ and $X_i(V'')$.

(g) Attrition Input

$$\int_{V_0}^{V_u} X_i(V) \left[\frac{2V_L(\tau)}{V_L(\tau)} \right] \times \int_{V+V_0}^{V_u} k_{V,b}(V', V, V'-V, \tau) \times F_{V,T}(V', \tau) dV' dV$$

$$= 2 \int_{V_0}^{V_u} \int_{V_0}^{V_u} k_{V,b}(V' + V, V, V', \tau) X_i(V) F_{V,T}(V' + V, \tau) dV' dV \dots (5.56)$$

(h) Attrition Output

$$\int_{V_0}^{V_u} X_i(V) \left[- \frac{V_L(\tau)}{V_L(\tau)} \right] \times \int_{V_0}^{V-V_0} k_{V,b}(V, V', V-V', \tau) \times F_{V,T}(V, \tau) dV' dV$$

$$= - \int_{V_0}^{V_u} \int_{V_0}^{V_u} k_{V,b}(V'+V, V, V', \tau) X_i(V'+V) F_{V,T}(V'+V, \tau) dV' dV \dots (5.57)$$

Combining the attrition in and out terms:

(i) Net Attrition

$$\int_{V_0}^{V_u} \int_{V_0}^{V_u} k_{V,b}(V'+V, V, V', \tau) [2 X_i(V) - X_i(V'+V)] F_{V,T}(V'+V, \tau) dV' dV \dots (5.58)$$

As noted, for the growth and agglomeration the feasibility of expressing (5.58) in terms of the pseudo moments, $\eta_i(\tau)$, will depend on the functional forms of $k_{V,b}(V'+V, V, V', \tau)$ and $X_i(V)$.

Collecting terms:

$$\begin{aligned} \frac{d}{d\tau} [\eta_i(\tau)] = & \\ & + G_D(\tau) \int_{V_0}^{V_u} \phi_g(V) F_{V,T}(V, \tau) \frac{d}{dV} [X_i(V)] dV \\ & + V_L(\tau) B F_{\lambda, n}(\tau) \int_{V_0}^{V_u} \phi_n(V) X_i(V) dV \\ & + \frac{1}{V_L(\tau)} \int_{V_0}^{V_u} \int_{V_0}^{V_u} k_{V,a}(V', V'', \tau) F_{V,T}(V', \tau) F_{V,T}(V'', \tau) \\ & \quad [X_i(V''+V') - X_i(V'')] dV'' dV' \\ & + \int_{V_0}^{V_u} \int_{V_0}^{V_u} k_{V,b}(V'+V, V, V', \tau) F_{V,T}(V'+V, \tau) [2X_i(V) - X_i(V'+V)] dV' dV \dots (5.59) \end{aligned}$$

, $i = 1, 2, 3, \dots, mp$

$$\text{I.C. } \eta_i(0) = \eta_{0(i)} \quad (5.60)$$

$$\text{where } \eta_i(\tau) \triangleq \int_{V_0}^{V_u} X_i(V) F_{V,T}(V, \tau) dV$$

Equation (5.59) is the i^{th} equation of the set of mp pseudo moment equations for a batch system with growth, nucleation, agglomeration, and attrition rate processes. The assumptions made in the derivation of this set of equations are the same as those for equation (5.34).

At this point it should be noted that in most cases a major difficulty arises in using these pseudo moment equations. This is because the functional form for $X_i(V'')$ that is 'desirable' for the agglomeration term is 'undesirable' for the growth term and vice versa. That is, when the term $\{\phi_g(V) \times \frac{d}{dV}[X_i(V)]\}$ equals a function of the $X_i(V)$'s the term $\{k_{V,a}(V',V'',\tau) \times [\frac{1}{2}X_i(V''+V') - X_i(V'')]\}$ can most often not be expressed as the product or sum of functions of the $X_i(V)$'s, while if the last condition can be met the first fails for most forms of $X_i(V)$. For example, a suitable form for $X_i(V)$ for the agglomeration term with $k_{V,a} = 1$ is: $X_i(V) = e^{-b_i V}$ where the b_i 's are positive parameters. With this form for $X_i(V)$ the agglomeration term becomes: $\{1 \times [\frac{1}{2} e^{-b_i(V''+V')} - e^{-b_i V''}]\}$ which equals:

$$\{\frac{1}{2} \times (e^{-b_i V''}) \times (e^{-b_i V'}) - (e^{-b_i V''}) \times (1)_{b_1}^* = 0\}$$

This shows that the agglomeration term can be written as the products and sums of the pseudo moments given by:

$$\int_{V_0}^V u e^{-b_i V} F_{V,T} dV$$

Thus for an agglomeration only process with $k_{V,a} = 1$ the population balance equation can be transformed to a set of closed pseudo moment

*To form a product in terms of the pseudo moments for this last term one of the b_i 's must be set to zero.

equations. However, it is seen that the growth rate term, which for $\phi_g(V) = V^{2/3}$, is equal to:

$$\{(V^{2/3}) \times (-b_i) \times (e^{-b_i V})\}$$

cannot be expressed in terms of $\int_{V_0}^{V_u} e^{-b_i V} F_{V,T} dV$ because of the $V^{2/3}$ factor. Other functions for $X_i(V)$, such as $X_i(V) = V^i$, with $\phi_g = V^{2/3}$, and $i = 0, 1/3, 2/3, \dots$, shows that a set of moment equations can be developed for a growth only process without difficulty. The real difficulty, however, is finding a function which is suitable for both growth and agglomeration processes simultaneously with realistic functions for ϕ_g and $k_{V,a}$.

Thus, although the usefulness of equation (5.60) might be limited in obtaining a closed set of pseudo moment equations, it can be used to advantage in the investigation of the constitutive expressions for G_D , $BF_{2,n}$, and $k_{V,a}$. That is, if for a process with negligible attrition the measured values of $F_{V,T}$ are weighted by a function X such that the nucleation and agglomeration term vanish, and the accumulation and growth rate integrals are calculated by numerical quadrature, then the only unknown remaining in equation (5.60) is the function G_D . This allows then for the investigation of and discrimination among different possible functions for G_D by means of a relatively small set of equations. Similarly $k_{V,a}$ and $BF_{2,n}$ can be investigated. Equation (5.60) is used in this context in Chapter 7. A few examples of different functions for $X_i(V)$ are given below.

Case I

$$X_i(V) = 1, \text{ zeroth moment}$$

$$\begin{aligned} \frac{d}{d\tau} \left[\int_{V_0}^{V_u} F_{V,T}(V,\tau) dV \right] &\triangleq \frac{d}{d\tau} [N_T(\tau)] - \\ &+ 0 \\ &+ V_L(\tau) B F_{2,n}(\tau) \int_{V_0}^{V_u} \phi_n(V) dV \\ &- \frac{1}{V_L(\tau)} \int_{V_0}^{V_u} \int_{V_0}^{V_u} k_{V,a}(V',V'',\tau) F_{V,T}(V',\tau) F_{V,T}(V'',\tau) dV'' dV' \\ &+ \int_{V_0}^{V_u} \int_{V_0}^{V_u} k_{V,b}(V'+V,V,V',\tau) F_{V,T}(V'+V,\tau) dV' dV \end{aligned} \quad \dots (5.61)$$

$$\text{I.C. } N_T(0) = N_{T,0} \quad (5.62)$$

Equation (5.61) is the expression for the rate of change of the total number of crystals, $N_T(\tau)$, in a batch system.

Case II

$$X_i(V) = \phi(V)V$$

This represents the first moment with respect to V , where $\phi(V)$ is a function that accounts for the solids density and volume shape factor such that the first moment is equal to the total weight of crystals in a batch system. Thus:

$$\begin{aligned}
& \frac{d}{d\tau} \left[\int_{V_0}^{V_u} \phi(V) V F_{V,T}(V, \tau) dV \right] - \frac{d}{d\tau} [W_T(\tau)] = \\
& + G_D(\tau) \int_{V_0}^{V_u} \phi_g(V) F_{V,T}(V, \tau) \frac{d}{dV} [\phi(V) V] dV \\
& + V_L(\tau) B F_{L,n}(\tau) \int_{V_0}^{V_u} \phi_n(V) \phi(V) V dV \\
& + 0 \\
& + 0
\end{aligned}
\tag{5.63}$$

$$\text{I:C. } W_T(0) = W_{T,0} \tag{5.64}$$

Equation (5.63) is the expression for the rate of change of the total weight of crystals, $W_T(\tau)$, in a batch system. This equation shows that volume (mass) is conserved in the agglomeration and attrition process models; which is in agreement with the concept of these physical processes.

Case III

The two previous cases are examples of commonly used weighting functions which for Case I relates the change of the total number of crystals in a system to the relevant rate processes; and for Case II relates the change of the total crystal weight to the rate processes. The weighting function presented below for Case III is not as common and is an illustration of the general applicability of equation (5.59). The first case allows one to investigate the nucleation rate expression since

that is the only unknown in equation (5.61) given values for $F_{V,T}$ and expressions for the agglomeration and attrition rates, while the second case provides for an investigation of the growth rate expression given that $F_{V,T}$ is known and the nucleation term in equation (5.63) is insignificant in comparison to the other terms in that equation. Case III provides an example of a weighting function which allows for the investigation of the agglomeration rate expression given that $F_{V,T}$ and the growth rate are known and that by particular choice of weighting functions the nucleation term equals zero and that the attrition rate in the process under investigation is relatively insignificant. Such a function is:

$$X_i(V) = C_{1i} V^2 e^{-C_{2i} V}, \quad i = 1, 2, \dots, mp$$

which, when substituted in equation (5.59), gives:

$$\begin{aligned} & \frac{d}{d\tau} \left[\int_{V_0}^{V_u} C_{1i} V^2 e^{-C_{2i} V} F_{V,T}(V, \tau) dV \right] \Delta \frac{d}{d\tau} [\eta_i(\tau)] = \\ & + G_D(\tau) \int_{V_0}^{V_u} \phi_g(V) F_{V,T}(V, \tau) \frac{d}{dV} [C_{1i} V^2 e^{-C_{2i} V}] dV \\ & + V_L(\tau) B F_{l,n}(\tau) \int_{V_0}^{V_u} \phi_n(V) [C_{1i} V^2 e^{-C_{2i} V}] dV \\ & + \frac{1}{V_L(\tau)} \int_{V_0}^{V_u} \int_{V_0}^{V_u} k_{V,a}(V', V'', \tau) F_{V,T}(V', \tau) F_{V,T}(V'', \tau) \times \\ & \quad \left[\frac{1}{2} C_{1i} \times (V' + V'')^2 \times e^{-C_{2i} \times (V' + V'')} - C_{1i} \times (V'')^2 \right. \\ & \quad \left. \times e^{-C_{2i} \times V''} \right] dV' dV'' \end{aligned}$$

.....(cont'd.)

$$\begin{aligned}
 & + \int_{V_0}^{V_u} \int_{V_0}^{V_u} k_{V,b}(V'+V, V, V', \tau) F_{V,T}(V'+V, \tau) \times \\
 & [2C1_i V^2 e^{-C2_i V} - C1_i \times (V'+V)^2 \times e^{-C2_i \times (V'+V)}] dV' dV \quad \dots (5.65)
 \end{aligned}$$

$$\text{I.C. } n_i(0) = n_{i,0}, \quad i = 1, 2, \dots, mp \quad (5.66)$$

Equation (5.65) is the i^{th} equation of a set of mp pseudo moment equations. The vector of parameters $C1$ and $C2$ can be chosen such that a set of equations result which describe the change of the number of particles in particular sections of the size distribution. Moreover, it is possible to choose these parameters so that the nucleation term can be eliminated from the set of equations. Furthermore, by proper choice of these parameters the change in the number of particles in each size range due to agglomeration can be represented by a relatively small set of equations which are still sensitive to the form and parameter values of the agglomeration effectiveness kernel. The vectors $C1$ and $C2$ could be chosen such that instead of a small set of equations only one equation resulted. The gain in ease of solution would, however, be offset by the insensitivity to the agglomeration rate expression. This expression by its very nature of agglomerating in and out of certain sections of the size distribution provides for the possibility of cancellation of negative and positive deviations over parts of the distribution such that a good overall fit is obtained for a poor agglomeration model.

A set of equations for the investigation of the agglomeration rate expression is solved in Chapter 7 where this solution method is explained in greater detail.

5.6 Mass Balances and Auxiliary Relations for the Batch Alumina Trihydrate System

The solution of the population balance equation provides the size distribution of the crystals in the batch crystallizer as a function of batch time. The population balance equation requires, however, constitutive relationships for the kinetic rate processes occurring in the system. These expressions will contain supersaturation as an independent variable which in turn varies with time. Thus it is necessary to obtain simultaneously the concentration of individual components in the solid and liquid phase. This requires solution of the equations which are formulated from the mass balances on each component. These balances are described below along with the required number of empirical relationships needed to ensure the same number of independent equations as system unknowns. Also, the relationship between the population balance and the mass balances is presented. Different sets of equations result depending on the assumptions made.

5.6.1 Mass Balances

The total and component mass balances for the batch alumina trihydrate system are:

(a) Total Mass Balance

$$\frac{d}{d\tau} [V_L \rho_L + W_T + V_S \sum_{i=1}^{k_p} CP_{s(i)}] = 0 \quad (5.67)$$

(b) Alumina Component Mass Balance

$$\frac{d}{d\tau} [V_L CA + .654 W_T] = 0 \quad (5.68)$$

(c) Caustic Component Mass Balance

$$\frac{d}{d\tau} [V_L CN] = 0 \quad (5.69)$$

(d) Water Component Mass Balance

$$\frac{d}{d\tau} [V_L CH + .346 W_T] = 0 \quad (5.70)$$

(e) Impurities Component Mass Balances

$$\frac{d}{d\tau} [V_L CP_{L(i)} + V_S CP_{s(i)}] = 0 \quad (5.79)$$

$$i = 1, 2, \dots, k_p$$

where k_p denotes the number of impurities.

The concentration of a component in solution is traditionally expressed as mass per unit solution volume, e.g. grams per liter. The concentration of the aluminum element or ion, Al^{3+} , in solution is commonly expressed as grams alumina, Al_2O_3 , per liter, while the sodium ion, Na^+ , is either expressed as grams sodium carbonate, Na_2CO_3 , or as grams

sodium oxide, Na_2O , per liter solution. To comply with existing constitutive relations, the caustic concentration is expressed in this work as sodium oxide. Note that, 1 gpl $\text{Na}_2\text{O} = 1.712$ gpl Na_2CO_3 . The 0.654 and 0.346 factors account for the stoichiometry of the chemical reaction, that is, 0.654 is the mass fraction of the solid alumina trihydrate, W_T , which is alumina; while 0.346 is the fraction of water in alumina trihydrate. The mass balances on the impurities need to be included and the equations solved if in fact impurities are present and some or all of these impurities affect the constitutive relations of the system, such as for instance solution density, solubility, growth, and nucleation rate.

5.6.2 Auxiliary and Empirical Relationships

An auxiliary relation for this system is the relationship between total slurry and solution volume, i.e.

$$V_T = V_L + W_T/\rho_S \quad (5.72)$$

while the solution density can be calculated from the following empirical correlation which was developed by Misra (m2).

$$\rho_L = 1.051 + (9.92 \times 10^{-4} - 1.1 \times 10^{-7} \times \text{CN}) \text{CN} \\ + 5.66 \times 10^{-4} \times \text{CA} + (-9.4 \times 10^{-4} + 5.1 \times 10^{-6} \times \theta) \theta \dots (5.73)$$

Misra (m4) also developed a semi-empirical relationship for alumina solubility in a system where impurities are absent; it is

$$CA_e = CN \times \exp\left\{6.2106 + \frac{(1.08753 \times CN) - 2486.7}{273.16 + \theta}\right\} \quad (5.74)$$

5.6.3 Relationships Between Population Balance and Mass Balances

The direct relationship between the mass balances and the population balance, that is, the number density function, is given by the following two equations:

(1) The relationship between the number density function, $F_{V,T}$, and the total solids weight at any instant is obtained by multiplying $F_{V,T}$ by $(\phi(V) \times V)$ and integrating over all crystal sizes, viz.:

$$W_T(\tau) = \int_{V_0}^{V_u} \phi(V) \cdot V F_{V,T}(V, \tau) dV \quad (5.75)$$

(2) The relationship between the rate of change of the total mass of solids with respect to time and the number density function is given by:

$$\begin{aligned} \frac{d}{d\tau}[W_T(\tau)] = & G_D(\tau) \int_{V_0}^{V_u} \phi_g(V) F_{V,T}(V, \tau) \frac{d}{dV} [\phi(V)V] dV \\ & + V_L(\tau) B F_{2,n}(\tau) \int_{V_0}^{V_u} \phi_n(V) \phi(V) V dV \quad \dots\dots(5.76) \end{aligned}$$

Thus, W_T can be calculated once the population balance equation has been solved and, therefore, is not an unknown in the 4+kp mass balance equations. However, there are still only 4+kp equations for 5+kp unknowns;

which indicates that an additional independent relationship or condition is required. An example of a realistic condition is the approximation of constant batch suspension volume, while an example of a relationship for a "pure" system is given by the solution density model which eliminates the unknown ρ_2 . Each of these possibilities are discussed in turn in the subsequent sub-sections.

5.6.4 Number of Independent Mass Balance Equations

A closer examination of the mass balance equations reveals that the sum of equations (5.68) to (5.71) is equal to equation (5.67). That is, $V_L CA + V_L CN + V_L CH + V_L \sum_{i=1}^{kp} CP_{2(i)} = V_L \rho_2$. This indicates that the $4+kp$ equations are not an independent set and that only $3+kp$ equations need to be solved. The equation which is usually eliminated from the set is the water component mass balance. Furthermore, it is shown below that for this batch system, it is not necessary to solve the set of $3+kp$ ordinary differential equations, but that it is only necessary to solve a set of $3+kp$ algebraic equations.

Equations (5.67) to (5.71) are differentials which can be integrated over any time interval. For instance, integrating

$$\frac{d}{dt} [V_L \rho_2 + W_T + V_S \sum_{i=1}^{kp} CP_{s(i)}] = 0$$

from state I to II gives:

$$\begin{aligned} & V_L(II)\rho_2(II) + W_T(II) + V_S(II) \sum_{i=1}^{kp} CP_{s(i)}(II) - V_L(I)\rho_2(I) \\ & - W_T(I) - V_S(I) \sum_{i=1}^{kp} CP_{s(i)}(I) = 0 \end{aligned}$$

where state I could be zero time and state II any other batch time.

That is,

$$\begin{aligned}
 & V_L(\tau) \rho_L(\tau) + W_T(\tau) + V_S(\tau) \sum_{i=1}^{kp} CP_{S(i)}(\tau) \\
 & = V_L(0) \rho_L(0) + W_T(0) + V_S(0) \sum_{i=1}^{kp} CP_{S(i)}(0) \quad \dots (5.77)
 \end{aligned}$$

The zero denotes initial condition values. In a similar manner, equations (5.68) to (5.71) are reduced to the following algebraic equations:

$$V_L(\tau) CA(\tau) + .654 W_T(\tau) = V_L(0) CA(0) + .654 W_T(0) \quad (5.78)$$

$$V_L(\tau) CN(\tau) = V_L(0) CN(0) \quad (5.79)$$

$$V_L(\tau) CP_{L(i)}(\tau) + V_S(\tau) CP_{S(i)}(\tau) = V_L(0) CP_{L(i)}(0) + V_S(0) CP_{S(i)}(0) \quad \dots (5.80)$$

Thus these $3+kp$ algebraic equations can be solved for the $3+kp$ unknowns given that the initial conditions are known and $W_T(\tau)$ has been obtained from the solution of the population balance equation. Here, the $3+kp$ unknowns are: $CA(\tau)$, $CN(\tau)$, $V_L(\tau)$ or $V_S(\tau)$, and $CP_{S(i)}(\tau)$ where $i = 1, 2, \dots, kp$.

5.6.5 Mass Balances for a Batch Alumina Trihydrate System with Approximate Constant Suspension Volume

For relatively dilute suspensions, small differences between solids and solution phase densities, and low supersaturations, it is reasonable to assume that the crystallizer suspension volume remains essentially constant during the crystallization process. Therefore, for $\frac{d}{dt} V_T(\tau) = 0$ and neglecting impurities, the mass balances that need to be solved simultaneously with the population balance equation are given by the following set of explicit algebraic equations (obtained from equations (5.67) to (5.75))

$$W_T(\tau) = \int_{V_o}^V \phi(V) V F_{V,T}(V, \tau) dV \quad (5.75)$$

$$V_L(\tau) = V_{L,o} + [W_{T,o} - W_T(\tau)]/\rho_s \quad (5.81)$$

$$CA(\tau) = [V_{L,o} CA_o + .654 W_{T,o} - .654 W_T(\tau)]/V_L(\tau) \quad (5.82)$$

$$CN(\tau) = [V_{L,o} CN_o]/V_L(\tau) \quad (5.83)$$

The zero subscript variables are the minimum number of initial conditions that need to be specified to define the batch system at the beginning of the batch process. The assumption of constant suspension volume also eliminates the need of having to develop an empirical solution density model. Also, note that $W_{T,o}$ can be calculated from:

$$W_{T,o} = \int_{V_o}^V \phi(V) V F_{V,T,o}(V) dV \quad (5.75)$$

Therefore, to initialize this batch system only the following variables need to be specified: $F_{V,T,0}(V)$, $V_{L,0}$, CA_0 , and CN_0 .

5.6.6 Mass Balances for a Batch Alumina Trihydrate System with a Given Empirical Solution Density Correlation

When the assumption of constant suspension volume cannot be made, then it is necessary to develop a solution density model which is a function of the concentration of components in solution and of the solution temperature. Given such a relationship the following set of implicit algebraic mass balance equations results:

$$W_T(\tau) = \int_{V_0}^V \phi(V) V F_{V,T}(V,\tau) dV \quad (5.75)$$

$$\rho_2(\tau) = \phi_0(CA, CN, CP_{2,i}, \theta) \quad (5.84)$$

$$V_L(\tau) = [V_{L,0} \rho_{2,0} + W_{T,0} - W_T(\tau)] / \rho_2(\tau) \quad (5.85)$$

$$CA(\tau) = [V_{L,0} CA_0 + .654 W_{T,0} - .654 W_T(\tau)] / V_L(\tau) \quad (5.82)$$

$$CN(\tau) = [V_{L,0} CN_0] / V_L(\tau) \quad (5.83)$$

Similar equations may be formulated for the impurities.

This set of equations can be transformed to an explicit set by incorporating the particular functional form of ρ_2 . For a 'pure' alumina trihydrate solution, Misra's equation (5.75) has been demonstrated to give a satisfactory representation of solution density with component

concentrations and temperature. If this equation is substituted into equation (5.67) the following set of explicit algebraic equations representing the mass balances may be derived:

$$W_T(\tau) = \int_{V_0}^{V_u} \phi(V) V F_{V,T}(V,\tau) dV \quad (5.75)$$

$$V_L(\tau) = \{ (C2 - W_T(\tau)) + [(C2 - W_T(\tau))^2 + (4 \times C1 \times C3)]^{1/2} \} / (2 \times C1) \quad (5.86)$$

$$CA(\tau) = [C4 - .654 W_T(\tau)] / V_L(\tau) \quad (5.87)$$

$$CN(\tau) = C5 / V_L(\tau) \quad (5.88)$$

The functions C1 to C5 are calculated from the initial conditions, namely:

$$C1(\tau) = 1.587715 \times [1051. + (.0051 \times \theta(\tau) - .94) \times \theta(\tau)] \quad (5.89)$$

$$C2 = 1.587715 \times \{ V_{L,0} \times [(\rho_{L,0} \times 1000.) - (.992 \times CN_0) - (.566 \times CA_0)] \} + W_{T,0} \quad (5.90)$$

$$C3 = 1.746486 \times 10^{-4} \times [V_{L,0} \times CN_0]^2 \quad (5.91)$$

$$C4 = (V_{L,0} \times CN_0) + (.654 \times W_{T,0}) \quad (5.92)$$

$$C5 = V_{L,0} \times CN_0 \quad (5.93)$$

For a non-isothermal operation, the temperature, θ , would vary with time and would have to be calculated simultaneously from an energy balance for this alumina trihydrate batch system. Note, the initial conditions, $W_{T,0}$ and $\rho_{L,0}$ are not specified but calculated from the following initially specified variables:

$$W_{T,0} = \int_{V_0}^{V_u} \phi(V) V F_{V,T,0}(V) dV \quad (5.75)$$

$$\rho_{L,0} = 1.051 + (9.92 \times 10^{-4} - 1.1 \times 10^{-7} \times CN_0) CN_0 \\ + 5.66 \times 10^{-4} \times CA_0 + (-9.4 \times 10^{-4} + 5.1 \times 10^{-6} \times \theta) \theta \quad (5.73)$$

Thus to initialize the system the following variables need to be specified:

$$F_{V,T,0}, V_{L,0}, CA_0, CN_0, \theta_0$$

5.6.7 Mass Balances for a Batch Alumina Trihydrate System with a Given Empirical Alumina Concentration Model

If one could predict the decrease in dissolved alumina concentration with time (say with some empirical model for the batch crystallizer operating under specified conditions) and also had an empirical expression relating density to system variables, then the performance of the batch crystallizer could be predicted. This would follow from the solution of the mass balance equations without recourse to the population, energy and momentum balance equations. Thus, given an empirical relationship which relates alumina concentration with time and an expression which relates solution density to solute concentrations (as, for example, presented by Misra (m2)) the following system of equations can be developed:

$$CA(\tau) = \phi_1(\tau, \theta) \quad (5.94)$$

$$CN(\tau) = \{-C3 + \{(C3)^2 - 4 \times C2 \times [CA(\tau) - .654 \times (1051. + CA(\tau) + C1)]\}^{1/2}} / (2 \times C2) \quad (5.95)$$

$$V_L(\tau) = V_{L,0} CN_0 / CN(\tau) \quad (5.96)$$

$$W_T(\tau) = \{[(V_{L,0} \times CA_0) - (V_{L,0} \times CN_0 \times CA(\tau) / CN(\tau))] / .654\} + W_{T,0} \quad (5.97)$$

where $C1 = (.0051 \theta(\tau) - .94)\theta(\tau)$

$$C2 = .654 \times .00011$$

$$C3 = .654 \times [1051./CN_0 - .00011 CN_0 + .566 CA_0 / CN_0 + C1 / CN_0] - CA_0 / CN_0$$

$V_{L,0}$, $W_{T,0}$, CA_0 , CN_0 , and θ_0 are initially specified variables.

From the above set of equations the crystallizer production rate, $W_T(\tau)$, can be calculated without, as mentioned, having to solve simultaneously the population, energy, and momentum balance. The advantage of not having to solve these equations in this model scheme is offset by

the disadvantage of not being able to predict the other important process variable, namely, the crystal size distribution. This solution scheme is applied in Chapter 7, Section 7.3.1.

CHAPTER 6

NUMERICAL SOLUTION OF THE MECHANISTIC BATCH CRYSTALLIZATION MODEL

6.1 Introduction

As shown in Chapter 5, the mechanistic model for a batch crystallizer involving nucleation, growth, agglomeration and attrition leads to a non-linear, integro-partial differential equation for the size distribution function, F_V . This equation is rather complex and, in general, is difficult to solve. Indeed, except for very special situations, the solution can only be effected by numerical methods. Since these numerical methods are approximations which can lead to inaccurate solutions if some care is not exercised and at the same time they may require excessive computer time, this difficult numerical problem requires considerable study and effort. The reward for this effort is considerable since not only is the crystal production rate, but also the size distribution, predicted as a function of time. Thus, the effect of controlled operating variables on all aspects of the performance of the crystallizer may be determined. In addition, the fundamental kinetic rate models together with their rate constants for the growth, nucleation, agglomeration and attrition can only be determined if the size distribution for the crystals at any instant is known. This fundamental information arises however at the expense of complexity and difficulties associated with the solution of the mathematical problem.

In this chapter, the solution of the crystallizer model equations is presented, including the method of solution of the integro-partial

differential equation. Specifically, the following topics are covered: a summary of the set of equations in the crystallizer model which must be solved, a review of the solutions which have been reported in the current literature, a number of different ways that the integro-partial differential equation was solved by the author; with their advantages, disadvantages and shortcomings, and finally, the strategy and numerical solution which was adopted for the crystallizer problem at hand. Since the population balance equation has widespread application, a general solution for this equation should have considerable interest here and in related fields.

6.2 Mechanistic Model for the Batch Crystallization of Alumina Trihydrate

The mathematical model for the batch crystallization of pure alumina trihydrate from a supersaturated solution of sodium aluminate consists of the following non-linear integro-partial differential equation and a set of explicit algebraic equations. These equations were derived and discussed in Chapter 5. They are repeated here as a set to allow a quick overview.

A. Conservation Equations

The conservation equations for the crystallization process are:

A1. Population Balance

$$\underbrace{\frac{\partial}{\partial \tau} H_T(V, \tau)}_{\text{accumulation}} + \underbrace{G_D(\tau) \phi_g(V)}_{\text{growth}} \frac{\partial}{\partial V} H_T(V, \tau) =$$

$$\begin{aligned}
& + \underbrace{\{V_L(\tau) BF_{V,\ell,n}(V,\tau,H_T)\}}_{\text{nucleation}} \\
& + \underbrace{\{V_L(\tau) BF_{V,\ell,a}(V,\tau,H_T)\}}_{\text{agglomeration in}} \\
& + \underbrace{\{V_L(\tau) DF_{V,\ell,a}(V,\tau,H_T)\}}_{\text{agglomeration out}} \\
& + \{\text{attrition term which is compounded in the nucleation} \\
& \quad \text{and agglomeration term}\} \quad (\text{number/h}) \quad \dots\dots(6.1)
\end{aligned}$$

$$\text{I.C. } H_T(V,0) = H_{T,0}(V) \quad (6.1a)$$

$$\text{B.C. } H_T(V_0,\tau) = 0 \quad (6.1b)$$

A2. Mass Balances

- Number-Mass Equality

$$W_T(\tau) = \int_{V_0}^{V_u} \phi(V) V F_{V,T}(V,\tau) dV \quad (\text{g}) \quad (6.2)$$

- Solution Volume*

$$\begin{aligned}
V_L(\tau) = & \{(C_2 - W_T(\tau)) + [(C_2 - W_T(\tau))^2 + \\
& (4 C_1 C_3)]^{1/2}\} / (2 C_1) \quad (\ell) \quad (6.3)
\end{aligned}$$

*This equation is conditional on the correctness of the solution density correlation as given by Misra (m2).

- Alumina Concentration

$$CA(\tau) = \{C4 - .654 W_T(\tau)\} / V_L(\tau) \text{ (g Al}_2\text{O}_3\text{/l sol.)} \quad (6.4)$$

- Caustic Concentration

$$CN(\tau) = CS / V_L(\tau) \text{ (g Na}_2\text{O/l sol.)} \quad (6.5)$$

- Impurities Concentration

For this work no mass balances are required to account for the impurities since chemically-pure alumina trihydrate and caustic were used and hence the impurity level was negligible.

In the above equations, the following functions pertain:

$$C1(\theta)^* = 1.5877\{1051 + (-.94 + (.0051\theta))\theta\} \quad (6.6)$$

$$C2 = 1.5877\{V_{L,o}(C6 - .992 CN_o - .566 CA_o)\} + W_{T,o} \quad (6.7)$$

$$C3 = 1.7465 \times 10^{-4} (V_{L,o} CN_o)^2 \quad (6.8)$$

$$C4 = V_{L,o} CN_o + .654 W_{T,o} \quad (6.9)$$

$$C5 = V_{L,o} CN_o \quad (6.10)$$

$$C6 = 1051 + .992 CN_o - .00011 CN_o^2 + .566 CA_o - .94 \theta_o + .0051 \theta_o^2 \quad (6.11)$$

*For an isothermal batch system C1 is a constant.

The 0 subscript denotes initial condition values.

A3. Energy Balance

An energy balance is not required here since all batch runs were carried out under isothermal conditions, therefore for batch p:

$$\theta_p(\tau) \approx \theta_{p,0} \text{ for all } \tau. \quad (6.12)$$

A4. Momentum Balance

A momentum balance is also not required because all runs were performed under identical agitation conditions. As a consequence, it is expected that the crystallization phenomena were influenced to the same extent throughout this study by liquid shear forces and particle-particle interaction. The effect of agitation on the crystallization process is of considerable importance and should be investigated.

B. Constitutive Relationships

The relationships which are presented below are shown in Chapter 7 to represent the kinetic behaviour of the alumina crystallization system quite well. The development of these relationships and the evaluation of the parameters contained within them is presented in Chapter 7.

B1. Growth Rate Kinetics

As discussed in Chapters 2 and 5, it is reasonable to represent volumetric growth rate by the product of a linear growth rate factor and a factor relating these two rates, viz.:

$$G_V(V, \tau) = G_D(\tau) \phi_g(V) \quad (\mu\text{m}^3/\text{h}) \quad (6.13)$$

where the linear growth rate, G_D , may be represented by a power law function of supersaturation

$$G_D(\tau) = BG_1(\theta) \Delta CA(\tau)^{BG_2} \quad (\mu\text{m}/\text{h}) \quad (6.14)$$

Other rate expressions as discussed and presented in Chapter 2 may be used as well. If it is assumed that the characteristic length of the crystal is the spherical volume equivalent diameter, then

$$\phi_g(V) = \frac{1}{2} \pi^{1/3} 6^{2/3} V^{2/3} \quad (\mu\text{m}^2) \quad (6.15)$$

On the other hand, if the volume-surface area relationship obtained from data published by Scott (gl) is valid, then:

$$\phi_g(V) = \frac{\pi D^2}{2} \psi(D) \quad (\mu\text{m}^2) \quad (6.16)$$

where D = diameter of a sphere with same volume as the particle
 ψ = Scott's angularity factor (correlated by equation (2.39))

It is to be noted that equation (6.13) assumes that the growth rate is independent of the selected linear growth rate variable, that is, McCabe's ΔL law pertains. If this is not the case, then equation (6.14) may be modified as follows:

$$G_D(\tau, D) = BG1(\theta) \Delta CA(\tau)^{BG2} \phi_D(D) \quad (\mu\text{m/h}) \quad (6.17)$$

where ϕ_D is a function that accounts for the dependence of the linear growth rate on some characteristic linear dimension of the growing crystals.

B2. Nucleation Rate Kinetics

Again, as discussed in Chapter 2, the nucleation rate is usually expressed as the product of two factors, viz.:

$$BF_{V,\ell,n}(V, \tau) = BF_{\ell,n}(\tau) \phi_n(V) \quad (6.18)$$

where $BF_{\ell,n}(\tau)$ expresses the dependence of nucleation on system conditions and $\phi_n(V)$ indicates the probability of a new nuclei being of size V .

Typical functional relationships are:

- (a) a power law relationship for $BF_{\ell,n}(\tau)$ (number $\text{h}^{-1}(\ell \text{ sol.})^{-1}$):

$$BF_{\ell,n}(\tau) = BN1(CA(\tau) - CA_e(\tau))^{BN2} \quad (6.19)$$

- (b) a log-normal function for $\phi_n(V)$ (μm^{-1}):

$$\phi_n(V) = \frac{1}{BN4\sqrt{2\pi} V} e^{-\frac{1}{2(BN4)^2} (\ln V - BN5)^2} \quad (6.20)$$

B3. Agglomeration Rate Kinetics

As shown in Chapter 5, a reasonable model to express the agglomeration rate is:

$$BF_{V,\ell,a}(V,\tau,H_T) = \frac{1}{(V_L(\tau))^2} \int_{V_0}^{V/2} \int_{V'}^{V-V'} k_{V,a}(V',V'',\tau) F_{V,T}(V',\tau) F_{V,T}(V'',\tau) dV'' dV' \quad (\text{number } h^{-1}(\ell \text{ sol.})^{-1})$$

.....(6.21)

$$DF_{V,\ell,a}(V,\tau,H_T) = \frac{1}{(V_L(\tau))^2} \int_{V_0}^V \int_{V_0}^{V-u} k_{V,a}(V',V'',\tau) F_{V,T}(V',\tau) F_{V,T}(V'',\tau) dV'' dV' \quad (\text{number } h^{-1}(\ell \text{ sol.})^{-1})$$

.....(6.22)

where $F_{V,T}(V,\tau) = \frac{\partial}{\partial V} H_T(V,\tau) \quad (\text{number } \mu\text{m}^{-1}) \quad \text{.....(6.23)}$

The function, $k_{V,a}$, accounts for the effect of operating conditions (e.g. supersaturation) and the efficiency of agglomeration when particles of different size contact each other (the effect of crystal size on the agglomeration rate). One possible form for this kinetic rate constant is:

$$k_{V,a}(V',V'',\tau) = BA1 \sigma^{BA2} \phi_{V,a}(V',V'') \quad (\text{number}^{-1} h^{-1} \ell \text{ sol.})$$

.....(6.24)

where the size dependent factor could have a form which indicates that the agglomeration process occurs more readily with smaller particles, viz.:

$$\phi_{V,a}(V',V'') = \{(V')^{1/3} + (V'')^{1/3}\}^2 |(V')^{2/3} - (V'')^{2/3}| e^{-BA3\{(V')^{2/3} + (V'')^{2/3}\}} \quad \text{.....(6.25)}$$

This functional relationship can account (through parameter BA3) for the observation in practice that larger crystals of alumina trihydrate do not agglomerate as readily as smaller ones. Moreover, as discussed earlier, the parameter $k_{V,a}$ should depend on the crystallization apparatus and the degree of agitation within it.

B4. Attrition Rate Kinetics

In Chapter 2, it was shown that when dealing with the population balance of crystal sizes, the attrition or crystal break-up process had to be considered. This process probably occurs to some extent in any mixed suspension system. Unfortunately, if it occurs simultaneously with agglomeration, it is only the net effect of attrition and agglomeration which can be measured for any particular crystal size; hence the attrition process is confounded by the agglomeration process. In this crystallizer system, the agitation in the system was designed to minimize attrition as much as possible while still maintaining a homogeneous suspension. Consequently, because attrition is relatively small, modelling of the attrition process was not attempted.

C. Empirical Correlations

The empirical correlations which are required for this crystallization system are the following:

C1. Solute Solubility

The equation used in this work was developed by Misra (m4); it is:

$$CA_e = CN \exp\left\{6.2106 + \frac{(1.08753 CN - 2486.7)}{273.16 + \theta}\right\} \text{ (g Al}_2\text{O}_3\text{/l sol.)} \quad \dots (6.26)$$

This correlation is only valid for pure sodium aluminate solutions, while its ranges of applicability are:

$$\begin{aligned} \theta & 25 + 100^\circ\text{C} \\ CN & 30 + 320 \text{ g Na}_2\text{O/l sol.} \end{aligned}$$

During the course of this study this equation was checked from time to time and found to be satisfactory (Table 4.2.1-A).

C2. Solution Density

Misra (m2) also developed a correlation relating solution density to aluminate and caustic concentrations and temperature. This correlation is:

$$\begin{aligned} \rho_l = & 1.051 + 9.92 \times 10^{-4} CN - 1.1 \times 10^{-7} CN^2 + 5.66 \times 10^{-4} CA - \\ & 9.4 \times 10^{-4} \theta + 5.1 \times 10^{-6} \theta^2 \quad \text{(g/cm}^3\text{)} \quad \dots (6.27) \end{aligned}$$

It is valid over the ranges of:

$$\begin{aligned} \theta & 20 + 100^\circ\text{C} \\ CN & 50 + 250 \text{ g Na}_2\text{O/l sol.} \\ CA & 15 + 300 \text{ g Al}_2\text{O}_3\text{/l sol.} \end{aligned}$$

A number of spot checks of this correlation indicated that it was quite satisfactory. Equation (6.27) is not required explicitly in this model solution, but it is needed to develop an explicit set of algebraic equations for the mass balances.

C3. Crystal Geometry Relationships

The function, $\phi(V)$, which is needed in the number mass equality (equation (6.2)), is given by:

$$\phi(V) = \rho_s \times 10^{-2} \times \psi_{VV} \quad (\text{g/cm}^3) \quad (6.28)$$

where ρ_s - solids density which for Gibbsite equals 2.42 g/cm^3
 ψ_{VV} - measured to 'true' crystal volume relationship
 (dimensionless)
 10^{-12} - dimensions conversion factor ($\text{cm}^3/\mu\text{m}^3$)

The value of 1.0 is used in this study for ψ_{VV} . This is probably a good approximation since for this work $F_{V,T}$ was obtained from Coulter Counter measurements which measures crystal volume directly. Therefore, $\phi(V)$ is independent of V and equal to 2.42×10^{-12} .

The other geometric relationship needed in this work is a function which relates measured crystal volume to crystal surface area. This need arises because the overall crystal growth phenomena is related to crystal surface area. In the population balance equation, this surface area must be related to crystal volume. The function is denoted here by ϕ_g (equation (6.12)). A detailed discussion on this function is contained in Appendix D.

The equations presented in this sub-section constitute a complete model for the batch crystallization of alumina trihydrate. The model is subject to those assumptions expressed here and in Chapter 5. These equations are presented in summary form in Table 6.2-A.

TABLE 6.2-A Summary of Model EquationsInitial Conditions

$$F_{V,T}(V,o), V_{L,o}, CA_o, CN_o, \theta_o$$

Constants

$$\theta = \theta_o$$

$$W_{T,o} = 2.42 \times 10^{-12} \int_{V_o}^{V_u} V F_{V,T}(V,o) dV$$

$$C6 = 1051 + (.992 - .00011)CN_o + .566 CA_o + (.0051 \theta_o - .94)\theta_o$$

$$C5 = V_{L,o} CN_o$$

$$C4 = C5 + .654 W_{T,o}$$

$$C3 = 1.7465 \times 10^{-4} (C5)^2$$

$$C2 = 1.5877 \{ V_{L,o} (C6 - .992 CN_o - .566 CA_o) \} + W_{T,o}$$

$$C1 = 1.5877 \{ 1051 + (-.94 + .0051 \theta) \theta \}$$

Mass Balances

$$W_T(\tau) = 2.42 \times 10^{-12} \int_{V_o}^{V_u} V F_{V,T}(V,\tau) dV$$

.....(cont'd.)

TABLE 6.2-A (cont'd.)

$$V_L(\tau) = \{(C2 - W_T) + ((C2 - W_T)^2 + (4 C1 C3))^{1/2}\} / (2 C1)$$

$$CA(\tau) = (C4 - .654 W_T) / V_L$$

$$CN(\tau) = C5 / V_L$$

Empirical Correlation

$$CA_e(\tau) = CN \exp\left\{6.2106 + \frac{1.08753 CN - 2486.7}{273.16 + \theta}\right\}$$

Crystal Volume - Area Relationship

$$\phi_g(V) = \frac{1}{2}\pi^{1/3} 6^{2/3} V^{2/3}$$

Constitutive Relations

$$G_D(\tau) = BG1(CA - CA_e)^{BG2}$$

$$BF_{V,\ell,n}(V,\tau) = \{BN1(CA - CA_e)^{BN2}\} \left\{ \frac{1}{BN4 \sqrt{2\pi} V} e^{-\frac{1}{2} \left(\frac{\ln V - BN3}{BN4} \right)^2} \right\}$$

$$BF_{V,\ell,a}(V,\tau,H_T) = \frac{1}{V_L^2} \int_{V_0}^{V/2} \int_{V_0}^{V-V'} k_{V,a}(V',V'',\tau) F_{V,T}(V',\tau) F_{V,T}(V'',\tau) dV'' dV'$$

$$DF_{V,\ell,a}(V,\tau,H_T) = \frac{1}{V_L^2} \int_{V_0}^V \int_{V_0}^{V-V'} k_{V,a}(V',V'',\tau) F_{V,T}(V',\tau) F_{V,T}(V'',\tau) dV'' dV'$$

with $F_{V,T}(V',\tau) = \frac{\partial H_T(V,\tau)}{\partial V} / V'$

$$k_{V,a}(V',V'',\tau) = \{BA1 \sigma^{BA2}\} \{(V')^{1/3} + (V'')^{1/3}\}^2 \{(V')^{2/3} - (V'')^{2/3}\} \\ \times e^{-BA3\{(V')^{2/3} + (V'')^{2/3}\}}$$

.....(cont'd.)

TABLE 6.2-A (cont'd.)

Population Balance

$$\frac{\partial}{\partial \tau} H_T(V, \tau) + G_D(\tau) \phi_g(V) \frac{\partial}{\partial V} H_T(V, \tau) = V_L(\tau) \{ BF_{V, \ell, n}(V, \tau) \\ + BF_{V, \ell, a}(V, \tau, H_T) \\ - DF_{V, \ell, a}(V, \tau, H_T) \}$$

with I.C. $H_T(V, 0) = H_{T, 0}(V)$

B.C. $H_T(V_0, \tau) = 0$

6.3 Solution of the Model Equations

6.3.1 General

The solution of the model equations summarized in Table 6.2-A provides the desired model response. Solution of the model is in essence effected by solving the population balance. The ease or difficulty in solving the population balance equation depends on the choice of the constitutive equations. The particular choice of the agglomeration model transforms the partial differential equation into an integro-partial differential equation. In addition, the integro part has the special characteristic in that one of the integrals is a convolution integral.

6.3.2 Solution of the Population Balance Equation

Substitution of the agglomeration rate terms into the population balance results in the following non-linear integro-partial differential equation:

$$\begin{aligned} \frac{\partial}{\partial \tau} F_{V,T}(V,\tau) + G_D(\tau) \frac{\partial}{\partial V} \phi_g(V) F_{V,T}(V,\tau) - \\ + V_L(\tau) B F_{2,n}(\tau) \phi_n(V) \\ + \frac{1}{V_L(\tau)} \int_{V_0}^{V/2} k_{V,a}(V',V-V',\tau) F_{V,T}(V',\tau) F_{V,T}(V-V',\tau) dV' \\ - \frac{1}{V_L(\tau)} F_{V,T}(V,\tau) \int_{V_0}^{V_u} k_{V,a}(V,V',\tau) F_{V,T}(V',\tau) dV' \dots (6.29a) \end{aligned}$$

$$\text{I.C. } F_{V,T}(V,0) = F_{V,T,0}(V)$$

$$\text{B.C. } F_{V,T}(V_0,\tau) = 0$$

or written in terms of the cumulative number distribution function this equation is:

$$\begin{aligned}
 & \frac{\partial}{\partial \tau} H_T(V, \tau) + G_D(\tau) \phi_g(V) \frac{\partial}{\partial V} H_T(V, \tau) - \\
 & + V_L(\tau) B F_{l,n}(\tau) \int_{V_0}^V \phi_n(V') dV' \\
 & - \frac{1}{V_L(\tau)} \int_{V_0}^{V/2} \int_{V'}^{V-V'} k_{V,a}(V', V'', \tau) F_{V,T}(V', \tau) F_{V,T}(V'', \tau) dV'' dV' \\
 & - \frac{1}{V_L(\tau)} \int_{V_0}^V \int_{V_0}^u k_{V,a}(V', V'', \tau) F_{V,T}(V', \tau) F_{V,T}(V'', \tau) dV'' dV' \\
 & \dots (6.29b)
 \end{aligned}$$

$$\text{I.C. } H_T(V, 0) = H_{T,0}(V)$$

$$\text{B.C. } H_T(V_0, \tau) = 0$$

Thus, to effect the model solution either equation (6.29a) or, alternatively, equation (6.29b) must be solved.

6.3.2.1 Survey of Previous Solutions of the Population Balance Equation

Considerable effort has been expended over the years in finding a solution of the population balance equation in its application to a number of different natural processes. Drake (d1,d2,h5) has examined this problem in great detail. In these references are presented some of his own work and an extensive literature survey summarizing the work of others. In his reviews he considered the following points:

- "- What are the various mathematical models proposed for determining the size spectra as functions of time?

- Are these models well posed with respect to such properties as the existence and uniqueness of solutions, the continuity of solutions with respect to the initial and boundary conditions and physical parameters of the system, the boundedness of solutions, and the positiveness of solutions?
- What are the proper choices of the physical parameters and the initial conditions in the various models?
- What is the time evolution of the power moments of the size spectrum?
- What exact solutions are known?
- What approximate solution techniques are known?"

One of Drake's main conclusions was that in the general case equation (6.29) can only be solved successfully by using numerical techniques which require large high speed computers. This is a generally well known fact. Since in this work the general case is considered it was recognized at the outset that equation (6.29) would need to be solved by numerical techniques. Although, several numerical schemes are presented in the literature (m10, b9, r4, p2, r9, s7), a particular method was developed for this study since none of the schemes had the flexibility of solution desired, and indeed required here. This flexibility requires that the method of solution be:

- (a) independent of the functional form of the agglomeration kernel;
- (b) suitable for any shape of size distribution;
- (c) applicable to the equation when it contains both growth and agglomeration acting together, along with nucleation.

6.3.2.2 Initial Investigation of Different Numerical Solutions

The numerical solution requires that starting from the initial distribution the function $F_{V,T}$ or H_T be evaluated at a sufficient number of two-dimensional grid points (independent variables V and τ) so that the continuous function $F_{V,T}$ or H_T be adequately represented by discrete approximations. A general type of 'marching forward' technique necessitates the repeated calculation of two quantities: (i) the agglomeration integrals and (ii) the growth partial differential, both at a sufficient number of discrete particle volumes V for each time step τ . The calculation of the agglomeration integrals is a time consuming process due to the convolution form of one of the integrals. This property results from the very characteristic of agglomeration, namely: that each particle has an opportunity to interact with any other particle in the crystallizer. Thus, in essence, the integration keeps track of all the particles in the crystallizer and this explains the laborious calculation involved. Moreover, this evaluation of the integral needs to be repeated a great number of times due to the relatively fast changing size distribution which has been observed with this crystallizing system. Thus, it is essential that the numerical evaluation of the agglomeration integrals be fast to keep the computer time requirements within practical limits.

In addition to being fast, the quadrature approximation should be relatively accurate, since quadrature truncation errors at each time step might add to or interact in some other way with the numerical integration errors of $F_{V,T}$ with respect to time. This means that the truncation errors of one time step become the input errors for the next time step. The combination of these errors might lead to very inaccurate

solutions and/or in some cases to unstable solutions if the input errors are magnified instead of damped at each integration step. This is a well-known behaviour for numerical solutions of partial differential equations, but here the problem is magnified due to the required quadrature calculations.

These combined requirements for both speed and accuracy led to investigating a number of possible numerical integration schemes. For background and to complete the presentation here, some of these attempts are outlined and discussed in the following sub-sections.

6.3.2.2.1 Successive Approximations Combined with the Method of Characteristics

In order to facilitate the use of the method of characteristics, it is more convenient to express equation (6.29a) in terms of variable L instead of V since, by assuming McCabe's ΔL law, the growth rate is assumed constant for all crystal diameters. The growth rate term can then be removed from the differential operator; thus equation (6.29a), transformed to variable L , may be written as:

$$\frac{\partial}{\partial \tau} F_{L,T}(L,\tau) = -\{G_L(F_{L,T}) \frac{\partial}{\partial L} F_{L,T}(L,\tau)\}$$

$$+\{V_L(F_{L,T}) B F_{L,2,n}(F_{L,T}, L)\}$$

$$+\left\{\frac{dV}{dL} \frac{1}{V_L(F_{L,T})} \int_{V_0}^{V/2} k_{V,a}(F_{L,T}, V', V-V')\right.$$

$$\left. \times F_{V,T}(V',\tau) F_{V,T}(V-V',\tau) dV'\right\} \quad (\text{cont'd...})$$

$$- \left\{ \frac{1}{V_L(F_{L,T})} F_{L,T}'(L,\tau) \int_{V_0}^{V_u} k_{V,a}(F_{L,T},V',V) \right. \\ \left. \times F_{V,T}(V',\tau) dV' \right\} \dots\dots (6.30)$$

For solution by successive approximations, this equation can be written in terms of averages over small intervals of τ and L , namely:

$$\frac{\partial}{\partial \tau} F_{L,T} + G_L \frac{\partial}{\partial L} F_{L,T} = - C1 F_{L,T} + C2 \quad (6.31)$$

where. $F_{L,T} = F_{V,T} \frac{dV}{dL}$

$L =$ some function of V

$$G_L = G_V \frac{dL}{dV}$$

$$C1 = \frac{1}{V_L} \int_{V_0}^{V_u} k_{V,a} F_{V,T} dV$$

$$C2 = V_L B F_{L,\ell,n} + \frac{1}{V_L} \frac{dV}{dL} \int_{V_0}^{V/2} k_{V,a}(V',V-V') F_{V,T}(V') \times F_{V,T}(V-V') dV'$$

Equation (6.31) can now be solved analytically by the method of characteristics (a2). This integration method applies to hyperbolic-type partial differential equations. The method transforms the integration of the partial differential equation to that of integration of ordinary differential equations along certain lines called characteristics. In this case, application of this method to equation (6.31) leads to the requirement that equation (6.32), given by:

$$\frac{d}{dx}(F_{L,T}) = - C1 F_{L,T} + C2 \quad (6.32)$$

be integrated along the characteristic x , where x is related to τ and L by:

$$\Delta L = \Delta x \cos\theta \quad (6.32a)$$

$$\Delta \tau = \Delta x \sin\theta \quad (6.32b)$$

$$\text{with } \theta = \arctan(1/G_L) \quad (6.32c)$$

The integration of equation (6.32) is easily effected analytically if C_1 and C_2 can be assumed constant. This solution is:

$$F_{L,T} = \frac{C_2}{C_1} + C \exp(-C_1 \Delta x) \quad (6.33)$$

The constant of integration is evaluated from the initial condition as:

$$C = F_{L,T/x} - 0 - \frac{C_2}{C_1}$$

and thus:

$$F_{L,T} = \frac{C_2}{C_1} \{1 - \exp(-C_1 \Delta x)\} + F_{L,T/x} - 0 \exp(-C_1 \Delta x) \quad (6.35)$$

Equation (6.35) can be solved along a grid of lines which may be equally spaced in L (line specified by integer i), while marching in the direction of increasing time, τ (each time interval specified by integer j). This method of solution for $F_{L,T}$ requires knowledge of representative constant values of C_1 and C_2 over the integration interval, but it is to

be noted (equation (6.31)) that these constants contain $F_{V,T}$; thus an iterative procedure is required. Also, the integration interval, Δx , itself depends on a changing value, namely G_L (equation (6.32a)). Fortunately, the change of G_L is very small for small integration intervals so that the growth rate at i,j may be used without significant error.

In this case:

$$\Delta x = \Delta L / \cos \theta = \frac{\Delta B \{G_L^2(i,j) + 1\}^{1/2}}{G_L(i,j)}$$

After calculation of $F_{L,T}$ at all grid points i at time $(j+1)$ the updated values for $C1(i,j+1)$ and $C2(i,j+1)$ can be evaluated by numerical integration. These new values are then to be compared to those assumed and if they do not agree within a specified tolerance the calculation procedure must be repeated.

If this iterative procedure converges and if $C1$ and $C2$ are relatively slow changing functions of both L and τ , this method should be very attractive. It was not pursued further in this case since it was known that in the crystallization of alumina trihydrate, the agglomeration process takes place to quite a significant extent and consequently $C1$ and especially $C2$ should vary considerably over a small interval of Δx . Moreover, some doubt also exists with regard to the convergence of the iterative process because of the strong interactions of all $F_{L,T}$ values through the agglomeration integrals.

6.3.2.2.2 Method of Moments and Pseudo Moments

Solution of special forms of equation (6.29) by the method of moments is a standard type of solution procedure (h4). It is a very

attractive method of solution if it is possible to convert the integro-partial differential equation into a small bounded set of coupled ordinary differential equations. This allows for accurate and very fast solutions and consequently this method is suitable for parameter estimation and investigation of different constitutive models.

The general pseudo moment equation was derived in Chapter 5, equation (5.59). For the purpose of this discussion it can be written as:

$$\begin{aligned} \frac{d}{d\tau} \left\{ \int_{V_0}^V X_i(V) F_{V,T}(V, \tau) dV \right\} = & + G_D(\tau) \int_{V_0}^V \phi_g(V) \left\{ \frac{d}{dV} X_i(V) \right\} F_{V,T}(V, \tau) dV \\ & + V_L(\tau) B F_{\ell, n}(\tau) \int_{V_0}^V \phi_n(V) X_i(V) dV \\ & + \frac{1}{V_L(\tau)} \phi_{E, a}(\tau) \int_{V_0}^V \int_{V_0}^{V'} \phi_{V, a}(V', V'') \\ & \times \{ \frac{1}{2} X_i(V''+V') - X_i(V'') \} \\ & \times F_{V,T}(V', \tau) F_{V,T}(V'', \tau) dV' dV'' \\ & i = 1, 2, \dots, mp \quad \dots (6.37) \end{aligned}$$

where X_i is the i^{th} weighting function.

An attempt was made in this work to select a set of X_i 's such that:

$$\phi_g(V) \frac{d}{dV} \{ X_i(V) \} \approx \sum_{\ell=1}^{mp} C_{1\ell} X_{\ell}(V) \quad (6.38)$$

and

$$\phi_{V,a}(V', V'') \{ \frac{1}{2} X_i(V'''+V') - X_i(V'') \} \approx \sum_{\ell=1}^{mp} C2_{\ell} \sum_{p=1}^{mp} C2_p X_{\ell}(V') X_p(V'') \dots (6.39)$$

Here the $C1$ and $C2$'s are a set of constants such that the right-hand side of these equations is a close approximation of the left-hand functions. These are not the only type of possible approximations. If these series approximations can be effected, equation (6.37) reduces to a bounded set of pseudo moment equations (i.e. a set consisting of mp moments and mp independent equations). This was accomplished in this work but due to stability problems and the complexity of finding suitable approximations for each different kernel $\phi_{V,a}$, this approach was abandoned.

6.3.2.2.3 Finite Difference Solutions Using a Fixed Grid

Equation (6.29) was solved in terms of finite difference approximations along a fixed rectangular grid with respect to V and τ . That is, the $\frac{\partial}{\partial V}$ term was approximated by finite differences, the integral terms calculated from sectional approximations of $F_{V,T}$, and the $\frac{\partial}{\partial \tau}$ term obtained by 'marching' along the grid lines in the direction of increasing τ . Thus approximating $\frac{\partial}{\partial V}$ by finite differences transformed the integro-partial differential equation to a coupled set of integro-ordinary differential equations. This set of equations was then solved using a "Runge Kutta Merson" algorithm (c2,c3) which provides for automatic step-size adjustment. This step-size adjustment is needed here because of the wide range of time constants for the equations within the set and also since these time constants change dramatically with time.

It was found, however, that forward and central difference approximations for $\partial/\partial V$ for certain step sizes led to instabilities, while the use of backward differences, although stable, resulted in gross inaccuracies. The inaccuracies were most pronounced at the tail ends of the size distribution. The instability problem with these finite difference approximations in first-order hyperbolic partial differential equations is well known and has been discussed in detail by Mitchell (m9).

Solution of the equation in terms of the cumulative distribution, H_T , markedly improved the accuracy and no further attempts were made to solve equation (6.29) in terms of the number density function, $F_{V,T}$. However, in spite of this improvement the solution was still unsatisfactory due to inaccuracies. Thus, this 'standard' way of solution by approximating the $\frac{\partial H_T}{\partial V}$ term by backward differences, and solving for $\frac{\partial H_T}{\partial \tau}$ by the RKM fourth order approximation with error estimate was not applicable to this problem.

6.3.3 Strategy for Obtaining a Solution for the Population Balance Equation

As numerical schemes for the solution of the complete population balance equation ran into difficulties involving either long solution times, gross inaccuracies, or instability problems, it was decided to attack the problem in a more systematic way by investigating solutions of specific parts of the equation separately. As a first-step in effecting the solution, the partial differential part and the integral part were considered separately.

The accuracy of the various numerical solution methods which were tried was checked by solving, by numerical techniques, parts of the equa-

tion for which analytical solutions are known to exist, and then comparing the numerical with the analytical solution. Thus the population balance, equation (6.29b), was solved for a growth-only process and then separately for an agglomeration-only process. This uncoupled the partial differential and the convolution type integral parts of the equation. These numerical solution methods were then combined to form a numerical solution for the 'full' population balance.

6.3.3.1 Solution of the Integro Part of the Integro-Partial Differential Equation

In this sub-section an efficient quadrature scheme is developed for the integro-part of equation (6.29b); thus the equation to be considered is:

$$\frac{\partial}{\partial \tau} H_T(V, \tau) = \frac{1}{V_L(\tau)} \int_{V_0}^{V/2} \int_{V'}^{V-V'} k_{V,a}(V', V'', \tau) F_{V,T}(V', \tau) F_{V,T}(V'', \tau) dV'' dV' - \frac{1}{V_L(\tau)} \int_{V_0}^V \int_{V_0}^{V-u} k_{V,a}(V', V'', \tau) F_{V,T}(V', \tau) F_{V,T}(V'', \tau) dV'' dV' \quad \dots (6.40)$$

I.C. $H_T(V, 0) = H_{T,0}(V)$

and

$$F_{V,T}(V', \tau) = \frac{\partial}{\partial V} H_T(V, \tau) / V'$$

This is essentially the standard type of model for an unsteady state agglomeration process. Because of the dependence of H_T on the variables V and τ the right-hand side of this equation must be computed at a sufficient number of V size intervals and batch time, τ , steps. The

number of steps is determined by how fast H_T changes with respect to V and τ . Moreover, the number or size of steps is also determined by the need to provide a good approximation for the continuous variable H_T when interpolating between the discrete values of H_T which are calculated by the numerical methods. In general, for the same accuracy, a complex interpolation function requires few discrete H_T evaluations and vice versa.

A complication unique to this type of equation is the convolution character of the first integral expression. This is not obvious when the term is expressed in cumulative form by the double integral but it is nevertheless present in the integration limits. When expressed in terms of the density function (see equation (6.29a) it is seen that in evaluating the integrand, which represents the interaction between pairs of crystals, it is necessary that for each $F_{V,T}(V')$ a corresponding $F_{V,T}(V-V')$ be found. If $F_{V,T}(V-V')$ is not one of the calculated grid values it would need to be approximated by interpolation after location of straddling grid values. This would require a search and interpolation scheme just to be able to evaluate the integrand at one particular size V' . This procedure would need to be repeated for each V' over the range V_0 to $V/2$ in order to evaluate the integrand in the convolution integral corresponding to size V . After evaluation of the discrete integrand values the integral could then be approximated by a quadrature scheme. This procedure would need to be repeated for each volume grid point at each particular time step. The same complicated procedure arises in evaluating the double integral since again a search and interpolation procedure is required in evaluating the integrand because the integration boundaries do not fall on particular grid points.

A further complication arises with the agglomeration process in that the range of particle volumes can become relatively large. In the process under study, the particle volume can vary from 10^{-6} to 10^{+6} μm^3 (particle diameter ca. 10^{-2} to 10^{+2} μm), or twelve orders of magnitude. This is a natural consequence of the agglomeration process. Combination of particles results in rapid discrete increases of particle volumes and consequently rapid spreading of the particle size distribution. In addition, for this process the size distribution with respect to particle volume is very much skewed towards the smaller end, and therefore for a 'proper' presentation of the distribution by discrete values it is necessary to use an unequally spaced grid with the grid density decreasing with increasing particle volume.

6.3.3.1.1 Special Grid and Quadrature Expressions
for the Evaluation of the Agglomeration Term

The above discussion points out the need for developing a numerical method which would avoid the complications arising out of any interpolation scheme and the search for matching convolution number density functions. The scheme should also be able to handle the problem of a wide particle-size distribution and the rapidly varying density function over the small particle sizes which arises because of the skewed nature of the distribution. A particle volume grid which avoids or resolves all of these difficulties is the following:

$$V_l = \left(2^{k_2} + \left(\frac{2^{k_2}}{k_1} \times (l - 1 - (k_1 \times k_2)) \right) \right) \times V_0 \quad (6.41)$$

where $\ell = 2, 3, 4, \dots, m+1$

$$k_1 = 2^{(na-1)}$$

$$na = 1, 2, 3, \dots$$

$$k_2 = \lceil (\ell-1)/k_1 \rceil^*$$

The variable $(m+1)$ denotes the number of grid points with respect to crystal volume and na is a variable which determines the grid density.

For $na = 1$ the grid has a logarithmic characteristic given by $V_\ell = 2^{\ell-1} V_0$

while for $2^{(na-1)} \leq m$ the grid becomes an equal volume interval grid.

The latter spacing is used for narrow-sized, non-skewed distributions while the former is suitable for wide-spread distributions which are skewed towards the small end.

The advantages of this particular grid spacing for the crystal volume are:

- (I) It reduces to an equal interval grid for narrow size distributions.
- (II) It has a logarithmic characteristic for widespread distributions.
- (III) It achieves a good approximation to the crystal size distribution by a sequence of discrete values, or in other words, it has a good resolution for either wide-spread or narrow size distributions.
- (IV) It allows for the selection of a coarse or fine grid in an automatic manner.

*The double square bracket is an integer operator symbol, i.e. $\lceil x \rceil$ is the integer value of x .

- (V) It allows the convolution integral to be expressed exclusively in terms of a set of discrete grid point values and thus provides a fast and convenient algorithm for numerical quadrature.

The derivation of quadratures based on this special grid is as follows: First, the dependence of H_T on τ has been dropped here for convenience since it is not relevant to this derivation; second, V' and V'' are treated as two independent variables as is shown in the following discussion. Furthermore, referring to Figure 6.3.3.1-A, it is seen that:

$$I_i(V_k) = \Delta \int_{V_0}^{V_k/2} \int_{V'}^{V_k - V'} \{ \dots \} dV'' dV' = A_k \quad (6.42)$$

where $\{ \dots \} = k_{V,a}(V', V'') F_{V,T}(V') F_{V,T}(V'')$.

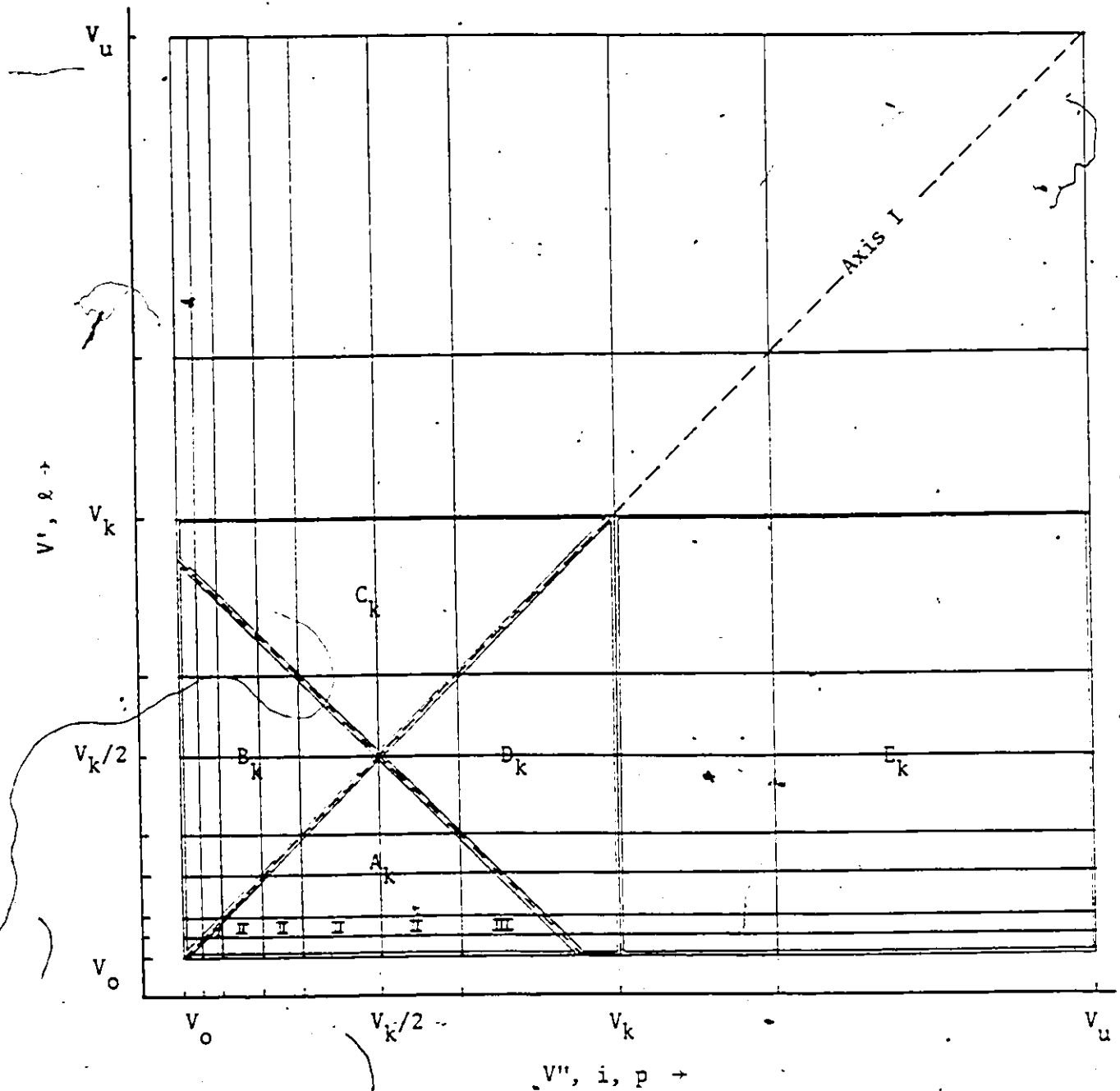
$$\text{and } I_o(V_k) = \Delta \int_{V_0}^{V_k} \int_{V_0}^{V_u} \{ \dots \} dV'' dV' = A_k + B_k + C_k + D_k + E_k \quad \dots (6.43)$$

Moreover, since the integrands of both integrals are symmetric with respect to axis I, the integral I_o also equals:

$$I_o(V_k) = 2(A_k + D_k) + E_k \quad (6.44)$$

This shows that the integrands need to be evaluated only on one side of the axis I. Thus, for the evaluation of I_i and I_o it is necessary to calculate A, D, and E which is done here by sectionalizing the integrals over each grid interval and integrating along strips parallel to the V'' axis as follows:

FIGURE 6.3.3.1-A Grid to Facilitate The Repeated Calculation of the Agglomeration Rate Expression



(i) For $\ell = 1, 2, \dots, (m-2^{na-1})$, calculate:

$$\phi_1(\ell+1) = \int_{V_\ell}^{V_{\ell+1}} \int_{V'}^{V_{\ell+1}} \{ \dots \} dV'' dV' \quad (6.45)$$

$$\phi_1(i) = \phi_1(i-1) + \int_{V_\ell}^{V_{\ell+1}} \int_{V_{i-1}}^{V_i} \{ \dots \} dV'' dV' , \quad i = \ell+2, \ell+3, \dots, m+1 \quad \dots (6.46)$$

$$\phi_2(p) = \phi_1(i) + \int_{V_\ell}^{V_{\ell+1}} \int_{V_i}^{V_p - V'} \{ \dots \} dV'' dV' , \quad p = \ell+1+2^{na-1}, \ell+2+2^{na-1}, \dots, m+1 \quad \dots (6.47)$$

where $i = \begin{cases} p-1 \\ p-2 \\ \vdots \\ p-2^{na-1} \end{cases}$

for $0 < V_{\ell+1} \leq (V_p - V_{p-1})$

$- p-2$

$(V_p - V_{p-1}) < V_{\ell+1} \leq (V_p - V_{p-2})$

$- p-2^{na-1}$

$(V_p - V_{p+1-2^{na-1}}) < V_{\ell+1} \leq (V_p - V_{p-2^{na-1}})$

These are the integrals evaluated over the I, II's, and III, domains, respectively, while the integrals denoted by A, D, and E are equal to:

$$(A + D)_i = (A + D)_i + \phi_1_i , \quad i = \ell+1, \ell+2, \dots, m+1 \quad \dots (6.48)$$

$$A_i = A_i + \phi_2_i , \quad i = \ell+1+2^{na-1}, \ell+2+2^{m-1}, \dots, m+1 \quad \dots (6.49)$$

$$E_i = E_i + \phi_1_{m+1} - \phi_1_i , \quad i = \ell+1, \ell+2, \dots, m \quad (6.50)$$

with the sequence initiated by initially setting the vectors $(A + D)$, A , and E equal to zero.

(ii) Similarly for $\ell = m+1-2^{na-1}, m+2-2^{na-1}, \dots, m$, calculate:

$$\phi_1(\ell+1) = \int_{V_\ell}^{V_{\ell+1}} \int_{V'}^{V_{\ell+1}} \{ \dots \} dV'' dV' \quad (6.51)$$

$$\phi_1(i) = \phi_1(i-1) + \int_{V_\ell}^{V_{\ell+1}} \int_{V_{i-1}}^V \{ \dots \} dV'' dV', \quad i = \ell+2, \ell+3, \dots, m+1$$

.....(6.52)

and

$$(A + D)_i = (A + D)_i + \phi_1_i, \quad i = \ell+1, \ell+2, \dots, m+1 \quad (6.53)$$

$$E_i = E_i + \phi_1_{m+1} - \phi_1_i, \quad i = \ell+1, \ell+2, \dots, m \quad (6.54)$$

After these calculations the integrals $I_i(V_k)$ and $I_o(V_k)$ can thus be evaluated directly, i.e.

$$I_i(V_k) = A_k \quad (6.55)$$

$$I_o(V_k) = 2(A + D)_k + E_k \quad (6.56)$$

The above scheme involves the minimum number of calculations for I_i and I_o .

The next step is the development of sectional approximations for $k_{V,a}$ and $F_{V,T}$ over each grid interval. Simple approximations will probably require a large number of grid points while the reverse is probably true for more complicated approximations. For this work low order approximations were used since:

- (i) for higher order approximations the computation time becomes excessive, and
- (ii) higher order functions might magnify instead of dampen errors in the integrand grid values (s6).

The number of grid points needed to achieve a certain accuracy for low order approximations is evaluated later in this chapter.

The approximations used in this work are:

- (i) First order collocation for H_T , i.e.

$$H_T^{\ell+1} \approx \alpha_\ell + \beta_\ell V \quad (6.57)$$

- (ii) Zero order collocation for the size dependent factor of

$k_{V,a}$ which is $\phi_{V,a}$, i.e.

$$\phi_{V,a}^{\ell+1/p+1} \approx C_{\ell,p} \quad (6.58)$$

With these approximations the integrals needed in the calculation for ϕ_1 and ϕ_2 are equal to:

$$\int_{V_\ell}^{V_{\ell+1}} \int_{V'}^{V_{\ell+1}} \{ \dots \} dV'' dV' \approx \phi_{E,a}(\tau) C_{\ell,\ell} \beta_\ell^2 \frac{\Delta V_\ell^2}{2} \quad (6.59)$$

$$\int_{V_\ell}^{V_{\ell+1}} \int_{V_{i-1}}^{V_i} \{ \dots \} dV'' dV' \approx \phi_{E,a}(\tau) C_{\ell,i-1} \beta_\ell \beta_{i-1} \Delta V_\ell \Delta V_{i-1} \quad (6.60)$$

$$\int_{V_\ell}^{V_{\ell+1}} \int_{V_i}^{V_p - V'} \{ \dots \} dV'' dV' \approx \phi_{E,a}(\tau) C_{\ell,i} \beta_\ell \beta_i \Delta V_\ell$$

$$\times \left\{ V_p - V_i - \frac{V_{\ell+1} + V_\ell}{2} \right\} \dots \quad (6.61)$$

Being able to approximate the first and last integrals by these simple expressions (equations (6.59) and (6.61)) is a direct consequence of the special grid which takes into account the special nature of the convolution integral. That is, the 135° boundary line of the integral I_i only crosses the vertical grid lines at node points, which means that the number of evaluations of the most time consuming integral, equation (6.61) is minimized. The expressions for I_i and I_0 are exact given that the functions ϕ_a and $F_{V,T}$ are equal to the respective sectional approximations. This sectional approximation feature makes this a very powerful method suitable for any shape of size distribution.

In general, the advantages of this special grid and sectional approximation method are:

- (I) It provides for an accurate solution.
- (II) It is relatively fast because it involves a minimum number of computer operations.
- (III) It requires a relatively small amount of computer storage.
- (IV) It does not place any restrictions on the form of the initial distribution or on the functional form of the kernel.
- (V) It places no restriction on the form of the distribution at any instant in time; for example, the distribution may be bimodal or have any other shape.

6.3.3.1.2 Investigation of the Numerical Accuracy of the Quadrature Expressions for the Agglomeration Term

Although an analytical solution does not exist for the general case of the agglomeration-only process (equation (6.40)), it can be solved

for specific cases where the functions $k_{V,a}$ and $H_{T,o}$ have special forms. This allows for a comparison between the solution obtained by the numerical scheme and that obtained analytically and thus provides a test of the accuracy of the method.

As an example, consider the following form for $k_{V,a}$ and $H_T(V,o)$:

$$k_{V,a} = C V_L(\tau) \quad (6.62)$$

$$H_T(V,o) = -N_o (\exp(-V/V_{ave}) - \exp(-V_o/V_{ave})) \quad (6.63)$$

The analytical solution of equation (6.40) is then (s5):

$$H_T(V,\tau) = \left(\frac{N_o}{V_{ave}}\right) \frac{4}{(T+2)^2} \frac{1}{a} \{\exp(a V) - \exp(a V_o)\} \quad (6.64)$$

where $T = C N_o \tau \quad (6.65)$

$$a = -\frac{2}{(T+2)V_{ave}} \quad (6.66)$$

C = agglomeration rate constant

N_o = initial total number of particles

τ = batch time

V_{ave} = average initial particle volume

The comparisons between H_T obtained analytically by equation (6.64) and that calculated by quadratures (6.59) to (6.61) and numerical integration by means of the Runge-Kutta-Merson method (c2), is shown in

Table 6.3.3.1.2-A. In this calculation, the agglomeration process was allowed to proceed over a long time period so that any accumulation of truncation errors in approximating the function H_T would become apparent. In this period, the total number of particles changed from 1.0×10^{11} to 7.9×10^8 and thus this problem should provide a good test of the numerical method. It should also be noted that this magnitude of change is expected in the alumina crystallization process.

The maximum accumulated error with 61 grid points is approximately 9.46%; while with 121 grid points this was reduced to 2.45%. Increasing the numerical integration routine error tolerance from 0.1% to 0.001% increased the number of agglomeration term evaluations from 250 to 635 for a 61 grid point system, but the maximum accumulated error was still 9.46%. This indicates that the error is not due to numerical integration but instead results from accumulated errors of the quadrature approximation. Since a relative numerical error of 9.46% is not acceptable for this study, it follows that the number of grid points with respect to crystal volume should be at least 121. Note also that without checks, numerical solutions of equation (6.40), or of more complicated population balance equations, might be misleading as a result of numerical errors. These would be superimposed on the fit of any proposed model (constitutive relationship) for the agglomeration rate kernel. This could lead to misleading models or a poor fit of a good model.

TABLE 6.3.3.1.2-A Comparison between the Analytical and Developed Numerical Approximation Solution of an Unsteady State Agglomeration Model.

Particle Diameter (µm)	Initial Cumulative Size Distribution Values		Analytical Solution (equation (6.62))		Numerical Solution			
	H = 60 I _T	H = 120 I _T	H = 60 I _T (anal.)	H = 120 I _T (anal.)	I _T (num.)	% Deviation	ε = 0.001 H = 60 N = 635 I _T (num.) % Deviation	ε = 0.1 H = 120 N = 250 I _T (num.) % Deviation
0.100	0.	0.	0.	0.	0.	0.	0.	0.
0.108	5.00x10 ⁴	2.50x10 ⁴	3.15	1.57	3.15	8.1x10 ⁻²	5.9x10 ⁻²	3.1x10 ⁻²
0.114	7.50x10 ⁴	5.00x10 ⁴	4.30	3.15	6.30	8.1x10 ⁻²	5.9x10 ⁻²	3.1x10 ⁻²
0.126	1.00x10 ⁵	1.00x10 ⁵	6.30	6.30	6.30	8.1x10 ⁻²	5.9x10 ⁻²	3.0x10 ⁻²
0.136	2.00x10 ⁵	1.50x10 ⁵	1.26x10 ¹	9.45	1.26x10 ¹	8.1x10 ⁻²	5.9x10 ⁻²	3.0x10 ⁻²
0.144	3.00x10 ⁵	2.00x10 ⁵	1.89x10 ¹	1.57x10 ¹	1.89x10 ¹	8.1x10 ⁻²	5.9x10 ⁻²	3.0x10 ⁻²
0.159	4.00x10 ⁵	3.00x10 ⁵	2.52x10 ¹	1.89x10 ¹	2.52x10 ¹	8.1x10 ⁻²	5.9x10 ⁻²	3.0x10 ⁻²
0.182	5.00x10 ⁵	4.00x10 ⁵	3.15x10 ¹	2.52x10 ¹	3.15x10 ¹	8.1x10 ⁻²	5.9x10 ⁻²	3.0x10 ⁻²
0.191	6.00x10 ⁵	5.00x10 ⁵	3.78x10 ¹	3.15x10 ¹	3.78x10 ¹	8.1x10 ⁻²	5.9x10 ⁻²	3.0x10 ⁻²
0.200	7.00x10 ⁵	6.00x10 ⁵	4.41x10 ¹	3.78x10 ¹	4.41x10 ¹	8.1x10 ⁻²	5.9x10 ⁻²	3.0x10 ⁻²
0.215	9.00x10 ⁵	7.00x10 ⁵	5.67x10 ¹	4.41x10 ¹	5.67x10 ¹	8.1x10 ⁻²	5.9x10 ⁻²	3.0x10 ⁻²
5.81	1.78x10 ¹⁰	1.78x10 ¹⁰	1.24x10 ⁶	1.24x10 ⁶	1.24x10 ⁶	6.6x10 ⁻²	4.47x10 ⁻²	2.6x10 ⁻²
6.12	2.05x10 ¹⁰	2.05x10 ¹⁰	1.65x10 ⁶	1.44x10 ⁶	1.65x10 ⁶	6.1x10 ⁻²	4.0x10 ⁻²	2.5x10 ⁻²
6.40	2.31x10 ¹⁰	2.31x10 ¹⁰	2.06x10 ⁶	1.65x10 ⁶	2.06x10 ⁶	6.1x10 ⁻²	4.0x10 ⁻²	2.6x10 ⁻²
6.89	2.79x10 ¹⁰	2.79x10 ¹⁰	2.47x10 ⁶	2.06x10 ⁶	2.47x10 ⁶	2.0x10 ⁻²	5.4x10 ⁻³	1.9x10 ⁻²
7.33	3.25x10 ¹⁰	3.25x10 ¹⁰	3.0x10 ⁶	2.47x10 ⁶	3.0x10 ⁶	7.7x10 ⁻³	-1.2x10 ⁻²	1.3x10 ⁻²
7.71	4.08x10 ¹⁰	4.08x10 ¹⁰	4.94x10 ⁶	3.0x10 ⁶	4.94x10 ⁶	-1.1x10 ⁻¹	-1.3x10 ⁻¹	1.5x10 ⁻²
8.06	5.45x10 ¹⁰	5.45x10 ¹⁰	6.58x10 ⁶	4.94x10 ⁶	6.58x10 ⁶	-1.7x10 ⁻¹	-1.9x10 ⁻¹	1.5x10 ⁻²
8.69	7.30x10 ¹⁰	7.30x10 ¹⁰	9.85x10 ⁶	6.58x10 ⁶	9.85x10 ⁶	-5.2x10 ⁻¹	-5.4x10 ⁻¹	1.5x10 ⁻²
9.23	8.40x10 ¹⁰	8.40x10 ¹⁰	1.31x10 ⁷	9.85x10 ⁶	1.31x10 ⁷	-6.9x10 ⁻¹	-7.1x10 ⁻¹	1.5x10 ⁻²
10.2	9.27x10 ¹⁰	9.27x10 ¹⁰	1.63x10 ⁷	1.31x10 ⁷	1.63x10 ⁷	-6.9x10 ⁻¹	-7.1x10 ⁻¹	1.5x10 ⁻²
11.6								
12.2								
12.8								
13.8								

.....(cont'd.)

TABLE 6.3.3.1.2-A (cont'd.)

Particle Diameter (µm)	Initial Cumulative Size Distribution Values		Analytical Solution (equation (6.62))		Numerical Solution		
	H = 60 H _T	H = 120 H _T	H = 60 H _T (anal.)	H = 120 H _T (anal.)	ε = 0.1 M = 60 N = 250	ε = 0.001 M = 60 N = 635	ε = 0.1 M = 120 N = 250
14.6	9.57x10 ¹⁰	9.57x10 ¹⁰	1.96x10 ⁷	1.96x10 ⁷	1.93x10 ⁷	1.93x10 ⁷	1.95x10 ⁷
15.4	9.85x10 ¹⁰	9.57x10 ¹⁰	2.28x10 ⁷	2.28x10 ⁷	2.55x10 ⁷	2.55x10 ⁷	2.27x10 ⁷
16.1	9.85x10 ¹⁰	9.85x10 ¹⁰	2.60x10 ⁷	2.60x10 ⁷	3.23x10 ⁷	3.23x10 ⁷	2.59x10 ⁷
17.4	9.98x10 ¹⁰	9.95x10 ¹⁰	3.86x10 ⁷	3.86x10 ⁷	3.75x10 ⁷	3.75x10 ⁷	3.84x10 ⁷
18.5	1.00x10 ¹¹	1.00x10 ¹¹	4.49x10 ⁷	4.49x10 ⁷	4.92x10 ⁷	4.92x10 ⁷	4.45x10 ⁷
20.3	1.00x10 ¹¹	1.00x10 ¹¹	5.11x10 ⁷	5.11x10 ⁷	7.16x10 ⁷	7.16x10 ⁷	5.07x10 ⁷
21.9	1.00x10 ¹¹	1.00x10 ¹¹	6.34x10 ⁷	6.34x10 ⁷	7.16x10 ⁷	7.16x10 ⁷	6.26x10 ⁷
23.2	1.00x10 ¹¹	1.00x10 ¹¹	7.54x10 ⁷	7.54x10 ⁷	9.32x10 ⁷	9.32x10 ⁷	7.44x10 ⁷
24.5	1.00x10 ¹¹	1.00x10 ¹¹	8.73x10 ⁷	8.73x10 ⁷	1.33x10 ⁸	1.33x10 ⁸	8.61x10 ⁷
25.6	1.00x10 ¹¹	1.00x10 ¹¹	9.89x10 ⁷	9.89x10 ⁷	1.71x10 ⁸	1.71x10 ⁸	9.75x10 ⁷
27.6	1.00x10 ¹¹	1.00x10 ¹¹	1.22x10 ⁸	1.22x10 ⁸	2.38x10 ⁸	2.38x10 ⁸	1.20x10 ⁸
29.3	1.00x10 ¹¹	1.00x10 ¹¹	1.44x10 ⁸	1.44x10 ⁸	2.98x10 ⁸	2.98x10 ⁸	1.41x10 ⁸
30.9	1.00x10 ¹¹	1.00x10 ¹¹	1.86x10 ⁸	1.86x10 ⁸	3.95x10 ⁸	3.95x10 ⁸	1.62x10 ⁸
32.2	1.00x10 ¹¹	1.00x10 ¹¹	2.25x10 ⁸	2.25x10 ⁸	4.73x10 ⁸	4.73x10 ⁸	1.82x10 ⁸
34.7	1.00x10 ¹¹	1.00x10 ¹¹	2.61x10 ⁸	2.61x10 ⁸	5.82x10 ⁸	5.82x10 ⁸	2.20x10 ⁸
36.9	1.00x10 ¹¹	1.00x10 ¹¹	2.96x10 ⁸	2.96x10 ⁸	6.54x10 ⁸	6.54x10 ⁸	2.55x10 ⁸
40.6	1.00x10 ¹¹	1.00x10 ¹¹	3.85x10 ⁸	3.85x10 ⁸	7.29x10 ⁸	7.29x10 ⁸	2.89x10 ⁸
43.8	1.00x10 ¹¹	1.00x10 ¹¹	4.37x10 ⁸	4.37x10 ⁸	7.64x10 ⁸	7.64x10 ⁸	3.20x10 ⁸
46.5	1.00x10 ¹¹	1.00x10 ¹¹	5.20x10 ⁸	5.20x10 ⁸	7.87x10 ⁸	7.87x10 ⁸	3.76x10 ⁸
49.0	1.00x10 ¹¹	1.00x10 ¹¹	6.33x10 ⁸	6.33x10 ⁸	7.92x10 ⁸	7.92x10 ⁸	4.26x10 ⁸
51.2	1.00x10 ¹¹	1.00x10 ¹¹	6.99x10 ⁸	6.99x10 ⁸	7.92x10 ⁸	7.92x10 ⁸	4.70x10 ⁸
55.2	1.00x10 ¹¹	1.00x10 ¹¹	7.61x10 ⁸	7.61x10 ⁸	7.92x10 ⁸	7.92x10 ⁸	5.08x10 ⁸
58.6	1.00x10 ¹¹	1.00x10 ¹¹	8.22x10 ⁸	8.22x10 ⁸	7.92x10 ⁸	7.92x10 ⁸	5.71x10 ⁸
61.7	1.00x10 ¹¹	1.00x10 ¹¹	8.73x10 ⁸	8.73x10 ⁸	7.92x10 ⁸	7.92x10 ⁸	6.20x10 ⁸
64.5	1.00x10 ¹¹	1.00x10 ¹¹	9.22x10 ⁸	9.22x10 ⁸	7.92x10 ⁸	7.92x10 ⁸	6.59x10 ⁸
69.5	1.00x10 ¹¹	1.00x10 ¹¹	9.93x10 ⁸	9.93x10 ⁸	7.92x10 ⁸	7.92x10 ⁸	6.89x10 ⁸
73.8	1.00x10 ¹¹	1.00x10 ¹¹	1.00x10 ¹¹	1.00x10 ¹¹	7.92x10 ⁸	7.92x10 ⁸	7.29x10 ⁸
77.7	1.00x10 ¹¹	1.00x10 ¹¹	1.00x10 ¹¹	1.00x10 ¹¹	7.92x10 ⁸	7.92x10 ⁸	7.54x10 ⁸
81.3	1.00x10 ¹¹	1.00x10 ¹¹	1.00x10 ¹¹	1.00x10 ¹¹	7.92x10 ⁸	7.92x10 ⁸	7.69x10 ⁸
87.6	1.00x10 ¹¹	1.00x10 ¹¹	1.00x10 ¹¹	1.00x10 ¹¹	7.92x10 ⁸	7.92x10 ⁸	7.79x10 ⁸
93.0	1.00x10 ¹¹	1.00x10 ¹¹	1.00x10 ¹¹	1.00x10 ¹¹	7.92x10 ⁸	7.92x10 ⁸	7.88x10 ⁸
97.9	1.00x10 ¹¹	1.00x10 ¹¹	1.00x10 ¹¹	1.00x10 ¹¹	7.92x10 ⁸	7.92x10 ⁸	7.91x10 ⁸
102.4	1.00x10 ¹¹	1.00x10 ¹¹	1.00x10 ¹¹	1.00x10 ¹¹	7.92x10 ⁸	7.92x10 ⁸	7.91x10 ⁸

Legend: ε -- relative Runge-Kutta-Merson error tolerance
 H -- number of size grid intervals
 N -- number of right-hand side of equation (6.40) evaluations

6.3.3.2 Solution of the Partial Differential Part of the Integro-Partial Differential Equation

In order to develop a suitable numerical scheme for the partial differential part of the population balance equation, a growth-only process was studied. For such a process the population balance equation (6.29b) reduces to:

$$\frac{\partial}{\partial \tau} H_T(V, \tau) + G_D(H_T, \tau) \phi_g(V) \frac{\partial}{\partial V} H_T(V, \tau) = 0 \quad (6.67)$$

with I.C. $H_T(V, 0) = H_{T,0}$
 B.C. $H_T(V_0, \tau) = 0$

This is a homogeneous quasilinear hyperbolic, first-order partial differential equation. A method of solution for this equation, which is not only natural but also very powerful is by the method of characteristics (a2). In this scheme, the function H_T is solved along the characteristics of the equation by a set of ordinary differential equations. The non-linearity introduces an additional complication in that the characteristic grid changes as the solution progresses. This change must be accommodated as the solution progresses. This obviates an analytical solution but poses no real difficulties for a numerical method.

One drawback of the method of characteristics is, however, that the numerical solution along a 'characteristic grid' provides H_T values which do not fall on any rectangular grid with respect to the independent variables V and τ . As discussed in the previous sub-section, a rectangular grid with special spacings is the heart of the solution method for the integral part. Therefore, for a solution of the 'full' equation it will

either be necessary to develop an interpolation scheme between the characteristic and special rectangular grid, or abandon the method of characteristics and solve along the special grid by approximating the partial derivative with respect to V by a stable accurate finite difference approximation. The latter scheme is preferred since it requires less complex programming.

6.3.3.2.1 Evaluation of the Accuracy of the Numerical Solution of the Population Balance for a Growth-Only Process

Different numerical solution schemes were evaluated by comparing the numerical solutions to the analytical solution of a particular form of equation (6.67). To effect an analytical solution, equation (6.67) is first transformed to the simpler form

$$\frac{\partial}{\partial \tau} H_T(D, \tau) + G_D(H_T, \tau) \frac{\partial H_T}{\partial D}(D, \tau) = 0 \quad (6.68)$$

which follows from the following identities:

$$G_D(H_T, \tau) \phi_g(V) = G_V(H_T, V, \tau) = \frac{dV}{d\tau} \quad (6.69)$$

and

$$\left(\frac{dV}{d\tau}\right) \frac{\partial H_T}{\partial V} = \left(\frac{dD}{d\tau} \frac{dV}{dD}\right) \frac{\partial H_T}{\partial V} = \frac{dD}{d\tau} \frac{\partial H_T}{\partial D} = G_D \frac{\partial H_T}{\partial D} \quad (6.70)$$

Equation (6.68) is also a homogeneous quasilinear hyperbolic first-order partial differential equation. Again, no analytical solution exists for such an equation. However, if the growth rate, G_D , is assumed equal to a function of τ only the equation is linear and analytical solutions can be derived.

Of the many analytical solution techniques available, such as: by Z-transforms for a discrete form of (6.68), by the method of characteristics, or by means of Laplace transforms, the latter was used here to effect a solution. With G_D given by:

$$G_D(\tau) = C_1 e^{C_2 \tau} \quad (6.71)$$

with C_1 and C_2 as constants, the analytical solution of equation (6.68) is:

$$H_T(\tau, D) = H_{T,0} (D - C_1(1 - \exp(C_2 \tau))/C_2) \quad (6.72a)$$

for all $D \geq (D_0 + C_1(\exp(C_2 \tau) - 1)/C_2)$

$$\text{and } H_T(\tau, D) = 0 \quad (6.72b)$$

for all $D < (D_0 + C_1(\exp(C_2 \tau) - 1)/C_2)$

$H_{T,0}$ is some arbitrary initial size distribution and D is the spherical equivalent diameter. Thus, equation (6.72) provides a means of evaluating the accuracy of a numerical solution of equation (6.68).

In effecting a numerical solution by finite differences, certain restrictions arise in its application which are well-known (m9). As was found previously in attempting a finite difference solution of the full model (Section 6.3.2.3) using the usual differencing schemes for $\partial H_T / \partial D$, the explicit forward and central differences, for large step sizes, led to instabilities, while backward differences, although stable, led to gross inaccuracies.

Analysis of the following finite difference forms of equation (6.68)

$$\frac{H_T(i,j+1) - H_T(i,j)}{\Delta\tau} = -G_D \frac{\{H_T(i+1,j) - H_T(i,j)\}}{\Delta D} \quad (6.68a)$$

and

$$\frac{H_T(i,j+1) - H_T(i,j)}{\Delta\tau} = -G_D \frac{\{H_T(i+1,j) - H_T(i-1,j)\}}{2\Delta D} \quad (6.68b)$$

by the Fourier method (c1) showed that the forward and central difference approximations, equations (6.68a) and (6.68b) respectively, are unstable. Their amplification factors* are:

$$|\xi|_{\text{forward}} = 1 + \{1 + 2 G_D \frac{\Delta\tau}{\Delta D} (1 + G_D \frac{\Delta\tau}{\Delta D})\}^{1/2}$$

$$|\xi|_{\text{central}} = 1 + \{1 + (G_D \frac{\Delta\tau}{\Delta D})^2\}^{1/2}$$

This shows that the RKM (Runge-Kutta-Merson) solution (which is a higher order explicit forward finite difference approximation) is more robust with regard to stability than this explicit first order forward approximation. That is, the RKM central difference solution exhibited conditional stability while only the forward difference solution was unstable.

To solve the inaccuracy and instability problem, a weighted central difference approximation was developed which in combination with the Runge-Kutta-Merson method of solution was also conditionally stable.

It is:

*See reference (c1) for a definition and discussion of this amplification factor. For stability, this factor should obey the condition $|\xi| \leq 1$.

$$\frac{\partial y}{\partial x}_i \approx C_i U_{i-1} + (1-C_i)U_i \quad (6.73)$$

$$\text{where } U_{i-1} = (y_i - y_{i-1})/\Delta x \quad (6.74)$$

$$C_i = (U_i + \lambda)/(U_i + U_{i-1} + \lambda) \quad (6.75)$$

The use of the constant, λ , (here $\lambda = 0.0001$) avoids the problem of dividing by zero when both U_i and U_{i-1} are zero. The variables y and x are transformations of H_T and V , respectively, and are given by:

$$(G_V) \frac{\partial H_T}{\partial V} = (G_D) \frac{\partial H_T}{\partial D} = (G_D) \frac{dH_T}{dy} \frac{dV}{dD} \frac{dx}{dV} \frac{\partial y}{\partial x} \quad (6.76)$$

In this case, the transformations which were used are:

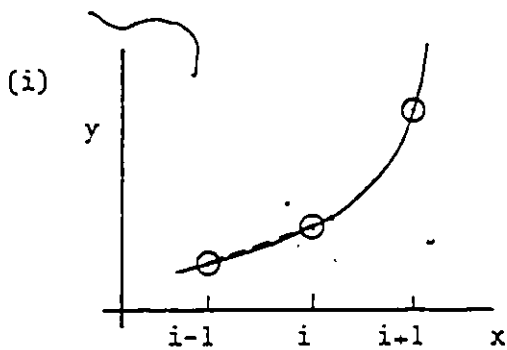
$$y = \ln(H_T + 1)$$

$$x = a + bV + C \ln V$$

$$D = \left(\frac{6}{\pi}\right)^{1/3} V^{1/3}$$

These transformations provide scaling of H_T and transforms the unequally spaced V -grid into an equally spaced x -grid.

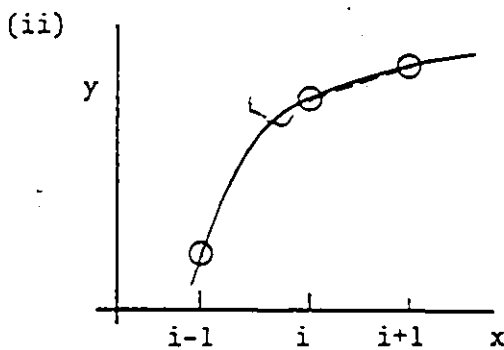
The actual differencing scheme used through choice of C_i is best illustrated graphically as follows:



$$U_i \gg U_{i-1}$$

$$C_i \approx 1$$

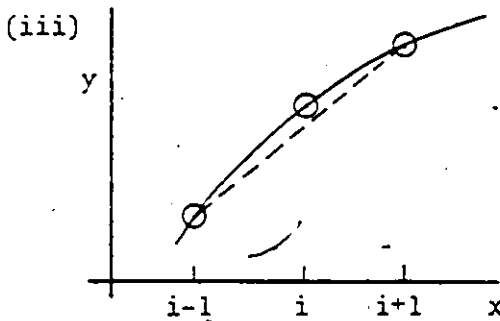
backward difference



$$U_i \ll U_{i-1}$$

$$C_i \approx 0$$

forward difference



$$U_i \approx U_{i-1}$$

$$C_i \approx 1/2$$

central difference

Note that the approximation of the derivative by equation (6.73) at point i appears close to the true derivative based on smooth lines drawn through the points.

Comparison between the analytical solution (equation (6.72)) and the numerical solution of equation (6.68) by means of this weighted central difference approximation and the Runge-Kutta-Merson integration method showed that:

- (I) The deviation between the WCD (weighted central difference) solution and the analytical solution was most pronounced at the 'tail' ends of the size distribution, as was the case with the BD (backward difference) and CD (central difference) solutions.
- (II) The deviation of the WCD method was less than either the BD or CD deviations.
- (III) Using the first moment of the size distribution as a criteria for accuracy, after a certain integration time, the BD and CD methods exhibited errors of +16 and +9%, respectively, while the error was -5% for the WCD method using 121 size grid points and the same Runge-Kutta-Merson routine integration error tolerance. Moreover, the number of function evaluations required for the WCD, BD, and CD methods were 1618, 1678, and 2188, respectively.

Thus, the WCD approximation is more accurate than either the first order BD approximation or the second order CD approximation. Furthermore, it requires less function evaluations than either the stable BD or the conditionally stable CD approximation. This is important when considering the computer time requirements for a solution of the full model.

A still more accurate solution of equation (6.68) can be obtained by means of the method of characteristics. Such a solution is very accurate since the only differential equations which need to be solved are the ones along the characteristic lines as given by (a2):

$$\frac{dD_i}{dS} = G_D(\tau) / (G_D^2(\tau) + 1)^{1/2}, \quad i = 1, 2, \dots, m+1 \quad (6.78)$$

$$\frac{d\tau}{dS} = 1 / (G_D^2(\tau) + 1)^{1/2} \quad (6.79)$$

$$\frac{dH_{T,i}}{dS} = 0, \quad i = 1, 2, \dots, m+1 \quad (6.80)$$

where S is the characteristic.

The difference between this numerical solution scheme and the analytical solution was negligible. Unfortunately, as shown in the next sub-section, this latter method of solution, when used in combination with the integral part of the equation, requires a means of relating the solution at one set of grid points to that at another set. This can lead to interpolation errors which can be significant.

As a general point, it is to be noted that the use of backward or central differences might result in gross numerical inaccuracies. The magnitude of the errors would depend on the number of grid points used and the rapidity with which the cumulative size distribution changes with time and size. Such inaccuracies would confound any modelling work based on a population balance with a growth rate term.

6.4 Solution of the Full Model

After investigation of the growth and agglomeration parts of the population balance the separate most accurate solution schemes were combined to form a numerical solution for the full model. Thus, full model solutions were developed based on the weighted central difference approximation in combination with integrating along the agglomeration

grid, and secondly a solution was devised based on the method of characteristics in combination with interpolation between the characteristic and the special rectangular grid for agglomeration. This last solution method, in spite of the required complex programming, was developed here since numerical interpolation should be inherently more accurate than numerical differentiation.

The full model in terms of characteristics S is:

$$\frac{d\tau}{dS} = 1/(G_D^2(\tau) + 1)^{1/2} \quad (6.79)$$

$$\frac{dD_i}{dS} = G_D(\tau)/(G_D^2(\tau) + 1)^{1/2} \quad (6.78)$$

$$\begin{aligned} \frac{dH_{T,i}}{dS} &= V_L(\tau) B F_{\ell,n}(\tau) \int_{V_0}^{V_i} \phi_n(V') dV' \\ &\pm \frac{1}{V_L(\tau)} \int_{V_0}^{V_i/2} \int_{V'}^{V_i-V'} k_{V,a}(V',V'',\tau) F_{V,T}(V',\tau) F_{V,T}(V'',\tau) dV'' dV' \\ &- \frac{1}{V_L(\tau)} \int_{V_0}^{V_i} \int_{V_0}^{V_i+1} k_{V,a}(V',V'',\tau) F_{V,T}(V',\tau) F_{V,T}(V'',\tau) dV'' dV' \end{aligned}$$

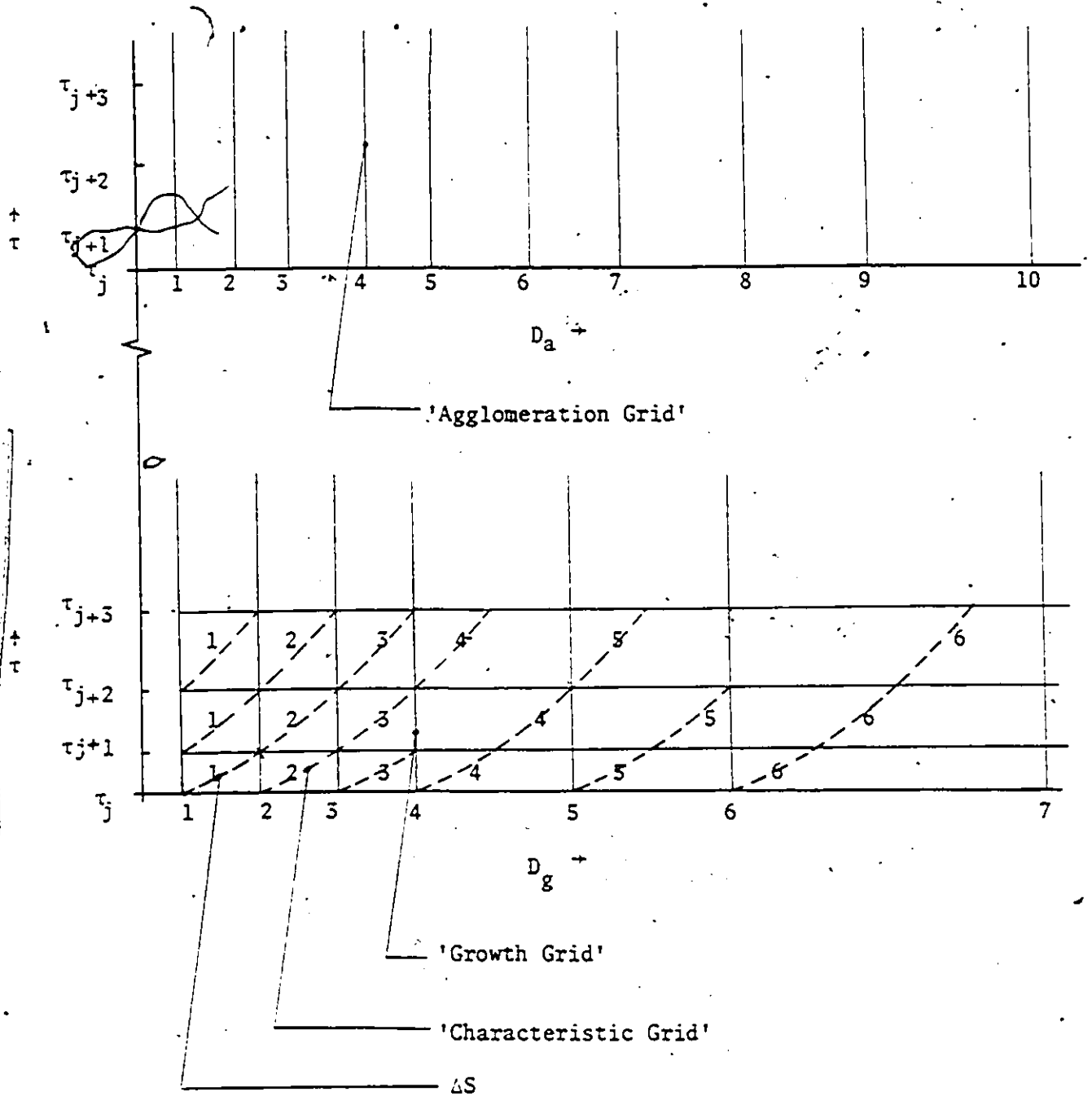
$$i = 1, 2, \dots, m+1 \quad (6.81)$$

This system of equations was solved along the characteristic grid lines, S , as shown in Figure 6.4-A.

The 'agglomeration grid' denoted by D_a , is calculated from equation (6.41) while the 'growth-rate grid', D_g , is determined such that:

$$\Delta D_g(i+1) = \Delta D_g(i) \quad (6.82)$$

FIGURE 6.4-A Grid for the Solution of the Full Model



if the corresponding ΔD_a interval is less than $\Delta D_g(i)$, or

$$\Delta D_g(i+1) = 2\Delta D_g(i) \quad (6.83)$$

if it is greater. This sequence is started by setting $\Delta D_g(1) = C\Delta D_a(1)$ where C is a constant. Selection of the vector D_g in this particular way assures a grid density of approximately equal density for the characteristic and special quadrature (agglomeration) grids. In addition, it has as a result that when one of the 'characteristic grid' D values, by equation (6.78), reaches a D_g grid line, the other D values either fall also on their corresponding D_g grid lines or will simultaneously coincide subsequently. Therefore, the characteristic grid can be 'updated' so as to maintain the same number of changing characteristic grid values as fixed growth grid values. This is illustrated in Figure 6.4-A and assures a constant characteristic grid density.

With this selection of grids the method of solution proceeds as follows: First, the vector of S values ($S(1), S(2), \dots, S(m)$) are set to zero. Also, from the boundary condition, the values of $H_T(1)$ are zero along vertical growth grid line 1 since this line corresponds to V_0 . Secondly, with these boundary and initial conditions the problem resolves itself into numerically integrating equations (6.79), (6.78), and (6.81) by the Runge-Kutta-Merson method along the characteristic grid lines. To carry out this integration requires evaluation of the right-hand side of equation (6.81) at the values of S specified by the step size in the integration routine. This, in turn, requires the numerical evaluation of the two agglomeration integrals which in this case for fast integration, by the quadratures developed in Section 6.3.3.1.1, requires the H_T values

at the agglomeration grid corresponding to a given value of time. These are obtained by interpolating between characteristic lines. The special quadrature formulas are then applied to evaluate the rate of change of H_T due to the agglomeration process at the agglomeration grid values corresponding to the same value of time. After that, these rate of change values are interpolated from the agglomeration to the characteristic grid providing the right-hand side values of the set of dH_T/dS equations. This interpolation between the two grids allows thus for the application of the method of characteristics by integrating along the characteristic grid and at the same time for the efficient calculation of the agglomeration integrals.

The integration along S is stopped when $D(1)$ by equation (6.78) reaches $D_g(2)$. At this point in time, say τ_{j+1} , the \underline{S} vector and 'new' $H_T(1)$ are set equal to zero again and the new $H_T(2)$ is set equal to the 'old' $H_T(1)$ obtained by integrating along S over the interval τ_j to τ_{j+1} . The other H_T values, depending on whether the characteristic grid coincides with the growth grid, are also updated as shown in Figure (6.4-A). This means that the H_T values along the characteristics are continuous while maintaining the same number of discrete H_T values by introducing at each time step a new $H_T(1)$ and dropping a H_T as shown in Figure (6.4-A).

The practical implementation of the characteristic grid interpolation solution scheme requires that for each integration step the value of ΔS needs to be calculated before-hand. Now ΔS is related to ΔD_g through equation (6.78), which in finite difference form is:

$$\Delta S_j^{j+1} = \Delta D_g(1) \frac{(G_D^2(\tau) + 1)^{1/2}}{G_D(\tau)} \Big|_j^{j+1} \quad (6.84)$$

while from (6.79) the corresponding $\Delta\tau_j$ is related in turn to ΔS_j by:

$$\Delta\tau_j = \Delta S_j (G_D^2(\tau) + 1)^{1/2} / j^{j+1} \quad (6.85)$$

At the start of an integration step from τ_j to τ_{j+1} , $G_D(\tau_j)$ is known but $G_D(\tau_{j+1})$ is not. Since G_D changes relatively slowly, the average growth rate over the interval is taken as $G_D(\tau_j)$. This practice leads to negligible error.

6.4.1 Correction for Quadrature Approximation Errors

After some initial numerical solutions either by means of the characteristic interpolation scheme or by the fixed grid weighted central difference approximation method, it became apparent that small approximation errors in the calculation of the agglomeration integrals by quadratures resulted in very small changes in the total crystal weight for an agglomeration only process at each time step calculation. For a pure agglomeration process with a bounded kernel the total mass or volume of particles is invariant. Any observed weight changes are thus the result of numerical approximations of the 'true' solution. Although, the approximation error for each quadrature calculation was very small, of the order of a few hundredths of a percent, it was found that this resulted in significant total weight errors after these quadratures are calculated several thousand times. This delineates one of the main difficulties in solving this type of equation. Total weight errors in turn result in errors in the calculation of the agglomeration term, since the agglomeration rate equation is a strong function of supersaturation which is directly

related to the crystal weight change. In addition, for a crystallization process the other rate processes such as growth and nucleation are functions of supersaturation as well, and therefore are also affected by the seemingly very small agglomeration quadrature approximation errors. It became apparent that for the type of fast changing size distribution encountered in this work this propagation of approximation errors led to erroneous numerical solution results.

To resolve this problem the following empirical correction expression for the agglomeration integral terms was developed. It is based on the fact that for an agglomeration-only process, total crystal weight is invariant. Starting with the equation for total crystal weight:

$$W_T = \int_{V_0}^V \phi(V) V F_{V,T}(V, \tau) dV$$

with $\phi(V) = 1 \times 10^{-12} \rho_s$ (see Appendix D), this integral may be approximated by:

$$W_T \approx 1 \times 10^{-12} \rho_s \sum_{i=1}^m \frac{\Delta H_T(i)}{\Delta V(i)} \Delta V(i) \left(\frac{V_{(i+1)} + V_{(i)}}{2} \right) \quad (6.87)$$

where $F_{V,T}$ has been approximated by $\Delta H_T / \Delta V$. More sophisticated approximations for the differential of H_T with respect to V could be applied as long as they would not introduce instabilities into the solution. Now in an agglomeration-only process, it is seen that the derivative of equation (6.87) with respect to τ must be zero, except for the quadrature approximation errors denoted here by ϵ . Thus

$$\begin{aligned} \frac{dW_T}{d\tau} / \text{aggl. only} &= \frac{1 \times 10^{-12}}{2} \rho_s \sum_{i=1}^m (V_{(i+1)} + V_{(i)}) \frac{d}{d\tau} \frac{\Delta H_T(i)}{\Delta V(i)} / \text{aggl. only} \\ &= 0 + \epsilon \end{aligned}$$

Letting $\frac{1 \times 10^{-12}}{2} \rho_s (V_{(i+1)} + V_{(i)}) = C_i$ shows that:

$$\sum_{i=1}^m C_i \frac{d}{d\tau} \Delta H_T(i) / \text{aggl. only} = 0 + \epsilon \quad (6.88)$$

This derivative term is in turn related to the agglomeration birth and death terms by:

$$\frac{d}{d\tau} \Delta H_T(i) / \text{aggl. only} = \{BH_{l,a}(i+1) - DH_{l,a}(i+1)\} - \{BH_{l,a}(i) - DH_{l,a}(i)\} \quad \dots (6.89)$$

since

$$\frac{\partial H_T(i)}{\partial \tau} / \text{aggl. only} = BH_{l,a}(i) - DH_{l,a}(i)$$

If it is assumed now that the 'true' $BH_{l,a}$ and $DH_{l,a}$ values (denoted by superscript *) are related to calculated values by expressions of the form:

$$BH_{l,a}^*(i) = (1-\lambda_i) BH_{l,a}(i) \quad (6.90)$$

$$DH_{l,a}^*(i) = (1-\lambda_i) DH_{l,a}(i) \quad (6.91)$$

with λ_i given by:

$$\lambda_i = b \times DH_{l,a}(i) \quad (6.92)$$

where b is determined as shown below. Although these relationships are entirely empirical they are based on the reasoning that the errors are

probably proportional to the magnitudes of $BH_{l,a}$ and $DH_{l,a}$. The result of this procedure is that the largest adjustment to the cumulative particle size distribution occurs over the upper size range of the distribution. This, in turn, means that only a very small correction needs to be made since the crystal weight is most sensitive to changes in the upper part of the distribution.

Substitution of (6.90) and (6.91) into equation (6.89) for the true birth and death values and summing as required by expression (6.88) with $\epsilon = 0$ for the true values gives:

$$\sum_{i=1}^m C_i \{ [(1-\lambda_{i+1})BH_{l,a}(i+1) - (1-\lambda_{i+1})DH_{l,a}(i+1)] - [(1-\lambda_i)BH_{l,a}(i) - (1-\lambda_i)DH_{l,a}(i)] \} = 0 \quad \dots\dots(6.93)$$

which after substitution of $b \times DH_{l,a}(i)$ for λ_i provides an expression for the only unknown b , i.e.

$$b = \frac{\sum_{i=1}^m C_i \{ (BH_{l,a}(i+1) - DH_{l,a}(i+1)) - (BH_{l,a}(i) - DH_{l,a}(i)) \}}{\sum_{i=1}^m C_i \{ DH_{l,a}(i+1)(BH_{l,a}(i+1) - DH_{l,a}(i+1)) - DH_{l,a}(i)(BH_{l,a}(i) - DH_{l,a}(i)) \}} \quad \dots\dots(6.94)$$

The empirically corrected values can then be calculated from:

$$BH_{l,a}^*(i) = (1 - b \times DH_{l,a}(i))BH_{l,a}(i) \quad (6.95)$$

$$DH_{l,a}^*(i) = (1 - b \times DH_{l,a}(i))DH_{l,a}(i) \quad (6.96)$$

This empirical numerical correction relationship is valid regardless of the significance of the other rate processes. The birth and death terms so corrected will change H_T due to agglomeration such that dW_T/dt as a result of agglomeration equals zero. It is required however that the agglomeration kernel be bounded, otherwise this correction would also compensate for the number of particles being agglomerated out of the solution domain. Another requirement for the validity of equations (6.95) and (6.96) is that the relationship between W_T and H_T must be consistent with the relationship used in the mass balance set of equations. Given that these conditions are met this correction is exact and thus eliminates the problem of the agglomeration quadrature approximation errors.

6.5 Investigation of the Two Numerical Solution Methods

The two numerical solution schemes proposed here are:

- (i) The method of characteristics combined with interpolation between the characteristic and rectangular agglomeration grids, and
- (ii) The solution along the rectangular grid using the weighted central difference approximation for $\partial H_T / \partial V$.

The first is denoted by CICR (Characteristics with Interpolation between Characteristics and Rectangular grids) and the second by RWCD (Rectangular grid with Weighted Central Difference). To demonstrate and evaluate the two schemes, a number of different cases were considered as shown in Table 6.5-A. The computer time required in each case is a measure of the 'ease' by which the solution is effected. It is seen that these times

TABLE 6.5-A Number of Required Function Evaluations and Required Central Processing Time for the Numerical Solution over an Integration Interval of Fifteen Minutes

TYPE OF BATCH CRYSTALLIZATION SYSTEM		Numerical Solution Accuracy Control			TYPE OF NUMERICAL SOLUTION WITH A CYBER 170 COMPUTER			
Crystallization Processes	Form of Initial Distribution	Number of Grid Points	RKM Relative Error Tolerance ϵ	Solution Along the Rectangular Grid	Solution by the RMCN Method	Solution Along the Characteristic Grid	Solution by the CICR Method	
				#/CP	#/CP	#/CP	#/CP	
nucleation only	exponential exponential	120 60	0.1 0.1	52/ 5.0 52/ 2.5	NA NA	NA NA	NA NA	
agglomeration only	exponential in normal in normal	120 120 60	0.1 0.1 0.1	77/50 72/46 117/19	NA NA NA	NA NA NA	NA NA NA	
agglomeration with empirical correction (aggl. cor.)	exponential	120	0.1	62/38	NA	NA	NA	
nucleation and aggl. cor.	exponential exponential	120 60	0.1 0.1	62/39 62/11	NA NA	NA NA	NA NA	
growth only	exponential	120	0.1	NA	2447/150	223/ 6.5	NA	
growth and nucleation	exponential	120	0.1	NA	1267/124	1493/108	NA	
growth and aggl. cor.	exponential in normal	120 120	0.1 0.1	NA NA	12000/7748* NI	NA NA	4294/2773* 458/296	
growth and nucleation & aggl. cor. (full model)	exponential exponential in normal	120 60 120	0.1 0.1 0.1	NA NA NA	1267/818 1242/201 762/492	NA NA NA	4043/2610* 3997/ 645 4593/2881	

Legend: RKM - Runge-Kutta-Morsion
 # - number of required function evaluations
 CP - computer central processing time(s)
 NA - not applicable
 NI - not investigated
 * - extrapolated from a shorter integration interval

depend on the type of crystallization process taking place and on the shape of the initial crystal size distribution. In situations where the birth and death processes predominate (nucleation-only, agglomeration-only or nucleation plus agglomeration), the solution is naturally along the rectangular grid. The method of characteristics is most appropriate for a process where the crystal growth rate is significant.

For a process with agglomeration the solution times increase by a factor of four with an increase of the number of grid points with respect to particle volume of two. This is to be expected since the agglomeration term consists of double integrals with respect to particle volume. If the process has an insignificant agglomeration rate, solution times pose no problem and the solution is naturally along the characteristics. As seen from Table 6.5-A, the solution of a growth only process is very fast if solved along the characteristics, while for a growth plus nucleation process the solution times are of the same order of magnitude for the CICR and RWCD solution methods. The characteristic solution in this case has, however, an advantage in that it is slightly more accurate, as discussed in sub-section 6.3.3.2.1 for a growth only process. Thus, for a process with only growth and/or nucleation the recommended solution method is by the CICR method.

Solution of an agglomeration only or an agglomeration plus nucleation process poses also no problem with regard to solution times. Introduction of the agglomeration empirical correction expression does not increase solution times, but instead results in a slight decrease of solution times, while as discussed in the previous sub-section, it greatly enhances the accuracy of the solution. In all subsequent solutions the agglomeration term was calculated with the empirical correction procedure included.

The type of initial size distribution influences the solution times only marginally and a significant nucleation rate has no effect on the computer time in an agglomeration plus nucleation process.

Unfortunately, the solution of the problem is more difficult by orders of magnitude, both with regard to computer time and accuracy, when a growth process is included with agglomeration or with agglomeration plus nucleation (the full model required here). This means that the interpolation procedure in the CICR method or the central weighted difference approximation for $\partial H_T / \partial V$ in the RWCD method adds significant complexity to the problem. Moreover, the results shown in Table 6.5A demonstrate that for a growth plus agglomeration process the shape of the initial size distribution profoundly influences the solution times for both solution methods. The essential difference between the log-normal distribution and the exponential distribution is that the latter introduces a step change at size V_0 , whereas the former does not. Thus, the solution times for an initial log-normal distribution are much faster because much larger step sizes can be tolerated in both numerical interpolation and numerical differentiation. It is interesting to note the behaviour of the step size used in the Runge-Kutta-Merson routine. The numerical integration method has an automatic step-size adjustment depending upon the estimated error (the Merson contribution) in integrating over the step size. With the same criterion in both methods the following observations were made:

- (a) For an agglomeration plus growth process, the step size allowed by the Runge-Kutta-Merson scheme was greater for the CICR solution than for the RWCD method.

- (b) For an agglomeration plus growth plus nucleation process, the reverse was true; that is, the step size was larger with the RWCD than with the CICR method.

No explanation can be offered for this behavior.

It is also to be noted that the RWCD method became unstable if the step size in the Runge-Kutta-Merson integration routine was automatically increased beyond a certain limit. Experience with this method here suggested that the maximum allowable step size was of the order of:

$$\Delta\tau \leq \frac{4\Delta D}{G}$$

(6.97)

This empirical expression was used to control the maximum step size and solved the instability problem. The reason for this conditional stability criterion is unknown.

6.6 Solution Procedure for the Alumina Trihydrate System

The observations and experiences of Section 6.5 suggested the following procedure for solving the full model (that is, with all crystallization processes involved): Start with the RWCD method and carry out the solution until the nucleation process becomes very small, that is, the process becomes one of essentially growth plus agglomeration. This solution then provided the initial conditions and size distribution for solution by the CICR method. With the constitutive rate relationships developed for the alumina trihydrate system under study here, this change-over point occurred at four hours crystallization time. This procedure resulted in a stable and accurate solution with a significant decrease in overall computer time.

From this experience, it can be concluded that both numerical solution methods can provide a practical solution to this difficult problem. The preferred solution method depends on the initial size distribution and the relative significance of each of the rate processes to the overall crystallization behaviour. Probably, as demonstrated, a combination of the two is the best compromise.

6.7 Comments on and Problems Arising out of the Solution Difficulties of the Full Model

Considerable effort was directed to establishing a satisfactory finite difference approximation for $\partial H/\partial V$ and this led to the weighted central difference approximation recommended here. On the other hand, different types of interpolating approximations for use in the CICR method have only been looked at superficially. It was found that linear interpolation between the two grids lead to gross accumulated errors when a fast changing size distribution (with respect to V or τ) was involved. On the other hand, using more complex interpolating schemes, such as piecewise continuous splines, resulted in instabilities. Thus, to realize the full potential of the CICR method, this interpolation problem for certain kinds of size distributions needs to be resolved. Certainly the CICR method is preferred over the RWCD method since numerical interpolation should be faster and more accurate than numerical differentiation.

The long computer time required to effect a solution of the population balance equation has serious ramifications for this research program. Note that constitutive equations relating the rates of growth, nucleation, and agglomeration with supersaturation and other system variables are required. Not only are the parameters in these relation-

ships unknown but also, as has been discussed in Chapter 2, a number of possible forms of these relationships can be postulated. Thus, a program for discriminating among the models for the various crystallization processes must be carried out and then the parameters in the 'best' models must be estimated. Note also, that even with the simplest of constitutive relationships, the dimensionality of the problem becomes very high (in the order of ten parameters at least). Moreover, the interaction among the parameters is expected to be severe.

In carrying out the model discrimination and parameter estimation exercise, the required objective function must be minimized or maximized depending upon the criterion used. This requires many evaluations of the objective function. One evaluation of the objective function requires the complete solution of the full model with one set of constitutive relationships and one set of parameters in them. Given the computer time required for each solution, the use of the full model in this exercise is most impractical. Thus, other methods for model discrimination and parameter estimation must be found. The development of suitable methods is described in Chapter 7. Finally, the predictions of the full model relative to the experimental observations are presented in Chapter 8.

CHAPTER 7

DEVELOPMENT OF CONSTITUTIVE RELATIONSHIPS- BY MEANS OF THE METHOD OF PSEUDO MOMENTS

7.1 Introduction

Since the straightforward method of discriminating among different constitutive relationships and evaluating parameters, through use of the full model and minimizing the sum of the squares of the residuals, requires impractically long computer times; a revised scheme was needed to circumvent this difficulty. This was achieved, as described below, through mathematical manipulation of the full model so as to obtain a mathematical expression which is independent of one or more of the processes which contribute to the crystal size distribution. Thus the full model was 'broken' into parts, such that each process could be considered in turn. The degree of difficulty in effecting a solution of each part increases as each new process is considered. The advantage of this scheme is that it allows model discrimination and parameter estimation in a relatively fast and easy way. The final constitutive relationships along with the parameters estimated for them are then used in the full model which is required to predict the crystal size distribution at any time during the batch crystallization.

7.2 Method of Pseudo Moments

The basic principle of the method is to transform the population balance equation to a pseudo-moment equation through use of a weighting function. This weighting function is so chosen that the effect of one of.

the processes of growth, agglomeration or nucleation is magnified while the effect of the others is suppressed. Thus, this method provides a means of extracting from the overall change of the size distribution that change which is specifically due to one particular crystallization process.

The general pseudo-moment equation, which was developed in Chapter 5, is repeated here for convenience:

$$\begin{aligned}
 \frac{d}{d\tau} \left\{ \int_{V_0}^{V_u} X_i(V) F_{V,T}(V, \tau) dV \right\} &= \frac{d}{d\tau} \{ \eta_i(\tau) \} - \\
 &+ G_D(\tau) \int_{V_0}^{V_u} \phi_g(V) F_{V,T}(V, \tau) \frac{d}{dV} \{ X_i(V) \} dV \\
 &+ V_L(\tau) B F_{l,n}(\tau) \int_{V_0}^{V_u} \phi_n(V) X_i(V) dV \\
 &+ \frac{1}{V_L(\tau)} \int_{V_0}^{V_u} \int_{V_0}^{V_u} k_{V,a}(V', V'', \tau) \{ X_i(V''+V') - X_i(V'') \} \\
 &\times F_{V,T}(V', \tau) F_{V,T}(V'', \tau) dV'' dV' \dots\dots (7.1)
 \end{aligned}$$

with initial conditions:

$$\eta_i(0) = \eta_{0,i} \quad (7.2)$$

where $i = 1, 2, 3, \dots, m_p$

m_p = number of pseudo-moment equations

This equation demonstrates the essence of this method of solution: If the variable $F_{V,T}$ is available from experimental data and the weighting

function X_i is, for instance, of a form such that the nucleation and agglomeration terms integrate out of the resulting expression, then the only process left to be described by this equation is the growth phenomenon. The parameters in the appropriate constitutive equation for this growth process may be easily estimated by standard least squares procedures whether the resulting expression is non-linear or not. In principle, the same procedure can be followed to obtain the kinetic models for the agglomeration and then the nucleation process; in these cases different weighting functions, X_i , are required.

Thus, the advantage of this method is that it decreases the dimensionality of the problem considerably and consequently the computer time for solution is reduced considerably. Moreover, the interaction among models and the correlation among the parameters is minimized.

7.2.1 Change in the Crystal Size Distribution Due to the Growth Process

To emphasize the effect of the growth process on the crystal size distribution and to suppress the effect of agglomeration and nucleation, the weighting function, X_i , was chosen to be:

$$X = \phi(V)V \quad (7.3)$$

Integration of equation (7.1) with X equal to this function gives:

$$\begin{aligned} \frac{d}{d\tau} \int_{V_0}^{V_u} \phi(V)V F_{V,T}(V,\tau) dV &= G_D(\tau) \int_{V_0}^{V_u} \phi_g(V) F_{V,T}(V,\tau) \frac{d}{dV} [\phi(V)V] dV \\ &+ V_L(\tau) B F_{L,n}(\tau) \int_{V_0}^{V_u} \phi_n(V) \phi(V) V dV \\ &+ 0 \quad \dots (7.4) \end{aligned}$$

The factor ϕ is chosen such that:

$$\int_{V_0}^{V_u} \phi(V) V F_{V,T}(V, \tau) dV = W_T(\tau) \quad (7.5)$$

If it is assumed that the solids density is 2.42 g/cm^3 , as suggested by Sakamoto (gl), and that the Coulter Counter measures true crystal volume*, then with the experimental $F_{V,T}$ values, the factor ϕ equals 2.42×10^{-12} . The factor 10^{-12} is required to maintain dimensional consistency for the dimensions used in this study,

Estimation of the area-volume shape factor in equation (7.4) poses a more difficult problem*. For spherical equivalent crystals (that is, spheres with the same volume as the crystals), the function ϕ_g as defined by:

$$G_V(V, \tau) \Delta \frac{dV}{d\tau} = G_D(\tau) \phi_g(V) \quad (7.6)$$

becomes:

$$\phi_g(V) = 0.5 \pi^{1/3} 6^{2/3} V^{2/3} \quad (7.7)$$

Thus, in this way, the crystal growth rate, $G_D(\tau)$, is defined on the basis of a spherical equivalent crystal area. This does not restrict the usefulness of any constitutive relationships since the growth rate relationship will absorb any differences between actual areas and assumed ones.

*These problems are discussed in detail in Appendix D.

The last term in equation (7.4) is zero because volume is conserved in the agglomeration process and the expression vanishes upon integration over the whole size range. This is a direct result of the definition of the agglomeration process. Moreover, if it is assumed that the rate of change of total crystal weight due to nucleation is negligibly small as compared to the change due to growth, this term in equation (7.4) can be set equal to zero. Therefore, incorporating this assumption along with the expressions for $\phi(V)$ and $\phi_g(V)$, equation (7.4) reduces to the following:*

$$\frac{d}{d\tau} \left\{ 2.42 \times 10^{-12} \int_{V_0}^{V_u} V F_{V,T}(V, \tau) dV \right\} \approx G_D(\tau) \left\{ 5.8515 \times 10^{-12} \int_{V_0}^{V_u} V^{2/3} F_{V,T}(V, \tau) dV \right\} \quad \dots (7.8)$$

or, in short form:

$$\frac{d}{d\tau} \{ \phi W(\tau) \} = G_D(\tau) \{ \phi A(\tau) \} \quad (7.9)$$

In applying the method which is proposed here to obtain a model for the growth rate along with its parameters, it would be necessary, in using equation (7.8), to differentiate experimental data from which ϕW is obtained. Differentiation of experimental data leads to high inaccuracies and, in general, should be avoided. (h6).

*Note that the growth rate, $G_D(\tau)$, in equation (7.8) is indicated as a function of time; in fact, the kinetic model for growth rate is a function of supersaturation which is a function of time for a batch system.

To circumvent this practical difficulty, equation (7.9) is integrated with respect to τ to give:

$$\phi W(\tau_j) = \int_0^{\tau_j} G_D(\tau) \phi A(\tau) d\tau + \phi W(0) \quad (7.10)$$

Equation (7.10) may be used to determine a kinetic model for the crystal growth rate using experimental data from a batch crystallization in the following way: at any time, τ_j , a numerical value of $\phi W(\tau_j)$ may be determined by performing the indicated integration (numerically) using the experimental crystal size distribution data obtained at that time. Call this value ϕW_j . At the same time, given a model for $G_D(\tau)$ along with the parameters in it, the right-hand side of equation (7.10) may be evaluated by numerical quadrature at time τ_j as well. Note that this requires the experimental size distribution data as well; also, $W(0)$ must be evaluated, numerically, from experimental data. Call this numerical value of the right-hand side ϕW_j^* . Thus, equation (7.10) may be written in the form:

*In this study the overheads $\hat{\sim}$ and \sim denote best estimate and expected values, respectively. Thus for any model:

$$\underline{Z}(x,y) = \hat{\underline{Z}}(x,y,b) + \underline{\epsilon}(Z) \quad (7.15)$$

where

- \underline{Z} - vector of 'observations' or experimental measurements
- $\hat{\underline{Z}}$ - vector of expected model values
- $\underline{\epsilon}$ - vector of errors associated with the measurements
- \underline{b} - vector of model parameters
- $\underline{x}, \underline{y}$ - vectors of experimental variables

with the 'predicted' model values denoted by $\hat{\underline{Z}}(x,y,\hat{\underline{b}})$. The vector $\hat{\underline{b}}$ is the 'best' estimate of \underline{b} with 'best' depending upon the criterion used to define it. Here use is made of the least-squares estimation procedure.

$$\phi W_j = \phi \tilde{W}_j + \epsilon_j \quad j = 1, 2, \dots, n \quad (7.11)$$

and n is the number of experimental observations at known times, τ_j , with:

$$\phi \tilde{W}_j = 5.8515 \times 10^{-12} \int_0^{\tau_j} G_D(\tau) \int_{V_0}^{V_u} V^{2/3} F_{V,T}(V, \tau) dV d\tau + \phi W(0) \quad \dots (7.12)$$

and

$$\phi W_j = 2.42 \times 10^{-12} \int_{V_0}^{V_u} V F_{V,T}(V, \tau_j) dV \quad (7.13)$$

with ϵ_j an unknown error associated with measurement j.

Unfortunately both $\phi \tilde{W}_j$ and ϕW contain experimental measurements (in this case functions of the same random variable) so that writing equation (7.11) in this form is not correct in the usual statistical sense. However, in the absence of a better method, the best set of parameters in any given model for the growth rate were estimated by the least-squares procedure, namely by choosing the parameters such that S_g as defined by:

$$S_g = \sum_{j=1}^n W_j (\phi W_j - \phi \tilde{W}_j)^2 \quad (7.14)$$

was minimized. Note $\phi \tilde{W}_j$ contains the growth rate model and thus is considered the expected value of ϕW_j ; it also contains the experimentally measured $\phi W(0)$. The weighting functions, W_j , are included to account for the different variances which may exist for the different ϕW values. This weighting allows those values which exhibit the greatest error to contribute the least to the numerical value of S_g .

Thus, this scheme provides a method for selecting the best growth model and evaluating the parameters in it without confounding the estimation procedure with the nucleation and agglomeration processes which interact with it. Moreover, the difficulties associated with obtaining a solution to the integro-partial differential equation are avoided. The only disadvantage is that the errors associated with the integral expressions are difficult to evaluate.

7.2.2 Change in the Crystal Size Distribution Due to the Agglomeration Process

As was done in extracting the crystal growth rate, an attempt was made to integrate the growth and nucleation rate terms out of the integro-differential equation and leave only the agglomeration terms. Unfortunately, a way to do this was not found. By proper choice of weighting functions, however, it was possible to eliminate the effect of nucleation and minimize the effect of growth. This was done by selecting m_p weighting functions of the form:

$$X_k = C1 \times \{H(V-\alpha_k) - H(V-\beta_k)\} \quad (7.17)$$

$$k = 1, 2, 3, \dots, m_p$$

where $C1$ is a scaling constant given by, for example,

$$C1 = 1000 / \int_{V_0}^{V_u} F_{V,T}(V,0) dV \quad (7.18)$$

and $H(V)$ is a unit step function which takes on the following values:

$$\begin{aligned}
 H(V) &= 0 && \text{for } V < 0 \\
 &= 1 && \text{for } V \geq 0
 \end{aligned}$$

Graphically, these weighting functions have the shape as shown by the broken lines in Figure 7.2.2-A. This figure also indicates how these functions weight the crystal size distribution. It can be seen that together these mp equations represent the whole size distribution and not merely a small section or a global average. The use of a set instead of only one was found to be advantageous in discriminating among various agglomeration kernel models. This advantage results because a possible poor fit of a particular model would show up in some or all of the mp moment equations. With the use of only one global weighting function this might have gone unnoticed due to cancellation of negative and positive deviations between changes in the size distribution and changes predicted by the agglomeration model.

The parameters in the weighting functions, that is α_k and β_k in the mp weighting functions given by equation (7.17), are chosen such that the nucleation term in equation (7.1) is always zero. This means

that

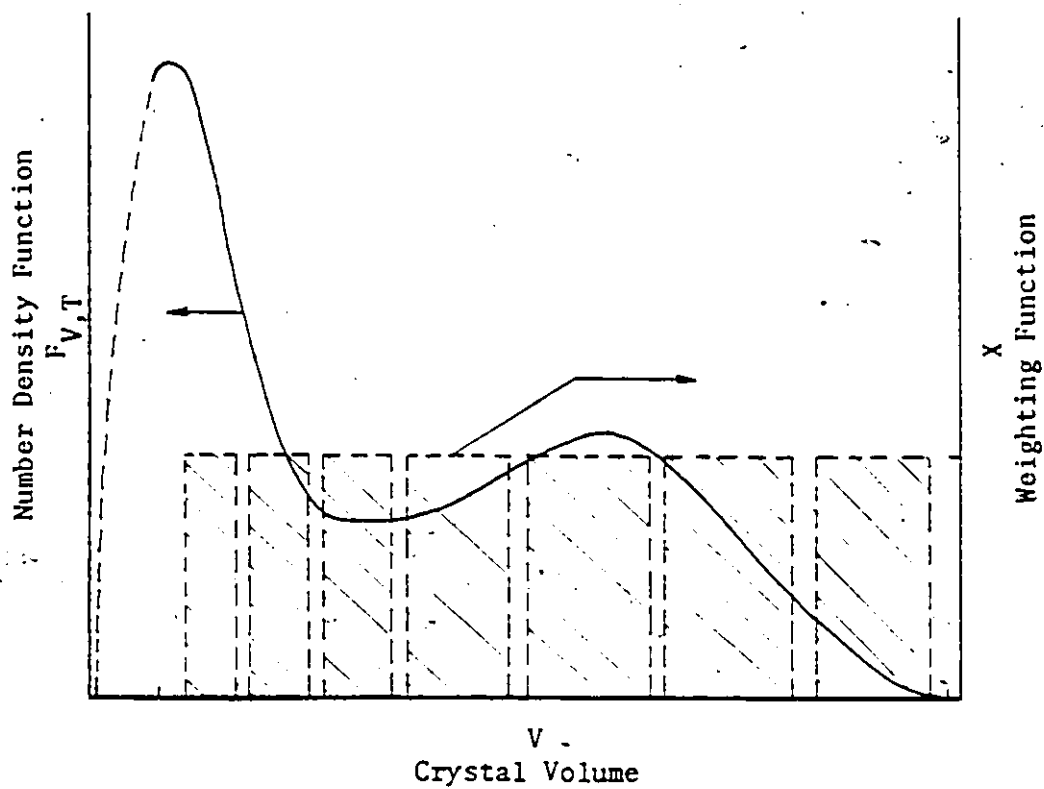
$$\int_{V_0}^{V_u} \phi_n(V) X_k(V) dV = 0 \quad (7.19)$$

since, over the region where $\phi_n(V) > 0$, the weighting function, $X_k(V) = 0$; while, where $X_k(V) > 0$, the nucleation term, $\phi_n(V) = 0$.

The growth rate term which from equation (7.1) is equal to

$$G_D(\tau) \int_{V_0}^{V_u} \phi_g(V) F_{V,T}(V, \tau) \frac{d}{dV} \{X_k(V)\} dV \quad (7.20)$$

FIGURE 7.2.2-A Schematic of the Weighting Functions used in the Investigation of Agglomeration Kernel Models Superimposed on a Number Density Function



is evaluated for this particular set of X_k functions as follows: First, by definition of $\phi_g(V)$

$$G_V(V, \tau) = G_D(\tau) \phi_g(V)$$

and by substitution into equation (7.20) for G_D and ϕ_g this equation can be expressed through integration by parts as the equality:

$$\int_{V_0}^{V_u} X_k(V) \frac{\partial}{\partial V} \{G_V(V, \tau) F_{V,T}(V, \tau)\} dV = X_k(V) G_V(V, \tau) F_{V,T}(V, \tau) \Big|_{V_0}^{V_u} - \int_{V_0}^{V_u} G_V(V, \tau) F_{V,T}(V, \tau) \frac{d}{dV} \{X_k(V)\} dV \quad \dots (7.21)$$

The last term is equivalent to equation (7.20), while the first term on the right is equal to zero since $F_{V,T}(V_0, \tau)$ and $F_{V,T}(V_u, \tau)$ are zero.

Thus:

$$(7.20) = - \int_{V_0}^{V_u} X_k(V) \frac{\partial}{\partial V} \{G_V(V, \tau) F_{V,T}(V, \tau)\} dV \quad (7.22)$$

Second, it is seen that for these X_k functions equation (7.22) is zero for $V < \alpha_k$ and for $V > \beta_k$, while for $\alpha_k \leq V \leq \beta_k$

$$(7.20) = - C1 \int_{\alpha_k}^{\beta_k} \frac{\partial}{\partial V} \{G_V(V, \tau) F_{V,T}(V, \tau)\} dV \quad (7.23)$$

since $X_k = C1$ over this interval. The solution of this integral is:

$$\{G_V(\alpha_k, \tau) F_{V,T}(\alpha_k, \tau) - G_V(\beta_k, \tau) F_{V,T}(\beta_k, \tau)\}$$

Back substitution of $G_D(\tau) \cdot \phi_g(V)$ for $G_V(V, \tau)$ in this expression and including the spherical equivalent expression for $\phi_g(V)$ yields:

$$(7.20) = 2.418 C1 G_D(\tau) \{ \alpha_k^{2/3} F_{V,T}(\alpha_k, \tau) - \beta_k^{2/3} F_{V,T}(\beta_k, \tau) \} \dots (7.24)$$

$k = 1, 2, 3, \dots, mp$

Note that if the two terms in equation (7.24) are approximately equal, the growth term in equation (7.1) becomes very small relative to the agglomeration term for the mp pseudo moments. Moreover, since the nucleation term is zero, the choice of this particular set of pseudo moments leads to a set of equations which describe the change in the size distribution which arises essentially from the agglomeration process only.

The general pseudo moment equation (7.1) for the set of weighting functions given by equation (7.17) thus reduces to:

$$C1 \frac{d}{d\tau} \int_{\alpha_k}^{\beta_k} F_{V,T}(V, \tau) dV = 2.418 C1 G_D(\tau) \{ \alpha_k^{2/3} F_{V,T}(\alpha_k, \tau) - \beta_k^{2/3} F_{V,T}(\beta_k, \tau) \} + \frac{1}{V_L(\tau)} \int_{V_0}^V \int_{V_0}^u k_{V,a}(V', V'', \tau) F_{V,T}(V', \tau) F_{V,T}(V'', \tau) \times [\frac{1}{2} X_k(V''+V') - X_k(V'')] \dots (7.25)$$

$k = 1, 2, 3, \dots, mp$

which is written, for convenience, in short form through the definition of the following variables:

$$\frac{d}{d\tau} nA_k(\tau) = nG_k(\tau) + nC_k(\tau) \quad (7.26)$$

$$k = 1, 2, 3, \dots, mp$$

This set of equations can be used to obtain a constitutive relationship for $k_{V,a}$ as a function of system variables through the following procedure: Again, as for the expression for the growth rate, the differential is removed by the integration of equation (7.26) with respect to batch time, τ , to give the following set of equations

$$nA_{k,j} = \tilde{n}A_{k,j}(\underline{b}_a) + \epsilon_{k,j} \quad (7.27)$$

$$\text{where } \tilde{n}A_{k,j}(\underline{b}_a) = \int_0^{\tau_j} nG_k(\tau) d\tau + \int_0^{\tau_j} n\tilde{C}_k(\tau, \underline{b}_a) d\tau + nA_{k,1} \quad (7.27a)$$

$$\text{with } n\tilde{C}_k(\tau, \underline{b}_a) = \frac{1}{V_L(\tau)} \int_{V_0}^{V_u} \int_{V_0}^{V_u} k_{V,a}(V', V'', \tau, \underline{b}_a) F_{V,T}(V', \tau) F_{V,T}(V'', \tau) \\ \times \left\{ \frac{1}{2} X_k(V'+V'') - X_k(V'') \right\} dV' dV'' \quad \dots (7.27b)$$

In this expression, $k_{V,a}(V', V'', \tau, \underline{b}_a)$ is the constitutive relationship expressing the agglomeration rate kernel as a function of system variables which are a function of time and crystal sizes. Note that this relationship also contains the parameters, \underline{b}_a , which must be estimated for this crystallization system.

The other terms in equation (7.27a) are obtained as follows:

Note that the experimental size distribution data are available as a function of time. Using these data the integral:

$$\eta A_{k,j} = C_1 \int_{\alpha_k}^{\beta_k} F_{V,T}(V,\tau) dV \quad (7.28)$$

may be evaluated by numerical quadrature. Similarly, the growth rate term in each of the mp equations:

$$\eta G_k(\tau) = 2.418 C_1 \hat{G}_D(\tau) \{ \alpha_k^{2/3} F_{V,T}(\alpha_k, \tau) - \beta_k^{2/3} F_{V,T}(\beta_k, \tau) \} \quad \dots (7.29)$$

may be evaluated given the model for $G_D(\tau)$ and the parameters which were estimated previously by the method described earlier. The double integration indicated in equation (7.27b) is carried out by numerical quadrature as well, using the experimental data for the size distribution as a function of time. Again, this does introduce a problem associated with evaluating the error term in equation (7.27), since the expected value, $\eta \tilde{A}_{k,j}(\underline{b}_a)$, as well as the observations, $\eta A_{k,j}$ contain experimental data which are subject to considerable error.

As in the case of estimating the parameters in the model for the growth rate, the ~~parameters~~ in any agglomeration rate model are estimated by minimizing S_a given by:

$$S_a = \sum_{j=1}^n \sum_{k=1}^{mp} W(k,j) \{ \eta A(k,j) - \eta \tilde{A}(k,j, \underline{b}_a) \}^2 \quad (7.30)$$

The weighting functions $W(k,j)$ should be related to the unknown error term; thus, again, a problem does arise in using this scheme to estimate the parameters.

This method does, however, provide a means of obtaining a model for the agglomeration effectiveness kernel, $k_{V,a}$, without strong interaction with the other rate processes. Indeed, this model is only weakly correlated with the growth rate and is completely independent of the nucleation rate. The problem of having to solve an integro-partial differential equation with a large number of parameters in different models has been avoided by this procedure. The solution does require evaluation of a considerable number of integrals including the double integral for n_k^2 through a numerical quadrature technique, a process which may consume considerable computer time. This computer time, however, is not so excessive as to discourage investigation of a number of different size dependent models for $k_{V,a}$. These attempts are discussed later in this chapter.

7.2.3 Change in the Crystal Size Distribution Due to the Nucleation Process

The method of pseudo-moments was also used to separate the effect of the nucleation rate on the crystal size distribution. In this case the weighting function was chosen as:

$$X(V) = C_1 \quad (7.31)$$

where C_1 is a scaling parameter which, for example, may be given by:

$$Cl = 1000 \int_{V_0}^{V_u} F_{V,T}(V,0) dV \quad (7.32)$$

The choice of this particular weighting function results in a moment equation which is very sensitive to the nucleation rate and also 'integrates out' the growth term in equation (7.1). This latter result is easily demonstrated by the same procedure which gave rise to equation (7.24) except that $F_{V,T}(V,\tau) = 0$ at both the upper and lower integration limit. Thus equation (7.1) becomes:

$$\begin{aligned} Cl \frac{d}{d\tau} \int_{V_0}^{V_u} F_{V,T}(V,\tau) dV &= V_L(\tau) BF_{\ell,n}(\tau) Cl \int_{V_0}^{V_u} \phi_n(V) dV \\ &- \frac{1}{2} Cl \frac{1}{V_L(\tau)} \int_{V_0}^{V_u} \int_{V_0}^{V_u} k_{V,a}(V',V'',\tau) \\ &F_{V,T}(V',\tau) F_{V,T}(V'',\tau) dV'' dV' \dots (7.33) \end{aligned}$$

Note that this equation relates the rate of change of total particle number to the birth term (via nucleation) minus the death term (via agglomeration). Equation (7.33) indicates that the change in number of crystals is independent of crystal growth as is expected.

As was done in the previous cases, equation (7.33) can be used in conjunction with the experimental data to estimate the parameters in any nucleation model, $BF_{\ell,n}(\tau)$, which relates nucleation rate to the system operating conditions which are a function of time. The procedure outlined below was followed:

Equation (7.33) is integrated with respect to time and for convenience rewritten in terms of new variables:

$$\xi A_j = \int_0^{\tau_j} \xi N(\tau) d\tau - \int_0^{\tau_j} \xi C(\tau) d\tau + \xi A_1 \quad (7.34)$$

where $\xi A_j = Cl \int_{V_0}^V F_{V,T}(V, \tau_j) dV$

$$\xi C(\tau) = \frac{Cl}{2V_L(\tau)} \int_{V_0}^V \int_{V_0}^V k_{V,a}(V', V'', \tau) F_{V,T}(V', \tau) F_{V,T}(V'', \tau) dV'' dV'$$

$$\xi N(\tau) = Cl V_L(\tau) BF_{\ell,n}(\tau) \int_{V_0}^V \phi_n(V) dV$$

with ξA_1 being the initial number of seed crystals in the crystallizer.

To use this equation to estimate the parameters in a nucleation model for $BF_{\ell,n}(\tau)$ and $\phi_n(V)$ requires evaluation of the term, $\xi C(\tau)$, which accounts for the effect of agglomeration on crystal number. This term may be evaluated, if an appropriate model for the agglomeration kernel, $k_{V,a}$, which may be developed by the scheme presented earlier, provides a satisfactory representation of this phenomenon. Thus, the expected value of the particle number at any time, τ_j , may be written:

$$\begin{aligned} \xi \tilde{A}_j(\underline{b}_n) &= Cl \int_0^{\tau_j} V_L(\tau) BF_{\ell,n}(\tau, \underline{b}_n) d\tau \int_{V_0}^V \phi_n(V, \underline{b}_n) dV \\ &\quad - \frac{Cl}{2} \int_0^{\tau_j} \frac{1}{V_L(\tau)} \int_{V_0}^V \int_{V_0}^V k_{V,a}(V', V'', \tau, \underline{b}_n) F_{V,T}(V', \tau) \\ &\quad \quad \quad F_{V,T}(V'', \tau) dV' dV'' d\tau + \xi A_1 \end{aligned} \quad \dots (7.35)$$

and

$$\xi A_j = \xi \tilde{A}_j + \epsilon_j \quad j = 1, 2, 3, \dots, n \quad (7.36)$$

Here \underline{b}_n is the vector of parameters in the model for nucleation which relate the nucleation process to the changing environment (supersaturation)

and to a particle size function, respectively, as will be shown later in this chapter. This expected value, ξA_j , may be determined for any given set of parameters by evaluating the indicated integrals by numerical methods. The experimental particle size distribution and agglomeration model are required to evaluate the agglomeration term. The 'experimental' value, ξA_j , may be determined using the experimental size distribution data at time, τ_j .

As was done previously, the parameters in the nucleation models are estimated by minimizing S_N , as given by:

$$S_N = \sum_{j=1}^n W_j (\xi A_j - \xi A_j)^2 \quad (7.37)$$

where the weights, W_j , should be related to the error function ϵ_j . Herein lies the problem for now this error function contains not only the experimental errors associated with measuring $F_{V,T}$ but also contains the error associated with the model for the agglomeration phenomenon. If this compounded error is the same for each experimental point, then the weighting is the same for each point and minimizing the sum of squares of the residuals is the correct procedure to use to estimate the parameters in the nucleation model. In the absence of any way to evaluate the correct weighting, this procedure was adopted here.

The advantages of using this method to determine a nucleation model are:

- (1). The evaluation of the expected value requires numerical integration of a small set of integrals.

- (2) The interaction with the growth rate is eliminated.
- (3) The agglomeration rate term is evaluated using a model which was determined from an independent scheme.

The main disadvantage is that the experimental errors are not accounted for properly.

7.5 Constitutive Relationships for Growth, Agglomeration and Nucleation

Models (7.11), (7.27), and (7.36), along with their parameters, for the rate of crystal growth, agglomeration and nucleation are, in principle, relatively easily obtained by the methods already described. Unfortunately, two practical problems associated with this method arise: First, the errors in the measurements are not able to be accounted for, since the expected model values need to be calculated from experimental measurements, such as supersaturation and crystal size distribution for example, which are subject to measurement errors. Note also, that the 'experimental response' itself is a transformation of the primary response from the experiment. This situation is atypical of normal modelling procedures. Secondly, because a numerical integration technique is required to obtain both the experimental and expected value, the integrands of the integrals need to be evaluated at specific values of the integration variable. Since in general these values do not coincide with the experimentally measured ones, interpolation between the experimental measurements is required.

It was found that the interpolation between the raw experimental measurements led to difficulties during the parameter estimation procedures since such interpolations among 'noisy' experimental data gave rise

to expected values which were not a slowly changing function of the model parameters. Particularly, it was difficult to discriminate among the various suggested constitutive relationships because of these interpolation problems. Using smoothed experimental data alleviated this problem. If more accurate methods for carrying out the experimental measurements (particularly the size distribution measurements) are devised this smoothing procedure may not be necessary.

7.3.1 Smoothing of Experimental Data

The empirical regression equations used to smooth the experimental measurements and to allow interpolation are described in the following sub-sections.

7.3.1.1 Solution Concentration Variables

Empirical equations for the solution concentration variables such as, alumina, caustics, and solids weight are required since they are either directly or indirectly part of the constitutive relations for growth, agglomeration, and nucleation. It will be seen that once a smoothing equation has been developed for the alumina concentration, all the other dependent variables which are a function of time follow from this equation and initial conditions (c.f. Chapter 5, Section 5.6.6).

(A) Smoothing Formula for the Alumina Solution Concentration

Of the possible smoothing formulas to express the alumina solution concentration as a function of time, the following were investigated:

- cubic splines with minimum second derivatives,
- cubic splines with variable 'knots',
- weighted orthogonal polynomials,
- non-linear, exponential-type formulas.

These are all purely empirical formulas. Their 'goodness' was judged by the sum of squares of the residuals, by the random distribution of the residuals about zero, by the variation of the expected value between data points and by the behaviour of the derivative of the dependent variable as a function of batch time, τ . Any empirical function which did not exhibit a monotonically increasing or decreasing behaviour between data points was judged to be poor for the purposes intended for its use here.

The spline formula provided reasonable fits, but unfortunately the interpolated values (those predicted by the formula) usually tended to oscillate about a smooth curve drawn through the data points. Moreover, the derivatives indicated this rapidly changing behaviour. The orthogonal polynomials did not provide as good fits and also showed even more variation between the data points than that observed for the cubic spline fit. The exponential-type formula removed this oscillatory behaviour. They provided the 'best' fit according to the criteria as stated above. The best of those tried is given by:

$$C_A^2 = b_1 + b_2 \exp\{-(\tau + b_3)^{b_4}\} \quad (7.38)$$

with $b_3 \geq 0$ for all τ . This smoothing formula for the dissolved alumina concentration provides a representation which decreases monotonically with time. The parameter estimation scheme is presented at the end of the next section.

(B) Relationship between the Alumina and Caustic Solution Concentrations

Equation (7.38) also indirectly defines the smoothed rate of change of caustic concentration with respect to time since these compounds are both related to the solution volume change. The relationship is derived in Chapter 5, Section 5.6.7. The resulting equation for caustic concentration as a function of batch time is:

$$\tilde{CN} = \{-C3 - (C3^2 - 4C2C4)^{1/2}\} / (2C2) \quad (7.39)$$

where $C1 = (CA_o - 654 \rho_{l,o}) / CN_o$

$$\rho_{l,o} = b6 + b7CN_o + b8CN_o^2 + b9CA_o$$

$$C2 = b8$$

$$C3 = C1/654 + b7$$

$$C4 = b6 + (b9 - .001529)CA$$

The o subscripts denote initial conditions, while the parameters, b6 to b9, are those which were suggested by Misra (m2) in his solution density model; their numerical values are:

$$b6 = 1.051 + 5.1 \times 10^{-6} \theta^2 - 9.4 \times 10^{-4} \theta$$

$$b7 = 9.92 \times 10^{-4}$$

$$b8 = -1.1 \times 10^{-7}$$

$$b9 = 5.66 \times 10^{-4}$$

From equation (7.39) it is seen that CN_0 needs to be known before this equation can be solved for CN. If CN_0 were known relatively accurately as compared to CN, it could be treated as a deterministic constant. This is the usual situation where it is possible to accurately measure the initial conditions. In this case, however, an accurate measurement of the initial concentration was not possible because of the ill-defined actual starting time; hence CN_0 was considered as an unknown parameter. That is, in equation (7.39), $\rho_{2,0}$ and C1 were calculated with the parameter $b5 \equiv CN_0$, which was then estimated along with the parameters b1 through b4 of equation (7.38).

The five parameters in equations (7.38) and (7.39) were obtained by minimization of S_s as defined by:

$$S_s = \sum_{j=1}^n \{W1_j (CA_j - \hat{CA}_j)^2 + W2_j (CN_j - \hat{CN}_j)^2\} \quad (7.40)$$

where the weight vectors W1 and W2 were set equal to one since the variances of the experimental observations CA and CN are of approximate equal absolute magnitude (g3). The minimization was carried out by means of the Marquardt non-linear estimation technique, and the estimated parameters were found to be:

$$\hat{b}_1 = 92.46$$

$$\hat{b}_2 = 79.62$$

$$\hat{b}_3 = 0.3856$$

$$\hat{b}_4 = 0.4218$$

$$\hat{b}_5 = 120.1$$

(C) Other Process Variables Required in the Crystallizer Model

The other variables involved in the crystallization process follow directly through mass balances once the alumina and caustic concentrations are known. The relationships are derived in Chapter 5 and repeated here for convenience. They are:

(i) Solution Volume

$$V_L(\tau) = V_{L,o} \text{CN}_o / \text{CN}(\tau) \quad (7.41)$$

(ii) Solids Weight

$$W_T(\tau) = (V_{L,o} \text{CA}_o - \frac{V_{L,o} \text{CN}_o \text{CA}(\tau)}{\text{CN}(\tau)}) / .654 + W_{T,o} \quad (7.42)$$

(iii) Suspension Volume

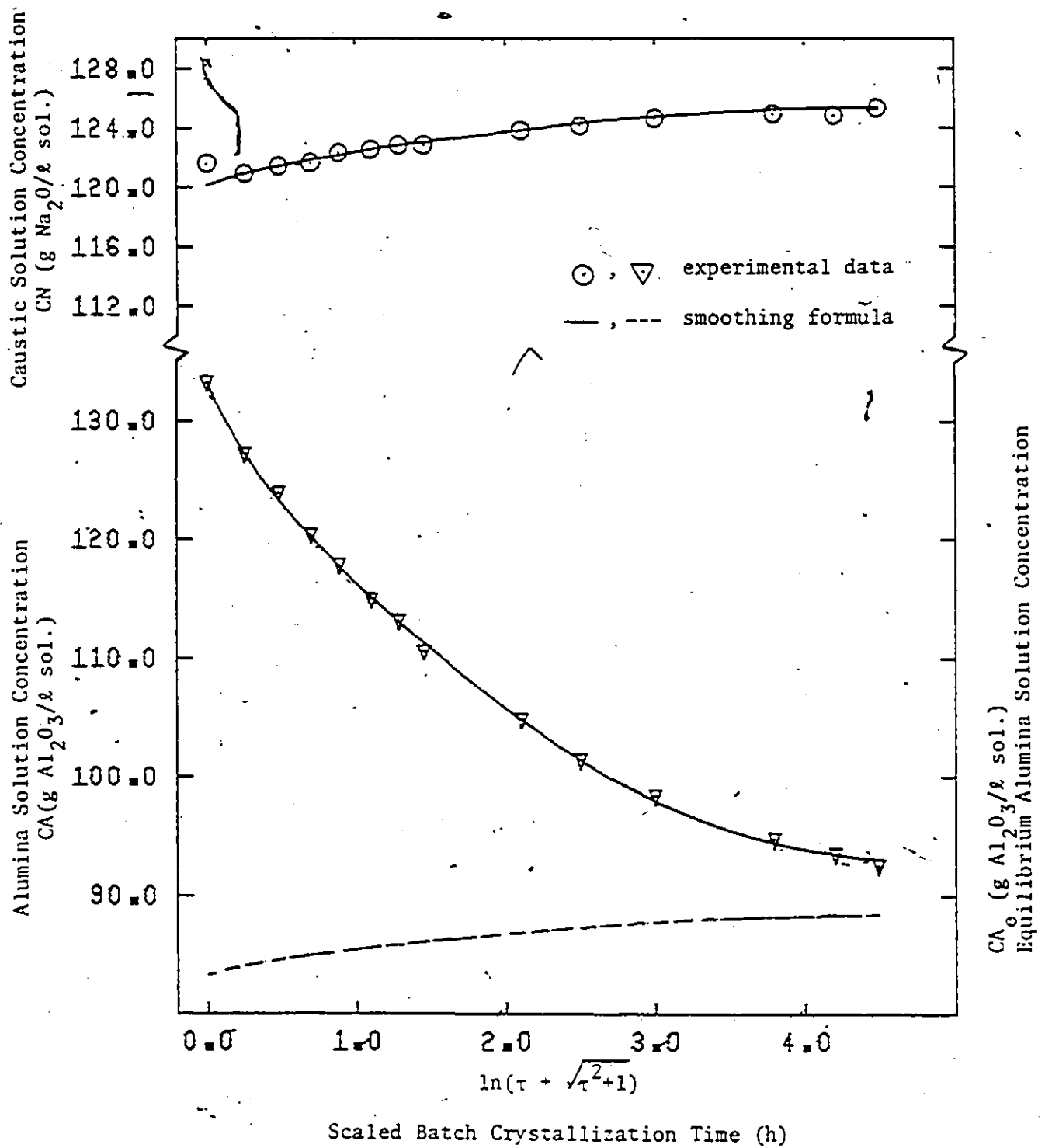
$$V_T(\tau) = V_L(\tau) + \frac{W_T(\tau)}{1000 \rho_s} \quad (7.43)$$

In addition, the equilibrium concentration of alumina is required in the model. The expression derived by Misra (m2) is assumed to be correct over the concentration ranges of these experiments:

$$\text{CA}_e(\tau) = \text{CN}(\tau) \exp\left\{6.2106 + \frac{(1.08753 \text{CN}(\tau) - 2486.7)}{273.16 + \theta}\right\} \quad (7.44)$$

The computer program used in the parameter estimation procedure for equations (7.38) and (7.39) is listed in Appendix E. The comparisons between the smoothed values and experimental data are shown in Figure 7.3.1.1-A.

FIGURE 7.3.1.1-A Experimental and Smoothed Alumina and Caustic Solution Concentrations



7.3.1.2 Smoothing Formula for the Experimental Crystal Size Distribution Data

As indicated earlier numerical values of the density function $F_{V,T}$ at specified times and crystal volumes are required to evaluate the objective function in the procedure used to evaluate the parameters in models for the nucleation, growth and agglomeration. Moreover, smoothing of the experimental data helped to shorten the computer time required in these parameter estimation programs. Thus, a mathematical representation for the experimental measurements for the crystal-size density function as a function of particle size (volume) and time is required.

The crystal size distribution varies rapidly with size over the region of small crystal size, but then changes slowly over the larger size region. A similar behaviour is observed with batch time. To facilitate the finding of a suitable smoothing formula these two independent variables and the dependent variable were transformed in an identical way, namely:

$$x^t = \ln(x + \sqrt{x^2+1})$$

where x may be time, τ , crystal volume, V , or density function, $F_{V,T}$.

These transformations scaled the independent variables in such a way that the density function changed at about the same rate over the full range of the two variables. It was found that a satisfactory smoothing formula for $F_{V,T}$ could not be found if these transformations were not used.

The process of obtaining a satisfactory two-dimensional mathematical representation for the experimental data consisted of first finding one with respect to the transformed crystal size variable at each time at which the experimental measurements were made. The values as predicted by these equations were then fitted with respect to the transformed batch time.

A number of formula have been tried, including a set of orthogonal polynomials, cubic spline approximations specially developed for smoothing, and cubic splines least-square approximations over the whole domain of both independent variables. These smoothing schemes all proved inadequate in that large non-random deviations between predicted and experimental values occurred over the ranges of the two independent variables. This indicated that these smoothing approximations were not correct.

It was found, however, that an approximation consisting of cubic splines with variable knot locations (subroutine ICSVKH of the IMSL Library 3, by International Mathematical and Statistical Libraries, Inc.) fitted only over the domain where the density function values are greater than zero gave a reasonable fit. In this case, the only parameter which was varied was the total number of knots. In the fitting of crystal size, it was found that seven knots gave a good fit, while in the time dimension the number of knots was a variable function depending on the number of data points, viz.:

$$NXT_i = NJ_i/7 + 2$$

where NXT_i is the number of knots used in the variable-knots location, cubic spline formula; NJ_i is the number of data points in the time domain at crystal volume V_i where the density function is greater than zero.

The percentage differences between experimental data and smoothed predictions are presented in Table 7.3.1.2-A. It is seen that the deviations are randomly distributed about zero and are not correlated with either crystal volume or time.

TABLE 7.3.1.2-A Relative Percentage Difference between Experimental Density Function Data and Smoothed Predictions

Crystal Size, D	Batch Time, τ														
	0.0	.3	.5	.8	1.0	1.3	1.7	2.0	4.0	6.0	10.0	22.0	33.0	44.0	
4.2	0	-2.1	7.4	-2.8	-1.3	-1.5	49.9	-6.1	12.0	-5.6	12.4	-7.4	22.8	9.4	
4.3	4.7	-1.6	6.2	-2.7	-1.2	-6.8	25.0	-12.3	9.0	-10.3	1.0	-12.2	10.4	9.8	
4.4	1.6	-2.0	5.9	-1.0	-1.0	-7.0	14.2	-13.0	4.7	-11.0	-3.2	1.0	7.5	14.3	
4.5	1.7	-2.2	5.6	-3.7	-6.2	-7.0	32.0	-9.7	13.2	-8.8	5.4	-8.6	26.4	12.0	
4.6	1.1	-2.0	5.5	-5.0	-3.0	-9.0	25.0	-14.7	13.0	-12.5	2.5	-9.5	15.0	12.5	
4.8	1.7	-4.0	5.4	-7.1	-3.4	-6.7	17.0	-2.2	16.0	-17.0	-4.5	-5.8	11.0	11.5	
5.0	1.5	-3.0	5.2	-1.0	-5.3	0.0	0.3	-0.9	17.0	-24.0	7.3	17.3	13.0	13.0	
5.2	1.4	-3.0	5.0	-0.3	-5.3	0.0	1.4	-0.0	17.0	-26.0	13.0	17.0	13.0	13.0	
5.3	1.5	-3.0	5.0	-7.0	-5.1	-7.0	13.0	-4.0	19.0	-9.0	19.0	-15.0	15.0	15.0	
5.4	1.5	-3.0	5.0	-4.0	-3.0	-7.0	10.0	-10.0	19.0	-18.0	11.0	-12.0	13.0	13.0	
5.5	1.5	-3.0	5.0	-7.0	-2.0	-7.0	9.0	-10.0	19.0	-27.0	18.0	-25.0	13.0	13.0	
5.6	1.5	-3.0	5.0	-7.0	-2.0	-7.0	9.0	-10.0	19.0	-27.0	18.0	-25.0	13.0	13.0	
5.7	1.5	-3.0	5.0	-7.0	-2.0	-7.0	9.0	-10.0	19.0	-27.0	18.0	-25.0	13.0	13.0	
5.8	1.5	-3.0	5.0	-7.0	-2.0	-7.0	9.0	-10.0	19.0	-27.0	18.0	-25.0	13.0	13.0	
5.9	1.5	-3.0	5.0	-7.0	-2.0	-7.0	9.0	-10.0	19.0	-27.0	18.0	-25.0	13.0	13.0	
6.0	1.5	-3.0	5.0	-7.0	-2.0	-7.0	9.0	-10.0	19.0	-27.0	18.0	-25.0	13.0	13.0	
6.1	1.5	-3.0	5.0	-7.0	-2.0	-7.0	9.0	-10.0	19.0	-27.0	18.0	-25.0	13.0	13.0	
6.2	1.5	-3.0	5.0	-7.0	-2.0	-7.0	9.0	-10.0	19.0	-27.0	18.0	-25.0	13.0	13.0	
6.3	1.5	-3.0	5.0	-7.0	-2.0	-7.0	9.0	-10.0	19.0	-27.0	18.0	-25.0	13.0	13.0	
6.4	1.5	-3.0	5.0	-7.0	-2.0	-7.0	9.0	-10.0	19.0	-27.0	18.0	-25.0	13.0	13.0	
6.5	1.5	-3.0	5.0	-7.0	-2.0	-7.0	9.0	-10.0	19.0	-27.0	18.0	-25.0	13.0	13.0	
6.6	1.5	-3.0	5.0	-7.0	-2.0	-7.0	9.0	-10.0	19.0	-27.0	18.0	-25.0	13.0	13.0	
6.7	1.5	-3.0	5.0	-7.0	-2.0	-7.0	9.0	-10.0	19.0	-27.0	18.0	-25.0	13.0	13.0	
6.8	1.5	-3.0	5.0	-7.0	-2.0	-7.0	9.0	-10.0	19.0	-27.0	18.0	-25.0	13.0	13.0	
6.9	1.5	-3.0	5.0	-7.0	-2.0	-7.0	9.0	-10.0	19.0	-27.0	18.0	-25.0	13.0	13.0	
7.0	1.5	-3.0	5.0	-7.0	-2.0	-7.0	9.0	-10.0	19.0	-27.0	18.0	-25.0	13.0	13.0	
7.1	1.5	-3.0	5.0	-7.0	-2.0	-7.0	9.0	-10.0	19.0	-27.0	18.0	-25.0	13.0	13.0	
7.2	1.5	-3.0	5.0	-7.0	-2.0	-7.0	9.0	-10.0	19.0	-27.0	18.0	-25.0	13.0	13.0	
7.3	1.5	-3.0	5.0	-7.0	-2.0	-7.0	9.0	-10.0	19.0	-27.0	18.0	-25.0	13.0	13.0	
7.4	1.5	-3.0	5.0	-7.0	-2.0	-7.0	9.0	-10.0	19.0	-27.0	18.0	-25.0	13.0	13.0	
7.5	1.5	-3.0	5.0	-7.0	-2.0	-7.0	9.0	-10.0	19.0	-27.0	18.0	-25.0	13.0	13.0	
7.6	1.5	-3.0	5.0	-7.0	-2.0	-7.0	9.0	-10.0	19.0	-27.0	18.0	-25.0	13.0	13.0	
7.7	1.5	-3.0	5.0	-7.0	-2.0	-7.0	9.0	-10.0	19.0	-27.0	18.0	-25.0	13.0	13.0	
7.8	1.5	-3.0	5.0	-7.0	-2.0	-7.0	9.0	-10.0	19.0	-27.0	18.0	-25.0	13.0	13.0	
7.9	1.5	-3.0	5.0	-7.0	-2.0	-7.0	9.0	-10.0	19.0	-27.0	18.0	-25.0	13.0	13.0	
8.0	1.5	-3.0	5.0	-7.0	-2.0	-7.0	9.0	-10.0	19.0	-27.0	18.0	-25.0	13.0	13.0	
8.1	1.5	-3.0	5.0	-7.0	-2.0	-7.0	9.0	-10.0	19.0	-27.0	18.0	-25.0	13.0	13.0	
8.2	1.5	-3.0	5.0	-7.0	-2.0	-7.0	9.0	-10.0	19.0	-27.0	18.0	-25.0	13.0	13.0	
8.3	1.5	-3.0	5.0	-7.0	-2.0	-7.0	9.0	-10.0	19.0	-27.0	18.0	-25.0	13.0	13.0	
8.4	1.5	-3.0	5.0	-7.0	-2.0	-7.0	9.0	-10.0	19.0	-27.0	18.0	-25.0	13.0	13.0	
8.5	1.5	-3.0	5.0	-7.0	-2.0	-7.0	9.0	-10.0	19.0	-27.0	18.0	-25.0	13.0	13.0	
8.6	1.5	-3.0	5.0	-7.0	-2.0	-7.0	9.0	-10.0	19.0	-27.0	18.0	-25.0	13.0	13.0	
8.7	1.5	-3.0	5.0	-7.0	-2.0	-7.0	9.0	-10.0	19.0	-27.0	18.0	-25.0	13.0	13.0	
8.8	1.5	-3.0	5.0	-7.0	-2.0	-7.0	9.0	-10.0	19.0	-27.0	18.0	-25.0	13.0	13.0	
8.9	1.5	-3.0	5.0	-7.0	-2.0	-7.0	9.0	-10.0	19.0	-27.0	18.0	-25.0	13.0	13.0	
9.0	1.5	-3.0	5.0	-7.0	-2.0	-7.0	9.0	-10.0	19.0	-27.0	18.0	-25.0	13.0	13.0	
9.1	1.5	-3.0	5.0	-7.0	-2.0	-7.0	9.0	-10.0	19.0	-27.0	18.0	-25.0	13.0	13.0	
9.2	1.5	-3.0	5.0	-7.0	-2.0	-7.0	9.0	-10.0	19.0	-27.0	18.0	-25.0	13.0	13.0	
9.3	1.5	-3.0	5.0	-7.0	-2.0	-7.0	9.0	-10.0	19.0	-27.0	18.0	-25.0	13.0	13.0	
9.4	1.5	-3.0	5.0	-7.0	-2.0	-7.0	9.0	-10.0	19.0	-27.0	18.0	-25.0	13.0	13.0	
9.5	1.5	-3.0	5.0	-7.0	-2.0	-7.0	9.0	-10.0	19.0	-27.0	18.0	-25.0	13.0	13.0	
9.6	1.5	-3.0	5.0	-7.0	-2.0	-7.0	9.0	-10.0	19.0	-27.0	18.0	-25.0	13.0	13.0	
9.7	1.5	-3.0	5.0	-7.0	-2.0	-7.0	9.0	-10.0	19.0	-27.0	18.0	-25.0	13.0	13.0	
9.8	1.5	-3.0	5.0	-7.0	-2.0	-7.0	9.0	-10.0	19.0	-27.0	18.0	-25.0	13.0	13.0	
9.9	1.5	-3.0	5.0	-7.0	-2.0	-7.0	9.0	-10.0	19.0	-27.0	18.0	-25.0	13.0	13.0	
10.0	1.5	-3.0	5.0	-7.0	-2.0	-7.0	9.0	-10.0	19.0	-27.0	18.0	-25.0	13.0	13.0	
10.1	1.5	-3.0	5.0	-7.0	-2.0	-7.0	9.0	-10.0	19.0	-27.0	18.0	-25.0	13.0	13.0	
10.2	1.5	-3.0	5.0	-7.0	-2.0	-7.0	9.0	-10.0	19.0	-27.0	18.0	-25.0	13.0	13.0	
10.3	1.5	-3.0	5.0	-7.0	-2.0	-7.0	9.0	-10.0	19.0	-27.0	18.0	-25.0	13.0	13.0	
10.4	1.5	-3.0	5.0	-7.0	-2.0	-7.0	9.0	-10.0	19.0	-27.0	18.0	-25.0	13.0	13.0	
10.5	1.5	-3.0	5.0	-7.0	-2.0	-7.0	9.0	-10.0	19.0	-27.0	18.0	-25.0	13.0	13.0	
10.6	1.5	-3.0	5.0	-7.0	-2.0	-7.0	9.0	-10.0	19.0	-27.0	18.0	-25.0	13.0	13.0	
10.7	1.5	-3.0	5.0	-7.0	-2.0	-7.0	9.0	-10.0	19.0	-27.0	18.0	-25.0	13.0	13.0	
10.8	1.5	-3.0	5.0	-7.0	-2.0	-7.0	9.0	-10.0	19.0	-27.0	18.0	-25.0	13.0	13.0	
10.9	1.5	-3.0	5.0	-7.0	-2.0	-7.0	9.0	-10.0	19.0	-27.0	18.0	-25.0	13.0	13.0	
11.0	1.5	-3.0	5.0	-7.0	-2.0	-7.0	9.0	-10.0	19.0	-27.0	18.0	-25.0	13.0	13.0	

TABLE 7.3.1.2-A (cont'd.).....

Crystal Size, D	Batch Time, τ													
	0.0	.3	.5	.8	1.0	1.3	1.7	2.0	4.0	6.0	10.0	22.0	33.0	44.0
12.0	35.0	3.0	4.0	3.0	3.0	4.0	3.0	3.0	2.0	1.0	2.0	1.0	7.0	25.0
12.0	38.0	4.0	5.0	4.0	4.0	5.0	4.0	4.0	3.0	2.0	3.0	2.0	8.0	26.0
13.0	31.0	5.0	6.0	5.0	5.0	6.0	5.0	5.0	4.0	3.0	4.0	3.0	9.0	28.0
13.0	32.0	6.0	7.0	6.0	6.0	7.0	6.0	6.0	5.0	4.0	5.0	4.0	10.0	29.0
14.0	33.0	7.0	8.0	7.0	7.0	8.0	7.0	7.0	6.0	5.0	6.0	5.0	11.0	30.0
14.0	34.0	8.0	9.0	8.0	8.0	9.0	8.0	8.0	7.0	6.0	7.0	6.0	12.0	31.0
15.0	35.0	9.0	10.0	9.0	9.0	10.0	9.0	9.0	8.0	7.0	8.0	7.0	13.0	32.0
15.0	36.0	10.0	11.0	10.0	10.0	11.0	10.0	10.0	9.0	8.0	9.0	8.0	14.0	33.0
16.0	37.0	11.0	12.0	11.0	11.0	12.0	11.0	11.0	10.0	9.0	10.0	9.0	15.0	34.0
16.0	38.0	12.0	13.0	12.0	12.0	13.0	12.0	12.0	11.0	10.0	11.0	10.0	16.0	35.0
17.0	39.0	13.0	14.0	13.0	13.0	14.0	13.0	13.0	12.0	11.0	12.0	11.0	17.0	36.0
17.0	40.0	14.0	15.0	14.0	14.0	15.0	14.0	14.0	13.0	12.0	13.0	12.0	18.0	37.0
18.0	41.0	15.0	16.0	15.0	15.0	16.0	15.0	15.0	14.0	13.0	14.0	13.0	19.0	38.0
18.0	42.0	16.0	17.0	16.0	16.0	17.0	16.0	16.0	15.0	14.0	15.0	14.0	20.0	39.0
19.0	43.0	17.0	18.0	17.0	17.0	18.0	17.0	17.0	16.0	15.0	16.0	15.0	21.0	40.0
19.0	44.0	18.0	19.0	18.0	18.0	19.0	18.0	18.0	17.0	16.0	17.0	16.0	22.0	41.0
20.0	45.0	19.0	20.0	19.0	19.0	20.0	19.0	19.0	18.0	17.0	18.0	17.0	23.0	42.0
20.0	46.0	20.0	21.0	20.0	20.0	21.0	20.0	20.0	19.0	18.0	19.0	18.0	24.0	43.0
21.0	47.0	21.0	22.0	21.0	21.0	22.0	21.0	21.0	20.0	19.0	20.0	19.0	25.0	44.0
21.0	48.0	22.0	23.0	22.0	22.0	23.0	22.0	22.0	21.0	20.0	21.0	20.0	26.0	45.0
22.0	49.0	23.0	24.0	23.0	23.0	24.0	23.0	23.0	22.0	21.0	22.0	21.0	27.0	46.0
22.0	50.0	24.0	25.0	24.0	24.0	25.0	24.0	24.0	23.0	22.0	23.0	22.0	28.0	47.0
23.0	51.0	25.0	26.0	25.0	25.0	26.0	25.0	25.0	24.0	23.0	24.0	23.0	29.0	48.0
23.0	52.0	26.0	27.0	26.0	26.0	27.0	26.0	26.0	25.0	24.0	25.0	24.0	30.0	49.0
24.0	53.0	27.0	28.0	27.0	27.0	28.0	27.0	27.0	26.0	25.0	26.0	25.0	31.0	50.0
24.0	54.0	28.0	29.0	28.0	28.0	29.0	28.0	28.0	27.0	26.0	27.0	26.0	32.0	51.0
25.0	55.0	29.0	30.0	29.0	29.0	30.0	29.0	29.0	28.0	27.0	28.0	27.0	33.0	52.0
25.0	56.0	30.0	31.0	30.0	30.0	31.0	30.0	30.0	29.0	28.0	29.0	28.0	34.0	53.0
26.0	57.0	31.0	32.0	31.0	31.0	32.0	31.0	31.0	30.0	29.0	30.0	29.0	35.0	54.0
26.0	58.0	32.0	33.0	32.0	32.0	33.0	32.0	32.0	31.0	30.0	31.0	30.0	36.0	55.0
27.0	59.0	33.0	34.0	33.0	33.0	34.0	33.0	33.0	32.0	31.0	32.0	31.0	37.0	56.0
27.0	60.0	34.0	35.0	34.0	34.0	35.0	34.0	34.0	33.0	32.0	33.0	32.0	38.0	57.0
28.0	61.0	35.0	36.0	35.0	35.0	36.0	35.0	35.0	34.0	33.0	34.0	33.0	39.0	58.0
28.0	62.0	36.0	37.0	36.0	36.0	37.0	36.0	36.0	35.0	34.0	35.0	34.0	40.0	59.0
29.0	63.0	37.0	38.0	37.0	37.0	38.0	37.0	37.0	36.0	35.0	36.0	35.0	41.0	60.0
29.0	64.0	38.0	39.0	38.0	38.0	39.0	38.0	38.0	37.0	36.0	37.0	36.0	42.0	61.0
30.0	65.0	39.0	40.0	39.0	39.0	40.0	39.0	39.0	38.0	37.0	38.0	37.0	43.0	62.0
30.0	66.0	40.0	41.0	40.0	40.0	41.0	40.0	40.0	39.0	38.0	39.0	38.0	44.0	63.0
31.0	67.0	41.0	42.0	41.0	41.0	42.0	41.0	41.0	40.0	39.0	40.0	39.0	45.0	64.0
31.0	68.0	42.0	43.0	42.0	42.0	43.0	42.0	42.0	41.0	40.0	41.0	40.0	46.0	65.0
32.0	69.0	43.0	44.0	43.0	43.0	44.0	43.0	43.0	42.0	41.0	42.0	41.0	47.0	66.0
32.0	70.0	44.0	45.0	44.0	44.0	45.0	44.0	44.0	43.0	42.0	43.0	42.0	48.0	67.0
33.0	71.0	45.0	46.0	45.0	45.0	46.0	45.0	45.0	44.0	43.0	44.0	43.0	49.0	68.0
33.0	72.0	46.0	47.0	46.0	46.0	47.0	46.0	46.0	45.0	44.0	45.0	44.0	50.0	69.0
34.0	73.0	47.0	48.0	47.0	47.0	48.0	47.0	47.0	46.0	45.0	46.0	45.0	51.0	70.0
34.0	74.0	48.0	49.0	48.0	48.0	49.0	48.0	48.0	47.0	46.0	47.0	46.0	52.0	71.0
35.0	75.0	49.0	50.0	49.0	49.0	50.0	49.0	49.0	48.0	47.0	48.0	47.0	53.0	72.0

Representative plots of the transformed density function versus transformed time are shown on Figure 7.3.1.2-A. It can be seen that this spline formula provides a very good representation and the necessary smoothing of the data.

The computer program (Program BC) for this smoothing scheme is listed in Appendix E.

7.3.1.3 Estimation of the Number of Crystals with a Size Less than the Cut-off Size

As indicated previously, a serious limitation of the Coulter Counter is its inability to detect particles less than a certain size (the cut-off size). If the particles to be measured have a size range beyond the capability of the orifice tube used in it, then some lower part of the distribution will be unknown. The extent of this unknown region is related to the maximum particle size expected in the distribution. In the present case, because agglomeration occurs to an appreciable extent, rather large particles can be expected (ca. 60 μm) and, as a consequence, the cut-off size is fairly large (ca. 4 μm). Unfortunately, because of the secondary nucleation process, an appreciable number of crystals exist below this cut-off size during the early part of the crystallization at least.

In order to establish a nucleation model and estimate the parameters in it, it is important to have measurements of the total number of particles as a function of time (see equation (7.36)). Fortunately, it is possible to estimate the unknown part of the size distribution (particle size density function) using the experimental measurements of the alumina concentration and the crystal size distribution which were

FIGURE 7.3.1.2-A Experimental Density Function Data and Smoothed Cubic Splines Predictions

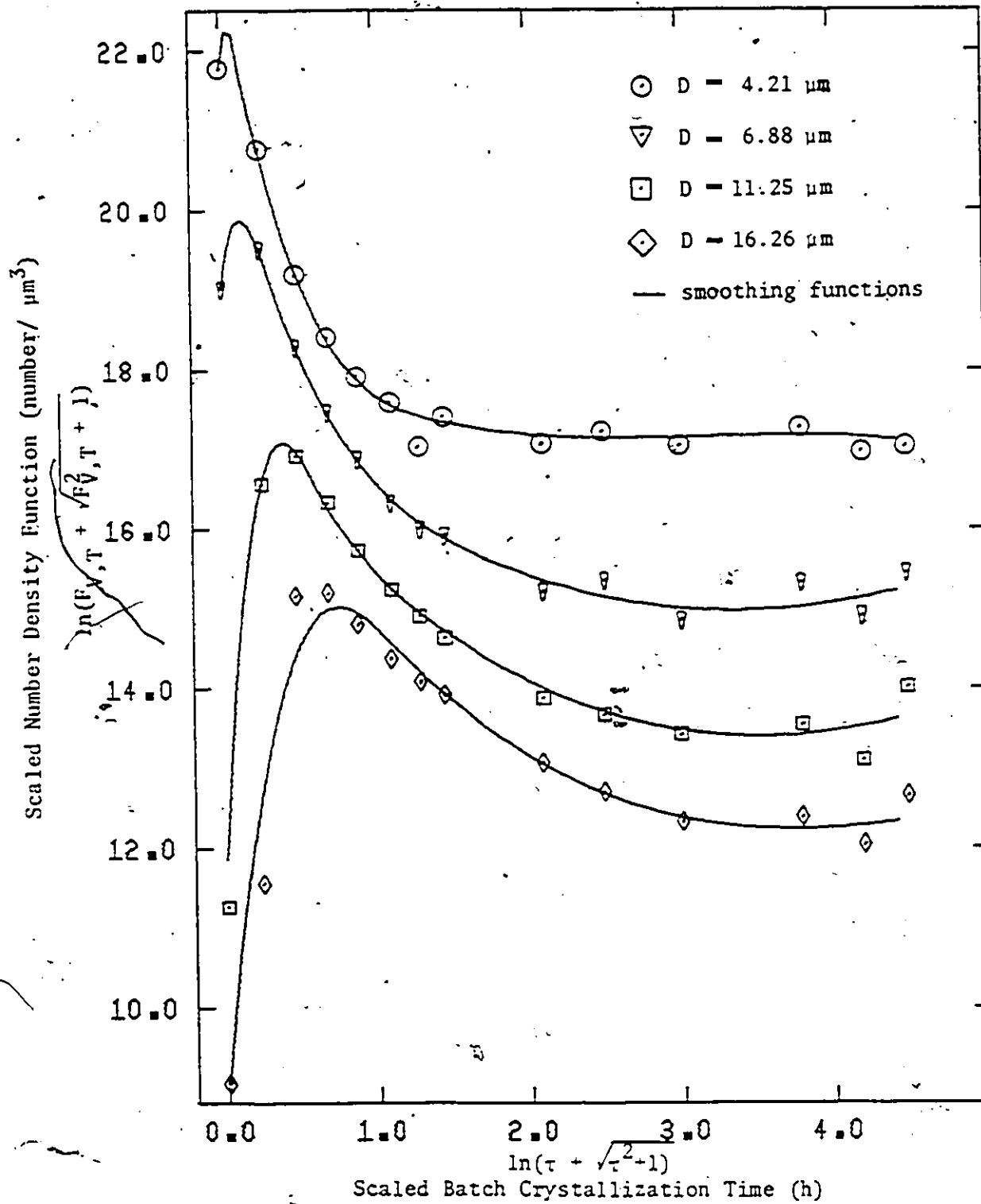
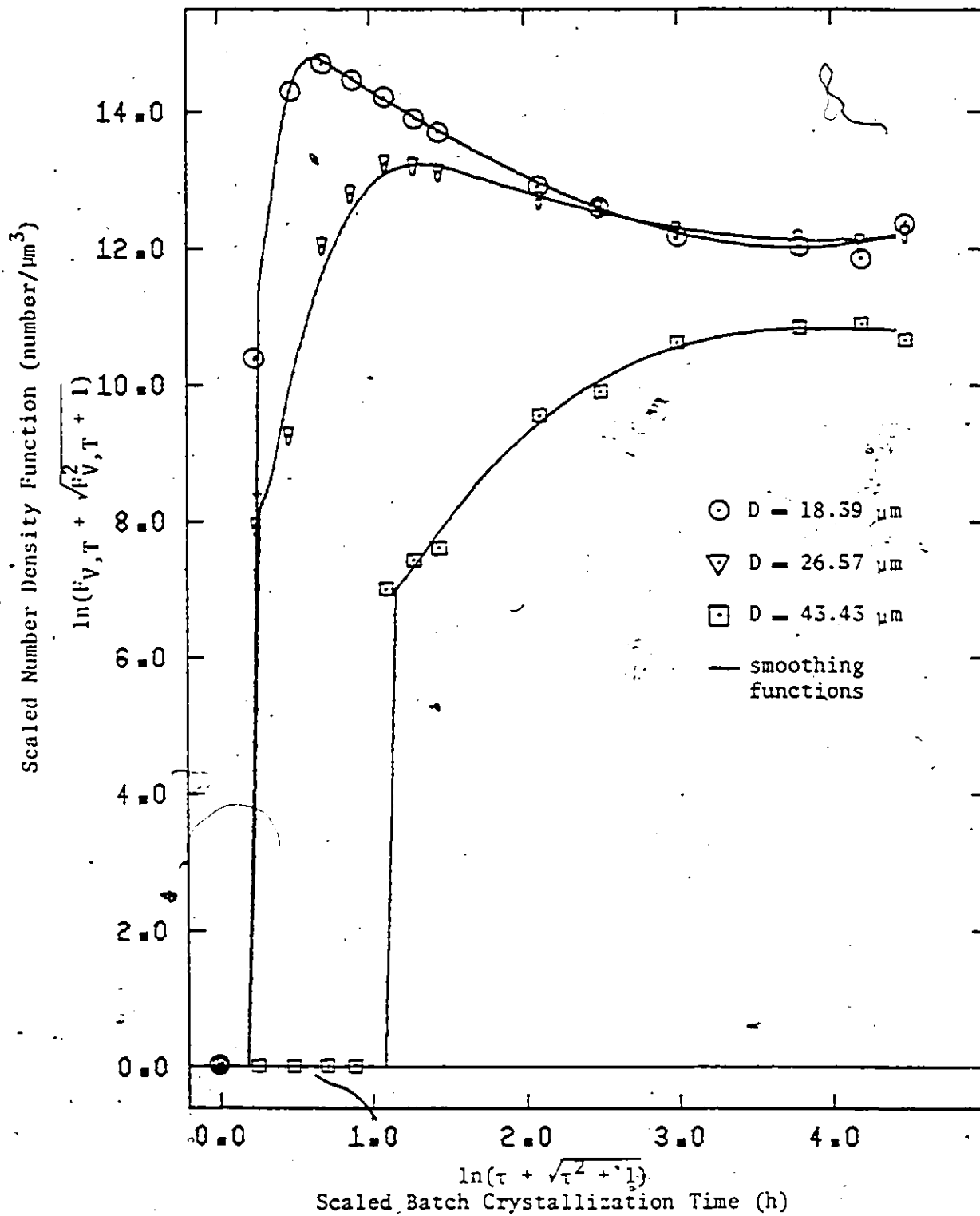


FIGURE 7.3.1.2-A (cont'd.)



made at specific times during the experiment. This estimation procedure is described below.

In Chapter 4, it was shown that the mass of solid per unit volume of solution could be calculated at any time in two independent ways:

- (i) From the initial seed charge and alumina concentration and the alumina concentration at any time during the crystallization suitably corrected for changing solution volume.
- (ii) From the crystal size density function which was measured on an absolute concentration basis.

Thus, the total mass of solid expressed in terms of the crystal density function is given by:

$$W_{T,S}(\tau) = 2.42 \times 10^{-12} \left\{ \int_{V_0}^{V_c} V F_{V,T}(V,\tau) dV + \int_{V_0}^{V_u} V F_{V,T}(V,\tau) dV \right\} \quad \text{.....(7.45)}$$

where the integration limits V_0 , V_c , V_u are the smallest, the Coulter Counter cut-off size, and the largest crystal volume, respectively. The mass of solid expressed in terms of solute concentrations is:

$$W_{T,S}(\tau) = CS_1(\tau) V_T(\tau) \quad (7.46)$$

where $CS_1(\tau)$ is given by equation (4.8) as presented in Chapter 4.

Thus, the unknown distribution is expressed in terms of experimental measurements, viz.:

$$N_{o,c}(\tau) = CS_1(\tau)V_T(\tau) - \int_{V_c}^u V F_{V,T}(V,\tau)dV/2.42 \times 10^{12} \quad (7.46a)$$

with the expected value of $N_{o,c}$ given by:

$$\tilde{N}_{o,c}(\tau) = \int_{V_o}^{V_c} V \tilde{F}_{V,T}(V,\tau)dV/2.42 \times 10^{12} \quad (7.46b)$$

An empirical equation for the unknown distribution (i.e. the $\tilde{F}_{V,T}$ values over the range V_o to V_c) may be suggested by the following reasoning: since no prior information was available with regard to the number of crystals below the cut-off size other than that their number is significant, the first expression tested for $\tilde{F}_{V,T}/V_o^c$ was a constant times $F_{V,T}(V_c,\tau)$. This provided a poor fit; the estimate at small τ values was too small and at large τ values it was too large. Therefore, a time dependence was put in the expression which after some trials resulted in the following empirical expression for the size distribution below the cut-off size:

for $0 < \tau \leq \tau e(2)$,

$$\tilde{F}_{V,T}(\tau) = [a(1)\tau + b(1)]F_{V,T}(V_c,\tau) \quad (7.47a)$$

for $\tau e(2) < \tau \leq \tau e(4)$,

$$\tilde{F}_{V,T}(\tau) = [a(2)\tau + b(2)]F_{V,T}(V_c,\tau) \quad (7.47b)$$

and for $\tau > \tau_e(4)$,

$$\tilde{F}_{V,T}(\tau) = bs(3)F_{V,T}(V_c, \tau) \quad (7.47c)$$

where $a(1) = \{bs(2) - bs(1)\}/\{\tau_e(2) - \tau_e(1)\}$

$a(2) = \{bs(3) - bs(2)\}/\{\tau_e(4) - \tau_e(2)\}$

$b(1) = bs(1) - \{a(1)\tau_e(1)\}$

$b(2) = bs(2) - \{a(2)\tau_e(2)\}$

$\tau_e =$ batch sample times (h)

$\tau =$ batch times (h)

The vector of parameters, \underline{bs} , in the empirical expression for the crystal density function below the cut-off size was estimated by minimizing the sum of squares of the residuals:

$$S_F = \sum_{j=1}^n \{N_{o,c}(j) - \tilde{N}_{o,c}(\xi_j, \underline{bs})\}^2 \quad (7.48)$$

The empirical expression $\tilde{N}_{o,c}(\xi_j, \underline{bs})$ provides the expected value under experimental conditions, $\underline{\xi}$:

$$\tilde{N}_{o,c}(j) = 2.42 \times 10^{-12} \int_{V_o}^{V_c} V \tilde{F}_{V,T}(\tau_j, \underline{bs}) dV$$

Note, there are n measurements during a batch experiment, each giving an experimentally derived function, $N_{o,c}(j)$ and an expected value $\tilde{N}_{o,c}(j)$.
Again, the Marquardt procedure was used to search for the minimum.

The best estimates of the \underline{bs} vector were found to be:

$$\hat{b}_s(1) = 2.3$$

$$\hat{b}_s(2) = 7.1$$

$$\hat{b}_s(3) = 1.0$$

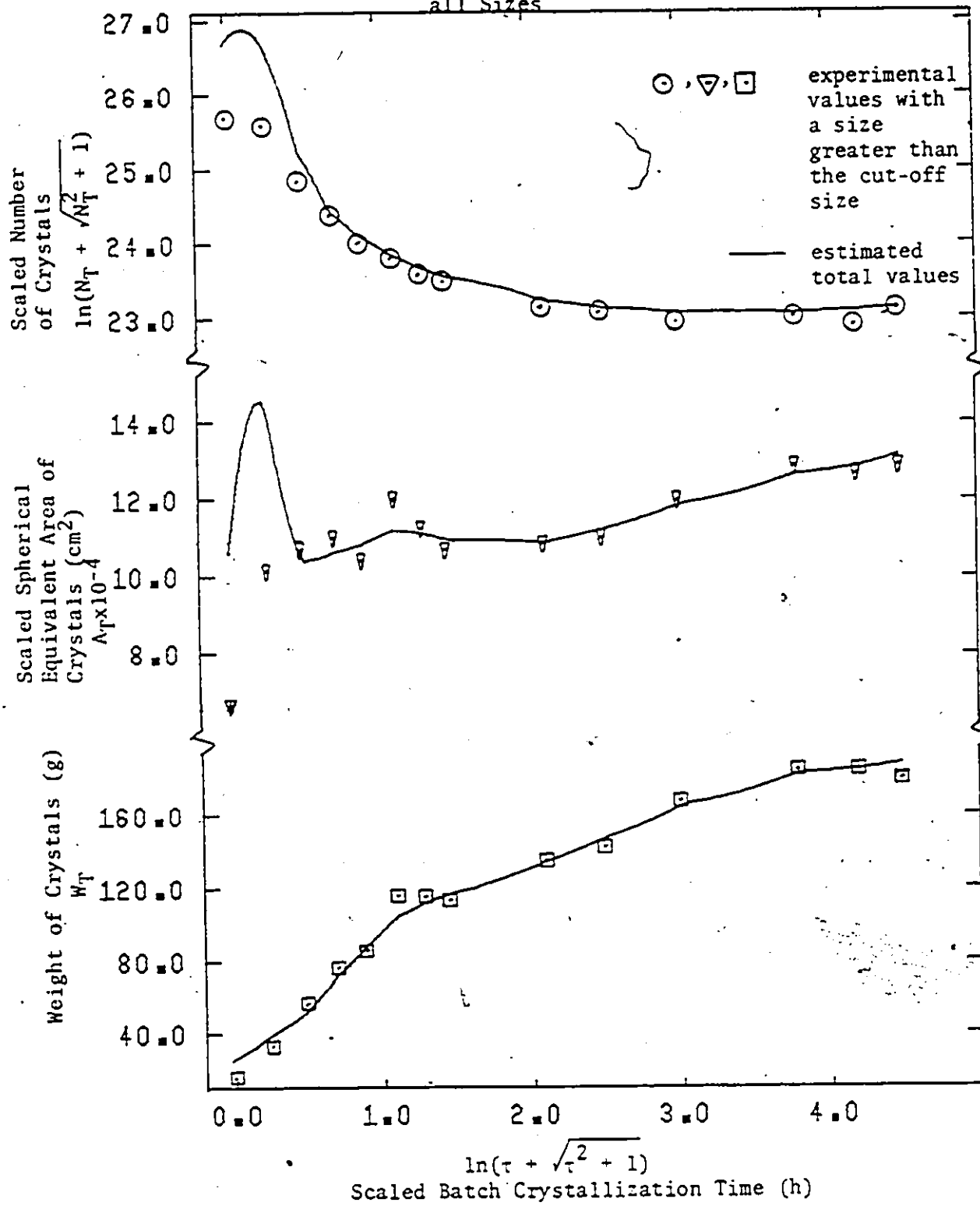
Figure 7.3.1.3-A shows the comparison between the measured number of crystals with sizes larger than the cut-off size and the estimated total number of crystals as a function of time. The same is shown for the spherical equivalent area and weight in Figure 7.3.1.3-A. This figure demonstrates that a significant proportion of the total crystals (or equivalently their area and mass) had crystal sizes less than the cut-off size only during the initial stages of this batch run. As expected, the effect of cut-off size affected the total number most and the solids mass least. Note that this simple extrapolating expression reduced the maximum relative deviation between measured and predicted mass from 29 to 11 percent.

The computer listing of this estimation procedure may be found in Program CA, Appendix E.

7.3.2 Implementation of the Pseudo Moment Equations

Now that the practical limitations have been resolved through the development of smoothing and extrapolation formulas, equations (7.11), (7.27), and (7.36) provide a means for independent investigation of the growth rate expression G_D , the agglomeration effectiveness kernel $k_{V,a}$, and the nucleation rate expression $BF_{l,n} \times \phi_n$, respectively. Different functions are investigated in the next sub-sections and their suitability evaluated by means of the minimum sum of squares criterion and by inspection of residuals. The effect of the cut-off size is investigated by

FIGURE 7.3.1.3-A Measured Number, Area, and Weight of Crystals with Sizes Greater than the Cut-off Size and Estimated Values Over all Sizes



calculating the pseudo moments under two situations: First, it is assumed that no crystals existed with sizes less than the cut-off size and then, that the number of crystals in this size interval is equal to the number predicted by formula (7.47).

Unfortunately, the computer time required to estimate the parameters in any model of the agglomeration effectiveness kernel by the method of pseudo moments is still very high. Indeed, even with this method, one model evaluation with a crystal size dependent kernel required about 13 seconds of central processor time on a CDC 6400 computer. Although this imposes some restriction on the number of different models that could be investigated, the computer times required are not excessive. Certainly if the integro partial differential equation were used directly in this model discrimination-parameter estimation step, the computer time would have been beyond the resources of this project.

The steps which were taken to develop suitable kinetic rate models for each of the phenomena occurring in this crystallization system using the methods already described are presented below.

7.3.2.1 Kinetic Growth Rate Expression

The following constitutive rate expressions for the growth rate were considered as reasonable given the physical models for the crystal growth process which were presented in Section 2.4.5.

- (1) $G_D = BG_1 \Delta C A^{BG_2}$
- (2) $G_D = BG_1 \sigma^{BG_2}$
- (3) $G_D = BG_1 \sigma^2 \tanh(BG_2/\sigma)$
- (4) $G_D = BG_1 \sigma^{5/6} \exp(-BG_2/\sigma)$

where $\Delta CA = CA - CA_e$

$\sigma = \Delta CA / CA_e$

CA = smoothed experimental alumina concentration (g Al_2O_3 /l sol.)

CA_e = equilibrium alumina concentration from equation (7.44)
with smoothed experimental values (g Al_2O_3 /l sol.)

The parameter BGl is expected to be a function of temperature; this functional relationship should be an Arrhenius type.

Each of the models is non-linear and contains two parameters. All are explicit functions of supersaturation and implicit functions of temperature through the parameter BGl. Recall that models (1) and (2) are empirical power law models; (3) is the BCF or Burton, Cabrera, Frank model which is based on the notion of growth occurring at screw-dislocation steps; and (4) is the birth and spread, two-dimensional nucleation model.

The results of the model discrimination/parameter estimation work using the four models for the growth rate are summarized in Table 7.3.2.1-A. In this case, the initial solid concentration used in equation (7.16) was obtained from the smoothed experimental data by equation (7.15). The total number of crystals and size distribution included the experimentally measured distribution and the number predicted below the cut-off size by equation (7.47).

It must be pointed out that the growth rate parameters depend directly on the basis for estimating crystal area. In this the crystal area is calculated from the measured and estimated part of the crystal density function assuming the crystals are spheres of equivalent volume. If this calculation scheme is in serious error, the parameters in each of the crystal growth rate models will be incorrect. Certainly, it would be most desirable to have as independent measurement of the crystal surface area which is appropriate for crystal growth.

TABLE 7.3.2.1-A Fit of Different Growth Rate Models

Model	Estimated Parameter Values		Sum of Squares after Regression	Predicted Growth Rate Range \hat{G}_D ($\mu\text{m/h}$)
	$\hat{BG1}$	$\hat{BG2}$		
(1) $G_D = BG1 \Delta CA^{BG2}$	6.80×10^{-4}	2.37	486	$7.09 + 2.6 \times 10^{-2}$
(2) $G_D = BG1 \sigma^{BG2}$	23.3	2.30	501	$7.20 + 2.7 \times 10^{-2}$
(3) $G_D = BG1 \sigma^2 x \tanh\left(\frac{BG2}{\sigma}\right)$	13.2	1.00	8151	$4.42 + 3.7 \times 10^{-2}$
(4) $G_D = BG1 \sigma^{5/6} x \exp\left(-\frac{BG2}{\sigma}\right)$	15.2	0.340	652	$5.64 + 2.1 \times 10^{-3}$

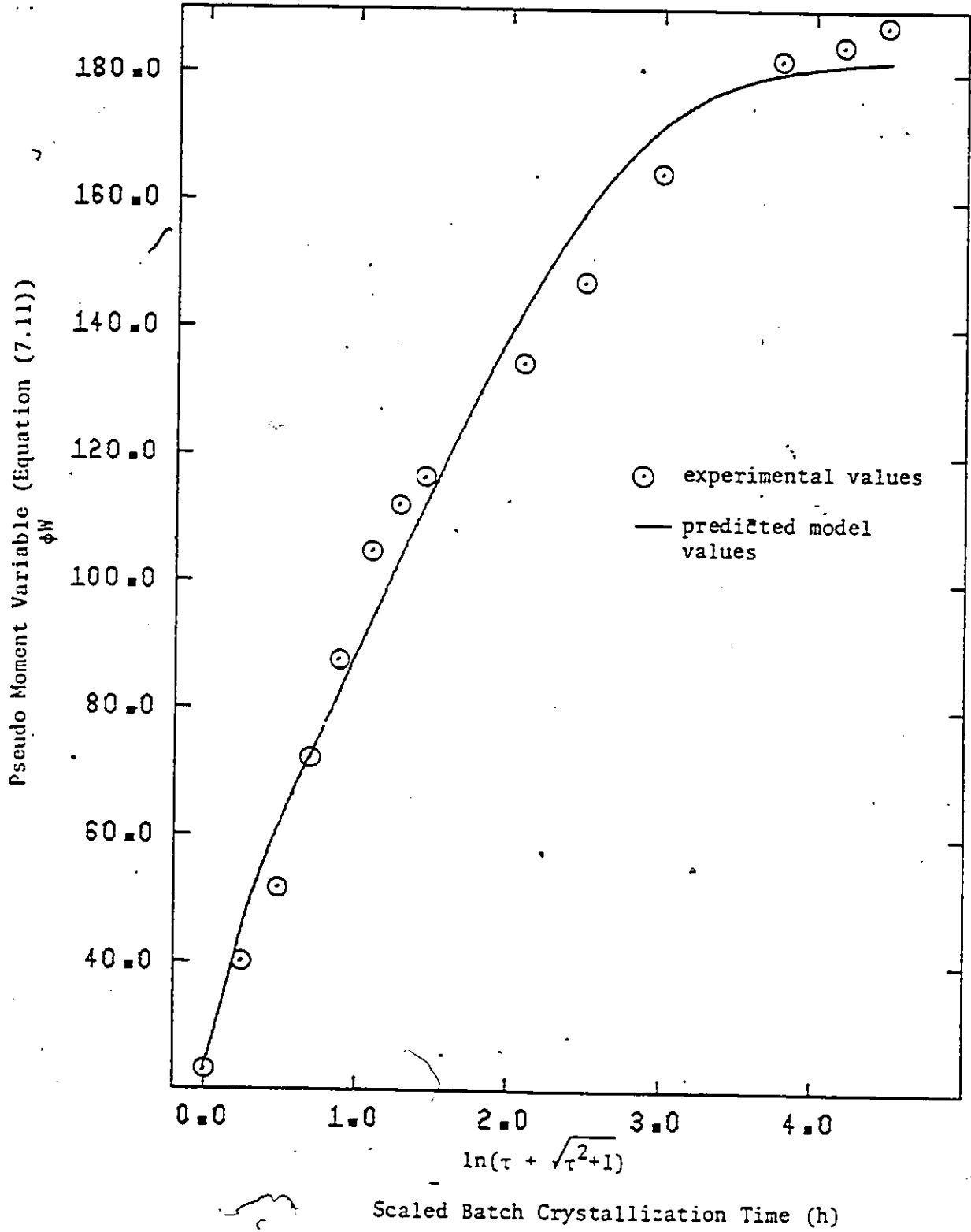
The results shown in Table 6.3.2.1-A also indicate that the BCF screw dislocation or spiral propagation model provides the worst fit. This result is consistent with direct microscopic observation of crystals (b7) which do not show such spirals or other evidence of a screw dislocation mechanism. It is not possible to discriminate among the other three models on the basis of the results of this experiment. Direct observations (b7) have suggested that the surface (two-dimensional) nucleation and spread model, model 4, is appropriate for this crystallizing system. Since this model has some theoretical basis, it is selected here for use in the agglomeration modelling work to be presented next. The fit of this growth rate model in terms of the variables of pseudo moment equation (7.11) is shown in Figure 7.3.2.1-A.

It is to be noted that, in the case of Model 4, including the estimated crystal size density function below the cut-off size improved the degree of fit of the model. In this case, the sum of squares of the residuals after regression was reduced from 894 to 652. In addition, the predicted growth rate for all models was approximately the same only when the estimated crystals below the cut-off size were included. Thus, the estimated density function below the cut-off size is certainly better than disregarding those crystals and probably provides a reasonable estimate of the true distribution. Thus, in the estimation procedures for the agglomeration rate and nucleation rate kinetic models, the estimated density function below the cut-off size will be included.

In summary, the growth rate model as obtained under the conditions of this experiment is:

$$\tilde{G}_D(\tau) = BG1 \sigma(\tau)^{5/6} \exp(-BG2/\sigma(\tau)) \quad (7.49)$$

FIGURE 7.3.2.1-A Fit of the Growth Rate Model in Terms of the Pseudo Moments



where \hat{G}_D - expected linear, spherical-equivalent growth rate ($\mu\text{m}/\text{h}$)

while the model parameters (at 85°C) were estimated to be:

$$\hat{BG1} - 15.22 \pm 3.0$$

$$\hat{BG2} - 0.3397 \pm .058$$

The limits on these parameters are those estimated on the basis of a linearized model using the 95% confidence level.

The computer programs used in this modelling of the growth rate are listed in Appendix E (Program CA).

7.3.2.2 Kinetic Agglomeration Rate Expression

As indicated in Chapter 2, very little fundamental or experimental work has been done on the appropriate model form for the agglomeration effectiveness kernel. The only guidance might come from plant personnel who have observed that small crystals agglomerate more effectively than large ones in this crystallizing system. This observation suggests that the effectiveness kernel may be considered a product of two functions, one which depends only on crystal environment (supersaturation) and the other only on the size of the crystals which come together. Thus, one may write:

$$k_{V,a} - \phi_{E,a}(\tau) \phi_{V,a}(V', V'') \quad (7.50)$$

The different functional forms of these functions which have been investigated here through use of the pseudo moment procedure are shown in Table 7.3.2.2-A. The rationale behind these models is as follows:

A. The Environmental Function, $\phi_{E,a}$

The model to account for the crystal environment was chosen as a simple power-law function of the solution supersaturation. This is consistent with the concept that after two crystals collide, the effectiveness with which they stick together to form one crystal depends on the rate at which the crystals grow. The following reasoning suggests this: If two crystals are to collide and stay together, a crystal bridge must form between them within the time that they are in contact. This bridge may be broken if it is not strong enough to withstand the local forces on it. The rate at which the bridge forms and the strength of the bridge will be functions of the crystal growth rate. Since it has been shown that growth rate may be well represented as a simple power law of supersaturation, this representation has been used here.

B. The Size Dependent Function, $\phi_{V,a}$

Some of the functional forms for $\phi_{V,a}$ have been suggested from agglomeration studies of other systems. The first model in Table 7.3.2.2-A represents the simplest function possible, that is, that the process is independent of the contacting crystals. This has been observed by Turkevich (t5) for the initial agglomeration rate of hydrosols which initially had a narrow size distribution. This model along with the functional form for $\phi_{E,a}$ (model 2) was claimed by Halfon (h2) to represent the agglomeration

TABLE 7.3.2.2-A Fit of Different Agglomeration Effectiveness Kernel Models

Model	Estimated Parameter Values			Sum of Squares after Regression
	BA1	BA2	BA3	
(1) $\phi_{E,a} = BA1 \sigma^{BA2}$ $\phi_{V,a} = 1$	9.94×10^{-20}	10.3	-	587.1
(2) $\phi_{E,a} = BA1 S^4$ $\phi_{V,a} = 1$	3.8×10^{-25}	-	-	587.1
(3) $\phi_{E,a} = BA1 \sigma^{BA2}$ $\phi_{V,a} = \frac{\{V(\ell)^{1/3} + V(p)^{1/3}\}^2}{x / V(\ell)^{2/3} - V(p)^{2/3}}$	1.10×10^{-10}	11.4	-	185.1
(4) $\phi_{E,a} = BA1 \sigma^{BA2}$ $\phi_{V,a} = \frac{\{V(\ell)^{1/3} + V(p)^{1/3}\}^2}{x / V(\ell)^{1/3} - V(p)^{1/3}}$	1.48×10^{-10}	7.96	-	273.4
(5) $\phi_{E,a} = BA1 \sigma^{BA2}$ $\phi_{V,a} = \frac{\{V(\ell)^{1/3} + V(p)^{1/3}\}^2}{x V(\ell)^{2/3} - V(p)^{2/3} }$ $\times e^{-BA3(V(\ell)^{2/3} + V(p)^{2/3})}$	1.05×10^{-12}	3.06	6.58×10^{-3}	88.0

of alumina trihydrate although, as will be discussed later, there were serious shortcomings in his experiments and analysis.

The forms for $\phi_{V,a}$ shown in models 3 and 4 follow if an inertial impaction mechanism is considered (d1). The general concept is explained as follows: Particles move about by virtue of turbulent, gravity or other forces. If two particles of volume $V(l)$ and $V(p)$, respectively, are to collide they must be in the cross-sectional area proportional to the term, $\{V(l)^{1/3} \pm V(p)^{1/3}\}^2$, that is proportional to the area of a circle circumscribing both particles. In addition, the difference in velocities of the two particles must be accounted for in some way, and the functional form should take into account the type of fluid and the magnitude of the particle motion. For example, if the fluid is highly viscous and the particles are very small, the particles are in the 'creeping motion' regime and the particle velocities are proportional to $V^{1/3}$. On the other hand, where the particle movement is relatively fast, the drag coefficient may be considered essentially constant (Newton's law regime) and the velocity is proportional to the cross-sectional area or $V^{2/3}$. In any event, crystals of widely different sizes should collide more frequently than crystals of approximately the same size and this is reflected in the functional forms:

$$|V(l)^{2/3} - V(p)^{2/3}| \quad \text{or} \quad |V(l)^{1/3} - V(p)^{1/3}|$$

which reflect the difference in particle velocities under these two conditions.

It is to be noted that the concentration of particles of various sizes is already accounted for in the agglomeration rate term through the product of the particle density functions.

7.3.2.2.1 Estimation of the Parameters in the Models

In applying the method of pseudo-moments to this problem it was essential to scale the responses in equation (7.27) because the integrated number density function (variable $nA_{k,j}$) changed by several orders of magnitude over all k and j . If scaling had not been applied a relatively few of the responses $nA_{k,j}$ would have 'overwhelmed' the objective function, S_a , and the others would not have been effective in determining the parameter estimates. The scaling was achieved through the transformation

$$Y_{k,j} = \ln\{nA_{k,j} + (nA_{k,j}^2 + 1)^{1/2}\} \quad (7:51)$$

The unknown error structure was still not accounted for, but since this transformation is essentially logarithmic, this transformation assumes that the errors in the integrated density functions are proportional to the magnitude of the value of that integral. This certainly is not unreasonable.

Table 7.3.2.2-A indicates the results of the parameter estimating program for these models using the method of pseudo-moments. It can be seen that the first two models, which assume the agglomeration effectiveness kernel is independent of the size of the crystals which contact, provide relatively poor fit for this system. This is in direct contradiction to the results of Halfon (h2) who claimed that model 2 provided a good fit for the data he obtained from experiments on this crystallization system. On the other hand, there are a number of criticisms which can be made concerning Halfon's work:

- (i) In Halfon's experiments, the size distribution changed very little with batch time (he operated at very low supersaturations) and consequently the agglomeration rate was very small. Thus, the agglomeration model was not put to a severe test.
- (ii) In analyzing his results, Halfon only considered crystals greater than the cut-off size of his Coulter Counter. As will be shown later, this procedure can lead to very poor models and estimated parameters in them.
- (iii) Halfon only considered the change in the total number of measured crystals above the cut-off size. In order to discriminate among various models it is important to consider the change in number of crystals in different size intervals. Unless this is done, no information is obtained about the cancelling of positive and negative deviations within the model, that is an overall good fit may be obtained fortuitously because of the cancelling of local errors.

Models 3 and 4 which do contain the size dependent function, $\phi_{V,a}$, provide relatively good fits for the data; certainly they are a great improvement over the size-independent models. The data, however, do not allow a discrimination between model 3 and 4; thus, on the basis of this data, it is impossible to state which exponent (2/3 or 1/3) should be used in the model.

Note that in models 3 and 4, the term $\phi_{V,a}$ predicts a small agglomeration rate for small crystals. This minimizes the sensitivity of the model parameters to the estimate of the number of crystals below the cut-off size. Also, it is surprising to observe such a large exponent

on the supersaturation, since the mechanism should be related to growth rate and the growth rate exponents are usually not this large. Part of this problem might be because of the high correlation between $\phi_{E,a}$ and $\phi_{V,a}$. That is, the function $\phi_{V,a}$ might provide an agglomeration rate which is too large for the larger crystals as the distribution widens with batch time and then this rate might be compensated for by a rapidly decreasing environmental function, $\phi_{E,a}$.

On the basis of this latter observation, that is, the large crystals seem to be agglomerating faster than expected, and also on the basis that the models are not bounded at the upper end, that is, this model suggests that large crystals can continue to agglomerate up to very large crystals (which is inconsistent with observations), it was decided that the models could be refined to remedy these shortcomings. An empirical term of the following form (as a multiplying factor) was suggested by the above considerations:

$$e^{-BA3\{V(l)^m + V(l)^m\}} \quad (7.52)$$

Such a term provides for a slowing down of the agglomeration rate as the crystal size increases. This is consistent with a mechanism in which it is visualized that large crystals are subjected to greater shear forces because of their size and thus are more susceptible to break-up after their initial collision. One might also reason that the large crystals may not have been in contact for sufficient time to allow a strong bridge between particles to develop. In any event, term (7.52) should provide the desired effect. Several exponents (m) were investigated in expression (7.52); $m = 2/3$ provided the best fit of those tried.

Of all the models investigated, model 5 for the agglomeration effectiveness kernel, namely:

$$k_{V,a}(V(l),V(p),\tau) = \phi_{E,a}(\tau) \phi_{V,a}(V(l),V(p))$$

with

$$\phi_{E,a}(\tau) = BA1 \sigma^{BA2}$$

and

$$\begin{aligned} \phi_{V,a}(V(l),V(p)) = & \{V(l)^{1/3} + V(p)^{1/3}\}^2 \times |V(l)^{2/3} - V(p)^{2/3}| \\ & \times \exp\{-BA3(V(l)^{2/3} + V(p)^{2/3})\} \end{aligned}$$

provided the best fit. In this model for $\phi_{V,a}$, the first two factors are related to the collision frequency and the third accounts for the efficiency of the collision as it relates to the agglomerates' ability to maintain the agglomerated form. The model parameters were estimated to be (at 85°C):

$$\hat{BA1} = 1.025 \times 10^{-12} \pm .014 \times 10^{-12}$$

$$\hat{BA2} = 3.062 \pm .117$$

$$\hat{BA3} = 6.579 \times 10^{-3} \pm .280 \times 10^{-3}$$

Again the limits are estimated using a linearized form of the model and the 95% confidence level. In obtaining these parameter estimates, the estimated particle size distribution below the cut-off size was included with the measured distribution for use in equation (7.27(b)).

Comparisons of the experimental transformed η_A function with the corresponding transformed functions predicted by the model are shown in

Figure 7.3.2.2.1-A. It is seen that the fit is very good for the crystals of small size but deviates after the first half hour for crystals with diameter greater than about 11 μm ; thus some refinement is still possible although it was not done here. It is important to realize that the search for a particular model is a tedious process, even by the method of pseudo-moments. This time-consuming search is complicated by the very nature of the agglomeration process which means that a change over a certain size range affects all other size ranges, thus making it very difficult to 'sectionally-improve' on a model.

A three-dimensional plot of the size-dependent term, $\phi_{V,a}$, versus the size of participating crystals, Figure 7.3.2.2.1-B, shows a very interesting result, namely: small as well as large crystals do not agglomerate as effectively with themselves or with each other as do crystals of intermediate size (range 10 to 30 μm). This is consistent with plant observations since the rate at which very small crystals agglomerate would be difficult to detect by the operators.

A listing of the computer programs which were used in the parameter estimation process is presented in Appendix E.

7.3.2.3 Kinetic Nucleation Rate Expressions

Of the three crystallization rate processes, the least is known about the nucleation process, particularly with respect to calculating the rate of nucleation, a priori. Common models for the rate of nucleation have been presented in Section 2.5. These models have provided some guidance in formulating the potential form of the models for this system.

FIGURE 7.3.2.2.1-A Fit of the Agglomeration Rate Model
in Terms of the Pseudo Moments

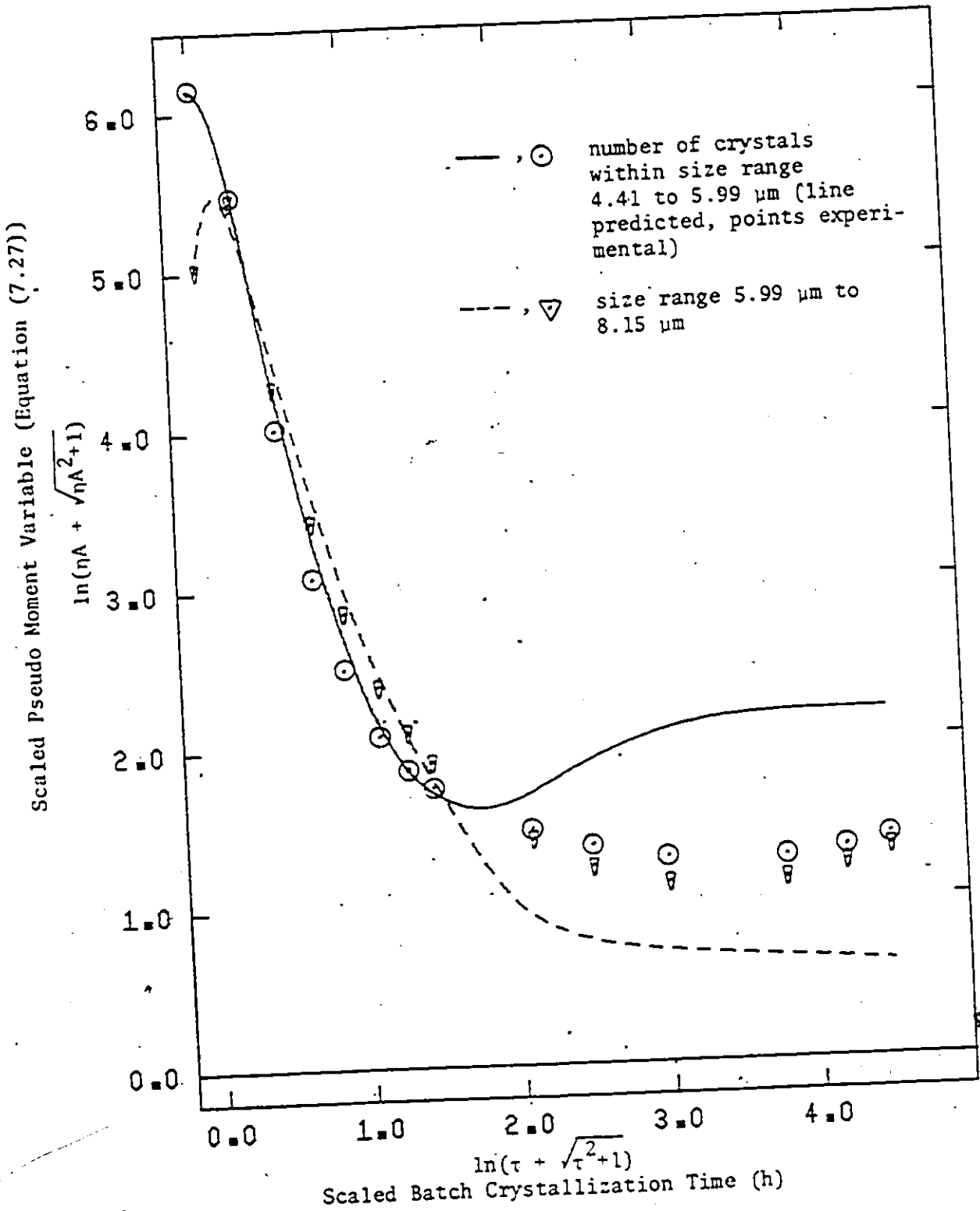


FIGURE 7.3.2.2.1-A (cont'd.)

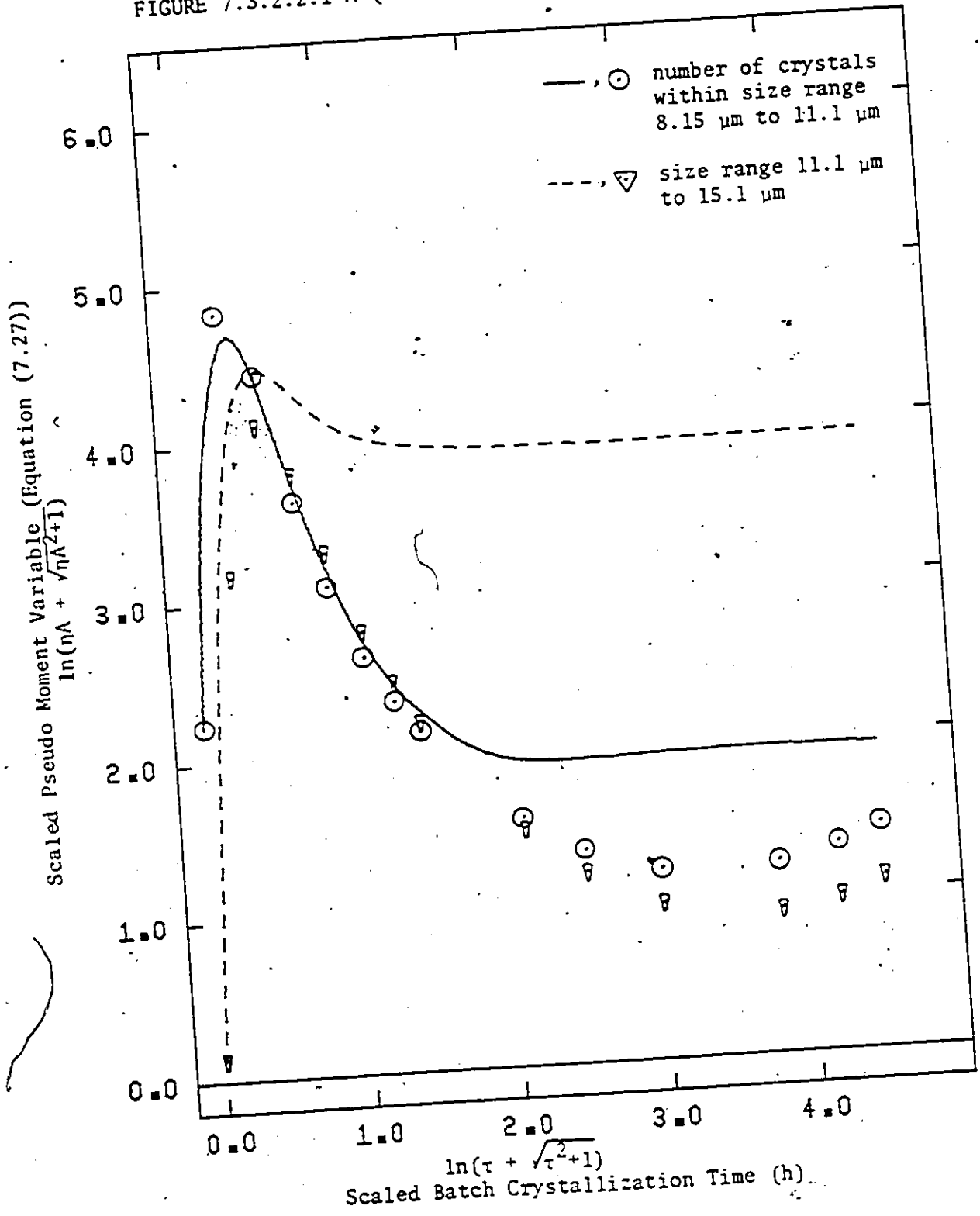


FIGURE 7.3.2.2.1-A (cont'd.)

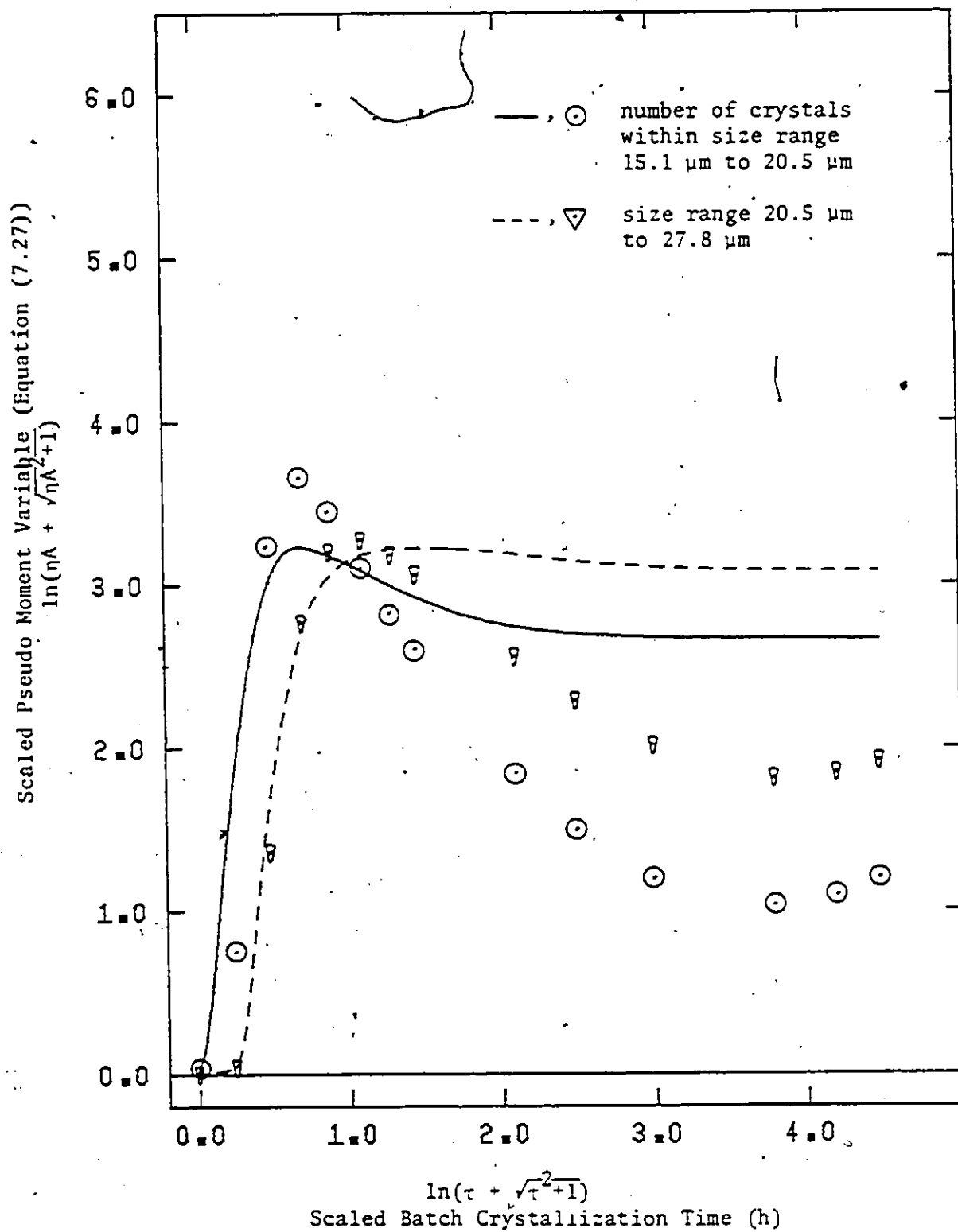


FIGURE 7.3.2.2.1-A (cont'd.)

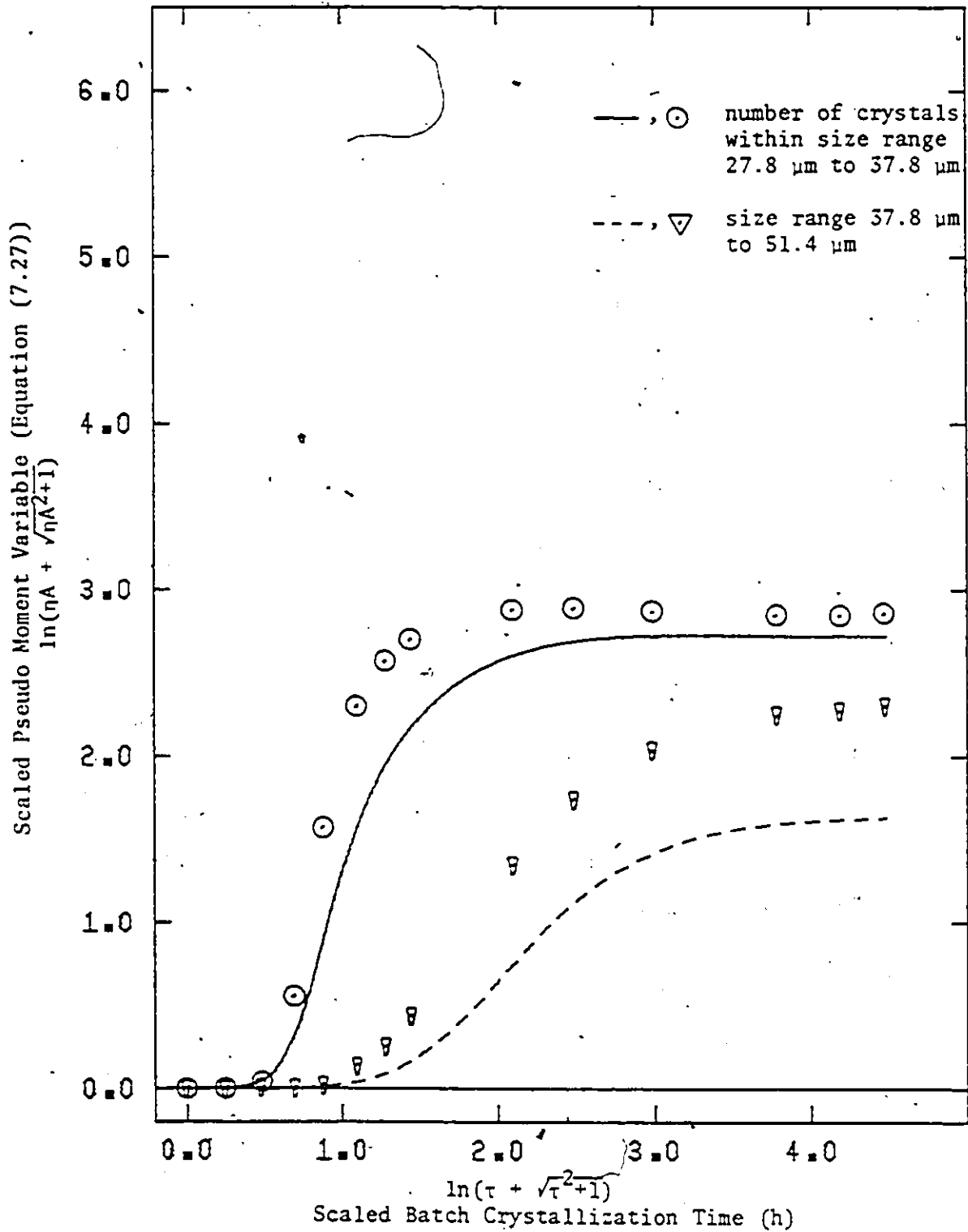


FIGURE 7.3.2.2.1-B Size Dependent Term of the Agglomeration Effectiveness Kernel, $\phi_{v,a}$ vs. $D(l)$ and $D(p)$

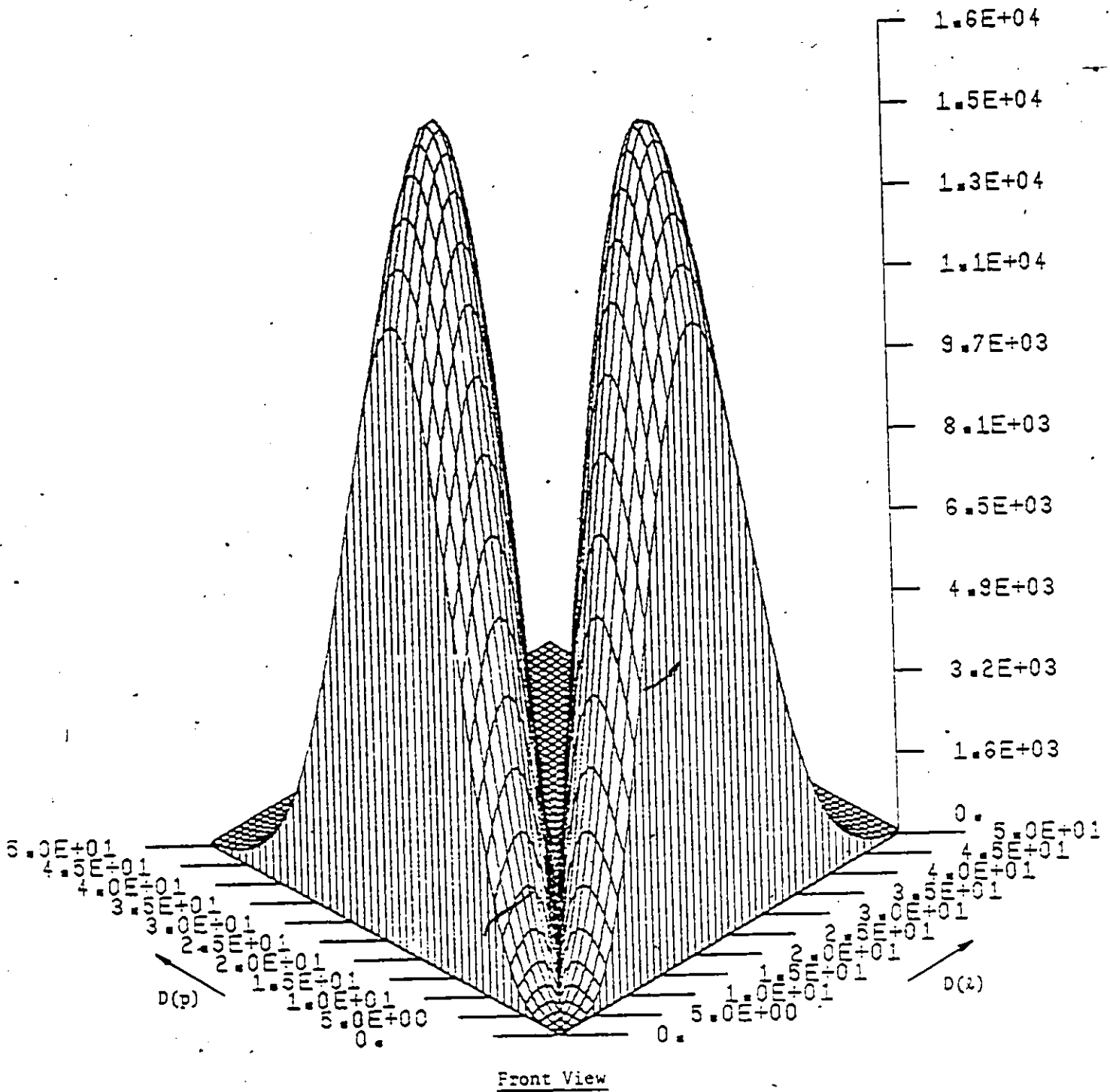
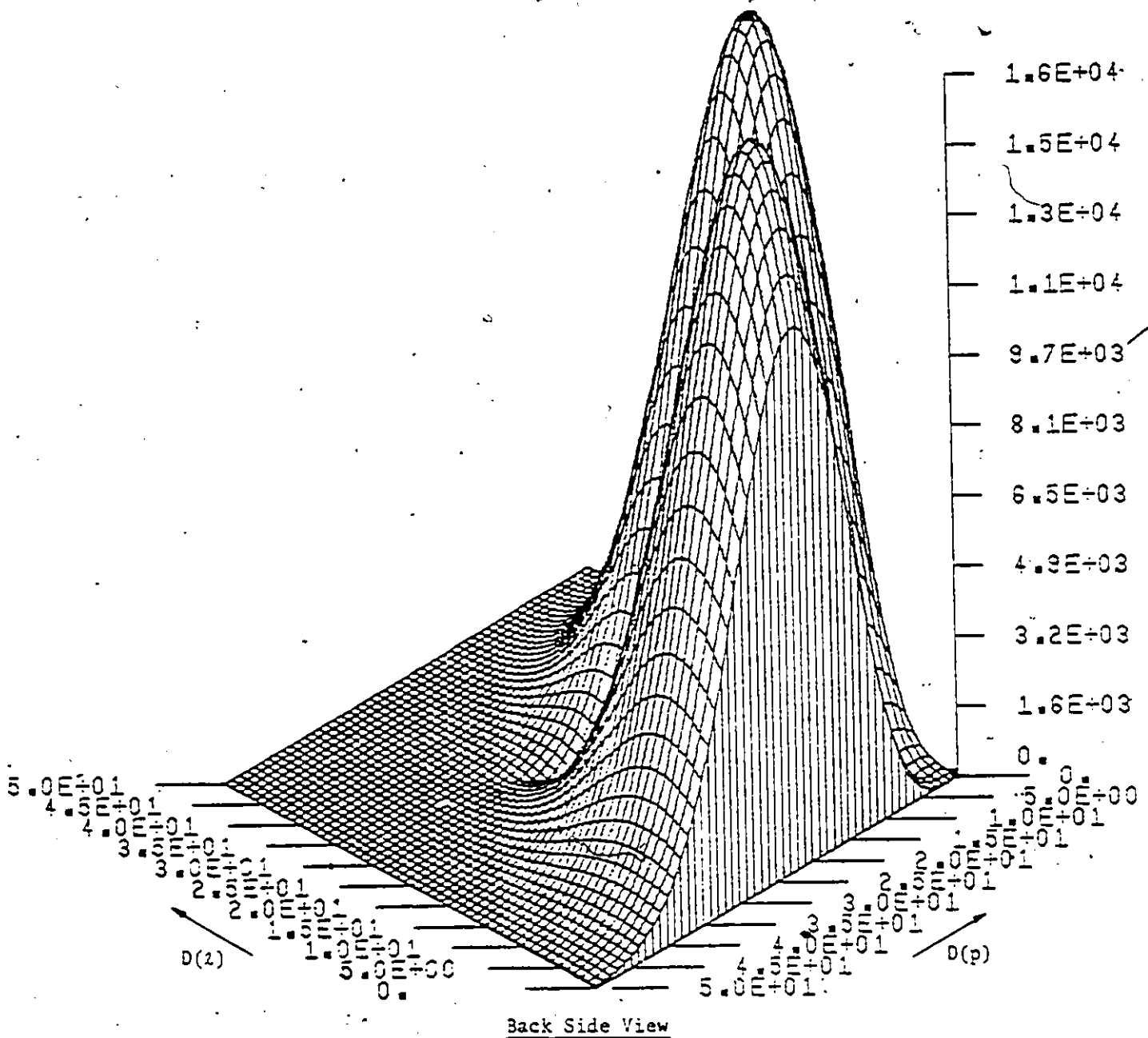


FIGURE 7.3.2.2.1-B Size Dependent Term of the Agglomeration Effectiveness Kernel, $\phi_{v,a}$ vs. $D(l)$ and $D(p)$



In formulating an expression for the nucleation rate function $BF_{V,\ell,n}(\tau,V)$, one must include a rate dependent function $\phi_{E,n}(\tau,V)$ and a particle size density function of the nuclei formed during the process, $\phi_{V,n}(V)$. Thus, we may write

$$BF_{V,\ell,n}(\tau,V) = \phi_{E,n}(\tau,V) \phi_{V,n}(V) \quad (7.52)$$

In this case the rate dependent function will depend on those environmental factors which determine the rate of secondary nucleation. These factors may be expected to include supersaturation, concentration of crystals in suspension, the size distribution of the crystals in suspension and other apparatus related factors.

Some estimate of the size distribution of the nuclei as they are formed is required here since the nucleation is not included as a boundary condition, but is included in the population balance equation. Since no conclusive information is available from other workers with regard to the size distribution of the nuclei for the alumina trihydrate system, or for other crystallization systems, it is assumed here to be log-normal. The two parameters in this distribution cannot be estimated from the data obtained from this experiment, but must be determined in some other way. Here, the two parameters were estimated by assuming that the size range of the nuclei, when formed, was in the range of stable nuclei as predicted by equation (2.21), Section 2.5.5. Thus:

$$\phi_{V,n}(V) = \frac{1}{BNS \sqrt{2\pi} V} \exp\left\{-\frac{1}{2}\left(\frac{\ln V - BN^4}{BNS}\right)^2\right\} \quad (7.53)$$

with $\hat{BN4} = -4.10$

$\hat{BN5} = 1.15$

The various assumed forms of the environmental function, $\phi_{E,n}(\tau, V)$, are shown in Table 7.3.2.3-A. These models were investigated in turn and the number of the model indicates its order in the model development process. All models consider that nucleation is some function of supersaturation; they differ in the way they attempt to take into account the effect of crystal contact which is expected to affect the rate of secondary nucleation. The first two models follow from the conceptual mechanisms of secondary nucleation with model 1 accounting for either crystal-wall collisions (c1,o2) and/or crystal-crystal collisions due to fluid turbulence, and model 2 accounting for these collisions arising from gravitational forces (e1). Model 3 represents an attempt to include the effect of the particle size of the contacting crystals (through the x_c term). This functional form attempts to account for the inertial-impaction mechanism which was discussed in the previous sub-section relating to agglomeration. Finally, models 4, 5 and 6 were suggested from the results found during the parameter estimation procedures on models 1, 2 and 3. These models include only the effect of solution supersaturation; that is, there is neither a dependence on crystal concentration nor particle size distribution.

7.3.2.3.1 Estimation of Parameters

The parameter estimation procedure as presented in Section 7.2.3 was used for each model in turn. As in the previous case for agglomeration, the transformation

TABLE 7.3.2.3-A Fit of Different Models for the Crystals Environment Term of the Nucleation Rate Expression

Model	Estimated Values of the Parameters			Sum of Squares after Regression
	$\hat{BN1}$	$\hat{BN2}$	$\hat{BN3}$	
(1) $\phi_{E,n} = BN1 S^{BN2} \left(\frac{W_T}{V_L}\right)^1$	1.76×10^5	2.81	-	201
(2) $\phi_{E,n} = BN1 S^{BN2} \left(\frac{W_T}{V_L}\right)^2$	4.21×10^3	3.00	-	271
(3)* $\phi_{E,n} = BN1 S^{BN2} X_c$	1.73×10^{-19}	2.78	-	82.5
(4) $\phi_{E,n} = BN1 S^{BN2} \sigma$	6.47×10^3	5.06	-	58.2
(5) $\phi_{E,n} = BN1 \cdot e^{BN2}$	1.31×10^8	13.1	-	46.8
(6) $\phi_{E,n} = \frac{BN1}{1 + e^{BN2(1/\sigma - BN3)}}$	1.73×10^{12}	8.50	1.61	0.196

$$* X_c = \int_{V_0}^{V_u} \int_{V_0}^{V_u} \phi_{VCN}(V', V'') \frac{F_{V,T}(V', \tau)}{V_L(\tau)} \frac{F_{V,T}(V'', \tau)}{V_L(\tau)} dV'' dV'$$

$$\text{where } \phi_{VCN}(l, p) = \{V(l)^{1/3} + V(p)^{1/3}\}^2 |V(l)^{2/3} - V(p)^{2/3}|$$

$$Y_j = \ln\{EA_j + (EA_j^2 + 1)^{1/2}\} \quad (7.54)$$

was employed to ensure that all data points were effective in determining the value of S_N . The particle size distribution function, equation (7.47), which was developed to predict the particle size distribution below the cut-off size was used in equation (7.36). This distribution is important here because of the significant number of particles contained in the region below the cut-off size.

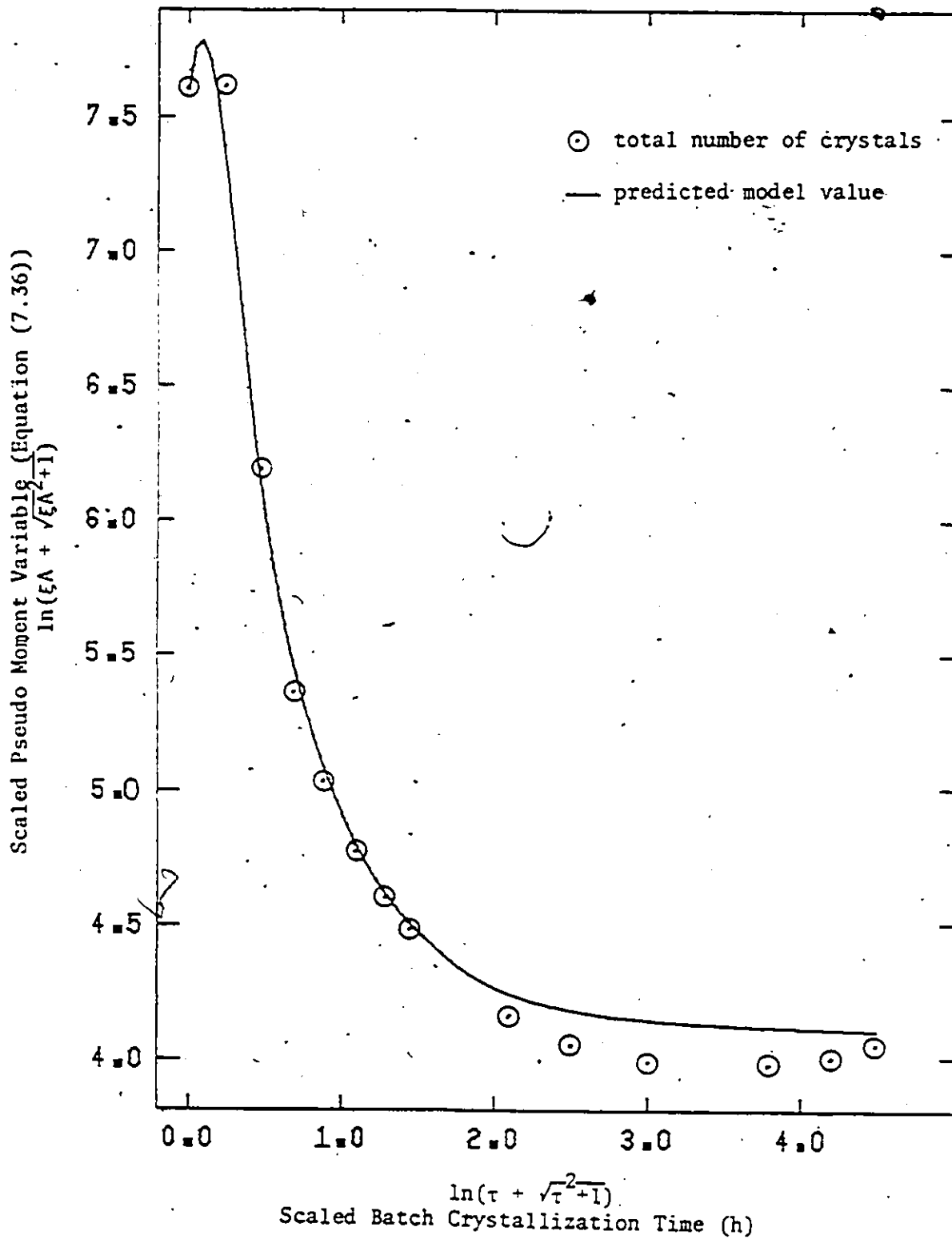
The results of the parameter estimation work with each of the models are presented in Table 7.3.2.3-A. It is seen that models 1 and 2 provide relatively poor fits for the data (note the magnitude of the residual sum of squares) with model 2 being worse than model 1. The fit was equally poor if the particles below the cut-off size were ignored. At this point in the model development, the exponent on the solid concentration was allowed to be a parameter in the model. The minimizing routine drove this parameter to values near zero and, therefore, the solids concentration was ignored in the later models.

Including the crystal-crystal collision function in the model (model 3) did not improve the model significantly. This result essentially substantiated the earlier finding, with model 1 and 2, that including any function relating to a crystal collision mechanism was not beneficial in providing a good fit to the data. Thus, in models 4 and 5, the nucleation rate was made a function of supersaturation only. This reduced the sum of squares after regression as compared to models 1, 2 and 3 but a plot of predicted values and experimental data showed that these models still provided a poor fit.

After a thorough inspection of the experimental data expressed in terms of pseudo moments, it became apparent that to fit the data it would be necessary to introduce essentially all nuclei at the beginning of the batch experiment, and none or a very small number during the rest of the batch run. Model 6 is such a function; in essence, it is a 'smoothed' step function of the relative supersaturation. From the reduction in the sum of squares after regression and the comparison of experimental and predicted as shown in Figure 7.3.2.3-A, it can be concluded that this empirical model does indeed provide a very good fit of the data.

This finding allows the very interesting hypothesis to be made that at the temperature of this experiment, namely 85°C, nucleation by whatever mechanism did not take place. This observation is in agreement with Misra's observations (m5), and suggests that the large number of nuclei that is observed initially results in some way from the seed crystals. It may be that very small crystals of nuclei size are loosely attached to the seed crystals and when these seed crystals are introduced into a supersaturated solution, the small nuclei are dislodged from them. This would suggest that mechanical stresses develop in the crystal as a result of the initial crystal growth process. A detailed examination of the crystal habit during these early stages of crystal growth would be illuminating on this point. The phenomenon of a large number of initial nuclei has been observed and discussed for other systems by Strickland-Constable (s2). He termed it a 'dusting' of the seed crystals. On the other hand, the observed appearance of a large number of crystals at very high supersaturation levels might well be a particular nucleation mechanism.

FIGURE 7.3.2.3-A Fit of the Nucleation Rate Model
in Terms of the Pseudo Moments



For example, homogeneous nucleation is expected to be extremely sensitive to supersaturation so that it would appear that all nuclei were formed only during the initial stages of crystallization. Here, the supersaturation function in model 6 provides for the type of behaviour to be expected if homogeneous nucleation were to prevail. However, as mentioned in Chapter 2, it is generally accepted that homogeneous nucleation does not occur in this system even at the supersaturation levels used in this study. These opinions are based on direct observations here and elsewhere that highly supersaturated solutions are very stable; moreover, indirect support comes from the fact that this chemical system has a high solid-solution interfacial tension (m^3). Thus, a homogeneous nucleation mechanism does seem highly improbable. Instead, model 6 with its very strong dependence on supersaturation may express a form of secondary nucleation which is very sensitive to supersaturation. In fact, if the concept of mechanical stress development in the seed were to be accepted, then these stresses (and hence the rate of formation of nuclei) should be a strong function of supersaturation.

The extent of this study is insufficient to allow definite conclusions to be made on the nucleation mechanism prevailing here. This study does suggest, however, that a somewhat unique nucleation mechanism seems to exist in a seeded alumina trihydrate crystallizing system at 85°C .

Thus, the recommended model for the nucleation function is as follows:

$$BF_{V,\ell,n}(V,\tau) = \phi_{E,n}(\tau) \phi_{V,n}(V) \quad (7.55)$$

with

$$\phi_{V,n}(V) = \frac{1}{\sqrt{2\pi}} \frac{1}{BN5} \frac{1}{V} e^{-\frac{1}{2(BN5)^2}(\ln V - BN4)^2} \quad (7.53)$$

$$\phi_{E,n}(\tau) = \frac{BN1}{1 + e^{BN2(1/\sigma - BN3)}} \quad (7.56)$$

and parameter estimates at 85°C equal to:

$$\widehat{BN1} = 1.725 \times 10^{12} \pm .003 \times 10^{12}$$

$$\widehat{BN2} = 8.504 \pm .064$$

$$\widehat{BN3} = 1.606 \pm .005$$

$$\widehat{BN4} = -4.10$$

$$\widehat{BN5} = 1.15$$

with the limits calculated from a linearized form of the model at a 95% confidence level.

It should be pointed out that this nucleation model, along with the parameter estimates, is conditional on how well the formula for the number of crystals below the cut-off size and/or the agglomeration rate model represent the truth. If either of these are in serious error, the form of the nucleation model and/or the parameter estimates will be incorrect.

The computer program used in this nucleation rate model development and identified by the letters 'CC' is listed in Appendix E.

7.4 Summary of the Rate Models for Growth, Agglomeration and Nucleation

To summarize the presentations in this chapter, the constitutive rate models along with their parameter estimates which have been developed from the experimental data using the method of pseudo moments are listed below:

Growth Rate: (linear spherical equivalent rate)

$$G_D(\tau) = BG1 \sigma^{5/6} \exp(-BG2/\sigma) \quad (7.G)$$

with $\hat{BG1} = 15.22$ @ 85°C

$\hat{BG2} = 0.3397$

Agglomeration Rate:

$$k_{V,a}(V(l), V(p), \tau) = \{BA1 \sigma^{BA2}\} \{V(l)^{1/3} + V(p)^{1/3}\}^2 |V(l)^{2/3} - V(p)^{2/3}| \exp\{-BA3(V(l)^{2/3} + V(p)^{2/3})\} \quad \dots (7.A)$$

with $\hat{BA1} = 1.025 \times 10^{-12}$ @ 85°C

$\hat{BA2} = 3.062$

$\hat{BA3} = 6.579 \times 10^{-3}$

Nucleation Rate:

$$BF_{V,l,n}(\tau, V) = \left\{ \frac{BN1}{1 + e^{BN2(\frac{1}{\sigma} - BN3)}} \right\} \left\{ \frac{1}{BN5 \sqrt{2\pi V}} e^{-\frac{1}{2} \left(\frac{\ln V - BN4}{BN5} \right)^2} \right\} \quad (7.N)$$

with $\widehat{BN1} = 1.725 \times 10^{12}$
 $\widehat{BN2} = 8.504$
 $\widehat{BN3} = 1.606$
 $\widehat{BN4} = -4.10$
 $\widehat{BN5} = 1.15$

where $V =$ crystal volume (μm^3)
 $\sigma =$ relative supersaturation (S/CAE)
 $S =$ solution supersaturation ($\text{g Al}_2\text{O}_3/\text{l sol.}$)
 $\text{CAE} =$ equilibrium alumina concentration ($\text{g Al}_2\text{O}_3/\text{l sol.}$)
 $G_D =$ growth rate ($\mu\text{m}/\text{h}$)
 $k_{V,a} =$ agglomeration rate effectiveness kernel ($\text{l sol.}/$
 $(\text{number } \mu\text{m}^3\text{h})$)
 $BF_{V,\ell,n} =$ nucleation rate ($\text{number}/(\mu\text{m}^3\text{h } \text{l sol.})$)

The main advantage in the use of this method of pseudo moments is that it allows for model discrimination and parameter estimation of each rate process independently of the other processes. This greatly reduces the dimensionality of the problem and eliminates the bothersome interaction between the different rate processes. However, the method suffers from the fact that experimental errors are not properly accounted for in the estimation procedure, and that it is affected by the cut-off problem. These weaknesses of this estimation method affect the rate process models to a different degree with growth being least affected and nucleation most.



CHAPTER 8

BATCH CRYSTALLIZATION MODEL FOR THE ALUMINA TRIHYDRATE SYSTEM: COMPARISON WITH EXPERIMENTAL OBSERVATIONS AND RESULTS FROM OTHER STUDIES

8.1 Introduction

A mechanistic model for a seeded batch crystallizer for alumina trihydrate was formulated in Chapter 5. This model was based upon mass balances and the population balance equation. The latter provided a method for predicting the crystal size distribution as a function of time. The numerical solution of the resulting integro-partial differential equation proved to be a formidable task because of the form of the equation and the potential computer requirements. Two satisfactory solution methods were suggested in Chapter 6, each having certain advantages depending upon the predominance of the growth, agglomeration and nucleation rates in the crystallization process. The model requires the constitutive relationships which relate the rates of growth, agglomeration and nucleation to the process variables. In Chapter 7, these constitutive relationships were derived from experimental measurements through use of the pseudo-moment method. Thus the combined results of Chapters 6 and 7 allow a direct comparison of the model predictions with the experimental observations of the crystal size distribution at specific times.

The overall mechanistic model predicts the evolution of the crystal size distribution with batch time for different operating conditions and different initial size distributions for a crystallization process with growth, nucleation, and agglomeration. Or, in other words, it shows the combined effect on the size distribution change due to these three crystal-

lization rate processes. A typical plot of a model solution is presented in Figure 8.1-A. It shows that a process with agglomeration in addition to growth and nucleation has a very different resultant size distribution as compared to either growth and/or nucleation. Agglomeration causes the distribution to 'widen' or 'spread out' very fast and it reduces the total number of crystals. As mentioned throughout this dissertation, the presence of significant growth and agglomeration rates complicates any crystallization process immensely. The alumina trihydrate system studied here is a system which exhibits significant growth and agglomeration.

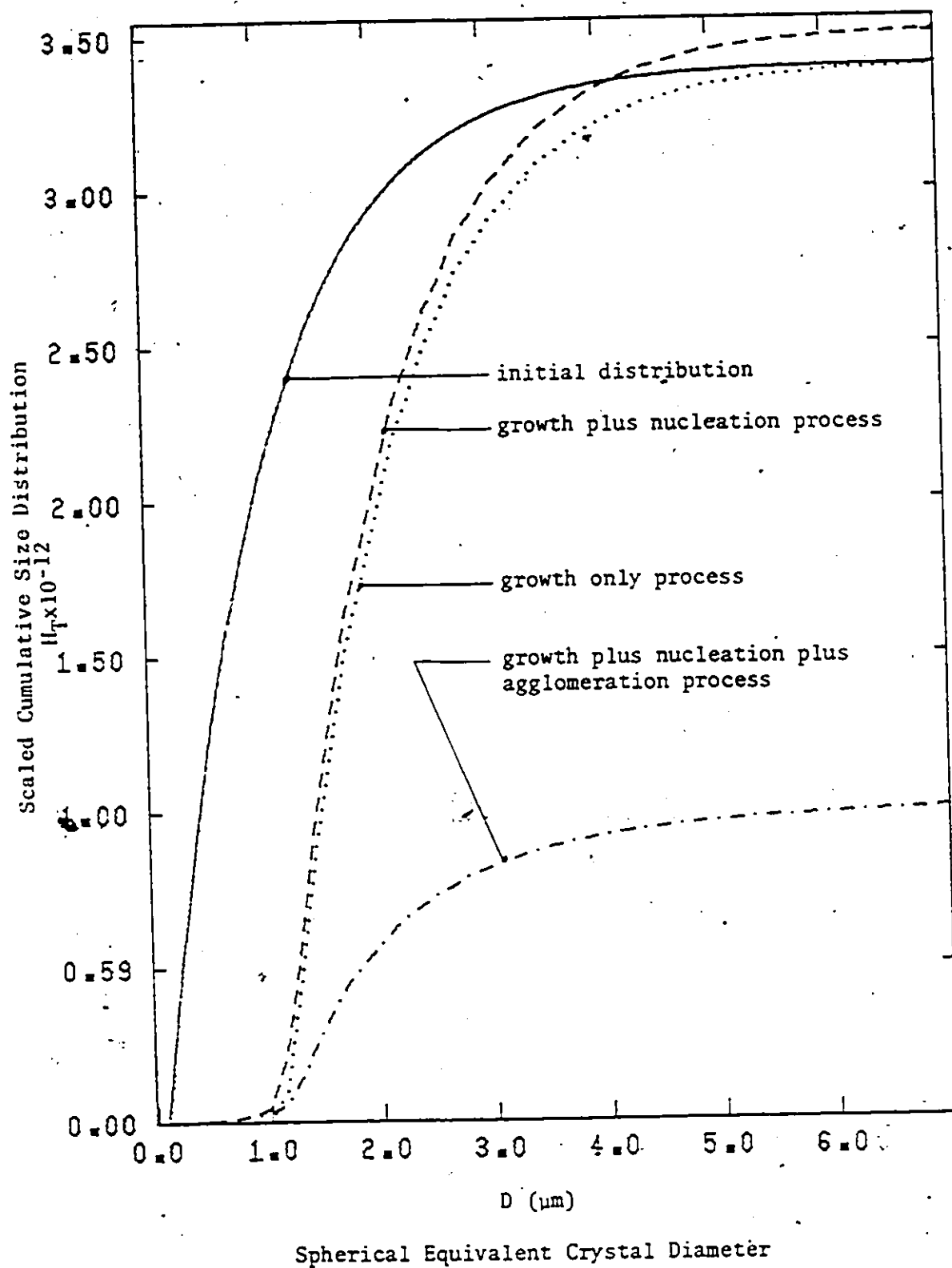
8.2 Size Distribution of Seed

In the development of the rate equations for growth, nucleation, and agglomeration processes, considerable difficulty was experienced because the Coulter Counter measures only part of the crystal size distribution at any time. This same difficulty exists with the initial size distribution of the seed crystals. Certainly, the entire initial size distribution is required in the modelling of the crystallizer since crystals smaller than the Coulter Counter cut-off size will eventually grow and/or agglomerate into the size range which is measured.

A way around this problem is to assume a distribution function and estimate the parameters in this function using the measured part of the seed size distribution and the total mass of seed crystals. The Marquardt non-linear optimization technique was used to estimate the parameters by minimizing the following sum of squares:

$$S_1 = \sum_{i=1}^{m+1} (Y_i - \hat{Y}_i)^2 \quad (8.1)$$

FIGURE 8.1-A Change in the Crystal Size Distribution due to Different Crystallization Processes



$$\text{with } Y(i) = \ln(F_{V,T,o}(i) + 1) \quad \text{for } i = 1, 2, \dots, m_e \quad (8.1a)$$

$$Y(m_e+1) = W_{T,o} \quad (8.1b)$$

where m_e = number of measured crystal size intervals
 $F_{V,T,o}(i)$ = measured number density function value for size interval i
 $W_{T,o}$ = total weight of the seed crystals
 \sim = overhead which denotes expected model values

Underlying the logarithmic transformation is the assumption that the errors in the measurements of $F_{V,T,o}$ are proportional to the magnitude of the density function values, and in addition it provides for suitable scaling with respect to the values of the vector $F_{V,T,o}$ and $W_{T,o}$.

A number of size distribution functions such as log-normal, normal, and exponential with respect to spherical equivalent crystal diameter, and normal with respect to crystal volume were investigated. Of these, the log-normal and exponential functions provided the best fit based on the least squares criterion. Their equations and estimated parameter values are:

(A) Log-Normal

$$\tilde{F}_{V,T,o}(i) = \left(\frac{2}{\pi} D_i^2\right) \frac{BI(1)}{\sqrt{2\pi} BI(2) D_i} \exp \left\{ -\frac{1}{2(BI(2))^2} (\ln D_i - BI(3))^2 \right\} \quad \dots (8.2)$$

$$\text{and } \tilde{H}_{T,o}(i) = \frac{1}{2} BI(1) \{ \text{erf}(Q_i) - \text{erf}(Q_1) \} \quad (8.3)$$

with $Q_i = \frac{\ln D_i - BI(3)}{\sqrt{2} BI(2)}$ (8.4)

erf(x_i) = error function $\Delta \frac{2}{\sqrt{\pi}} \int_0^{x_i} e^{-x^2} dx$

$\widehat{BI}(1) = 2.18 \times 10^{11}$

$\widehat{BI}(2) = 0.291$

$\widehat{BI}(3) = 1.37$

(B) Exponential

$$\widehat{F}_{V,T,o}(i) = \left(\frac{2}{\pi} D_i^2\right) BI(1) BI(2) \exp\{-BI(2) D_i\} \quad (8.5)$$

and $\widehat{H}_{T,o}(i) = BI(1) \{\exp(-BI(2) D_i) - \exp(-BI(2) D_{i+1})\}$ (8.6)

with $\widehat{BI}(1) = 3.77 \times 10^{12}$

$\widehat{BI}(2) = 1.04$

In both cases the predicted crystal weight was calculated from:

$$\widehat{W}_{T,o} = 1.21 \times 10^{-12} \sum_{\ell=1}^m \{\widehat{H}_{T,o}(\ell+1) - \widehat{H}_{T,o}(\ell)\} \{V(\ell+1) + V(\ell)\} \quad \dots (8.7)$$

where m = number of model size intervals

$V(\ell)$ = crystal volume value at grid number ℓ

Note that this summation includes all the model distribution function values, including those below the Coulter Counter cut-off size. In addition, $W_{T,o}$ is approximated by equation (8.7) and not calculated from

the respective mathematical functions for the logarithmic and exponential distributions, so as to be consistent with the subsequent model solution. In that solution the continuous H_T function was approximated between the H_T grid values by a first order collocation function. Such an approximation leads to equation (8.7) for the relationship between W_T and H_T .

Figures 8.2-A and 8.2-B show the excellent fit of these models to the measured part of the seed size distribution. However, as the solution progresses from zero time to two hours, it is seen (Figure 8.2-A) that the solution using the initial exponential distribution deviates more and more from the measured distribution as time progresses. On the other hand, when the initial size distribution of the seed is represented by the log-normal distribution (Figure 8.2-B), the differences between the model predictions and the experimental observations are much less. The relatively large difference between predicted and observed particle size distributions after two hours batch time when the exponential distribution is used can be explained in the main by the large number of crystals less than the cut-off size which are assumed to exist initially with this distribution. These crystals agglomerate and show up in the measured size range later; thus the predicted size distribution is much higher than the measured in the intermediate size range (ca. $15 \mu\text{m}$ at $\tau = 2.0$). On the other hand, with the log-normal distribution, although the predictions show some deviations which are correlated with time and size, the fit is much better. Of course, this deviation between predictions and observations may also arise to some extent because of the inadequacies of the nucleation, growth and agglomeration constitutive rate equations. This ambiguity would be removed if the seed size distribution were known over

FIGURE 8.2-A Fit of the Full Model with an Exponential Initial Distribution

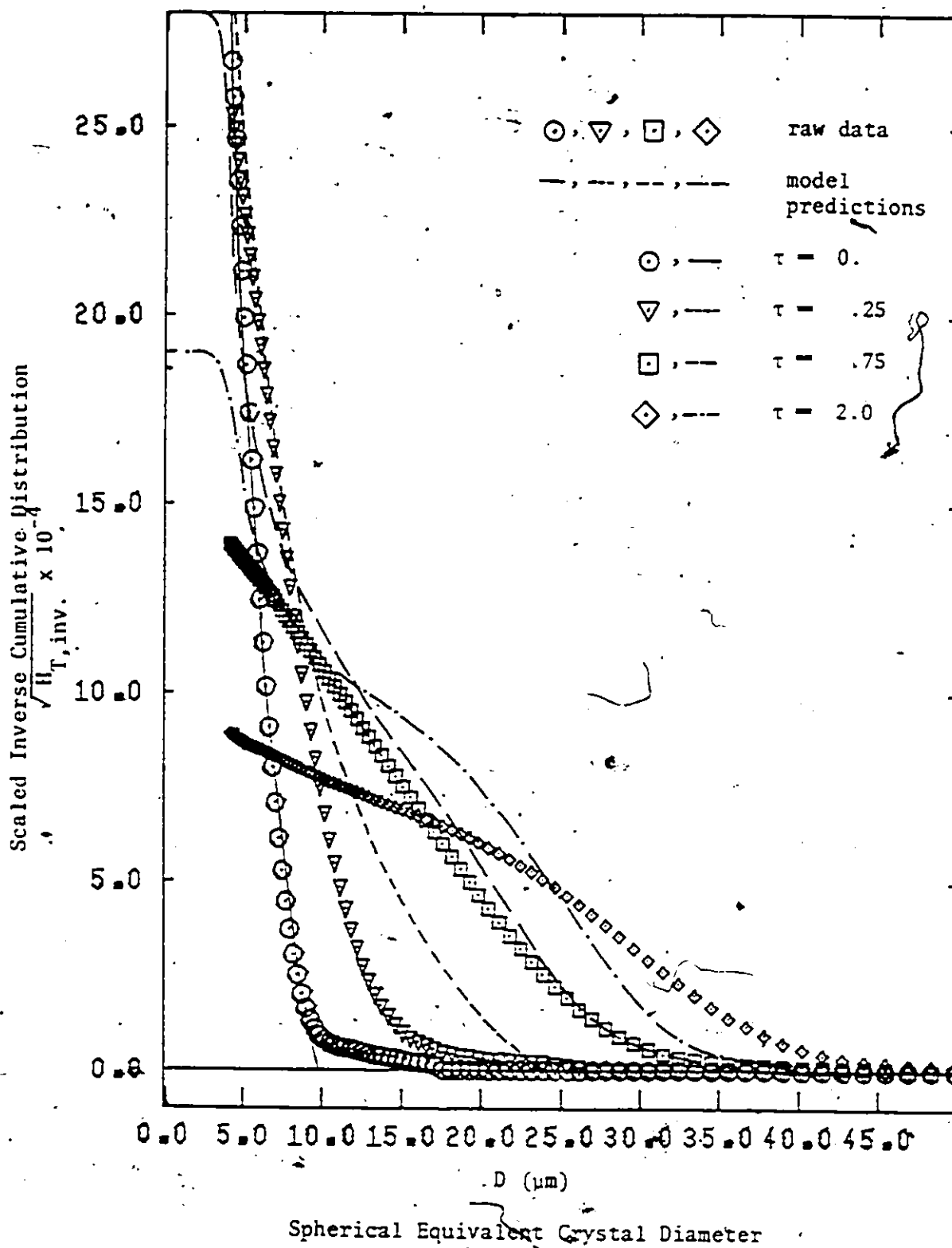
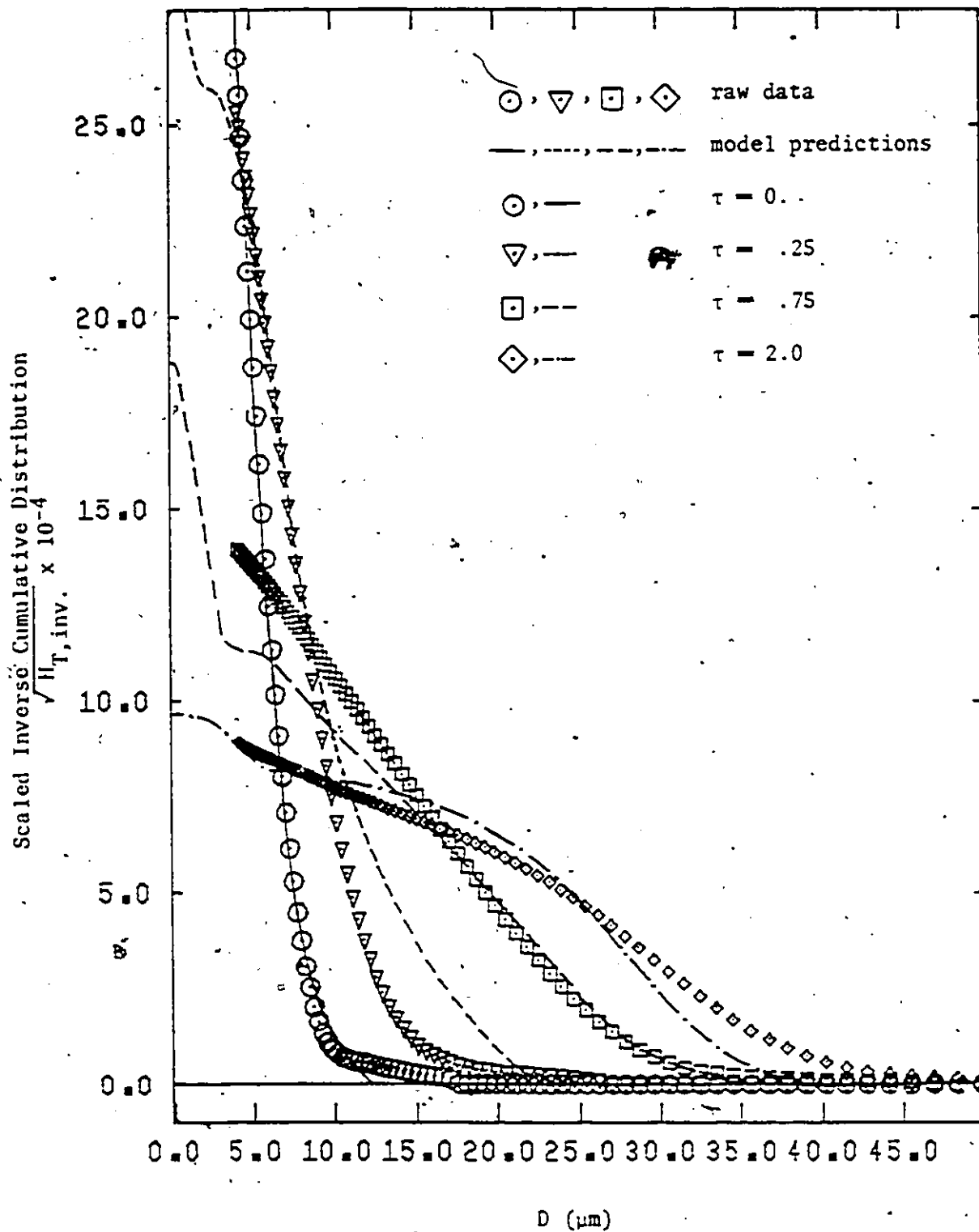


FIGURE 8.2-B Fit of the Full Model with a Log-Normal Initial Distribution



the entire size range of seed crystals. Again the limitation of the Coulter Counter leads to a problem in this research program. Given the difficulty of measuring the small crystal sizes when a broad range of crystal sizes exists, it thus seems much better to use seed which has been preprocessed to limit its smallest crystal size to that which can be measured conveniently with available equipment.

Although the log-normal representation of the initial seed distribution was shown to be somewhat inadequate, of the formulations tested it did provide the best agreement between predictions and observations. Thus, for the purposes of illustration here, equation (8.2) was used to represent the initial crystal size distribution of the seed.

8.3 Comparison between Predictions and Experimental Data

Using the log-normal representation for the initial size distribution of the seed, and the initial conditions for the experimental run, the computer solution provided the crystal size distribution as a function of time. These solutions along with the experimental data are shown in Figures 8.3-A to 8.3-I. Considering the relatively large change in the size distribution and the uncertainty in the initial distribution, the agreement between predicted and experimental data is quite good up to about two hours run time. After two hours the change in the size distribution is quite slow and relatively small. The predicted solution exhibits greater deviation from the observed results as time increases. The maximum deviation occurs at $\tau = 44$ h where the model fit is quite poor. It must be remembered, however, that the agglomeration rate equation which was developed in Chapter 7 exhibited greater deviation as time progressed.

FIGURE 8.3-A Mechanistic Batch Model Solution and Raw Size Distribution Data

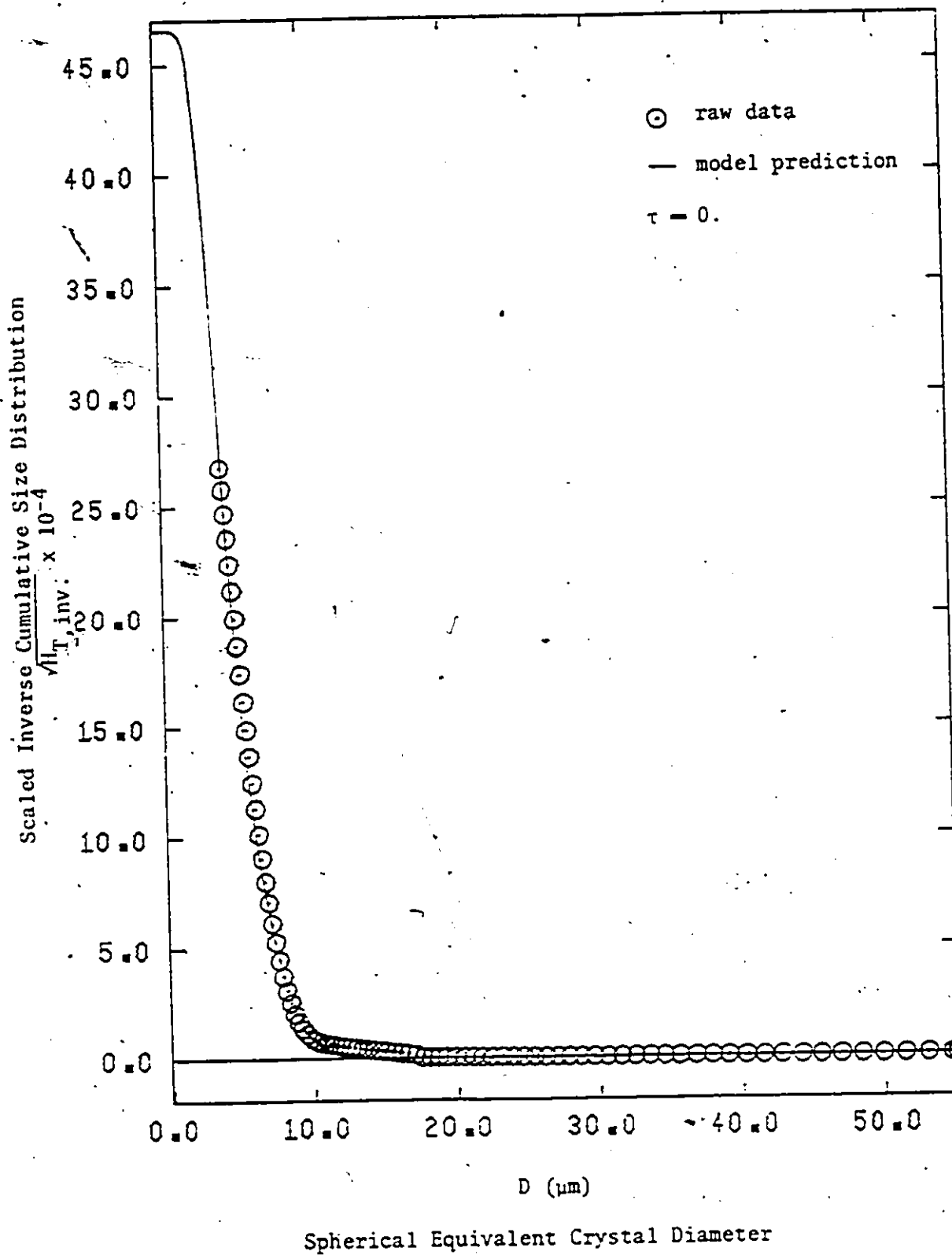
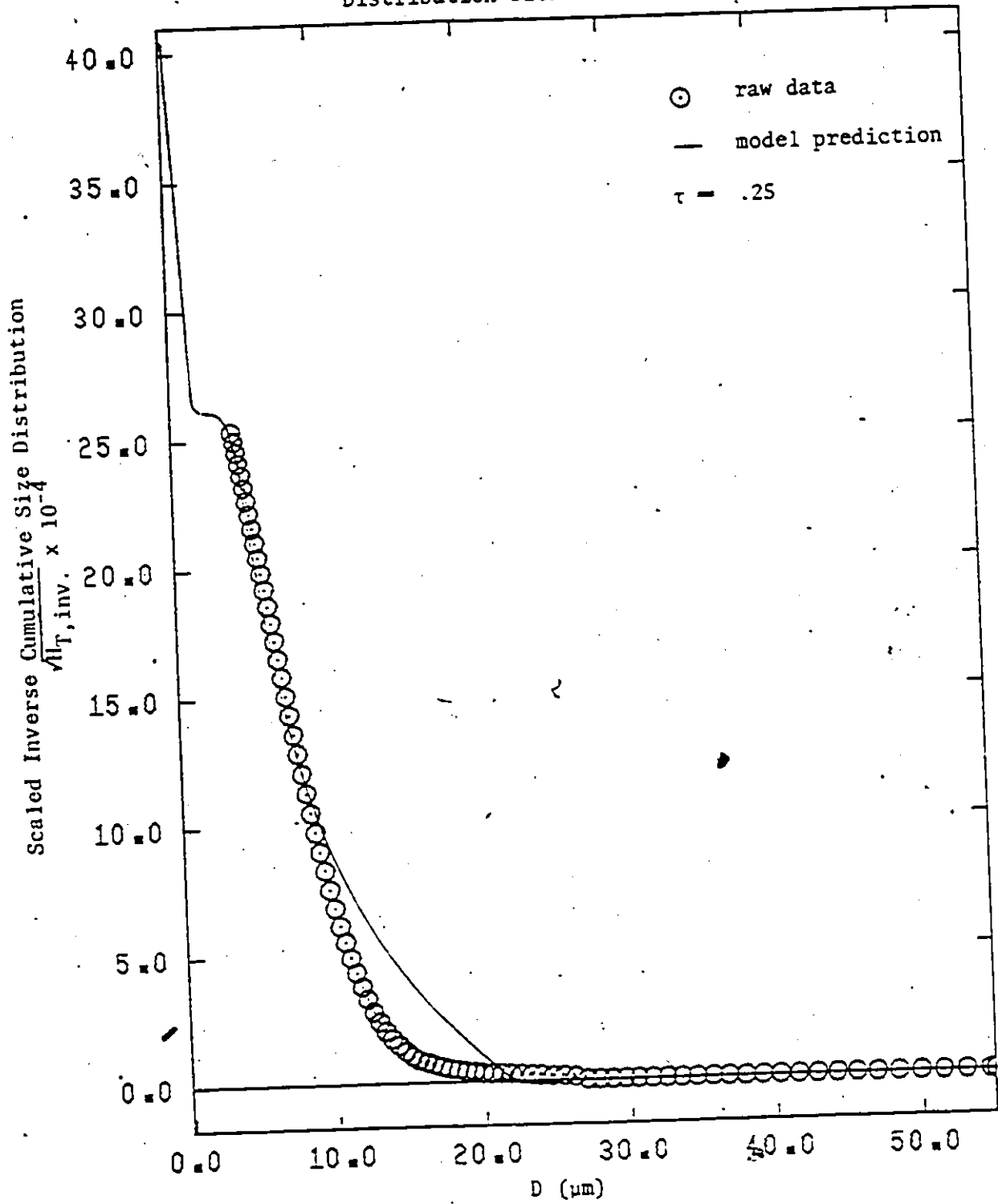


FIGURE 8.3-B Mechanistic Batch Model Solution and Raw Size Distribution Data



Spherical Equivalent Crystal Diameter

FIGURE 8.3-C Mechanistic Batch Model Solution and Raw Size Distribution Data

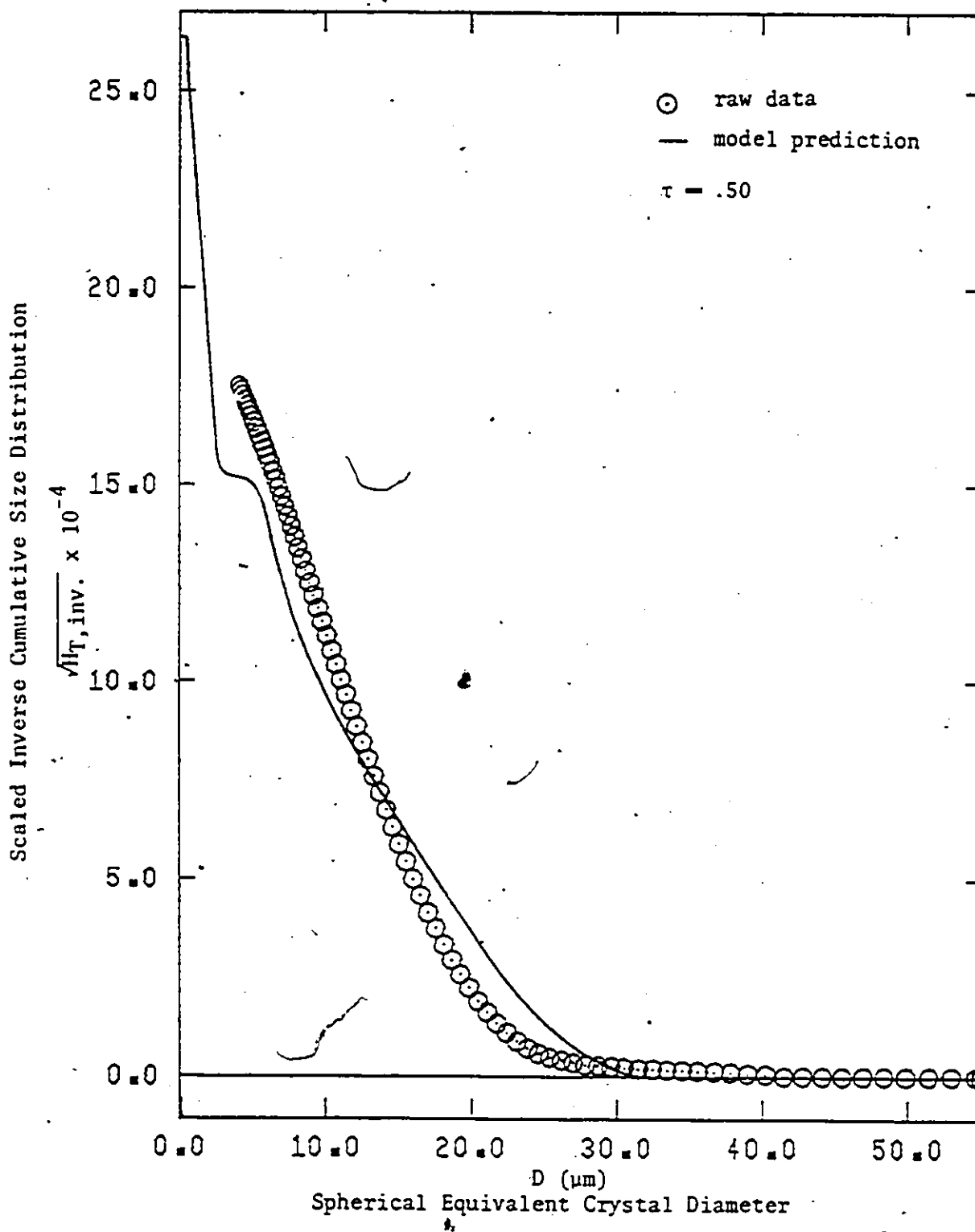


FIGURE 8.3-D Mechanistic Batch Model Solution and Raw Size Distribution Data

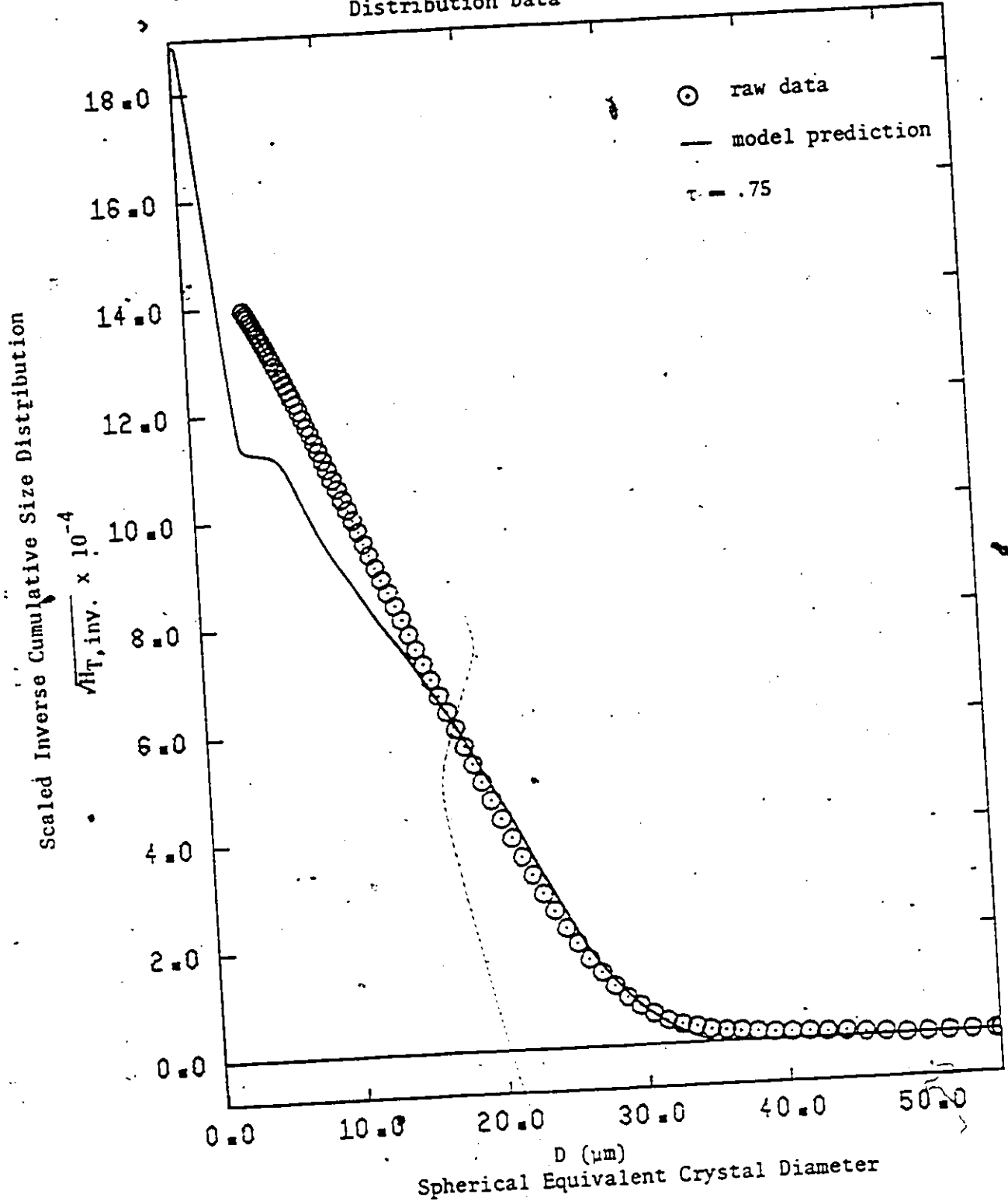


FIGURE 8.3-E Mechanistic Batch Model Solution and Raw Size Distribution Data

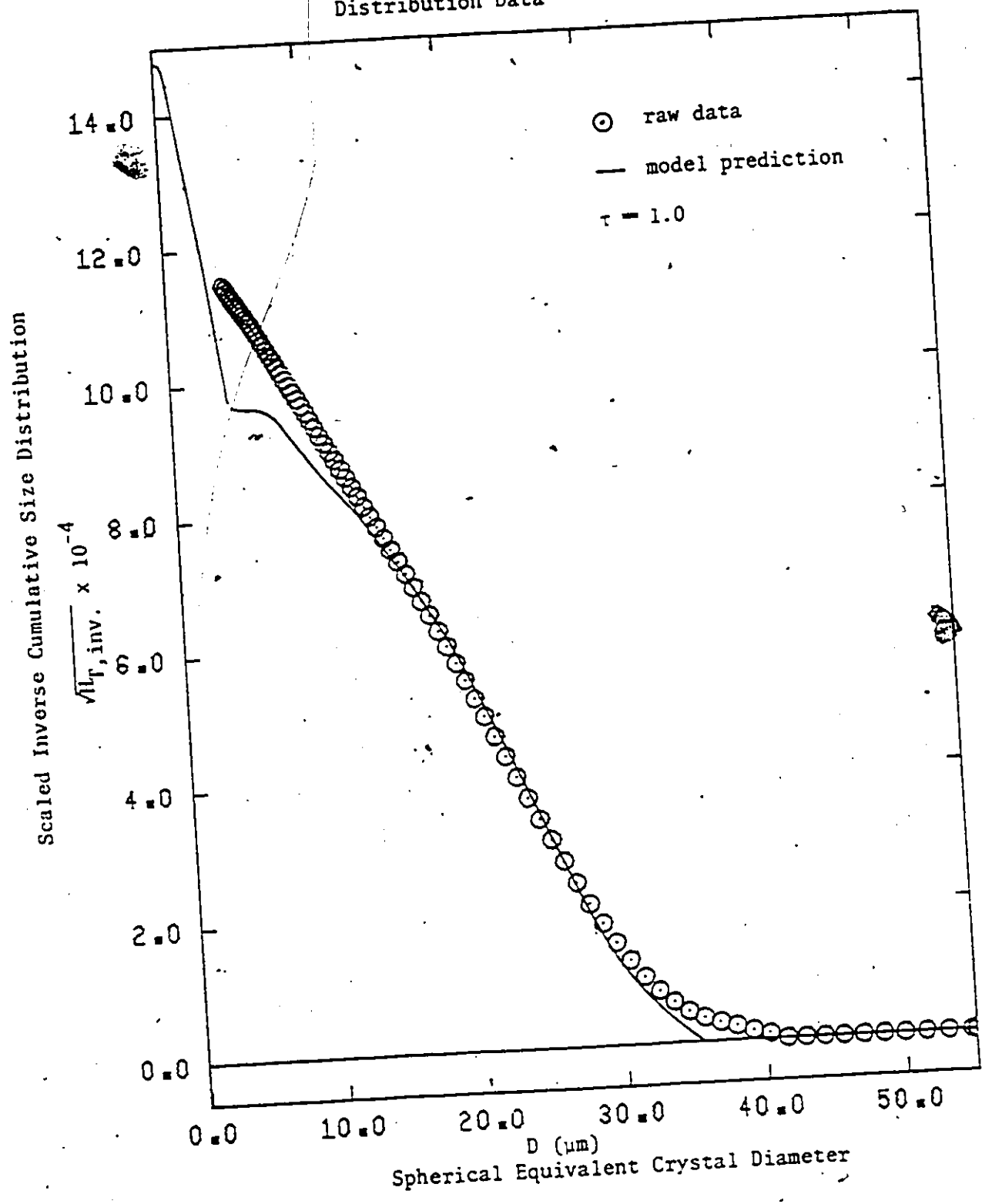


FIGURE 8.3-F Mechanistic Batch Model Solution and Raw Size Distribution Data

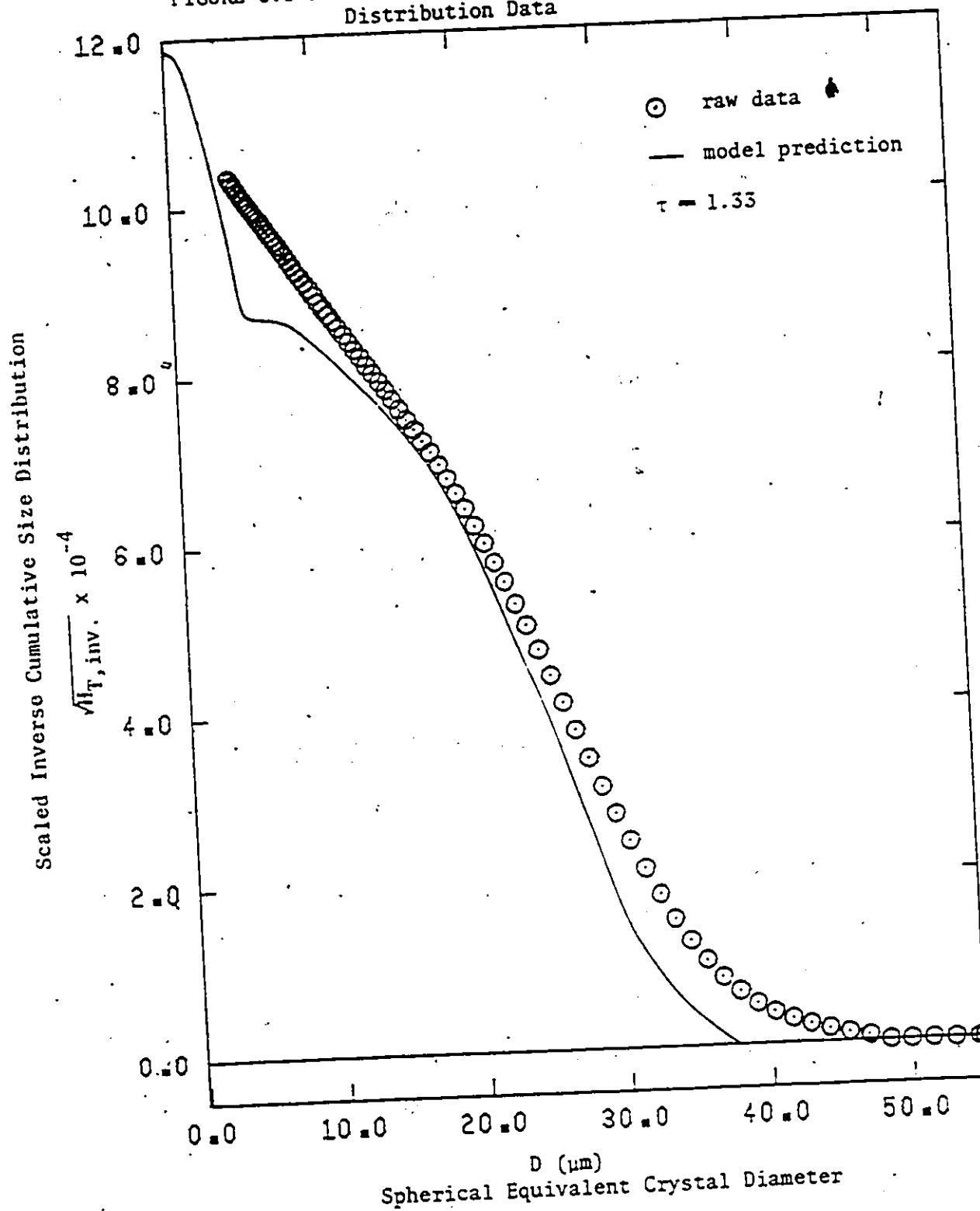


FIGURE 8.3-G Mechanistic Batch Model Solution and Raw Size Distribution Data

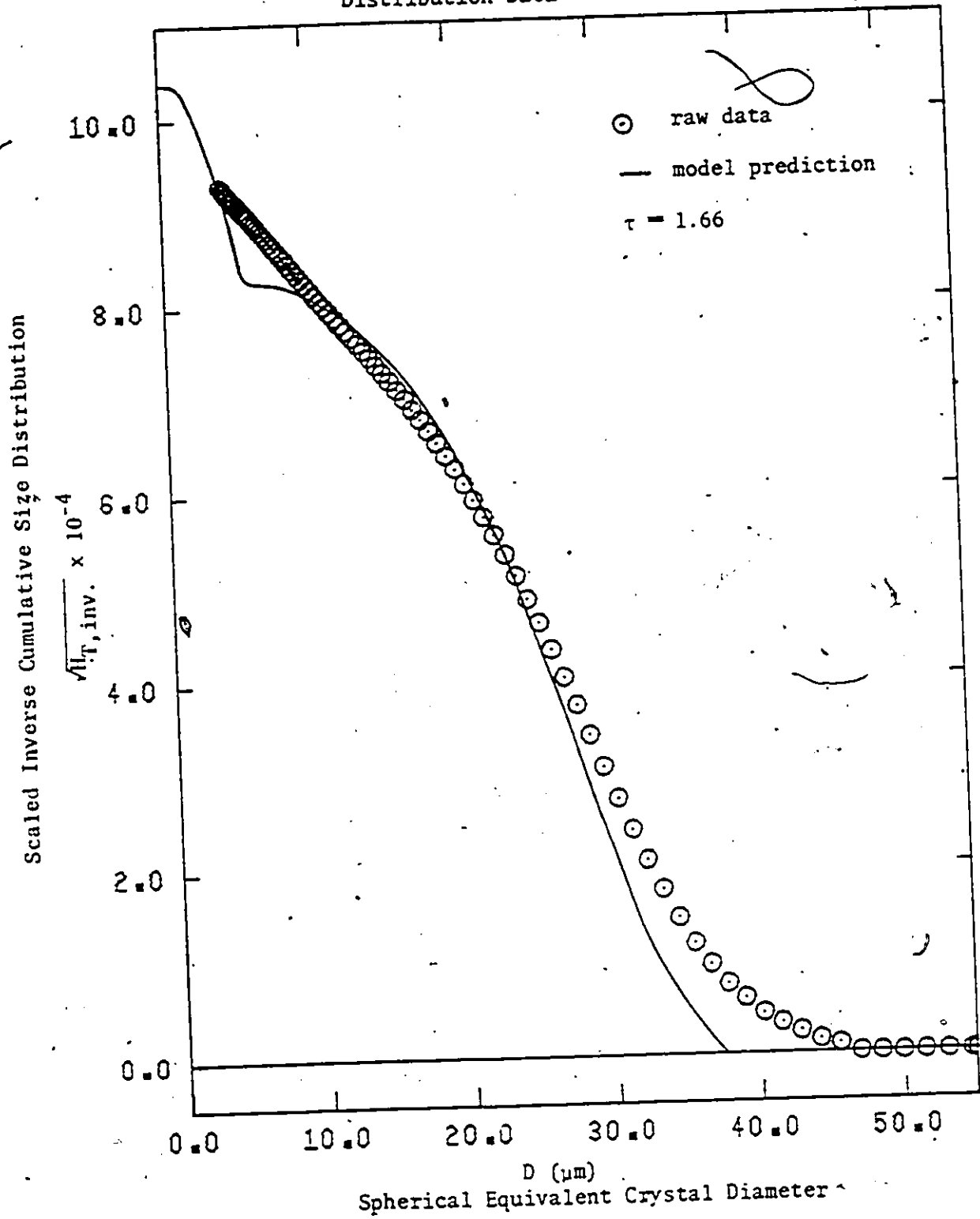


FIGURE 8.3-H Mechanistic Batch Model Solution and Raw Size Distribution Data

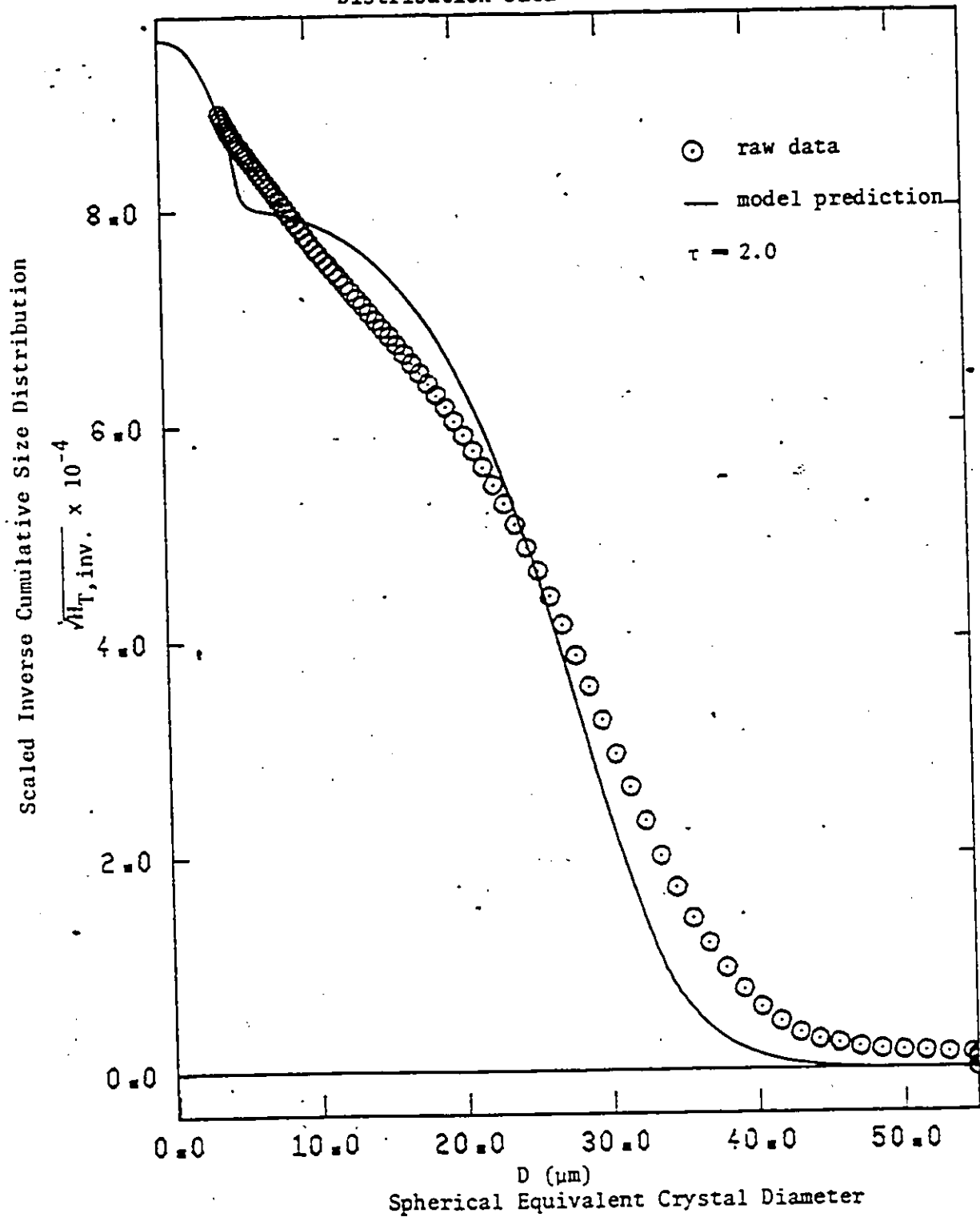
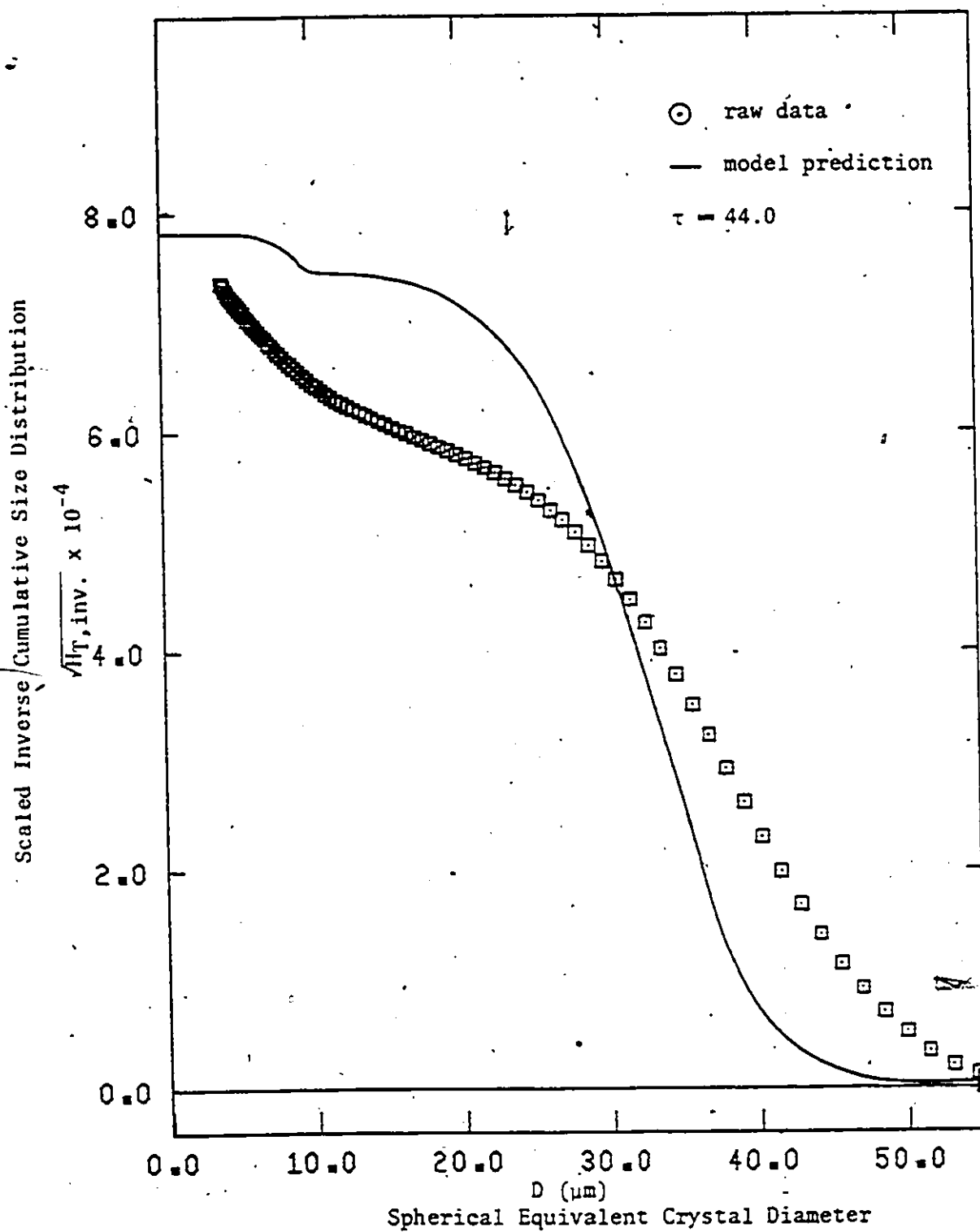


FIGURE 8.3-I Mechanistic Batch Model Solution and Raw Size Distribution Data



It was decided that because the experimental data was somewhat lacking at this time that little would be gained from a large expenditure of computer time to improve the agglomeration rate expression. The method of handling the data has been illustrated, the numerical method evaluated, and the difficulties associated with the experiment and the computer solution uncovered. The deviations observed here are explained, in part, by the inadequacy of the agglomeration rate model which could be improved with some effort. When more and improved data becomes available, certainly the additional effort would be warranted. Moreover, the experimental conditions under which agglomeration is maximized or minimized are suggested by this work and thus these preliminary results provide a very good starting point for designing future experiments.

8.3.1 The Problem of Correlation of Models and Model Parameters

Early in this work, before the pseudo-moment scheme was developed, considerable effort was directed toward finding suitable constitutive rate relationships by assuming certain forms for the various unknown expressions and adjusting the respective parameters to provide a fit of model predictions to experimental observations. At that stage, the exponential distribution for the initial seed was used. Agglomeration and nucleation rate equations were assumed and the parameters in these expressions were adjusted (crudely) to make the predictions agree with the experimental observations. The predictions were reasonably good, given the heuristic way in which the parameters were adjusted. Certainly a reasonably good fit could have been achieved after a very large expenditure of computer time. In the light of the analysis and results which have

been presented, this exercise demonstrated a number of shortcomings of this method and characteristics of the system; these are summarized as follows:

- (i) Although a poor distribution was used for the initial seed (the exponential distribution), a reasonable fit of the model to the experimental data could be achieved.
- (ii) The high number of crystals of size less than the cut-off size initially could be compensated by a very large agglomeration rate for these crystals.
- (iii) The high agglomeration rate for these small crystals would then require a very high nucleation rate to provide the required crystals later in the run.

Thus this scheme produced very high agglomeration rates and very high nucleation rates because of the high correlation among the three formulations for the initial distribution, agglomeration rate and nucleation rate. The pseudo-moment method minimizes this correlation and the current results using the pseudo-moment method indicate that the results of the earlier analysis were quite incorrect. Thus, without a method to minimize this high degree of correlation among the various processes, quite erroneous conclusions can result. It is to be noted that the pseudo-moment method also minimizes the effect of the unknown part of the seed size distribution.

8.4 Comparison with Other Studies

Since the previous studies on the crystallization of alumina trihydrate (m5,h1,h2,p1,b10) were carried out under quite different

conditions from those reported here, direct comparison of the results of those studies and this one cannot be made. Moreover, the apparatus used by each of these investigators was quite different and consequently, particularly because of the different level of mixing, the nucleation and agglomeration processes were quite different.

On the other hand, the growth rate should be independent of mixing level because the surface reaction is controlling in this system. Both Misra (m5) and Halfon (h1) proposed power law growth rate models. These models were found to predict the growth rate as measured in the present experiments quite well; however, since the birth and spread growth rate model was found to be equally adequate, has theoretical basis, and seems to be compatible with the direct observation of crystal habit, it was chosen as the model to be used in this work.

Misra (m5) stated that the growth rate of alumina trihydrate was independent of crystal size. This conclusion was based on the observation that the crystal size distribution retained the same shape but just moved to increasing sizes with time. In light of the importance of agglomeration in this system, it is surprising that agglomeration did not play a role in his experiments. On the other hand, the intensity of mixing may have been so high that agglomerates did not form or were broken as fast as they were formed.

The results of this investigation do not allow a definitive statement to be made whether this system really follows the McCabe ΔL law. Certainly, in this work, the crystal growth rate based on a spherical equivalent diameter was assumed to be independent of crystal size. The agglomeration rate expression could, however, compensate for the error

in this assumption or the fact that the spherical equivalent diameter is not the correct characteristic length to use in the ΔL law. Certainly, as indicated in Figure 4.4-C, alumina trihydrate crystals are far from spherical. Moreover, crystal growth is a surface phenomena and is related to the 'activity' of the surface. Thus, there is uncertainty as to the correct equivalent length to use.

Misra (m3) and Brown (b10) observed that the nucleation rate for the alumina trihydrate system was negligible at temperatures above 75°C. The results of this study agree with these observations, since the large initial production of crystal nuclei seems to have arisen from loosely adhered 'nuclei' on the surface of the seed crystals and not from a specific nucleation mechanism.

Nucleation rate expressions have been developed for this alumina-trihydrate system at temperatures below 75°C by Misra (m3) and at 60°C by Halfon (h1). However, Halfon obtained these rates from the change in alumina concentration in solution. This procedure is highly inaccurate since, even for very high nucleation rates, the change in the alumina concentration in solution due to nucleation is very small compared to the change due to growth. This was demonstrated in the model solutions presented in Chapter 6 on growth only and for nucleation plus growth. Halfon also used a 'vacant site' variable which was highly empirical and introduces another weakness in his analysis of nucleation rates. The greatest weakness in Halfon's analysis, however, is in the fact that he did not account for agglomeration in his analysis for a nucleation rate expression. Given all of these weaknesses in his analysis, one has little confidence that Halfon's expression for the nucleation rate represents the true rate even under the conditions of his experimental system.

Very little information is available on the agglomeration rates in the alumina trihydrate system. Using what now may be termed an inaccurate procedure, Halfon (h2) fitted his experimental data using an agglomeration kernel which was independent of crystal size. Such a kernel provided a very poor fit of the data from this study. The real weakness of this kernel, however, is that it is unbounded. Not only is it unrealistic but also does not agree with qualitative observations in the plant (p1) which indicate that large crystals do not agglomerate as readily as smaller ones. The agglomeration kernel recommended here, although requiring some moderate refinement, does suggest that crystals in the intermediate size range of 10 to 30 μm do agglomerate faster than either smaller or larger crystals. The slow rate of agglomeration of small particles ($D < 10 \mu\text{m}$) would be very difficult to detect during plant operation because particles in the intermediate range would always be present with the smaller ones. The slower rate for small particles can only be detected by analysis using mathematical methods like those presented in this thesis.

8.5 Summary

Presented in this chapter are the experimental size distribution data and mechanistic model predictions as a function of time. Considering the relatively large change in the size distribution and the uncertainty in the initial distribution, the agreement between predicted and experimental data is quite good up to about two hours run time. After that the size distribution changes quite slowly while the deviation between the predicted and experimental results worsens progressively as time increases. The deviations can in part be explained by the inadequacy of the agglomera-

tion rate expression which also exhibited greater deviation as time progressed. Because of the limited data available at this time it was decided that little would be gained from a large expenditure of computer time to improve the agglomeration rate expression. The method of handling the data has been illustrated, the numerical method evaluated, and the difficulties associated with the experiment and the computer solution uncovered.

Reasonably good agreement was also obtained with a different set of rate equations for growth, agglomeration, and nucleation obtained by solving for all three rate processes simultaneously. However, analysis by the method of pseudo moments showed that these rate equations were quite incorrect. Their overall good fit was due to the high correlation among the formulations for the initial distribution, agglomeration rate and nucleation rate. The pseudo-moment method minimizes this correlation.

No direct comparisons can be made between the experimental and model results of this study with previous studies since experimental conditions were quite different. However, the experimental results of this work and developed rate models for growth, agglomeration, and nucleation are in qualitative agreement with the widest held views on the behaviour of these crystallization processes. In particular, the agglomeration kernel recommended here (which still needs some moderate refinement) is the first quantitative agglomeration model that confirms the qualitative observations on agglomeration in the aluminum industry. They observed that large crystals do not agglomerate as readily as smaller ones. This model suggests that crystals in the intermediate size range of 10 to 30 μm do agglomerate faster than either smaller or larger crystals.

CHAPTER 9

SUMMARY, CONCLUSIONS, AND RECOMMENDATIONS

9.1 General

The overall objective of this research program was to develop experimental and mathematical techniques that would provide a method to obtain a mathematical model that would be representative of that for an industrial crystallizer. Indeed, it was the intention to develop these techniques on the bench-scale apparatus and then at some time in the future carry out similar tests on an industrial crystallizer to provide a mathematical model of it. In this regard, the experimental program dictated the model development program. At this stage the modelling program has delineated some of the shortcomings of the experimental techniques (for example, the need to measure particle size at diameters significantly smaller than the lower cut-off diameter of a Coulter Counter). In general, however, it can be said that this research program has been successful in attaining the above stated objective. The conclusions and contributions to knowledge as they relate to the experimental and modelling program are summarized below.

9.2 Experimental

(A) Summary and Conclusions

A bench-scale experimental crystallizer and special sampling and sample analysis system have been developed. This crystallizer was designed so that the gentle mixing action ensured that significant agglomeration

would take place. Thus, the nucleation, growth and agglomeration processes which occurred in the bench-scale crystallizer during the seeded-crystallization of alumina trihydrate were expected to proceed at about the same rate as those in the full-scale crystallizer.

The experimental procedures were very carefully planned. The sampling system and analytical procedures were shown, by means of mass balances and multiple replicates, to be representative, consistent and reproducible. The crystal size distribution was measured with a relatively new Coulter Counter equipped with Channelizer and Log-Transformer which provided 100 size intervals over the size range of about 4 to 80 μm . Although resolution and reproducibility were excellent, the use of this equipment did create serious limitations in the analysis of the data since a large number of crystals were produced and existed below the minimum size that could be measured with this wide size distribution.

(B) Recommendations

The general approach which was used for the study of the batch crystallization of alumina trihydrate should be continued and pursued further. The following improvements are suggested:

- (i) The modelling work would be considerably facilitated and improved if the crystal size distribution could be measured over a wider range of sizes, particularly at the small end. Unfortunately, this may require pretreatment of the sample to separate it into fractions which can be measured separately. The development of this technique is a formidable task and will require considerable effort and testing to ensure that the results are unbiased.

- (ii) Regardless of whether a more adequate procedure or apparatus for measuring crystal size is developed, it is recommended that the seed material used in the batch experiments be comprised of crystals with a narrow size distribution which is measureable over its entire size range. Such a seed could probably be obtained using wet screening techniques. The use of this type of seed with quite different average diameters should give greater insight into the crystallization rate processes. For example, crystals smaller than the smallest seed crystals can only appear through nucleation and/or attrition processes; the seed distribution can only broaden to larger sizes by growth and agglomeration. Moreover, if the seed is comprised of two narrow, but quite different distributions, the effect of agglomeration will be more readily observable and the pseudo-moment method should demonstrate its power in extracting the rate of agglomeration.
- (iii) A method needs to be devised which will give the total crystal area or the average area per particle which is effective in the crystal growth process. Adsorption techniques are probably appropriate.
- (iv) The experimental runs are quite long and require tedious manipulation of numerous valves. The sampling system, in particular, could easily be automated. Not only will this decrease the tedium and the need to be continuously present over long periods, but it will increase the flexibility and define the batch sampling times more sharply.

Given these improvements in the experimental system and procedures, it is recommended that the following be investigated:

- (1) A set of experiments should be carried out over the full range of experimental independent variables (seed charge, seed average diameter, supersaturation, etc.). These experiments should be designed on a statistical basis to allow an estimation of the parameters in an efficient and effective manner.
- (2) Selected experiments should be repeated with a different apparatus and/or mode of mixing. This will be another important step in understanding the alumina trihydrate system since it is expected that nucleation/attrition and agglomeration are strong functions of the intensity of agitation.
- (3) Some or all of the experiments should be repeated using plant liquor and seed; these experiments would provide information on the effect of known and unknown impurities on the rate processes.
- (4) The final step in this program would be to run similar experiments on the plant crystallizers. At this point, considerable insight into the form of the model (particularly the constitutive relationships) would have been obtained so that the effect of scale-up and agitation would be the main objectives of the in-plant program. The final model should be useful in understanding the crystallization process and hence afford better control of the particle size distribution.

All of the experiments recommended above should be analyzed by the mathematical methods developed in this work.

9.3 Determination of the Rate Equations

(A) Summary and Conclusions

A special mathematical method based on the population balance has been developed to determine appropriate rate constitutive relationships for growth, nucleation and agglomeration and estimate the parameters in these relationships. This method, termed here the pseudo-moment method, allows these expressions to be determined almost independent of the other process. Thus, this method circumvents the serious problem, which was present here, of confounding the models for the rate processes. Without a method to minimize the interaction among the rate processes, it was shown that very different and misleading results could be obtained from the experimental data.

The method of pseudo moments also allows the development of expressions for the crystallization rate processes with practical computer resources. The successful application of this pseudo-moment method has been demonstrated in this work in developing rate equations from the available data. Without this method it would have been very difficult if not impossible to determine the rate equations which were at least close to the 'true' ones.

(B) Recommendation

As discussed in the text the one remaining problem with the method of pseudo moments is that the experimental errors are not properly accounted

for; thus the experimental data are not properly weighted in the minimization of the sum of squares of the residuals. In this work the data were treated as having equal weight, that is they all had the same relative error. Because the experimental data are contained in the objective function in a very complicated way, it is important that the error be included in the correct way, probably in a manner similar to that suggested by Patino-Leal (p3). It is important that the model discrimination and parameter estimation procedures used in this work are based on sound statistical principles and methods.

9.4 Numerical Solution of a Population Balance for an Unsteady State Process with Growth, Nucleation and Agglomeration Terms

(A) General

The population balance equation may be used to predict the crystal size distribution as a function of time in an unsteady state crystallization process. In a numerical solution scheme, the probability density function, or alternatively, the cumulative density function, at each particle grid point is the dependent variable.

(B) Summary and Conclusions

Two numerical methods to effect the solution of this population balance equation were developed here. One of the methods, denoted here by RWCD, is based on a weighted central difference approximation to the partial derivative with respect to crystal volume. The other method, denoted here by CICR, exploits the fact that the population balance partial differential equation is of the hyperbolic type and therefore can be solved by the method of characteristics. In each case, the numerical

integration with respect to time was carried out using the Runge-Kutta-Merson, fourth-order, numerical integration routine with error estimate. This routine allows the step size to be adjusted automatically based on the estimated error.

One of the practical problems to be overcome here was that of obtaining a quadrature approximation to the integrals of the integro-partial differential population balance which would not only be fast but would also not require inordinate computer storage. Such a quadrature formula was developed in this work. It is based on special grid spacings with respect to crystal volume, which are adjustable depending upon the problem, and which account for the fact that one of the integrals is of a special convolution type.

For the RWCD method of solution integration with respect to time was along this special grid. For the CICR method this was not possible, since the characteristics (along which the solution was affected) only coincide with the special grid at points where the two grids cross. This meant that an interpolation program was required to provide the numerical value of the integrals at the grid points for the numerical integration with respect to time and the values of the dependent variable at the quadrature grid points for the evaluation of the integrals. It was found that linear interpolation between the two grids led to gross accumulated errors when a fast changing size distribution (with respect to V and τ) was involved, while use of more complex interpolation schemes, such as piecewise continuous splines, resulted in instabilities. However, for relatively slow changing size distributions, and in particular for growth and growth plus agglomeration processes, the CICR method is entirely satisfactory and vastly superior to the RWCD method.

Solution of the model by either of the solution methods showed that the effect of the propagation of very small errors (ca. 0.01%) in the numerical evaluation of the integrals at each time step led to gross inaccuracies (as measured by the mass balances) after several thousand time steps. This problem was overcome by developing an empirical correction expression based on the fact that for a bounded agglomeration kernel, the weight change for an agglomeration only process is zero (mass of crystals is constant). This expression is valid regardless of the contribution of the other processes to the overall crystallization process.

The accuracy of the weighted central difference approximation was evaluated by solving an unsteady growth only process by the RWCD method and comparing the numerical solution to an analytical solution. The numerical solution was conditionally stable and more accurate than either a first order backward difference or a second order central difference. The accuracy of the quadrature formulas within this solution scheme was checked against an analytical solution for a special unsteady state agglomeration-only process. Doubling the number of grid points with respect to particle volume reduced the maximum deviation from -9.5% to -2.4%. The overall average accuracy with 121 grid points was found to be very good.

In comparing the two methods for different processes and different initial size distributions; it was found that:

- (i) For a growth and for a growth plus agglomeration process the CICR method is vastly superior (with regard to solution time for relatively the same accuracy) to the RWCD method.

- (ii) For fast changing size distributions, especially fast local changes as due to a discontinuous initial size distribution and/or large nucleation rates, both methods require very long solution times; with the CICR method taking about four times as long as the RWCD method for the particular case investigated here.

No explanation can be offered for this behaviour of the two numerical solution schemes.

The full model developed here has a very large initial nucleation rate and essentially a zero rate subsequently in addition to growth and agglomeration. That is, the process was subject to fast local changes initially and then reduced to a growth plus agglomeration only process. Therefore, based on the above observations with regard to the behaviour of the two solution methods the model was solved first by the RWCD method and then for a growth plus agglomeration only process by the CICR method. This procedure resulted in an accurate solution with a significant decrease in overall computer time.

(C) Recommendation

Since the CICR method is based on interpolation techniques it should inherently be more accurate than the RWCD method which is based on numerical differentiation. Therefore, to realize the full potential of the CICR method, the interpolation problem as discussed in the text needs to be resolved. Once that is accomplished, the CICR method should, in general, be the preferred solution method.

9.5 Model for the Seeded Batch Crystallization of Alumina Trihydrate

(A) Summary and Conclusion

A dynamic model has been developed for the batch crystallization of alumina trihydrate from seeded supersaturated solutions. This model predicts the crystal mass produced and the crystal size-distribution as a function of time. This model includes the effects of nucleation, growth and agglomeration on the performance of the crystallizer. Constitutive relationships have been developed, using limited experimental data, to relate rates of crystal growth, nucleation and agglomeration to solution-supersaturation and crystal size distribution.

The equations which make up the model are summarized below:

(1) Population Balance

$$\begin{aligned} \frac{\partial H_T}{\partial \tau} (V, \tau) + G_D(\tau) \phi_g(V) \frac{\partial H_T}{\partial V} (V, \tau) = & +\{V_L(\tau)BF_{V,2,n}(V, \tau, H_T)\} \\ & +\{V_L(\tau)BF_{V,2,a}(V, \tau, H_T)\} \\ & +\{V_L(\tau)DF_{V,2,a}(V, \tau, H_T)\} \\ & \dots (9.1) \end{aligned}$$

$$\text{with the B.C. } H_T(V_0, \tau) = 0 \quad (9.2)$$

(2) Mass Balances

$$W_T(\tau) = \int_{V_0}^{V_u} \phi(V) V F_{V,T}(V, \tau) dV \quad (9.3)$$

$$V_L(\tau) = \{(C2 - W_T(\tau)) + [(C2 - W_T(\tau))^2 + (4C1C3)]^{1/2}\} / (2C1) \quad \dots (9.4)$$

$$CA(\tau) = \{C4 - .654 W_T(\tau)\} / V_L(\tau) \quad (9.5)$$

$$CN(\tau) = C5 / V_L(\tau) \quad (9.6)$$

where $F_{V,T} = \frac{\partial}{\partial V} H_T \quad (9.7)$

$$C1 = 1.5877\{1051 + (-.94 + (.0051 \theta))\theta\} \quad (9.8)$$

$$C2 = 1.5877\{V_{L,o}(C6 - .992 CN_o - .566 CA_o)\} + W_{T,o} \quad (9.9)$$

$$C3 = 1.7465 \times 10^{-4} (V_{L,o} CN_o)^2 \quad (9.10)$$

$$C4 = V_{L,o} CN_o + .654 W_{T,o} \quad (9.11)$$

$$C5 = V_{L,o} CN_o \quad (9.12)$$

$$C6 = 1051 + .992 CN_o - .00011 CN_o^2 + .566 CA_o - .94 \theta_o + .0051 \theta_o^2 \quad \dots (9.13)$$

with the following specified initial conditions:

$$H_T(V,o) = H_{T,o}(V), \theta_o, CA_o, CN_o, V_{L,o}$$

(3) Constitutive Relationships

$$G_D(\tau) = BG1 \sigma^{5/6} \exp(-BG2/\sigma) \quad (9.14)$$

$$BF_{V,\ell,n}(\tau,V) = \left\{ \frac{BN1}{1 + e^{BN2(\frac{1}{\sigma} - BN3)}} \right\} \left\{ \frac{1}{BNS V \sqrt{2\pi}} e^{-\frac{1}{2} \left(\frac{\ln V - BN4}{BNS} \right)^2} \right\} \quad \dots (9.15)$$

$$BF_{V,\ell,a}(\tau,V,H_T) = \frac{1}{(V_L(\tau))^2} \int_{V_0}^{V/2} \int_{V'}^{V-V'} k_{V,a}(V',V'',\tau) F_{V,T}(V',\tau) F_{V,T}(V'',\tau) dV'' dV' \quad \dots (9.16)$$

$$DF_{V,\ell,a}(\tau,V,H_T) = \frac{1}{(V_L(\tau))^2} \int_{V_0}^V \int_{V_0}^u k_{V,a}(V',V'',\tau) F_{V,T}(V',\tau) F_{V,T}(V'',\tau) dV'' dV' \quad \dots (9.17)$$

where $k_{V,a}(V',V'',\tau) = \{BA1 \sigma^{BA2}\} \{ (V')^{1/3} + (V'')^{1/3} \}^2$

$$\{ (V')^{2/3} - (V'')^{2/3} \} \exp\{-BA3((V')^{2/3} + (V'')^{2/3})\} \quad \dots (9.18)$$

with

$$\begin{aligned} \widehat{BG1} &= 15.22 @ 85^\circ\text{C} \\ \widehat{BG2} &= 0.3397 \\ \widehat{BN1} &= 1.725 \times 10^{12} @ 85^\circ\text{C} \\ \widehat{BN2} &= 8.504 \\ \widehat{BN3} &= 1.606 \\ \widehat{BN4} &= -4.10 \\ \widehat{BN5} &= 1.15 \end{aligned}$$

$$\hat{BA}_1 = 1.025 \times 10^{-12} \text{ @ } 85^\circ\text{C}$$

$$\hat{BA}_2 = 3.062$$

$$\hat{BA}_3 = 6.579 \times 10^{-3}$$

(4) Empirical Correlation for the Equilibrium Alumina Solution Concentration

$$CA_e = CN \exp\left\{6.2106 + \left(\frac{1.08753 CN - 2486.7}{273.16 + \theta}\right)\right\} \quad (9.19)$$

(5) Crystal Geometry Relationships

In this work it has been assumed that the crystals are spheres, therefore the shape factor relating volume to surface area is:

$$\phi_g(V) = \frac{1}{2} \pi^{1/3} 6^{2/3} V^{2/3} \quad (9.20)$$

and the factor relating volume (as measured in μm^3 to mass in g/cm^3 is:

$$\phi(V) \approx \phi = \rho_s \times 10^{-12} \quad (9.21)$$

Through this limited experimental study, some discrimination among the various proposed models for the various crystallization rate processes was possible. For example, the growth rate could be modelled very well considering the process to be governed by a two-dimensional birth and spread mechanism. The agglomeration rate kernel was found to require a size dependent term in addition to one relating this rate to supersaturation. The size dependence has been suggested to relate to an inertia impaction mechanism which accounts for collision frequency. The

other term in this expression (Equation (9.18)) accounts for the efficiency of the collision in bringing about agglomeration. The analysis of the experimental data indicates that the combined effect of these two terms is to make crystals in the intermediate size range (10 to 30 μm) the most effective in bringing about agglomeration. The development of the nucleation rate model, led naturally to one which suggested that the nucleation phenomena occurring in the experiment at 85°C was not via a normal homogeneous or heterogeneous mechanism. The model suggested a large burst of nuclei at the outset, probably arising from small, nuclei sized, particles adhering loosely to the seed crystals. No definite conclusions can be made from this work with regard to the nucleation mechanism at 85°C.

Qualitatively, the birth and spread model agrees with electron microscope observations by, among others, Brown (b7). The proposed agglomeration model is consistent with observations by plant personnel in the aluminum industry in that the rate of agglomeration of large crystals is less than that of small crystals. They were probably not able to observe that the rate for very small crystals is also smaller than that for crystals of intermediate size. The conjecture here that the large number of nuclei sized crystals at the initial stages of batch crystallization were merely the result of dusting of the seed, is consistent with observations by Misra (m3) and Brown (b10) of a negligible nucleation rate at temperatures above 75°C for the alumina trihydrate system.

The model proposed here provides a reasonable good fit to the raw data up to two hours batch time but deviates after that. The change in the crystallization process after two hours, however, was relatively small.

(B) Recommendations

From the fit of the model with the raw data it is seen that it needs further refinement, in particular with regard to the agglomeration effectiveness kernel. The model also needs to be expanded with regard to the effects of temperature, of the induction period experienced at lower temperatures, of the intensity of agitation, and of the modifications due to impurities. The experimental program required for this modelling work has already been described in Section 9.2.

NOTATION

A	surface area, cm^2
BF	particle birth rate density function, $\text{number h}^{-1} \mu\text{m}^{-1} (\text{l sol.})^{-1}$
BN	particle birth rate, $\text{number h}^{-1} (\text{l sol.})^{-1}$
b1, b2	model parameters, model dependent
CA	alumina solution concentration, $\text{g Al}_2\text{O}_3 (\text{l sol.})^{-1}$
CH	water solution concentration, $\text{g H}_2\text{O} (\text{l sol.})^{-1}$
CN	caustic solution concentration, $\text{g Na}_2\text{O} (\text{l sol.})^{-1}$
CNC	caustic solution concentration, $\text{g Na}_2\text{CO}_3 (\text{l sol.})^{-1}$
CP	impurities solution concentration, $\text{g impurity} (\text{l sol.})^{-1}$
CS	solids concentration, $\text{g} (\text{l susp.})^{-1}$
C1, C2, ...	constants, application dependent
D	spherical volume equivalent diameter, μm
DF	particle death rate density function, $\text{number h}^{-1} \mu\text{m}^{-1} (\text{l sol.})^{-1}$
Dlt	Coulter Counter sample dilution factor, dimensionless
F	particle number density function, $\text{number} \mu\text{m}^{-1}$, or $\text{number} \mu\text{m}^{-3}$
FA	particle area density function, $\text{cm}^2 \mu\text{m}^{-1}$
FW	particle weight density function, $\text{g} \mu\text{m}^{-1}$
G	particle growth rate, $\mu\text{m h}^{-1}$, or $\mu\text{m}^3 \text{h}^{-1}$
H	cumulative particle number distribution, number
k	rate constants, rate equation dependent
N	number of particles, number or $\text{number} (\text{l susp.})^{-1}$

PS	shape factor, dimensionless
Q	region in particle phase space, definition dependent
S	solute supersaturation, $\text{g Al}_2\text{O}_3 (\text{l sol.})^{-1}$
T	absolute temperature, $^{\circ}\text{K}$
U	volumetric flow rate, l h^{-1}
V	volume, l or m^3
v	particle phase-space velocity, (particle property) h^{-1}
W	weight, g

Greek Letters

θ	temperature, $^{\circ}\text{C}$
η	pseudo moment, definition dependent
η_A	pseudo moment variable, equation (7.26)
ϵ	internal particle property, definition dependent
ϵ_A	pseudo moment variable, equation (7.36)
ρ	density, g cm^{-3}
σ	relative solute supersaturation, dimensionless
τ	batch crystallization time, h
τ_e	batch sample time, h
ϕ, ϕ	function, definition dependent
ϕ_g	variable which relates the linear to the volumetric growth rate, m^2
ϕ_w	pseudo moment variable, equation (7.11)
X	pseudo moment weighing functions, dimensionless
ψ	number diffusive flux relative to the particle phase-space velocity v; definition dependent

ψ_{AV}	particle area volume shape factor, dimensionless
ψ_{DV}	particle diameter volume shape factor, dimensionless
ψ_{VV}	particle measured volume to 'true' volume shape factor, dimensionless

Subscripts

a	agglomeration process
b	attrition process
C	Coulter Counter cut-off size
CC	Coulter Counter
Ch	Channelyzer
D	with respect to spherical equivalent diameter
e	equilibrium
ext	external particle phase space
g	growth process
i,j,k,l	summation integers
int	internal particle phase space
l	unit of liquid phase
L	total liquid phase
n	nucleation process
o	boundary value, minimum value
p	particle, crystal
Q	particle phase space
s	unit of solids phase
S	total solids phase
spl	sample

t	unit of dispersed phase; suspension
T	total suspension phase
u	boundary value, maximum value
V	with respect to particle volume

Overscores

.	rate
ˆ	estimated value
˜	expected value
—	linear average value

Mathematical

≈	is approximately equal to
∝	is proportional to
Δ	is defined to be equal to
d	differential operator
∂	partial derivative operator
Δ	difference operator, increment
∇	vector differential operator, grad
.	dot product
/ /	absolute value
⌈ ⌋	real value to integer operator, equation (6.41)

REFERENCES

- a1 Anderssen, R.S., Bloomfield, P., Numer. Math., 22, p.157 (1974).
- a2 Aris, R., Amundson, N.R., "Mathematical Methods in Chemical Engineering", Vol.2, Prentice-Hall, Toronto (1973).
- a3 Aluminum Laboratories Ltd., Arvida, Que., "Determination of Caustic, Alumina, Ratio, and Total Titratable Soda in Bayer Plant Pregnant and Spent Liquor", Tentative Method 495-67, private communication (1967).
- b1 Botsaris, G.D., et al., Ind. and Eng. Chem., Vol.61, No.10, Oct., p.86 (1969).
- b2 Botsaris, G.D., Denk, Jr., E.G., Ind. Eng. Chem. Fundam., Vol.9, No.2, p.276 (1970).
- b3 Bennema, P., et al., 5th Symp. Ind. Crystallization, Prague, Czechoslovakia (1972).
- b4 Bauer, L.G., et al., AIChE J., Vol.20, No.4, p.653 (1974).
- b5 Botsaris, G.D., 5th Symp. Ind. Crystallization, Prague, Czechoslovakia (1972).
- b6 Brown, N., J. of Crystal Growth, 16, p.163-169 (1972).
- b7 Brown, N., ibid., 12, p.39-45 (1972).
- b8 Brown, N., Powder Technol., 4, p.232 (1970/71).
- b9 Bleck, R., J. of Geophysical Research, Vol.75, No.27, September 20, p.5165-5171 (1970).
- b10 Brown, N., J. of Crystal Growth, 29, p.309-315 (1975).
- c1 Carnahan, B., et al., "Applied Numerical Methods", John Wiley & Sons, Inc., N.Y. (1969).
- c2 Chai, A.S., Simulation, August, p.89-91 (1970).
- c3 Chan, Y.N.I., et al., Ind. Eng. Chem. Fundam., Vol.17, No.3, p.133-148 (1978).
- d1 Drake, R.L., A General Mathematical Survey of the Coagulation Equation, in International Reviews in Aerosol Physics and Chemistry, (by Hidy, G.M., Brock, J.R., eds.), Vol.3, p.203, Pergamon Press, N.Y. (1972).

- d2 Drake, R.L., AEC Symp. Ser. 22, "Precipitation Scavenging", p.385 (1970).
- d3 Davies, R., Ind. and Eng. Chem., Vol.62, No.12, p.87 (1970).
- d4 Davies, R., et al., Powder Technol., 12, p.157 (1975).
- e1 Evans, T.W., et al., AIChE J., Vol.20, No.5, p.959 (1974).
- f1 Faust, A.S., et al., "Principles of Unit Operations", John Wiley & Sons, Inc., N.Y. (1967).
- g1 Gerard, G., Stroup, P.T., eds., "Extractive Metallurgy of Alumina", Vol.1, Interscience Publ., N.Y. (1963).
- g2 Garside, J., et al., J. of Crystal Growth, 29, p.353 (1975).
- g3 Groeneweg, P.G., "The Crystallization of Alumina Trihydrate in a Batch Crystallizer", report to the Department of Chemical Engineering, McMaster Univ., Hamilton, Canada (1972).
- g4 Gnyra, B., "The Growth and Breakdown of Hydrates Produced under Varied Operating Conditions", private communication, February (1968).
- g5 Garside, J., et al., AIChE J., Vol.25, No.1, p.57-64 (1979).
- g6 Garside, J., Mullin, J.W., Chem. and Ind., November 26, p.2007 (1966).
- h1 Halfon, A., Kaliaguine, S., Can. J. of Chem. Eng., 54, June, p.160 (1976).
- h2 Ibid., p.168 (1976).
- h3 Hartman, P., ed., "Crystal Growth: an Introduction", North-Holland Publ. Co., Amsterdam (1973).
- h4 Hulbert, H.M., Katz, S., Chem. Eng. Sci., Vol.19, p.555 (1964).
- h5 Hidy, G.M., Brock, J.R., eds., "International Reviews in Aerosol Physics and Chemistry", Vol.1, Pergamon Press, N.Y. (1970).
- h6 Himmelblau, D.M., "Process Analysis by Statistical Methods", John Wiley & Sons, Inc., N.Y. (1970).
- j1 Janse, A.H., de Jong, E.J., 5th Symp. Ind. Crystallization, Prague, Czechoslovakia (1972).
- j2 Johnson, W.T., et al., AIChE Symp. Ser., No.121, Vol.68, p.31 (1972).

- k1 Kinsman, W.P.C., "Study of Alumina Hydrate Precipitation", An External Literature Survey, private communication, December (1966).
- k2 Kinsman, W.P.C., Chem. in Can., p.22, September (1971).
- k3 Karuhn, R., et al., Powder Technol., 11, p.157 (1975).
- l1 Klapunov, A.N., Kholmogortseva, E.P., J. Appl. Chem. USSR, p.1379 and p.1601 (1957).
- m1 Mullin, J.W., "Crystallization", 2nd ed., Butterworths, London (1972).
- m2 Misra, C., White, E.T., Chemeca 70, 52 (1970).
- m3 Misra, C., White, E.T., Chem. Eng. Prog. Symp. Series 110, 67, p.53 (1971).
- m4 Misra, C., Chem. and Ind., May 9, p.619 (1970).
- m5 Misra, C., White, E.T., J. of Crystal Growth, 8, p.172 (1971).
- m6 Megaw, H.D., "Crystal Structures: A Working Approach", W.B. Saunders Publ. Co., Philadelphia (1973).
- m7 Mullin, J.W., 5th Symp. Ind. Crystallization, Prague, Chechoslovakia (1972).
- m8 Misra, C., private communication, March (1970).
- m9 Mitchell, A.R., "Computational Methods in Partial Differential Equations", J. Wiley, N.Y. (1969).
- m10 Middleton, P., Brock, J., J. of Colloid and Interface Sci., Vol.54, No.2, February, p.249-264 (1976).
- n1 Nyvlt, J., "Industrial Crystallization from Solutions", Butterworths, London (1971).
- n2 Nielsen, A.E., 5th Symp. Ind. Crystallization, Prague, Czechoslovakia (1972).
- n3 Ness, J.N., White, E.T., AIChE Symp. Ser., No.153, Vol.72, p.64 (1976).
- o1 Ohara, M., Reid, R.C., "Modelling Crystal Growth Rates from Solution", Prentice-Hall, Toronto (1973).
- o2 Ottens, E.P.K., de Jong, E.J., 5th Symp. Ind. Crystallization, Prague, Czechoslovakia (1972).

- p1 Pearson, T.G., Monograph No.3, The Royal Institute of Chemistry, London (1957).
- p2 Pulvermacher, B., Ruchenstein, E., AIChE J., Vol.21, No.1, January, p.128-135 (1975).
- p3 Patino-Leal, H., "Advances in the Theory of Error in Variables Model with Applications in Chemical Engineering", Ph.D. Thesis, Dept. of Chem. Eng., Univ. of Waterloo (1979).
- r1 Randolph, A.D., Larson, M.A., "Theory of Particulate Processes", Academic Press, New York (1971).
- r2 Reid, R.C., et al., Ind. and Eng. Chem., Vol.62, Nos.11 and 12, Nov. and Dec., p.52 and 148 (1970).
- r3 Randolph, A.D., Chem. Eng., May 4, p.80 (1970).
- r4 Randolph, A.D., Cise, M.D., AIChE J., Vol.18, No.4, p.798 (1972).
- r5 Ross, S.L., "Measurements and Models of the Dispersed Phase Mixing Process", Ph.D. thesis, Univ. of Michigan (1971).
- r6 Remillard, M., et al., Can. J. of Chem. Eng., Vol.56, p.230 (1978).
- r7 Rivera, T., Randolph, A.D., Ind. Eng. Chem. Process Des. Dev., Vol.17, No.2, p.182-188 (1978).
- r8 Randolph, A.D., et al., AIChE J., Vol.23, No.4, p.500-520 (1977).
- r9 Ramabhadran, T.E., Seinfeld, J.H., Chem. Eng. Sci., Vol.30, p.1019-1025 (1975).
- s1 Strickland-Constable, R.F., "Kinetics and Mechanisms of Crystallization", Academic Press, N.Y. (1968).
- s2 Strickland-Constable, R.F., AIChE Symp. Ser., No.121, Vol.68, p.1 (1972).
- s3 Sastry, K.V.S., Fuerstenau, D.W., Ind. and Eng. Chem. Fundam., Vol.9, No.1, p.145 (1970).
- s4 Smith, C.L., et al., "Formulation and Optimization of Mathematical Models", Int. Textbk. Co., Scranton, Pennsylvania (1970).
- s5 Scott, W.T., J. of the Atm. Sci., Vol.25, January, p.54-65 (1968).
- s6 Scheid, F., "Numerical Analysis", Schaum's Outline Series, McGraw-Hill, N.Y. (1968).

- s7 Subramanian, G., Master's Thesis, Indian Institute of Technology, Kanpur (1969).
- t1 Tai, C.Y., et al., AIChE J., Vol.21, No.2, p.351 (1975).
- t2 Tsuchiya, A.C., et al., Advan. Chem. Eng., 6, p.192 (1966).
- t3 Turkevich, J., Am. Scient., 47, p.97-119 (1959).
- t4 Thompson, R.W., et al., Chem. Eng. Sci., Vol.53, p.386-390 (1978).
- v1 Van Hook, A., "Crystallization Theory and Practice", Reinhold, N.Y. (1961).
- w1 White, E.T., Powder Technol., 4, p.104 (1970/71).
- w2 White, E.T., Wright, P.G., Chem. Eng. Progr. Symp. Ser., No.110, Vol.67, p.81 (1971).
- w3 Wahi, E.F., Baker, C.G.J., Can. J. of Chem. Eng., Vol.49, p.742 (1971).
- w4 Waddel, H., J. Franklin Inst., 217, p.459 (1934).
- w5 Watts, H.L., Utley, D.W., Analy. Chem., Vol.25, No.6, p.864 (1953).
- w6 Watts, H.L., Utley, D.W., ibid., Vol.28, No.11, p.1731 (1956).
- S

10

APPENDIX A

Raw Data, Experiment #13

The raw data used for the model development work in this study is presented in the following tables, and the specific experimental conditions are listed in point form below.

(A) Experimental Conditions

(1) Seed Material

The seed was prepared in experiment number 8 (during the apparatus evaluation stage). After preparation, it was thoroughly stirred for about two hours, filtered, washed repeatedly, and dried at 110°C. The amount used for experiment number 13 was 24.8515 g.

(2) Initial Supersaturated Solution

The supersaturated solution of sodium aluminate was made up from:

- 394 g NaOH (analytical grade pellets)
- 505 g Al(OH)₃ (analytical grade crystals)
- 2109 ml H₂O (distilled)

and, after preparation, was analyzed to give:

- density at 25°C - 1.2275 g/cm³
- volume at 25°C - 2.3730 l
- caustic concentration at 25°C - 212.8 g Na₂CO₃/l
- alumina concentration at 25°C - 136.4 g Al₂O₃/l

TABLE A-1 Raw Data, Experiment #13

Column # Sample #	Batch Crystallization Time (hrs) (3)	Crystal- lizer Suspension Temperature (°C) (4)	Solution Analysis					Suspension Sample				Sample Weight				
			HCl (ml) (5)	Caustic Concentration (g Na ₂ CO ₃ /4 sol.) -- (5) x 26.5 (6)	NaOH (ml) (7)	Alumina Concentration (g Al ₂ O ₃ /4 sol.) -- (7) x 8.5 (8)	Weight of Sample Bottle 1 (g) (9)	Weight of Solution + Bottle 1 (g) (10)	Weight of Solution (g) -- (10) - (9) (11)	Weight of Filter Material (g) (12)	Weight of Solids + Filter Material (g) (13)	Weight of Solids (g) -- (13) - (12) (14)				
													(2)	(3)	(4)	(5)
1	1 ⁰⁰ p.m.	84.8	8.03	212.8	16.05	136.4	-	-	-	-	-	-	-	-	-	-
2	1 ¹⁵ p.m.	85.3	7.99	211.7	15.32	130.2	12.62400	22.77200	10.14800	1.15052	1.27585	0.12533				
3	1 ³⁰ p.m.	85.0	8.02	212.5	14.93	126.9	12.61561	22.64511	10.02930	1.16616	1.36300	0.19684				
4	1 ⁴⁵ p.m.	84.8	8.03	212.8	14.49	123.2	12.64741	23.01987	10.37246	1.15354	1.40703	0.25349				
5	2 ⁰⁰ p.m.	85.2	8.08	214.1	14.19	120.6	12.49148	22.53349	10.04201	1.16706	1.46753	0.30047				
6	2 ²⁰ p.m.	85.3	8.09	214.4	13.82	117.6	12.66054	22.69906	10.03852	1.17071	1.53029	0.35958				
7	2 ⁴⁰ p.m.	85.2	8.11	214.9	13.62	115.8	12.74704	22.59116	9.84412	1.17626	1.53552	0.35926				
8	3 ⁰⁰ p.m.	85.3	8.11	214.9	13.30	113.1	12.58300	22.30508	9.72208	1.13859	1.51720	0.37861				
9	5 ⁰⁰ p.m.	84.9	8.18	216.8	12.62	107.3	12.53332	21.95947	9.42615	1.14462	1.57003	0.42541				
10	7 ⁰⁰ p.m.	85.3	8.20	217.3	12.21	103.8	12.63500	22.18453	9.54953	1.17847	1.68660	0.50813				
11	11 ⁰⁰ p.m.	84.8	8.23	218.1	11.85	100.7	12.27400	21.77634	9.50234	1.16272	1.71471	0.55199				
12	11 ⁰⁰ a.m.	85.0	8.25	218.6	11.41	97.0	12.58745	21.97990	9.39245	0.39934	1.00644	0.60710				
13	10 ⁰⁰ p.m.	85.3	8.24	218.4	11.26	95.7	12.60980	21.01934	8.40954	0.40309	0.97472	0.57163				
14	9 ⁰⁰ a.m.	85.0	8.28	219.4	11.14	94.7	12.56583	22.06814	9.50233	0.40214	1.03646	0.63432				

(B) General Information on Experimental Procedure

- (I) The volume of extracted solution for solution analysis was 5 ml.
- (II) The solids for crystal size measurement by Coulter Counter model Z_B were obtained by taking about 0.01 g from the washed and dried suspension sample filter cake. This 0.01 g was then suspended in 200 cm³ of 'Isoton' (trade name of Coulter Electronics Inc.) electrolyte.
- (III) After each sample, the samplers, sample bottles, sample filter apparatus were rinsed with distilled water and dried in an oven at 75-80°C; they were then ready for the next sample.
- (IV) The crystallizer was tumbled back and forth through 360° in 38 sec. (9½ on the indicator of the variable speed transmission).
- (V) The room temperature during this experiment was about 23°C.

2502 2660 2826 2707 2628 2599 2407 2347 2185 2169
 1842 1815 1713 1581 1338 1154 1027 0902 0722 0646
 0477 0389 0263 0221 0173 0093 0075 0054 0043 0030
 0010 0011 0005 0006 0005 0001 0004 0002 0002 0002
 0002 0002 0000 0001 0001 0001 0001 0000 0000 0000
 0000 0002 0000 0000 0000 0001 0001 0000 0000 0000
 0001 0000 0000 0000 0000 0000 0000 0000 0000 0000
 0000 0000 0001 0000 0001 0000 0000 0000 0000 0000
 0000 0000 0000 0000 0000 0000 0000 0000 0000 0000
 0000 0000 0000 0000 0000 0000 0000 0000 0000 0000

2507 2788 2675 2731 2635 2511 2493 2379 2189 2119
 2000 1871 1637 1582 1325 1230 1013 0896 0808 0613
 0512 0429 0275 0266 0153 0118 0090 0051 0040 0021
 0014 0004 0006 0003 0003 0006 0000 0003 0003 0002
 0000 0000 0002 0001 0000 0001 0001 0000 0000 0001
 0001 0000 0001 0001 0001 0000 0000 0000 0000 0000
 0000 0001 0000 0000 0000 0000 0001 0000 0000 0000
 0000 0000 0000 0001 0000 0000 0000 0000 0000 0000
 0000 0000 0000 0000 0000 0000 0000 0000 0000 0000
 0000 0000 0000 0000 0000 0000 0000 0000 0000 0000

2535 2804 2730 2689 2558 2594 2404 2344 2274 2164
 1945 1807 1656 1566 1330 1217 1005 0895 0667 0658
 0483 0351 0290 0215 0138 0121 0072 0058 0027 0014
 0018 0006 0008 0006 0006 0001 0001 0001 0000 0005
 0001 0001 0002 0001 0000 0001 0002 0000 0000 0001
 0001 0000 0000 0002 0000 0000 0000 0001 0000 0000
 0000 0001 0000 0000 0000 0000 0000 0000 0000 0000
 0000 0001 0000 0000 0000 0000 0000 0000 0000 0000
 0000 0000 0000 0000 0000 0000 0000 0000 0000 0000
 0000 0000 0000 0000 0000 0000 0000 0000 0000 0000

2508 2702 2774 2796 2605 2613 2442 2307 2227 2115
 1844 1863 1649 1542 1352 1226 1010 0916 0734 0612
 0510 0396 0298 0220 0169 0121 0087 0057 0035 0017
 0016 0010 0003 0003 0002 0004 0003 0002 0000 0002
 0002 0001 0003 0002 0002 0002 0000 0000 0001 0000
 0001 0001 0000 0001 0000 0001 0000 0000 0000 0000
 0000 0001 0000 0000 0000 0001 0000 0000 0001 0000
 0000 0000 0000 0000 0000 0000 0000 0000 0000 0000
 0000 0000 0000 0000 0000 0000 0000 0000 0000 0000
 0000 0000 0000 0000 0000 0000 0000 0000 0000 0000

0169 0220 0181 0187 0208 0206 0224 0210 0212 0265
 0243 0240 0278 0259 0330 0320 0301 0336 0346 0356
 0367 0360 0325 0386 0358 0392 0443 0432 0378 0465
 0463 0456 0446 0492 0469 0445 0488 0466 0449 0484
 0459 0469 0471 0450 0483 0439 0422 0444 0410 0388
 0381 0375 0354 0314 0260 0262 0210 0202 0154 0139
 0106 0094 0057 0051 0024 0017 0007 0006 0009 0006
 0002 0002 0001 0000 0000 0000 0000 0001 0001 0001
 0000 0001 0000 0000 0000 0000 0000 0001 0000 0000
 0000 0000 0000 0000 0000 0000 0000 0000 0000 0000

0155 0178 0215 0186 0186 0199 0189 0226 0238 0232
 0248 0275 0294 0270 0301 0298 0330 0331 0294 0375
 0340 0408 0378 0350 0413 0379 0405 0428 0440 0474
 0415 0411 0457 0457 0506 0428 0446 0488 0483 0486
 0523 0437 0489 0446 0452 0442 0417 0448 0409 0411
 0376 0339 0366 0320 0259 0275 0205 0172 0132 0134
 0099 0090 0063 0042 0027 0020 0015 0004 0004 0003
 0003 0002 0000 0001 0001 0000 0001 0000 0001 0000
 0000 0000 0000 0000 0000 0000 0000 0000 0000 0000
 0000 0000 0000 0000 0000 0000 0000 0000 0000 0000

0194 0182 0185 0207 0169 0233 0201 0219 0236 0249
 0273 0274 0269 0291 0275 0312 0311 0355 0330 0345
 0359 0388 0352 0350 0395 0379 0378 0381 0364 0443
 0462 0434 0417 0454 0474 0465 0437 0457 0458 0496
 0455 0482 0437 0498 0457 0439 0463 0431 0427 0381
 0395 0357 0373 0348 0272 0245 0206 0194 0174 0135
 0090 0080 0064 0055 0025 0023 0009 0007 0006 0006
 0001 0000 0003 0001 0000 0000 0000 0000 0000 0000
 0000 0000 0002 0000 0000 0000 0000 0000 0000 0000
 0000 0000 0000 0000 0000 0000 0000 0000 0000 0000

0177 0159 0181 0196 0185 0218 0201 0228 0247 0243
 0263 0264 0266 0289 0284 0300 0336 0308 0305 0362
 0341 0396 0384 0429 0407 0414 0378 0418 0392 0430
 0408 0448 0463 0503 0465 0462 0434 0454 0472 0492
 0495 0463 0430 0503 0440 0453 0444 0482 0382 0380
 0350 0385 0350 0334 0274 0271 0215 0201 0159 0144
 0100 0093 0070 0034 0031 0024 0015 0009 0007 0002
 0002 0003 0001 0000 0000 0000 0000 0000 0000 0000
 0000 0000 0000 0001 0000 0000 0000 0000 0000 0000
 0000 0000 0000 0000 0000 0000 0000 0000 0000 0000

0065 0063 0044 0045 0055 0031 0038 0063 0047 0038
 0052 0047 0034 0058 0057 0065 0053 0061 0065 0071
 0059 0076 0078 0083 0076 0052 0072 0086 0106 0077
 0089 0092 0082 0090 0079 0121 0094 0109 0081 0096
 0105 0122 0112 0112 0092 0109 0113 0140 0149 0161
 0160 0139 0158 0175 0177 0187 0160 0164 0178 0162
 0164 0177 0137 0119 0076 0113 0077 0080 0042 0043
 0037 0009 0019 0006 0007 0002 0000 0000 0003 0001
 0001 0000 0001 0000 0000 0001 0000 0000 0000 0000
 0001 0000 0000 0000 0000 0000 0000 0000 0000 0000

0063 0059 0044 0037 0035 0051 0056 0050 0053 0055
 0049 0047 0060 0049 0065 0064 0061 0062 0056 0069
 0068 0082 0089 0077 0075 0064 0082 0081 0090 0078
 0076 0080 0083 0080 0094 0104 0088 0109 0077 0107
 0096 0109 0110 0111 0119 0105 0120 0142 0154 0153
 0152 0167 0170 0172 0158 0159 0160 0179 0173 0156
 0180 0173 0135 0131 0137 0087 0089 0063 0049 0035
 0018 0020 0009 0010 0002 0002 0000 0002 0000 0001
 0000 0002 0001 0000 0000 0000 0000 0000 0000 0000
 0000 0000 0000 0000 0000 0000 0000 0000 0000 0000

0075 0051 0052 0049 0051 0054 0053 0042 0043 0050
 0061 0067 0053 0058 0058 0077 0056 0068 0049 0078
 0066 0093 0086 0069 0071 0085 0058 0087 0093 0095
 0085 0087 0102 0098 0086 0081 0097 0097 0104 0088
 0096 0114 0117 0111 0112 0118 0132 0153 0139 0148
 0146 0164 0153 0161 0151 0163 0148 0183 0171 0180
 0197 0147 0128 0123 0104 0102 0086 0053 0050 0029
 0018 0023 0016 0005 0007 0004 0000 0003 0000 0001
 0000 0001 0000 0000 0000 0000 0000 0000 0000 0000
 0000 0000 0000 0000 0000 0000 0000 0000 0000 0000

0056 0055 0046 0051 0054 0043 0039 0045 0047 0038
 0044 0053 0051 0044 0065 0062 0062 0062 0065 0061
 0086 0064 0064 0083 0069 0074 0066 0089 0082 0091
 0089 0068 0091 0090 0093 0084 0104 0093 0095 0109
 0124 0111 0115 0120 0102 0121 0118 0141 0134 0132
 0158 0168 0154 0176 0176 0176 0186 0169 0156 0156
 0167 0159 0149 0109 0108 0095 0088 0055 0044 0031
 0026 0030 0010 0006 0003 0005 0003 0001 0002 0001
 0000 0000 0000 0000 0000 0000 0000 0000 0000 0000
 0000 0000 0000 0000 0000 0000 0000 0000 0000 0000

0028 0033 0029 0048 0027 0026 0024 0022 0039 0029
 0032 0028 0031 0036 0046 0040 0045 0035 0039 0046
 0053 0050 0041 0049 0055 0051 0042 0061 0058 0047
 0042 0051 0057 0061 0071 0073 0051 0071 0070 0071
 0060 0056 0070 0072 0072 0084 0089 0086 0098 0121
 0103 0108 0128 0129 0119 0143 0141 0153 0145 0154
 0154 0142 0126 0120 0140 0097 0092 0085 0061 0031
 0038 0020 0009 0011 0003 0004 0002 0000 0003 0000
 0000 0000 0000 0000 0000 0000 0000 0000 0001 0000
 0000 0000 0000 0000 0000 0000 0000 0000 0000 0000

0020 0025 0036 0035 0034 0029 0031 0023 0037 0034
 0037 0030 0040 0037 0033 0035 0036 0035 0056 0038
 0035 0049 0052 0065 0056 0035 0059 0052 0060 0070
 0060 0065 0063 0056 0052 0066 0055 0059 0068 0071
 0062 0090 0072 0085 0080 0080 0077 0098 0107 0125
 0097 0121 0127 0125 0143 0157 0120 0144 0155 0147
 0142 0143 0131 0120 0105 0098 0098 0080 0064 0041
 0026 0019 0010 0008 0010 0002 0003 0001 0000 0000
 0000 0000 0000 0000 0000 0000 0000 0001 0000 0000
 0000 0000 0000 0000 0000 0000 0000 0000 0000 0000

0031 0030 0036 0025 0019 0028 0032 0030 0033 0031
 0029 0025 0046 0040 0035 0030 0030 0038 0048 0047
 0039 0047 0037 0054 0049 0049 0057 0048 0061 0063
 0057 0062 0052 0054 0053 0066 0066 0067 0062 0059
 0076 0063 0071 0077 0081 0091 0093 0094 0099 0102
 0109 0125 0113 0141 0120 0130 0144 0145 0139 0157
 0135 0118 0133 0163 0124 0109 0071 0055 0047 0049
 0025 0022 0014 0007 0005 0001 0002 0001 0002 0001
 0000 0000 0000 0000 0000 0000 0000 0000 0000 0000
 0000 0000 0000 0000 0000 0000 0000 0000 0000 0000

0026 0031 0033 0032 0027 0024 0033 0019 0028 0035
 0031 0031 0035 0049 0037 0045 0047 0034 0038 0036
 0050 0049 0043 0054 0074 0067 0048 0053 0057 0058
 0057 0058 0074 0065 0058 0054 0073 0059 0052 0076
 0072 0067 0066 0085 0077 0085 0094 0110 0086 0113
 0108 0094 0124 0118 0123 0132 0143 0144 0135 0159
 0147 0145 0117 0134 0119 0111 0093 0075 0058 0036
 0026 0027 0014 0013 0007 0004 0003 0001 0000 0000
 0000 0000 0000 0000 0000 0001 0000 0000 0000 0000
 0000 0000 0000 0000 0000 0000 0000 0000 0000 0000

0025 0026 0036 0031 0034 0032 0030 0033 0037 0035
0041 0032 0029 0048 0039 0044 0032 0058 0037 0036
0047 0056 0053 0066 0053 0051 0059 0058 0046 0057
0068 0051 0054 0051 0052 0059 0049 0068 0057 0052
0083 0065 0080 0088 0085 0088 0093 0091 0117 0101
0107 0124 0120 0108 0132 0112 0148 0146 0145 0156
0139 0162 0138 0136 0112 0098 0082 0088 0054 0044
0037 0027 0012 0008 0005 0005 0001 0002 0000 0000
0001 0000 0000 0000 0000 0000 0000 0000 0000 0000
0000 0000 0000 0000 0000 0000 0000 0000 0000 0000

0032 0038 0032 0034 0031 0028 0030 0041 0032 0033
0031 0032 0032 0034 0038 0034 0048 0046 0055 0034
0041 0058 0045 0035 0061 0055 0055 0061 0056 0049
0063 0046 0063 0064 0065 0071 0050 0063 0070 0057
0079 0066 0074 0083 0080 0090 0087 0111 0087 0094
0107 0129 0106 0141 0138 0140 0144 0153 0148 0135
0140 0122 0143 0117 0115 0122 0071 0056 0060 0057
0029 0022 0014 0016 0005 0008 0003 0002 0000 0001
0000 0000 0000 0000 0000 0000 0000 0001 0000 0000
0000 0000 0000 0000 0000 0000 0000 0000 0000 0000

0081 0072 0073 0061 0058 0050 0051 0057 0056 0057
 0050 0057 0058 0062 0064 0064 0066 0062 0074 0086
 0092 0076 0064 0078 0082 0100 0090 0096 0088 0083
 0076 0102 0078 0085 0087 0099 0091 0122 0079 0113
 0111 0111 0101 0133 0133 0144 0122 0137 0142 0149
 0171 0191 0177 0182 0201 0193 0218 0241 0234 0238
 0247 0228 0242 0215 0207 0176 0176 0165 0127 0095
 0069 0050 0036 0029 0021 0006 0002 0004 0005 0000
 0001 0000 0001 0000 0000 0000 0000 0000 0000 0001
 0000 0000 0000 0000 0000 0000 0000 0000 0000 0000

0106 0085 0066 0084 0049 0053 0066 0056 0064 0061
 0048 0060 0071 0062 0063 0065 0077 0086 0055 0081
 0071 0079 0092 0069 0097 0083 0076 0088 0068 0092
 0100 0078 0097 0078 0090 0081 0105 0105 0097 0124
 0107 0108 0118 0126 0121 0106 0131 0120 0140 0130
 0156 0155 0167 0184 0206 0192 0196 0217 0220 0237
 0239 0223 0225 0244 0194 0207 0172 0160 0115 0104
 0073 0064 0033 0035 0012 0014 0004 0003 0002 0003
 0002 0001 0002 0000 0000 0001 0000 0000 0000 0000
 0000 0000 0000 0000 0000 0000 0000 0000 0000 0000

0097 0078 0068 0079 0066 0077 0060 0060 0044 0057
 0056 0070 0058 0064 0065 0075 0065 0062 0079 0060
 0095 0080 0080 0081 0089 0102 0078 0096 0116 0086
 0091 0070 0071 0081 0088 0117 0096 0098 0107 0118
 0123 0116 0111 0106 0120 0102 0135 0108 0138 0128
 0150 0157 0166 0182 0183 0214 0217 0218 0186 0230
 0226 0236 0210 0241 0207 0180 0188 0162 0129 0109
 0059 0057 0031 0018 0017 0013 0005 0002 0002 0002
 0000 0000 0000 0000 0000 0001 0000 0000 0000 0000
 0000 0000 0000 0000 0000 0000 0000 0000 0000 0000

0097 0097 0073 0059 0074 0062 0065 0067 0066 0066
 0062 0070 0061 0064 0061 0065 0067 0082 0072 0082
 0083 0084 0082 0086 0080 0085 0105 0110 0081 0104
 0082 0102 0070 0087 0102 0101 0108 0099 0105 0110
 0106 0108 0111 0114 0113 0116 0114 0132 0152 0152
 0166 0186 0179 0194 0180 0213 0207 0222 0221 0210
 0236 0257 0231 0224 0213 0203 0175 0133 0128 0075
 0061 0066 0043 0027 0013 0013 0007 0001 0001 0003
 0000 0000 0000 0000 0000 0001 0000 0001 0000 0000
 0000 0000 0000 0000 0000 0000 0000 0000 0000 0000

0066 0058 0041 0036 0037 0028 0035 0033 0031 0025
 0032 0026 0028 0023 0030 0032 0024 0033 0040 0040
 0027 0034 0039 0031 0033 0040 0035 0039 0033 0046
 0032 0043 0033 0042 0039 0039 0044 0037 0044 0040
 0036 0049 0038 0052 0048 0055 0036 0060 0062 0060
 0049 0082 0085 0097 0090 0101 0116 0137 0139 0155
 0148 0159 0174 0205 0185 0202 0224 0193 0168 0163
 0132 0122 0106 0074 0066 0045 0032 0024 0024 0005
 0001 0003 0000 0001 0002 0000 0000 0000 0000 0000
 0000 0000 0000 0000 0000 0000 0000 0000 0000 0000

0070 0057 0040 0039 0031 0036 0035 0029 0046 0031
 0037 0033 0028 0035 0033 0031 0033 0038 0033 0035
 0035 0038 0050 0045 0044 0044 0040 0040 0042 0039
 0041 0043 0030 0038 0043 0037 0028 0039 0044 0054
 0043 0044 0040 0050 0046 0054 0035 0051 0071 0077
 0076 0079 0072 0085 0099 0114 0105 0118 0134 0154
 0159 0153 0167 0171 0219 0200 0148 0201 0202 0168
 0142 0125 0123 0083 0057 0043 0029 0023 0014 0006
 0005 0001 0002 0000 0000 0001 0000 0000 0000 0001
 0000 0001 0000 0000 0000 0000 0000 0000 0000 0000

0052 0050 0047 0049 0043 0032 0034 0036 0035 0025
 0039 0033 0034 0030 0033 0029 0027 0036 0034 0037
 0037 0038 0037 0033 0044 0046 0038 0047 0052 0031
 0039 0052 0036 0053 0031 0045 0044 0042 0039 0056
 0047 0043 0047 0046 0046 0052 0044 0047 0046 0064
 0073 0071 0065 0084 0113 0101 0105 0137 0133 0151
 0128 0160 0153 0196 0211 0203 0216 0212 0168 0164
 0142 0126 0102 0067 0060 0041 0024 0035 0011 0012
 0005 0000 0000 0001 0001 0000 0000 0001 0000 0000
 0000 0000 0000 0000 0000 0000 0000 0000 0000 0000

0054 0054 0057 0054 0029 0030 0035 0035 0045 0031
 0030 0030 0044 0034 0037 0040 0030 0033 0036 0025
 0038 0046 0039 0047 0049 0035 0050 0049 0053 0045
 0044 0039 0045 0031 0034 0044 0034 0041 0049 0048
 0047 0054 0043 0059 0061 0049 0042 0059 0061 0067
 0073 0082 0071 0085 0093 0115 0117 0132 0138 0144
 0136 0173 0150 0189 0174 0187 0197 0198 0168 0163
 0114 0140 0095 0094 0051 0048 0033 0024 0019 0009
 0005 0001 0001 0001 0001 0000 0000 0001 0000 0000
 0000 0000 0000 0000 0000 0000 0000 0000 0000 0000

0065 0057 0046 0040 0045 0044 0051 0037 0029 0036
0046 0027 0035 0034 0028-0038 0029 0031 0048 0037
0043 0041 0044 0049 0044 0061 0038 0049 0040 0051
0043 0035 0043 0039 0033 0037 0039 0041 0041 0042
0050 0047 0059 0044 0056 0051 0068 0061 0066 0069
0074 0075 0085 0101 0090 0108 0115 0105 0132 0146
0145 0194 0150 0168 0171 0181 0200 0208 0192 0147
0143 0112 0096 0074 0070 0047 0019 0019 0011 0008
0004 0001 0001 0002 0001 0000 0000 0000 0000 0000
0000 0000 0000 0000 0000 0000 0000 0000 0000 0000

0068 0059 0066 0047 0053 0044 0048 0034 0033 0033
0039 0040 0043 0041 0041 0039 0041 0040 0039 0042
0038 0057 0053 0055 0056 0054 0054 0063 0052 0044
0041 0045 0030 0037 0033 0040 0040 0043 0036 0035
0043 0047 0051 0048 0045 0051 0057 0046 0056 0060
0073 0077 0069 0083 0088 0101 0094 0119 0130 0148
0140 0172 0163 0186 0190 0197 0188 0196 0153 0159
0109 0092 0088 0078 0061 0041 0030 0015 0014 0007
0007 0001 0001 0002 0000 0000 0000 0000 0000 0000
0000 0000 0000 0000 0000 0000 0000 0000 0000 0000

0074 0049 0046 0047 0030 0041 0031 0031 0038 0036
0029 0039 0033 0027 0038 0039 0033 0045 0030 0030
0032 0048 0041 0049 0035 0046 0053 0052 0035 0047
0039 0033 0023 0028 0030 0028 0020 0031 0026 0029
0035 0029 0031 0036 0026 0047 0036 0046 0034 0045
0047 0062 0062 0062 0066 0073 0078 0092 0114 0111
0129 0122 0133 0145 0175 0167 0151 0169 0149 0164
0143 0114 0113 0100 0058 0039 0038 0022 0012 0010
0005 0005 0004 0001 0002 0000 0001 0000 0000 0001
0000 0000 0000 0000 0000 0000 0000 0000 0000 0000

0066 0057 0043 0052 0046 0050 0037 0033 0047 0051
0031 0030 0037 0032 0036 0029 0037 0042 0032 0046
0035 0045 0042 0041 0046 0046 0047 0056 0039 0033
0050 0044 0019 0019 0031 0036 0029 0030 0021 0027
0030 0035 0033 0028 0034 0043 0028 0039 0036 0037
0046 0054 0058 0072 0062 0065 0072 0096 0090 0118
0103 0149 0110 0167 0148 0160 0160 0168 0141 0164
0113 0133 0100 0099 0068 0056 0033 0016 0017 0013
0006 0000 0001 0000 0001 0001 0000 0000 0000 0000
0000 0000 0000 0000 0000 0000 0000 0000 0000 0000

0064 0057 0039 0028 0031 0019 0023 0028 0023 0015
0011 0022 0022 0020 0012 0022 0012 0020 0021 0011
0020 0022 0020 0022 0024 0023 0019 0023 0019 0020
0020 0014 0016 0013 0014 0008 0019 0013 0020 0013
0013 0012 0019 0018 0020 0015 0023 0022 0015 0022
0014 0031 0025 0035 0026 0041 0043 0038 0046 0068
0074 0092 0082 0093 0110 0141 0118 0161 0154 0116
0149 0114 0114 0118 0086 0065 0056 0045 0031 0014
0012 0008 0004 0005 0000 0000 0000 0000 0000 0000
0000 0000 0000 0000 0000 0000 0000 0000 0000 0000

0061 0046 0038 0034 0021 0022 0021 0030 0020 0018
0015 0014 0012 0018 0016 0011 0023 0028 0026 0025
0020 0015 0016 0020 0021 0023 0020 0014 0021 0019
0026 0014 0017 0012 0015 0015 0009 0013 0017 0014
0016 0018 0023 0015 0013 0012 0027 0029 0035 0020
0022 0023 0028 0034 0033 0043 0033 0050 0045 0060
0068 0088 0098 0096 0100 0133 0114 0141 0121 0147
0119 0130 0128 0091 0078 0069 0052 0051 0025 0018
0013 0008 0003 0002 0000 0000 0000 0000 0000 0000
0000 0000 0000 0000 0000 0000 0000 0000 0000 0000

0049 0022 0017 0018 0024 0019 0014 0014 0017 0015
 0017 0018 0023 0023 0010 0014 0016 0019 0020 0019
 0014 0018 0017 0023 0018 0019 0024 0027 0025 0017
 0012 0025 0014 0017 0012 0013 0013 0011 0013 0019
 0013 0019 0011 0015 0013 0015 0014 0017 0013 0017
 0019 0022 0012 0018 0026 0027 0032 0029 0044 0044
 0051 0060 0063 0077 0081 0079 0116 0090 0095 0118
 0103 0104 0090 0093 0077 0062 0049 0048 0032 0023
 0011 0013 0006 0001 0004 0000 0001 0000 0000 0000
 0000 0000 0000 0000 0000 0000 0000 0000 0000 0000

0037 0030 0018 0024 0017 0021 0020 0018 0022 0015
 0012 0017 0017 0011 0013 0009 0018 0011 0018 0008
 0017 0013 0022 0019 0017 0021 0024 0026 0019 0015
 0022 0007 0016 0019 0009 0011 0014 0012 0010 0019
 0011 0011 0009 0017 0012 0014 0012 0021 0015 0012
 0017 0012 0014 0019 0016 0036 0029 0043 0032 0046
 0036 0040 0052 0094 0094 0105 0096 0116 0111 0113
 0109 0120 0106 0082 0087 0081 0054 0045 0024 0026
 0024 0015 0004 0002 0002 0000 0001 0001 0000 0000
 0001 0000 0000 0000 0000 0000 0000 0000 0000 0000

0036 0028 0024 0017 0028 0021 0014 0017 0010 0022
 0014 0013 0015 0018 0014 0012 0021 0015 0023 0020
 0020 0024 0018 0017 0016 0017 0020 0028 0022 0017
 0014 0023 0008 0014 0016 0010 0011 0014 0012 0009
 0007 0014 0011 0014 0015 0017 0018 0017 0015 0020
 0019 0019 0022 0022 0022 0023 0037 0036 0043 0041
 0042 0042 0048 0062 0082 0096 0090 0105 0110 0087
 0098 0100 0091 0095 0076 0083 0053 0045 0038 0026
 0017 0012 0004 0003 0001 0000 0000 0000 0000 0000
 0000 0000 0000 0000 0000 0000 0000 0000 0000 0000

0060 0040 0024 0031 0022 0020 0021 0021 0017 0023
 0012 0012 0016 0017 0012 0017 0022 0017 0013 0015
 0023 0024 0023 0017 0015 0022 0022 0028 0012 0021
 0023 0015 0022 0019 0013 0010 0013 0010 0009 0015
 0014 0009 0012 0012 0015 0016 0014 0018 0012 0019
 0016 0019 0019 0023 0017 0028 0034 0023 0034 0043
 0051 0058 0066 0056 0082 0086 0099 0122 0110 0098
 0109 0125 0107 0101 0079 0067 0050 0038 0038 0015
 0010 0011 0002 0000 0000 0002 0001 0000 0001 0000
 0001 0000 0000 0000 0000 0000 0000 0000 0000 0000

0069 0046 0036 0041 0023 0026 0030 0021 0024 0024
 0009 0018 0012 0020 0017 0028 0024 0026 0020 0021
 0019 0022 0027 0014 0017 0024 0030 0023 0024 0017
 0020 0014 0016 0023 0015 0012 0016 0007 0016 0010
 0014 0015 0008 0016 0025 0016 0013 0024 0020 0012
 0024 0023 0020 0032 0033 0045 0035 0042 0060 0074
 0074 0086 0099 0116 0121 0122 0146 0180 0191 0170
 0178 0185 0177 0152 0133 0138 0109 0083 0060 0043
 0033 0012 0005 0005 0003 0003 0002 0001 0000 0000
 0000 0000 0000 0000 0000 0000 0000 0000 0000 0000

0062 0049 0043 0036 0037 0037 0019 0032 0029 0022
 0027 0021 0026 0018 0029 0027 0019 0031 0029 0026
 0031 0029 0028 0034 0026 0034 0024 0032 0036 0024
 0028 0025 0017 0013 0012 0011 0015 0026 0014 0018
 0015 0014 0016 0016 0015 0013 0012 0022 0016 0018
 0024 0023 0020 0022 0023 0038 0040 0069 0051 0058
 0074 0094 0090 0110 0123 0135 0170 0189 0192 0162
 0172 0176 0155 0159 0113 0123 0096 0079 0064 0039
 0035 0014 0007 0009 0003 0002 0000 0000 0001 0002
 0000 0000 0000 0000 0000 0000 0000 0000 0000 0000

0070 0071 0037 0032 0027 0029 0033 0026 0024 0020
 0024 0028 0022 0029 0023 0019 0024 0031 0030 0023
 0026 0024 0034 0033 0028 0034 0033 0026 0032 0019
 0021 0021 0012 0017 0011 0011 0015 0009 0012 0016
 0017 0020 0018 0014 0021 0017 0015 0013 0014 0025
 0024 0025 0022 0031 0050 0038 0036 0040 0061 0059
 0082 0104 0094 0105 0135 0153 0159 0170 0176 0165
 0187 0182 0172 0156 0141 0112 0086 0090 0059 0036
 0030 0015 0009 0009 0002 0001 0000 0000 0000 0000
 0000 0000 0000 0000 0000 0000 0000 0000 0000 0000

0081 0040 0037 0030 0024 0027 0020 0026 0030 0033
 0025 0027 0021 0018 0024 0030 0027 0022 0028 0021
 0021 0023 0024 0024 0028 0038 0027 0026 0020 0020
 0023 0018 0019 0015 0014 0014 0013 0018 0022 0019
 0015 0012 0011 0019 0013 0015 0016 0014 0025 0015
 0025 0024 0029 0033 0036 0033 0046 0049 0064 0071
 0087 0083 0102 0106 0117 0129 0139 0194 0177 0174
 0165 0200 0170 0150 0126 0121 0093 0082 0059 0041
 0026 0015 0009 0003 0001 0001 0000 0000 0000 0000
 0000 0000 0000 0000 0000 0000 0000 0000 0000 0000

0023 0025 0024 0032 0021 0034 0031 0028 0021 0023
 0043 0044 0032 0029 0025 0033 0035 0025 0026 0031
 0029 0034 0027 0030 0032 0046 0037 0034 0032 0029
 0034 0032 0020 0031 0024 0026 0027 0027 0022 0019
 0034 0021 0018 0029 0016 0026 0019 0028 0022 0031
 0031 0023 0035 0036 0032 0049 0039 0056 0059 0072
 0071 0088 0081 0096 0110 0133 0116 0130 0134 0155
 0147 0140 0106 0101 0109 0077 0055 0057 0036 0026
 0014 0012 0004 0004 0002 0001 0000 0000 0000 0000
 0000 0000 0000 0000 0000 0000 0000 0000 0000 0000

0026 0036 0050 0034 0030 0024 0032 0037 0029 0030
 0029 0030 0028 0021 0022 0028 0027 0034 0029 0037
 0040 0031 0034 0033 0032 0032 0027 0018 0042 0036
 0026 0025 0033 0012 0024 0020 0018 0018 0022 0020
 0026 0032 0026 0025 0021 0024 0026 0023 0024 0032
 0028 0032 0032 0025 0037 0052 0046 0049 0046 0047
 0059 0066 0083 0120 0103 0119 0139 0146 0136 0140
 0119 0129 0134 0110 0095 0096 0056 0040 0041 0026
 0026 0014 0002 0001 0002 0001 0003 0000 0000 0000
 0000 0000 0000 0000 0000 0000 0000 0000 0000 0000

0035 0041 0026 0018 0035 0029 0028 0030 0036 0030
 0024 0028 0024 0035 0026 0036 0029 0035 0029 0037
 0029 0031 0040 0040 0032 0025 0041 0026 0039 0023
 0028 0016 0021 0030 0020 0022 0017 0024 0033 0025
 0019 0024 0023 0021 0029 0035 0023 0030 0024 0024
 0034 0033 0038 0031 0045 0046 0040 0067 0049 0078
 0052 0083 0076 0077 0102 0114 0125 0133 0122 0131
 0134 0130 0119 0114 0103 0069 0057 0053 0031 0024
 0012 0007 0002 0004 0000 0001 0000 0000 0000 0000
 0000 0000 0000 0000 0000 0000 0000 0000 0000 0000

0036 0039 0047 0041 0030 0021 0028 0029 0023 0039
 0020 0029 0025 0026 0034 0020 0024 0039 0026 0031
 0036 0028 0033 0038 0029 0025 0031 0027 0036 0030
 0037 0030 0030 0025 0020 0023 0026 0018 0015 0020
 0022 0026 0030 0025 0022 0019 0024 0043 0023 0020
 0033 0025 0034 0035 0032 0058 0039 0046 0056 0071
 0065 0072 0072 0115 0111 0101 0121 0134 0117 0132
 0119 0128 0110 0109 0086 0079 0060 0056 0032 0031
 0015 0011 0006 0002 0002 0001 0000 0000 0000 0000
 0000 0000 0000 0000 0000 0000 0000 0000 0000 0000

APPENDIX B

Preparation of and Analysis of a Supersaturated Solution of Sodium Aluminate

B.1 Preparation of a Supersaturated Solution of NaAlO₂

The first program listed in Appendix E calculates the required amounts of H₂O, NaOH, Al(OH)₃ needed to make up a supersaturated solution of a specified composition. Temperature effects are accounted for by means of a dilution factor. This factor is based on a solution density correlation developed by Misra (m2). The other equations were derived from mass balances.

To initialize the program the following variables need to be specified:

- * V_{T,2} - Suspension volume (cm³)
- CA₂ - alumina concentration (g Al₂O₃/ℓ sol.)
- CN₂ - caustic concentration (g Na₂O/ℓ sol.)
- θC₂ - operating temperature (°C)
- θC₁ - room temperature (°C)
- W_t - seed concentration (g/ℓ susp.)

The correction factor is based on the difference between the solution density at room and at the operating temperature, and resulting volume and concentration changes. This factor, denoted by α₂, is defined such that:

*Subscript 1 refers to room temperature conditions, while 2 refers to the conditions at the specified operating temperature.

$$CA_1 = \alpha_2 \times CA_2 \quad (B.1)$$

$$CN_1 = \alpha_2 \times CN_2 \quad (B.2)$$

$$\rho_{L,1} = \alpha_2 \times \rho_{L,2} \quad (B.3)$$

$$V_{L,1} = \frac{1}{\alpha_2} \times V_{L,2} \quad (B.4)$$

and is calculated from the solution density correlation at room temperature:

$$\rho_{L,1} = 1051 + .992 \times CN_1 - .00011 \times (CN_1)^2 + .566 \times CA_1 +$$

$$\{- .94 \times \theta C_1 + .0051 \times (\theta C_1)^2 \}$$

and relationships (B.1), (B.2), and (B.3), which when substituted in the density correlation give:

$$\alpha_2 = \{-C2 - [(C1)^2 - 4 \times C1 \times C3]^{1/2}\} / (2 \times C1) \quad (B.5)$$

where

$$C1 = -.00011 \times (CN_2)^2$$

$$C2 = .992 \times CN_2 + .566 \times CA_2 - \rho_{L,2}$$

$$C3 = 1051 + (.0051 \times \theta C_1 - .94) \times \theta C_1$$

$$\rho_{L,2} = 1051 + (-.00011 \times CN_2 + .992) \times CN_2 +$$

$$.566 \times CA_2 + (.0051 \times \theta C_2 - .94) \times \theta C_2$$

In addition to α_2 , the program calculates the variables:

(i) Seed weight and volume

$$W_S = .W_t \times V_{T,2} / 1000 \text{ (g)} \quad (B.6)$$

$$V_S = W_S / 2.42 \text{ (ml)} \quad (\text{B.7})$$

(ii) Volume and weight of the supersaturated solution

$$V_{L,2} = V_{T,2} - V_S \text{ (ml)} \quad (\text{B.8})$$

$$W_L = V_{L,2} / 1000 \times \rho_{L,2} \text{ (g)} \quad (\text{B.9})$$

(iii) Weights of the different components of the supersaturated solution

$$W_{Al} = CA_2 / 51 \times 78 \times V_{L,2} / 1000 \text{ (g Al(OH)}_3\text{)} \quad (\text{B.10})$$

$$W_{Na} = CN_2 / 31 \times 40 \times V_{L,2} / 1000 \text{ (g NaOH)} \quad (\text{B.11})$$

$$W_H = W_L - W_{Al} - W_{Na} \text{ (g H}_2\text{O)} \quad (\text{B.12})$$

After mixing of these amounts and digesting, the concentration of the supersaturated solution was checked by the following variables measured at room temperature and related to the variables at the operating temperature through the factor α_2 .

$$V_{L,1} = \frac{1}{\alpha_2} \times V_{L,2} \quad (\text{B.13})$$

$$CA_1 = \alpha_2 \times CA_2 \quad (\text{B.14})$$

$$CN_1 = \alpha_2 \times CN_2 \quad (\text{B.15})$$

The correction factor α_2 is typical of the order of about 2%. Although, these are not very large corrections, an attempt was made to control these variables as precisely as possible since they are treated as independent variables in subsequent model development. Accurate control of the independent variables will facilitate the use of statistical techniques in model development, and allow for a valid comparison between

repeat experiments.

B.2 Solution Concentration Analysis Procedure

The following liquor analysis procedure is in large part identical to the outline given by Aluminum Laboratories Ltd., Arvida (a3), and is also described in references (w5,w6). It is important that the final aliquot contains about 0.25 to 0.50 g of Al_2O_3 . Samples of different strengths should be diluted to be in this concentration range. For a description of the chemistry of these analytical reactions, references (w5,w6,k2) should be consulted. This volumetric procedure allows for a fast and accurate determination of the alumina and caustic concentration using phenolphthalein as indicator.

Required Reagents

(a) Phenolphthalein Indicator

Dissolve 5 g in 500 ml of acetone, dilute to 1000 ml with distilled water, and neutralize with 1 N NaOH to a faint pink colour.

(b) Barium Chloride Wash Solution

Dissolve 1.5 g of $BaCl_2 \cdot 2H_2O$ in water and dilute to 1000 ml. Normally this solution is neutral to phenolphthalein. If it is not, neutralize with 1 N NaOH or 1 N HCl, as required.

(c) Barium Chloride Solution

Same as previous, except 100 g of $BaCl_2 \cdot 2H_2O$.

(d) Sodium Tartrate Solution

Dissolve 250 g of $\text{Na}_2\text{C}_4\text{H}_4\text{O}_6 \cdot 2\text{H}_2\text{O}$ in water, and dilute to 1000 ml. Neutralize with 1 N NaOH or 1 N HCl as required.

(e) Potassium Fluoride Solution

Dissolve 617 g of KF or 998 g $\text{KF} \cdot 2\text{H}_2\text{O}$ in water and dilute to 1000 ml. Store in a polyethylene container. Check for acidity or alkalinity at regular intervals as follows: to 300 ml of water add 50 ml of potassium fluoride solution, and 6 drops of phenolphthalein indicator. Titrate with 1.00 N NaOH or 1.00 N HCl to a faint pink end point. Add or subtract this blank titration to or from the amount of 1 N HCl required for the alumina determination. Do not attempt to neutralize the potassium fluoride solution.

(f) 1.00 N HCl and NaOH Solutions

Dilute the contents of HCl and NaOH ampoules according to the indicated directions. Fresh 1.00 N solutions should be prepared before each experiment.

Analysis Procedure

The following steps are based on the Arvida works outline. This outline was slightly modified to suit the experimental conditions of this work. For some important notes on this procedure, reference (w5) should be consulted.

- (1) Pipette 5 ml (or other volume to obtain correct amount of Al_2O_3) of NaAlO_2 solution from the filtrate of the crystallizer sample into a polyethylene sample bottle and dilute with water to 50 ml.
- (2) Pipette 20 ml from the sample bottle into a 600 ml beaker.
- (3) Add 15 ml of barium chloride solution and fill beaker to 350-375 ml with barium chloride wash solution.
- (4) Add additional 15 ml of barium chloride solution, plus 25 ml of sodium tartrate and 6 drops of phenolphthalein indicator.
- (5) Titrate with 1.00 N HCl to the phenolphthalein end point.
- (6) Express caustic concentration as g/l Na_2CO_3 , which is equal to: $\{\text{ml of HCl}\} \times 26.50$.
- (7) To this solution add 20 ml of HCl (or less, see note 4, reference (w5), to give 3 to 5 ml back titration), and 50 ml of potassium fluoride while stirring.
- (8) Back titrate past end point with 1.00 N NaOH and just discharge colour with 1.00 N HCl.
- (9) Express aluminum concentration as g/l Al_2O_3 , which is equal to: $\{(20 \text{ ml of HCl or less}) - (\text{ml of NaOH step 8}) + (\text{ml of HCl step 8})\} \times 8.50$.

APPENDIX C

Crystal Size Analysis System

The apparatus used for measuring crystal size consisted of:

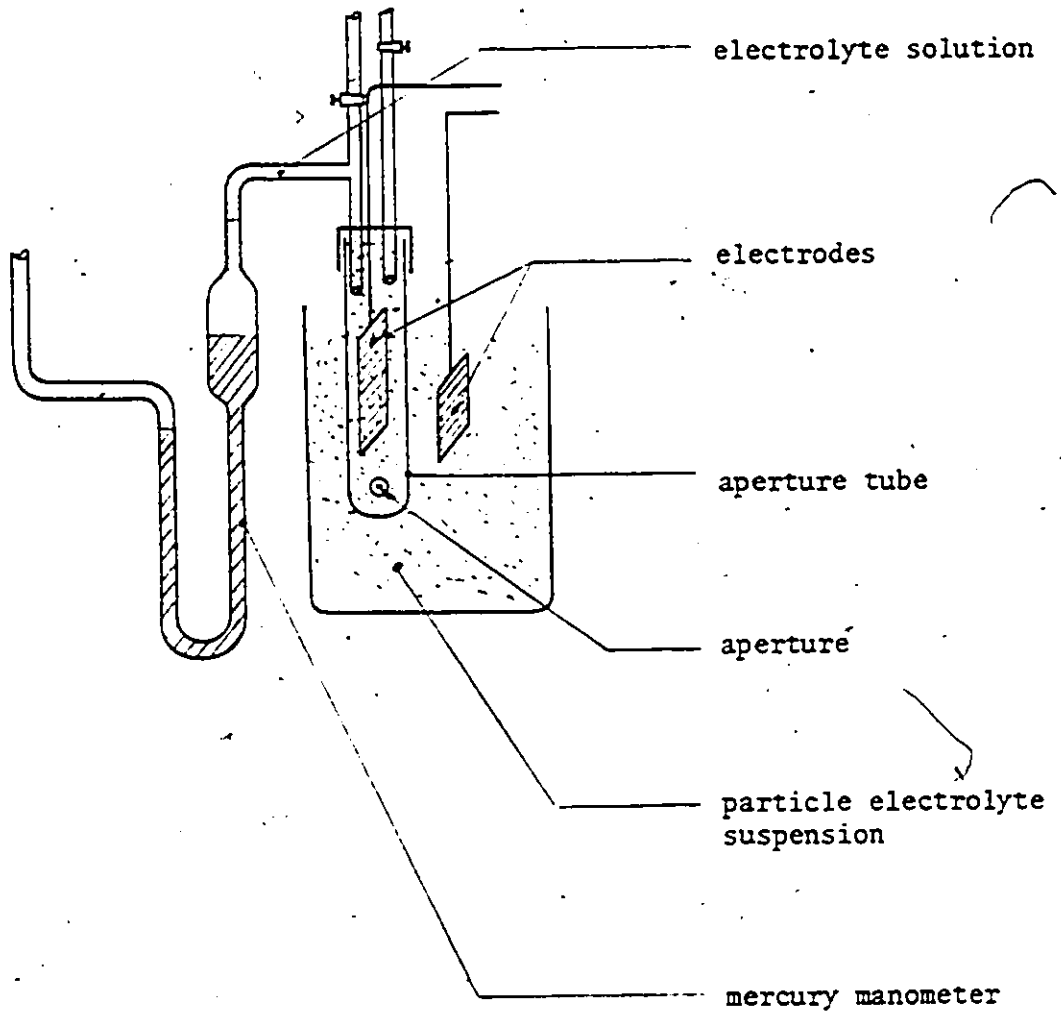
- Model Z_B Coulter Counter
- Model C-1000 Coulter Channelyzer
- Channelyzer Log Transformer
- Teleprinter Interface
- Teletype
- Constant Voltage Transformer

These devices are described, their operating principles explained, and the calibration procedure outlined in the following sub-sections.

C.1 Operating Principle of a Coulter Counter Apparatus (Model Z_B)

The operation of this type of apparatus is based on the difference in electrical conductivity between particles and common diluent (electrolyte). Particles act as insulators, the diluent as a good conductor. The particles, suspended in an electrolyte, are forced through a small aperture through which an electrical current path has been established. As each particle displaces the electrolyte in the aperture, a pulse proportional to the particle volume is produced; thus, the Coulter Counter measures particle volume. Particle volume is an unambiguous measure of particle size.

Schematic C-1 Coulter Counter Sampling Section



C.2 Function of Peripheral Coulter Counter Apparatuses

C.2.1 Coulter Channelyzer, Model C-1000

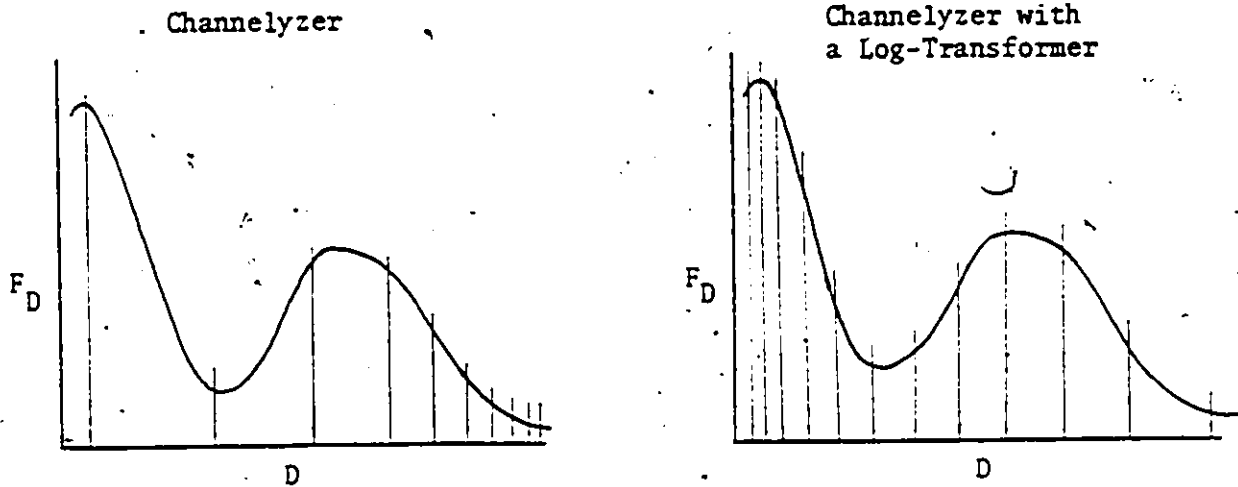
This apparatus accumulates the pulses from the Coulter Counter and automatically separates them into 100 channels at a rate of 5000 particles per second. This information is displayed graphically and digitally on the front panel and is stored for output to peripheral equipment.

The measurement range of the Channelyzer can be adjusted down to 10% of the dynamic range of the Coulter Counter. The Channelyzer 'sorts' the Coulter Counter data into 100 equal volume intervals.

C.2.1.1 Channelyzer Log Transformer

This peripheral Channelyzer device 'sorts' the Coulter Counter data into 100 channels or volume intervals. Each volume interval has a range such that $\log_{10} \Delta V_i = \text{constant}$, that is equal intervals on a logarithm basis. Dividing a wide spread distribution into equal volume intervals means that, when viewed on a spherical equivalent diameter basis, it has a very high resolution at the upper end of the distribution. The equal log volume interval division provides a very high resolution at the lower end of the distribution. This was required for this work (see schematic C-2). For a narrow size distribution this difference becomes insignificant.

Thus, the Channelyzer provides a very good resolution of narrow size distributions, while the Log Transformer makes it also suitable for widespread distributions. This means that the log transformer greatly enhances the versatility of this particle analysis system.



Schematic C-2

Different Resolution of a Crystal Size Density Function

C.2.1.2 Teleprinter Interface, Teletype

The teleprinter interface transmits the number count of each channel of the channelyzer to a teletype machine in a fixed format. The information is then automatically printed by a teletype and put on paper tape by means of the teletype tape punch. Thus, the teletype printout and paper tape provide the hard copies of the data.

The tape can be read by proper computer facilities, and the data manipulated by computer as desired. This whole procedure allows for fast, convenient, and versatile handling of a very voluminous amount of size distribution data.

C.2.2 Constant Voltage Transformer

The constant voltage transformer 'dampens' or reduces electrical input line noise to the Coulter Counter. This essentially eliminates 'noise', that is, false number counts in the lower channels.

C.3 Coulter Counter Channelyzer Calibration

To relate the control settings of the Coulter Counter and the Channelyzer to the volume of the analyzed particles the following procedure was adopted:

- (1) Based on prior knowledge of particle size to be expected in this crystallizing system, a 200 μm orifice tube was selected. This tube has a 'dynamic' or measuring range of between 2 and 40% of the 200 μm , i.e. 4 μm to 80 μm . Below 4 μm background noise interferes with the signal, and above 80 μm the Coulter Counter response is non-linear.
- (2) 'Isoton' (trade name from Coulter Counter Inc.) was selected as the electrolyte. This electrolyte had good dispersing properties and was inert towards the alumina trihydrate particles. Also, its conductivity was large enough to allow for the wide current range which was required when using the Channelyzer Log Transformer.
- (3) Once the aperture and electrolyte were selected the electrolyte resistance was measured following the procedure outlined in the Coulter Counter manual. For this set-up it was $11 \pm 1 \text{ k}\Omega$, and therefore, the Coulter Counter 'Matching Switch' was set at 10 k. Also, for this work, the 'Gain Trim Control' was set at 0.9.

- (4) A sample of a calibration standard of known 'mean' volume was then dispersed in the electrolyte. Dilution was enough so that no significant 'coincidence' occurred, and on the other hand was not too much so as to minimize count variations due to random events. Using these particles the Channelyzer was calibrated according to the procedure outlined in the Coulter Counter Channelyzer manual.
- (5) Once the controls were set, different calibration standards were measured. The results of these tests are shown in Table C-1. The calibration factor K was calculated as indicated in the following sub-sections.

C.3.1 Channelyzer in Linear Mode

$$K = \frac{V}{I \times A \times \left\{ (N \times \frac{NW}{100}) + BCT \right\}} \quad (C.1)$$

where K - calibration factor which is a function of: matching switch setting, gain control setting, electrolyte, orifice tube, and electronics; if any of these variables is changed K will change.

V - known mean volume of the calibration standard

I - Coulter Counter aperture current switch setting, i.e. the number as displayed on the front of the Coulter Counter cabinet

A - Coulter Counter amplification switch setting

TABLE C-1
Calibration of 200 (240 depth), Coulter Counter
Orifice Tube

Sample #	Standard		Z ₀ C.C.	Linear Mode						Log Mode											
	Calibration Standard	Diameter Range μm		Volume $V = \frac{4}{3}\pi r^3$	Total Count	Edite.	A	BCT	MW	N (modal channel)	Total Count	K	I	BCT	MW	N	log V	log I	Total Count	K	
1	*3 drops polystyrene	9.69	476.4	3349	/							.25	0	100	31-32	2.67761	-.6021	3279	2.020		
2				3265									.125	0	100	40		-.9031	3193	1.981	
3				3341	off	.125	1	0	100	21-22	3226	177.3		.5	0	100	23		-.3010	3303	2.059
4				3323	off	.126	.5	0	100	47	2733	162.2									
5				3301	on	.125	1	0	100	21	1876	181.5									
6				3619	on	.125	.5	0	100	46-47	1716	163.9									
7	**paper mulberry pollen	12-13 12.5	1022.6	21384								.25	0	100	36	5.009706	-.6021	19703	2.172		
8				21477									.125	0	100	44		-.9031	19634	2.153	
9				21242									.5	0	100	28		-.3010	19833	2.191	
10				21759	off	.25	1	0	100	15	20322	272.7									
11				21723	off	.25	.5	0	100	33	19605	247.9									
12				22107	on	.25	.5	0	100	32	10842	255.6									
13	*2 drops polystyrene	18.04	3074.0	4346	on	.25	2	0	100	34-35	2570	178.2									
14				4414	off	.25	2	0	100	34	4226	180.8									
15				4257										.125	0	100	60	3.48770	-.9031	4233	1.991
16				4254										.25	0	100	52		-.6021	4236	2.010
17				4254										.5	0	100	44-45		-.3010	4194	2.009
18				4254																	
19	**ragweed pollen	19-20 19.5	3882.4	1473								.5	0	100	46-47	3.58910	-.3010	1480	2.030		
20				1560									.25	0	100	54-55		-.6021	1649	2.011	
21				1688									.125	0	100	61-62		-.9031	1708	2.032	
22				1770	off	.25	2	0	100	38-42	1639	194.1									
23				1965	on	.25	2	0	100	39	1303	199.1									
24				1396																	
25	*sycopodium pollen 4 l drop of liquinox	27-28 27.5	10889.2	1382								.25	0	100	65-66	4.036988	-.6021	1413	2.019		
26				1372									.125	0	100	73		-.9031	1337	2.020	
27				1398	off	.25	4	0	100	70	73	155.6		.5	0	100	58		-.3010	1399	2.018
28				1447	on	.25	4	0	100	68	1037	160.1									
29				1493	on	.5	4	0	100	31	1109	175.6									
30				1930																	
31	**pecan pollen	45-50 47.5 45	56115.2 47713.0	2141								.5	0	100	72	4.74908	-.3010	1871	2.170		
32				1982									.25	0	100	72		-.3010	2083	2.170	
33				2057									.25	0	100	79		-.6021	1868	2.191	
34				1989	off	.5	8	0	100	59	1964	237.8									
35				2018	off	1	8	0	100	28	1983	250.5									

Notes:
 - new calibration standards *
 - old calibration standards **
 - electrolyte: Isoton
 - aperture electrolyte resistance 11 ± 1 kΩ
 - matching switch 10 K
 - gain control .9

N - modal channel number of the reference standard; it has been assumed that the largest number of particles has a mean volume equal to V

WW - Channelyzer window width setting

BCT - Channelyzer base channel threshold setting

The calculated calibration factor, using only new calibration standards, was 170.6. The old calibration standards were not included in the calculation of K because of their uncertain or poorly defined size distribution peak, and their known problem of 'swelling'. These factors probably were the cause of the large deviation in the value of K. In addition, it was observed by means of a sample weight check, that the size analyses based on these standards were consistently too large.

C.3.2 Channelyzer in Log Mode

$$K = \log\left(\frac{V}{I}\right) - \left(\left(N \times \frac{WW}{100}\right) + BCT\right)/25 \quad (C.2)$$

where K - calibration factor

V, I, N, WW, and BCT - are as defined previously

Note that the Coulter Counter amplification variable, A, is not in this equation since its setting has no effect on the Log Channelyzer output, that is the signal going to the log channelyzer is taken off before it enters the Coulter Counter amplification circuit.

Based on the new calibration standards, the calculated value of K was 2.014. The reasons for not including the old standards are given in the previous section.

C.4 Coulter Counter Count Corrections

In some counts, a loss of count may occur due to two or more particles entering the aperture simultaneously, and being registered as a single pulse and count. High dilutions will reduce this effect. However, when coincidence cannot be reduced by sample dilution, a correction factor must be applied.

C.4.1 Coincidence Correction Coulter Counter Equation

To correct for coincidence the manufacturer of the Coulter Counter recommends the following equations:

$$n_a = n_{cc} + n_l \quad (C.3)$$

$$n_l = p \times (n_{cc}/1000)^2 \quad (C.4)$$

$$p = 2.5 \times (D/100)^3 \times (500/V) \quad (C.5)$$

where n_a - 'actual' or corrected inverse cumulative number count
 n_{cc} - inverse cumulative number count as measured with the
 Coulter Counter
 n_l - inverse cumulative number of coincidence losses
 D - aperture diameter in μm
 V - manometer volume or sampled volume in μl

This correction is only valid when dealing with normal distributions with a narrow range of sizes.

C.4.2 An Agglomeration Type of Equation for Coincidence Correction

The equation presented below also corrects the Coulter Counter measurements for coincidence. It was developed based on the following postulates:

- (i) The number of particles of size V' which are not counted because they passed through the orifice simultaneously with particles of size V'' is proportional to the product of their respective number density functions.
- (ii) The number of particles which are counted as V' , and which are actually the sum of two smaller particles is proportional to the product of the number density functions of these smaller particles.
- (iii) The rate of passage through the orifice of the particles is only proportional to their respective number concentrations, and not to their sizes.

The equation is:

$$F_{V,a,i} = F_{V,CC,i} + b_{CC} \times (F_{V,CC,i} \times \int_{V_1}^V F_{V,CC}(V) dV - \frac{1}{2} \int_{V_1}^V F_{V,CC}(V_i - V) \times F_{V,CC}(V) dV) \quad \dots (C.6)$$

It can be approximated by:

$$\Delta n_{a,i} = \{ (\Delta n_{CC,i} / \Delta V_i) + b_{CC} \times [(\Delta n_{CC,i} / \Delta V_i) \times \sum_{l=1}^{99} \Delta n_{CC,l} - (\sum_{l=i-6}^i \Delta n_{CC,l} / \Delta V_l) / 7 \times \sum_{l=1}^{i-7} \Delta n_{CC,l}] \} \times \Delta V_i \quad \dots (C.7)$$

Within the limitations of the above postulates, equation (C.7) is valid for narrow as well as wide particle-size distributions. The coincidence correction parameter, b_{CC} , can be estimated by means of:

- (a) Comparisons between analysis of the same particle size distribution suspended in electrolyte samples of different concentration or dilution.
- (b) Calculation of the total weight concentration of particles and comparing this weight with the measured sample weight.

Although this last method for estimating b_{CC} is less sensitive than the first, this was the method used for this work. The samples were diluted to such an extent that only a small correction was required (ca. a few percent). The estimated value for b_{CC} was: 5×10^{-6} .

The approximation equation is only valid for a distribution measurement obtained with the Channelyzer in the log mode. It is based on the fact that with the Log Transformer the channel's volume relationship is given by:

$$V_{i+1} = 1.09647 \times V_i \quad (C.8)$$

and

$$V_{i+7} = 1.90536 \times V_i \approx 2 \times V_i \quad (C.9)$$

therefore

$$\begin{aligned} & \int_{V_1}^{V_i/2} F_{V,CC}(V_i - V) \times F_{V,CC}(V) dV \\ & \approx \{ \text{average } F_{V,CC}(V_i - V) \} \times \left\{ \int_{V_1}^{V_i/2} F_{V,CC}(V) dV \right\} \\ & = \left\{ \left(\sum_{l=1}^i F_{V,l} \right) / 7 \right\} \times \left\{ \sum_{l=1}^{i-7} F_{V,l} \times \Delta V_l \right\} \quad \dots (C.10) \end{aligned}$$

where $F_{V,i} = \frac{\Delta n_{a,i}}{\Delta V_i}$

$\Delta n_{a,i}$ - 'actual' or corrected number count of channel number i

$\Delta n_{CC,i}$ - Coulter Counter measured number of particles in channel i

ΔV_i - volume size interval of channel i

The equation presented in this sub-section was developed because it has the following advantages over the Coulter Counter equation:

- (a) It is suitable for narrow as well as wide-spread distributions.
- (b) It increases the number of particles in the smaller end of the distribution, while decreasing the number in the larger or upper end. The Coulter Counter equation increases the number over the whole size distribution. This latter procedure is not compatible with the concept of the actual coincidence process. That is, the Coulter Counter equation does not conserve the total mass of particles, which is a basic fact of the coincidence process. The equation presented in this section has this property. In general, it is felt that this coincidence correction equation is better.

C.4.3 Background Count Interference

Counts which arise due to events other than particles from the to-be-measured size distribution passing through the orifice are defined as 'background counts'. Background counts are caused by electrical interference and by dirt or foreign particles in the electrolyte. Since this count is rather unpredictable it should be reduced to relatively acceptable levels.

Electrical interference can be minimized by means of 'proper' instrument location and by assuring that the 110 volt A.C. supply is relatively stable at 110 volt and free of transients. Dirt or foreign matter in the electrolyte can be minimized by proper filtration of the electrolyte and by locating the Coulter Counter apparatuses in a relatively dust-free location. These measures were taken in this work. Moreover, direct measurements on electrolyte (without particles added) at various times during the analysis of samples indicated that background counts were very low.

C:5 Channelyzer Number Rejection Losses

The electronics of the Coulter Counter and Channelyzer are such that the Channelyzer cannot accept 'pulses' as fast as the Coulter Counter can send them. This situation arises because of the particle sizing circuitry in the Channelyzer. From Table C-2 and Graph C-3 it is seen that, except for very small counts where random events dominate, the Channelyzer total number count is consistently below the Coulter Counter count. Based on this rather sparse information, the following correction formula was developed:

$$N_{CC} = N_{Ch} + \left(\frac{bl_{Ch}}{100} \times N_{Ch}\right) \quad (C.11)$$

and

$$\Delta n_{CC} = \Delta n_{Ch} + \left(\frac{bl_{Ch}}{100} \times \Delta n_{Ch}\right) \quad (C.12)$$

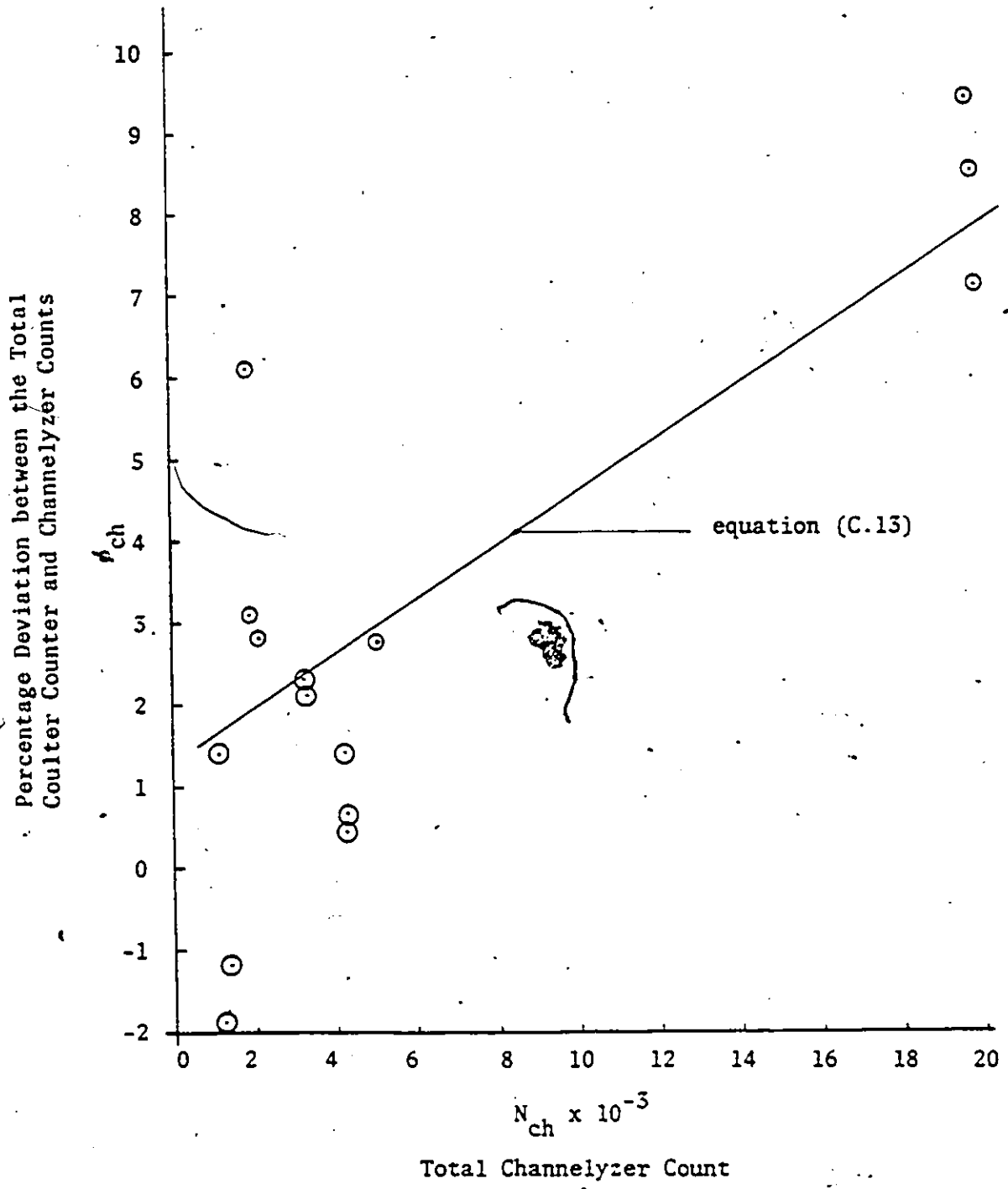
$$\text{where } bl_{Ch} = 1.3 + 3.3 \times 10^{-4} \times N_{Ch} = \phi_{Ch} \text{ predicted} \quad (C.13)$$

TABLE C-2

Channelyzer Number Rejection Losses

Total Coulter Counter Count (N_{CC})	Total Channelyzer Count (N_{Ch})	Percentage Deviation $(\phi_{Ch} = \frac{N_{CC} - N_{Ch}}{N_{Ch}} \times 100)$
1372	1399	-1.9
1382	1337	3.4
1396	1413	-1.2
1930	1871	3.1
1982	1868	6.1
2141	2083	2.8
3265	3193	2.3
3349	3279	2.1
4254	4236	0.42
4254	4194	1.4
4257	4233	0.57
21242	19833	7.1
21384	19703	8.5
21477	19634	9.4

Graph C-3 Channelyzer Number Rejection Losses



- N_{Ch} - total Channelyzer count
 N_{CC} - total Coulter Counter count
 n_i - counts in channel i

In the derivation of equation (C.13) it was assumed that the rejection losses are independent of pulse size.

These equations predict a rejection loss of ~ 2 to 3% for the smaller counts and $\sim 8\%$ for large counts. The Coulter Counter manufacturers state that the rejection loss is of the order of 2 to 3% . They do not mention that the correction depends on the total number count. Thus, these equations are in agreement with the manufacturer's suggestion for relatively small counts but deviate at large counts. From the data presented here it is felt that equations (C.11) and (C.12), which have a number dependence, are probably more accurate than the Coulter Counter correction of a global 2 to 3% .

C.6 Coulter Counter Electrolyte

A suitable electrolyte must have the following properties:

- (i) It must disperse the particles.
- (ii) It must not dissolve the particles.
- (iii) It must have low volatility, toxicity, and flammability.
- (iv) It must have the correct resistivity relative to the particles.
- (v) It must be miscible with any other liquids involved.
- (vi) It must have a relatively low cost.

The electrolyte used for this work was "Isoton". This is a standard type of electrolyte and is supplied by the manufacturer. It satisfied all of the above criteria.

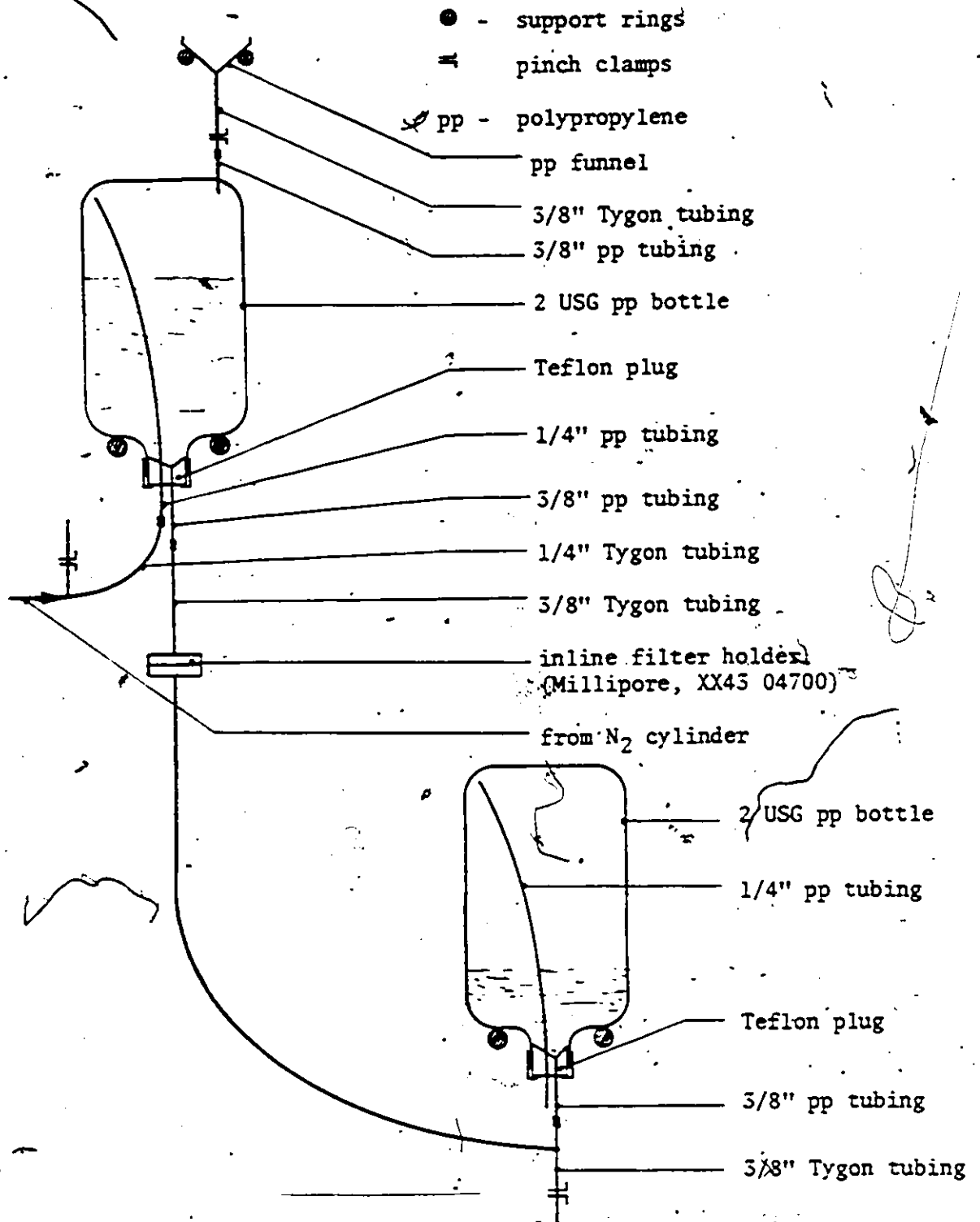
To assure that the electrolyte was free of dust and foreign matter, it was filtered through a 0.6 μm polyvinyl chloride filter. Sketch C-4 shows the filtration apparatus. After the top bottle was filled with electrolyte it was pressurized with nitrogen to about 5 psig. Under this pressure a batch of 2 gallons was filtered through the 0.6 μm filter in about 2 hours. Gravity filtration was not practicable. The filtered electrolyte was collected in the lower bottle and from there transferred to storage bottles.

C.7 Particle Size Distribution Measurement with a Coulter Counter Analysis System

Measurement of a particle size distribution with the previously described Coulter Counter apparatus and accessories can be done as follows:

- (1) Select and prepare a proper electrolyte. See Section C.6.
- (2) Select the correct size Coulter Counter orifice tube. This is done by knowing the upper size of the distribution a priori. An approximate estimate is sufficient.
- (3) Set the proper Coulter Counter controls as per Coulter Counter instruction manuals.
- (4) Determine the calibration factors for the linear and log mode using different calibration standards. See Section C.3.
- (5) Run several blank counts and determine that the counts are relatively free from 'background' interference. See Section C.4.3.

Sketch C-4 Automatic Batch Filtration Apparatus



- (6) Introduce a representative sample of the particles to be analyzed into the electrolyte which is contained in the sample beaker of the Coulter Counter. The concentration of particles in the electrolyte should be as concentrated as possible without increasing the coincidence correction above a few percent.
- (7) Run several repeat counts, taking care not to cause attrition of the particles by an excessively high rate of stirring or leaving the particles in the stirred electrolyte longer than the time required for analysis.
- (8) Have the particle size measurement data punched on the teletype paper tape. This paper tape may be read by a computer which, in turn, manipulates the data in the following manner:
 - (a) Correct for channelyzer number rejection losses, i.e.

$$\Delta n_{CC,i} = \Delta n_{Ch,i} + (bl_{Ch} \times \Delta n_{Ch,i})/100$$

$$i = 1, 2, 3, \dots, 100 \quad \dots (C.12)$$

where $bl_{Ch} = 1.3 + 3.3 \times 10^{-4} \times N_{Ch}$

N_{Ch} - total channelyzer number count

$\Delta n_{Ch,i}$ - number count in channelyzer channel i

$\Delta n_{CC,i}$ - rejection losses corrected count or the Coulter Counter measured number of particles in channel i

- (b) Correct for Coulter Counter coincidence losses*, i.e.

*This approximation equation is only valid for the 'log mode' setting of the channelyzer.

$$\Delta n_{a,i} = \{(\Delta n_{CC,i}/\Delta V_i) + b_{CC} \times$$

$$[(\Delta n_{CC,i}/\Delta V_i) \times \frac{100}{\sum_{l=1}^i \Delta n_{CC,l}}$$

$$- (\sum_{l=i-6}^i \Delta n_{CC,l}/\Delta V_l)/7 \times \sum_{l=1}^{i-7} \Delta n_{CC,l}] \} \times \Delta V_i$$

,.....(C.7)

- where $\Delta n_{CC,i}$ - Coulter Counter measured number of particles
in channel i
- $\Delta n_{a,i}$ - 'actual' or corrected number count for channel i
- ΔV_i - volume size interval of channel i
- b_{CC} - experimentally determined coincidence correction
parameter

- (9) Treat $\Delta n_{a,i}$ as the measured number of particles in size
interval V_i to V_{i+1} . This information along with the ΔV_i
of the interval gives the probability density function for
the mid-interval particle volume, that is:

$$F_V(i) = \frac{\Delta n_a(i)}{\Delta V_i}$$

APPENDIX D

Derivation of Auxiliary Equations and Relationships

D.1 Calculation of Crystallizer Solids Concentration

The crystallizer solids concentration was not measured directly. It was calculated in three different ways from different experimental measurements. Thus, these measurements provided a means of checking the consistency among the methods and of evaluating the mixing efficiency within the crystallizer, the sampling system and the analytical techniques. These methods for obtaining solids concentration are presented below.

(A) Method 1 Based on Solute Balance

The solids concentration, CS, at any time, may be calculated from the alumina and sodium carbonate analyses at time zero and at the specified time, and the initial weight of seed. The following analysis indicates the details.

The mass balance on alumina and caustic at any instant gives (nomenclature presented at the end of this section):

(a) Alumina:

$$\frac{d}{dt}(V_L(CA) + 0.654 W_T) = 0 \quad (D.1)$$

(b) Caustic:

$$\frac{d}{d\tau}(V_L(CN)) = 0 \quad (D.2)$$

Integrating from $\tau = 0$ to $\tau = \tau$ gives, respectively:

$$V_{L,0}(CA_0) - V_{L,\tau}(CA_\tau) + 0.654(W_{T,0} - W_{T,\tau}) = 0 \quad (D.3)$$

$$V_{L,0}(CN_0) - V_{L,\tau}(CN_\tau) = 0 \quad (D.4)$$

Now the total volume of the contents in the crystallizer at any time is

$$V_{T,\tau}^* = V_{L,\tau} + W_T/(R_S)(1000) \quad (D.5)$$

From (D.4)

$$V_{L,\tau}^* = V_{L,0}(CN_0)/(CN_\tau)$$

From (D.3) and (D.4)

$$W_{T,\tau} = \{V_{L,0}(CA_0)/.654\} - \{V_{L,0}(CN_0)(CA_\tau)/(.654 CN_\tau)\} + W_{T,0}$$

By definition:

$$CS_1(\tau) = W_{T,\tau}/V_{T,\tau} \quad (D.6)$$

Note: $V_{L,\tau}^$ is a hypothetical solution volume; i.e. this would not be the measured value at time τ but instead be the value at time τ as if no suspension had been removed through sampling. This is not equal to $V_{L,0}$.

which is the desired result.

In this derivation, the following nomenclature pertains:

CS_1 - crystallizer solids concentration calculated by method 1
(g/l susp.)

CA - alumina concentration (g Al_2O_3 /l sol.)

CN - caustic concentration (g Na_2O /l sol.)

W - solids weight (g)

ρ_s - density of solids (g/cm³)

V - volume (dm³)

o - subscript that denotes batch time zero (h)

τ - used as subscript here, it denotes batch time (h)

L - subscript that denotes total solution phase

T - subscript that denotes total suspension phase

(B) Method 2 Based on Direct Measurement of Mass of Solids and Solution

A sample was removed from the crystallizer and filtered. The weight of the sample filtrate, $W_{L,spl}$, and the weight of sample solids, $W_{S,spl}$, were determined. Then, the sample volume in l is:

$$V_{spl} = W_{L,spl}/(\rho_{L,2})(1000) + W_{S,spl}/(\rho_s)(1000)$$

Thus, the solids concentration is given by:

$$CS_2(\tau) = W_{S,spl}/V_{spl} \quad (D.7)$$

where CS_2 - crystallizer solids concentration calculated by method 2
(g/dm³ susp.)

$W_{L,sp1}$ - measured sample solution weight (g)

$W_{S,sp1}$ - measured sample solids weight (g)

$\rho_{l,2}$ - solution density at the crystallizer operating temperature
(g/cm³)

ρ_s - solids density (g/cm³)

(C) Method 3 Based on Crystal Size Distribution Measurements

Since the crystal size distribution was determined on an absolute basis (that is, the number of crystals per unit volume of slurry in a given particle volume interval), it is possible to calculate the solids concentration from the particle size measurement data.

The mass of crystals per unit volume of slurry in the particle volume interval $V_{p,i}$ to $V_{p,i+1}$ is given by:

$$\Delta W_i = \rho_s \times 10^{-12} \int_{V_{p,i}}^{V_{p,i+1}} \psi_{wV} \times V_p \times F_V dV_p \quad (D.8)$$

where ΔW_i - crystal weight in the crystal volume interval $V_{p,i+1} - V_{p,i}$
(g/l susp.)

V_p - crystal volume (μm^3)

* F_V - number density function (number/ μm^3 /l susp.)

*Note: $\int F_V \times dV_p \approx \Delta n_c \times Dlt$, which is the measured number of crystals corrected for Coulter Counter coincidence, and Channelizer rejection losses multiplied by the Coulter Counter dilution factor, Dlt.

- ψ_{WV} - volume weight function (dimensionless)
 ρ_s - density of solids (g/cm³)
 10^{-12} - multiplication factor to convert cm³ to μm^3

Equation (D.8) was calculated by relating it to the measured variables by the following approximation:

$$\Delta W_i \approx \rho_s \times 10^{-12} \times \psi_{WV,i} \times F_{V,i} \int_{V_{p,i}}^{V_{p,i+1}} V_p dV_p$$

which upon substitution of $F_{V,i}$ by $\Delta n_{a,i} \times Dlt / \Delta V_{p,i}$ is equal to:

$$\Delta W_i \approx \rho_s \times 10^{-12} \times \psi_{WV,i} \times \Delta n_{a,i} \times Dlt \times (V_{p,i+1} + V_{p,i}) / 2 \quad \dots (D.9)$$

The derivation of equation (D.9) is based on the assumption that the variables ψ_{WV} and F_V could be replaced by average values which could then be removed from the integral without causing serious error. This is a valid procedure given that the integration interval is relatively small and that the dependence of the variables on the integration variable is small over that interval. Since with the Coulter Counter system used for this work, the particle size distribution was divided into 100 intervals with correct resolution, this assumption is justified.

If, in addition, it is assumed that the function ψ_{WV} is constant and equal to 1, equation (D.9) becomes:

$$\Delta W_i \approx \rho_s \times 10^{-12} \times \Delta n_{a,i} \times Dlt \times (V_{p,i+1} + V_{p,i}) / 2 \quad (D.10)$$

This is again a good approximation because the Coulter Counter measures crystal volume directly. The only errors due to this approximation might result from Coulter Counter measurement 'effects', and from any solution 'inclusions' which would introduce an error in ρ_s .

Thus, the solids concentration by method 3 is:

$$CS_3 \approx \sum_{i=1}^m \Delta W_i \quad (D.11)$$

where CS_3 - crystallizer solids concentration calculated by method 3
(g/l susp.)

ΔW_i - variable calculated from equation (D.10)

In this summation, the weight which was not measured due to the Coulter Counter 'cut-off' size was neglected, or assumed to be zero. This was probably a poor assumption for those size distribution measurements which were made early in the experimental run, since a large proportion of the crystal mass were of a size less than the cut-off size.

D.2 Shape Factor Functions

A fundamental variable of importance in the crystal growth process is the crystal surface area. The crystal production rate of a crystallizer is directly related to the total crystal area in the crystallizer. This means that the crystallizer with the largest solid surface area would have the greatest production rate, all other things being equal.

Since surface area is so important in the crystal growth process, it should be measured directly in any experimental program in which growth

rates are measured. Unfortunately, it is difficult to measure the crystal surface area which is involved in the crystallization process and it is necessary to measure some particle property which can be related to its surface area by a shape factor or shape factor function.

In this work crystal volume was measured by the Coulter Counter assembly as described previously. Crystal volume is an unambiguous measurement and can be related to other crystal properties by the following relationships:

(A) Crystal Volume

The 'true' crystal volume may not be the volume as measured by the Coulter Counter. In this case, the two are related through ψ_{VV} as given by the following relationship:

$$V_p = \psi_{VV} \times V_{CC} \quad (D.12)$$

where V_p - true crystal volume
 V_{CC} - Coulter Counter measured crystal volume
 ψ_{VV} - shape factor relating V_p and V_{CC}

ψ_{VV} is probably equal to 1 over the measured size range provided that the Coulter Counter measurement errors were negligibly small. This requires that the 'proper' passage of the crystals through the orifice had occurred, and that calibration procedures were correct.

(B) Crystal Weight

The crystal weight is related to crystal volume through the solid density; thus:

$$W_p = \psi_{VV} \times \rho_s \times V_{CC} = \psi_{WV} \times V_{CC} \quad (D.13)$$

where W_p - crystal weight

ψ_{WV} - variable that relates the Coulter Counter volume measurement to the crystal weight

In this case, if $\psi_{VV} \approx 1$, and crystallization occurs in such a way as to minimize any inclusions, then the shape factor ψ_{WV} is probably close to ρ_s . The crystallization rate for the alumina trihydrate process is relatively 'slow', consequently inclusions probably do not occur to any significant extent.

(C) Crystal Surface Area

The crystal surface area can be related to crystal volume through a shape factor ψ_{AV} , viz.:

$$A_p = \psi_{AV} \times V^{2/3} \quad (D.14)$$

This is a less well 'defined' property as compared to V_p and W_p . The electron micrographs shown in Figure 4.4-C indicate a complex crystal geometry and hence the difficulty in estimating the area from the crystal volume measurements. The shape factor, ψ_{AV} , can only be obtained by direct

measurement of V and A_p and then modelling it as a function of V in an empirical way, assuming of course that it is only a function of V . This was not done for this initial investigative work.

For a spherical equivalent surface area $\psi_{AV} = \pi \times (6/\pi)^{2/3}$, while ψ_{AV} would be 6 if the crystals were cubic in shape. Scott (gl) measured the surface area of alumina trihydrate crystals by air permeability and related these measurements to the surface area calculated from particle size distribution measurements assuming perfect spheres. Particle sizes were determined by sieving and by sedimentation. He related these measurements by an 'angularity' factor, ψ , defined as:

$$\psi \triangleq \frac{\Delta}{V} \text{ (surface area of crystal) / (surface area of sphere of equivalent volume)}$$

This factor was correlated by:

$$\psi \approx 1.9055 - 1.0652 \times 10^{-2} \times D_p + 2.924 \times 10^{-5} \times (D_p)^2 \quad (D.15)$$

where D_p - spherical equivalent crystal diameter (μm)

The angularity factor as defined here is the inverse of the usual shape factor for surface area, namely 'sphericity' as used in particle hydrodynamics.

(D) Crystal Diameter

Given the shape of the crystals, as indicated in Figure 4.4-C, it is difficult to see how any one dimension could characterize the

particles in any way. It has meaning only when defined in relation to a certain process or to another crystal property. For example, equivalent Stokes diameter, equivalent sieve diameter, microscopic diameter, etc., are all measurements related to different processes or to different measurement techniques. Another definition of interest is the 'spherical volume equivalent' diameter. It is a hypothetical diameter obtained from crystal volume measurements.

For such a diameter

$$\psi_{DV} = (6/\pi \times \psi_{VV})^{1/3} \quad (D.16)$$

and

$$D_P = \psi_{DV} \bar{x} V^{1/3} \quad (D.17)$$

This was the diameter used in this work. Note that this diameter was not used in the model development work, only for presentation of data and model behaviour because of its favourable scaling effect.

APPENDIX E

Computer Listing of the Major Programs

The function of each program is described in each listing and the notation of the major variables is indicated at the beginning of each program. The equations which are used in the programs have been derived and discussed in the relevant sections of this thesis. The programs which are listed are:

	<u>Page</u>
(A) Program for Calculating the Chemicals Required for a Solution of a Specified Supersaturation	464
(B) Program Used to Manipulate Experimental Raw Data into a Form Used in Parameter Estimation (Program BA)	465
(C) Program for the Determination of the Parameters of an Empirical Model for the Solution Concentration Variables (Program BB)	473
(D) Program for the Determination of the Parameters of an Empirical Model for the Crystal Size Distribution (Program BC)	478
(E) Program Used to Estimate the Parameters in the Different Growth Rate Models by the Method of Pseudo Moments (Program CA)	484
(F) Program Used to Estimate the Parameters in the Agglomeration Rate Model by the Method of Pseudo Moments (Program CB)	492
(G) Program Used to Estimate the Parameters in the Nucleation Rate Model by the Method of Pseudo Moments (Program CC)	501
(H) Numerical Solution of the General Population Balance Model (the Full Model) by the RWCD Method or the CICR Method (Program DA)	509

PROGRAM TST (INPUT,OUTPUT,TAPES=INPUT,TAPE6=OUTPUT)

APRIL 24,74 MAKE UP OF SUPERSATURATED SOLUTION

CCCCCCCC

- SPECIFY AT OPER. TEMP.-----
VT2 SUSPENSION VOLUME ML
CA2 GM PER L SOLUTION AL2O3
CN2 GM PER L SOLUTION NA2O
TC2 OPER. TEMP. DEG. C
TC1 ROOM TEMP. DEG. C
WS SEED WEIGHT GM PER L SUSPENSION

JUNE 6,7-----
DATA VT2,CA2,CN2,TC2,TC1,WS/2500.,130.,120.,65.,25.,10./

```

C-----
CQZ2=CN2*EXP(6.2103+(-2480.7+1.04753*CN2)/(TC2+273.15))
RHOL2=1.051+(1.0011*CN2+.992)*CN2+.506*CA2+(1.0051*TC2-.9)*TC2
X1=-.00021*CN2*CN2
X2=.992*CN2+.506*CA2-RHOL2
X3=1.051+(.0051*TC1-.9)*TC1
ALPHA2=(-X2-SQRT(X2*X2-4.*X1*X3))/(2.*X1)
RHOL2=ALPHA2*RHOL2
CA2=ALPHA2*CA2
CN1=ALPHA2*CN2
CNC2=.7*CN1
HTS=WS*VT2/1000.
VTS=HTS/2.*2
VTL2=VT2-VTS
VTL1=VTL2/ALPHA2
HTL=VTL2/1000.*RHOL2
HTAL=CA2/51.*76.*VTL2/1000.
HTNA=CN2/51.*76.*VTL2/1000.
HTH=HTL-HTAL-HTNA
WRITE(6,100) VT2,CA2,CN2,TC2,TC1,WS
WRITE(6,102) ALPHA2,CQZ2,RHOL2,RHOL1,VTL2,VTL1,HTL,VTS,HTS,
CA1,CN1,CNC1

```

```

100 FORMAT(//,1X,*,--SPECIFIED AT OPERATING TEMP.--*,//,
F10.3,*, SUSPENSION VOLUME ML*,/
F10.3,*, GM PER L SOLUTION AL2O3*,/
F10.3,*, GM PER L SOLUTION NA2O*,/
F10.3,*, OPER. TEMP. DEG. C*,/
F10.3,*, ROOM TEMP. DEG. C*,/
F10.3,*, SEED WEIGHT GM PER L SUSPENSION*,/
)
102 FORMAT(//,1X,*, TEMP. DILUTION FACTOR*,/
F10.3,*, EQUIV. AL2O3 CONC. AT OPER. TEMP. GM PER L SOLUTION*,/
F10.3,*, SOLUTION DENSITY AT OPER. TEMP. GM PER L*,/
F10.3,*, SOLUTION DENSITY AT ROOM TEMP. GM PER L*,/
F10.3,*, SUPERSATURATED SOLUTION VOLUME AT OPER. TEMP. ML*,/
F10.3,*, SUPERSATURATED SOLUTION VOLUME AT ROOM TEMP. ML*,/
F10.3,*, SUPERSATURATED SOLUTION WEIGHT GMS*,/
F10.3,*, TOTAL SEED VOLUME ML*,/
F10.3,*, TOTAL SEED WEIGHT GMS*,/
F10.3,*, GM PER L SOLUTION AL2O3 AT ROOM TEMP. *,/
F10.3,*, GM PER L SOLUTION NA2O AT ROOM TEMP. *,/
F10.3,*, GM PER L SOLUTION NA2O3 AT ROOM TEMP. *)
104 FORMAT(//,1X,*,-- SUPERSATURATED SOLUTION IS MADE UP FROM--*,//
F10.3,*, GMS ALUMINUM TRI-HYDROXIDE*,/
F10.3,*, GMS SODIUM HYDROXIDE*,/
F10.3,*, GMS WATER*)
STOP
END

```

PROGRAM TST(INPUT,OUTPUT,PUNCH,TAPES=INPUT,TAPES=OUTPUT,
TAPET=7=PUNCH)

DATA MANIPULATION PROGRAM--BA-- THIS PROGRAM PRESENTS THE MEASURED OR PRIOR
VARIABLES, AND CALCULATES SECONDARY VARIABLES WHICH PROVIDE BASIC INFORMATION
WITH REGARD TO EXPERIMENTAL ACCURACY AND TYPE OF SUITABLE MECHANISTIC MODEL.

EXPERIMENTAL VARIABLES

N NUMBER OF SAMPLES
M NUMBER OF COULTER COUNTER SIZE INTERVALS
NS(J) SAMPLE NUMBER
TAU(J) SAMPLE OR BATCH TIME (H)
THETA1 ROOM TEMPERATURE (DEG. C)
THETA2(J) CRYSTALLIZER OPERATING TEMPERATURE (DEG. C)
CNC1(J) NA2CO3 CONCENTRATION AT ROOM TEMPERATURE (G/L SOL.)
CA1(J) AL2O3 CONCENTRATION AT ROOM TEMPERATURE (G/L SOL.)
WLSPL(J) HEIGHT OF SOLUTION OF (CRYSTALLIZER SAMPLE - CC SAMPLE) (G)
WSSPL(J) HEIGHT OF SOLIDS OF (CRYSTALLIZER SAMPLE - CC SAMPLE) (G)
WTO INITIAL CRYSTALS WEIGHT (G)
VLSO INITIAL SOLUTION VOLUME AT ROOM TEMPERATURE (L)
RHOS DENSITY OF CRYSTALS (G/CM**3)

COULTER COUNTER CALIBRATION AND INSTRUMENT SETTING VARIABLES (MODEL ZB
C/M CHANNELYZER AND LOG-TRANSFORMER)

RK LOG MODE CALIBRATION FACTOR
RI CC APERTURE CURRENT SWITCH SETTING
RH CHANNELYZER WINDOW WIDTH SETTING
BCT CHANNELYZER BASE CHANNEL THRESHOLD SETTING

COULTER COUNTER DILUTION FACTOR VARIABLES

V8(J) ELECTROLYTE VOLUME TO WHICH CC SAMPLE J IS ADDED (CM**3)
VH(J) VOLUME OF SAMPLED ELECTROLYTE SUSPENSION (CM**3)
CS2(J) CRYSTALLIZER SOLIDS CONCENTRATION CALCULATED BY METHOD 2
(G/CM**3 SUSP.)
WCC(S) WEIGHT OF SOLIDS ADDED TO CC ELECTROLYTE (G)

GENERAL COULTER COUNTER VARIABLES

RPT NUMBER OF REPEAT COULTER COUNTER MEASUREMENTS
BOC COULTER COUNTER COINCIDENCE CORRECTION PARAMETER
BCH CHANNELYZER NUMBER REJECTION LOSSES PARAMETER

OUTPUT CONTROL VARIABLE

NA(2) = 1 PRINT COULTER COUNTER VARIABLES, = 0 DO NOT
NP(2) = 1 PLOT COULTER COUNTER VARIABLES, = 0 DO NOT
NP(3) = 1 PUNCH COULTER COUNTER VARIABLES, = 0 DO NOT
NP(4) = 1 PRINT SOLUTION ANALYSIS VARIABLES, = 0 DO NOT
NP(5) = 1 PLOT SOLUTION ANALYSIS VARIABLES, = 0 DO NOT
NP(6) = 1 PUNCH SOLUTION ANALYSIS VARIABLES, = 0 DO NOT
NP(7) = 1 PUNCH VARIABLES FOR PLOTTING ROUTINE, = 0 DO NOT

DIMENSION NS(15),TAU(15),THETA2(15),CA(15),CNC(15),WSSPL(15),
WLSPL(15),V8(15),VH(15),WCC(15),CNC1(15),RHOL(15),CA2(15),CNC(15),
CNC2(15),RHOL2(15),CA(15),CNC(15),V8(15),VH(15),V1(15),V2(15),CS1(15),
CS2(15),CS3(15),VLSPL(15),VSSPL(15),VSPL(15),WTO(15),JLT(15),
RNT(15),RAT(15),RAT(15),CPL1(15),CPL2(15),
DIMENSION VP(15),UP(15),DELP(15),DELP(15),Z1(15),Z2(15),
SPF(15),RSPF(15),SP(15),RSP(15),FD(15),FAD(15),FWD(15)
DIMENSION DEIN(15),FV(15),FV(15)
DIMENSION ALABEL(35),INK(15),AKI(15),NP(15)


```

CC
C-PROGRAM INPUT DATA-----
CC
C PROGRAM OUTPUT CONTROL VARIABLE
  DATA (NP(K),K=1,7)/0,1,0,0,1,0,0/
C EXPERIMENTAL VARIABLES
C INITIAL CONDITIONS AND FREQUENCY OF SAMPLING
  DATA N,M,THETA1,RHOS,VL10,WT0/1+,100,23.0,2.42,2.3730,24.35155/
  DATA (NS(J),J=1,14)/1, 2, 3, 4, 5, 6, 7, 8, 9, 10, 11, 12, 13, 14/
C BATCH SAMPLING TIMES
  DATA (TAU(J),J=1,14)/0.0,0.25,0.50,0.75,1.0,1.333,1.667,2.0,4.0,
16.0,10.0,22.0,33.0,44.0,55.0/
C CRYSTALLIZER AND CRYSTALLIZER SAMPLE VARIABLES
  DATA (THET2(J),J=1,14)/84.8,85.3,85.0,84.8,85.2,85.3,85.2,85.3,
184.9,85.3,84.8,85.0,85.3,85.0/
  DATA (CA(J),J=1,14)/130.4,130.2,126.9,123.2,120.6,117.6,115.8,
1113.1,107.3,103.8,100.7,97.0,95.7,94.7/
  DATA (CNC1(J),J=1,14)/212.8,211.7,212.5,212.8,214.1,214.4,214.9,
121.9,216.8,217.6,218.1,218.6,218.4,219.4/
  DATA (WLSPL(J),J=2,14)/14.14800,14.62350,10.37246,10.04201,
110.03852,9.84412,9.72208,9.42615,9.54950,9.30234,9.39245,
28.40954,9.50232/
  DATA (WSSPL(J),J=2,14)/0.25330,0.19084,0.25349,0.33347,0.35958,
10.35926,0.37061,0.42541,0.50813,0.59199,0.60710,0.57103,0.63432/
CC
C COULTER COUNTER VARIABLES
  DATA BLANK,BCC,RK,RI,WH,BCT/1H ,5.E-06,2.014,0.25,100.,+.0/
  DATA (V9(J),J=1,14)/1+*200./
  DATA (VM(J),J=1,14)/1+*2./
  DATA (WCC(J),J=1,14)/0.0017+,0.00210,0.00638,0.00869,0.0114,0.0068
15.0,0.055+3,0.01262,0.01331,0.01397,0.01214,0.01031,0.01813,0.01333/
C AVERAGE BATCH OPERATING TEMPERATURE
  X1=0.
  DO 50 J=1,N
50 X1=X1+THET2(J)
  RN=N
  THETA2=X1/RN
C COULTER COUNTER VOLUME SETTINGS
  DO 52 I=1,101
  X3=I-1
  X4=ALOG10(RI)+RK+(((X3*WH/100.)+BCT)/25.)
  VP(I)=10.**X4
  Z1(I)=VP(I)**(5./3.)
  Z2(I)=VP(I)*VP(I)
C COULTER COUNTER SPHERICAL EQUIVALENT DIAMETERS
  52 DP(I)=CBRT(6./3.1-159*VP(I))
  DO 54 I=1,100
  DELVP(I)=VP(I+1)-VP(I)
  54 DELDP(I)=DP(I+1)-DP(I)
C CHANNELYZER NUMBER COUNT DATA
  DO 299 J=1,N
  DO 100 L1=1,80
100 ALABEL(L1)=BLANK
  READ(5,500) (ALABEL(L1),L1=1,80)
  READ(5,505) RPT
  KPT=RPT
  DO 102 L1=1,KPT
  READ(5,510) (INWK(I),I=1,100)
  DO 102 I=1,100
102 DELN(L1,I)=INWK(I)
  IF(NP(1).EQ.0) GO TO 103
  CALL WRT1(1,N,KPT,ALABEL,DELN)
103 CONTINUE
C-----

```

C TEMPERATURE CORRECTION OF SOLUTION CONCENTRATION MEASUREMENTS

```

CN1(J)=CNC1(J)*62./106.
RHOL1(J)=1.051+((( -1.1E-07*CN1(J))+9.92E-04)*CN1(J))
1 +(5.65E-04*CA1(J))+(((5.1E-06*THETA1)-9.4E-04)*THETA1)
C3=-1.1E-07*CN1(J)*CN1(J)
C2=(9.92E-04*CN1(J))+5.66E-04*CA1(J)-RHOL1(J)
C1=1.051+(((5.1E-06*THETA2)-9.4E-04)*THETA2)
ALPHA=(-C2+SQRT((C2*C2)-(4.*C1*C3)))/(2.*C1)
CA2(J)=CA1(J)/ALPHA
CN2(J)=CN1(J)/ALPHA
CNC2(J)=CN2(J)*106./62.
RHOL2(J)=1.051+((( -1.1E-07*CN2(J))+9.92E-04)*CN2(J))
1 +(5.65E-04*CA2(J))+(((5.1E-06*THETA2)-9.4E-04)*THETA2)

```

C SOLIDS CONCENTRATION FROM INITIAL CONDITIONS, CAUSTIC AND ALUMINA CONCENTRATION MEASUREMENTS

```

IF(J.EQ.1) VLG=VL0*ALPHA
IF(J.EQ.1) CA0=CA2(1)
IF(J.EQ.1) CNO=CN2(1)
CN(J)=CN2(J)
CA(J)=CA2(J)
VL(J)=VL0*CNO/CN(J)
HT(J)=(VL0*CA0/.65+)-((VL0*CNO/CN(J))*CA(J)/.654)+WTO
VT(J)=VL(J)+(HT(J)/(RHOS*1000.))
CS1(J)=HT(J)/VT(J)

```

C SOLIDS CONCENTRATION FROM CRYSTALLIZER SAMPLE SOLIDS CAKE AND SOLUTION WEIGHT MEASUREMENTS

```

IF(J.EQ.1) WLSPL(1)=VL(1)*RHOL2(1)*1000.
IF(J.EQ.1) WSSPL(1)=WTO
VLSPL(J)=WLSPL(J)/(RHOL2(J)*1000.)
VSSPL(J)=WSSPL(J)/(RHOS*1000.)
VSPL(J)=VLSPL(J)+VSSPL(J)
CS2(J)=WSSPL(J)/VSPL(J)

```

C COULTER COUNTER SAMPLE DILUTION FACTORS

```

DLT(J)=(VB(J)/VH(J))*(CS2(J)/HCC(J))

```

C CORRECTION FOR CHANNELYZER NUMBER REJECTION LOSSES

```

DO 108 L1=1,KPT
X1=0.
DO 107 I=1,100
107 X1=X1+DELN(L1,I)
SCH=1.3+(3.3E-04*X1)
DO 108 I=1,100
108 DELN(L1,I)=DELN(L1,I)*(1.+(SCH/100.))
IF(NP(1).EQ.0) GO TO 109
CALL WRT1(2,M,KPT,ALABEL,DELN)
109 CONTINUE

```

C CORRECTION FOR COULTER COUNTER COINCIDENCE LOSSES

```

DO 118 L1=1,KPT
X1=0.
DO 110 I1=1,M
110 X1=X1+DELN(L1,I1)
DO 118 I=1,100
X2=X3=0.
IF(I.LT.8) GO TO 115
KL=I-6
DO 112 I1=KL,I
112 X2=X2+(DELN(L1,I1)/DELVP(I1))
KU=I-7
DO 114 I2=1,KU
114 X3=X3+DELN(L1,I2)

```

```

116 CONTINUE
X4=DELN(L1,I)/DELVP(I)
DELN(L1,I)=(X4+(BCC*((X4*X4)-(X2/7.*X3))))*DELVP(I)
118 CONTINUE
IF(DELN(L1,I).LT.1.) DELN(L1,I)=0.
IF(NP(1).EQ.0) GO TO 119
CALL WRT1(3,M,KPT,ALABEL,DELN)
119 CONTINUE
C
C AVERAGED REPEAT COULTER COUNTER MEASUREMENTS
DO 124 I=1,100
X1=0.
DO 122 L1=1,KPT
122 X1=X1+DELN(L1,I)
124 WK1(I)=X1/RPT
DO 125 I=1,M
I1=1
IF(WK1(I).LE.0.) GO TO 126
125 CONTINUE
126 DO 127 I=I1,M
127 WK1(I)=0.
C
C AVERAGED COULTER COUNTER MEASUREMENTS ON AN ABSOLUTE BASIS
DO 130 I=1,100
130 WK1(I)=WK1(I)*DLT(J)
C
C NUMBER DENSITY FUNCTION WITH RESPECT TO CRYSTAL VOLUME
DO 132 I=1,100
132 FV(I,J)=WK1(I)/DELVP(I)
C
C RELATIVE VARIANCE OF THE NUMBER DENSITY MEASUREMENTS
DO 136 I=1,100
X1=SF2(I)=RSF2(I)=0.
IF(FV(I,J).LE.0.0) GO TO 136
DO 134 L1=1,KPT
X2=DELN(L1,I)*DLT(J)/DELVP(I)
X3=X2**V(I,J)
134 X1=X1+(X3*X3)
SF2(I)=1./(RPT-1.)*X1
RSF2(I)=SF2(I)/FV(I,J)*100.
136 CONTINUE
C
C RELATIVE STANDARD DEVIATION OF THE NUMBER DENSITY MEASUREMENTS
DO 138 I=1,100
SF(I)=RSF(I)=0.
IF(FV(I,J).LE.0.0) GO TO 138
SF(I)=SQRT(SF2(I))
RSF(I)=SF(I)/FV(I,J)*100.
138 CONTINUE
C
C NUMBER DENSITY FUNCTION WITH RESPECT TO SPHERICAL EQUIVALENT DIAMETER
DO 140 I=1,100
140 FD(I)=FV(I,J)*DELVP(I)/DELOP(I)
C
C AREA DENSITY FUNCTION WITH RESPECT TO SPHERICAL EQUIVALENT DIAMETER
X1=(3./5.)*CBRT(3.1+159)*(6.+(6./5.))*1.E-08
DO 142 I=1,100
142 FAD(I)=X1*FV(I,J)*(Z1(I+1)-Z1(I))/DELOP(I)
C
C WEIGHT DENSITY FUNCTION WITH RESPECT TO SPHERICAL EQUIVALENT DIAMETER
X1=RHOS/2.*1.E-12
DO 144 I=1,100
144 FWD(I)=X1*FV(I,J)*(Z2(I+1)-Z2(I))/DELOP(I)
C
C ZEROth MOMENT

```

```

X1=0.
DO 1+6 I=1,100
146 X1=X1+(FV(I,J)*DELVP(I))
RNT(J)=X1
C
C TWO-THIRDS MOMENT WITH RESPECT TO CRYSTAL VOLUME
X1=0.
DO 1+8 I=1,100
148 X1=X1+(FAD(I)*DELDP(I))
RAT(J)=X1
C
C FIRST MOMENT WITH RESPECT TO CRYSTAL VOLUME
X1=0.
DO 150 I=1,100
150 X1=X1+(FWD(I)*DELDP(I))
RWT(J)=X1
C
C SOLIDS CONCENTRATION FROM THE CRYSTAL SIZE DISTRIBUTION MEASUREMENTS
X1=0.
DO 152 I=1,100
152 X1=X1+(RHOS*1.E-12*FV(I,J)*DELVP(I)*(VP(I+1)+VP(I))/2.)
CS3(J)=X1
C
C PERCENTAGE DIFFERENCE BETWEEN THE CALCULATED CRYSTALLIZER SOLIDS
C CONCENTRATIONS
DEL21(J)=(CS2(J)-CS1(J))*100./CS1(J)
DEL31(J)=(CS3(J)-CS1(J))*100./CS1(J)
C-----
C
IF(NP(1).EQ.0) GO TO 202
WRITE(5,550) (ALABEL(L1),L1=1,80)
WRITE(6,500)
DO 200 I=1,M
X1=(VP(I+1)+VP(I))/2.
X2=CBRT(6./3.1+159*X1)
KWK1=I-1
200 WRITE(5,552) KWK1,X1,X2,DELVP(I),DELDP(I),FV(I,J),RSF2(I),RSF(I),
1 FDI,FAD(I),FWD(I)
202 CONTINUE
C
IF(NP(2).EQ.0) GO TO 250
DO 220 I=1,M
X1=(DP(I+1)+DP(I))/2.
220 CALL PLOTPT(X1,(((FDI)/1.E+05)+1.)**.25),24)
CALL RANGES(0.,100.,1.,10.)
CALL OUTPLT
DO 222 I=1,M
X1=(DP(I+1)+DP(I))/2.
222 CALL PLOTPT(X1,(((FAD(I)/1.E+01)+1.)**.35),21)
CALL RANGES(0.,100.,1.,10.)
CALL OUTPLT
DO 224 I=1,M
X1=(DP(I+1)+DP(I))/2.
224 CALL PLOTPT(X1,FWD(I),43)
CALL RANGES(0.,100.,0.,4.5)
CALL OUTPLT
GROOT=FV(1,J)
DO 225 I=2,M
IF(FV(I,J).GT.GROOT) GROOT=FV(I,J)
225 CONTINUE
DO 226 I=1,M
226 CALL PLOTPT(FV(I,J),RSF2(I),42)
CALL RANGES((GROOT*1.E-04),GROOT,5.E+04,3.5E+07)
CALL OUTPLT
DO 228 I=1,M

```

```

228 CALL PLOTPT(FV(I,J),RSF(I),39)
CALL RANGES((GROOT*1.E-04),GROOT,0.,50.)
CALL OUTPLT
DO 230 I=1,M,2
X1=I
X2=FV(I,J)
X3=X2+SF(I)
X4=X2-SF(I)
CALL PLOTPT(X1,X2,26)
CALL PLOTPT(X1,X3,3)
230 CALL PLOTPT(X1,X4,3)
CALL RANGES(0.,100.,0.,(FV(I,J)+SF(I)))
CALL OUTPLT
250 CONTINUE

```

```

C
IF(NP(3).EQ.0) GO TO 260
PUNCH(7,500) (ALABEL(L1),L1=1,80)
KWK1=M+1
PUNCH(7,576) (VP(I),I=1,KWK1)
DO 254 I=1,M
254 WK1(I)=FV(I,J)*VT(J)
PUNCH(7,576) (WK1(I),I=1,M)
260 CONTINUE

```

```

C
IF(NP(7).EQ.0.) GO TO 279
PUNCH(7,750) (FV(I,J),I=1,M)
PUNCH(7,752) (RSF2(I),I=1,M)
PUNCH(7,754) (RSF(I),I=1,M)
PUNCH(7,756) (FD(I),I=1,M)
PUNCH(7,758) (FAD(I),I=1,M)
PUNCH(7,760) (FWD(I),I=1,M)
279 CONTINUE

```

```

C
299 CONTINUE

```

```

C
IF(NP(4).EQ.0) GO TO 310
WRITE(6,602)
DO 300 J=1,N
300 WRITE(6,552) NS(J),TAU(J),THET2(J),CA1(J),CNC1(J),WLSPL(J),
1 WSSPL(J),VB(J),VM(J),WCC(J)
WRITE(6,604)
DO 302 J=1,N
302 WRITE(6,552) NS(J),TAU(J),CA(J),CN(J),VL(J),VT(J),HT(J),RHOL2(J)
WRITE(6,606)
DO 304 J=1,N
304 WRITE(6,552) NS(J),TAU(J),CS1(J),CS2(J),CS3(J),DEL21(J),DEL31(J)
WRITE(6,608)
DO 306 J=1,N
306 WRITE(6,552) NS(J),TAU(J),RNT(J),RAT(J),RWF(J)
310 CONTINUE

```

```

C
IF(NP(5).EQ.0) GO TO 380
DO 350 J=1,N
350 CALL PLOTPT(TAU(J),CA(J),21)
CALL OUTPLT
DO 352 J=1,N
352 CALL PLOTPT(TAU(J),CN(J),34)
CALL RANGES(0.,44.,100.,150.)
CALL OUTPLT
DO 354 J=1,N
354 CALL PLOTPT(TAU(J),THET2(J),40)
CALL RANGES(0.,44.,25.,100.)
CALL OUTPLT
DO 356 J=1,N
CALL PLOTPT(TAU(J),CS1(J),39)

```

```

CALL PLOTPT(TAU(J),CS2(J),25)
356 CALL PLOTPT(TAU(J),CS3(J),23)
CALL OUTPLT
DO 360 J=1,N
DO 358 I=1,M
X2=((FV(I,J)/1.E+01)+1.)**.15
X1=ALOG((VP(I+1)+VP(I))/2.)
358 CALL PLOTPT(X1,X2,+2)
CALL RANGES(3.,13.,1.,14.)
360 CALL OUTPLT
DO 362 J=1,N
362 CALL PLOTPT(TAU(J),RNT(J),34)
CALL OUTPLT
DO 364 J=1,N
364 CALL PLOTPT(TAU(J),RAT(J),21)
CALL OUTPLT
DO 366 J=1,N
366 CALL PLOTPT(TAU(J),RWT(J),43)
CALL OUTPLT
380 CONTINUE

```

```

C
IF(NP(5).EQ.0) GO TO 399
PUNCH(7,570) (TAU(J),J=1,N)
PUNCH(7,572) (CA(J),J=1,N)
PUNCH(7,574) (CN(J),J=1,N)
399 CONTINUE

```

```

C
IF(NP(7).EQ.0.) GO TO 449
PUNCH(7,700) (TAU(J),J=1,N)
PUNCH(7,702) (CA(J),J=1,N)
PUNCH(7,704) (CN(J),J=1,N)
PUNCH(7,706) (THET2(J),J=1,N)
PUNCH(7,708) (CS1(J),J=1,N)
PUNCH(7,710) (CS2(J),J=1,N)
PUNCH(7,712) (CS3(J),J=1,N)
PUNCH(7,714) (RNT(J),J=1,N)
PUNCH(7,716) (RAT(J),J=1,N)
PUNCH(7,718) (RWT(J),J=1,N)
M1=M+1
PUNCH(7,720) (VP(I),I=1,M1)
PUNCH(7,722) (DP(I),I=1,M1)
449 CONTINUE

```

```

C
500 FORMAT(80A1)
502 FORMAT(8F10.0)
510 FORMAT(I4,9I5)
550 FORMAT(1H1,/,1X,80A1)
552 FORMAT(1X,13,1PE12.4,10E12.4)
570 FORMAT(* TAU*,6X,7F10.3)
572 FORMAT(* CA*,7X,7F10.3)
574 FORMAT(* CN*,7X,7F10.3)
576 FORMAT(1PE10.3,7E10.3)
600 FORMAT(///,1X,*NCH*,2X,*VP*,10X,*DP*,10X,*DELVP*,7X,*DELOP*,7X,
1 *FV*,10X,*RVAR*,8X,*RSTD*,8X,*FD*,10X,*FAD*,9X,*FWD*,/)
602 FORMAT(1H1,/,1X,*INPUT DATA*,/,2X,*NS*,2X,*TAU*,9X,*THET2*,
1 7X,*CA*,9X,*CNCL*,9X,*WLSPL*,7X,*WSSPL*,7X,*VB*,10X,*VM*,
2 10X,*WCC*,/)
604 FORMAT(///,1X,*SOLUTION CONCENTRATION VARIABLES*,/,2X,*NS*,2X,
1 *TAU*,9X,*CA*,10X,*CN*,10X,*VL*,10X,*VT*,10X,*WT*,10X,*RHOL*,/)
606 FORMAT(///,1X,*CRYSTALLIZER SOLIDS CONCENTRATION*,/,2X,*NS*,
1 2X,*TAU*,9X,*CS1*,9X,*CS2*,9X,*CS3*,9X,*DEL1*,7X,*DEL2*,/)
608 FORMAT(///,1X,*MOMENTS OF CRYSTAL SIZE DISTRIBUTION*,/,2X,*NS*,
1 2X,*TAU*,9X,*RNT*,9X,*RAT*,9X,*RWT*,/)

```

```

C
700 FORMAT(* TAU *,1PE10.3,5E10.3)

```

```

702 FORMAT(* CA *,1PE10.0,0.0,0.0)
704 FORMAT(* CN *,1PE10.0,0.0,0.0)
706 FORMAT(* THET2 *,1PE10.0,0.0,0.0)
708 FORMAT(* CS1 *,1PE10.0,0.0,0.0)
710 FORMAT(* CS2 *,1PE10.0,0.0,0.0)
712 FORMAT(* CS3 *,1PE10.0,0.0,0.0)
714 FORMAT(* RNT *,1PE10.0,0.0,0.0)
716 FORMAT(* RAT *,1PE10.0,0.0,0.0)
718 FORMAT(* RRT *,1PE10.0,0.0,0.0)
720 FORMAT(* VPT *,1PE10.0,0.0,0.0)
722 FORMAT(* DP *,1PE10.0,0.0,0.0)
724 FORMAT(* FV *,1PE10.0,0.0,0.0)
726 FORMAT(* RSE2 *,1PE10.0,0.0,0.0)
728 FORMAT(* RSEF *,1PE10.0,0.0,0.0)
730 FORMAT(* TD *,1PE10.0,0.0,0.0)
732 FORMAT(* FAD *,1PE10.0,0.0,0.0)
734 FORMAT(* FWD *,1PE10.0,0.0,0.0)

```

C

STOP

END

SUBROUTINE WRT1(NP,M,KPT,ALABEL,DELN)

DIMENSION ALABEL(80),DELN(10,101)

WRITE(6,100) (ALABEL(L1),L1=1,80)

IF(NP.EQ.1) WRITE(6,200)

IF(NP.EQ.2) WRITE(6,202)

IF(NP.EQ.3) WRITE(6,204)

DO 10 I=1,M

KWK1=I-1

10 WRITE(6,102) KWK1,(DELN(L1,I),L1=1,KPT)

100 FORMAT(1H1, // ,1X,80A1)

102 FORMAT(1X,1I3,18F7.1)

200 FORMAT(// ,1X, *---RAW COULTER COUNTER DATA---*, // ,1X, *NCH*,
3X, *DELNCH*, /)202 FORMAT(// ,1X, *---COUNTS CORRECTED FOR CHANNELYZER NUMBER REJECTIO
N LOSSES---*, // ,1X, *NCH*, 3X, *DELNCC*, /)204 FORMAT(// ,1X, *---COUNTS CORRECTED FOR CHANNELYZER LOSSES AND COUL
TER COUNTER COINCIDENCE---*, // ,1X, *NCH*, 3X, *DELNA*, /)

C

RETURN

END


```

DATA (TH(K),K=1,9)/92.46,79.62,6.3856,0.+218,121.6,
1 0.,9.92E-04,-1.1E-07,5.66E-07

```

```

C ----- TH(6)=1.051+(((5.1E-06*TC)-9.4E-07)*TC) -----

```

```

C INPUT VARIABLES FOR THE MARQUARDT OPTIMIZATION ROUTINE

```

```

DO 10 K=1,9
10 TA(K)=TH(K)
DO 12 J=1,N
OMEGA1(J)=1.
OMEGA2(J)=1.
Z1(J)=OMEGA1(J)*CA(J)
12 Z1(N+J)=OMEGA2(J)*CN(J)
NOB=N+N
1+ CONTINUE
DO 16 K=1,NPAR
SIGNS(K)=1.
16 DIFF(K)=.005

```

```

C MARQUARDT OPTIMIZATION ROUTINE

```

```

CALL UHHAUS(NPROB,MODEL,NOB,Z1,NPAR,TH,DIFF,SIGNS,EPS1,EPS2,ITMAX,
1 RLM3DA,RNU,WK11)
CALL MODEL(NPROB,TH,WK1,NOB,NPAR)

```

```

C SUM OF SQUARES

```

```

SSE=0.
DO 20 J=1,N
EPSIL1(J)=CA(J)-ECA(J)
EPSIL2(J)=CN(J)-ECN(J)
X1=OMEGA1(J)*EPSIL1(J)
X2=OMEGA2(J)*EPSIL2(J)
20 SSE=SSE+(X1*X1)+(X2*X2)

```

```

C EMPIRICAL SOLUTION DENSITY MODEL

```

```

DO 22 J=1,N
22 ERHOL(J)=TH(6)+(((TH(6)+ECN(J))+TH(7))+ECN(J))+((TH(9)+ECA(J))

```

```

WRITE(6,200)
WRITE(6,205) NPAR,SSE
IF(NPAR.EQ.5) WRITE(6,210) (TH(K),K=1,5)
IF(NPAR.EQ.9) WRITE(6,210) (TH(K),K=1,9)
WRITE(6,215)
DO 30 J=1,N

```

```

30 WRITE(6,220) TAU(J),CA(J),ECA(J),EPSIL1(J),CN(J),ECN(J),EPSIL2(J)

```

```

C SOLUTION DENSITY MODEL CALCULATED WITH PARAMETERS ESTIMATED BY MISRA
C AND WITH PARAMETERS ESTIMATED HERE

```

```

IF(NPRG.EQ.1) GO TO 40
IF(NPAR.EQ.5) GO TO 32
IF(NPAR.EQ.9) GO TO 36

```

```

32 DO 34 J=1,N
34 Z2(J)=ERHOL(J)
GO TO 40

```

```

36 WRITE(6,225)
DO 38 J=1,N

```

```

X1=Z2(J)-ERHOL(J)
38 WRITE(6,220) TAU(J),Z2(J),ERHOL(J),X1
40 CONTINUE

```

```

C DISCRETE INDEPENDENT MODEL VARIABLE ,IT HAS NI-1 EXTRA VALUES
C BETWEEN THE DISCRETE DATA INDEPENDENT VARIABLE

```

```

IF(NPAR.EQ.9) GO TO 52
NI1=((N-1)*NI)+1
RNI=NI

```

```

NI=N-1
DO 50 J=1,N1
L1=((J-1)*NI)+1
L2=L1+NI
TAUI(L1)=TAU(J)
TAUI(L2)=TAU(J+1)
X1=(TAU(J+1)-TAU(J))/RNI
DO 50 K=2,NI
L=((J-1)*NI)+K
50 TAUI(L)=TAUI(L-1)+X1
52 CONTINUE

```

```

C
C PREDICTED MODEL VALUES
DO 60 L=1,NIT
60 ECAI(L)=TH(1)+TH(2)*EXP(-((TAUI(L)+TH(3))**TH(4)))
ECAU=ECAI(L)
ECNU=TH(5)
ERHOLD=TH(6)+(((TH(8)*ECNU)+TH(7))*ECNU)+(TH(9)*ECAU)
X1=(ECAU-(654.*ERHOLD))/ECNU
X2=TH(8)
X3=(X1/654.)+TH(7)
DO 62 L=1,NIT
X4=TH(5)+((TH(9)-.001529)*ECAI(L))
62 ECNI(L)=(-X3-SQRT((X3*X3)-(+.*X2*X4)))/(2.*X2)
DO 64 L=1,NIT
EVLI(L)=VLU/ECNI(L)*ECNU
EWTI(L)=((VLU*ECAU)-(VLU*ECNU*ECAI(L)/ECNI(L)))/.654)+WTS
EVTI(L)=EVLI(L)+(EWTI(L)/(RHOS*1000.))
ESCI(L)=EWTI(L)/EVTI(L)
ERHOLI(L)=TH(6)+(((TH(8)*ECNI(L))+TH(7))*ECNI(L))+(TH(9)*ECAI(L))
ECAEI(L)=ECNI(L)*EXP(6.2106+((1.0875*ECNI(L))-2+86.7)/(273.16+TC))
ESCI(L)=ESCI(L)-ECAEI(L)
ESAI(L)=ESCI(L)/ECAEI(L)
ESRI(L)=ECAI(L)/ECAEI(L)

```

```

C PREDICTED MODEL DERIVATIVE VALUES
EDCAI(L)=TH(4)*(-TH(2))*(((TAUI(L)+TH(3))**TH(4)-1.))
1 *EXP(-((TAUI(L)+TH(3))**TH(4)))
X1=(ECAI(L)*EVLI(L)/ECNI(L))+(.654*TH(7)*EVLI(L))+(1.308*TH(8)
1 *EVLI(L)*ECNI(L))-(.654*ERHOLI(L)*EVLI(L)/ECNI(L))
X2=EVLI(L)-(.654*TH(9)*EVLI(L))
EDCNI(L)=EDCAI(L)*X2/X1
EDVLI(L)=EDCNI(L)*(-EVLI(L))/ECNI(L)
64 EDWTI(L)=((EDCAI(L)*(-EVLI(L)))+(EDVLI(L)*(-ECAEI(L))))/.654

```

```

C
C PRINTED MODEL VARIABLES
WRITE(6,230)
DO 72 L=1,NIT
DO 70 J=1,N
IF(TAU(J).EQ.TAUI(L)) WRITE(6,235)
70 CONTINUE
72 WRITE(6,240) TAUI(L),ECAI(L),ECAEI(L),ESCI(L),ESAI(L),ESRI(L),
1 EWTI(L),ECNI(L),EVLI(L),EVTI(L),ERHOLI(L),EDWTI(L)

```

```

C
C PLOTTED MODEL VARIABLES
IF(NI.GT.10) NP=3
IF(NI.GT.5.AND.NI.LE.10) NP=2
IF(NI.LE.5) NP=1
DO 80 L=1,NIT,NP
80 CALL PLOTPT(TAUI(L),ECAI(L),+)
DO 82 J=1,N
82 CALL PLOTPT(TAU(J),CA(J),21)
DO 84 L=1,NIT,NP
84 CALL PLOTPT(TAUI(L),ECAEI(L),-)
CALL OUTPLT
CALL PRINTH(10H--CA,CAE--)

```

```

CALL OUTLIN
DO 86 L=1,NIT,NP
86 CALL PLOTPT(TAUI(L),ECNI(L),4)
DO 88 J=1,N
88 CALL PLOTPT(TAU(J),CN(J),34)
CALL OUTPLT
CALL PRINTW(6H--CN--)
CALL OUTLIN
DO 90 L=1,NIT,NP
90 CALL PLOTPT(TAUI(L),EHTI(L),4)
CALL OUTPLT
CALL PRINTW(6H--HT--)
CALL OUTLIN
DO 92 L=1,NIT,NP
92 CALL PLOTPT(TAUI(L),ECNI(L),4)
CALL OUTPLT
CALL PRINTW(6H--CN--)
CALL OUTLIN
DO 94 L=1,NIT,NP
94 CALL PLOTPT(TAUI(L),EVLI(L),4)
CALL OUTPLT
CALL PRINTW(6H--VL--)
CALL OUTLIN
DO 96 L=1,NIT,NP
96 CALL PLOTPT(TAUI(L),EVTI(L),4)
CALL OUTPLT
CALL PRINTW(6H--VT--)
CALL OUTLIN
DO 98 L=1,NIT,NP
98 CALL PLOTPT(TAUI(L),ERHOLI(L),4)
CALL OUTPLT
CALL PRINTW(6H--RHOL--)
CALL OUTLIN
DO 100 L=1,NIT,NP
100 CALL PLOTPT(TAUI(L),ESCI(L),4)
CALL OUTPLT
CALL PRINTW(10H- CA-CAE -)
CALL OUTLIN
DO 102 L=1,NIT,NP
102 CALL PLOTPT(TAUI(L),ESRI(L),4)
CALL OUTPLT
CALL PRINTW(10H- CA/CAE -)
CALL OUTLIN
DO 104 L=1,NIT,NP
104 CALL PLOTPT(TAUI(L),ESAI(L),4)
CALL OUTPLT
CALL PRINTW(10H DELCA/CAE)
CALL OUTLIN
DO 106 L=1,NIT,NP
106 CALL PLOTPT(TAUI(L),EDHTI(L),4)
CALL OUTPLT
CALL PRINTW(7H--DHT--)
CALL OUTLIN
C
IF(NPAR.EQ.5.AND.NPRG.EQ.2) GO TO 110
IF(NPAR.EQ.9.AND.NPRG.EQ.2) GO TO 110
NPAR=9
GO TO 14
C
110 CONTINUE
IF(NPNCH.EQ.6) GO TO 120
PUNCH(7,300) (TAUI(L),L=1,NIT,N)
PUNCH(7,302) (ECAI(L),L=1,NIT,N)
PUNCH(7,304) (ECNI(L),L=1,NIT,N)
PUNCH(7,306) (EVLI(L),L=1,NIT,N)

```

```

PUNCH(7,308) (EVTI(L),L=1,NIT,NI)
PUNCH(7,310) (EWTI(L),L=1,NIT,NI)
PUNCH(7,312) (ECSI(L),L=1,NIT,NI)
PUNCH(7,314) (ECAEI(L),L=1,NIT,NI)
PUNCH(7,316) (ERHOLI(L),L=1,NIT,NI)

```

```

120 CONTINUE

```

```

C
200 FORMAT(1H1,1X,+8H MODEL CA=B1+B2*EXP(-((TAU+EXP(B3))*B4)) + EPS)
205 FORMAT(///,1X,*NPAR=,I2,1X,*SSE=,PE12.3)
210 FORMAT(///,7X,*B1+,10X,*B2+,10X,*B3+,10X,*B4+,10X,*B5+,10X,*B6+,
1 10X,*B7+,10X,*B8+,10X,*B9+,//,1X,PE12.3,8E12.3)
215 FORMAT(///,4X,*TAU+,9X,*CA+,10X,*ECA+,9X,*CA-ECA+,6X,*CN+,10X,
1 *ECN+,9X,*CN-ECN+,//)
220 FORMAT(1X,1PE12.3,10E12.3)
225 FORMAT(1H1,1X,+X,*TAU+,9X,*ERHOL+,7X,*ERHOL+,5X,*DIFFR+,
1 /,17X,*MISRA+,7X,*THIS WRK+,//)
230 FORMAT(1H1,1X,*PREDICTED MODEL VALUES+,
1 //,3X,*TAU+,8X,*ECA+,8X,*ECAE+,7X,*DELCA+,6X,*DELCA/CAE+,2X,
2 *CA/CAE+,5X,*EWT+,8X,*ECN+,8X,*EVL+,8X,*EVT+,8X,*ERHOL+,6X,*EDWT+
3 ,//)
235 FORMAT(1X,1H)
240 FORMAT(1X,1PE11.3,11E11.3)

```

```

C
300 FORMAT(* ETAU * ,1PE10.3,6E10.3)
302 FORMAT(* ECA * ,1PE10.3,6E10.3)
304 FORMAT(* ECN * ,1PE10.3,6E10.3)
306 FORMAT(* EVL * ,1PE10.3,6E10.3)
308 FORMAT(* EVT * ,1PE10.3,6E10.3)
310 FORMAT(* EWT * ,1PE10.3,6E10.3)
312 FORMAT(* ECSI * ,1PE10.3,6E10.3)
314 FORMAT(* ECAE * ,1PE10.3,6E10.3)
316 FORMAT(* ERHOL * ,1PE10.3,6E10.3)

```

```

STOP
END
SUBROUTINE MODEL(NPROB,TH,WK1,NOB,NPAR)

```

```

C
C
C EMPIRICAL MODEL FOR THE ALUMINUM ION SOLUTION CONCENTRATION
C MODEL ECA=TH(1)+TH(2)*EXP(-((TAU(J)+EXP(TH(3)))*TH(4)))
C

```

```

C
C DIMENSION TH(4),WK1(1)
C COMMON /BL1/ TAU(20),TA(10),OMEGA1(20),OMEGA2(20)
C COMMON /BL2/ ECA(20),ECN(20)

```

```

C
N=NOB/2
DO 10 K=1,NPAR
10 TA(K)=TH(K)
DO 12 J=1,N
12 ECA(J)=TA(1)+TA(2)*EXP(-((TAU(J)+TA(3))*TA(4)))
ECA0=ECA(1)
ECN0=TA(5)
ERHOL0=TA(6)+(((TA(8)*ECN0)+TA(7))*ECN0)+(TA(9)*ECA0)
X1=(ECA0-(65+.*ERHOL0))/ECN0
X2=TA(8)
X3=(X1/65+.)+TA(7)
DO 14 J=1,N
14 X4=TA(5)+((TA(9)-1.529E-06)*ECA(J))
ECN(J)=(-X3-SQRT((X3+X3)-(X4+X4)))/(2.*X2)
DO 20 J=1,N
20 WK1(J)=OMEGA1(J)*ECA(J)
WK1(N+J)=OMEGA2(J)*ECN(J)
RETURN
END

```



```

      X10=ALOG(X1+SQRT(X1*X1+1.))
24  Y(I,J)=X10
C*****
C C
C SMOOTHING OF THE TRANSFORMED VARIABLE Y(I,J) WRT XV(I) BY MEANS
C OF LEAST SQUARES APPROXIMATION BY CUBIC SPLINES WITH VARIABLE KNOTS
      DO 50 J=1,N
C-NUMBER OF KNOTS AND INITIAL KNOT LOCATIONS, NXVK MAX=10 ---
      NXVK=7
C-----
      DO 25 I=1,M
      MWK=I
      IF(FVT(I,J).LT.1.) GO TO 26
25  CONTINUE
26  CONTINUE
      XVK(1)=XV(1)
      XVK(NXVK)=XV(MWK)
      INK=MWK/(NXVK-1)
      IE=NXVK-1
      DO 27 I=2,IE
27  XVK(I)=XV((I-1)*INK)
      DO 28 I=1,MWK
28  WK1(I)=Y(I,J)
      CALL ICSVKU(XV,WK1,MWK,XVK,NXVK,WK2,CV,9,ERROR,WK,IER)
C SMOOTHED VARIABLE
      K1=NXVK-1
      DO 32 I=1,MWK
      DO 29 L1=1,K1
      LK=L1
      IF(XV(I).GE.XVK(LK).AND.XV(I).LE.XVK(LK+1))GO TO 30
29  CONTINUE
30  DV=XV(I)-XVK(LK)
32  YH(I,J)=((CV(LK,3)*DV+CV(LK,2))*DV+CV(LK,1))*DV+WK2(LK)
      MWK1=MWK+1
      DO 34 I=MWK1,M
34  YH(I,J)=Y(I,J)
35  CONTINUE
C SMOOTHING OF THE SMOOTHED YH VARIABLE WITH RESPECT TO XTAU BY MEANS OF
C LEAST SQUARES APPROXIMATION BY CUBIC SPLINES WITH VARIABLE KNOTS
      DO 100 I=1,M
      DO 51 J=1,N
      J1=J
      IF(J1.GT.(N-2)) GO TO 98
      IF(FVT(I,J).GE.1.) GO TO 52
51  CONTINUE
52  JL(I)=J1
      NJ(I)=N-JL(I)+1
      NXT(I)=NJ(I)/7+2
      XTK(I)=XTAU(JL(I))
      XTK(NXT(I))=XTAU(N)
      IF(NXT(I).LE.2) GO TO 54
      JWK=NJ(I)/(NXT(I)-1)
      J1=NXT(I)-1
      DO 53 J=2,J1
53  XTK(J)=XTAU(JL(I)+((J-1)*JWK))
54  J1=NJ(I)
      DO 55 J=1,J1
      Z1(J)=XTAU(JL(I)+J-1)
55  Z2(J)=YH(I,JL(I)+J-1)
      CALL ICSVKU(Z1,Z2,NJ(I),XTK,NXT(I),WK2,CT,+,ERROR,WK,IER)
C SMOOTHED - SMOOTHED VARIABLE FUNCTION
      K1=NXT(I)-1
      DO 59 K=1,K1
      XI(I,K)=XTK(K)
      XU(I,K)=XTK(K+1)

```

```

      Y1(I,K)=WK2(K)
      Y2(I,K)=CT(K,1)
      Y3(I,K)=CT(K,2)
59     Y4(I,K)=CT(K,3)
      IJN(I)=1
      GO TO 100
98     IJN(I)=0
C     FOR X(J) BETWEEN XTK(LK) AND XTK(LK+1) WITH DT=X(J)-XTK(LK)
C     YHH(I,J)=((Y4(I,LK)*DT+Y3(I,LK))*DT+Y2(I,LK))*DT+Y1(I,LK)
100    CONTINUE
C
C     WRITE AND PLOT VARIABLES
C     EXPERIMENTAL DATA
      WRITE(5,550)
      WRITE(5,500) (TAU(J),J=1,N)
      WRITE(5,504)
      DO 102 I=1,M
102    WRITE(6,502) V(I),(FVT(I,J),J=1,N)
C
C     TRANSFORMED EXPERIMENTAL DATA
      WRITE(5,552)
      WRITE(5,500) (XTAU(J),J=1,N)
      WRITE(5,504)
      DO 106 I=1,M
106    WRITE(5,506) XV(I),(Y(I,J),J=1,N)
C
C     SMOOTHED DATA OR EMPIRICAL SIZE DISTRIBUTION MODEL VALUES
      WRITE(5,554)
      WRITE(5,500) (TAU(J),J=1,N)
      WRITE(5,504)
      DO 115 I=1,M
      IF(IJN(I).EQ.0) GO TO 113
      IF(JL(I)-1) 109,209,107
107    J1=JL(I)-1
      DO 108 J=1,J1
108    FVTMDL(I,J)=0.
109    K1=NXT(I)-1
      J1=JL(I)
      DO 112 J=J1,N
      X2=XTAU(J)
      DO 110 L1=1,K1
      LK=L1
      IF(X2.GE.XI(I,LK).AND.X2.LE.XU(I,LK)) GO TO 111
110    CONTINUE
111    DT=X2-XI(I,LK)
      X3=((Y4(I,LK)*DT+Y3(I,LK))*DT+Y2(I,LK))*DT+Y1(I,LK)
C*****
      X10=(EXP(X3)-EXP(-X3))/2.
112    FVTMDL(I,J)=X10
C*****
      GO TO 115
113    DO 114 J=1,N
114    FVTMDL(I,J)=0.
115    WRITE(6,502) V(I),(FVTMDL(I,J),J=1,N)
C
C     RELATIVE PERCENTAGE DIFFERENCE BETWEEN EXPERIMENTAL AND MODEL VALUES
      WRITE(5,556)
      WRITE(5,514) (TAU(J),J=1,N)
      WRITE(5,504)
      DO 118 I=1,M
      X1=CBRT(1.9098*V(I))
      DO 116 J=1,N
      WK1(J)=0.
      IF(FVT(I,J).GT.0.0) WK1(J)=(FVTMDL(I,J)-FVT(I,J))/FVT(I,J)*100.
116    CONTINUE

```

```

118 WRITE(6,516) X1,(HK2(J),J=1,N)
C MODEL VARIABLES
WRITE(5,558)
WRITE(5,562)
DO 120 I=1,M
IF(IJN(I).EQ.0) GO TO 120
K1=NXT(I)-1
WRITE(5,510) I,IJN(I),NXT(I),(XI(I,K),K=1,K1),(XU(I,K),K=1,K1)
WRITE(5,512) (Y1(I,K),K=1,K1),(Y2(I,K),K=1,K1)
WRITE(5,512) (Y3(I,K),K=1,K1),(Y4(I,K),K=1,K1)
120 WRITE(6,504)
C
DO 204 J=1,N
DO 200 I=1,M,2
X1=FVT(I,J)
X2=FVTMDL(I,J)
200 CALL PLOTPT(XV(I),X1,26)
CALL OUTPLT
WRITE(5,202) TAU(J)
202 FORMAT(/,1X,*FVT AND FVTMDL VS. XV*,10X,*TAU=*,1F6.2)
204 CONTINUE
C
DO 226 I=1,M,4
K1=NXT(I)-1
IF(IJN(I).EQ.0) GO TO 226
DELXT=(XTAU(N)-XTAU(1))/70
N1=70
X1=XTAU(1)-DELXT
DO 220 J1=1,N1
X1=X1+DELXT
DO 216 L1=1,K1
LK=L1
IF(X1.GE.XI(I,LK).AND.X1.LE.XU(I,LK)) GO TO 218
216 CONTINUE
GO TO 220
218 DT=X1-XI(I,LK)
X2=((Y4(I,LK)*DT+Y3(I,LK))*DT+Y2(I,LK))*DT+Y1(I,LK)
CALL PLOTPT(X1,X2,*)
Z1(J1)=X1
Z2(J1)=X2
220 CONTINUE
DO 222 J=1,N
X1=Y(I,J)
222 CALL PLOTPT(XTAU(J),X1,26)
CALL OUTPLT
I1=I
X5=CBRT(.19098*V(I))
WRITE(5,224) I1,XV(I),X5,V(I)
224 FORMAT(/,1X,*Y AND YHH VS. XTAU*,10X,*I=*,15,5X,*XV=*,
1PE11.3,5X,*D=*,1E11.3,5X,*V=*,1E11.3)
IF(NPNCH.NE.1) GO TO 225
PUNCH(7,612) (Z1(J1),J1=1,N1)
PUNCH(7,614) (Z2(J1),J1=1,N1)
PUNCH(7,616) (XTAU(J),J=1,N)
PUNCH(7,618) (Y(I,J),J=1,N)
225 CCNTINUE
226 CONTINUE
C PUNCH MODEL VARIABLES
IF(NPNCH.NE.1) GO TO 250
PUNCH(7,602) (JL(I),I=1,M)
PUNCH(7,604) (NJ(I),I=1,M)
PUNCH(7,606) (NXT(I),I=1,M)

```



```

PUNCH(7,608) (IJN(I),I=1,M)
DO 234 I=1,M
IF(IJN(I).EQ.0) GO TO 232
K1=NXT(I)-1
DO 230 K=1,K1
230 PUNCH(7,610) I,K,XI(I,K),XU(I,K),Y1(I,K),Y2(I,K),Y3(I,K),Y4(I,K)
232 CONTINUE
234 CONTINUE
230 CONTINUE
C
C PUNCH SMOOTHED DENSITY FUNCTION VALUES
IF(NPNCHE.NE.1) GO TO 262
DO 260 J=1,N
PUNCH(7,520) (ALABEL(L1,J),L1=1,80)
PUNCH(7,522) (VP(I),I=1,M)
260 PUNCH(7,522) (FVTMDL(I,J),I=1,M)
262 CONTINUE
C
C MOMENTS
Z2(1)=VP(1)**1.666667
Z3(1)=VP(1)*VP(1)
DO 270 I=1,M
Z1(I)=VP(I+1)-VP(I)
Z2(I+1)=VP(I+1)**1.666667
270 Z3(I+1)=VP(I+1)*VP(I+1)
C ZERO TH MOMENT
DO 282 J=1,N
X1=X2=0
DO 280 I=1,M
X1=X1+FVT(I,J)*Z1(I)
280 X2=X2+FVTMDL(I,J)*Z1(I)
RNT(J)=X1
282 RNTMDL(J)=X2
C TWO-THIRDS MOMENT WRT CRYSTAL VOLUME
DO 286 J=1,N
X1=X2=0
DO 284 I=1,M
X3=2.90158E-08*(Z2(I+1)-Z2(I))
X1=X1+FVT(I,J)*X3
284 X2=X2+FVTMDL(I,J)*X3
RAT(J)=X1
286 RATMDL(J)=X2
C FIRST MOMENT WRT CRYSTAL VOLUME
DO 290 J=1,N
X1=X2=0
DO 288 I=1,M
X3=1.21E-12*(Z3(I+1)-Z3(I))
X1=X1+FVT(I,J)*X3
288 X2=X2+FVTMDL(I,J)*X3
RWT(J)=X1
290 RWTMDL(J)=X2
C
C PRINT AND PLOT MOMENTS
WRITE(5,530)
DO 300 J=1,N
300 WRITE(5,532) RNT(J),RNTMDL(J),RAT(J),RATMDL(J),RWT(J),RWTMDL(J)
DO 302 J=1,N
CALL PLOTPT(XTAU(J),RNT(J),34)
302 CALL PLOTPT(XTAU(J),RNTMDL(J),4)
CALL OUTPLT
DO 304 J=1,N
CALL PLOTPT(XTAU(J),RAT(J),21)
304 CALL PLOTPT(XTAU(J),RATMDL(J),4)
CALL OUTPLT
DO 306 J=1,N

```

```

306 CALL PLOTPT(XTAU(J),RNT(J),3)
CALL PLOTPT(XTAU(J),RNTMDL(J),4)
CALL OUTPLT

```

```

C
500 FORMAT(9X,14F9.3)
502 FORMAT(1X,1PE9.2,1+E9.2)
504 FORMAT(1X,1H )
506 FORMAT(1X,15F9.3)
510 FORMAT(3I5,1PE12.4,9E12.4)
512 FORMAT(15X,1PE12.4,9E12.4)
514 FORMAT(7X,14F6.1)
516 FORMAT(1X,15F6.1)

```

```

C
520 FORMAT(80A1)
522 FORMAT(1PE10.3,7E10.3)
524 FORMAT(10X,7F10.3)
530 FORMAT(1H1,5X,*RNT*,9X,*RNTMDL*,6X,*RAT*,9X,*RATMDL*,6X,*RWT*,
1 9X,*RWTMDL*,/)
532 FORMAT(1X,1PE12.4,10E12.4)

```

```

C
550 FORMAT(1H1,1X,*EXPERIMENTAL DATA*,// ,11X,*TAU(J)*,/ ,2X,*V*,8X,
1 *FVT(I,J)*,/)
552 FORMAT(1H1,1X,*TRANSFORMED EXPERIMENTAL DATA*,// ,13X,*XTAU(J)*,
1 / ,5X,*XV(I)*,3X,*Y(I,J)*,/)
554 FORMAT(1H1,1X,*EMPIRICAL SIZE DISTRIBUTION MODEL VALUES*,// ,11X,
1 *TAU(J)*,/ ,2X,*V*,8X,*FVTMDL(I,J)*,/)
556 FORMAT(1H1,1X,*RELATIVE PERCENTAGE DIFFERENCE BETWEEN*,/ ,2X,
1 *EXPERIMENTAL AND MODEL VALUES*,// , 3X,*TAU(J)*,/,
2 *X*,0*, 5X,*EPSRLT(I,J)*,/)
558 FORMAT(1H1,1X,*MODEL VARIABLES*,//)
562 FORMAT(/ ,+X,*I*,2X,*IUN*,2X,*NXT*,5X,*XI*,20X,*XU*,/ ,
1 20X,*Y1*,20X,*Y2*,/ ,20X,*Y3*,20X,*Y4*,/ )

```

```

C
602 FORMAT(* JL *,15I5)
604 FORMAT(* NJ *,15I5)
606 FORMAT(* NXT *,15I5)
608 FORMAT(* IUN *,15I5)
610 FORMAT(* K *,15I5,5X,*K=*,112,5X,1PE10.3,5E10.3)
612 FORMAT(* XTAUMDL *,1PE10.3,6E10.3)
614 FORMAT(* YHH *,1PE10.3,6E10.3)
616 FORMAT(* XTAU *,1PE10.3,6E10.3)
618 FORMAT(* Y *,1PE10.3,6E10.3)
STOP
END

```

PROGRAM TST(INPUT,OUTPUT,PUNCH,TAPES=INPUT,TAPE6=OUTPUT,
1 TAPE7=PUNCH)

C-EMPIRICAL GROWTH RATE MODEL--CA--THIS PROGRAM ESTIMATES THE PARAMETERS
OF A GIVEN EMPIRICAL GROWTH RATE MODEL BY MEANS OF THE METHOD OF
PSEUDO MOMENTS AND AUXILIARY EMPIRICAL MODELS

DESCRIPTION OF PRINCIPAL VARIABLES

M NUMBER OF CRYSTAL SIZE INTERVALS , NUMBER OF DISCRETE SIZES =M+1
N NUMBER OF DISCRETE BATCH SAMPLE TIME INTERVALS,NUMBER OF DISCRETE
BATCH TIMES =N+1
NT NUMBER OF DISCRETE BATCH MODEL TIME INTERVALS,
NUMBER OF DISCRETE BATCH MODEL TIMES =NT+1
NI NUMBER OF MODEL TIME INTERVALS BETWEEN EACH TWO SUCCESSIVE
BATCH TIMES , MIN NI=2
RNCT VARIABLE RELATED TO THE ESTIMATED NUMBER OF CRYSTALS
WITH A SIZE LESS THAN THE CUT-OFF SIZE
PHIW(J) VARIABLE RELATED TO TOTAL CRYSTAL WEIGHT
PHIA(J) VARIABLE RELATED TO TOTAL CRYSTAL AREA
PHIG(J) GROWTH RATE CRYSTAL AREA SHAPE FUNCTION
NCTL(K) PROGRAM CONTROL VARIABLE
1 =1 ESTIMATE THE NUMBER OF CRYSTALS WITH A SIZE LESS THAN THE
CUT-OFF SIZE, =0 DO NOT
2 =1 ESTIMATE THE VALUE OF PHIIH(1) ALONG WITH THE GROWTH RATE
PARAMETERS, =0 PHIIH(1) IS TREATED AS A KNOWN DETERMINISTIC
VARIABLE AND THEN EQUALS PHIW(1)

DIMENSION TH(5),SIGNS(5),DIFF(5),Y(20),WK(900),NPR(5),TG(5,5)
DIMENSION CRN0(200),CRN1(200),CRA0(200),CRA1(200),CRWJ(200),
1 CRW1(200),WTSLT(200)
COMMON/BL1/M,M1,N,N1,NI,NT,NT1,NCTL(5)
COMMON/BL2/TAUE(20),TAU(200),V(102),D(102),TTR(200),RNCT(4)
COMMON/BL3/CA(200),CAE(200),CN(200),WT(200),VL(200),VT(200)
COMMON/BL4/PHIG(102),PHIA(200),PHIW(200),GO(200),PHIIH(200)
COMMON/BL5/Z1(200),Z2(200),Z3(200),OMEGA(20)
INTEGER H
EXTERNAL HOLGRT,HOLNCT

C
DATA 00,NI/1,0E-01,7/
DATA NPUNCH/1/
DATA (NCTL(H),H=1,2)/1,J/
DATA (NPR(H),H=1,5)/1,1,1,1,0/
DATA (RNCT(H),H=1,4)/0,0,0,0/
DATA (TG(1,H),H=1,2)/3.30E-03,2.00/
DATA (TG(2,H),H=1,2)/15.0,2.00/
DATA (TG(3,H),H=1,2)/0.0,0.00/
DATA (TG(4,H),H=1,2)/9.21,0.25+/
DATA (WTSLT(J),J=1,14)/2.85,1.89,53.67,72.75,84.8+,96.25,
1 103.7,113.4,137.6,150.9,163.3,177.2,181.4,186.5/

C READ-IN CRYSTAL SIZE DISTRIBUTION
CALL EMP5DR(1,J,M,N1,Z1,1,TAUE,J,X1)
M=M+1
N=N1+1
NT=(N1-1)*NI
NT1=NT+1

C ESTIMATED MINIMUM CRYSTAL SIZE
V(1)=.323599*DU*DU

C DISCRETE CRYSTAL SIZES
DO 40 I=2,M1
+0 V(I)=Z1(I-1)
DO 41 I=1,M1

```

41 D(I)=1.2407*CBRT(V(I))
C DISCRETE BATCH MODEL TIMES
  RNI=NI
  NI1=NI+1
  TAU(1)=TAUE(1)
  DO 46 J=2,N
  X1=(TAUE(J+1)-TAUE(J))/RNI
  NIWK=(J-1)*NI
  DO 46 JWK=2,NI1
46 TAU(NIWK+JWK)=TAU(NIWK+JWK-1)+X1
  DO 47 J=1,NT1
47 TTR(J)=ALOG(TAU(J)+SQRT(TAU(J)*TAU(J)+1.))
C CRYSTAL ENVIRONMENT MODEL VALUES
  CALL EMPENV(0,TAU(1),CA(1),CAE(1),CN(1),WT(1),VL(1),VT(1))
  DO 50 J=2,NT1
50 CALL EMPENV(1,TAU(J),CA(J),CAE(J),CN(J),WT(J),VL(J),VT(J))
C ESTIMATE OF THE NUMBER OF CRYSTALS WITH A SIZE LESS THAN THE CUT-OFF SIZE
  DO 55 J=1,NT1
55 Z1(J)=WTSLT(J)
  DO 58 L=1,NT1
  DO 56 J=1,N
  JT=J
  IF(TAU(L).GE.TAUE(J).AND.TAU(L).LE.TAUE(J+1)) GO TO 57
56 CONTINUE
57 X1=(Z1(J+1)-Z1(J))/(TAUE(J+1)-TAUE(J))
  X2=Z1(J)-(X1*TAUE(J))
58 WTSLT(L)=X2+(X1*TAU(L))
  IF(NCTL(1),EQ.0) GO TO 52
  DO 51 H=1,3
  TH(H)=1.
  DIFF(H)=0.01
51 SIGNS(H)=1.
  CALL UHHAUS(9,MOLNCT,NT1,WTSLT,3,TH,DIFF,SIGNS,1.E-10,1.E-04,
  1,100,0.01,10.0,WK)
  DO 53 H=1,3
53 RNCT(H)=TH(H)+1.
  WRITE(6,606) (RNCT(H),H=1,3)
C EFFECT OF THE CUT-OFF SIZE
  DO 10 H=1,4
10 Z1(H)=0.
  DO 14 J=1,NT1
  XS0=XS1=0.
  DO 12 I=1,M
  CALL EMPSDR(0,Z1,H,N1,Z2,I,TAUE,TAU(J),X0)
  CALL EMPSDR(0,RNCT,H,N1,Z2,I,TAUE,TAU(J),X1)
  XS0=XS0+(X0*(V(I+1)-V(I)))
12 XS1=XS1+(X1*(V(I+1)-V(I)))
  CRNB(J)=XS0
14 CRN1(J)=XS1
  X2=5.8515E-12
  DO 18 I=1,M1
18 Z3(I)=.6*(V(I)**1.66667)
  DO 22 J=1,NT1
  XS0=XS1=0.
  DO 20 I=1,M
  CALL EMPSDR(0,Z1,H,N1,Z2,I,TAUE,TAU(J),X0)
  CALL EMPSDR(0,RNCT,H,N1,Z2,I,TAUE,TAU(J),X1)
  XS0=XS0+(X0*(Z3(I+1)-Z3(I)))
20 XS1=XS1+(X1*(Z3(I+1)-Z3(I)))
  CRA0(J)=X2*XS0
22 CRA1(J)=X2*XS1

```

```

X2=2.42E-12
DO 24 I=1,M1
2+ Z3(I)=.5*V(I)*V(I)
DO 28 J=1,NT1
XS0=XS1=0.
DO 26 I=1,M
CALL EMPSDR(0,Z1,M,N1,Z2,I,TAUE,TAU(J),X0)
CALL EMPSDR(0,RNCT,M,N1,Z2,I,TAUE,TAU(J),X1)
XS0=XS0+(X0*(Z3(I+1)-Z3(I)))
26 XS1=XS1+(X1*(Z3(I+1)-Z3(I)))
CRW0(J)=X2*XS0
28 CRW1(J)=X2*XS1
DO 30 J=1,NT1,3
XC=ALOG(CRW0(J)+SQRT(CRW0(J)*CRW0(J)+1.))
X1=ALOG(CRW1(J)+SQRT(CRW1(J)*CRW1(J)+1.))
CALL PLOTPT(TTR(J),X0,10)
30 CALL PLOTPT(TTR(J),X1,34)
CALL OUTPLT
DO 32 J=1,NT1,3
CALL PLOTPT(TTR(J),CRA0(J),10)
32 CALL PLOTPT(TTR(J),CRA1(J),21)
CALL OUTPLT
DO 34 J=1,NT1,3
CALL PLOTPT(TTR(J),CRW0(J),10)
CALL PLOTPT(TTR(J),CRW1(J),43)
34 CALL PLOTPT(TTR(J),WTSLT(J),39)
CALL OUTPLT
IF(NPNCH.EQ.1) PUNCH(7,612) (TAU(J),J=1,NT1)
IF(NPNCH.EQ.1) PUNCH(7,614) (CRW1(J),J=1,NT1)
IF(NPNCH.EQ.1) PUNCH(7,616) (CRA1(J),J=1,NT1)
IF(NPNCH.EQ.1) PUNCH(7,618) (CRW1(J),J=1,NT1)

```

C

52 CONTINUE

C

C CRYSTAL WEIGHT TERM

```

DO 54 H=1,3
54 TH(H)=RNCT(H)
CALL MDLNCT(9,TH,Z1,NT1,3)

```

C

C-CRYSTAL AREA SHAPE FUNCTION

```

DO 60 I=1,M1
60 PHIG(I)=2.418*(V(I)**.66667)

```

C

C CRYSTAL AREA TERM

```

X1=5.8515E-12
DO 61 I=1,M1
61 Z2(I)=.6*(V(I)**1.66667)
DO 64 J=1,NT1
XS=0.
DO 62 I=1,M
CALL EMPSDR(0,RNCT,M,N1,Z1,I,TAUE,TAU(J),X3)
62 XS=XS+(X3*(Z2(I+1)-Z2(I)))
64 PHIA(J)=X1*XS

```

C

C WRITE AND PLOT

```

WRITE(6,600)
WRITE(6,602)
DO 65 I=1,M1
X1=3.1*10**D(I)*D(I)/(PHIG(I)+2.)
WRITE(6,600) D(I),V(I),PHIG(I),X1
65 CALL PLOTPT(D(I),X1,39)
CALL RANGES(D(1),D(M1),0.,2.)
CALL OUTPLT
WRITE(6,604)
DO 67 J=1,NT1

```

```

X1=0
DO 66 L=1,N1
IF (ABS(TAU(J)-TAUE(L)).LT.1.E-04) X1=1.
66 CONTINUE
X2=(PHIW(J)-WTSLT(J))/WTSLT(J)*100.
IF (X1.EQ.1.) WRITE(6,608)
WRITE(5,500) TAU(J),PHIA(J),PHIW(J),WTSLT(J),X2
IF (X1.EQ.1.) WRITE(6,608)
CALL PLOTPT(TTR(J),PHIW(J),23)
67 CALL PLOTPT(TTR(J),WTSLT(J),4)
CALL OUTPLT
DO 68 J=1,NT1
68 CALL PLOTPT(TTR(J),PHIA(J),21)
CALL OUTPLT

```

C
C
C-MARQUARDT OPTIMIZATION OF THE GROWTH RATE MODELS PARAMETERS

```

71 CONTINUE
IF (NPR(1).EQ.1) GO TO 72
IF (NPR(2).EQ.1) GO TO 73
IF (NPR(3).EQ.1) GO TO 74
IF (NPR(4).EQ.1) GO TO 75
GO TO 110
72 NPR(1)=0
NPROB=1
NPAR=2
GO TO 78
73 NPR(2)=0
NPROB=2
NPAR=2
GO TO 78
74 NPR(3)=0
NPROB=3
NPAR=2
GO TO 78
75 NPR(4)=0
NPROB=4
NPAR=2
78 ITMAX=100
EPS1=1.E-10
EPS2=1.E-04
RLAMBDA=0.01
RNU=10.0
NOB=N1
DO 79 KP=1,NPAR
SIGNS(KP)=1.
DIFF(KP)=0.01
79 TH(KP)=TG(NPROB,KP)
DO 82 J=1,N1
82 OMEGA(J)=1.
DO 84 J=1,NOB
X1=PHIW((J-1)*NI+1)
84 Y(J)=OMEGA(J)*X1
IF (NCTL(2).EQ.0) GO TO 90
NPAR=NPAR+1
SIGNS(NPAR)=1.
DIFF(NPAR)=0.01
TH(NPAR)=PHIW(1)
90 CONTINUE

```

C
C
C
CALL UHHAUS(NPROB,MOLGRT,NOB,Y,NPAR,TH,DIFF,SIGNS,EPS1,EPS2,
1 ITMAX,RLAMBDA,RNU,WK)
CALL MOLGRT(NPROB,TH,Z1,NOB,NPAR)

```

L=2
WRITE(5,610)
DO 92 J=1,NT1
X3=0.
DO 91 L=1,N1
IF(ABS(TAU(J)-TAUE(L)).LT.1.E-04) X3=1.
91 CONTINUE
X1=(PHIW(J)-PHIWH(J))/PHIW(J)*100.
IF(X3.EQ.1.) WRITE(6,608)
WRITE(5,500) TAU(J),PHIW(J),PHIWH(J),X1,GO(J)
IF(X3.EQ.1.) WRITE(6,608)
92 CALL PLOTP(TTR(J),PHIWH(J),4)
DO 93 J=1,NT1
JWK=(J-1)*N1+J
Z1(J)=PHIW(JWK)
93 CALL PLOTP(TTR(JWK),PHIW(JWK),4)
CALL OUTPLT
IF(NPNCH.EQ.1) PUNCH(7,622) (Z1(J),J=1,N1)
IF(NPNCH.EQ.1) PUNCH(7,626) (PHIWH(J),J=1,NT1)
C
DO 108 H=1,5
IF(NPR(H).EQ.1) GO TO 71
108 CONTINUE
110 CONTINUE
C
500 FORMAT(1X,1PE12.+,1CE12.+)
600 FORMAT(1H1,3X,*CRYSTAL AREA SHAPE FUNCTION*,/)
602 FORMAT(3X,*0*,11X,*V*,11X,*PHIG*,3X,*SPHR*,/)
604 FORMAT(1H1,3X,*TAU*,9X,*PHIA*,8X,*PHIW*,3X,*WT*,10X,*RLDVT*,/)
606 FORMAT(///,1X,*ESTIMATED NUMBER CUT-OFF PARAMETER RNCT=*,F10.3)
608 FORMAT(1X,1H)
610 FORMAT(1H,6X,*TAU*,3X,*PHIW*,3X,*PHIWH*,7X,*RLDVT*,7X,*GO*,/)
612 FORMAT(* TAUCR * ,1PE10.0,0E10.3)
614 FORMAT(* CRN1 * ,1PE10.0,0E10.3)
616 FORMAT(* CRA1 * ,1PE10.0,0E10.3)
618 FORMAT(* CRW1 * ,1PE10.0,0E10.3)
620 FORMAT(* PHIWH * ,1PE10.0,0E10.3)
622 FORMAT(* PHIW * ,1PE10.0,0E10.3)
C
STOP
END
SUBROUTINE MGLNCT(NPROB,TH,YH,NOB,NPAR)
C
C TOTAL CRYSTAL WEIGHT CALCULATED FROM CRYSTAL SIZE DISTRIBUTION MEASUREMENTS C
C FROM SIZE DISTRIBUTION MODEL VALUES
C
DIMENSION TH(NPAR),YH(NOB)
COMMON/BL1/M,M1,N,N1,NI,NT,NT1,NCTL(5)
COMMON/BL2/TAUE(20),TAU(200),V(102),D(102),TTR(200),RNCT(4)
COMMON/BL3/CA(200),CAE(200),CN(200),WT(200),VL(200),VT(200)
COMMON/BL4/PHIG(102),PHIA(200),PHIW(200),GO(200),PHIWH(200)
COMMON/BL5/Z1(200),Z2(200),Z3(200),OMEGA(20)
DO 8 K=1,5
RNCT(K)=TH(K)+1.
X1=2.425-12.
DO 10 I=1,M1
Z2(I)=.5*V(I)*V(I)
DO 14 J=1,NT1
XS=0.
DO 12 I=1,M
CALL ZMPSOR(0,RNCT,M,N1,Z1,I,TAUE,TAU(J),X3)
12 XS=XS+(X3*(Z2(I+1)-Z2(I)))
14 PHIW(J)=X1*XS
DO 16 J=1,NT1
16 YH(J)=PHIW(J)

```

```

RETURN
END
SUBROUTINE MDLGR(TH, YH, NOB, NPAR)

```

```

C THIS SUBROUTINE CALCULATES GROWTH RATE MODEL VALUES GIVEN THE MODEL
C PARAMETER VALUES

```

```

DIMENSION TH(NPAR), YH(NOB)
COMMON/BL1/H, M1, N, N1, NI, NT, NT1, NCTL(5)
COMMON/BL2/TAU(20), TAU(200), V(102), D(102), TTR(200), RNCT(4)
COMMON/BL3/CA(200), CAE(200), CN(200), WT(200), VL(200), VT(200)
COMMON/BL4/PHIG(102), PHIA(200), PHIW(200), GD(200), PHIWH(200)
COMMON/BL5/Z1(200), Z2(200), Z3(200), OMEGA(20)

```

```

C
GO TO (10, 14, 18, 22), NPROB
10 BG1=TH(1)
   BG2=TH(2)
   DO 11 J=1, NT1
      X1=CA(J)-CAE(J)
11  GD(J)=BG1*(X1**BG2)
   GO TO 30
14  BG1=TH(1)
   BG2=TH(2)
   DO 15 J=1, NT1
      X1=(CA(J)-CAE(J))/CAE(J)
15  GD(J)=BG1*(X1**BG2)
   GO TO 30
18  BG1=TH(1)
   BG2=TH(2)
C PARAMETER CONSTRAINT BG2.LT.1. AND .GT.0.
   BG2MX=1.
   IF(BG2-BG2MX) 60, 50, 50
50  DO 52 J=1, NT1
      X1=(CA(J)-CAE(J))/CAE(J)
52  GD(J)=BG1*X1*X1*TANH((2.*BG2MX-BG2)/X1)
   GO TO 30
60  CONTINUE
   DO 19 J=1, NT1
      X1=(CA(J)-CAE(J))/CAE(J)
19  GD(J)=BG1*X1*X1*TANH(BG2/X1)
   GO TO 30
22  BG1=TH(1)
   BG2=TH(2)
   DO 23 J=1, NT1
      X1=(CA(J)-CAE(J))/CAE(J)
23  GD(J)=BG1*(X1**(5./6.))*EXP(-BG2/X1)
30  CONTINUE
   PHIWH(1)=PHIW(1)
   IF(NCTL(2).EQ.1) PHIWH(1)=TH(3)
   DO 31 J=1, NT1
31  Z1(J)=GD(J)*PHIA(J)
   DO 32 J=2, NT1
32  PHIWH(J)=PHIWH(J-1)+((TAU(J)-TAU(J-1))*(Z1(J)+Z1(J-1)))/2.)
   DO 34 J=2, N1
34  YH(J)=OMEGA(J)*PHIWH((J-1)*NI+1)
RETURN
END
SUBROUTINE EMPENV(NCLC, TAU, CA, CAE, CN, WT, VL, VT)

```

```

C EMPIRICAL MODEL FOR THE SOLUTION CONCENTRATION VARIABLES

```

```

DIMENSION TH(9)
INTEGER H

```

```

C IF(NCLC.EQ.0) GO TO 10

```



```

GO TO 12
10 CONTINUE
DATA VLD,WT0,THETA,RHOS,X2,+30.2+.85,85.1,2.42/
DATA (TH(1),M=1,9),92.48,79.82,-0.9529,0.4218,120.1,0.1008E+01,
1 0.9920E-03,-0.1180E-06,0.5660E-03/
CA0=TH(1)+TH(2)*EXP(-(EXP(TH(3))**TH(4)))
CN0=TH(5)
RHOL0=TH(6)+(((TH(8)*CN0)+TH(7))*CN0)+(TH(9)*CA0)
X1=(CA0-(654.*RHOL0))/CN0
X2=TH(8)
X3=(X1/654.)+TH(7)
C
12 CONTINUE
Z1=EXP(TH(3))
CA=TH(1)+TH(2)*EXP(-((TAU+Z1)**TH(4)))
X4=TH(5)+((TH(9)-.901529)*CA)
CN=(-X3-SQRT((X3*X3)-(4.*X2*X4)))/(2.*X2)
CAE=CN*EXP(6.2106+((-2+86.7+(1.08753*CN))/(273.15+THETA)))
VL=VL0*CN0/CN
WT=((VL0*CA0)-(VL)*CN0*CA/CN)/.654+WT0
VT=VL+(WT/(1000.*RHOS))
RETURN
END
SUBROUTINE EMPSDR(NCLC,RNCT,M1,NX,VP,L,TAUE,TAU,FVTH)
C
C CRYSTAL SIZE DISTRIBUTION
C
DIMENSION FVT(100,14),ALABEL(80)
DIMENSION VP(M1),TAUE(NX),RNCT(4),AN(4),BN(4)
C
IF(NCLC.EQ.0) GO TO 20
C-----
DATA M,N/100,14/
M1=M+1
NX=N
N1=N-1
READ(5,582) (TAUE(J),J=1,N)
DO 18 J=1,N
READ(5,504) (ALABEL(L1),L1=1,80)
READ(5,500) (VP(I),I=1,M1)
18 READ(5,560) (FVT(I,J),I=1,M)
C-----
20 CONTINUE
C IF L=1, V IS LESS THAN THE CUT-OFF SIZE AND THE DENSITY FUNCTION
C VALUE IS ESTIMATED AS FOLLOWS
LW=L-1
IF(L.GT.1) GO TO 28
LW=L
C INTERPOLATE WRT TAUE
28 DO 30 J=1,N1
J1=J
IF(TAU.GE.TAUE(J).AND.TAU.LE.TAUE(J+1)) GO TO 32
30 CONTINUE
32 X1=(FVT(LW,J1+1)-FVT(LW,J1))/(TAUE(J1+1)-TAUE(J1))
X2=FVT(LW,J1)-(X1*TAUE(J1))
FVTH=X2+(X1*TAU)
IF(L.GT.1) GO TO 40
AN(1)=(RNCT(2)-RNCT(1))/(TAUE(2)-TAUE(1))
AN(2)=(RNCT(3)-RNCT(2))/(TAUE(4)-TAUE(2))
BN(1)=RNCT(1)-(AN(1)*TAUE(1))
BN(2)=RNCT(2)-(AN(2)*TAUE(2))
IF(TAU.GE.TAUE(1).AND.TAU.LT.TAUE(2)) FVTH=(AN(1)*TAU+BN(1))*FVTH
IF(TAU.GE.TAUE(2).AND.TAU.LT.TAUE(4)) FVTH=(AN(2)*TAU+BN(2))*FVTH
IF(TAU.GE.TAUE(4)) FVTH=RNCT(3)*FVTH
40 CONTINUE

```

C
500 FORMAT(1PE10.3,7E10.3)
502 FORMAT(14X,7F10.3)
504 FORMAT(80A1)

C
RETURN
END

```
PROGRAM TST(INPUT,OUTPUT,PUNCH,TAPES=INPUT,TAPE6=OUTPUT,
1 TAPE7=PUNCH)
```

```
C-EMPIRICAL AGGLOMERATION RATE MODEL--CB-- THIS PROGRAM ESTIMATES THE
C PARAMETERS OF A GIVEN EMPIRICAL AGGLOMERATION RATE MODEL BY MEANS OF
C THE METHOD OF PSEUDO MOMENTS AND AUXILIARY EMPIRICAL MODELS
```

```
C DESCRIPTION OF PRINCIPAL VARIABLES
```

```
C M NUMBER OF CRYSTAL SIZE INTERVALS , NUMBER OF DISCRETE
C SIZES =M+1
C MP NUMBER OF DIFFERENT PSEUDO MOMENTS WHICH EQUALS THE NUMBER
C OF INTEGRATED INTERVALS WRT THE VARIABLE V
C N NUMBER OF DISCRETE BATCH SAMPLE TIME INTERVALS, NUMBER OF
C BATCH TIMES =N+1
C NT NUMBER OF DISCRETE BATCH MODEL TIME INTERVALS, NUMBER OF DISCRETE
C BATCH MODEL TIMES =NT+1
C NI NUMBER OF MODEL TIME INTERVALS BETWEEN EACH TWO SUCCESSIVE
C BATCH TIMES , MIN NI=2
C RNCT VARIABLE RELATED TO THE ESTIMATED NUMBER OF CRYSTALS IN THE
C CUT-OFF SIZE INTERVAL
C NPRB NUMBER OF PROBLEMS
C NPR(U) NUMBER OF PARAMETERS
C ETAA(K,Q) ACCUMULATION TERM RELATED VARIABLE
C ETAG(K,Q) GROWTH RATE TERM RELATED VARIABLE
C ETAC(K,Q) AGGLOMERATION RATE TERM RELATED VARIABLE
```

```
C DIMENSION TH(5),SIGNS(5),DIFF(5),Y(126),NPR(3),WK(250)
C DIMENSION RNCT(4)
C COMMON/BL1/M,M1,N,N1,NI,NT,NT1,MP,NFLAG1,C1
C COMMON/BL2/TAUE(14),TAU(53),V(52),V23(52),DELV(5),ONT(5,53)
C COMMON/BL3/CA(53),CAE(53),CN(53),WT(53),VL(53),VT(53),GD1(53)
C COMMON/BL4/PHIEA(53),ETAA(9,53),ETAAM(9,53),ETAG(9,53),ETAG1(9,53)
C COMMON/BL5/ETAC(9,53),ETAC1(9,53),PHION(9,53)
C COMMON/BL6/ALPHA(9),BETA(9),KL(9),KU(9),TA(5),TAO(5)
C COMMON/BL7/Z1(102),Z2(102),Z3(102),OMEGA(9,14)
C INTEGER Q,H,P
C EXTERNAL MDLAGL
```

```
C *****
C DATA MP,NI/9,+/
C DATA NPNCH/1/
C DATA DO/1.0E-01/
C DATA NPR(1),NPRB/3,1/
C DATA (RNC(H),H=1,+)/2.33,7.09,1.30,0./
C DATA (TA(KP),KP=1,5)/.2018E-11, .30+6E+01, .6601E-02, 0. , 0./
```

```
C *****
C DO 10 H=1,5
C 10 TAO(H)=TA(H)
```

```
C READ-IN CRYSTAL SIZE DISTRIBUTION
C CALL EMPSDR(1,0,M9,N1,Z1,1,TAUE,0.,X1)
C N=N1-1
C NT=(N1-1)*NI
C NT1=NT+1
```

```
C ESTIMATED MINIMUM CRYSTAL SIZE
C V(1)=0.523599*00*00*00
C X1=CBRT(V(1))
C V23(1)=X1*X1
```

```
C DISCRETE CRYSTAL SIZES
C M91=M9+1
C Z2(1)=V(1)
C DO 40 I=2,M91
```

```

      Z2(I)=Z1(I-1)
+0 Z3(I-1)=Z2(I)-Z2(I-1)
C DISCRETE BATCH MODEL TIMES
  RNI=NI
  NI1=NI+1
  TAU(1)=TAUE(1)
  DO 45 J=1,N
    X1=(TAUE(J+1)-TAUE(J))/RNI
    NIWK=(J-1)*NI
    DO 46 JWK=2,NI1
      46 TAU(NIWK+JWK)=TAU(NIWK+JWK-1)+X1
C CRYSTAL ENVIRONMENT MODEL VALUES
  CALL EMPENV(1,TAU(1),CA(1),CAE(1),CN(1),WT(1),VL(1),VT(1))
  DO 50 J=2,NT1
    50 CALL EMPENV(J,TAU(J),CA(J),CAE(J),CN(J),WT(J),VL(J),VT(J))
C SIZE DISTRIBUTION MODEL VALUES
  M=(M9-1)/2+1
  M1=M+1
  DO 52 J=1,NT1
    CALL EMPSDR(0,RNCT,M9,N1,Z1,1,TAUE,TAU(J),X1)
    DNT(1,J)=X1*Z3(1)
    L=1
    DO 52 I=2,M
      XS=0.
      DO 51 K=1,2
        L=L+1
        CALL EMPSDR(0,RNCT,M9,N1,Z1,L,TAUE,TAU(J),X1)
      51 XS=XS+X1*Z3(L)
      52 DNT(I,J)=XS
      V(2)=Z2(2)
      L=2
      DO 53 I=3,M1
        L=L+2
      53 V(I)=Z2(L)
      DO 54 I=2,M1
        X1=CBRT(V(I))
        V23(I)=X1*X1
      54 DELV(I-1)=V(I)-V(I-1)
C AGGLOMERATION WEIGHTING FUNCTION AND TO BE INTEGRATED WRT V INTERVALS
  IL=-2
  DO 55 K=1,MP
    IL=IL+5
    IU=IL+5
    ALPHA(K)=V(IL)
    BETA(K)=V(IU)
    KL(K)=IL
    55 KU(K)=IU
C AGGLOMERATION WEIGHTING FUNCTION CONSTANT
  XS=0.
  DO 56 I=1,M
    56 XS=XS+DNT(I,1)
  C=1000./XS
C ACCUMULATION TERM RELATED VARIABLE
  DO 58 J=1,NT1
    DO 58 K=1,MP
      IL=KL(K)
      IU=KU(K)-1
      XS=0.
      DO 57 I=IL,IU

```

```

57 XS=XS+DNT(I,J)
58 ETAA(K,J)=C1*XS
C GROWTH RATE MODEL VALUES
DO 62 J=1,NT1
62 CALL GTRT(CA(J),CAE(J),GOI(J))
C GROWTH RATE TERM RELATED VARIABLE
X1=2.418*C1
DO 64 K=1,MP
KV1=KL(K)
KV2=KU(K)
LL=KV1*2-2
LU=KV2*2-2
IF(KV1.LE.2) LL=KV1
IF(KV2.LE.2) LU=KV2
DO 64 J=1,NT1
CALL EMPSDR(0,RNCT,M9,N1,Z1,LL,TAUE,TAU(J),X2)
CALL EMPSDR(0,RNCT,M9,N1,Z1,LU,TAUE,TAU(J),X3)
64 ETAG(K,J)=X1*GOI(J)*((X2*V23(KV1))-(X3*V23(KV2)))
DO 66 K=1,MP
ETAGI(K,1)=0.
DO 66 J=2,NT1
DLTAU=TAU(J)-TAU(J-1)
66 ETAGI(K,J)=ETAGI(K,J-1)+(.5*DLTAU*(ETAG(K,J)+ETAG(K,J-1)))
C
C-MARQUARDT OPTIMIZATION
DO 130 LL=1,NPRB
NPAR=NPR(LL)
NPROB=LL
NFLAG1=1
ITMAX=100
EPS1=1.E-10
EPS2=1.E-04
RLAMBDA=0.01
RNU=10.0
NOB=N1*MP
DO 80 KP=1,NPAR
SIGNS(KP)=1.
80 DIFF(KP)=0.01
DO 82 Q=1,N1
DO 82 K=1,MP
82 OMEGA(K,Q)=1.
H=0
DO 84 Q=1,N1
DO 84 K=1,MP
H=H+1
X1=ETAA(K,(Q-1)*N1+1)
84 Y(H)=OMEGA(K,Q)*ALOG(X1+SQRT(X1*X1+1.))
CPA1=SECONO(CP)
DO 85 H=1,NPAR
85 TH(H)=TA(H)
CALL MDLAGL(NPROB,TH,Z1,NOB,NPAR)
CPA2=SECONO(CP)
X1=CPA2-CPA1
WRITE(6,66) X1
86 FORMAT(1H1,1X,*ONE MODEL EVALUATION TAKES*,1F8.3,3X,*CP SEC.*,/)
NPRT=1
IF(NPRT.EQ.1) GO TO 90
88 CONTINUE
-----
C
C OPTIMIZATION BY MEANS OF THE MARQUARDT METHOD
CALL UNHAUS(NPROB,MDLAGL,NOB,Y,NPAR,TH,DIFF,SIGNS,EPS1,EPS2,
1 ITMAX,RLAMBDA,RNU,WK)

```

```
CALL MDLAGL(NPROB,TH,Z1,NOB,NPAR)
```

```

C PRINTED VARIABLES
90 CONTINUE
DO 104 K=1,MP
X1=1.2407*CBRT(ALPHA(K))
X2=1.2407*CBRT(BETA(K))
WRITE(5,500) K,ALPHA(K),BETA(K),X1,X2
WRITE(6,502)
DO 102 J=1,NT1
X1=0.
DO 100 L=1,N1
IF(ABS(TAU(J)-TAUE(L)).LT.1.E-04) X1=1.
IF(ABS(TAU(J)-TAUE(L)).LT.1.E-04) LJ=L
100 CONTINUE
IF(X1.EQ.1.) WRITE(6,502)
X2=0.
IF(ETAA(K,J).GT.2.E-04) X2=(ETAA(K,J)-ETAAH(K,J))/ETAA(K,J)*100.
X3=ETAA(K,J)
X4=ALOG(X3+SQRT(X3*X3+1.))
X5=ETAAH(K,J)
X6=ALOG(X5+SQRT(X5*X5+1.))
WRITE(5,500) TAU(J),ETAG(K,J),ETAC(K,J),ETAA(K,J),ETAAH(K,J),
1 X2,ETAGI(K,J),ETACI(K,J),ETAA(K,1),X4,X6
IF(X1.EQ.1.) WRITE(6,502)
X7=ALOG(TAU(J)+SQRT(TAU(J)*TAU(J)+1.))
IF(X1.EQ.1.) Z1(LJ)=X7
IF(X1.EQ.1.) Z2(LJ)=X4
IF(X1.EQ.1.) CALL PLOTPT(X7,X4,26)
X8=ETAGI(K,J)+ETAA(K,1)
X9=ALOG(X8+SQRT(X8*X8+1.))
IF(X1.EQ.1.) CALL PLOTPT(X7,X9,10)
Z3(J)=X7
WK(J)=X6
102 CALL PLOTPT(X7,X6,4)
IF(NPRT.EQ.1) GO TO 103
IF(NPNCH.EQ.1) PUNCH(7,610) (Z1(J),J=1,N1)
IF(NPNCH.EQ.1) PUNCH(7,612) (Z2(J),J=1,N1)
IF(NPNCH.EQ.1) PUNCH(7,614) (Z3(J),J=1,NT1)
IF(NPNCH.EQ.1) PUNCH(7,616) (WK(J),J=1,NT1)
103 CONTINUE
CALL RANGES(0.,5.,0.,7.)
104 CALL OUTPLT
NPRT=NPRT+1
IF(NPRT.EQ.2) GO TO 88
130 CONTINUE
C
500 FORMAT(1X,1PE12.4,10E12.4)
502 FORMAT(1X,1H )
600 FCRMAT(1H1,1X,*K=*,1I2,5X,*ALPHA=*,1E12.4,5X,*BETA=*,1E12.+,
1 5X,*DL=*,1F6.2,5X,*DU=*,1F6.2)
602 1 FORMAT(///,3X,*TAU*,9X,*ETAG*,8X,*ETAC*,8X,*ETAA*,8X,*ETAAH*,
1 7X,*RLTDVT*,6X,*ETAGI*,7X,*ETACI*,7X,*ETAA(1)*,5X,*Y*,11X,*YH*,/)
610 FCRMAT(* XTAU *,1PE10.3,6E10.3)
612 FCRMAT(* XETAH *,1PE10.3,6E10.3)
614 FCRMAT(* XTAUI *,1PE10.3,6E10.3)
616 FCRMAT(* XETAAH *,1PE10.3,6E10.3)

```

```

C STOP
END
SUBROUTINE MDLAGL(NPROB,TH,YH,NOB,NPAR)

```

```

C THIS SUBROUTINE CALCULATES MODEL VALUES GIVEN MODEL PARAMETER VALUES
C DIMENSION TH(NPAR),YH(NOB)

```

```

COMMON/BL1/M,M1,N,N1,NI,NT,NT1,MP,NFLAG1,C1
COMMON/BL2/TAU(14),TAU(53),V(52),V23(52),DELV(51),DNT(51,53)
COMMON/BL3/CA(53),CAE(53),CN(53),HT(53),VL(53),VT(53),GOT(53)
COMMON/BL4/PHIEA(53),ETA(9,53),ETAH(9,53),ETAG(9,53),ETAG1(9,53)
COMMON/BL5/ETAC(9,53),ETAC1(9,53),PHIDN(9,53)
COMMON/BL6/ALPHA(9),BETA(9),KL(9),KU(9),TA(5),TAO(5)
COMMON/BL7/Z1(102),Z2(102),Z3(102),OMEGA(9,14)
INTEGER Q,H,P,QWK

```

```

C
C*****
DO 85 H=1,NPAR
85 TA(H)=TH(H)
C*****
BA1=TA(1)
BA2=TA(2)
BA3=TA(3)
BA4=TA(4)
BA5=TA(5)

C
C AGGLOMERATION RATE EFFECTIVENESS KERNEL
C ENVIRONMENT ONLY DEPENDENT FACTOR
DO 100 J=1,NT1
100 CALL AGGKT(BA1,BA2,CA(J),CAE(J),PHIEA(J))
C
IF(NFLAG1) 104,104,105
104 CONTINUE
IF((TA(3).EQ.TAO(3)).AND.(TA(4).EQ.TAO(4)).AND.(TA(5).EQ.TAO(5)))
1 GO TO 112
105 NFLAG1=0

C
C SIZE DEPENDENT FUNCTION
CALL AGGKRV(1,1,1,M1,V,BA3,BA4,BA5,GROOT,X1)
PHVMN=1.E-06*GROOT
DO 110 K=1,MP
DO 106 J=1,NT1
106 PHIDN(K,J)=J.
DO 110 P=1,M
DO 110 L=1,M
CALL AGGWF(V(L),V(L+1),V(P),V(P+1),DELV(L),DELV(P),ALPHA(K),
1 BETA(K),AWO,AWI,PHICHI)
IF(ABS(PHICHI).LT.1.E-03) GO TO 110J
CALL AGGKRV(0,L,P,M1,V,BA3,BA4,BA5,GROOT,PHIVA)
IF(PHIVA.LT.PHVMN) GO TO 110
X2=PHIVA*PHICHI
DO 108 J=1,NT1
X1=DNT(L,J)*DNT(P,J)
IF(X1.LT.1.E-01) GO TO 108
PHIDN(K,J)=PHIDN(K,J)+(X2*X1)
108 CONTINUE
110 CONTINUE
112 CONTINUE
DO 114 J=1,NT1
114 Z1(J)=C1*PHIEA(J)/VL(J)
DO 116 J=2,NT1
116 Z2(J)=TAU(J)-TAU(J-1)
DO 120 K=1,MP
DO 118 J=1,NT1
118 ETAC(K,J)=Z1(J)*PHIDN(K,J)
ETAC1(K,1)=U.
DO 120 J=2,NT1
120 ETAC1(K,J)=ETAC1(K,J-1)+(.5*Z2(J))*(ETAC(K,J)+ETAC(K,J-1))
DO 124 K=1,MP
DO 124 J=1,NT1
124 ETAH(K,J)=ETAG1(K,J)+ETAC1(K,J)+ETA(K,1)

```

```

H=0
DO 130 Q=1,N1
  QWK=(Q-1)*NI+1
  DO 135 K=1,MP
    H=H+1
    X1=ETAAM(K,QWK)
  130 YH(H)=OMEGA(K,Q)*ALOG(X1+SQRT(X1*X1+1.))
C
DO 148 H=1,5
  140 TAO(H)=TA(H)
  RETURN
  END
SUBROUTINE AGGKT(BA1,BA2,CA,CAE,PHIEA)
C
C AGGLOMERATION RATE EFFECTIVENESS KERNEL
C ENVIRONMENT DEPENDENT FACTOR
C
C-MODEL AGGE1-----
  X1=(CA-CAE)/CAE
  PHIEA=BA1*(X1**BA2)
C-----
  RETURN
  END
SUBROUTINE AGGKRV(NCLC,L,P,M1,V,BA3,BA4,BA5,GROOT,PHIVA)
C
C AGGLOMERATION RATE EFFECTIVENESS KERNEL
C CRYSTAL SIZE DEPENDENT FACTOR
C
  DIMENSION V(M1)
  DIMENSION U(200),U1(200),U2(200)
  INTEGER P
C
C-MODEL AGGV5-----
  IF(NCLC.EQ.1) GO TO 10
  GO TO 16
  10 CONTINUE
  M=M1-1
  DO 12 I=1,M
    X1=CBRT((V(I+1)+V(I))/2.)
    U(I)=X1
  12 U1(I)=X1*X1
  GROOT=1.E-10
  16 CONTINUE
  X1=U(L)+U(P)
  PHIVA=X1*X1*ABS(U1(L)-U1(P))*EXP(-BA3*(U1(L)+U1(P)))
C-----
  RETURN
  END
SUBROUTINE EMPENV(NCLC,TAU,CA,CAE,CN,WT,VL,VT)
C
C EMPIRICAL MODEL FOR THE SOLUTION CONCENTRATION VARIABLES
C
  DIMENSION TH(9)
  INTEGER H
C
  IF(NCLC.EQ.1) GO TO 10
  GO TO 12
  10 CONTINUE
  DATA VLO,WT0,THETA,RHOS/2,+50,24.85,85.1,2.42/
  DATA (TH(H),H=1,9)/92.46,79.82,-0.9529,0.4218,120.1,0.1008E+01,
  1 0.9920E-03,-0.1100E-06,0.5660E-03/
  CA0=TH(1)+TH(2)*EXP(-(EXP(TH(3))**TH(4)))
  CN0=TH(5)
  RHOL=TH(6)+((TH(8)*CN0)+TH(7))*CN0+(TH(9)*CA0)
  X1=(CA0-(654.*RHOL))/CN0

```



```

X2=TH(8)
X3=(X1/654.)+TH(7)

```

```

C 12 CONTINUE

```

```

Z1=EXP(TH(3))
CA=TH(1)+TH(2)*EXP(-((TAU+Z1)**TH(4)))
X4=TH(5)+(LH(9)-.001529)*CA
CN=(-X3-SQRT((X3**X5)-(4.*X2*X4)))/(2.*X2)
CAE=CN*EXP(6.2106+(T-24.867+(1.08753*CN))/(273.15+THETA)))
VL=VL0*CN0/CN
WT=((VL0*CA0)-(VL0*CN0*CA/CN))/654)+HT0
VT=VL+(WT/(1000.*RHOS))
RETURN
END
SUBROUTINE EMPSDR(NCLC,RNCT,M1,NX,VP,L,TAUE,TAU,FVTH)

```

```

C C C CRYSTAL SIZE DISTRIBUTION

```

```

DIMENSION FVT(100,14),ALABEL(80)
DIMENSION VP(M1),TAUE(NX),RNCT(4),AN(4),BN(4)

```

```

C IF(NCLC.EQ.0) GO TO 20

```

```

C -----
DATA M,N/100,1+

```

```

M1=M+1

```

```

NX=N

```

```

N1=N-1

```

```

READ(5,502) (TAUE(J),J=1,N)

```

```

DO 18 J=1,N

```

```

READ(5,504) (ALABEL(L),L=1,80)

```

```

READ(5,500) (VP(I),I=1,M1)

```

```

C 18 READ(5,500) (FVT(I,J),I=1,M)

```

```

C -----
20 CONTINUE

```

```

C IF L=1, V IS LESS THAN THE CUT-OFF SIZE AND THE DENSITY FUNCTION
C VALUE IS ESTIMATED AS FOLLOWS

```

```

LH=L-1

```

```

IF(L.GT.1) GO TO 28

```

```

LH=L

```

```

C INTERPOLATE WRT TAUE

```

```

28 DO 30 J=1,N1

```

```

J1=J

```

```

IF(TAU.GE.TAUE(J).AND.TAU.LE.TAUE(J+1)) GO TO 32

```

```

30 CONTINUE

```

```

32 X1=(FVT(LH,J1+1)-FVT(LH,J1))/(TAUE(J1+1)-TAUE(J1))

```

```

X2=FVT(LH,J1)-(X1*TAUE(J1))

```

```

FVTH=X2+(X1*TAU)

```

```

IF(L.GT.1) GO TO 40

```

```

AN(1)=(RNCT(2)-RNCT(1))/(TAUE(2)-TAUE(1))

```

```

AN(2)=(RNCT(3)-RNCT(2))/(TAUE(4)-TAUE(2))

```

```

BN(1)=RNCT(1)-(AN(1)*TAUE(1))

```

```

BN(2)=RNCT(2)-(AN(2)*TAUE(2))

```

```

IF(TAU.GE.TAUE(1).AND.TAU.LT.TAUE(2)) FVTH=(AN(1)*TAU+BN(1))*FVTH

```

```

IF(TAU.GE.TAUE(2).AND.TAU.LT.TAUE(4)) FVTH=(AN(2)*TAU+BN(2))*FVTH

```

```

IF(TAU.GE.TAUE(4)) FVTH=RNCT(3)*FVTH

```

```

C 40 CONTINUE

```

```

503 FORMAT(1PE10.3,7E10.3)

```

```

502 FORMAT(10X,7F10.3)

```

```

504 FORMAT(80A1)

```

```

C RETURN

```

```

END

```

```

C SUBROUTINE GRTRT(CA,CAE,GDI)

```

C ISOTHERMAL GROWTH RATE MODEL

C DIMENSION BG(2)
C INTEGER H

C DATA (BG(H),H=1,2)/15.22,0.3397/
C X1=(CA-CAE)/CAE
C X2=5./5.
C GOI=BG(1)*(X1**X2)*EXP(-BG(2)/X1)

C RETURN
C END
C SUBROUTINE AGGWF(VL,VL1,VP,VP1,DELVL,DELVP,ALPHAK,BETAK,
C 1 AWO,AWI,AW)

C AGGLOMERATION WEIGHTING FUNCTION FOR ONE ELEMENT BOUNDED
C BY (V(L),V(L+1) , AND (V(P),V(P+1))

C AGGLOMERATION OUT TERM
C AWO=0.
C IF (VP.GE.ALPHAK.AND.VP1.LE.BETAK) AWO=1.

C AGGLOMERATION IN TERM
C X11=VL1+VP1
C IF (X11.LE.ALPHAK) GO TO 50
C X00=VL+VP
C IF (X00.GE.BETAK) GO TO 50
C IF (X00.GE.ALPHAK.AND.X11.LE.BETAK) GO TO 52
C X10=VL1+VP
C X01=VL+VP1
C IF (X00.GE.ALPHAK.AND.X11.GT.BETAK) GO TO 10
C IF (X11.LE.BETAK.AND.X00.LT.ALPHAK) GO TO 20
C WRITE(6,200) VL,VL1,VP,VP1,ALPHAK,BETAK
C 200 FORMAT(1H1,/,/,1X,1P13.4,5E13.4,/,/,1X,*,AGGL.WGTFT.CALC.NON OF THE
C 1 CONDITIONS WERE SATISFIED*)
C STOP

10 CONTINUE
C IF (DELVP.GE.DELVL) GO TO 12
C GO TO 14

12 CONTINUE
C IF (BETAK.LE.X10) GO TO 54
C IF (BETAK.GE.X01) GO TO 56
C GO TO 38

14 CONTINUE
C IF (BETAK.LE.X01) GO TO 54
C IF (BETAK.GE.X10) GO TO 56
C GO TO 30

20 CONTINUE
C IF (DELVP.GE.DELVL) GO TO 22
C GO TO 24

22 CONTINUE
C IF (ALPHAK.LE.X10) GO TO 62
C IF (ALPHAK.GE.X01) GO TO 64
C GO TO 66

24 CONTINUE
C IF (ALPHAK.LE.X01) GO TO 62
C IF (ALPHAK.GE.X10) GO TO 64
C GO TO 68

C 50 AWI=0.
C GO TO 160
C 52 AWI=.5
C GO TO 100
C 5+ Z1=BETAK-X00
C AWI=.5*(Z1*Z1/2.)/(DELVP*DELVL)

```
GO TO 100
56 Z1=X11-BETAK
   AWI=.5*(1.-((Z1*Z1/2.)/(DELVP*DELVL)))
   GO TO 100
58 Z1=BETAK-X10
   Z2=BETAK-X00
   AWI=.5*(DELVL/2.*(Z1+Z2)/(DELVP*DELVL))
   GO TO 100
60 Z1=BETAK-X00
   Z2=BETAK-X01
   AWI=.5*(DELVP/2.*(Z1+Z2)/(DELVP*DELVL))
   GO TO 100
62 Z1=ALPHAK-X00
   AWI=.5*(1.-((Z1*Z1/2.)/(DELVP*DELVL)))
   GO TO 100
64 Z1=X11-ALPHAK
   AWI=.5*(Z1*Z1/2.)/(DELVP*DELVL)
   GO TO 100
66 Z1=X01-ALPHAK
   Z2=X11-ALPHAK
   AWI=.5*(DELVL/2.*(Z1+Z2)/(DELVP*DELVL))
   GO TO 100
68 Z1=X10-ALPHAK
   Z2=X11-ALPHAK
   AWI=.5*(DELVP/2.*(Z1+Z2)/(DELVP*DELVL))
100 AW=AWI-AW0
   RETURN
END
```

PROGRAM TST(INPUT,OUTPUT,PUNCH,TAPES=INPUT,TAPE6=OUTPUT,
1 TAPE7=PUNCH)

EMPIRICAL NUCLEATION RATE MODEL--CC-- THIS PROGRAM ESTIMATES THE
PARAMETERS OF A GIVEN EMPIRICAL NUCLEATION RATE MODEL BY MEANS OF THE
METHOD OF PSEUDO MOMENTS AND AUXILIARY EMPIRICAL MODELS

DESCRIPTION OF PRINCIPAL VARIABLES

M NUMBER OF CRYSTAL SIZE INTERVALS, NUMBER OF DISCRETE
SIZES=M+1
N NUMBER OF DISCRETE BATCH SAMPLE TIME INTERVALS, NUMBER OF
BATCH TIMES =N+1
NT NUMBER OF DISCRETE BATCH MODEL TIME INTERVALS, NUMBER OF DISCRETE
BATCH MODEL TIMES =NT+1
NI NUMBER OF MODEL TIME INTERVALS BETWEEN EACH TWO SUCCESSIVE
BATCH TIMES, MIN NI=2
RNCT VARIABLE RELATED TO THE ESTIMATED NUMBER OF CRYSTALS IN THE
CUT-OFF SIZE INTERVAL
PHIP(J) ACCUMULATION TERM RELATED VARIABLE/
PHIN(J) NUCLEATION TERM \$ \$
PHIA(J) AGGLOMERATION TERM \$ \$
NCTL(K) PROGRAM CONTROL VARIABLE
1 =1 ESTIMATE THE VALUE OF PHIPH(1) ALONG WITH THE NUCLEATION
RATE PARAMETERS, =0 PHIPH(1) IS TREATED AS A KNOWN DETERMINISTIC
VARIABLE AND THEN EQUALS PHIP(1)
2 =1 ENVIRONMENT DEPENDENT FACTOR IS PROPORTIONAL TO THE TOTAL
NUMBER OF CRYSTAL-CRYSTAL COLLISIONS, =0 IS NOT

DIMENSION DELV(101),DNT(101,100)
DIMENSION TH(5),SIGNS(5),DIFF(5),WK(300),Y(20),PHIEA(100)
DIMENSION RNCT(4)
COMMON/BL1/M,M1,N,N1,NI,NT,NT1,NCTL(5),C1
COMMON/BL2/TAUE(20),TAU(100),V(102),D(102)
COMMON/BL3/CA(100),CAE(100),CN(100),WT(100),VL(100),VT(100)
COMMON/BL4/PHIVN(102),SFLN(100),PHIN(100),PHINI(100)
COMMON/BL5/PHIA(100),PHIAI(100),PHIP(100),PHIPH(100)
COMMON/BL6/Z1(200),Z2(200),TN(5),OMEGA(20)
COMMON/BL7/CHIC(100),ARTR(100)
INTEGER P,PL
EXTERNAL MDLNCL

DATA NI/7/
DATA DD/1.0E-01/
DATA NPAR/3/
DATA (NCTL(H),H=1,2)/0,0/
DATA NPNCH/1/
DATA (TN(KP),KP=1,5)/2.53+E+12,6.154,1.536,1.15,-4.10/
DATA (RNCT(H),H=1,4)/2.33,7.09,1.00,0.7

READ-IN CRYSTAL SIZE DISTRIBUTION
CALL EMPSORT(1,0,M,NI,Z1,1,TAUE,0.,X1)
M1=M+1
N=N1-1
NT=(N1-1)*NI
NT1=NT+1

ESTIMATED MINIMUM CRYSTAL SIZE:
V(1)=0.523599*DD*DD*DD

DISCRETE CRYSTAL SIZES
MVK=M+1
DO 60 I=2,MVK

```

V(I)=Z1(I-1)
+0 DELV(I-1)=V(I)-V(I-1)
DO 41 I=1,M1
+1 D(I)=1.2407*CBRT(V(I))

```

```

C DISCRETE BATCH MODEL TIMES

```

```

RNI=NI
NI1=NI+1
TAU(1)=TAUE(1)
DO 45 J=1,N
X1=(TAUE(J+1)-TAUE(J))/RNI
NIWK=(J-1)*NI
DO 46 JWK=2,NI1
+6 TAU(NIWK+JWK)=TAU(NIWK+JWK-1)+X1

```

```

C CRYSTAL ENVIRONMENT MODEL VALUES

```

```

CALL EMPENV(0,TAU(1),CA(1),CAE(1),CN(1),WT(1),VL(1),VT(1))
DO 50 J=2,NT1
50 CALL EMPENV(1,TAU(J),CA(J),CAE(J),CN(J),WT(J),VL(J),VT(J))

```

```

C SIZE DISTRIBUTION MODEL VALUES

```

```

DO 52 I=1,M
L=I
DO 52 J=1,NT1
CALL EMPSDR(0,RNCT,M,NI,Z1,L,TAUE,TAU(J),DNT(I,J))
52 DNT(I,J)=DNT(I,J)*DELV(I)

```

```

C TERM PROPORTIONAL TO THE NUMBER OF CRYSTAL-CRYSTAL COLLISIONS

```

```

DO 200 I=1,M
Z1(I)=CBRT((V(I+1)+V(I))/2.)
200 Z2(I)=Z1(I)*Z1(I)
M9=M-1
DO 220 J=1,NT1
XS=0.
DO 210 L=1,M
X1=Z1(L)+Z1(L)
X2=X1*X1*ABS(Z2(L)-Z2(L))
210 XS=XS+(.5*X2*DNT(L,J)*DNT(L,J))
DO 214 L=1,M9
PL=L+1
DO 214 P=PL,M
X1=Z1(L)+Z1(P)
X2=X1*X1*ABS(Z2(L)-Z2(P))
214 XS=XS+(X2*DNT(L,J)*DNT(P,J))
220 CHIC(J)=XS

```

```

C C TOTAL CRYSTAL AREA

```

```

DO 230 I=1,M1
230 Z1(I)=V(I)**1.6666667
DO 234 J=1,NT1
XS=0.
DO 232 I=1,M
232 XS=XS+(2.90E-08*DNT(I,J)/DELV(I)*(Z1(I+1)-Z1(I)))
234 ARTR(J)=XS

```

```

C PSEUDO MOMENT

```

```

XS=0.
DO 54 I=1,M
54 XS=XS+DNT(I,1)
C1=1000./XS

```

```

C ACCUMULATION TERM

```

```

DO 62 J=1,NT1
XS=0.
DO 60 I=1,M

```

```

60 XS=XS+DNT(I,J)
62 PHIP(J)=C1*XS
C AGGLOMERATION RATE TERM
CPA1=SECOND(CP)
CALL AGGKRN(0,1,NT1,M1,CA,CAE,PHIEA,V,1,1,X1)
CALL AGGKRN(1,J,NT1,M1,CA,CAE,PHIEA,V,1,1,X1)
DO 64 J=1,NT1
64 Z1(J)=SQRT(PHIEA(J)/VL(J))
DO 66 J=1,NT1
DO 66 L=1,M
56 DNT(L,J)=DNT(L,J)*Z1(J)
CALL AGGKRN(1,1,NT1,M1,CA,CAE,PHIEA,V,M,M,PHIVA)
X1=.5*C1*PHIVA
DO 68 J=1,NT1
68 PHIA(J)=X1*DNT(M,J)*DNT(M,J)
M9=M-1
DO 72 L=1,M9
CALL AGGKRN(1,1,NT1,M1,CA,CAE,PHIEA,V,L,L,PHIVA)
X1=.5*C1*PHIVA
DO 70 J=1,NT1
70 PHIA(J)=PHIA(J)+(X1*DNT(L,J)*DNT(L,J))
PL=L+1
DO 72 P=PL,M
CALL AGGKRN(1,1,NT1,M1,CA,CAE,PHIEA,V,L,P,PHIVA)
X1=C1*PHIVA
DO 72 J=1,NT1
72 PHIA(J)=PHIA(J)+(X1*DNT(L,J)*DNT(P,J))
CPA2=SECOND(CP)
X1=CPA2-CPA1
WRITE(6,300) X1
300 FORMAT(//,1X,*TIME TO CALCULATE AGGLOMERATION TERM CP SEC.=*,
1 1F8.3,/)

```

C-MARQUARDT OPTIMIZATION-----

```

NPROB=1
ITHAX=100
EPS1=1.E-10
EPS2=1.E-06
RLAMBDA=0.01
RNU=10.0
NOB=N1
DO 80 KP=1,NPAR
SIGNS(KP)=1.
80 DIFF(KP)=0.01
DO 82 J=1,NOB
82 OMEGA(J)=1.
DO 84 J=1,NOB
X0=PHIP((J-1)*NI+1)
X1=ALOG(X0+SQRT(X0*X0+1.))
84 Y(J)=OMEGA(J)*X1
DO 86 KP=1,NPAR
86 TH(KP)=TN(KP)
IF(NCTL(1).EQ.0) GO TO 90
NPAR=NPAR+1
SIGNS(NPAR)=1.
DIFF(NPAR)=0.01
TH(NPAR)=PHIP(1)
90 CONTINUE

```

```

C-----
C CALL UHHAUS(NPROB,MOLNCL,NOB,Y,NPAR,TH,DIFF,SIGNS,EPS1,EPS2,
1 ITHAX,RLAMBDA,RNU,*K)
C CALL MOLNCL(NPROB,TH,Z1,NOB,NPAR)

```

```

C WRITE AND PLOT
  WRITE(6,600)
  WRITE(6,602)
  DO 100 I=1,M1
100  WRITE(6,500) D(I),V(I),PHIVN(I)
  WRITE(6,604)
  DO 104 J=1,NT1
  X1=0.
  DO 102 L=1,N1
  IF(ABS(TAU(J)-TAUE(L)).LT.1.E-04) X1=1.
102  CONTINUE
  X2=(PHIP(J)-PHIPH(J))/PHIP(J)*100.
  X3=-PHIAI(J)
  IF(X1.EQ.1.) WRITE(6,502)
  WRITE(6,500) TAU(J),BFLN(J),PHIN(J),PHIA(J),PHIP(J),PHIPH(J),
  X2,PHINI(J),X3,PHIPH(1)
  IF(X1.EQ.1.) WRITE(6,502)
  X4=ALOG(TAU(J)+SQRT(TAU(J)*TAU(J)+1.))
  X5=ALOG(PHIPH(J)+SQRT(PHIPH(J)*PHIPH(J)+1.))
  Z1(J)=X4
  Z2(J)=X5
104  CALL PLOTPT(X4,X5,4)
  IF(NPNCH.EQ.1) PUNCH(7,610) (Z1(J),J=1,NT1)
  IF(NPNCH.EQ.1) PUNCH(7,612) (Z2(J),J=1,NT1)
  DO 105 J=1,N1
  JWK=(J-1)*NI+1
  X4=ALOG(TAU(JWK)+SQRT(TAU(JWK)*TAU(JWK)+1.))
  X5=ALOG(PHIPH(JWK)+SQRT(PHIPH(JWK)*PHIPH(JWK)+1.))
  Z1(J)=X4
  Z2(J)=X5
105  CALL PLOTPT(X4,X5,3+1)
  IF(NPNCH.EQ.1) PUNCH(7,614) (Z1(J),J=1,N1)
  IF(NPNCH.EQ.1) PUNCH(7,616) (Z2(J),J=1,N1)
  CALL OUTPLT

C
500  FORMAT(1X,1PE12.4,10E12.4)
502  FORMAT(1X,1H )
600  FORMAT(1H1,3X,*NUCLEATION RATE CRYSTAL SIZE DEPENDENT FACTOR*)
602  FORMAT(/,3X,*0*,11X,*V*,11X,*PHIVN*,/)
604  FORMAT(1H1,3X,*TAU*,9X,*BFLN*,8X,*PHIN*,8X,*PHIA*,8X,*PHIP*,8X,
  1 *PHIPH*,7X,*RLTDVT*,6X,*PHINI*,7X,*-PHIAI*,6X,*PHIPH(1)*,/)
610  FORMAT(* XTAUI      *,1PE10.3,6E10.3)
612  FORMAT(* XPHIPH     *,1PE10.3,6E10.3)
614  FORMAT(* XTAU       *,1PE10.3,6E10.3)
616  FORMAT(* XPHIP      *,1PE10.3,6E10.3)

C
  STOP
  END
  SUBROUTINE MOLNCL(NPROB,TH,YH,NOB,NPAR)

C THIS SUBROUTINE CALCULATES NUCLEATION RATE MODEL VALUES GIVEN MODEL
C PARAMETER VALUES
  DIMENSION TH(NPAR),YH(NOB)
  COMMON/BL1/M,M1,N,N1,NI,NT,NT1,NCTL(5),C1
  COMMON/BL2/TAUE(20),TAU(100),V(102),D(102)
  COMMON/BL3/CA(100),CAE(100),CN(100),WT(100),VL(100),VT(100)
  COMMON/BL4/PHIVN(102),BFLN(100),PHIN(100),PHINI(100)
  COMMON/BL5/PHIA(100),PHIAI(100),PHIP(100),PHIPH(100)
  COMMON/BL6/Z1(200),Z2(200),TN(5),OMEGA(20)
  COMMON/BL7/CHIC(100),ARTR(100)
  REAL MU

  PHIPH(1)=PHIP(1)
  IF(NCTL(1).EQ.1) PHIPH(1)=TH(NPAR)

```

```

NWK=NPAR
IF(NCTL(1).EQ.1) NWK=NPAR-1
DO 5 K=1,NWK
5 IN(K)=TH(K)
DATA NCLC/0/
IF(NWK.LT.4.AND.NCLC.EQ.1) GO TO 20
NCLC=NCLC+1
C SIZE DEPENDENT FACTOR OF THE NUCLEATION RATE MODEL
BN4=SIGMA=TN(4)
BN5=MU=TN(5)
X1=.398942/SIGMA
X2=-1./(2.*SIGMA*SIGMA)
DO 10 I=1,M1
Y=ALOG(V(I))
X3=Y-MU
X4=X1*EXP(X2*X3*X3)
10 PHIVN(I)=X4/V(I)
XL=ALOG(V(1))
XU=ALOG(V(2))
RM1=M1-1
XST=(XU-XL)/RM1
DO 11 I=1,M1
RI=I
YI=XL+((RI-1.)*XST)
VI=EXP(YI)
X3=YI-MU
X4=X1*EXP(X2*X3*X3)
Z1(I)=VI
11 Z2(I)=X4/VI
CALL QDRLIN(Z1,Z2,M1,XSUM1)
K=0
DO 12 I=2,M1
K=K+1
MK=K
Z1(K)=V(I)
12 Z2(K)=PHIVN(I)
CALL QDRLIN(Z1,Z2,MK,XSUM2)
SDRFCT=XSUM1+XSUM2
WRITE(6,14) SDRFCT,XSUM1,XSUM2
14 FORMAT(///,1X,*INTEGRATED WRT V SIZE DEPENDENT FACTOR OF THE NUCLE
ATION RATE MODEL*,/ ,1X,*SDRFCT=*,1PE12.4,10X,*XSUM1=*,1E12.4,
2 10X,*XSUM2=*,1E12.4,5X,*-----*,///)
C
20 CONTINUE
C CRYSTAL ENVIRONMENT DEPENDENT FACTOR OF THE NUCLEATION RATE MODEL
BN1=TN(1)
BN2=TN(2)
BN3=TN(3)
C-----
DO 30 J=1,NT1
X1=CA(J)-CAE(J)
X2=WT(J)/VL(J)
X3=X1/CAE(J)
IF(NCTL(2).EQ.0) BFLN(J)=BN1*(1.+EXP(BN2*(-BN3+(1./X3))))
IF(NCTL(2).EQ.1) BFLN(J)=BN1*(X1**BN2)*(CHIC(J)**BN3)
IF(NCTL(2).EQ.2) BFLN(J)=BN1*(X1**BN2)*(ARTR(J)**BN3)
30 CONTINUE
C-----
DO 32 J=1,NT1
32 PHIN(J)=C1*VL(J)*BFLN(J)*SDRFCT
PHINI(1)=PHIAI(1)=0.
DO 3+ J=2,NT1
DLTAU=TAU(J)-TAU(J-1)
PHINI(J)=PHINI(J-1)+(.5*DLTAU*(PHIN(J)+PHIN(J-1)))
PHIAI(J)=PHIAI(J-1)+(.5*DLTAU*(PHIA(J)+PHIA(J-1)))

```



```
34 PHIPH(J)=PHINI(J)-PHIAI(J)+PHIPH(1)
```

```
DO 36 J=1,N1
```

```
X0=PHIPH((J-1)*NI+1)
```

```
X1=ALOG(X0+SQRT(X0*X0+1.))
```

```
36 YH(J)=OMEGA(J)*X1
```

```
RETURN
```

```
END
```

```
SUBROUTINE EMPENV(NCLC,TAU,CA,CAE,CN,WT,VL,VT)
```

```
C  
C  
C
```

```
EMPIRICAL MODEL FOR THE SOLUTION CONCENTRATION VARIABLES
```

```
DIMENSION TH(9)
```

```
INTEGER H
```

```
C
```

```
IF(NCLC.EQ.0) GO TO 10
```

```
GO TO 12
```

```
10 CONTINUE
```

```
DATA VLG,WT0,THETA,RHOS/2.430,24.85,85.1,2.42/
```

```
DATA (TH(H),H=1,9)/92.46,79.62,-0.9529,0.4218,120.1,0.1008E+01,
```

```
0.9920E-03,-0.1100E-06,0.5660E-03/
```

```
CA0=TH(1)+TH(2)*EXP(-(EXP(TH(3))*TH(4)))
```

```
CN0=TH(5)
```

```
RHOLD=TH(6)+(((TH(8)*CN0)+TH(7))*CN0)+(TH(9)*CA0)
```

```
X1=(CA0-(65+.*RHOLD))/CN0
```

```
X2=TH(8)
```

```
X3=(X1/654.)+TH(7)
```

```
C
```

```
12 CONTINUE
```

```
Z1=EXP(TH(3))
```

```
CA=TH(1)+TH(2)*EXP(-((TAU+Z1)**TH(4)))
```

```
X4=TH(6)+((TH(9)-.001529)*CA)
```

```
CN=(-X3-SQRT((X3*X3)-(4.*X2*X4)))/(2.*X2)
```

```
CAE=CN*EXP(6.2106+((-2486.7+(1.08753*CN))/(273.15+THETA)))
```

```
VL=VL0*CN0/CN
```

```
WT=((VL0*CA0)-(VL0*CN0*CA/CN))/654+WT0
```

```
VT=VL+(WT/(1000.*RHOS))
```

```
RETURN
```

```
END
```

```
SUBROUTINE EMPSDR(NCLC,RNCT,M1,NX,VP,L,TAUE,TAU,FVTH)
```

```
C
```

```
C
```

```
CRYSTAL SIZE DISTRIBUTION
```

```
C
```

```
DIMENSION FVT(100,14),ALABEL(80)
```

```
DIMENSION VP(M1),TAUE(NX),RNCT(4),AN(4),BN(4)
```

```
C
```

```
IF(NCLC.EQ.0) GO TO 20
```

```
C
```

```
DATA M,N/100,14/
```

```
M1=M+1
```

```
NX=N
```

```
N1=N-1
```

```
READ(5,502) (TAUE(J),J=1,N)
```

```
DO 18 J=1,N
```

```
READ(5,504) (ALABEL(L1),L1=1,80)
```

```
READ(5,506) (VP(I),I=1,M1)
```

```
18 READ(5,508) (FVT(I,J),I=1,M)
```

```
C
```

```
20 CONTINUE
```

```
C
```

```
C
```

```
IF L=1, V IS LESS THAN THE CUT-OFF SIZE AND THE DENSITY FUNCTION  
VALUE IS ESTIMATED AS FOLLOWS
```

```
LW=L-1
```

```
IF(L.GT.1) GO TO 28
```

```
LW=L
```

```
C
```

```
INTERPOLATE WRT TAUE
```

```
28 DO 30 J=1,N1
```

```

J1=J
IF(TAU.GE.TAUE(J).AND.TAU.LE.TAUE(J+1)) GO TO 32
30 CONTINUE
32 X1=(FVT(LW,J1+1)-FVT(LW,J1))/(TAUE(J1+1)-TAUE(J1))
X2=FVT(LW,J1)-(X1*TAUE(J1))
FVTM=X2+(X1*TAU)
IF(L.GT.1) GO TO 40
AN(1)=(RNCT(2)-RNCT(1))/(TAUE(2)-TAUE(1))
AN(2)=(RNCT(3)-RNCT(2))/(TAUE(3)-TAUE(2))
BN(1)=RNCT(1)-(AN(1)*TAUE(1))
BN(2)=RNCT(2)-(AN(2)*TAUE(2))
IF(TAU.GE.TAUE(1).AND.TAU.LT.TAUE(2)) FVTM=(AN(1)*TAU+BN(1))*FVTM
IF(TAU.GE.TAUE(2).AND.TAU.LT.TAUE(4)) FVTM=(AN(2)*TAU+BN(2))*FVTM
IF(TAU.GE.TAUE(4)) FVTM=RNCT(3)*FVTM
40 CONTINUE

```

```

C 500 FORMAT(1PE10.3,7E10.3)
502 FORMAT(10X,7F10.3)
504 FORMAT(60A1)

```

```

C -RETURN
END

```

```

SUBROUTINE AGGKRN(NCLC1,NCLC2,NT1,M1,CA,CAE,PHIEA,V,L,P,PHIVA)

```

```

C C C AGGLOMERATION KERNEL MODEL

```

```

C DIMENSION V(M1),CA(NT1),CAE(NT1),PHIEA(NT1),U(200),U1(200)
C INTEGER P

```

```

C IF(NCLC1.EQ.0) GO TO 10
IF(NCLC2.EQ.0) GO TO 14
GO TO 20

```

```

10 CONTINUE

```

```

C ENVIRONMENT ONLY DEPENDENT FACTOR

```

```

DATA BA1,BA2/1.025E-12,5.062/

```

```

DO 12 J=1,NT1

```

```

X1=(CA(J)-CAE(J))/CAE(J)

```

```

12 PHIEA(J)=BA1*(X1**BA2)

```

```

RETURN

```

```

14 CONTINUE

```

```

C CRYSTAL SIZE ONLY DEPENDENT FACTOR

```

```

DATA BA3/6.579E-03/

```

```

M=M1-1

```

```

DO 16 I=1,M

```

```

X1=CBRT((V(I+1)+V(I))/2.)

```

```

U(I)=X1

```

```

16 U1(I)=X1*X1

```

```

RETURN

```

```

20 CONTINUE

```

```

X1=U(L)+U(P)

```

```

PHIVA=X1*X1*ABS(U1(L)-U1(P))*EXP(-BA3*(U1(L)+U1(P)))

```

```

RETURN

```

```

END

```

```

SUBROUTINE QDRLIN(X,Y,N,AREA)

```

```

C C C QUADRATURE , TRAPEZOIDAL EQUATION FOR UNEQUAL INTERVALS

```

```

C DIMENSION X(N),Y(N)

```

```

C C C AREA=SUM OF (.5*(X(I+2)-X(I))*(Y(I+2)+Y(I)) ,I=1,2,...,N-1)
C C C MIN. N=2

```

```

C N1=N-1

```

```

AREA=0.

```

```

DO 10 I=1,N1

```

```
10 AREA=AREA+((X(I+1)-X(I))*(Y(I+1)+Y(I)))  
   AREA=.5*AREA  
   RETURN  
   END
```

PROGRAM TST (INPUT,OUTPUT,PUNCH,TAPES=INPUT,TAPES=OUTPUT,TAPE7=
1 PUNCH)

PROGRAM --DA--

NUMERICAL SOLUTION OF GENERAL POPULATION BALANCE MODEL (THE FULL MODEL)
THE FULL MODEL IS SOLVED NUMERICALLY BY MEANS OF A SPECIALLY DEVELOPED
NUMERICAL ALGORITHM.
THE NUMERICAL SOLUTION CAN BE COMPARED TO ANALYTICAL SOLUTIONS FOR
SIMPLIFIED MODEL CASES
THE COMPARISON ALLOWS FOR A RELATIVE CHECK ON THE ACCURACY AND THE NUMBER
OF REQUIRED SOLUTION GRID POINTS OF THE NUMERICAL ALGORITHM
THE MODEL PARAMETERS CAN BE OPTIMIZED IN CASE OF MODEL COMPARISON WITH
AVAILABLE EXPERIMENTAL DATA

PROGRAM VARIABLES

EXPERIMENTAL MEASUREMENTS RELATED VARIABLES
ME NUMBER OF MEASURED CRYSTAL SIZE INTERVALS , NUMBER OF MEASURED
AVERAGE DENSITY FUNCTION VALUES AND ASSOCIATED MEAN CRYSTAL
VOLUME VALUES =ME
NE1 NUMBER OF EXPERIMENTAL BATCH SAMPLES
FVTE(IE,JE) EXPERIMENTAL NUMBER DENSITY FUNCTION WRT VE , IE=1,...,ME ,
JE=1,...,NE1
TAJE(JE) EXPERIMENTAL BATCH TIMES , JE=1,...,NE1
VE(IE) EXPERIMENTAL AVERAGE CRYSTAL VOLUME , IE=1,...,ME

NUMERICAL MODEL VARIABLES

M NUMBER OF MODEL CRYSTAL SIZE INTERVALS , NUMBER OF DISCRETE
MODEL SIZES OR GRID POINTS WRT V=M+1 , THE NUMBER OF GRID POINTS
WRT TAU IS DETERMINED AUTOMATICALLY BY THE INTEGRATION ROUTINE
RUNGE-KUTTA-MERSON
FVT(I) NUMERICAL SOLUTION NUMBER DENSITY FUNCTION WRT V , I=1,...,M+1
TAJ NUMERICAL SOLUTION BATCH TIME
V(I) NUMERICAL ALGORITHM CRYSTAL VOLUME GRID VALUES , I=1,...,M+1
BI(K) INITIAL SIZE DISTRIBUTION MODEL PARAMETERS , K=1,...,NPI
BS(K) GROWTH RATE MODEL PARAMETERS , K=1,...,NPG
BN(K) NUCLEATION RATE MODEL PARAMETERS , K=1,...,NPN
BA(K) AGGLOMERATION RATE MODEL PARAMETERS , K=1,...,NPA

PROGRAM CONTROL VARIABLES

BGF =1 PROCESS WITH GROWTH , =0 WITHOUT
BNL =1 PROCESS WITH NUCLEATION , =0 WITHOUT
BAS =1 PROCESS WITH AGGLOMERATION , =0 WITHOUT
NCTL(1) =1 OPTIMIZE INITIAL SIZE DISTRIBUTION MODEL PARAMETERS , =0 DO NOT
NCTL(2)
NCTL(3) =1 PRINT MODEL VALUES , =0 DO NOT
NCTL(4) =1 COMPARE MODEL AND EXPERIMENTAL NUMBER DENSITY FUNCTION
WRT V , =0 DO NOT
NCTL(5) =1 APPLY THE EMPIRICAL AGGLOMERATION TERM CORRECTION
EXPRESSION , =0 DO NOT

MINIMUM REQUIRED DIMENSIONS

NCTL(J), TAUM(NM1), Y(MC1+1), DYX(MC1+1), ERR(MC1+1), SIGNSI(NPI),
DIFFI(NPI), YI(ME+1), TAU(NE1), VS(ME1), VE(ME), DE(ME),
FVTE(ME,NE1), VG(MG1), CG(MG1), VA(MA1), JA(MA1), VC(MC1),
DC(MC1), VCO(MC1), DCO(MC1), V(MG), D(MG), FVT(MG), HTC(MC1),
BG(NPG), BN(NPN), BA(NPA), BI(NPI), GRTC(MC1), PHIVN(MC1),
RNC(LC(MC1), HTA(MA1), PHIVA(MA*(MA+1)/2), BHLA(MC1),
DHLA(MC1), AGERW(MC1), AGGC(MC1), DELVA(MA), SMVA(MA),
PHI1(MA1), PHI2(MA1), A(MA1), AD(MA1), E(MA1), Z1(MG1),
Z2(MG1), Z3(MG1), Z4(MG1), Z5(MG1), WK1(UWHAUS)

DIMENSION TAUM(14), Y(152), YO(152), DYX(152), WK1(605)
DIMENSION SIGNSI(3), DIFFI(3), YI(101)

COMMON/BL E/NE1,ME1,ME,TAUE(14),VE(101),DE(101),HTIE(101,14)
COMMON/BL M1/MG,MG1,MA,MA1,MC,MC1,FVT(150),HTC(161),HTA(151)
COMMON/BL M2/VG(151),DG(151),VA(151),DA(151),VC(151),DC(151)
COMMON/BL M3/C1,C2,C3,C4,C5,C6,WT,VL,CA,CAE,CN,THETA,TAU,TAUO
COMMON/BL M4/YWFACT,DCO(151),DVD(151),DXV(151)
COMMON/BL PR/NPG,NPN,NPA,NPI,BG(3),BN(5),BA(5),BI(3)
COMMON/BL CS1/GL,GLO,GRIC(151),PHIEN,PHIVN(151),RNCLC(151)
COMMON/BL CS2/PHIEA,PHIYA(11325),BHLA(151),JHLA(151),AGERW(151)
COMMON/BL CS3/AGGC(151),DELVA(150),SMVA(150),PHI1(151),PHI2(151),
1 A(151),AD(151),E(151)
COMMON/BL CT/EGT,BNL,BAG,FIXGRD,NCASE,NCTL(5),TIMX2,NPNCH
COMMON/BL R/NCFN,COFN,MWK1,NGA,ERR(151),HST,HSTMN,HSTMX
COMMON/BL I/XWI
COMMON/BL W/Z1(151),Z2(151),ZS1(151),ZS2(151)
EXTERNAL OPTINL
EXTERNAL DFN

C-PROGRAM INPUT DATA-----
C SPECIFIED INITIAL PROCESS CONDITIONS
C DATA DD,VLD,CAO,CNO,WTO,THETA0/1.0E-01,2.430,133.2,120.1,24.85,
C 1 85.1/
C GRID WRT CRYSTAL SIZE RELATED VARIABLES
C DATA MA,NGA,CAG1,CAG/120,3,5.,1.10/
C MWK1=MA*(MA+1)/2
C NUMBER OF EXPERIMENTAL DATA POINTS, IF NON SET =0
C DATA ME1,NE1/101,14/
C ME=NE1-1
C MODEL PARAMETERS VALUES OR INITIAL ESTIMATES IF THEY ARE TO BE OPTIMIZED
C IF NOT REQUIRED SET =0
C INITIAL SIZE DISTRIBUTION MODEL
C DATA (BI(K),K=1,3)/2.0E+11,0.7225,0./
C DATA NPI/2/
C GROWTH RATE MODEL
C DATA (BG(K),K=1,2)/15.22,0.3397/
C DATA NPG/2/
C NUCLEATION RATE MODEL
C DATA (BN(K),K=1,5)/1.725E+12,8.504,1.606,1.15,-4.10/
C DATA NPN/5/
C AGGLOMERATION RATE MODEL
C DATA (BA(K),K=1,5)/1.025E-12,3.062,6.579E-03,0.,0./
C DATA NPA/5/
C PROGRAM CONTROL VARIABLES
C DATA (NCTL(KW),KW=1,5)/0,0,1,1,1/
C DATA BGT,BNL,BAG/1.,1.,1./
C DATA JM,NM1,NPNCH,FIXGRD,TAU,TIMX1,TIMX2/1,14,1,1.,0.,1800.,2020./
C NUMERICAL OPTIMIZATION DATA FOR INITIAL SIZE DISTRIBUTION
C DATA NPROBI,MITI/1,200/
C DATA EPS1I,EPS2I,FLAMI,FNUI/1.0E-10,1.0E-05,0.01,10.0/
C NUMERICAL INTEGRATION DATA
C DATA EPSR/1.E-01/
C DATA (TAUM(J),J=1,14)/0.0,0.25,0.50,0.75,1.0,1.3333,1.6667,
C 1 2.0,4.0,6.0,10.0,22.0,33.0,44.0/
C DATA NOFN/0/

C ISOTHERMAL BATCH OR UNSTEADY STATE MODEL

THETA=THETA0

C IF REQUIRED READ IN EXPERIMENTAL DATA

KW=0

IF(NCTL(1).EQ.1) KW=1

IF(NCTL(2).EQ.1) KW=1

IF(NCTL(4).EQ.1) KW=1

IF(KW.EQ.1) CALL EXMLDT(1,ME,ME1,NE1, TAUE,VE,JE,HTIE,WTBE)

C DIFFERENT PROBLEMS AND OR SOLUTION METHODS VARIABLE

NCASE=2

IF((3GT.EQ.1.).AND.(FIXGRD.NE.1.)) NCASE=1

C SPECIAL GRIDS WRT CRYSTAL SIZE

C GRID FOR THE REPEATED CALCULATION OF THE AGGLOMERATION TERM

JA(1)=D0

MA1=MA+1

VA0=VA(1)=.523598*DA(1)*DA(1)*DA(1)

K1=2**(NGA-1)

RK1=K1

DO 10 I=2,MA1

X2=(I-1)/K1

X1=2.*K2

X2=I-1-(K1*K2)

VA(I)=(X1+(X1/RK1*X2))*VA0

10 JA(I)=1.2407*CBRT(VA(I))

C GRID FOR THE METHOD OF CHARACTERISTICS

IF(NCASE.EQ.1) GO TO 20

MG=MA

MG1=MG+1

DO 15 I=1,MG1

VG(I)=VA(I)

15 DG(I)=DA(I)

GO TO 32

20 JG(1)=DA(1)

DELOG=CAG1*(DA(2)-DA(1))

DG(2)=DG(1)+DELOG

KP=1

L=2

22 L=LP

IF(DG(L).GT.DA(MA1)) GO TO 28

DO 24 K=KP,MA

KWK=K

IF((DG(L).LE.DA(K+1)).AND.(DG(L).GE.DA(K))) GO TO 26

24 CONTINUE

25 KP=KWK

X1=CAG*(DA(KP+1)-DA(KP))

X2=2.*DELOG

IF(X1.GE.X2) DELOG=X2

JG(L+1)=DG(L)+DELOG

LP=L+1

GO TO 22

28 MG=L

MG1=MG+1

JG(L+1)=DG(LP)+DELOG

DO 30 I=1,MG1

30 VG(I)=.523599*DG(I)*DG(I)*DG(I)

32 CONTINUE

C GRID EQUAL TO THE PROJECTION OF THE CHARACTERISTICS ON THE TAU-D PLANE

IF(NCASE.EQ.1) GO TO 44

MC=MA

```

MC1=MC+1
DO 42 I=1,MC1
VC(I)=VA(I)
42 JC(I)=DCO(I)=DA(I)
GO TO 50
44 MC1=MG1-1
MC=MC1-1
DO 46 I=1,MC1
VC(I)=VG(I)
46 JC(I)=DCO(I)=DG(I)
50 CONTINUE

```

C TRANSFORMATIONS WRT CRYSTAL SIZE

```

Z1(I)=ALOG(VC(I))
DO 54 I=2,MC1
Z1(I)=ALOG(VC(I))
54 Z2(I-1)=VC(I)-VC(I-1)
DO 56 I=2,MC
DVO(I)=1.570796*DC(I)*DC(I)
X1=1./((Z1(I+1)-Z1(I))/Z2(I))-((Z1(I)-Z1(I-1))/Z2(I-1))
1 *((1./Z2(I))-(1./Z2(I-1)))
X2=(1./Z2(I-1))-X1*(Z1(I)-Z1(I-1))/Z2(I-1)
56 DXV(I)=X2+(X1/VC(I))

```

C CALCULATED INITIAL SIZE DISTRIBUTION

```
IF(NCTL(1))58,58,60
```

```

58 CONTINUE
READ(5,600) JM,TAU
READ(5,602) C1,C2,C3,C4,C5
READ(5,602) C6,GL,HST,HSTMN,HSTMX
READ(5,602) (DC(I),I=1,MC1)
READ(5,602) (HTC(I),I=1,MC1)
GO TO (224,203),NCASE

```

50 CONTINUE

C CALCULATED INITIAL SIZE DISTRIBUTION WITH OPTIMIZED PARAMETERS
C MARQUARDT OPTIMIZATION ROUTINE IS USED

```

DO 52 K=1,NPI
SIGNSI(K)=1.
62 JIFFI(K)=0.01
NOBI=ME1
XWI=1.
DO 54 I=1,ME
X1=(HTIE(I,1)-HTIE(I+1,1))/(VE(I+1)-VE(I))
64 YI(I)=XWI*ALOG(X1+1.)
YI(ME1)=WDE
CAL UMHAUS(NPROBI,OPTINL,NOBI,YI,NPI,BI,DIFFI,SIGNSI,EPS1I,EPS2I,
1 MITI,FLAMI,FNUI,WK1)
CALL INLSOR(ME1,NPI,BI,VE,DE,Z1,Z2,X1)
Z1(ME1)=0.
DO 56 I=1,ME
56 Z1(ME1-I)=Z1(ME1-I+1)+Z2(ME1-I+1)-Z2(ME1-I)
C COMPARISON BETWEEN EXPERIMENTAL AND MODEL INITIAL SIZE DISTRIBUTION VALUES
WRITE(6,68) (BI(K),K=1,NPI)
68 FORMAT(1H1,2X,*OPTIMIZED INITIAL SIZE DISTRIBUTION PARAMETER VALUE
15*,//,3X,*BI(K)=*,1PE12.4,5E12.4)
WRITE(5,70)
70 FORMAT(//,3X,*COMPARISON BETWEEN EXPERIMENTAL AND MODEL INITIAL S
1ZE DISTRIBUTION VALUES*,//,3X,*DE*,10X,*VE*,10X,*HTIE*,8X,
2*HTI*,9X,*EPS*,9X,*RLT CVT*,/)
DO 72 I=1,ME1
X1=4TIE(I,1)-Z1(I)
X2=0.

```

```

IF(4*IE(I,1).GT.0.) X2=X1/HTIE(I,1)*100.
72 WRITE(6,500) DE(I),VE(I),HTIE(I,1),Z1(I),X1,X2
CALL INLSOR(MC1,NPI,BI,VC,DC,FVT,HTC,WTO)
WRITE(6,74) WTOE,WTO
74 FORMAT(//,1X,*WTOE =*,1PE12.4,10X,*WTO =*,1E12.4)
90 CONTINUE

```

C MASS BALANCE CONSTANTS

```

WTO=0.
DO 100 I=1,MC
100 WTO=WTO+(HTC(I+1)-HTC(I))*(VC(I+1)+VC(I))
WTO=1.21E-12*WTO
BO1=1051.+((-0.94+(5.1E-03*THETA0))*THETA0)
BO2=9.92E-01
BO3=-1.1E-04
BO4=5.66E-01
C5=VLO*CN0
C4=(VLO*CA0)+(.654*WTO)
C3=BO3*C5*C5
C2=1.-(.654*BO4)
C1=BO1
RHOL0=BO1+(BO2*CN0)+(BO3*CN0*CN0)+(BO4*CA0)
C6=- (VLO*RHOL0)-WTO+(BO2*C5)+(BO4*C4)

```

C NUMERICAL INTEGRATION

```

GO TO (220,200),NCASE
200 CONTINUE
TAJ0=TAU
HST=(TAUM(2)-TAUM(1))/1.E+03
HSTM=TAUM(NM1)
HSTMN=HST/100.
202 CONTINUE
YWFCT=1.E+02/HTC(MC1)
DO 204 I=1,MC1
Y(I)=HTC(I)*YWFCT
204 CONTINUE
X=TAJ
CALL DFN(Y,X,MC1,DYX)
IF(NCTL(3).EQ.1) WRITE(6,300) NDFN,COFY,HST,HSTMN,HSTMX
IF(NCTL(3).EQ.1) CALL PRMGL(MC1,MC,MA1,MA,MC1,TAJM(JM),
1 WT,VL,CA,CN,CAE,GE,GRIC,PHIEN,PHIVN,RVCLC,PHIEA,AGERW,BHLA,DHLA,
2 AGGC,Y,ERR,DYX,HTC,DC,VC,HTA,DA,VA,NPNCH)
IF(NCTL(4).EQ.1) CALL EXMDL(JM,ME1,ME1,ME,MC1,MC,TAUE,VE,DE,
1 VC,JC,HTIE,HTC,Z1,Z2,NPNCH)
IF(JM.GE.NM1) GO TO 250
GO TO 205
203 CONTINUE
YWFCT=1.E+02/HTC(MC1)
X=TAJ
DO 201 I=1,MC1
Y(I)=HTC(I)*YWFCT
201 CONTINUE
205 XL=X
XU=XL+HST
IF(XU.GT.TAUM(JM+1)) XU=TAUM(JM+1)
IF(BST.EQ.1.) HSTMX=(DC(2)-DC(1))/GL*4.
IF(HST.GT.HSTMX) HST=HSTMX
CALL RNGMRS(DFN,MC1,Y,XL,XU,HST,HSTMN,HSTMX,EPSR,ERR,Z1,Z2,WK1)
DO 206 I=1,MC1
HTC(I)=Y(I)/YWFCT
IF(HTC(I).LT.0.) HTC(I)=0.
206 CONTINUE
-----
C IF(CDFN.LT.TIMX1) GO TO 604
PUNCH(7,600) JM,TAU

```



```

3 UNCH(7,602) C1,C2,C3,C4,C5
3 UNCH(7,502) C6, GL, HST, HSTMN, HSTMX
3 UNCH(7,602) (DC(I), I=1, MC1)
3 UNCH(7,602) (HTC(I), I=1, MC1)
WRITE(6,300) NDFN, CDFN, HST, HSTMN, HSTMX
CALL PRMTDL(MC1, MC, MA1, MA, M9, TAU, WT, VL, CA, CN, CAE, GL, GRTC,
1 PHIEN, PHIVN, RNCLC, PHIEA, AGERW, BHLA, DFLA, AGGC, Y, ERR, DYX, HTC, DC,
2 VC, HTA, DA, VA, 0)
STOP

```

504 CONTINUE

```

C-----
IF(XU.GE.TAUM(JM+1)) GO TO 207
X=TAU
GO TO 205
207 JM=JM+1
GO TO 202
220 CONTINUE
TAUO=TAU
YWFCT=1.E+02/HTC(MC1)
DO 222 I=1, MC1
Y(I)=HTC(I)*YWFCT
222 CONTINUE
CALL DFN(Y, 0., MC1, DYX)
HST=1.E-04
HSTMN=HST/10.
224 CONTINUE
TAUO=TAU
GLO=GL
XL=0.
XU=(JG(2)-JG(1))*SQRT((GLO*GLO)+1.)/GLO
HST=X-XJ-XL
IF(HST.GT.(HSTMX/2.)) HST=HSTMX
YWFCT=1.E+02/HTC(MC1)
DO 226 I=1, MC1
DC(I)=DC(I)
Y(I)=HTC(I)*YWFCT
226 YO(I)=Y(I)
CALL RNMRS(DFN, MC1, Y, XL, XU, HST, HSTMN, HSTMX, EPSR, ERR, Z1, Z2, WK1)
CALL DFN(Y, XU, MC1, DYX)
IF(TAU.LT.TAUM(JM)) GO TO 244
DO 232 I=1, MC1
ZS1(I)=DC(I)
232 ZS2(I)=Y(I)
XS1=TAU
IF(ABS(TAU-TAUO).LT.1.E-04) GO TO 236
X=XJ*(TAUM(JM)-TAUO)/(TAU-TAUO)
DO 234 I=1, MC1
234 Y(I)=YO(I)+((ZS2(I)-YO(I))*X/XU)
GO TO 240
235 X=0.
DO 238 I=1, MC1
235 Y(I)=YO(I)
240 CALL DFN(Y, X, MC1, DYX)
IF(NCTL(3).EQ.1) WRITE(6,300) NDFN, CDFN, HST, HSTMN, HSTMX
IF(NCTL(3).EQ.1) CALL PRMTDL(MC1, MC, MA1, MA, (MC1+1), TAUM(JM),
1 WT, VL, CA, CN, CAE, GL, GRTC, PHIEN, PHIVN, RNCLC, PHIEA, AGERW, BHLA, DFLA,
2 AGGC, Y, ERR, DYX, HTC, DC, VC, HTA, DA, VA, NPNCH)
IF(NCTL(4).EQ.1) CALL EXMDL(JM, NE1, ME1, ME, MC1, MC, TAUE, VE, DE,
1 VC, DC, HTIE, HTC, Z1, Z2, NPNCH)
JM=JM+1
IF(JM.GT.NM1) GO TO 250
DO 242 I=1, MC1
DC(I)=ZS1(I)
242 Y(I)=ZS2(I)
TAU=XS1

```

```

244 DO 245 I=1,MC1
245 Z1(I)=Y(I)
      DO 248 I=2,MC1
      IF(ABS(DC(I)-DG(I+1)).LT.1.E-04) GO TO 246
      GO TO 248
246 JC(I)=DG(I)
      Y(I)=Z1(I-1)
248 CONTINUE
      DC(I)=DG(I)
      Y(I)=0.
      DO 249 I=1,MC1
      HTC(I)=Y(I)/YWFCT
      IF(HTC(I).LT.0.) HTC(I)=0.
249 CONTINUE
-----
      IF(CDFN.LT.TIMX1) GO TO 260
      PUNCH(7,500) JM,TAU
      PUNCH(7,602) C1,C2,C3,C4,C5
      PUNCH(7,602) C6,GL,HST,HSTMN,HSTMX
      PUNCH(7,602) (DC(I),I=1,MC1)
      PUNCH(7,502) (HTC(I),I=1,MC1)
      WRITE(6,300) NDFN,CDFN,HST,HSTMN,HSTMX
      CALL PRMCL(MC1,MC,MA1,MA,M9,TAU,NT,VL,CA,CN,CAE,GL,GRTC,
1 PHEN,PHIVN,RNCLC,PHIEA,AGERW,BHLA,DHLA,AGGC,Y,ERR,DYX,HTC,DC,
2 VC,HTA,DA,VA,0)
      STOP

```

```

250 CONTINUE
-----
      GO TO 224
250 CONTINUE

```

```

300 FORMAT(1H1,1X,*NDFN=*,I4,10X,*CDFN=*,1PE12.4,5X,*HST=*,1E12.4,
1 5X,*HSTMN=*,1E12.4,5X,*HSTMX=*,1E12.4)
500 =ORFAT(1X,1PE12.4,10E12.4)
600 =ORFAT(1I5,1E16.10)
602 =ORFAT(5E13.10)

```

```

STOP
END
SUBROUTINE DFN(Y,X,M9,DYX)

```

RIGHT HAND SIDE VALUES OF THE SET OF ORDINARY DIFFERENTIAL MODEL EQUATIONS

```

DIMENSION Y(M9),DYX(M9)
COMMON/BLM1/MG,MG1,MA,MA1,MC,MC1,FVT(150),HTC(151),HTA(151)
COMMON/BLM2/VG(151),DG(151),VA(151),DA(151),VC(151),DC(151)
COMMON/BLM3/C1,C2,C3,C4,C5,C6,WT,VL,CA,CAE,CN,THETA,TAU,TAUO
COMMON/BLM4/YWFCT,DCO(151),DVD(151),DXV(151)
COMMON/BLP2/NPG,NPN,NPA,NPI,BG(3),BN(5),BA(5),BI(3)
COMMON/BLCS1/GL,GLO,GRTC(151),PHEN,PHIVN(151),RNCLC(151)
COMMON/BLCS2/PHIEA,PHIVA(11325),BHLA(151),DHLA(151),AGERW(151)
COMMON/BLCS3/AGGC(151),DELVA(150),SMVA(150),PHI1(151),PHI2(151),
1 A(151),AD(151),E(151)
COMMON/BLCT/BGT,BNL,BAG,FXGRC,NCASE,NCTL(5),TIMX2,NPNCH
COMMON/BLR/NDFN,CDFN,MWK1,NGA,ERR(151),HST,HSTMN,HSTMX
COMMON/BLW/Z1(151),Z2(151),ZS1(151),ZS2(151)

```

```

CENTRAL PROCESSING TIME.
CD=N=SECOND(CP)

```

```

NUMBER OF CALLS TO SUBROUTINE DFN
ND=N=NDFN+1

```

```

IF(NDFN.GT.1) GO TO 28
IF(3GT.NE.0.) GO TO 10

```

```

31 = 0.
DO 8 I=1,MC1
8 GRTC(I)=0.
10 CONTINUE
IF(3VL.NE.0.) GO TO 14
PHIEA=0.
DO 12 I=1,MC1
12 PHIVN(I)=RNCLC(I)=0.
14 CONTINUE
IF(3AG.NE.0.) GO TO 20
PHIEA=0.
DO 15 I=1,MA1
15 BHLA(I)=DBHLA(I)=AGERW(I)=0.
DO 19 I=1,MC1
19 AGGC(I)=0.
20 CONTINUE
25 CONTINUE
GO TO (30,40),NCASE
3) TAU=TAUO
IF(X.GT.0.) TAU=TAUO+X/SQRT(GLO*GLO+1.)
X1=0.
IF(X.GT.0.) X1=X*GLO/SQRT(GLO*GLO+1.)
DO 32 I=1,MC1
DC(I)=DCO(I)+X1
VC(I)=.523598*DC(I)*DC(I)*DC(I)
HTC(I)=Y(I)/YWFCT
32 CONTINUE
DO 33 I=1,MC1
IF(ABS(HTC(I)).GT.(1.1*HTC(MC1))) GO TO 80
IF(HTC(I).LT.0.) HTC(I)=0.
33 CONTINUE
CALL MSSBLC(MC,MC1,VC,MA1,VA,HTC,C1,C2,C3,C4,C5,C6,THETA, WT,
1 VL,CA,CN,CAE,Z1)
CALL GRTRT(NPG,BG,CA,CAE,TAU, GL)
IF(3AG.EQ.1.) CALL AGGLRT(NCTL(5),TAU,CA,CAE,VL,WT,MC,MC1,MA,
1 MA1,NPA,MWK1,NGA,BA,NCASE,VC,VA,HTC, HTA,PHIEA,PHIVA,BHLA,DBHLA,
2 AGERW,AGGC,Z1,Z2,DELVA,SMVA,PHI1,PHI2,A,AD,E)
IF(3NL.EQ.1.) CALL NCLRT(MC,MC1,VC,MA1,VA,NPN,BN,CA,CAE,VL,WT,
1 PHIEN,PHIVN,RNCLC,Z1)
DO 34 I=1,MC1
DYX(I)=(AGGC(I)+RNCLC(I))*YWFCT
34 CONTINUE
IF((CA-(CAE*1.05)).LE.0.) GO TO 80
IF(CJFN.GE.TIMX2) GO TO 80
RETJRN
40 TAU=X
DO 42 I=1,MC1
42 HTC(I)=Y(I)/YWFCT
CONTINUE
DO 43 I=1,MC1
IF(ABS(HTC(I)).GT.(1.1*HTC(MC1))) GO TO 80
IF(HTC(I).LT.0.) HTC(I)=0.
43 CONTINUE
CALL MSSBLC(MC,MC1,VC,MA1,VA,HTC,C1,C2,C3,C4,C5,C5,THETA, WT,
1 VL,CA,CN,CAE,Z1)
IF(3AG.EQ.1.) CALL AGGLRT(NCTL(5),TAU,CA,CAE,VL,WT,MC,MC1,MA,
1 MA1,NPA,MWK1,NGA,BA,NCASE,VC,VA,HTC, HTA,PHIEA,PHIVA,BHLA,DBHLA,
2 AGERW,AGGC,Z1,Z2,DELVA,SMVA,PHI1,PHI2,A,AD,E)
IF(3VL.EQ.1.) CALL NCLRT(MC,MC1,VC,MA1,VA,NPN,BN,CA,CAE,VL,WT,
1 PHIEN,PHIVN,RNCLC,Z1)
IF(3GT.NE.1.) GO TO 50
CALL GRTRT(NPG,BG,CA,CAE,TAU, GL)
DO 44 I=1,MC1
44 Z1(I)=ALOG(HTC(I)+1.)
DO 46 I=2,MC1

```

```

46 Z2(I-1)=Z1(I)-Z1(I-1)
DO 48 I=2,MC
X1=(Z2(I)+.0001)/(Z2(I)+Z2(I-1)+.0001)
X2=(X1*Z2(I-1))+((1.-X1)*Z2(I))
48 GRTC(I)=GL*(HTC(I)+1.)*DVO(I)*DXV(I)*X2
GRTC(I)=0.
GRTC(MC1)=GL*(HTC(MC1)-HTC(MC))/(DC(MC1)-DC(MC))
DO 49 I=1,MC1
IF(GRTC(I).LT.1.E-04) GRTC(I)=0.
49 CONTINUE
50 DO 52 I=1,MC1
JYX(I)=(AGGC(I)+RNCLC(I)-GRTC(I))*Y.WFST
52 CONTINUE
IF((CA-(CAE*1.05)).LE.0.) GO TO 80
IF(CJFN.GE.TIMX2) GO TO 80
RETURN
80 CONTINUE
WRITE(6,300) NDFN,COFN,HST,HSTMN,HSTMX
CALL PRMDEL(MC1,MC,MA1,MA,M9,TAU,WT,VL,CA,CN,CAE,GL,GRTC,
1 PHEN,PHIVN,RNCLC,PHIEA,AGERW,BHLA,DOLA,AGGC,Y,ERR,DYX,HTC,DC,
2 VC,HTA,JA,VA,0)
300 FORMAT(1H1,1X,*NDFN=*,I4,10X,*COFN=*,1PE12.4,5X,*HST=*,1E12.4,
1 5X,*HSTMN=*,1E12.4,5X,*HSTMX=*,1E12.4)
STOP
END
SUBROUTINE OPTINL(NPROB1,Y9,YIM,NOBI,NP9)

```

INITIAL SIZE DISTRIBUTION SCALED MODEL VALUES FOR OPTIMIZATION ROUTINE UI

```

DIMENSION Y9(NP9),YIM(NOBI)
COMMON/BLE/NE1,ME1,ME,TAUE(14),VE(101),DE(101),HTIE(101,14)
COMMON/BLM1/MG,MG1,MA,MA1,MC,MC1,FVT(150),HTC(151),HTA(151)
COMMON/BLM2/VG(151),DG(151),VA(151),DA(151),VC(151),DC(151)
COMMON/BL1/XWI
COMMON/BLW/Z1(151),Z2(151),ZS1(151),ZS2(151)

CALL INLSDR(MG1,NP9,Y9,VG,DG,Z1,Z2,HTD)
CALL INLSDR(ME1,NP9,Y9,VE,DE,Z1,Z2,X1)
DO 12 I=1,4E
X1=(Z2(I+1)-Z2(I))/(VE(I+1)-VE(I))
12 YI4(I)=XWI*ALOG(X1+1.)
YI4(4E1)=WTD

RETURN
END
SUBROUTINE INLSDR(M,NPI,BI,V,C,FVT,HT,HTD)

```

EMPIRICAL INITIAL SIZE DISTRIBUTION MODEL

```

DIMENSION BI(NPI),V(M),D(M),FVT(M),HT(4)

```

EXPONENTIAL DENSITY FUNCTION WRT D-----

```

X1=EXP(-BI(2)*D(1))
DO 10 I=1,M
VT(I)=.63662/(D(I)*D(I))*BI(1)*BI(2)*EXP(-BI(2)*D(I))
10 HT(I)=BI(1)*(X1-EXP(-BI(2)*D(I)))

```

INITIAL CRYSTAL WEIGHT

```

41=4-1
WTD=0.
DO 12 I=1,M1
12 WTD=WTD+(HT(I+1)-HT(I))*(V(I+1)+V(I))
WTD=1.21E-12*WTD

```

```

RETURN
END
SUBROUTINE MSSBLC(MC,MC1,VC,MA1,VA,HTC,C1,C2,C3,C4,C5,C6,THETA,
1  WT,VL,CA,CN,CAE,Z1)
C MASS BALANCE VARIABLES , EMPIRICAL CORRELATION
C DIMENSION VC(MC1),VA(MA1),HTC(MC1),Z1(MC1)
C MASS BALANCE VARIABLES
WT=0.
DO 10 I=1,MC
11  WT=WT+(HTC(I+1)-HTC(I))*(VC(I+1)+VC(I))
    WT=WT+HTC(1)*(VC(1)+VA(1))
    AT=1.21E-12*WT
    X1=C5+(WT*C2)
    VL=(-X1+SQRT((X1*X1)-(4.*C1*C3)))/(2.*C1)
    CA=(C4-(.654*WT))/VL
    CN=C5/VL
C EMPIRICAL CORRELATION
CAE=CN*EXP(6.2106+(((1.0875*CN)-2486.7)/(273.16+THETA)))
RETURN
END
SUBROUTINE GRTRT(NPG,BG,CA,CAE,FAU, G_)
C GROWTH RATE
C DIMENSION BG(NPG)
C-CONSTITUTIVE EQUATION-----
X1=(CA-CAE)/CAE
GL=BG(1)*(X1**(5./6.))*EXP(-BG(2)/X1)
RETURN
END
SUBROUTINE NCLRT(MC,MC1,VC,MA1,VA,NPN,BN,CA,CAE,VL,WT,
1  PHIEN,PHIVN,RNCLC,Z1)
C NUCLEATION RATE
C DIMENSION BN(NPN),VC(MC1),VA(MA1),PHIVN(MC1),RNCLC(MC1),Z1(MC1)
C-CONSTITUTIVE EQUATIONS-----
C ENVIRONMENT DEPENDENT FACTOR
X1=(CA-CAE)/CAE
PHIEN=BN(1)/(1.+EXP(BN(2)*(-BN(3)+(1./X1))))
C SIZE DEPENDENT FACTOR (LOG NORMAL WRT V)
DO 10 I=1,MC1
10  Z1(I)=ALOG(VC(I))
    X1=1./(2.50663*BN(4))
    X2=-1./(2.*BN(4)*BN(4))
    DO 12 I=1,MC1
    X3=Z1(I)-BN(5)
12  PHIVN(I)=X1/VC(I)*EXP(X2*X3*X3)
    X1=1.41421*BN(4)
    J0=(ALOG(VA(1))-BN(5))/X1
    X2=ERF(U0)
    X3=VL*PHIEN/2.
    DO 14 I=1,MC1
    J=(Z1(I)-BN(5))/X1
14  RNCLC(I)=X3*(ERF(U)-X2)
RETURN

```

```

END
SUBROUTINE AGGLRT(NCLT,TAU,CA,CAE,VL,WT,MC,MC1,MA,MA1,NPA,MWK,
1 NGA,BA,NCASE,VC,VA,HTC,HTA,PHIEA,PHIVA,BHLA,DHLA,AGERW,AGGC,
2 Z1,Z2,DELVA,SMVA,PHI1,PHI2,A,AD,E)

```

```

AGGLOMERATION RATE

```

```

MWK      =MA*(MA+1)/2
NCLT     =1 APPLY THE EMPIRICAL AGGLOMERATION TERM CORRECTION
          EXPRESSION, =0 DO NOT

```

```

DIMENSION BA(NPA),VA(MA1),VC(MC1),HTA(MA1),HTC(MC1),PHIVA(MWK),
1 BHLA(MC1),DHLA(MC1),AGERW(MC1),AGGC(MC1),Z1(MC1),Z2(MC1),
2 DELVA(MA),SMVA(MA),PHI1(MA1),PHI2(MA1),A(MA1),AD(MA1),E(MA1)
INTEGER P,PMN

```

```

C-----CONSTITUTIVE EQUATIONS-----
C SIZES DEPENDENT FACTOR

```

```

DATA NFLG1/0/
NFLG1=NFLG1+1
IF(NFLG1.GT.1) GO TO 8
DO 4 I=1,MA
Z1(I)=CBRT((VA(I+1)+VA(I))/2.)
* Z2(I)=Z1(I)*Z1(I)
K=0
DO 5 P=1,MA
DO 6 L=P,MA
K=K+1
X1=Z1(L)
X2=Z1(P)
X3=Z2(L)
X4=Z2(P)
X5=X1+X2
5 PHIVA(K)=X5*X5*ABS(X3-X4)*EXP(-BA(3)*(X3+X4))
6 CONTINUE

```

```

C ENVIRONMENT DEPENDENT FACTOR
PHIEA=BA(1)*(((CA-CAE)/CAE)**BA(2))

```

```

C-----ONCE TO BE CALCULATED VARIABLES-----

```

```

IF(NFLG1.GT.1) GO TO 14
DO 10 I=1,MA
DELVA(I)=VA(I+1)-VA(I)
10 SMVA(I)=(VA(I+1)+VA(I))/2.
LPR=2** (NGA-1)
MX=MA1-LPR-1
K=0
DO 12 P=1,MA
DO 12 L=P,MA
K=K+1
12 PHIVA(K)=PHIVA(K)*DELVA(P)*DELVA(L)
14 CONTINUE

```

```

C-----INTERPOLATION FROM THE VC GRID TO THE VA GRID-----

```

```

GO TO (20,16),NCASE
15 DO 13 I=1,MA1
13 HTA(I)=HTC(I)
GO TO 32
20 CONTINUE
Z1(1)=VA(1)
Z2(1)=0.
DO 22 I=2,MC1
Z1(I)=VC(I-1)
22 Z2(I)=HTC(I-1)
DO 24 I=1,MC1
24 Z2(I)=ALOG(Z2(I)+1.E-14)

```

```

HTA(1)=0.
KWK=1
DO 3J I=2,MA1
DO 25 L=KWK,MC
L1=L
IF(VA(I).LE.Z1(L+1).AND.VA(I).GE.Z1(L)) GO TO 28
25 CONTINUE
23 Z2=0.
X1=Z1(L1+1)-Z1(L1)
IF(ABS(X1).GT.1.E-08) C2=(Z2(L1+1)-Z2(L1))/X1
Z1=Z2(L1)-(C2*Z1(L1))
HTA(I)=EXP(C1+(C2*VA(I)))
30 KWK=L1
32 CONTINUE

```

GGGGG EXACT SOLUTION OF THE AGGLOMERATION INTEGRAL EXPRESSIONS GIVEN A PARTICULAR SECTIONAL APPROXIMATION OF HTA FIRST ORDER COLLOCATION APPROXIMATION OF HTA AND ZERO ORDER COLLOCATION OF PHIVA

```

BHLA(1)=OHLA(1)=AGGC(1)=0.
DO 40 I=1,MA
40 Z2(I)=(HTA(I+1)-HTA(I))/DELVA(I)
DO 42 I=1,MA1
42 A(I)=AD(I)=E(I)=0.
DO 50 P=1,LMX
KWK1=(MA*P)-((P-1)*P/2)-MA
L=P
K=KWK1+L
PHI1(L+1)=PHIVA(K)*Z2(L)*Z2(L)/2.
LMN=P+1
DO 44 L=LMN,MA
K=KWK1+L
Z1(L)=PHIVA(K)*Z2(L)*Z2(P)
44 PHI1(L+1)=PHI1(L)+Z1(L)
LMN=P+LPR+1
IWK=LPR
DO 45 L=LMN,MA1
X1=VA(L)-VA(P)
45 I=L-IWK
IF(X1.GE.VA(I).AND.X1.LE.VA(I+1)) GO TO 48
IWK=IWK-1
GO TO 46
48 PHI2(L)=PHI1(I)+(Z1(I)*(VA(L)-VA(I)-SMVA(P))/DELVA(I))
LMN=I+1
DO 50 L=LMN,MA1
AD(L)=AD(L)+PHI1(L)
50 E(L)=E(L)+PHI1(MA1)-PHI1(L)
LMN=P+LPR+1
DO 52 L=LMN,MA1
52 A(L)=A(L)+PHI2(L)
51 CONTINUE
PHV=LMX+1
DO 70 P=PMN,MA
KWK1=(MA*P)-((P-1)*P/2)-MA
L=P
K=KWK1+L
PHI1(L+1)=PHIVA(K)*Z2(L)*Z2(L)/2.
IF(L.EQ.MA) GO TO 66
LMN=P+1
DO 52 L=LMN,MA
K=KWK1+L
52 PHI1(L+1)=PHI1(L)+(PHIVA(K)*Z2(L)*Z2(P))
DO 54 L=LMN,MA1
AD(L)=AD(L)+PHI1(L)
64 E(L)=E(L)+PHI1(MA1)-PHI1(L)

```

```

GO TO 70
66 AD(L+1)=AD(L+1)+PHI1(L+1)
70 CONTINUE
DO 72 I=2,MA1
BHLA(I)=PHIEA/VL*A(I)
72 JHLA(I)=PHIEA/VL*(AD(I)+AD(I)+E(I))

```

BACK INTERPOLATION FROM THE VA TO THE VC GRID

```

GO TO (120,140),NCASE
120 DO 122 I=1,MA1
Z1(I)=BHLA(I)
122 Z2(I)=DHLA(I)
KWK=1
DO 128 L=1,MC1
L1=L
IF(VC(L1).GT.VA(MA1)) GO TO 130
DO 124 I=KWK,MA
I1=I
IF(VC(L).GE.VA(I).AND.VC(L).LE.VA(I+1)) GO TO 126
124 CONTINUE
125 C2=(Z1(I1+1)-Z1(I1))/(VA(I1+1)-VA(I1))
C1=Z1(I1)-(C2*VA(I1))
BHLA(L)=C1+C2*VC(L1)
C2=(Z2(I1+1)-Z2(I1))/(VA(I1+1)-VA(I1))
C1=Z2(I1)-(C2*VA(I1))
JHLA(L)=C1+C2*VC(L1)
128 KWK=I1
130 DO 132 L=L1,MC1
BHLA(L)=BHLA(L-1)
132 JHLA(L)=JHLA(L-1)
140 CONTINUE

```

EMPIRICAL AGGLOMERATION TERM WEIGHT CORRECTION

```

IF(NCLT) 100,100,80
81 DO 82 I=1,MC1
82 Z1(I)=BHLA(I)-DHLA(I)
X1=1.
XS1=XS2=0.
DO 84 I=1,MC
X2=X1*(VC(I+1)+VC(I))
XS1=XS1+(X2*(Z1(I+1)-Z1(I)))
84 XS2=XS2+(X2*((DHLA(I+1)*Z1(I+1)-(DHLA(I)*Z1(I))))
C=XS1/XS2
DO 85 I=1,MC1
AGERW(I)=1.-(C*DHLA(I))
BHLA(I)=AGERW(I)*BHLA(I)
85 JHLA(I)=AGERW(I)*JHLA(I)
100 CONTINUE

```

```

DO 142 I=1,MC1
142 AGGC(I)=BHLA(I)-DHLA(I)

```

```

RETURN
END

```

SUBROUTINE NMTHG1(M1,TAU,V,D,HTC,C1,SISMA,ETA,BG1,BG2,HTCTHG)

ANALYTICAL SOLUTION OF GROWTH ONLY PROCESS WITH-----

```

GD=BG1*EXP(BG2*TAU)

```

```

DIMENSION V(M1),D(M1),HTC(M1),HTCTHG(M1)
REAL L

```



```

FLTD(C1,SIGMA,ETA,L)=C1/(2.506628*SIGMA*L*EXP(-1./(2.*SIGMA*SIGMA)
1 *ALOG(L)-ETA)*(ALOG(L)-ETA))

```

ANALYTICAL SOLUTION

```

J0=J(1)
X1=J0+(BG1/BG2*(EXP(BG2*TAU)-1.))
Q1=(ALOG(D0)-ETA)/(1.4142136*SIGMA)
DO 12 I=1,M1
HTCTHG(I)=0.
IF(D(I).LT.X1) GO TO 12
X2=J(I)-(BG1/BG2*(EXP(BG2*TAU)-1.))
QI=(ALOG(X2)-ETA)/(1.4142136*SIGMA)
HTCTHG(I)=.5*C1*(ERF(QI)-ERF(Q1))

```

12 CONTINUE

COMPARISON BETWEEN NUMERICAL AND ANALYTICAL SOLUTIONS

```

GD=3G1*EXP(BG2*TAU)
WRITE(6,600) TAU,GD
DO 20 I=1,M1
X1=HTC(I)-HTCTHG(I)
X2=0.
IF(HTCTHG(I).GT.0.) X2=X1/HTCTHG(I)*100.
20 WRITE(6,602) D(I),V(I),HTC(I),HTCTHG(I),X1,X2

```

600 FORMAT(1H1,1X,*-COMPARISON BETWEEN NUMERICAL AND ANALYTICAL SOLUTI

```

10N-*,//,1X,*GROWTH ONLY PROCESS*,
2 //,1X,*TAU =*,1PE12.4,10X,*GD =*,1E12.4,
3 ///,3X,*J*,11X,*V*,11X,*HTC*,9X,*HTCTHG*,
4 6X,*EPS*,9X,*RLT DVT*,/)

```

602 FORMAT(1X,1PE12.4,10E12.4)

RETURN

END

SUBROUTINE NMTHA1(M1,TAU,V,HTC,NO,VAVE,C,HTCTH1)

ANALYTICAL SOLUTION OF AGGLOMERATION ONLY PROCESS WITH----

INITIAL SIZE DISTRIBUTION $FVT(I,0) = \exp(-V(I)/VAVE) * NO / VAVE$
 AGGLOMERATION EFFECTIVENESS KERNEL $KP = PHIEA * PHIVA / VL = C$

```

DIMENSION V(M1),HTC(M1),HTCTH1(M1)
REAL NO

```

ANALYTICAL SOLUTION

```

T=C*NO*TAU
X1=T+2
X2=4.*NO/(VAVE*X1*X1)
X3=-2./(X1*VAVE)
X4=EXP(X3*V(1))
DO 10 I=1,M1
10 HTCTH1(I)=X2/X3*(EXP(X3*V(I))-X4)

```

COMPARISON BETWEEN NUMERICAL AND ANALYTICAL SOLUTIONS

```

WRITE(6,600) TAU,T
DO 20 I=1,M1
X1=CBRT(1.90986*V(I))
X2=HTC(I)-HTCTH1(I)
X3=0.
IF(HTCTH1(I).GT.0.) X3=X2/HTCTH1(I)*100.
20 WRITE(6,602) X1,V(I),HTC(I),HTCTH1(I),X2,X3

```

600 FORMAT(1H1,1X,*-COMPARISON BETWEEN NUMERICAL AND ANALYTICAL SOLUTI

```

10N-*,//,1X,*AGGLOMERATION ONLY PROCESS*,
2 //,1X,*FVT(V,0)=EXP(-V/VAVE).NO/VAVE*,
3 //,1X,*K=C*,//,1X,*TAU =*,1PE12.4,10X,*T =*,1E12.4,

```

```

4  ///,3X,*D*.11X,*V*.11X,*HTC*.9X,*HTCTH1*.5X,
5      *EPS*.9X,*RLI DVT*,/)
602  FORMAT(1X,1PE12.4,10E12.4)
      RETURN
      END
      SUBROUTINE PRTMDL(MC1,MC,MA1,MA,MWK,TAU,WT,VL,CA,CN,CAE,
1  GL,GRTC,PHIEN,PHIVN,RNCLC,PHIEA,AGERW,BHLA,J4LA,AGGC,
2  Y,ERR,DYT,HTC,DC,VC,HTA,DA,VA,NPNCH)

MODEL VALUES

      DIMENSION JC(MC1),VC(MC1),DA(MA1),VA(MA1),HTC(MC1),HTA(MA1),
1  GRTC(MC1),PHIVN(MC1),RNCLC(MC1),BHLA(MC1),DHLA(MC1),AGERW(MC1),
2  AGGC(MC1),Y(MWK),DYT(MWK),ERR(MWK)

      WRITE(6,200) TAU
      WRITE(6,202) WT,VL,CN,CA,CAE
      WRITE(6,204) GL,PHIEN,PHIEA
      WRITE(6,205)
      DO 10 I=1,MC1
10  WRITE(6,302) DC(I),VC(I),Y(I),DYT(I),ERR(I),HTC(I),
1  GRTC(I),RNCLC(I),AGGC(I),PHIVN(I),BHLA(I),DHLA(I),AGERW(I)
      WRITE(6,208)
      DO 12 I=1,MA1
12  WRITE(6,300) DA(I),VA(I),HTA(I)
      DO 20 I=1,MC1
      X1=JC(I)
      X2=SQRT(HTC(I))
20  CALL PLOTPT(X1,X2,4)
      CALL OUTPLT
      WRITE(6,210) TAU
      IF(NPNCH.EQ.0) GO TO 100
      PUNCH(7,304) (DC(I),I=1,MC1)
      PUNCH(7,305) (HTC(I),I=1,MC1)
100  CONTINUE

200  FORMAT(///,2X,*MODEL VALUES*,//,2X,*TAU=*,1PE12.4,//)
202  FORMAT(2X,*WT*,10X,*VL*,10X,*CN*,10X,*CA*,10X,*CAE*,//,1PE12.4,
1  4E12.4,//)
204  FORMAT(2X,*GL*,10X,*PHIEN*,7X,*PHIEA*,//,1PE12.4,2E12.4,//)
206  FORMAT(4X,*DC*.3X,*VC*.8X,*Y*.9X,*DYT*.7X,*ERR*.7X,*HTC*.7X,
1  *GRTC*.6X,*RNCLC*.5X,*AGGC*.6X,*PHIVN*.5X,*BHLA*.6X,*DHLA*.
2  6X,*AGERW*)
208  FORMAT(//,4X,*DA*.3X,*VA*.8X,*HTA*)
210  FORMAT(//,15X,*TAU=*,1F6.2,25X,*HCT VS. DC*,//,
1  30X,*-----*)
300  FORMAT(1X,1F6.2,1PE10.2,11E10.2)
302  FORMAT(1X,1F6.2,1PE10.2,10E10.2,1E18.10)
304  FORMAT(1X,*DC=*,1PE10.3,6E10.3)
306  FORMAT(1X,*HTC=*,1PE10.3,6E10.3)
      RETURN
      END
      SUBROUTINE EXMLDT(NCTP,ME,ME1,NE1,TAUE,VE,DE,HTIE,WTDE)

EXPERIMENTAL DATA

NCTP      =1 PRINT EXPERIMENTAL DATA , =0 DO NOT

      DIMENSION TAUE(NE1),VE(ME1),DE(ME1),HTIE(ME1,NE1)
      DIMENSION ALABEL(80)

      DATA X1/24.85/
      WTDE=X1
      READ(5,500) (TAUE(J),J=1,NE1)
      DO 20 J=1,NE1

```

```

      READ(5,502) (ALABEL(L1),L1=1,80)
      READ(5,504) (VE(I),I=1,ME1)
20    READ(5,504) (HTIE(I,J),I=1,ME)
      DO 22 I=1,ME1
22    DE(I)=1.240701*CBRT(VE(I))
      DO 24 J=1,NE1
      HTIE(ME1,J)=0.
      DO 24 I=1,ME
24    HTIE(ME1-I,J)=HTIE(ME1-I+1,J)+(HTIE(ME1-I,J)*(VE(ME1-I+1)-
1    VE(ME1-I)))

```

```

C    PRINT DATA

```

```

      IF(NCTP) 34,34,30
30    WRITE(6,600) (TAUE(J),J=1,NE1)
      DO 32 I=1,ME
32    WRITE(6,650) DE(I),VE(I),(SQRT((HTIE(I,J)-HTIE(I+1,J))/(VE(I+1)-
1    VE(I))))),J=1,NE1)
34    CONTINUE

```

```

C    500 FORMAT(10X,7F10.3)

```

```

      502 FORMAT(80A1)

```

```

      504 FORMAT(1PE10.3,7E10.3)

```

```

      600 FORMAT(1H1,1X,*EXPERIMENTAL DATA*,

```

```

1    //,20X,*TAUE(J)*, //,17X,14F8.3,

```

```

2    //,3X,*DE*,8X,*VE*,4X,*SQRT(FVTE(I,J))* ,/)

```

```

      650 FORMAT(1X,1F6.2,2X,15F8.1)

```

```

      RETJRN

```

```

      ENJ

```

```

      SUBROUTINE EXMDL(JE,NE1,ME1,ME,MC1,MC,TAUE,VE,DE,VC,DC,

```

```

1    HTIE,HTC,HTIM,Z1,NPNCH)

```

```

C    COMPARISON BETWEEN MODEL AND EXPERIMENTAL INVERSE CUMULATIVE NUMBER
DISTRIBUTION

```

```

      DIMENSION TAUE(NE1),VE(ME1),DE(ME1),VC(MC1),DC(MC1),

```

```

1    HTIE(ME1,NE1),HTC(MC1),HTIM(ME1),Z1(MC1)

```

```

C    INTERPOLATION OF MODEL VALUES BY MEANS OF FIRST ORDER APPROXIMATING FUNCTIONS
IT IS ASSUMED THAT THE MODEL VALUES STRADDLE THE EXPERIMENTAL DATA

```

```

      Z1(MC1)=0.

```

```

      DO 30 I=1,MC

```

```

30    Z1(MC1-I)=Z1(MC1-I+1)+HTC(MC1-I+1)-HTC(MC1-I)

```

```

      DO 40 I=1,ME1

```

```

      DO 34 L=1,MC

```

```

      M9=L

```

```

      IF((VC(L).LE.VE(I)).AND.(VC(L+1).GE.VE(I))) GO TO 36

```

```

34    CONTINUE

```

```

35    X1=Z1(M9)+((Z1(M9+1)-Z1(M9))/(DC(M9+1)-DC(M9))*(DE(I)-DC(M9)))

```

```

40    HTIM(I)=X1

```

```

C    COMPARISON BETWEEN EXPERIMENTAL AND MODEL VALUES

```

```

      WRITE(6,600) TAUE(JE)

```

```

      DO 70 I=1,ME1

```

```

      X1=HTIE(I,JE)-HTIM(I)

```

```

      X2=J.

```

```

      IF(HTIE(I,JE).GT.0.) X2=X1/HTIE(I,JE)*100.

```

```

70    WRITE(6,602) DE(I),VE(I),HTIE(I,JE),HTIM(I),X1,X2

```

```

      X1=0.

```

```

      DO 72 I=1,ME

```

```

      X2=HTIE(I,JE)-HTIM(I)

```

```

72    X1=X1+(X2*X2)

```

```

      SSELCL=X1

```

```

      WRITE(6,604) SSELCL

```

```

      DO 74 I=1,ME1

```

```

X1=JE(I)
X2=SQRT(HTIM(I))
X3=SQRT(HTIE(I,JE))
CALL PLOTPT(X1,X2,4)
74 CALL PLOTPT(X1,X3,28)
X1=SQRT(HTIE(I,JE))
IF(HTIM(I).GT.HTIE(I,JE)) X1=SQRT(HTIM(I))
CALL RANGES(0.,50.,0.,X1)
CALL OUTPLT
WRITE(6,608) TAU(JE)
DO 78 I=1,MC
IF(DC(I).LT.DE(I)) GO TO 78
CALL PLOTPT(DC(I),(HTC(I+1)-HTC(I)),4)
75 CONTINUE
DO 80 I=1,ME
80 CALL PLOTPT(DE(I),(HTIE(I,JE)-HTIE(I+1,JE)),26)
CALL OUTPLT
IF(NPNCH.EQ.0) GO TO 200
PUNCH(7,301) JE
PUNCH(7,300) (DE(I),I=1,ME1)
PUNCH(7,302) (HTIE(I,JE),I=1,ME1)
PUNCH(7,304) (HTIM(I),I=1,ME1)
200 CONTINUE
300 FORMAT(1X,*JE=      *,1PE10.3,6E10.3)
301 FORMAT(1X,*JE=      *,1I5)
302 FORMAT(1X,*HTIE=    *,1PE10.3,6E10.3)
304 FORMAT(1X,*HTIM=    *,1PE10.3,6E10.3)
600 FORMAT(1H1,1X,*-COMPARISON BETWEEN EXPERIMENTAL AND MODEL VALUES--
1 // ,3X,*TAU =*,1F6.2,/// ,3X,*DE*,10X,*VE*,10X,*HTIE*,8X,
2 *4TIM*,8X,*EPS*,9X,*RLT DVT*,/)
602 FORMAT(1X,1PE12.4,10E12.4)
604 FORMAT(// ,3X,*LOCAL SUM OF SQUARES*,10X,*SSELCL =*,1PE12.4)
603 FORMAT(// ,15X,*TAU=*,1F6.2,25X,*HTIE AND HTIC VS. D*,
1 //)
RETRN
END
SUBROUTINE RNGMRS(DFN,N,Y1,X3,X2,H1,HMIN,HMAX,EPS,ERR,Z1,Z2,WK)

```

```

-----
-RUNGE KUTTA MERSON SUBROUTINE-----
SOLVES A SYSTEM OF FIRST ORDER ORDINARY DIFFERENTIAL EQUATIONS
WRITTEN JAN ,74

```

```

DFN  EXTERNAL SUBROUTINE THAT EVALUATES THE DERIVATIVES OF Y1 W.R.T X
N    NUMBER OF SIMULTANEOUS ORDINARY DIFFERENTIAL EQUATIONS
Y1   VALUES OF THE DEPENDENT VARIABLES AT THE BEGINNING AND END OF AN
      INTEGRATION INTERVAL
X3   INITIAL VALUE OF THE INDEPENDENT VARIABLE
X2   END VALUE OF THE INDEPENDENT VARIABLE
H1   INITIAL AND UPDATED STEP SIZE
HMIN  MINIMUM ALLOWABLE STEP SIZE
HMAX  MAXIMUM ALLOWABLE STEP SIZE
EPS   MAXIMUM PERCENTAGE RELATIVE ERROR
ERR   ABSOLUTE ERROR ESTIMATES
Z1    WORKING VECTOR
Z2    WORKING VECTOR
WK    WORKING VECTOR
      MIN. DIMENSIONS  Y1(N),ERR(N),Z1(N),Z2(N),WK(5*N)

```

```

DIMENSION Y1(1),ERR(1),Z1(1),Z2(1),WK(1)

```

```

X1=X3
I=1
1 IF((X1+H1).GT.X2) H=X2-X1
CALL DFN(Y1,X1,N,Z2)
2 GO TO J=1,N

```

```

WK(N+J)=H/3.*Z1(J)
4 WK(J)=Y1(J)+WK(N+J)
X=X1+H/3.
CALL DFN(WK,X,N,Z1)
DO 5 J=1,N
WK(2*N+J)=4/3.*Z1(J)
5 WK(J)=Y1(J)+.5*(WK(N+J)+WK(2*N+J))
CALL DFN(WK,X,N,Z1)
DO 6 J=1,N
WK(3*N+J)=H/3.*Z1(J)
6 WK(J)=Y1(J)+.375*WK(N+J)+1.125*WK(3*N+J)
X=X1+H/2.
CALL DFN(WK,X,N,Z1)
DO 7 J=1,N
WK(4*N+J)=H/3.*Z1(J)
7 WK(J)=Y1(J)+1.5*WK(N+J)-4.5*WK(3*N+J)+5.*WK(4*N+J)
X=X1+H
CALL DFN(WK,X,N,Z1)
DO 8 J=1,N
WK(2*N+J)=H/3.*Z1(J)
8 WK(J)=WK(N+J)-4.5*WK(3*N+J)+4.*WK(4*N+J)-.5*WK(2*N+J)
WK(N+J)=Y1(J)+.5*WK(N+J)+2.*WK(4*N+J)+.5*WK(2*N+J)
C RELATIVE ERROR
GROOT=0.
DO 10 J=1,N
Z11=ABS(WK(J))/(ABS(WK(N+J))+1.E-14)*100.
IF(Z11.GT.GROOT) GROOT=Z11
10 CONTINUE
C STEP SIZE ADJUSTMENT
IF(GROOT.LT.EPS) GO TO 12
IF(H1.GT.HMIN) GO TO 11
H1=HMIN
WRITE(6,50) H1,X,GROOT
GO TO 12
11 H1=H1/2.
IF(H1.LT.HMIN) H1=HMIN
GO TO 1
12 DO 14 J=1,N
IF(H.GE.(X2-X3)) ERR(J)=WK(J)
IF(H.EQ.H1) ERR(J)=WK(J)
14 Y1(J)=WK(N+J)
IF(GROOT.LE.(EPS/16.)) H1=2.*H1
IF(H1.GT.HMAX) H1=HMAX
IF(X.GE.(X2-1.E-08)) RETURN
X1=X
GO TO 1
50 FORMAT(///,1X,*---REACHED MINIMUM STEP SIZE---*,1E10.2,/,
1 1X,*---VALUE OF THE INDEPENDENT VARIABLE---*,1E10.2,/,
2 1X,*---MAXIMUM RELATIVE PERCENTAGE ERROR---*,1E10.2,/)
END

```